WILEY-VCH

Peter Haseley and Georg-Wilhelm Oetjen

Freeze-Drying

Third, Completely Revised and Enlarged Edition

Freeze-Drying

Freeze-Drying

Third, Completely Revised and Enlarged Edition

Peter Haseley and Georg-Wilhelm Oetjen

WILEY-VCH
Verlag GmbH & Co. KGaA

Authors

Peter Haseley
Alfons-Auer-Str. 8e
93053 Regensburg
Germany

Georg-Wilhelm Oetjen*
Lübeck
Germany

Cover
The cover photograph shows a production freeze-drying plant with slot door for loading and unloading at the front and main service door at the right hand side.

(Photograph: Austar Group, China)

*deceased

Library of Congress Card No.: applied for

British Library Cataloguing-in-Publication Data A catalogue record for this book is available from the British Library.

Bibliographic information published by the Deutsche Nationalbibliothek The Deutsche Nationalbibliothek lists this publication in the Deutsche Nationalbibliografie; detailed bibliographic data are available on the Internet at <http://dnb.d-nb.de>.

Print ISBN: 978-3-527-34306-5
ePDF ISBN: 978-3-527-80891-5
ePub ISBN: 978-3-527-80893-9
Mobi ISBN: 978-3-527-80892-2
oBook ISBN: 978-3-527-80894-6

Cover Design Adam Design, Weinheim, Germany
Typesetting Thomson Digital, Noida, India
Printing and Binding Weinheim

Printed on acid-free paper

10 9 8 7 6 5 4 3 2 1

Contents

Preface to Third Edition and Acknowledgment

This third, revised edition I would like to dedicate to Dr. Georg-Wilhelm Oetjen, who passed away in 2015. He introduced me to Freeze-Drying and essentially influenced my professional career.

I would like to acknowledge my supporters who helped me to complete this book. Without their continued support and effort I probably would have not been able to bring my work to a successful completion. I would like to thank Mr. Mars Ho – CEO Austar Group, Hong Kong; Mr. Austin McDonald – CEO Sterile Technology LLC, USA; Mr. Manfred Steiner – GEA Lyophil GmbH, Germany; and Mr. Anton Mangold – CEO iQ-mobil solutions, Germany.

Without the professional support of Mrs. Regine Fisher, MD Semicom Media & Communications, Germany, I would have had difficulties to finish the book. She was responsible for the text finalization and proofreading as well as for the editing and handling of images, tables, and graphics.

Peter Haseley
Dipl.-Ing.(FH)

Preface to the Second Edition

Drying of food and herbs is one of the oldest preservation methods of humanity.

Freeze-drying was first carried out, as K.H. Neumann wrote in his book *Grundriß der Gefriertrocknung,* 1954, by Altmann, who freeze-dried parts of organs in 1890. In 1932, Gersh designed an effective vacuum plant for freeze-drying of histological preparations with the help of the diffusion pump just invented by Gaede at that time. Sawyer, Lloyd, and Kitchen successfully freeze-dried yellow fiber viruses in 1929. Industrial freeze-drying began, as E.W. Flosdorf shows in his book *Freeze-Drying,* 1949, with the production of preserved blood plasma and penicillin.

Vacuum technology and penicillin were also my own first encounter with freeze-drying. After my studies of physics at the university in Göttingen, I worked in the development department of E. Leybold's Nachf. where I had to build a freeze-drying plant for penicillin. Since that time I was engaged in vacuum process technology for almost 25 years, from 1952 on as managing director of Leybold Hochvakuum Anlagen GmbH. From this time I know Peter Haseley, whom I employed for the freeze-drying department. Later, as "Geschäftsführer" of Steris GmbH, he was actively involved with engineering modern freeze-drying plants with all their complex requirements of documentation and qualification. Together we have developed an old idea of mine to control the freeze-drying process not by predetermined time, pressure, and temperature data, but by the data measured during the process. Therefore, I was very happy when Peter Haseley agreed to rewrite the chapters "Installation and Equipment Technique" and "Trouble-Shooting and Regulatory Issues" for this second edition.

Freeze-drying has always fascinated me as the most complex vacuum process. Mechanical and chemical engineering, chemistry and biology, and sterility and regulatory issues are all part of the freeze-drying process.

After my retirement from the managing board of Drägerwerke AG, I had the time to write the German edition of this book, *Gefriertrocknen,* published in 1997, and the first English edition in 1999. In 2004, a translation into Japanese has also been published.

When I started to write the German edition, Mr. Wolfgang Suwelack, managing partner of Dr. Otto Suwelack Nachf. GmbH & Co., asked me to work for him as consultant in freeze-drying, and I have to thank him for the permission to use some of the results achieved in the last years. This activity was the new start of my

work in freeze-drying, and I would therefore like to dedicate this book to Mr. Wolfgang Suwelack out of gratitude for a harmonic cooperation lasting for over a decade.

Several companies and publishing houses have granted permission to use drawings and photographs to which they own the copyright. Mr. Haseley and I are grateful to all of them because they have thus made it possible to present freeze-drying under many aspects.

We have tried to show the interconnection between the properties of the product, the goal to make it stable, and the necessary processes to achieve this. The problems of the different process steps are discussed with examples and the parameters influencing each step are described. We have avoided to follow the many theoretical attempts to describe one or more of the freeze-drying steps, but have restricted ourselves to a few equations that permit calculating process and product data with sufficient accuracy, or to at least allow an estimate based on measuring some of the data.

The freezing of a product is a very important step. The structure in the frozen product decides whether the product can be freeze-dried at all, and under which conditions it can be done. Therefore, the consequences of freezing rate, layer thickness of the product, and excipients are discussed in some detail. The second main point is the measurement and control of the two drying phases, the main and secondary drying, and the third point concentrates on the residual moisture content, its measurement, and the consequences during storage of the dry product. There will be critical opinions that some of the processes are unilaterally represented. I have tried to show the limits and advantages of certain procedures to enable the reader to decide for himself whether the ideas of the quoted authors or my own can be applied best to his particular task.

The approximately 270 literature references in the 1999 edition have been in part replaced and furthermore supplemented to a new total of 370.

Dr. Georg-Wilhelm Oetjen

1

Foundations and Process Engineering

Freeze-drying or lyophilization is a drying process in which the solvent and/or the suspension medium is crystallized at low temperatures and thereafter sublimed from the solid state directly into the vapor phase.

Freeze-drying is mostly done with water as solvent. Figure 1.1 shows the phase diagram of water and the area in which this transfer from solid to vapor is possible.

Table 1.1 shows the relation of temperature (°C), mTorr, and mbar.

This step is relatively straightforward for pure water. If the product contains two or more components in true solutions or suspensions, the situation can become so complicated that simplified model substances have to be used to make the process more understandable. Such complex systems occur ubiquitously in biological substances.

The drying transforms the ice or water in an amorphous phase into vapor. Owing to the low vapor pressure of the ice, the vapor volumes become large, as can be seen in Figure 1.2. During the second step of the drying, the water adsorbed on the solids is desorbed.

The goal of freeze-drying is to produce a substance with good shelf stability and which is unchanged after reconstitution with water, although this depends also very much on the last step of the process: the packing and conditions of storage.

The advantages of freeze-drying can be summarized as follows:

- The drying at low temperatures reduces degradation of heat-sensitive products.
- The liquid product can be accurately dosed.
- The moisture content of the final product can be controlled during the process.
- The dry product can have an appealing physical form.
- The dry product with a high specific surface area is rapidly reconstituted.

The disadvantages are as follows:

- The high investment, operating and maintenance costs.
- The complexity of the process and the equipment requires a team of skilled and permanently trained collaborators.

Freeze-Drying, Third Edition. Peter Haseley and Georg-Wilhelm Oetjen.

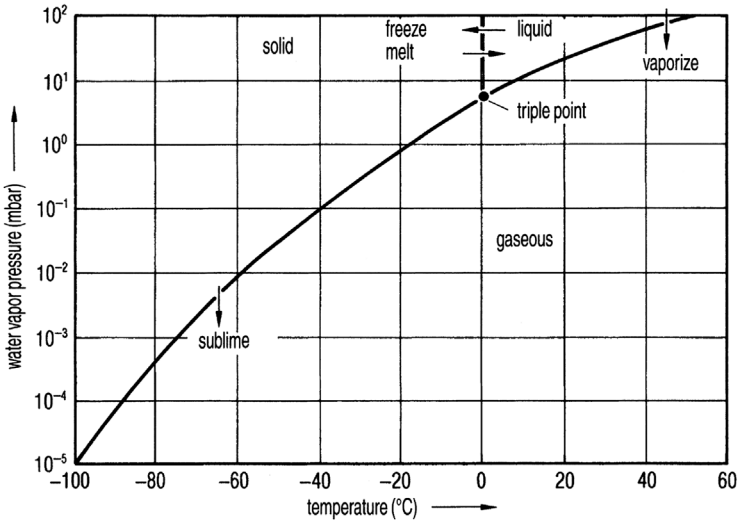

Figure 1.1 Phase diagram of water.

1.1 Freezing

To freeze a substance, it must be cooled to a temperature at which the water and the solids are fully crystallized or at which areas of crystallized ice and solids are enclosed in zones in which amorphous concentrated solids and water remain in a mechanically solid state (see Section 1.1.2). In the zone of freezing, the ice crystals first grow, thus concentrating the remaining solution, which can vary the pH value. In many substances an eutectic temperature can be determined, but in many others this value does not exist. The crystallization depends on several

Table 1.1 Vapor pressure of water.

Temperature (°C)	mTorr	mbar	Temperature (°C)	mTorr	mbar
0	4579	6.108	−40	96.6	0.1238
−4	3280	4.372	−44	60.9	0.0809
−8	2326	3.097	−48	37.8	0.0502
−12	1832	2.172	−52	23.0	0.0300
−16	1132	1.506	−56	13.8	0.0183
−20	930	1.032	−60	8.0	0.0107
−24	526	0.6985	−64	4.6	0.0061
−28	351	0.4669	−68	2.8	0.0034
−32	231	0.3079	−72	1.4	0.0018
−36	150	0.2020			

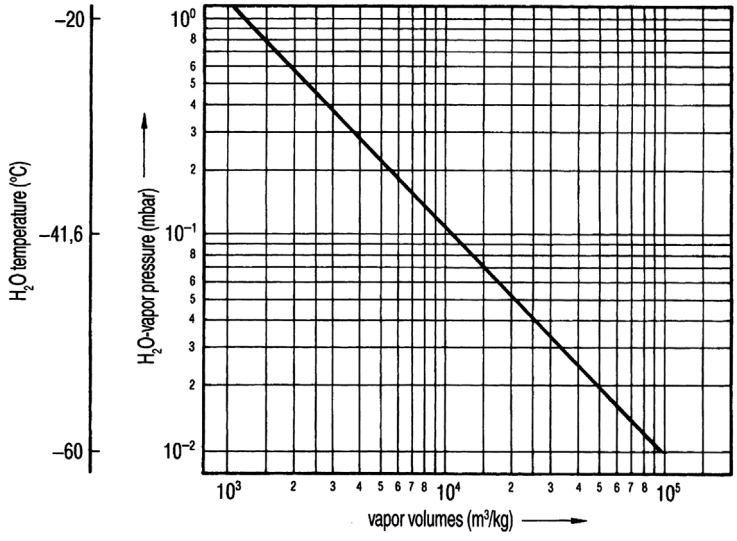

Figure 1.2 Specific volume of water vapor as a function of the water vapor pressure. The temperature of the vapor in this diagram is that of ice.

factors that influence each other: cooling rate, initial concentration, end temperature of cooling, and the time at this temperature. In several products, no crystallization takes place and the product remains in an amorphous, glass-like phase or a mixture of both occurs.

1.1.1 Amount of Heat, Heat Conductivity, Heat Transfer, and Cooling Rate

For pure water, the melting heat to be withdrawn for freezing (Q_{tot}) can be calculated by Eq. (1.1), if the starting and the desired final temperatures are known:

$$Q_{tot} = c_w(T_1 - T_0) + Q_e + c_e(T_0 - T_2) \quad (kJ/kg) \tag{1.1}$$

where

c_w = specific heat capacity of water;
Q_e = melting heat of ice;
c_e = specific heat capacity of ice;
T_0 = freezing temperature of ice;
T_1 = initial temperature of water;
T_2 = final temperature of ice.

The temperature dependences of c_w between +20 and 0 °C and c_e between 0 and −50 °C have to be adopted as average values.

For solutions and suspensions, the solid content has to be recognized. This is reflected in Eq. (1.2):

$$Q_{tot} = [(c_w x_w + c_{f'} x_f)(T_1 - T_0)] + x_w Q_e + [(c_e x_w + c_f x_{w'})(T_0 - T_2)] \tag{1.2}$$

where

x_w = part of water above 0 °C;
c_f = specific heat of solids, for example:
for animal products ≈ 1.47 kJ/kg °C
for plant products ≈ 1.34 kJ/kg °C
for some solids:
carbohydrates ≈ 1.42 kJ/kg °C
proteins ≈ 1.55 kJ/kg °C
fats ≈ 1.7 kJ/kg °C
salts ≈ 0.8 kJ/kg °C;
x_f = part of solids;
$x_{w'}$ = part of ice, which freezes until temperature T_2 is reached. If not all water is frozen at T_2, an additional term has to be introduced, which reflects the cooling of the unfrozen water.

Table 1.2 shows the unfreezable water (UFW) in various foods. The reasons and the consequences are described in Sections 1.1.3 and 1.1.4. In comparing these data with other publications, for example, Ref. [1], smaller values may be found. This can depend not only on the different raw materials and the history of the probe until measurement but also on the methods of measurement.

For meat with less than 4% fat content, Riedel [2] has published an enthalpy diagram (shown in Figure 1.3). For some other foods, Table 1.3 shows enthalpy data at various temperatures. At −40 °C the enthalpy is set at 0 kJ/kg.

Table 1.2 Percentage of water frozen out at various temperatures for some foods.

Product	Frozen out water at °C (% of the total water)				UFW (% of total water)
	– 10	– 15	– 20	– 30	
Lean beef	82	85	87	88	12
Haddock	84	87	89	91	9
Whole eggs, liquid	89	91	92	93	7
Yolk	85	86	87	87	13
Egg white	91	93	94		6
Yeast	80	85	88	89	11
Fruit juice	85	90	93	96	(3)
Peas	80	86	89	92	(7)

Part of Table 1.1 in Refs [2,3].

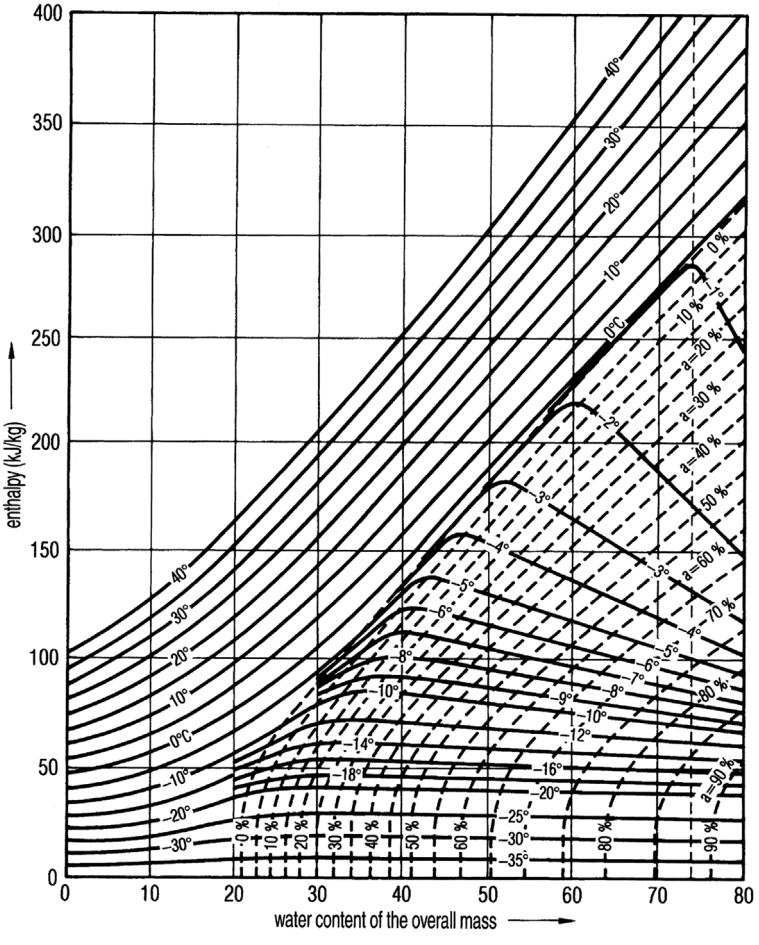

Figure 1.3 Enthalpy of lean beef meat as a function of its water content (0 kJ/kg at −40 °C). The temperatures at the beginning of cooling and the desired end temperatures for freezing are plotted as parameters. The dotted lines indicate the percentage of water frozen at the end temperatures (see also Figure 1 from Refs [2,3]). *Example*: Beef meat has 74% water. At +10 °C, the enthalpy is ~325 kJ/kg; at −20 °C, the enthalpy is ~40 kJ/kg; therefore, 285 kJ/kg have to be removed and 83% of the water frozen. The maximum possible (88%) (see Table 1.1) is reached at ≃30 °C.

In Table 1.4 the UFW data for products used in pharmaceuticals are listed in Ref. [6] of Chapter 3.

The transport of the calculated energy from the freezing zone of the product to the cooling medium can be described in a simplified way by the following steps: the product is an infinite plate, which is cooled from one site only, and the energy flows only perpendicular to its infinite expansion. The crystallization energy flows from the crystallization zone, through the already frozen ice, through the container bottom to a shelf, and finally into the cooling brine.

Table 1.3 Enthalpy of meat, fish, and egg products.

Product	Water content (weight %)	Enthalpy (kJ/kg) at a temperature of °C					
		−30	−20	−10	0	+5	+20
Beef, 8% fat	74.0	19.2	41.5	72.4	298.5	314.8	368.4
Cod	80.3	20.1	41.9	74.1	322.8	341.2	381.0
Egg white	86.5	18.4	38.5	64.5	351.3	370.5	427.1
Whole egg	74.0	18.4	38.9	66.2	308.1	328.2	386.9

Part of Table 1.3 in Refs [2,3].

The freezing time (t_e) is approximately given by Eq. (1.3) [4]:

$$t_e = \Delta J / \Delta T \rho_g (d^2/2\lambda_g + d/K_{su}) \tag{1.3}$$

$$t_e = \Delta J / \Delta T \rho_g (w + u) \tag{1.3a}$$

where

t_e = freezing time;
ΔJ = enthalpy difference between the initial freezing point and the final temperature;
ΔT = difference of temperature between the freezing point and the cooling medium;
D = thickness of the product parallel to direction of prevailing heat transfer;
ρ_g = density of the frozen product;
λ_g = thermal conductivity of the frozen product;
K_{su} = surface heat transfer coefficient between cooling medium and the freezing zone.

Table 1.4 Percentage of unfrozen water (UFW) , which cannot be frozen by lower temperature (see Figure 1.20).

Excipient	UFW (%)
Trehalose	16.7
Sorbitol	18.7
Maltose	20
Glycerin	27
Glucose	29.1
Sucrose	35.9
Lactose	40.8
Glycerol	45.9
Fructose	49.0

The thermal conductivity of ice and of dried products are relatively well known, but the surface heat transfer coefficient K_{su} during freezing and the total heat transfer coefficient K_{tot} during freeze-drying vary largely, as described in the various chapters. Table 1.5 gives a survey of some data of interest in freeze-drying.

The influence of the variables in Eq. (1.3) can be studied by an example. A slice of lean beef with a thickness that is small compared with its horizontal dimensions is to be frozen to −20 °C. The influences of the border of the slice are neglected. The thickness of the slice is $d = 2$ cm. As can be seen in Figure 1.3, the enthalpy difference for beef with 74% water is approximately 240 kJ/kg. If the freezing process starts between 0 and −3 °C and is mostly finished at −20 °C, the cooling medium has a temperature of −43 °C and an average $\lambda = 1.38 \times 10^{-2}$ J/°C cm s is used when the slice is in contact with a liquid, having a similar behavior to water at 20 °C, $K_{su} = 4.61 \times 10^{-2}$ J/°C cm^2 s can be used for the calculation. The freezing time is

$$t^{fl}_{e\,d20} = 5.4(0.725 \times 10^2 + 0.43 \times 10^2) \approx 12 \text{ min} \tag{1.4}$$

As shown in Eqs. (1.3) and (1.3a), the thickness d has a major influence if the conductivity term w, which includes d^2, is large compared with the transfer term u, which includes only d.

Table 1.5 Surface heat transfer coefficient, total heat transfer coefficient, and thermal conductivity.

K_{su}	From gases to a solid surface (kJ/m^2 h °C): free convection	17–21
	Laminar flow 2 m/s	50
	Laminar flow 5 m/s	100
K_{su}	Between the shelf of a freeze-drying plant and a product in vials or trays during freezing (kJ/m^2 h °C)	200–400
K_{su}	Between a liquid and a solid surface (kJ/m^2 h °C): oil in tubes, laminar	160–250
	LN_2 by drops on the product[a)]	900
	From liquids similar to water[b)]	1600
	From water at 1 bar, temperature difference <7 °C[c)]	3600
K_{tot}	Between the shelf of a freeze-drying plant and the sublimation front in the product contained in vials or trays under vacuum[d)] (kJ/m^2 h °C)	60–130
λ	Thermal conductivity (kJ/m^2 h °C)	
λ_g	Frozen product (ice)[e)]	5.9–6.3
λ_{tr}	Dry product[f)]	0.059–0.29

a) Reinsert, A.P.: Factors affecting the erythrocyte during rapid freezing and thawing. *Ann. N. Y. Acad. Sci.* **85**, 576–594, 1960.
b) From Ref. [3].
c) From VDI- = Wärmeatlas 5. Auflage, Bild 38, P. A 26, VDI-Verlag, Düsseldorf, 1988.
d) Figures 1.116 and 1.117.
e) From Ref. [3].
f) From Refs [5–8].

In Eq. (1.4), $w{:}u = 1.7{:}1$, showing that the influence of the conductivity is almost double that of the transfer. Assuming that d is only 0.2 cm, the freezing time falls to

$$t^{\mathrm{fl}}_{\mathrm{e\,d2}} = 5.4(0.725 + 4.35) \approx 28\ \mathrm{s} \tag{1.5}$$

In this case, $w{:}u = 1{:}6$ and the transfer term is overwhelming. The freezing time is neither reduced by d^2 nor by d, since the importance of w and u has changed. An increase in d by a factor of 3, to 6 cm, prolongs the freezing time:

$$t^{\mathrm{fl}}_{\mathrm{e\,d60}} \approx 70\ \mathrm{min} \tag{1.6}$$

Here $w{:}u = 5{:}1$, and the freezing time depends mostly on the heat conductivity of the material.

The freezing of a slice of beef in direct contact with a model liquid has been used to demonstrate the influence of the two terms w and u. To freeze a product for freeze-drying, two methods are mainly used: (i) freezing of the product in trays or in vials on cooled surfaces; or (ii) in a flow of cold air. If these methods do not result in a sufficient freezing rate, liquid nitrogen (LN_2) in direct contact with the vials is used (see Figures 2.2 and 2.3) or droplets of the product are sprayed into LN_2 (see Section 2.1.4).

The heat transfer coefficient K_{su} in air varies strongly with the gas velocity, surface conditions of the product, and the geometry of the installation. In practical operations, it will be difficult to achieve K_{su} values of $1.7–2.5 \times 10^{-3}$ J/cm^2 s °C or ~75 kJ/m^2 h °C and in many applications only half of this value (or less) may be possible. However, even with this high K_{su}, the above-discussed slice of beef (2 cm thick) has a freezing time

$$t^{\mathrm{lu}}_{\mathrm{e\,d20}} = 5.4(0.72 \times 10^2 + 9.5 \times 10^2) \approx 92\ \mathrm{min} \tag{1.7}$$

compared with 12 min when cooled by a liquid, since the K_{su} of a gas is ≤10% that of a liquid.

The time to reach a desired temperature level can be expressed as freezing rate v_{f}, the change in temperature per unit time, for example, °C/min. Thus, the results of Eqs. (1.4)–(1.7) are approximately as follows:

(4) $v_{\mathrm{f}} = 1.7$ °C/min (5) $v_{\mathrm{f}} = 43$ °C/min
(6) $v_{\mathrm{f}} = 0.3$ °C/min (7) $v_{\mathrm{f}} = 0.2$ °C/min

These data are calculated by using 0 °C as the start and −20 °C as the end temperature to show the relative data. The exact calculation requires more information, as given below.

Figure 1.4 is the cooling curve of vials filled with a solution of 4% solid content and 27 mm filling height. From the curve, v_{f} can be estimated:

0 to −10 °C	~0.15 °C/min
0 to −14° C	~0.18 °C/min
−14 to −30 °C	~0.73 °C/min
0 to −30 °C	~0.3 °C/min

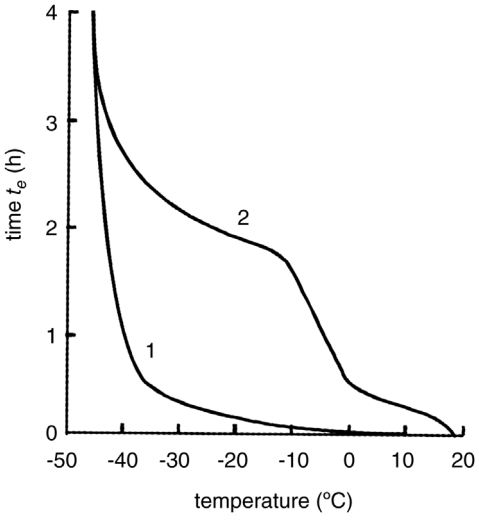

Figure 1.4 Temperatures during freezing as a function of time. 1, shelf temperature; 2, product temperatures in a product with $d = 2.7$ cm, solid content ~4%. (From Steris GmbH, 50354 Hürth, Germany.)

During the freezing of the main part of the water, v_T is only 25% compared with the value after most of the water is crystallized. Taking the average value between 0 and −30 °C can therefore be misleading: The intention to freeze at a rate of 0.3 °C/min has not occurred during an important part of the operation. The difference between 0.15 and 0.7 °C/min influences the structure of the product. How important the change is has to be checked from case to case, but the difference between 0.15 and 0.7 °C/min is most likely important.

With Eq. (1.3), it is also possible to estimate $K_{su.}$ The uncertainties are the differences between the freezing of the product around the temperature sensor and in the undisturbed product, the position of the sensors, the correlation between time and temperature, and occasionally also the actual amount of frozen water. From Figure 1.4, the estimated K_{su} is approximately 480 kJ/m^2 h °C with a possible error of ±10% and maximum error of ±20%. Such high values can only be expected if the vials are carefully selected for their uniformity, especially with respect to a very even and flat bottom. Otherwise, the K_{su} can be much smaller, for example, 230 kJ/m^2 h °C as calculated from data shown in Table 1.6.

If the vials are placed in trays and these are loaded on the shelves, K_{su} will be reduced, very likely to <100 kJ/m^2 h °C, with the consequence that the freezing time is twice or three times longer and freezing rates of 1 °C/min cannot be achieved.

Equation (1.3) can be used to estimate the influence of the variation of the layer thickness and the shelf temperature, if the K_{su} values are measured for the type of vials used.

As shown, for example, in Figures 1.5–1.7, the temperature as a function of time can vary. Therefore, the calculation of freezing rates and the resulting K_{su} contain a certain error. Table 1.7 shows a comparison of cooling rates [9]. Run 1 is from Figure 1.5, run 3 from Figure 1.6, and run 5 from Figure 1.7. The percentage indicates the maximum differences between the measurements with three temperature sensors in three vials.

Table 1.6 Cooling time and freezing rate as a function of layer thickness for well manufactured vials, not selected for the flatness of the bottom.

Layer (mm)	Time from 0 °C to – 10 °C (min)	Cooling rate (°C/min)	Time from – 10 °C to – 30 °C (min)[a)]	Cooling rate (°C/min)	Cooling rate from 0 °C to – 30 °C (°C/min)
6	14	0.71	9.3	2.1	1.29
12	32	0.31	12.9	1.6	0.67
20	60	0.17	19.0	1.1	0.38
30	105	0.095	28.3	0.7	0.23

a) In this time the cooling of the glass of the vials from 0 °C to −30 °C is included.

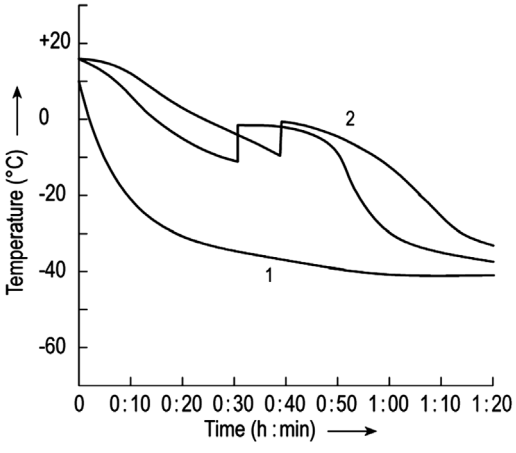

Figure 1.5 Temperatures during freezing as a function of time for two different runs in the same plant, with the same product, T_{sh} cooled as quickly as possible. 1, shelf temperature; 2, product temperature.

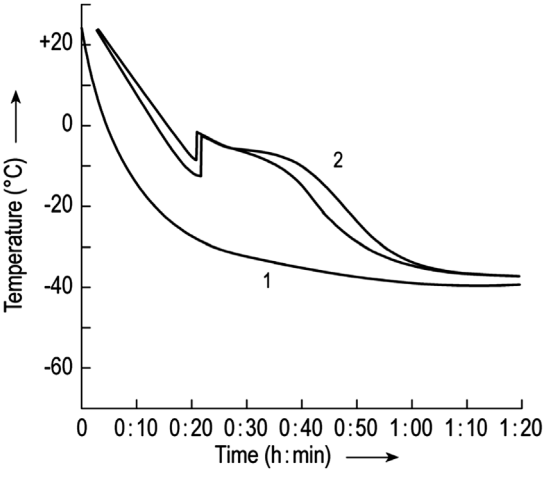

Figure 1.6 See Figure 1.5.

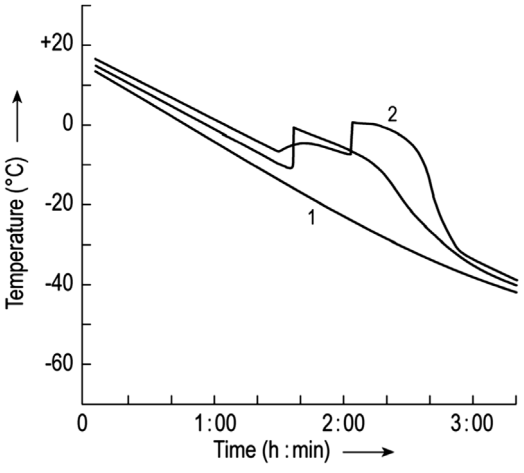

Figure 1.7 As Figure 1.5, but T_{sh} cooled controlled. (From Ref. [9].)

To increase ν_t, the following possibilities can be used: (i) reducing d; (ii) reducing the shelf temperature; (iii) precooling of the vials, for example, to −80 °C, and filling the precooled product, for example, +4 °C, into the cold vials; (iv) cooling of the vials directly with LN_2; and (v) dropping the product into LN_2. With precooled vials, ν_t can be on the order of 10–20 °C/min, and with direct cooling by LN_2 40–60 °C/min and more is possible. With droplet freezing, up to 1000 °C/min can be achieved.

For laboratory work, different cooling liquids can be used as shown in Table 1.8. However, these substances are not easy to use, they boil and are partially explosive. The cooling method shown in Figure 1.8 can be helpful. LN_2 is evaporated under vacuum, freezing part of the N_2 as a solid. In this mixture

Table 1.7 Comparison of cooling rates, measured in the same installation, with comparable vials and comparable d.

Run	Time from 0 °C to − 10 °C (min)	Cooling rate (°C/min)	Time from − 10 °C to − 30 °C (min)	Cooling rate (°C/min)
1	34 ± 5	0.29 ± 15%	13 ± 5	1.5 ± 38%
2	25	0.4	17	1.2
3	23 ± 1.5	0.4 ± 6%	15 ± 2	1.3 ± 13%
4[a)]	19 ± 2.5	0.5 ± 13%	21 ± 3.5	0.95 ± 17%
5[b)]	79 ± 7	0.13 ± 9%	38 ± 5	0.5 ± 13%

a) During the cooling phase −10 to −30 °C $\Delta T \approx 13$ °C instead of ≈ 20 °C in run 1–3; taking this into account, the value of 0.95 corresponds to 1.4 in run 1–3.

b) The shelf temperature was constantly lowered at ≈10 °C/30 min. Therefore, ΔT is only ≈ 8 °C during the freezing phase, compared with ≈ 30 °C in run 1–3. 0.13 °C/min therefore corresponds to ≈ 0.48 °C/min. The same applies to the 0.5 °C/min during the cooling phase, making it comparable to 1.3 °C/min.

Table 1.8 Physical data of cooling liquids.

Medium	Boiling point, T_s (°C)	c_p of liquid at T_s (kJ/kg °C)	λ of liquid at T_s (kJ/mh °C)	Heat of vaporization at T_s (kJ/kg)
Helium (He^4)	−268.9	4.41	0.098	20.5
Nitrogen	−195.8	2.05	0.506	197.6
Propane	−42.3	2.19		426.2
n-Pentane	+36.1	2.2		234.1
(Figure 2 from Umrath, W. Kurzbeitrag für die Tagung Raster-Elektronenmikroskopie in Medizin and Biologie, unpublished, Brühl.)				

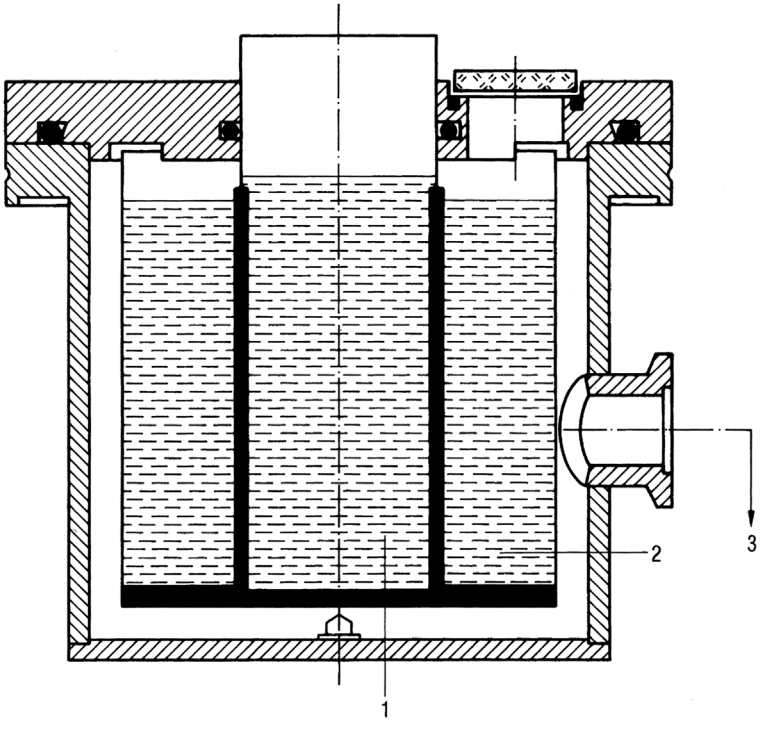

Figure 1.8 Apparatus to produce a mixture of liquid and solid nitrogen. 1, inner container with LN_2; 2, external container with LN_2 connected to a vacuum pump; 3, the container 2 is evacuated to ~124 mbar and kept at that pressure. The evaporating nitrogen reduces the temperature in 2 and thereby also in 1, since the two containers are in close thermal contact. A temperature of −210 °C is reached in container 1 after ~5 min. (From Umrath, 1974 [10]. Reproduced with permission of John Wiley & Sons.)

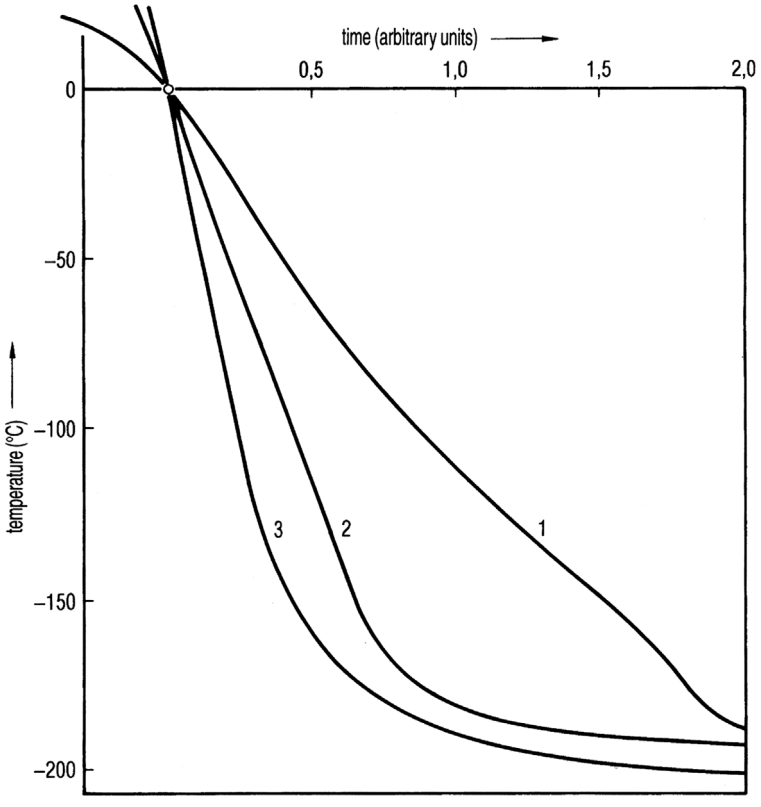

Figure 1.9 Relative cooling rate of a small sample in different forms of N_2. (The plot for LN_2 depends mostly on the successful removal of the nitrogen gas.) Melting solid nitrogen reduces the formation of gaseous N_2, since the crystallization energy melts the solid nitrogen and does not evaporate the liquid. (*Note*: Theoretically, cooling in solid N_2 would be the fastest method, but liquid N_2 will be formed and the heat transfer is not stable.) 1, LN_2; 2, LN_2 + solid N_2; 3, melting of solid N_2. (See also Umrath, W., unpublished results, Brühl.)

the solid melts, if energy is produced from cooling and crystallization. Thus, the formation of gaseous N_2 is greatly reduced, which otherwise limits the heat transfer. Figure 1.9 shows the relative cooling rates for different forms of N_2.

Riehle [11] has calculated the theoretically possible cooling velocities for small objects between 1 and 10^{-3} mm as shown in Figure 1.10. These calculations are made for a substance consisting of water only and K_{su} is assumed to be infinitely large for the geometric dimensions shown in (a) a sphere, (b) a square cylinder of infinite length, and (c) a plate of infinite length and the thickness X, cooled only from one side. For the plate (c), v_f is also calculated for three limited K_{su}: 10^3, 10^4, and 10^5 W/m^2 s (Chain lines). The purpose of this calculation is to show that freezing rates of 10^3–10^4 °C/s (6×10^4–6×10^5 °C/min) cannot be achieved. However, these rates are necessary to reduce the velocity of crystal growth in pure water sufficiently to obtain water in a glass-like phase with irregular particle size $<10^{-8}$ m.

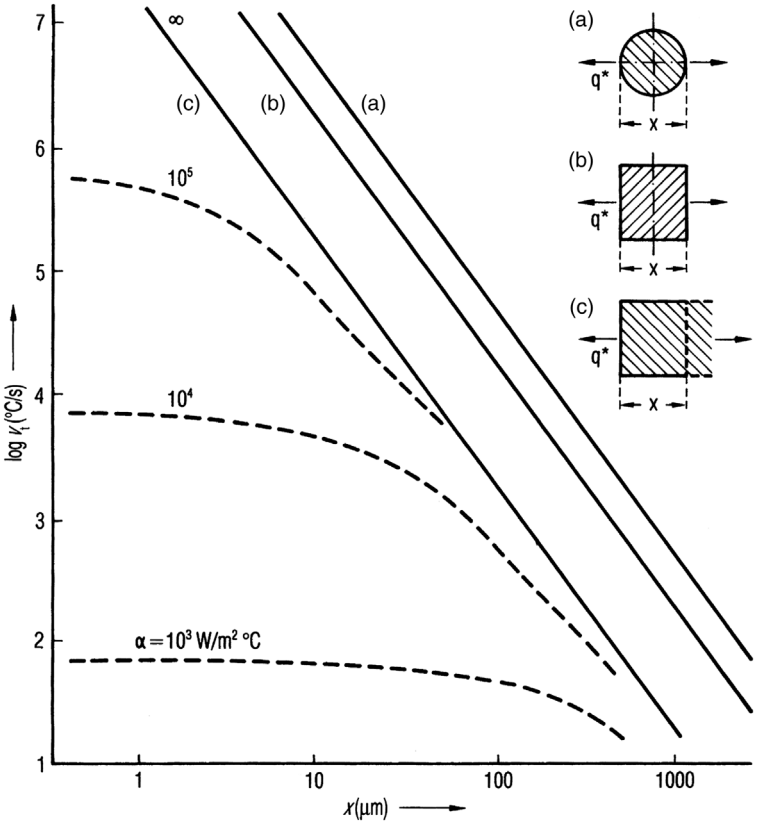

Figure 1.10 Maximum theoretical cooling rate for different geometric configurations (a–c) of water by cooling with LN_2, if α is assumed to be ∞. The dotted lines are calculated for three values: $\alpha = 10^3$, 10^4, 10^5 W/m^2 s. (From Riehle, 1986 [11]. Reproduced with permission of John Wiley & Sons.)

Riehle showed that such freezing rates can only be reached for layers of <0.1 mm under a pressure of 1.5–2.5 kbar.

A different way of obtaining short cooling and freezing times is to evaporate part of the water in the product under vacuum. The evaporation energy of water at 0 °C is approximately 2.5×10^3 kJ/kg. To cool 1 kg of beef from 0 to −20 °C, 240 kJ have to be removed, which corresponds to ~0.1 kg of water to be evaporated or 15% of the water in the beef. This quick evaporation will produce foam or bubbles in the product. This is unacceptable in most cases, since the original structure is changed and that part of the product that is vacuum dried will have different qualities to the freeze-dried part. Often the product frozen in this way cannot be freeze-dried at all.

1.1.2 Structure of Ice, Solutions, and Dispersions

The water molecule has a configuration as shown in Figure 1.11 [12], having a pronounced dipole moment, which produces the liquid phase at relatively high

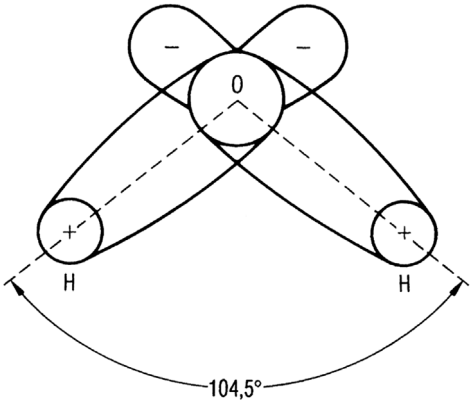

Figure 1.11 Configuration of the electrical charges in a water molecule. (From de Quervain, 1975 [12]. Reproduced with permission of Elsevier.)

temperatures and ensures a structure in the envelope of molecules that surrounds ions [13]. However, clusters are also in water without ions; these consist of approximately 10 water molecules in a tetrahedral geometry surrounded by O—H—O groups. The clusters are not stable units with always the same molecules and they are constantly exchanging molecules with their surroundings, having an average lifetime of between 10^{-10} and 10^{-1} s. The number of clusters decreases as the temperature is lowered until freezing occurs.

In water that is very well cleared of all foreign particles, the clusters begin to crystallize in the subcooled water at −39 °C; this is called homogeneous nucleation. Foreign, undissolved particles in water act as nuclei for the crystallization of ice and this is called heterogeneous nucleation. In normal water there exist approximately 10^6 particles per cm^3 and these act as nuclei for crystallization. They become increasingly effective if their structure is similar to that of water. If a nucleus has formed, it grows faster at the outside than at the inside, producing (depending on subcooling and cooling velocity) structures of ice stars (Figure 1.12). During further freezing, branches grow at an angle of 60°, well known as frost flowers. For a crystal of $1 \times 10^{-9}\,mm^3$, 2.7×10^{10} molecules have to be brought into position. It is difficult to visualize how such a crystal can be formed in a small fraction of a second, but it is obvious that the growth of such a crystal will be influenced or disturbed by many factors.

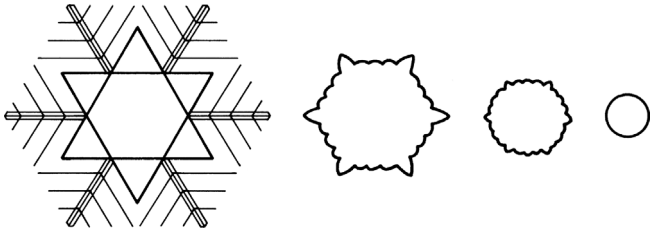

Figure 1.12 Growth of ice crystals in water. The subcooling is increased from left to right. (From de Quervain, 1975 [12]. Reproduced with permission of Elsevier.)

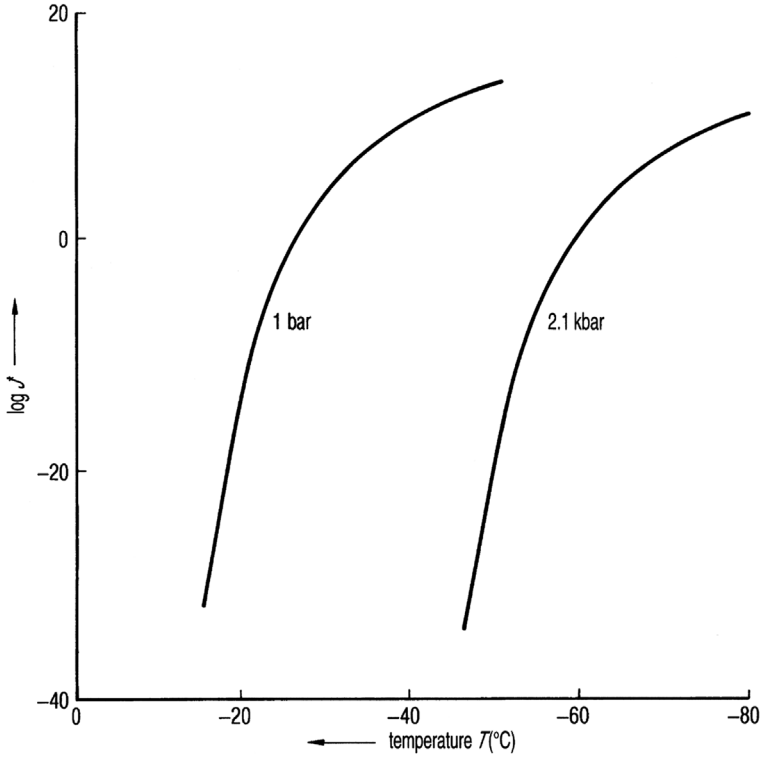

Figure 1.13 Nucleation rate J^* (nuclei/volume time) as a function of the temperature of the water–ice phase transformation. (From Riehle, 1986 [11]. Reproduced with permission of John Wiley & Sons.)

Figure 1.13 shows logJ^* (J^* = nuclei per unit time and volume) as a function of the temperature of the water–ice phase transition at different pressures of 1 and 2100 bar according to Riehle. At 2100 bar, J^* is comparable to J^* at an approximately 35 °C higher temperature. Under pressure, water can be subcooled further, with a delayed formation of nuclei.

The growth of crystals is determined by the diffusion of molecules to the surface of the nucleus, the finding of a proper place, and the distribution of the freed energy to the surroundings. Under normal conditions (cooling speed $v_f < 10^2$ °C/s and subcooling $T_{sc} < 10$ °C), Eq. (1.8) can be used:

$$v_k = \text{constant} \times T_{sc}^n \tag{1.8}$$

where $n = 1$ if the energy transport and $n = 1.7$ if the surface reactions are decisive (Hillig and Turnbull, *J. Chem. Physiol.*, **1956**, *24*, 914). If $T_{sc} > 10$ °C, the diffusion process has to be taken into account. Since v_k is furthermore dependent on the concentration, the calculation of v_k is insecure.

To summarize, the following can be stated:

To produce large crystals,

- the rate of nucleation should be small, therefore the subcooling should be small;
- the freezing should take place in a quasi-equilibrium situation between solution and crystals;
- the temperature should be as high as possible, since the crystals grow with the function $e^{-1/T}$;
- the time given for crystallization has to be increased, since v_K is inversely proportional to the size of the crystal.

To produce only very few or no crystals,

- freezing should take place under high pressure (Figure 1.13);
- the freezing rate should be as high as possible, to produce a large degree of subcooling.

As can be seen from Figure 1.14, in pure water Ic and the other phases can only be reached under high pressures.

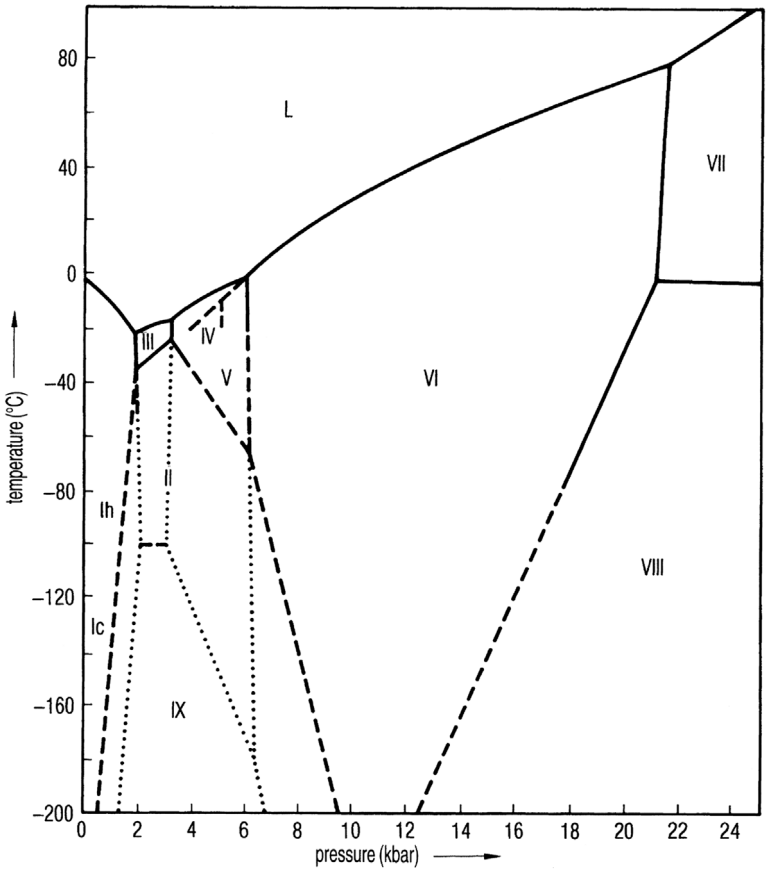

Figure 1.14 Phase diagram of water. L = liquid water; Ih = hexagonal ice; Ic = cubic ice; III–IX crystal configurations of ice. (From de Quervain, 1978 [12]. Reproduced with permission of Elsevier.)

Dowell and Rinfret [14] demonstrated that the phase at temperatures above −160 °C consists of small crystals ~400 Å in size and having cubic and pseudo-hexagonal structures.

Figure 1.15 shows the three phases of ice that exist under normal pressure as a function of temperature, indicating also the time it takes to change from one type to another. If water vapor is condensed on a cold surface in a very thin film, amorphous ice is formed and remains stable at −160 °C for a long time. As shown in Figure 1.15, the change from amorphous to cubic ice will take $\sim 5 \times 10^5$ min or more than a year. The rate of change depends very much on the temperature: at

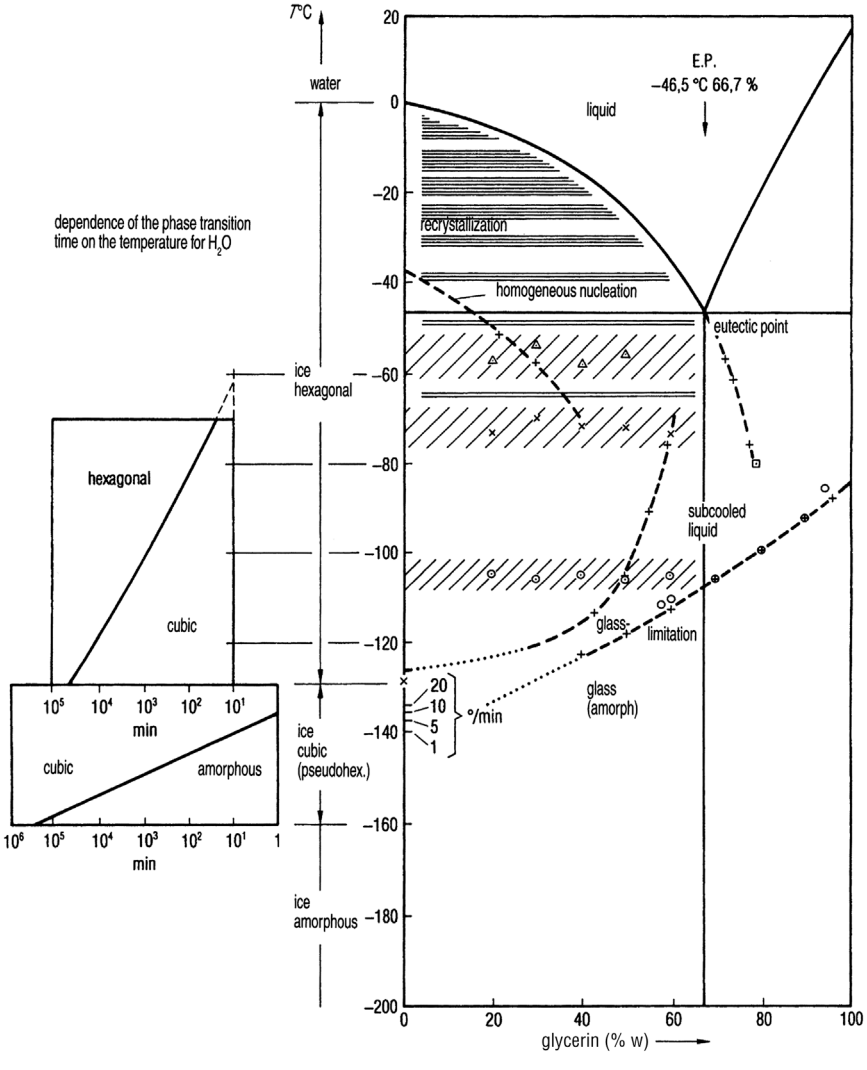

Figure 1.15 Water–glycerin phase diagram. On the left-hand side, the dependence of the phase transformation time on the ice temperature is shown: At −140 °C, amorphous ice transforms into cubic ice in ~10 min. (See also Figure 8 from Ref. (Umrath, W., Kurzbeitrag für die Tagung Raster-Elektronenmikroskopie in Medizin and Biologie, unpublished, Brühl.))

−135 °C the same change takes only 1 min. This change is called devitrification. At −125 °C the change from cubic to hexagonal ice takes ∼1000 h, while at −65 °C only hexagonal ice is stable.

To summarize, amorphous ice is stable below −160 °C, until −125 °C when cubic ice is formed irreversibly from the amorphous phase; above this temperature, hexagonal ice develops. Between −160 and −130 °C, cubic ice can be embedded in an amorphous surrounding. During warming, it is likely that some amorphous ice changes directly into the hexagonal form. Between −130 and −65 °C all three phases could be present, depending on the time–temperature function. This behavior of pure water changes if water solutions, suspensions in water, and mixtures with water are studied, as will be the case for virtually all products to be freeze-dried.

The freezing process will be discussed with model substances, which will be used as cryoprotective agents (CPAs). If a solution of water and glycerol is cooled quickly, a 10% solution in a layer of 3×10^{-3} mm and $\nu_f = 10^6$ °C/s can be vitrified ([11], p. 218), but in a 5% solution crystals of 1000 Å are formed. At high pressures (1.5–2.1 kbar), 4×10^3 °C/s is sufficient for a 10% solution and 2×10^4 C/s for a 5% solution to achieve vitrification. For these measurements, the absence of foreign particles must be presumed in order to use the subcooling effect fully. Foreign particles could also come from containers, holding devices, and so on.

Riehle has proved the existence of such vitrification by electron microscopy. With higher concentrations of glycerol, vitrification becomes simpler. Luyet [15] showed diagrammatically (Figure 1.16) how various phase changes take place at different glycerol concentrations. At 60% glycerol devitrification takes place at ≃115 °C and increases with increasing glycerol concentration to ≃85 °C. However, such high concentrations of glycerol can normally not be used to freeze-dry organic substances.

As shown for pure water, the phase transitions depend on the cooling rate, the end temperature of cooling, and the temperature and time of the treatment after cooling. The rate of rewarming is especially critical. One has to differentiate between quasi-static situations, which are independent of time and all other dynamic states, in which the history of the present situation and the rate of the further changes play an important role.

Freezing processes can be divided into two categories: one type is so slow that they run under almost equilibrium conditions; others are too fast to approach the equilibrium situation. Figures 1.17–1.19 show the effect of the freezing rate on the structure of the dried product. In Figure 1.17, milk has been frozen slowly (0.2–0.4 °C/min) in trays. In Figure 1.18, mannitol solution has been frozen in vials at a rate of ∼1 °C/min; the arch at the bottom represents the vial bottom. In Figure 1.19, γ-globulin has been frozen in LN_2 (∼10–15 °C/min). This shows only the upper part of the dry product. The cake has been frozen so quickly from the bottom and the walls that the concentrated liquid has been pushed to the center, where it has been pressed to form a cone. The cake is cut and in the center of the cone a channel can be seen, in which highly concentrated solution has been included, leaving a channel. Since the solids of this part are agglomerated to the surrounding areas, the structure of the channel is partially collapsed during drying.

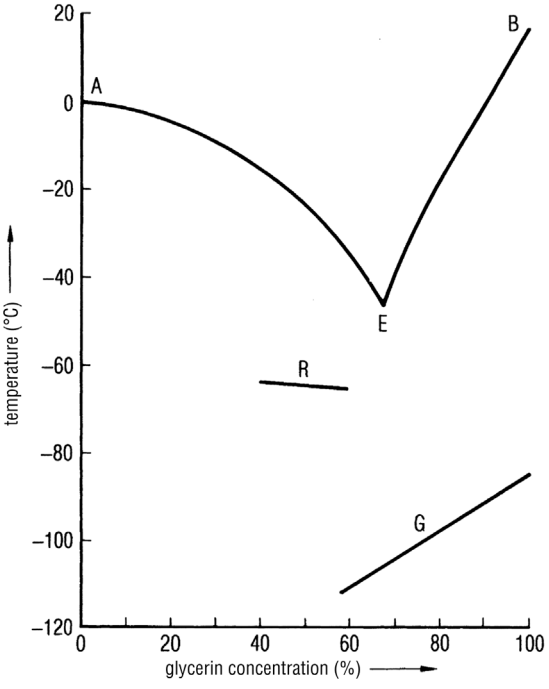

Figure 1.16 Temperature as a function of the concentration of water–glycerin mixture at which phase transformations occur. (Figure 14 from Ref. [15].) Definitions by Luyet: AE, formation of small crystals or molecular groups; E, eutectic point; EB, formation of clusters; R, eruptive recrystallization; G, glass transition.

The nonequilibrium status can be seen during a slow cooling of a water–glycerol solution. Starting with a 20% glycerol solution, pure ice crystals will first be formed until at −46.5 °C when the glycerol concentration has reached 66.7%. At this temperature, the eutectic should solidify. However, it is possible to reduce

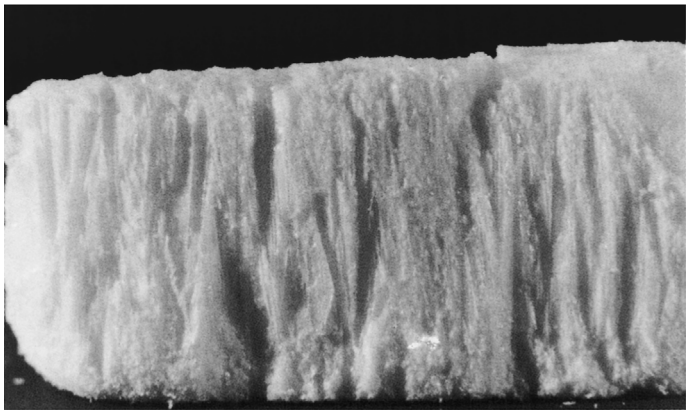

Figure 1.17 Milk frozen slowly (0.2–0.4 °C/min) in a tray. (Courtesy of Steris GmbH, Hürth, Germany.)

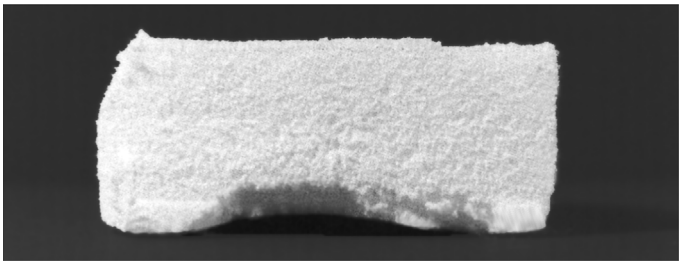

Figure 1.18 Mannitol solution frozen at ~1 °C/min in a vial on precooled shelf. (Courtesy of Steris GmbH, Hürth, Germany.)

the temperature to −58 °C with a glycerol concentration of 73%. A further decrease in temperature does not crystallize any more water. The solution is so highly concentrated and viscous and the mobility of the water molecules is so much reduced that the remaining water is unfreezable (UFW) in an amorphous state between the glycerol and ice molecules.

Figure 1.20 ([16], p. 286) shows diagrammatically at a given starting concentration which parts will be ice, unfrozen water, and glycerol at a freezing temperature actually used under equilibrium conditions. A solution of 20% initial glycerol contains, when cooled to −50 °C, 70% ice, 10% UFW, and 20% glycerol. At −58 °C, the line marked UFW is effective; 72% is glycerol and 27% UFW.

The fact that a certain amount of water cannot crystallize in a highly concentrated solution, and that the molecules cannot move any more to the existing crystals, is important during the freezing of biological substances. Tables 1.2 and 1.4 show this for some food products and CPAs.

The combination of this knowledge and the results of quick-freezing processes provide a theoretical opportunity to freeze products into a solid, amorphous state. If the freezing velocity is smaller than required for vitrification, but large enough to avoid an equilibrium state, an amorphous mixture will result of hexagonal ice, concentrated solids, and UFW.

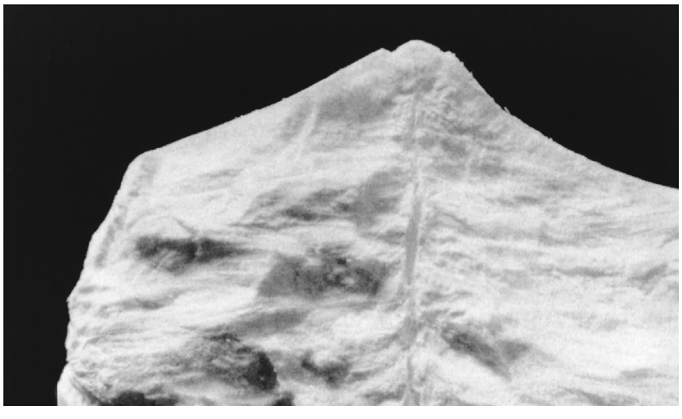

Figure 1.19 γ-Globulin solution frozen in a vial by LN_2 at ~10 °C/min (only the upper part of the product is shown). (Courtesy of Steris GmbH, Hürth, Germany.)

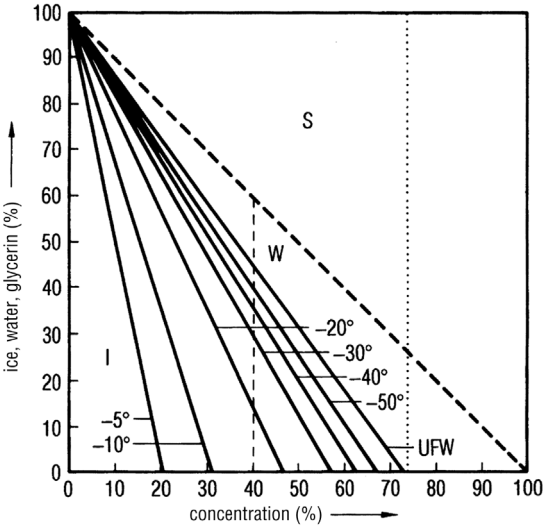

Figure 1.20 Rate of ice, water, and dissolved substance in the state of equilibrium of a glycerin–water solution as a function of the initial glycerin concentration, plotted at different freezing temperatures between −5 and −50 °C. A 40% glycerin solution frozen at −30 °C contains in the state of equilibrium ~32% ice, 30% water, and 38% glycerin. The line marked UFW represents the temperature at which the glycerin concentration becomes so high that no more water can be frozen (the water molecules become highly unmovable). The glycerin concentration is ~73% and the UFW concentration 27%. The diagram shows the equilibrium conditions, which may not exist during quick freezing. (See also Figure 1 from Ref. [16].)

1.1.3 Influence of Excipients

The freezing of complex organic solutions and suspensions is often difficult to predict theoretically. The methods to analyze the freezing process and the structure formed are described in Section 1.1.5. The freezing is influenced by several factors, which often act in opposing directions:

1) Freezing rate
   – slow: quasi-equilibrium
   – very fast: dynamically governed
2) Number and geometry of foreign particles, which influence the heterogeneous nucleation: the closer their structure is similar to the ice structure, the better is their effectiveness as nuclei.
3) The degree of subcooling, which depends on the substance, but is strongly influenced by the two points above.
4) The rate of growth of the ice crystals, which depends on temperature and the viscosity of the solution; the latter increases strongly with increasing concentration of the solution.
5) That part of the water that is not frozen due to high freezing rate forms highly viscous occlusions in between the ice crystals.
6) The crystallization of the solved substance(s) (or part of it) or the subcooling and the delay of this crystallization, which depends again not only on the temperature but also very much on the viscosity of mixture.

By adding excipients not only is it possible to influence the cooling and solidification processes, but also they may be necessary to obtain one or more of the following objectives:

- To grow stable structures if the amount of solids is small, for example, <3% in the solution, to prevent solid particles from being carried out of the vials by the water vapor stream (bulking agents).
- To adjust pH data (buffers).
- To avoid or induce crystallization.
- To protect the active constituent during freezing (cryoprotectants).
- To protect the active constituent during freeze-drying (lyoprotectants).
- To reduce changes of the active constituent during storage (e.g., unfolding or aggregation of proteins.

An example of avoiding crystallization of sucrose by adding polyvinylpyrrolidone (PVP) was given by Shamblin and Zografi [17] even if a significant level of absorbed water is present. Zeng *et al.* [18] described the effect of the molecular weight (MW) and the added amount of PVP on the glass transition temperature T_g and the crystallization of sucrose; 5% of PVP of MW 300 K increased T_g from 48.3 °C for freeze-dried sucrose alone to 58.8 °C; 2.5% of PVP of MW 24 K or 40 K showed smaller or no effects on T_g. Shalaev *et al.* [19] freeze-dried sucrose in the presence of citric acid (citric acid:sucrose 1: 10) to RM <0.1% w/w. At 50 °C, the sucrose undergoes significant inversion in spite of the low RM. The rate of inversion is directly related to the citric acid concentration in the solution before freeze-drying. The authors concluded that the freeze-drying of sucrose with acidic substances may lead to substances that could react with other ingredients. Kouassi and Roos [20] freeze-dried maltodextrin–sucrose (2: 1) and maltodextrin–lactose–sucrose solutions (1: 1: 1) with invertase (10 mg/17.2 g). Sorption isotherms and T_g values of the amorphous dried products were measured. Sucrose hydrolysis was observed significantly at 24 °C and 0.662 aw. Saleki-Gerhardt and Zografi [21] studied the crystallization of sucrose from the amorphous state, influenced by absorbed water and additives (lactose, trehalose, and raffinose). Table 1.9 shows the data for T_g and T_c with absorbed water, and Table 1.10 the respective data with additives.

Mannitol, a frequently used excipient, shows complexity in its application. Yu *et al.* [22] reported the formation of a metastable mannitol hydrate during freeze-drying. The amount of mannitol hydrate varies from vial to vial in one batch. It reduces the drying rate, it can be converted to anhydrous polymorphs, redistributing the residual hydrate water, and it shows varying moisture levels from vial to vial. Cannon and Trappler [23] found at least three different polymorphs of mannitol. Under all studied process conditions, all three polymorphs were present, but in different ratios, strongly dependent on the freezing technique.

Pyne and Suryanarayanan [24] followed the phase transitions of glycine during freeze-drying among other methods in the sample chamber of an X-ray diffractometer. Freezing rates of 20 and 2 °C/min of a 15% wt/wt glycin solution resulted in the crystallization of 2-glycin with an increasing amount after annealing to −10 °C. Glycin immersed in LN_2 formed an amorphous product. Upon heating to −65 °C, an unidentified crystalline phase of glycin was observed, which

Table 1.9 Glass transition temperature T_g and crystallization temperature T_c for amorphous sucrose, trehalose, lactose, raffinose, and amorphous sucrose in the presence of absorbed water.

Product	T_g (°C)	T_c (°C)
Sucrose	74	130
Sucrose, 0.99% H_2O	60	125
Sucrose, 1.47% H_2O	58	115
Sucrose, 1.98% H_2O	50	100
Sucrose, 3.13% H_2O	32	92
Trehalose	115	–[a)]
Lactose	108	185
Raffinose	102	–[a)]

a) Did not crystallize.
Table I and II from Ref. [23].

transformed at ≃55 °C to 2-glycin. After annealing, 3-glycin appeared to an extent that depended on the annealing temperature. Cooling rate, annealing, and the temperature during MD influence the solid state of glycin.

Hinrichs *et al.* [25] compared inulin of various degrees of polymerization with trehalose as glass-forming agents. Inulin above a certain degree of polymerization, $DP_n/DP_w > 5.5/6.0$ and trehalose stabilize alkaline phosphatase equally well. The T_g and T'_g values for inulin of <5.5/6.0 were higher than those for trehalose.

Glucose-6-phosphate dehydrogenase (G6PDH) freeze-dried with sucrose/raffinose at different mass ratios showed a higher T_g at higher mass ratios of raffinose than sucrose [26]. Different mass ratios did not influence the recovery of G6PDH after freeze-drying, but during storage low sucrose offered the best enzyme stability.

Fakes *et al.* [27] evaluated the moisture sorption behavior of mannitol, anhydrous lactose, sucrose, D-(+)-trehalose, dextran 40, and povidine (PVP K24) as bulking agents. Mannitol was found to be crystalline and nonhygroscopic

Table 1.10 Crystallization temperature of sucrose with various proportions of additives.

Additives (% w/w)	Crystallization temperature (°C)		
	Lactose	Trehalose	Raffinose
0.0	130	130	130
1.0	131	128	128
5.0	137	145	148
10.0	156	161	160

Table IV in Ref. [23].

Table 1.11 Size and number of pores in chicken meat as a function of freezing rate.

Freezing rate (°C/min)	Size of pores (μm)[a)]	Rate of pores (%)
0.5	≥10	95
9	≥10	65
230	≥10	25
0.5	≥30	85
9	≥30	22
230	≥30	12

a) $1\ \mu m = 10^{-3}\ mm = 10^{-6}\ m$.

before and after freeze-drying with RM 0.1–0.3% w/w at 25 °C and 10–60% RH. Anhydrous lactose, sucrose, and trehalose were crystalline and relatively non-hygroscopic with RM 0.86, 0.15, and 9.2%, respectively. After freeze-drying, they were amorphous with RM 1.6, 2.5, and 1.2%, respectively, and adsorbed moisture in an increasing RH atmosphere. Lactose adsorbed 10% water and formed its crystalline hydrate at 55% RH.

The cooling rate directly influences the size of the ice crystals, which can be measured after drying by the size of the pores in the product. Thijssen and Rulkens [28] gave the size of the pores in chicken meat (Table 1.11). Figure 1.21 shows the average size of pores in 20% dextrose solution as a function of the

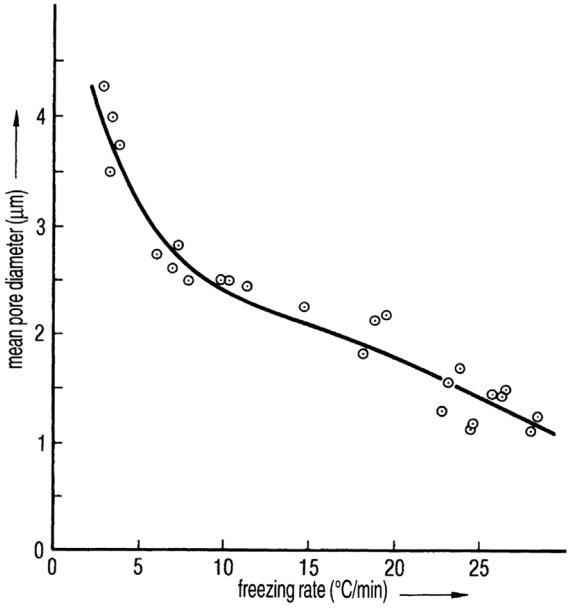

Figure 1.21 Pore diameter as a function of freezing rate in 20% dextran solution. (See also Figure 3 from Ref. [28].)

freezing rate. Godward *et al.* [29] used NMR to measure the pore size distribution in freeze-dried starch gels. They used the fact that starch surfaces change the relaxation for acetone proton transverse magnetization and recommended this method for pore size measurements in food systems. The pore size influences the drying rate and the retention of aroma (see Section 1.2.5).

Reid *et al.* [30] described the effect of the addition of 1% of certain polymers on the heterogeneous nucleation rate: At −18 °C, the rate was 30 times greater than in distilled, microfiltered water and at −15 °C, the factor was still 10-fold higher. All added polymers (1%) influenced the nucleation rate in a more or less temperature-dependent manner. However, the authors could not identify a connection between the polymer structure and nucleation rate. Nonetheless, it became clear that the growth of dendritic ice crystals depended on two factors: (i) the concentration of the solution (5–30% sucrose) and (ii) the rate at which the water–ice crystals phase boundary moved. However, the growth was found to be independent of the freezing rate. (*Note:* The freezing rate influences the rate of boundary movement.) The chances of a water molecule reaching dendritic ice decrease as sucrose concentration increases and the distance between the points of the ice stars increases. The addition of polymers reinforces this effect.

Burke and Lindow [31] showed that certain bacteria (e.g., *Pseudomonas syringae*) can act as nuclei for crystallization if their surface qualities and their geometric dimensions are close to those of ice. Rassmussen and Luyet [32] developed a connection for solutions of water with ethylene glycol (EG) , glycerol (GL) , and polyvinylpyrrolidone (PVP) between the subcooling to the heterogeneous and the homogeneous nucleation of ice.

The heterogeneous and homogeneous temperatures of nucleation during cooling (5 °C/min) and the melting temperatures during rewarming may be measured by differential thermal analysis (DTA). Figure 1.22 shows the resulting phase diagram for water–glycerol and Figure 1.23 for water–PVP. Glycerol reduces the temperature of homogeneous crystallization to a much greater extent than PVP; the melting temperatures follow the same tendency. Figures 1.22 and 1.23 also show the temperatures of devitrification: 50% PVP is sufficient to avoid crystallization at ≃68 °C, while 50% glycerol reaches this effect only at ≃132 °C.

PVP decreases the temperatures of crystallization less than GL, the temperatures of devitrification being higher with PVP than with GL. With GL, crystallization can be avoided until ≃70 °C, but PVP pushes devitrification in an amorphous product to higher temperatures.

Sutton [33] studied the question of how quickly solutions with certain CPAs (GL, dimethyl sulfoxide (DMSO) , and others) have to be cooled in order to avoid crystallization. At 100 °C/min, concentrations of 42.1% DMSO and 48.5% GL are necessary to achieve the glass phase. With a 32.5% solution of (2*R*,3*R*)-(−)-butane-2,3-diol, the same effect can be accomplished at ∼50 °C/min. Sutton showed (see Figure 1.24) that polyethylene glycol with a molecular weight of 400 (PEG 400) reduced the critical cooling rate to ∼25 °C/min. The addition of PEG 8000 [34] improved the protection of lactate dehydrogenase (LDH) by maltodextrins, if maltodextrins with low dextrose equivalents are used.

Levine and Slade [36] investigated the mechanics of cryostability by carbohydrates. Figure 1.25 shows an idealized phase diagram developed from differential

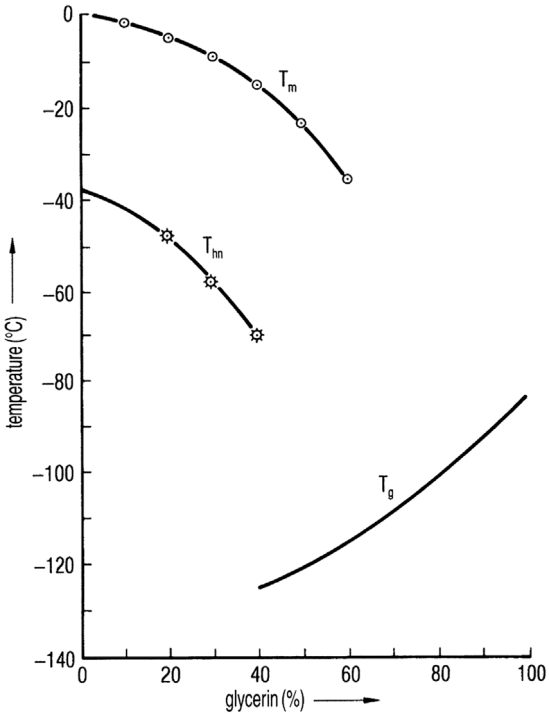

Figure 1.22 Phase diagram for glycerin–water. T_m, melting temperature; T_{hn}, temperature of homogeneous crystallization; T_g, devitrification temperature. (See also Figure 3 from Ref. [32].)

scanning calorimetry (DSC) measurements for hydrolyzed starch (MW >100) and for polyhydroxy combinations having a low molecular weight. With slow cooling (quasi-equilibrium conditions), no water crystallizes below the T_g curve.

The terms "antemelting" and "incipient melting" describe phenomena that occur at temperatures near T_g. Also the "eruptive" crystallization, during the main drying of the freeze-drying process, is the consequence of a collapse of the matrix, allowing the water molecules to diffuse to the ice crystals. This may also free volatile substances, enclosed in the amorphous phase. These phenomena can also occur only in a part of the product, especially if the temperature gradient in the product is substantial. Measurements of T_r and T_c by other authors agree well with T'_g measurements made by Levine and Slade [36], for example, for sucrose −32/−32 °C, for maltose −32.2/−29.5 °C, for lactose −32/−28 °C (Tables 5 and 6 in Ref. [36]). T'_g, c'_g, and g UFW/g carbohydrate are characteristic data for such solutions. Shalaev and Kaney [37] investigated the solid–liquid state diagram of the ternary system water–glycine–sucrose with DTA and X-ray diffraction. Figure 1.26 shows the isoplethal section of the solid–liquid state diagram for a glycine/sucrose ratio of $R = 0.1$. The line EE' divides the two-phase (ice + amorphous phase) and single-phase (amorphous phase) fields. The lines ABB' and CDD' subdivide the fields with different states of the amorphous phase. Below T'_g (line ABB), the amorphous phase is in a structural solid state and the translational

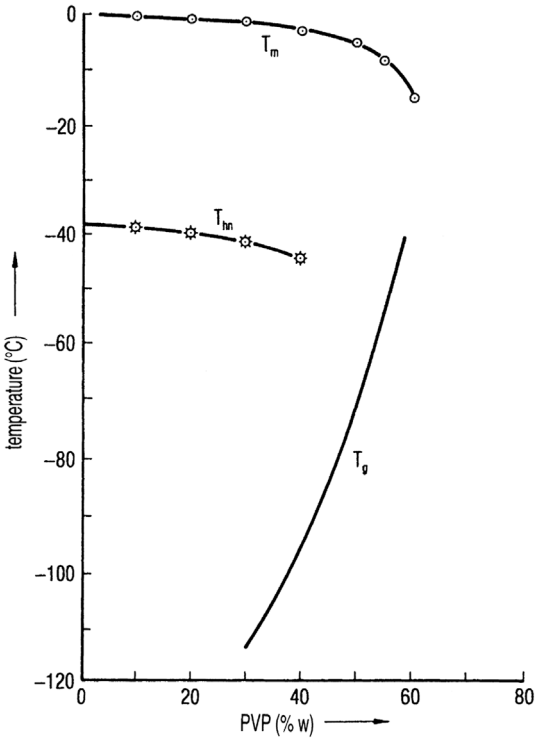

Figure 1.23 Phase diagram for polyvinylpyrrolidone (PVP)–water. For explanation, see Figure 1.22. (See also Figure 4 from Ref. [32].)

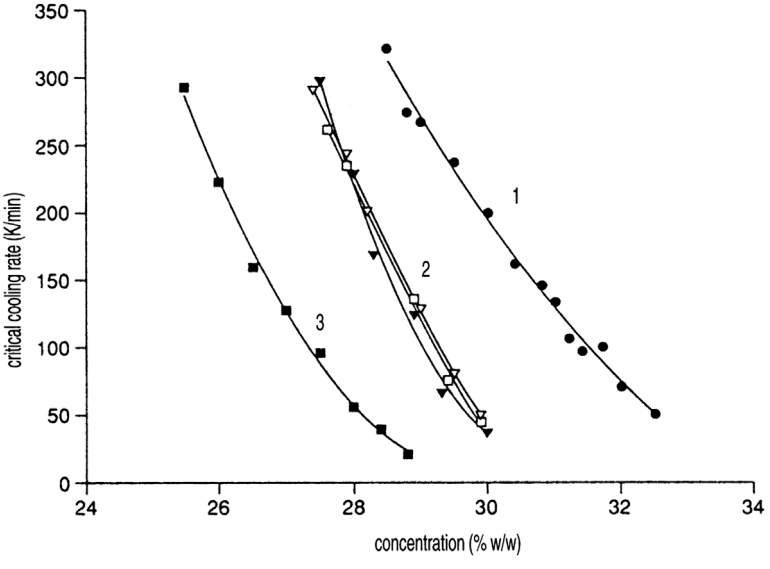

Figure 1.24 Critical cooling rates for butane-2,3-diol and dextran as a function of butane-2,3-diol concentration. 1, butane-2,3-diol; 2, butane-2,3-diol and dextran 20; 3, butane-2,3-diol and PEG 400. (From Sutton, 1992 [35]. Reproduced with permission of Elsevier.)

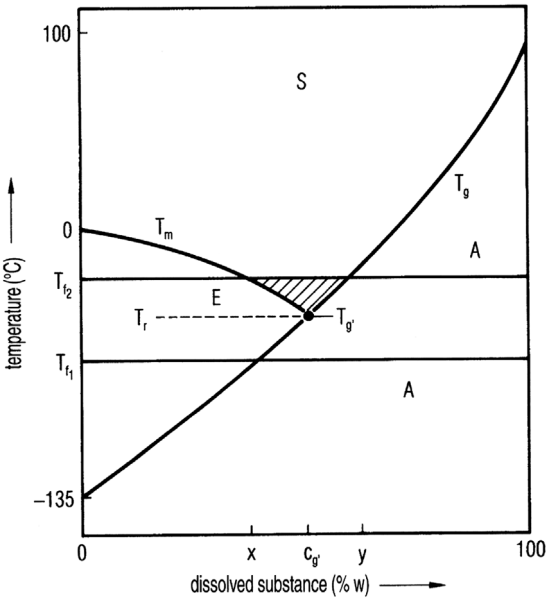

Figure 1.25 Idealized diagram to show generally the dependence of the phase on temperature and concentration. The dissolved, hypothetical substance consists of small carbohydrates as found in food. The figure illustrates the meaning of T'_g. If a temperature range between T_{f1} and T_{f2} is applied, the product can, above T'_g, recrystallize, start melting, or remain in the amorphous phase, depending on the concentration of the dissolved substance. Below T'_g and at concentrations lower than c'_g, crystallization is possible. A, amorphous solid; E, ice; S, solution area. (See also Figure 1 from Ref. [36].)

motion of the molecules is retarded. Above T'_g, the product transforms into a structural liquid state, but the sample keeps its form because the viscosity is so high. At $R = 1$, devitrification is observed at −30 °C and ≥50% water.

Jang *et al.* [38] investigated the glass transition temperature T'_g for FK 906 (a synthetic peptide) during rewarming from the frozen state and T_g of the dry product in the presence of sucrose, maltose, trehalose, and lactose and also polymers with different molecular weights and three salts. For the first group of disaccharides, the Gordon–Taylor equation [39] describes the glass transition temperatures as a function of the FK906 content if the T_g of each component is known. The three salts have approximate eutectic temperatures of NaCl −21 °C, NaBr −31 °C, and KCl −11 °C, and FK 906 −19 °C. NaCl (0.1–0.3%) lowers the T'_g of a 10% FK 906 solution from −19 to −27 °C. NaBr (0.1–1%) solutions have approximately the same effect, while KCl induces a small decrease from −19 to −23 °C at concentrations of 0.1–0.2% in 10% FK 906 solution. However, on increasing the concentration to 1.5%, T_g increases by approximately 2 °C. The glass transition temperature of the freeze-dried product is not changed by NaCl contents up to 0.6%. Nicolajsen and Hvidt [40] described a similar effect of NaCl in the trehalose–NaCl–water system. At trehalose concentrations above 3.5% frozen to −70 °C and heated at 2 °C/min, no eutectic transition was found, indicating that all the NaCl is trapped in the glass phase. However, the lower the

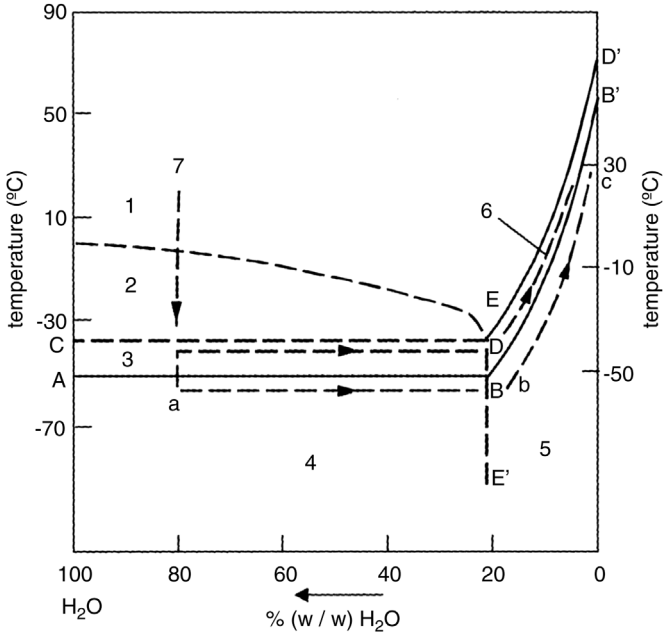

Figure 1.26 Isoplethal section of the solid–liquid state diagram for $R = 0.1$. Section fields: 1, solution (viscous-flow state); 2, ice; 3, ice and amorphous phase (mechanical properties of a solid); 4, ice + glass; 5, glass; 6, amorphous phase (mechanical properties of a solid); 7, freeze-drying pathway. (From Shalaev, 1994 [37]. Reproduced with permission of Elsevier.)

glass transition temperature, the larger the % NaCl/% trehalose ratio. NaCl appears to be a destabilizing factor in the glass phase.

As shown in Section 1.1.5, DSC, MDSC, and TMDSC have provided a better understanding of changes in glass, amorphous, and crystalline phases.

For freeze-drying, one can summarize as follows:

- If the product temperature approaches T'_g from lower temperatures, the viscosity changes rapidly (within a few degrees) by several decimal powers. Since the product temperature can also be measured only with a certain accuracy (see Section 1.2.3), one has to account for both uncertainties. It is recommended that the maximum product temperature during main drying be chosen 3–5 °C below T'_g.
- The addition of certain carbohydrates increases, by varying degrees, the values and decreases the amount of UFW. These stabilize the glass phase to higher temperatures and permit higher drying temperatures. They can also bind volatile components.

Carpenter *et al.* [41] showed that the stabilization of proteins, using the enzymes phosphofructokinase (PFK) and lactate dehydrogenase (LDH) as models, during freezing and thawing and freeze-drying is based on two different mechanisms. In Table 1.12, nine substances provide relatively good protection against denaturation during freezing and thawing (40–85% of the activity

Table 1.12 Activity of lactate dehydrogenase after freezing and thawing in the presence of dissolved substances, which are mostly repelled by proteins.

Dissolved substance	Highest tested concentration (mol/L)	Remaining activity (%)
None	0.0	21.5
Sucrose	1.0	85.4
Lactose	0.5	74.2
Glucose	1.0	60.2
Glycerin	1.0	71.4
Sorbitol	1.0	75.3
Mannitol	1.0	67.3
Glycine	2.0	39.1
Sodium acetate	2.0	81.2
$MgSO_4$	2.0	61.7
NaCl	3.0	20.7

See also Table III in Ref. [41].

remains). This does not apply for 3 mol/L NaCl (the 10 substances listed are a selection of 28 substances studied).

Timasheff *et al.* [42] explained the stabilizing or destabilizing effect of the additives by the combination of the additive molecule with the protein (destabilizing) or its rejection by the protein (stabilizing). The predominant effect of the additive depends on its chemical qualities and the surface structure of the protein. For example, NaCl bounds predominantly to the LDH and destabilizes it. Urea had the same effect on LDH during freezing.

A different effect stabilized PFK during freeze-drying and subsequent storage. As shown in Table 1.13, only disaccharide can protect PFK. Since only a special group of CPAs is effective, one can assume that these CPAs combine with the protein. If water molecules of the hydrated envelope of the protein are removed during freeze-drying, the molecules of the effective CPA can replace these water molecules, keeping the protein stable. Prestrelski *et al.* [43] demonstrated by infrared spectroscopy that the addition of 10 mM mannitol, lactose, trehalose, or 1% PEG to lactate dehydrogenase and phosphofructokinase attenuated the unfolding, but spectral differences in the dried state were still observed. However, a combination of 1% PEG with 10 mM mannitol, lactose, or trehalose preserved full enzymic activity upon reconstitution of the freeze-dried product.

Carpenter *et al.* [44] found that certain polymers (e.g., PVP) could stabilize multimeric enzymes during freezing and freeze-drying by a different mechanism: they cannot replace water molecules in the dried state, and therefore it is assumed that they inhibited the dissociation of the enzymes molecules induced by freezing and freeze-drying.

Rey [45] developed a theoretical diagram of the low-temperature behavior of a system susceptible to present glass formation (Figure 1.27). The diagram

Table 1.13 Activity of phosphofructokinase after freeze- and air-drying in the presence of different CPAs.

CPA (0.5 M)	Remaining activity freeze-dried	Air-dried
None	0.0	
Trehalose	56.0	68.4
Maltose	69.2	51.4
Sucrose	56.3	67.7
Glucose	3.3	2.1
Glycerin	0.0	
Glycine	0.0	2.8

See also Table IV in Ref. [41].

summarizes (a) the behavior of excipients, which can form a glass phase when they are slowly or quickly frozen, and (b) the events that can take place during warming of the glass.

1.1.4 Freezing of Cells and Bacteria

In 1968, Meryman [46] presented his ideas about the "minimum cell volume" and hypothesized that during freezing, cells are damaged in two steps. Initially water

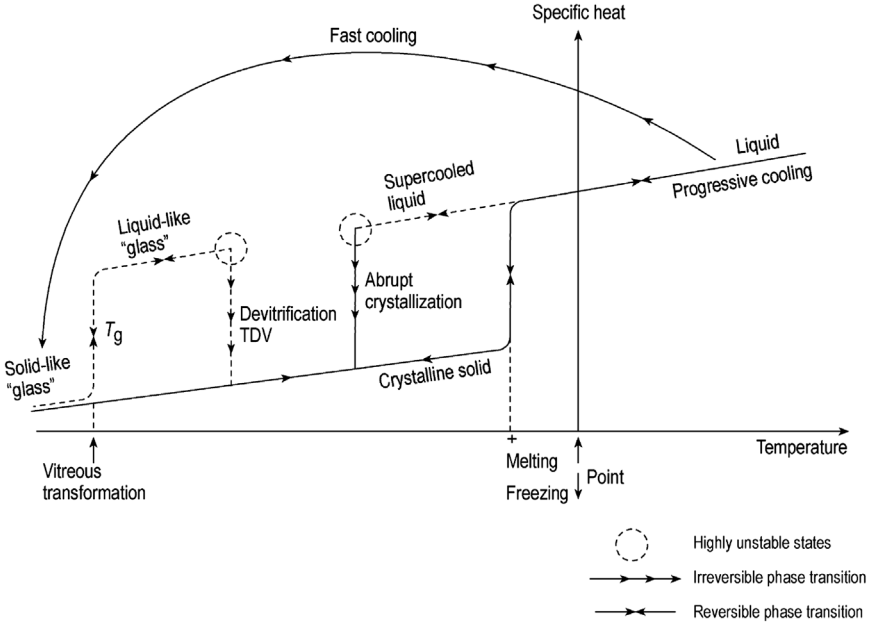

Figure 1.27 Theoretical diagram of the low-temperature behavior of a system susceptible to present glass formation. (See also Figure 9 from Ref. [45].)

diffuses from the cell to the surrounding, the freezing solution concentrating the solution in the cell. However, only a certain amount of water can be withdrawn from the cell until it has shrunk so much (minimum cell volume) that any further withdrawal takes water from the membrane molecules, which are an essential part of the cell's structure. The removal of this water leads to an irreversible change in the membrane structure.

As shown in Section 1.1.3, these structural changes can be avoided if certain sugars or other CPAs replace the water molecules. Pushkar and Itkin [47] showed by cryomicroscopy and X-ray analysis of structures that 15% glycerol in suspensions of marrow cells lowered the beginning of ice nucleation to −15 °C. Down to −10 °C, no nucleation in the cells was observed. With polyethylene oxide (10–15%), a few crystals of 10^{-3}–10^{-4} cm have been detected in an amorphous surrounding. Under these conditions, the function of the cells after thawing remained mostly normal. Nei [48] studied the nucleation of ice crystals during rapid freezing (100–1000 °C/min) using electron microscopy. Ice crystals can be observed in the cells of yeast, whereas in most bacteria (e.g., *coli* forms) almost no ice crystals could be detected. In Nei's opinion, ice crystals were more likely to have been produced in animal cells than in those of microorganisms. Cosman *et al.* [49] showed, using photographs taken with a cryomicroscope, that the volume of mouse islet cells shrank to 40% during cooling from 0 to −10 °C. Figure 1.28 indicates how many cells in rat liver contained ice as a function of cooling rate. The cells were cooled from −1 to −21 °C: Up to 50 °C/min, no ice was formed in the cells, whereas at ~160 °C/min all cells contained ice crystals.

De Antoni *et al.* [50] demonstrated that the addition of trehalose during freezing and thawing of two strains of *Lactobacillus bulgaricus* improved the survival rate differentially, but in both cases considerably. The samples (1 mL) were frozen at 18 °C/min to −60 °C and thawed to 37 °C at 15 °C/min. The

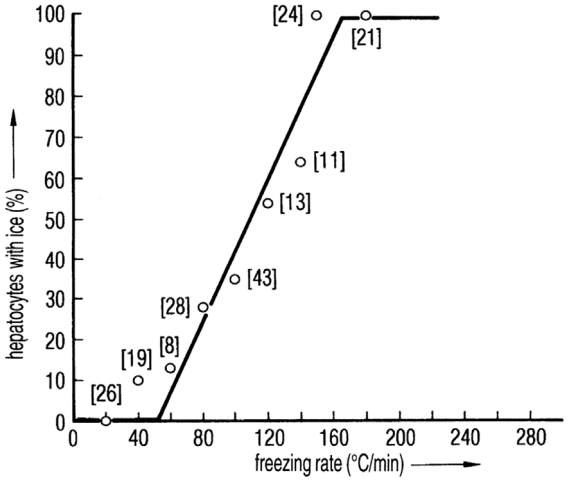

Figure 1.28 Percentage of hepatocytes of rats, which show intracellular ice as a function of freezing rate in the range of −1 to −21 °C. The numbers in brackets indicate the number of hepatocytes participating in each test. (See also Figure 8 from Ref. [49].)

solution consisted of distilled water, culture medium, and 10% milk with or without trehalose. It was shown that after three freeze–thaw cycles, milk alone resulted in a survival rate of 24 or 65%, whereas with trehalose this was could be improved to 32 and 100%, respectively. The efficacy in the case of both strains was clearly different. De Antoni *et al.* suggested that the efficiency of milk was related to its Ca^{2+} content, whereas the trehalose could replace water molecules in the phospholipids of the membranes. However, no mention was made of whether other sugar molecules in milk showed any effect.

1.1.5 Methods of Structure Analysis

The knowledge that successful freeze-drying depends largely on the structure of the frozen product has inspired the development of methods to analyze and understand these structures more quantitatively. Rey [51] has shown that in addition to the electrical resistance (ER) of a freezing substance, the thermodynamic behavior can also be used to study the freezing process and the frozen product.

1.1.5.1 Measurements of Electrical Resistance (ER)

Measurement of ER is done in an apparatus (Figure 1.29) in which the sample is cooled by LN_2 and electrically heated. Two electrodes are immersed in the sample, which is placed in a vial. The resistance between the two electrodes is measured with an alternating current of 50 Hz. For complete information, high

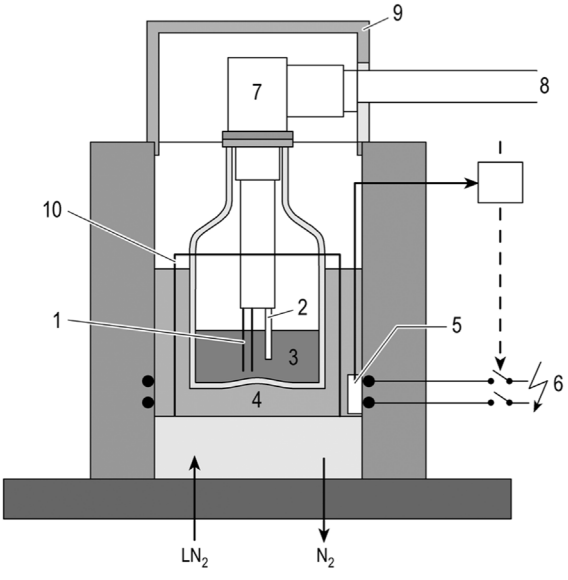

Figure 1.29 Schematic drawing of an instrument to measure the electrical resistance (ER) of a sample during cooling and rewarming. (Figure 1 from Ref. [52].) 1, platinum electrodes; 2, temperature sensor in the product; 3, product sample; 4, heat transfer medium; 5, temperature sensor in the heat transfer medium; 6, resistance heating; 7, highly insulated sensor head; 8, shielded cable; 9, electrical and magnetic shield; 10, vial holder.

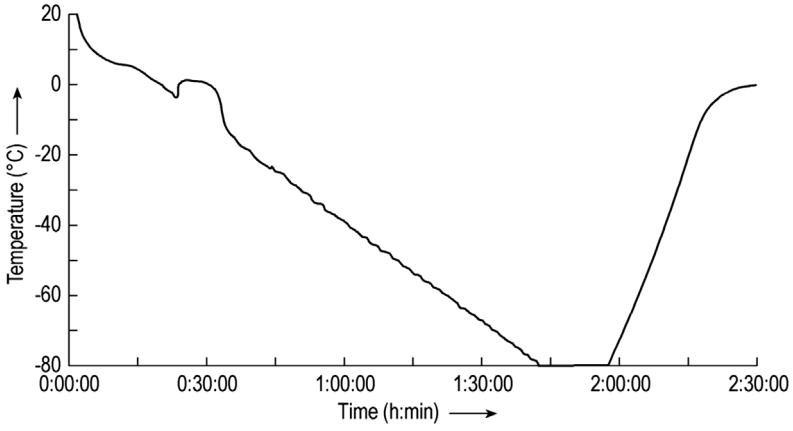

Figure 1.30 Check of cooling and heating rate. Preset data in this example: cooling 1.0 °C/min ±10%, warming 3 °C/min ±10%.

resistance up to 10^{11} Ω should be measurable. This requires high resistance, up to 10^{12} Ω, not only between the electrodes itself but also in the temperature sensor and surroundings. In addition to high insulation between the electrodes, the preset cooling and heating rates should be qualified as shown in Figure 1.30. The cooling rate is 1 °C/min between 0 and −50 °C and the heating rate is 3.3 °C/min between −80 and −10 °C. The measurement and interpretation of ER plots should consider the following:

- ER data reflect the mobility of the ions as a function of temperature.
- The sample size is comparable to a product in vials.
- The cooling rates chosen should be smaller than, the same as, and larger than in the pilot and production plant, for example, if the cooling rate in the production plant is 0.8 °C/min, then a minimum of three measurements at 0.4, 0.8, and 1.6 °C/min are recommended, each repeated three times, if the plots are practically identical.
- The first derivative of the ER plot should also be calculated and printed.
- If the product is frozen on the shelves of the plant, the cylindrical part of the sample vial in the instrument should be isolated from the heat transfer medium.

The use of an ER measuring system and the interpretation of the results require some familiarization with the possibilities and limitations of the method.

Solutions of salts, for example, 0.9% NaCl, will normally show the eutectic temperature, but the event can be at lower temperatures during cooling owing to the degree of supercooling and the cooling rate: For example, the event has been found with 1 °C/min (average of six measurements) at −24.1 °C, standard deviation (SA) 1.2 °C; with 3 °C/min at −30.2 °C, SA 2.3 °C. During rewarming, the event can be close to the expected temperature: −21.5 °C, SA 0.5 °C at 1 °C/min and 21.3 °C at 3 °C/min. Figure 1.31 shows a complete plot down to −120 °C at 3 °C/min. The behavior below −80 °C can be speculated as a reversible change in the crystal structure. Above 1×10^{12} Ω, the measurement is inaccurate, the

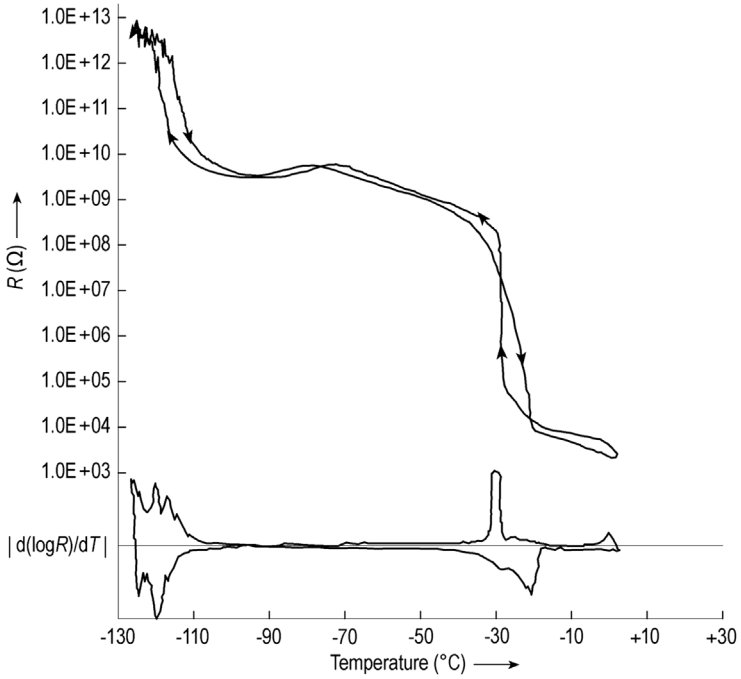

Figure 1.31 Electrical resistance as a function of temperature of 1% NaCl solution. Cooling rate 3 °C/min, warming rate 3 °C/min, and the first derivative d(log*R*)/d*T* measured down to −120 °C.

resistance of the sensor and its cable is $\sim 10^{12}$ Ω. The crystallization delay during cooling to −28/−30 °C is visible (see Figure 1.32), and also some event starting at −28 °C during warming. Figure 1.33 is a typical plot for 0.9% NaCl solution at a cooling rate of 1 °C/min (all rewarming plots are at 3 °C/min) and Figure 1.34 shows the enlarged derivative. Figure 1.35 presents the average of 22 0.9% NaCl measurements at 1 °C/min between −10 and −70 °C and the minimum and maximum data at each temperature. The resistance change covers six decades and the frequency distribution of the resistance data at each temperature (Figure 1.36a–g) reflects the very different or uniform development of the structure during freezing and rewarming: If the freezing of this solution at a rate of 1 °C/min were terminated at −30 °C, the resistance of the product would vary substantially, improving at −40 °C and becoming statistically predictable below −50 °C. The freezing of a product is not a uniform operation, it is influenced by several factors that can only be judged by sufficient statistical data.

One of the advantages of ER compared with other methods discussed later is the dimensions of the sample, especially its thickness of 10–15 mm. This is comparable to frequently used filling heights of vials for pharmaceutical products. If the cake thickness is substantially larger, for example, 40 mm, the freezing rates in a study should be chosen accordingly: 1 °C/min cannot be expected with freezing on the shelves: 0.2 or 0.3 °C/min is more likely. Therefore, tests for these thicknesses may be carried out, for example, at 0.15, 0.25, and 0.35 °C/min.

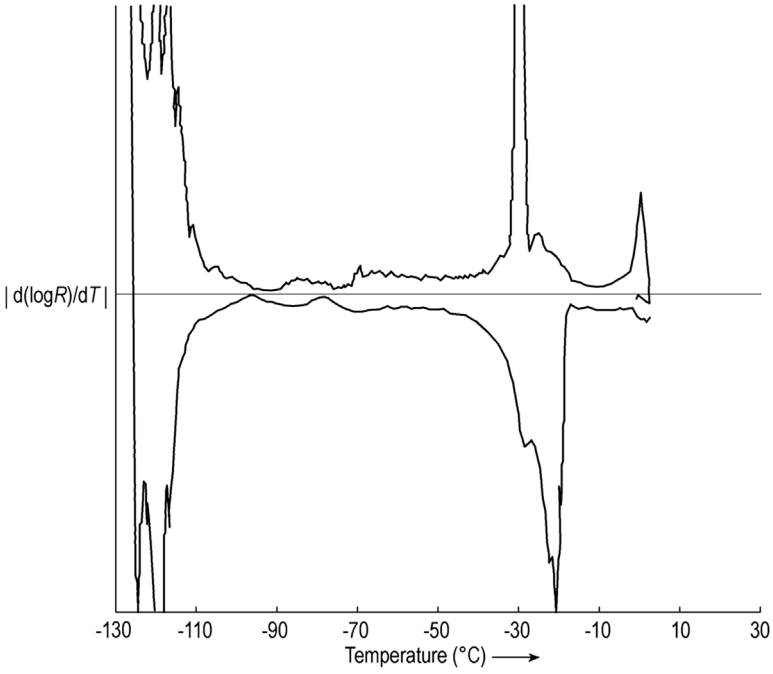

Figure 1.32 The first derivative of Figure 1.31 (approximately five times linearly enlarged).

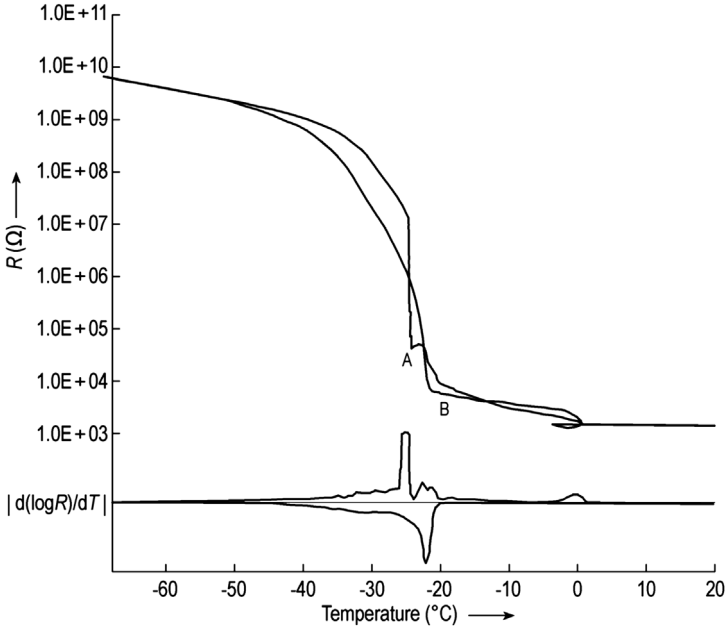

Figure 1.33 Typical electrical resistance plot of 1% NaCl solution with 1 °C/min cooling: event A at −24.5 °C during cooling and event B at 21.8 °C during warming.

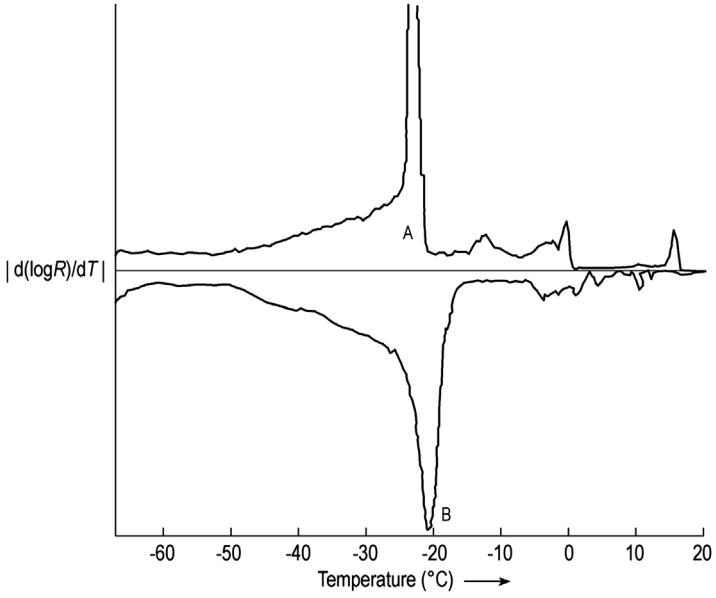

Figure 1.34 Enlarged derivative of Figure 1.33.

As can be seen from Figures 1.31–1.34, the derivative plots are helpful in determining the temperatures of changes in the slopes of log$R$ more accurately. Enlarged derivative plots may show some undulation, which can be disregarded. The main events can still be clearly detected.

If the product in vials is frozen on the shelves, the energy flow is mostly through the bottom of the vial and not through the wall. To simulate this condition, the wall of the sample vial can be isolated from the heat transfer medium by a layer of, for example, glass-fiber material. The difference in the cooling and warming behavior can be seen in Figures 1.37 and 1.38 as an example. In Figure 1.39, the influence of the isolation is typical for this product. The suspension subcools twice at events 1 and 2. Also, event 3 is a mixture of subcooling and crystallization. During rewarming, no event can be detected, since the water has been frozen to the maximum possible content. The product then starts to melt at $\simeq$12 °C.

The resistance plot of a 10% egg albumin solution with a freezing rate of 1 °C/min is completely different, as shown in Figure 1.40. The reproducibility of several measurements is within the drawing accuracy of the plots, except the degree of subcooling, which varies with the freezing rate. In pharmaceutical and food products, one finds mixtures of the two extremes shown above. Examples of ER measurements are given in Figures 1.40 and 1.42. In Figures 1.41 and 1.42, the influence of the freezing rate on two human blood derivatives is shown. The slow freezing in Figure 1.41 (1 °C/min) leads to larger crystals with larger inclusions of high-viscosity concentrates between them. This results in a softening of the structure during rewarming at a lower temperature: d(log$R$)/dT drops from −60 °C to a minimum at −47 °C; in the fast-cooled product, the inclusions

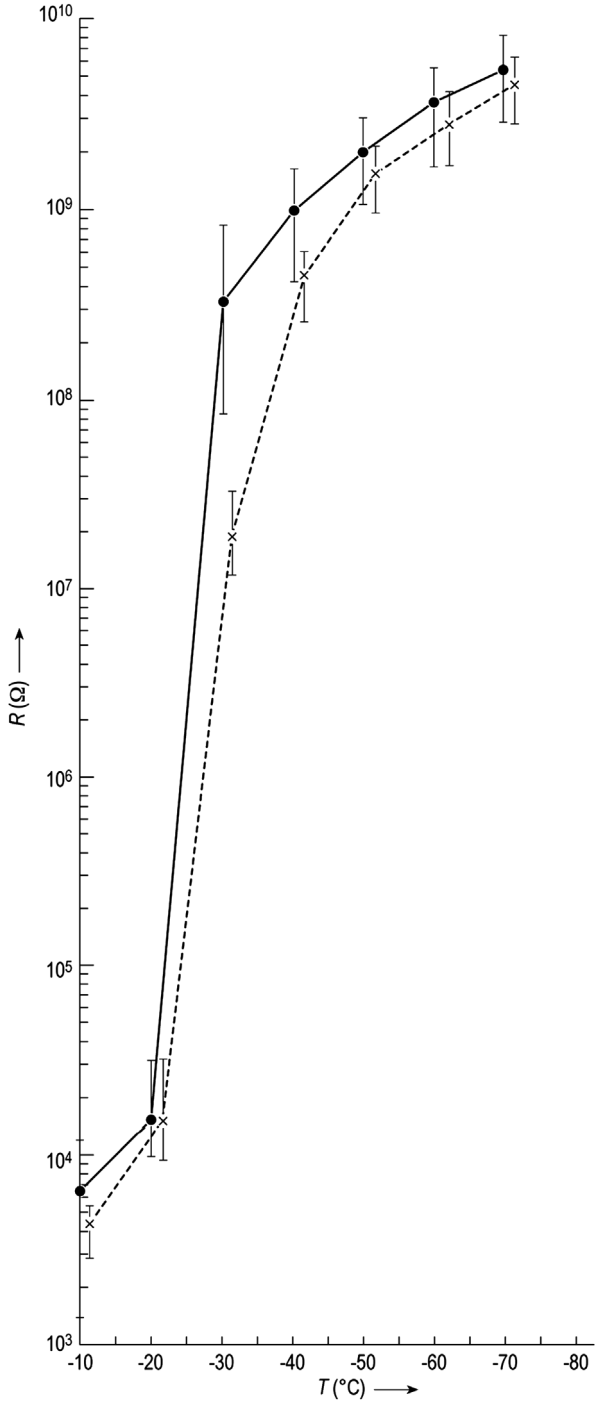

Figure 1.35 Average of 22 electrical resistance plots of 1% NaCl solution (1 °C/min cooling) from −10 to −70 °C. Solid line, cooling; vertical bars, average ± SD. Dashed line, warming; vertical bars, average ± SD.

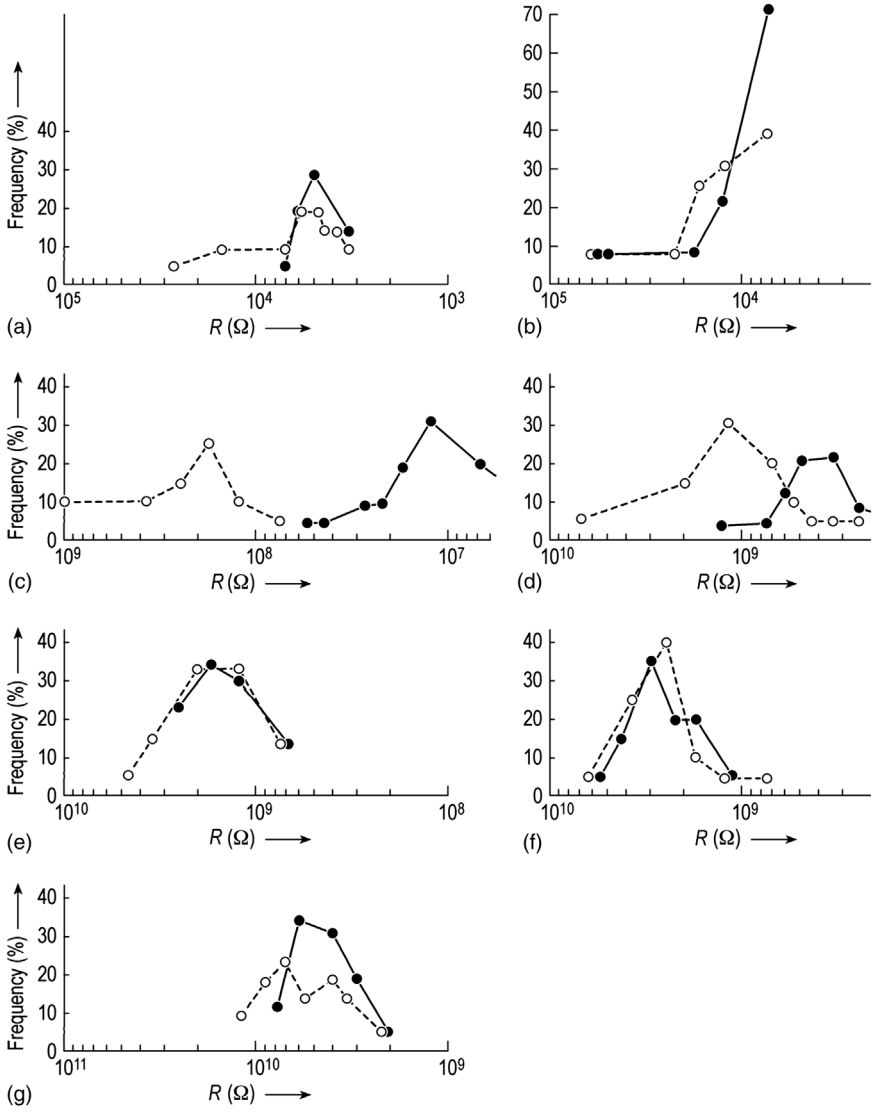

Figure 1.36 Frequency distribution (% of all measurements) of the 22 resistance measurements at (a) −10; (b) −20; (c) −30; (d) −40; (e) −50; (f) −60; (g) −70 °C. Cooling and warming as in Figure 1.35: (•) average resistance of all measurements during cooling and (×) average resistance of all measurements during rewarming.

remain smaller and more evenly distributed, and the minimum of $d(\log R)/dT$ is at −40 °C. A similar result can be seen in Figure 1.42: The difference in the freezing rate seems to be small (1 and 0.4 °C/min), but the consequences for the drying process are substantial. The temperature at the sublimation front for plot 1 should be ≃54 °C and for the product of plot 2 ≃45 °C (see the note below). As shown in Section 1.2.1, the operating pressure (p_c) for plot 1 will be in the region of 1×10^{-2}

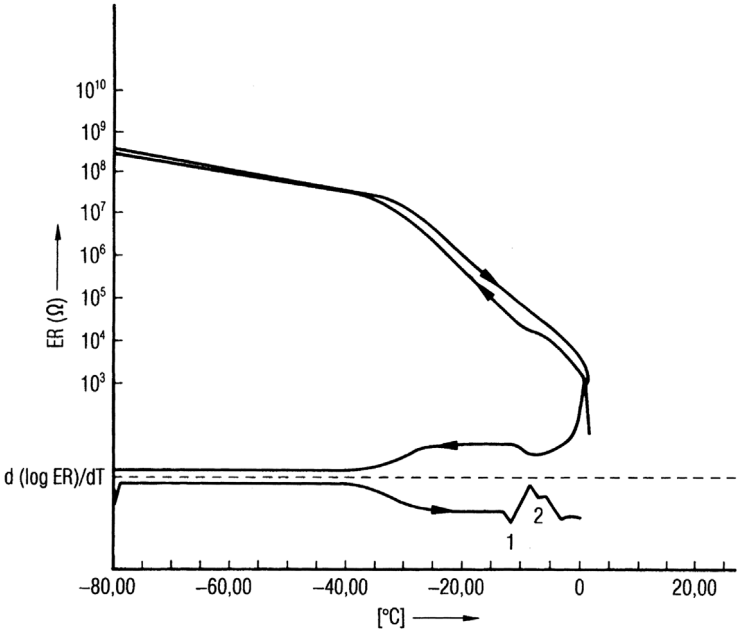

Figure 1.37 Electrical resistance of a pharmaceutical product as a function of temperature during cooling at 1 °C/min and rewarming at 3 °C/min. Heat transfer medium and product are approximately uniformly heated.

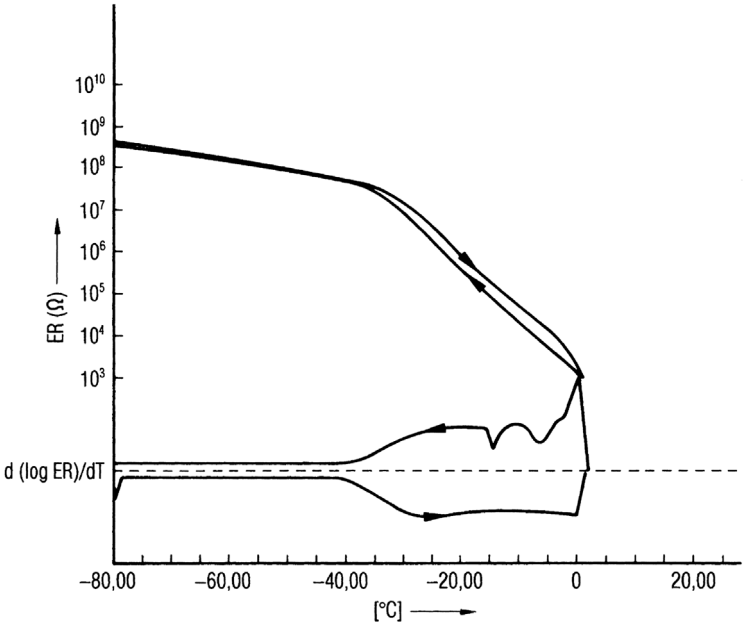

Figure 1.38 Measurement of the electrical resistance as in Figure 1.37 except that the wall of the vial is insulated by a plastic tape up to the filling height of the product. Therefore, the heat is mostly removed through the bottom of the vial (see also (Willemer, H. unpublished results, Köln)).

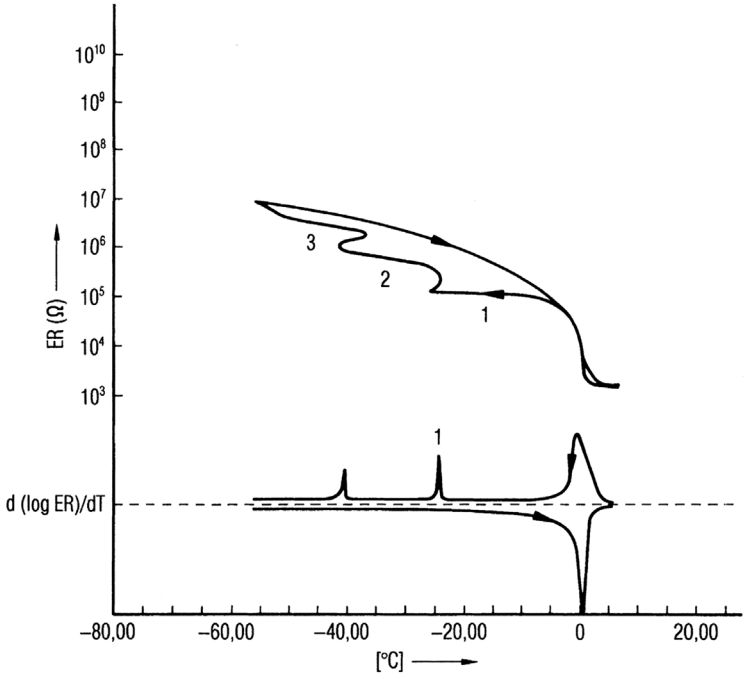

Figure 1.39 Electrical resistance as a function of temperature of a suspension cooled at 0.8 °C/min and heated at 3 °C/min. The vial is insulated as described in Figure 1.38 (see also (Willemer, H. unpublished results, Köln)).

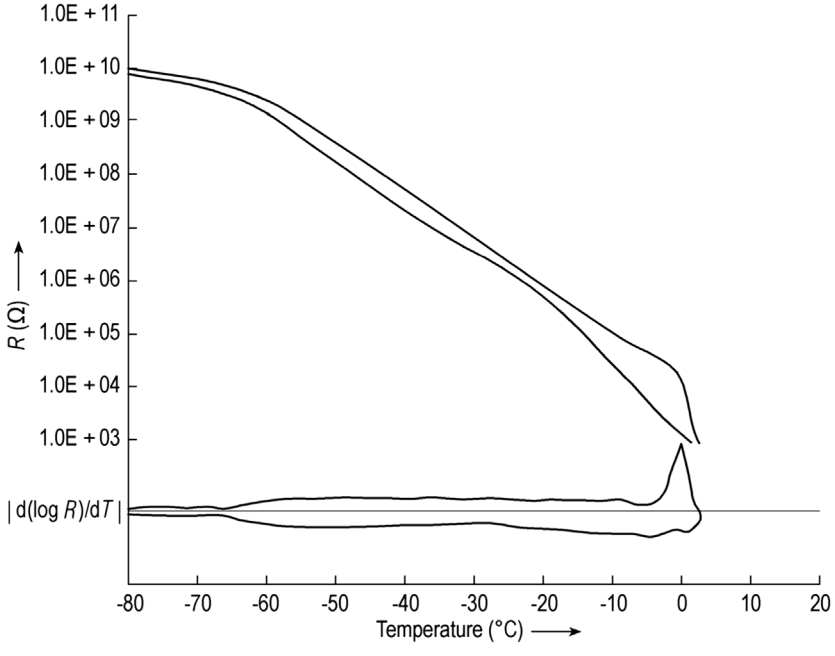

Figure 1.40 Electrical resistance of a 10% egg–albumin solution.

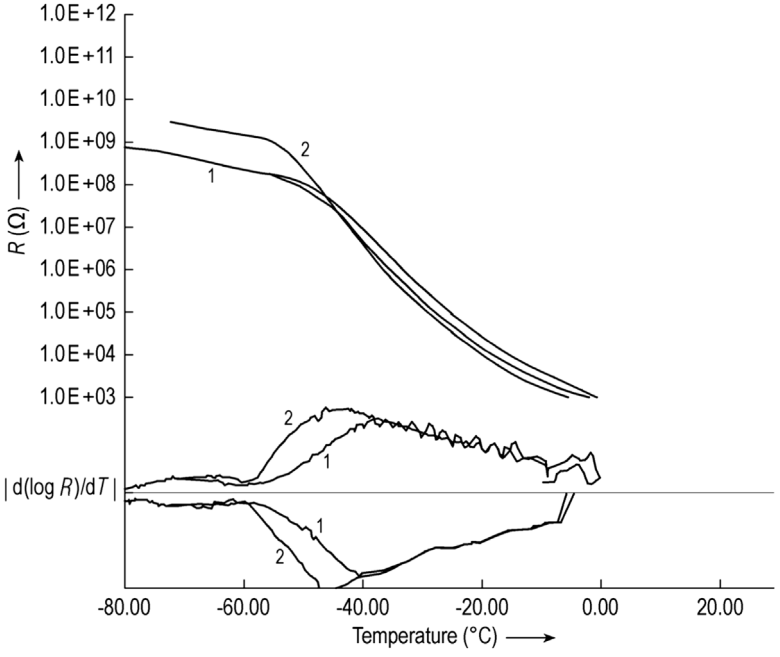

Figure 1.41 Electrical resistance of a human blood derivative. Cooling rate: (1) 14 and (2) 1 °C/min.

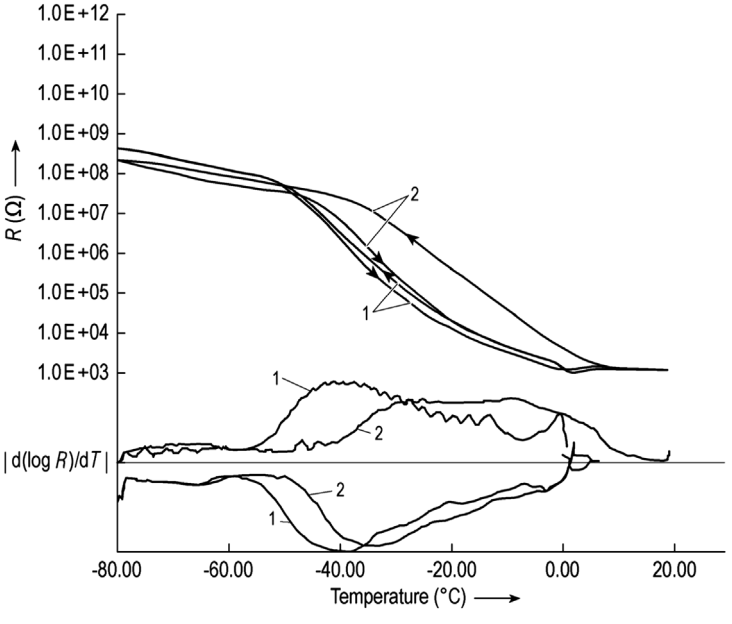

Figure 1.42 Electrical resistance of a different human blood derivative to Figure 1.41. Cooling rate: (1) 0.4 and (2) 1 °C/min.

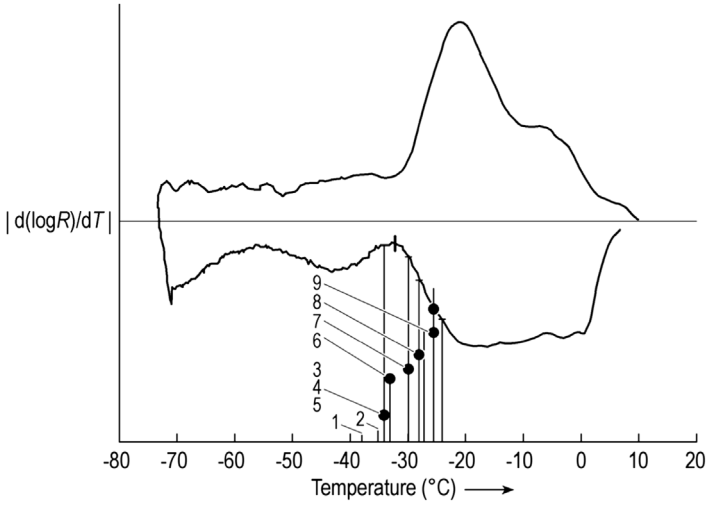

Figure 1.43 Electrical resistance of a human protein solution. The numbers 1–9 refer to photographs taken with a cryomicroscope (see text and note).

mbar and for plot 2 at $\sim 4 \times 10^{-2}$ mbar. For many production, freeze-drying installations $p_c \approx 10^{-2}$ mbar will be difficult or uneconomical to operate on, whereas 4×10^{-2} mbar is usually operable in a modern plant. The limitation will not only be in the shelf and chamber design, but also in the vapor transportation from the chamber to the condenser (Section 1.2.4). Structure analysis of the product during its development phase can help to avoid costly operations or changes later. (*Note:* Comparisons of protein ER measurements with cryomicroscope observations have led to a rule of thumb: In Figure 1.42 the $d(\log R)/dT$ plot 2 starts to change at −50 °C with a minimum at −34 °C, difference 16 °C, 1/3 of 16

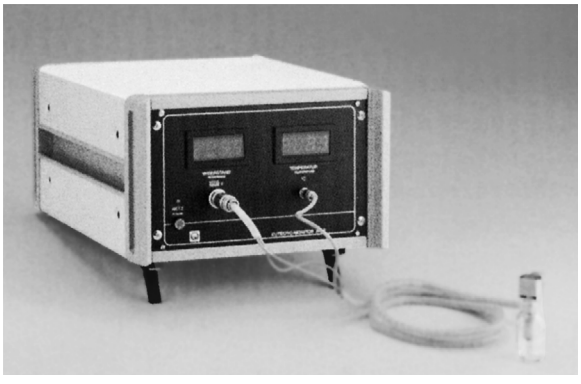

Figure 1.44 Monitor AW 2. In the foreground, right: sample vial with measuring electrodes and resistance thermometer. Behind, to the left: the control and analysis unit. The storage of LN_2 and its control valve are not shown. The resistance in the sensor head has to be large compared with the resistances to be measured, for example, 10^{11} Ω. (Steris GmbH, Hürth, Germany.)

≈ 5, stable freeze-drying should be possible at −50 °C minus 5 °C = −45 °C. With the same rule for plot 1, one arrives at −54 °C. Figure 1.43 shows the enlarged plot of d(log$R$)/dT for a different protein. With the rule, one would arrive at $T_{ice} \approx$ −28 °C. The numbers 1–9 indicate the photographs taken with the cryomicroscope. In photographs 1–7, no structure change is visible. In photographs 9 and later, the structure softens visibly. The temperature in photograph 8 is regarded as acceptable, which is between −28 and −27 °C.)

Figure 1.44 shows an instrument to measure log$R = f(T)$ and calculate d(log$R$)/dT.

1.1.5.2 Differential Thermal Analysis (DTA)

Another method to study structures during cooling and warming is differential thermal analysis (Figure 1.45). It measures the different course of temperature

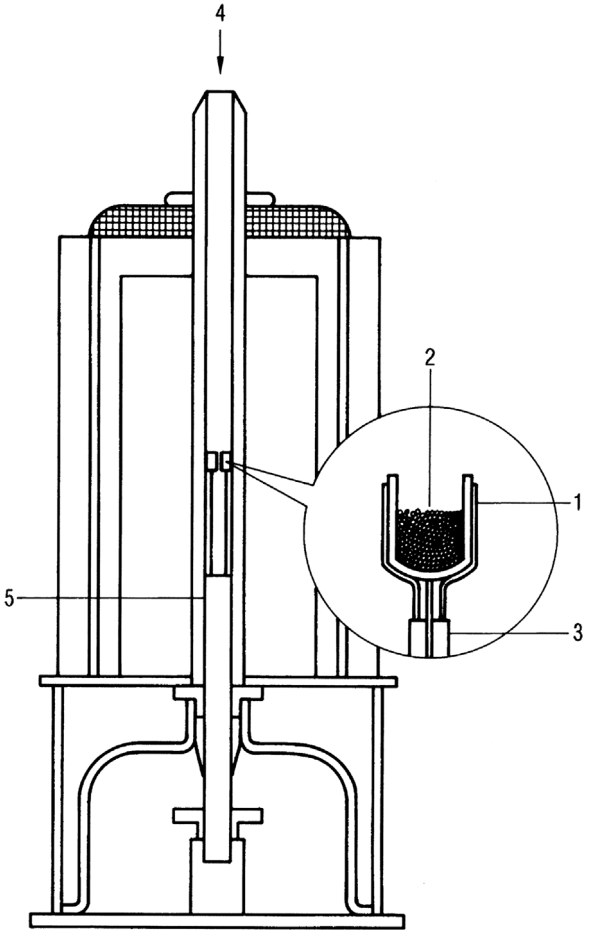

Figure 1.45 Scheme of a DTA measuring cell. 1, crucible with sample; 2, sample; 3, thermocouple (reference crucible not enlarged); 4, gas inlet; 5, ceramic support. (See also TA Instruments, New Castle, DE, USA.)

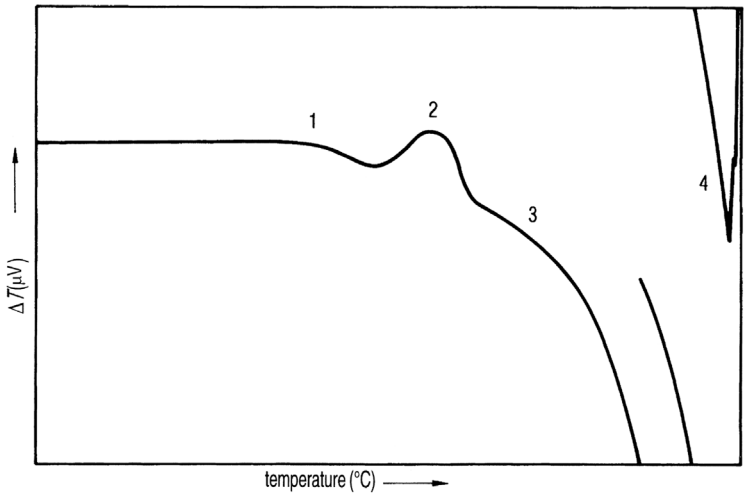

Figure 1.46 DTA measurement of a 24% sucrose–6% NaCl solution during slow rewarming after quick (200 °C/min) freezing. 1, glass transition at ≃78 °C; 2, growth of crystals (exothermic) at ≃52 °C; 3, increase of c_p, water is formed between the crystals; 4, ice melts at ≃7 °C. (See also Figure 1 from Ref. [53].)

between the sample and a probe, which changes its thermal behavior uniformly but does not have a phase transition in the measured temperature range.

Using DTA and ER measurements of quickly frozen (200 °C/min) sucrose–NaCl solutions, MacKenzie presented the different events occurring during slow rewarming [53]. Among others, two sucrose–NaCl solutions were studied: a 24% sucrose solution with 6% NaCl (sucrose:NaCl ratio = 80: 20) (Figure 1.47) and a 10% sucrose solution with 10% NaCl (ratio 1: 1) (Figure 1.48). In Figure 1.46, event

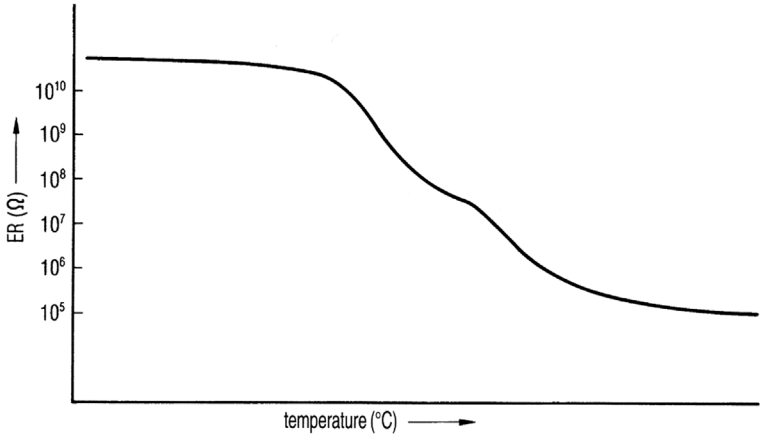

Figure 1.47 Electrical resistance (ER) measurement of the same solution as in Figure 1.46; identical temperature scale. (See also Figure 2 from Ref. [53].)

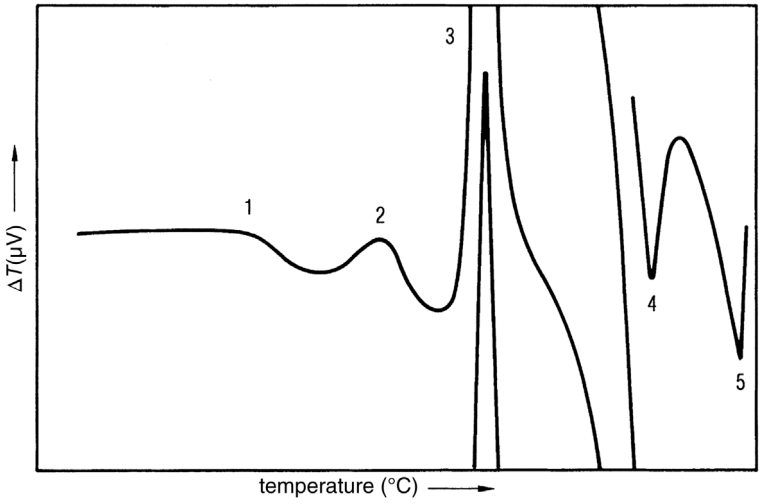

Figure 1.48 DTA measurement of a 10% sucrose–10% NaCl solution during slow rewarming after quick (200 °C/min) freezing. 1, glass transition at ≃93 °C; 2, crystal growth (exothermic) at −65 °C; 3, significant exothermic event, crystallization of NaCl at ≃44 °C; 4, eutectic melting at ≃22 °C; 5, melting of ice at ≃7 °C. (See also Figure 5 from Ref. [53].)

1 at ≃78 °C can be explained as a glass transition. In Figure 1.47, event 1 reduces the ER significantly. In event 2 at ≃50 °C, the mobility of the molecules has increased so much as to allow the growth of crystals (exothermic) and the resistance drops more slowly. At event 3, some water is formed between the crystals and c_p rises. The c_p of water is about twice that of ice. At event 4 (at ≃7 °C) the ice melts.

In Figure 1.48, event 1 is at ≃93 °C, event 2 at ≃66 °C, and the exothermic event 3 at ≃44 °C results from the crystallization of NaCl. Event 4 at ≃22 °C represents the eutectic melting and event 5 corresponds to event 4 in Figure 1.46.

In Figure 1.49, the softening of the glass phase can be seen in the change of the ER, whereas at event 2 the resistance changes more slowly, corresponding to Figure 1.48. The crystallization of NaCl can be seen from the increase in ER at event 3, which does not exist in Figure 1.47. Events 4 and 5 cannot be observed in the ER curves shown. The interpretation of ER measurements is substantially improved by using the derivative of the ER curve, as shown in Figures 1.32 and 1.34.

The results of several measurements by MacKenzie [53] are shown in Figure 1.50. The glass transition line 4 exists over the whole concentration range studied, while lines 2 and 3 are absent in the area of high sucrose and high NaCl concentrations, respectively. Later measurements proved that the mobility in the solid matrix is too reduced to observe the events during the observation time used. Only the rotation of the water molecules is still possible. With an increase in temperature (line 3), the energy increases sufficiently to allow some movements of the molecules, which can also be seen as a decrease in

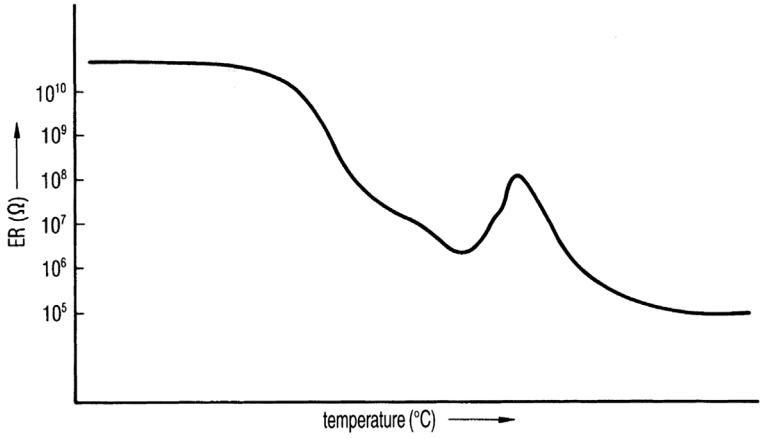

Figure 1.49 ER measurement of the same solution as in Figure 1.48; identical temperature scale. (See also Figure 6 from Ref. [53].)

ER. MacKenzie denoted this temperature "antemelting," although he subsequently suggested (note in Ref. [54] that the term should not be used, but should be replaced by "collapse temperature" (T_c, for alternative opinions on the subject, see Section 1.1.3).

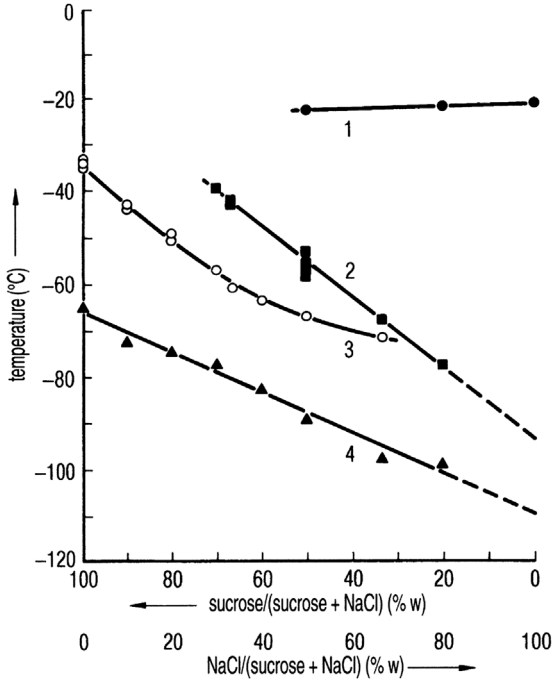

Figure 1.50 Behavior of a sucrose–NaCl solution at different sucrose–NaCl concentrations and temperatures after quick freezing (200 °C/min) during slow rewarming. (Figure 8 from Ref. [53].) 1, eutectic melting temperature of NaCl; 2, crystallization temperature of NaCl; 3, temperature at which the glass phase starts to soften; 4, glass transition temperature.

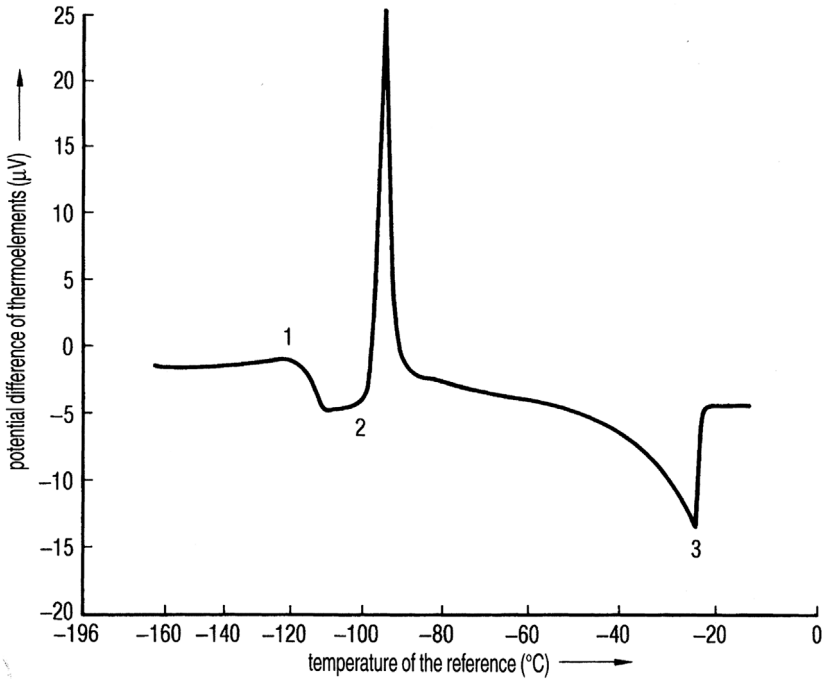

Figure 1.51 Plot of the DTA measurement of a 50% glycerin solution during slow rewarming after quick freezing at 75–200 °C/min. 1, T_g; 2, T_d; 3, T_m. (See also Figure 1 from Ref. [55].)

Another event called "incipient melting" at a temperature T_{im} is the melting of ice crystals between crystallized eutectic mixtures or the dissolution of crystals surrounded by highly concentrated inclusions, known as interstitial melting of ice. Luyet and Rasmussen [55] have studied the phase transitions by DTA of quickly frozen (75 or 200 °C/min) water solutions of glycerol, ethylene glycol, sucrose, and glucose during warming (5 °C/min). Figure 1.51 shows a typical DTA curve, if measurable amounts of amorphous product have been formed during freezing, which starts to crystallize after T'_g is exceeded at a temperature T_d (exothermic event). At the temperature T_d, one can expect a viscosity of $\sim 10^9$ P. At T'_g, the viscosity, in agreement with other authors, is on the order of 10^{13} P. This concept is shown in Figure 1.52: If the solution freezes relatively slowly (3 °C/min), all freezable water is crystallized; if the rewarming is interrupted before the melting starts and the product cooled again to, for example, −150 °C, the rewarming curves resemble that in Figure 1.52. There is no water left that can crystallize at T_d. There are only two events that are denoted (according to MacKenzie) antemelting and incipient melting.

From DTA measurements, phase diagrams can be constructed as shown for ethylene glycol in Figure 1.53. A solution of 40% ethylene glycol is only stable in the glass phase below ≃135 °C; at ≃120 °C, unfrozen water starts to crystallize, at ≃65 °C recrystallization is observed, and at ≃45 °C, melting will start. As recrystallization is the growth of existing crystals and not the nucleation of new ones, this event cannot be detected by DTA, but can be observed under a microscope when a transparent area becomes opaque.

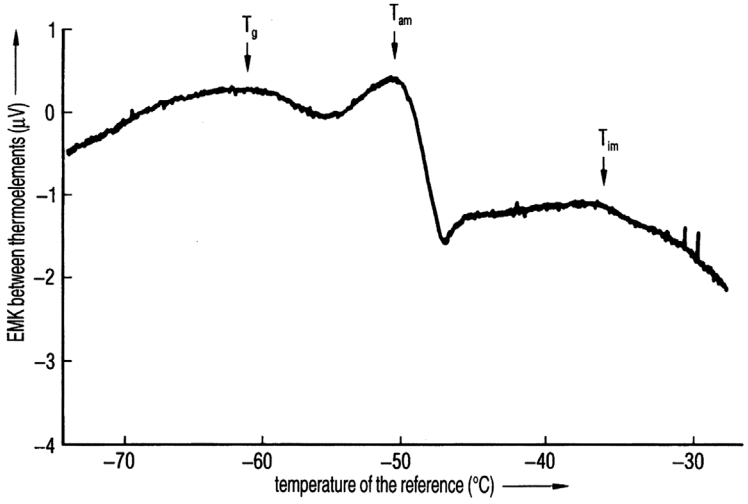

Figure 1.52 DTA plot of a 50% glucose solution, frozen at 3 °C/min during rewarming. T_g, start of devitrification; T_{am}, start of ante-melting; T_{im}, start of incipient melting. (See also Figure 1 from Ref. [56].)

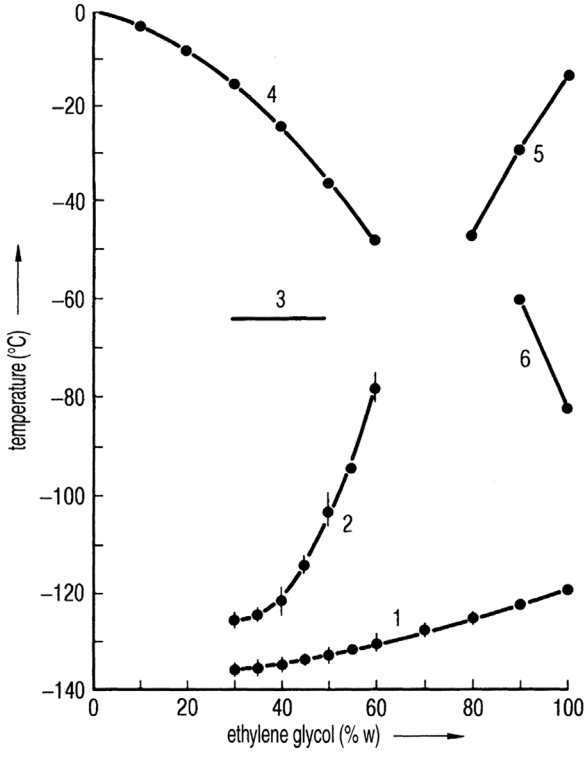

Figure 1.53 Phase diagram of ethylene glycol, in which the following events are shown: 1, glass transition; 2, devitrification; 3, recrystallization; 4, melting; 5 and 6, devitrification and melting of ethylene glycol. (See also Figure 4 from Ref. [55].)

1.1.5.3 Cryomicroscopy

Hsu *et al.* [57] observed recrystallization on the recombinant CD4-IgG with a cryomicroscope cooled to −60 °C by a cascade of four Peltier modules. The observation cell can also be evacuated for freeze-drying studies.

Willemer [52] compared ER measurements with photographs made by a cryomicroscope, a scheme of which is shown in Figure 1.54. ER measurements of complex products are sometimes difficult to interpret. Figure 1.55 shows the ER curve of a cryoprotectant solution for a virus. The solution freezes partially by cooling to −10 °C, subcools thereafter down to ≃46 °C, and crystallizes at ≃65 °C. Upon rewarming, the resistance changes rapidly at ≃32.5 °C. The photographs taken using a cryomicroscope show at −40 °C a uniform structure in both the already dried and the frozen parts. At −30 °C, both parts show a mix of dark and gray zones, indicating that some ice is melted and is also diffused into the dried part. In such cases, ER measurements can be used as a relatively quick method to study the influences of different CPAs, varying their concentrations and selecting an optimal freezing rate. The finally selected combination can be tested in the cryomicroscope. Figures 1.56–1.58 show the structural changes of a pharmaceutical product in a cryomicroscope during freezing, during the thermal treatment, and before drying. Figures 1.56–1.58 are from one experiment showing different details in one sample. Figure 1.56a is during quick cooling at ≃25 °C, Figure 1.56b during first warming from −50 to ≃35 °C, and Figure 1.56c during second cooling at −50 °C. In Figure 1.56a, the crystals (dark) are mostly uniformly distributed between the amorphous concentrated solids (lighter color). In Figure 1.56b, the crystals have grown and some water from the concentrate has crystallized. In Figure 1.56c, the boundaries between crystals and glass inclusions are more clearly visible, especially in the upper right corner. In Figure 1.57, another part of the microscope sample close to the border of the samples is shown at comparable temperatures: (a) at ≃23 °C, (b) during first warming at ≃30 °C, and (c) after second cooling at −60 °C. In Figure 1.57b, the crystals have grown without much change in their general structure, especially in the upper left corner. In Figure 1.57c, the boundaries between crystals and glass have become clearer.

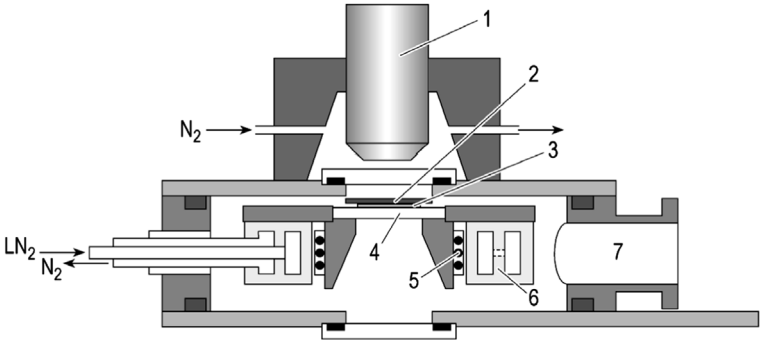

Figure 1.54 Scheme of a cryomicroscope. 1, objective of the microscope; 2, cover-glass; 3, sample; 4, sample support; 5, electrical heating; 6, cooling chamber with LN_2 connection; 7, vacuum connection. (See also Figure 1 from Ref. [52].)

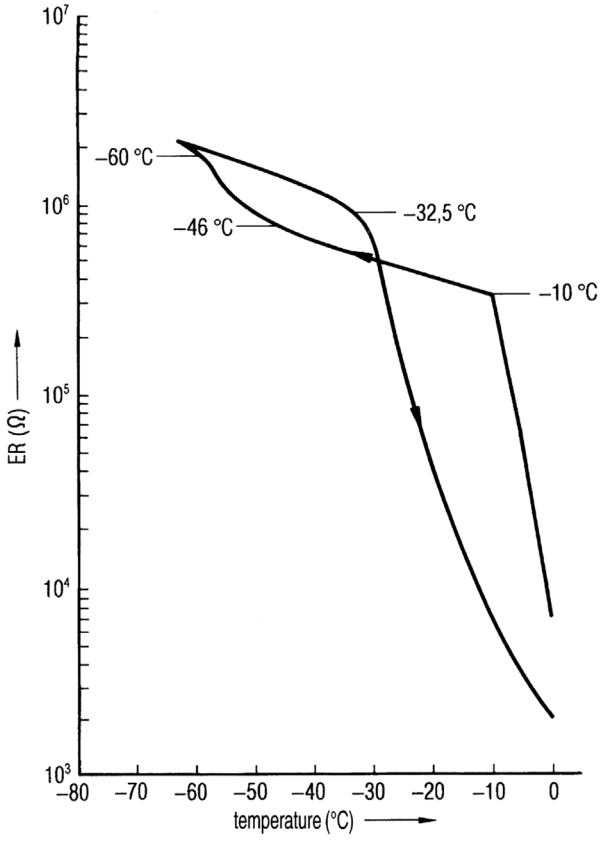

Figure 1.55 Electrical resistance as function of temperature during cooling and rewarming of a virus suspension. The suspension subcools from −10 to ≃46 °C and freezes at −60 to −65 °C. During rewarming, the resistance drops clearly at ≃33 °C. This product should be freeze-dried at $T_{ice} = -40$ °C or slightly higher. (See also Figure 7 from Ref. [52].)

Figure 1.58 represents a third part of the sample: (a) after cooling to −65 °C and (b) after thermal treatment, a second cooling to −60 °C and the beginning of freeze-drying at −40 °C. Again the overall structure has not been changed by the thermal treatment, but the structure of the crystals is clearer, indicating that water molecules between the glass phase and the crystals have migrated to the crystals. The photographs in Figure 1.57 show that the quick freezing does not produce a uniform structure throughout the sample; it is influenced by boundary effects. Nevertheless, the effect of thermal treatment can be seen in all parts of the sample. Figure 1.59 shows the effect of crystal growth without thermal treatment during the temperature rise from the end of freezing (−60 °C) to the beginning of drying at −42 °C. This is of interest during automatic loading on cold shelves. The product in the first vials loaded will have a structure different from those loaded, for example, 2 or 3 h later.

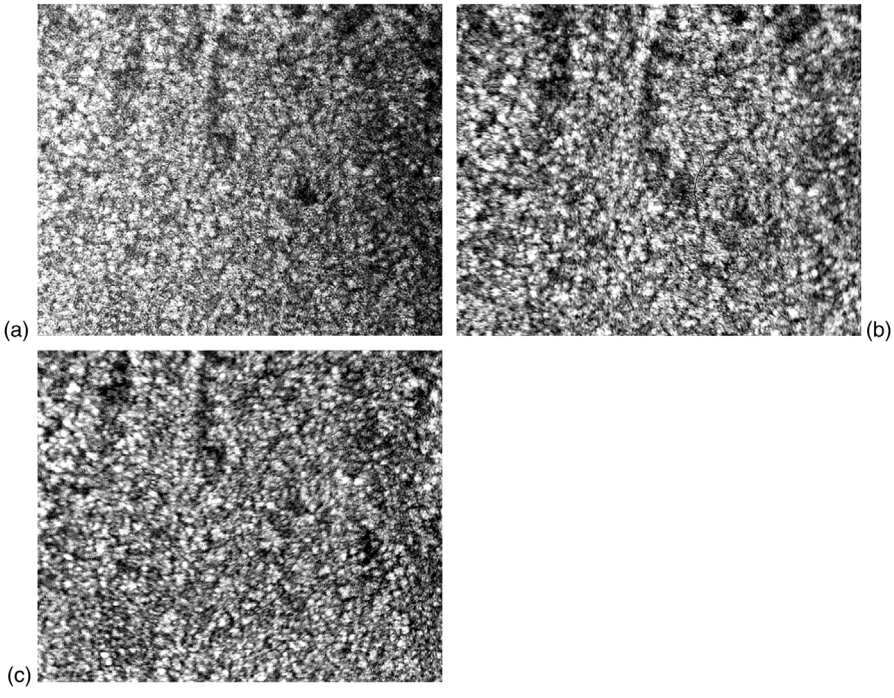

Figure 1.56 Cryomicroscope photograph of a pharmaceutical product frozen at a rate of ~4 °C/min: (a) during cooling at ≃24 °C; (b) after cooling to −54 °C and thermal treatment (TT) at −36 °C; (c) after cooling again to −55 °C. (Steris GmbH, Hürth, Germany).

Cryomicroscope studies have the advantage of showing pictures of the structural changes and the frozen product can be freeze-dried in most instruments. The product layer is very thin and the product is quickly frozen. The behavior of the product during warming and drying therefore corresponds exactly only to a quickly frozen product. To simulate a thermal treatment is difficult because of the thin layer. However, experience shows that critical temperatures taken from such studies are valuable, especially if they are supported by, for example, ER data of a more slowly frozen product.

Nunner [58] photographed with a special cryomicroscope the changes of the planar front of 0.9% NaCl solution during directional freezing in 360 s to a stable dendritic ice structure (Figure 1.60). The concentrated NaCl (dark border) can be seen on the surface of the ice crystals.

A cryomicroscope that permits quantitative evaluation of the pictures was described by Cosman *et al.* [49]. The unit has four distinctive features:

- Temperature generation, measurement, and control are programmable.
- The picture of the microscope is documented for later use.
- The documentation can be partially used for automatic picture recognition.

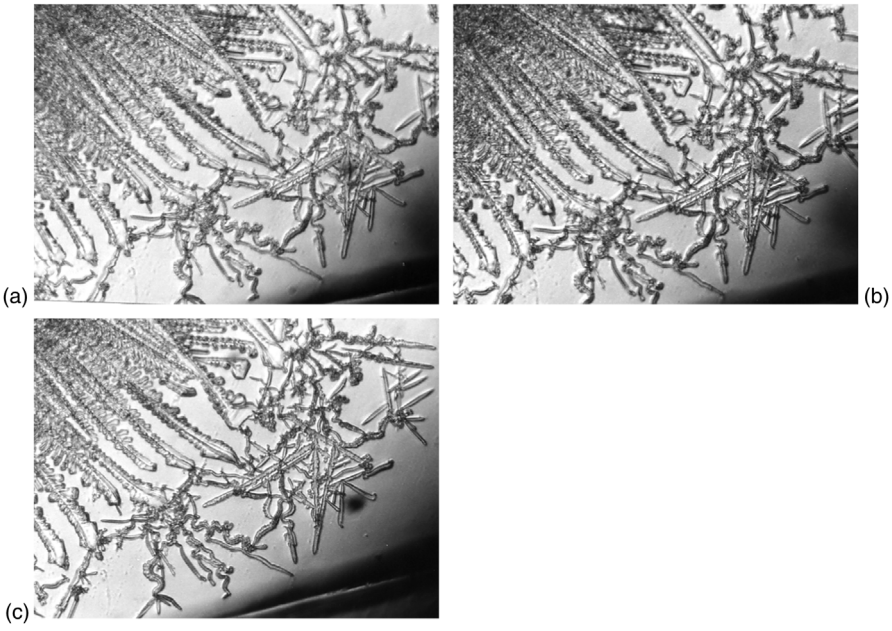

Figure 1.57 As Figure 1.56, showing a different part of the sample, close to the border: (a) during freezing at ≃24 °C; (b) after cooling to −54 °C and TT at −36 °C; (c) after cooling again to −60 °C. (Steris GmbH, Hürth, Germany.)

- The amount of data can be reduced in such a way that a freezing process can be described mathematically and the behavior of cells predicted.

Figure 1.61 shows the layout of the system. By the use of a very good heat-conducting sapphire window and a cooling system with LN_2, the authors achieved cooling rates of several hundred degrees per minute down to −60 °C and temperature gradients in the sample of 0.1 °C at a temperature of ∼0 °C.

Three examples will show how freezing processes can be studied quantitatively and documented using this microscope system. Figure 1.62 shows the change in volume of an isolated islet cell of a mouse as a function of temperature. The

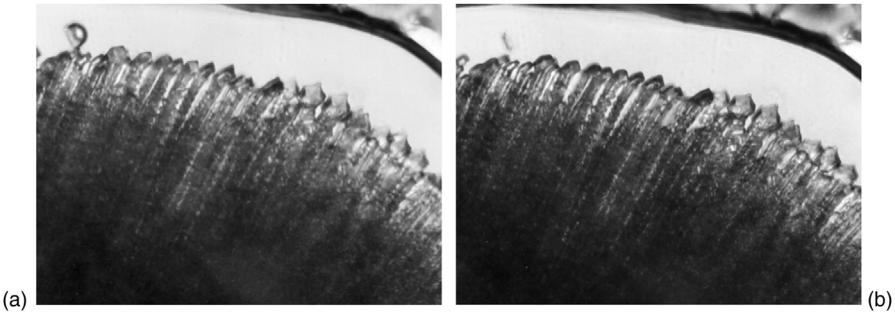

Figure 1.58 As Figure 1.56, showing a third part of the sample: (a) after freezing to −64 °C; (b) after TT at the beginning of drying at ≃45 °C. (Steris GmbH, Hürth, Germany.)

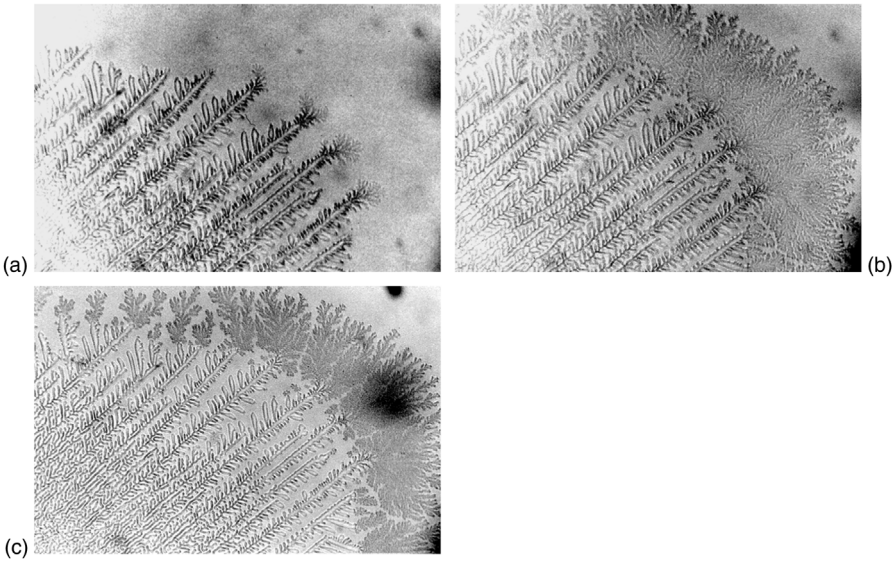

Figure 1.59 Cryomicroscope photograph of a pharmaceutical product (different from Figure 1.56) frozen at a rate of ~4 °C/min without TT: (a) cooled to −60 °C; (b) during warming for drying at −48 °C, the recrystallization of unfrozen water is visible; (b) at −42 °C, the softening of the structure starts, especially in the left lower corner and the newly formed crystals start to disappear. The product frozen at this rate should be thermally treated. (Steris GmbH, Hürth, Germany.)

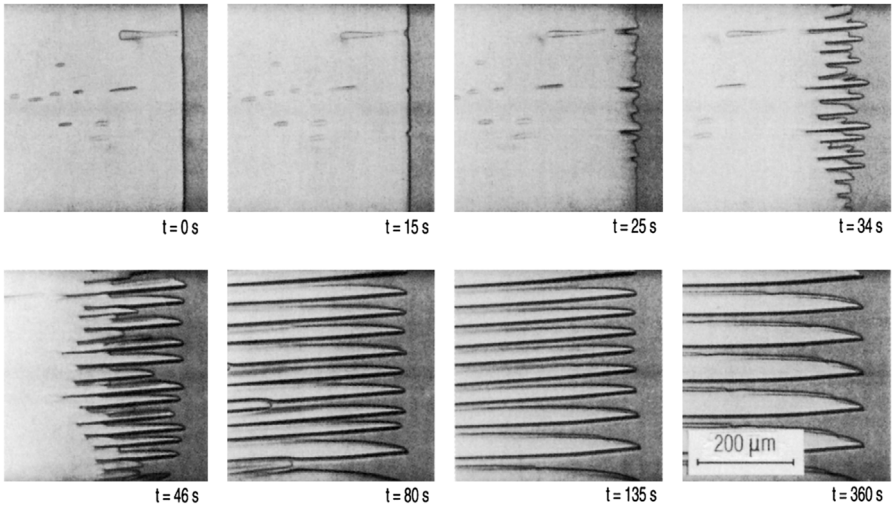

Figure 1.60 Change of the planar front of ice ($t = 0$ s) through an unstable phase ($t = 34$ s) into a dendritic structure. A 0.9% NaCl solution is directionally frozen in a temperature field having a gradient of 67 K/cm. The sample is moved at a rate of 15 µm/s through the temperature field. (From Ref. [58].)

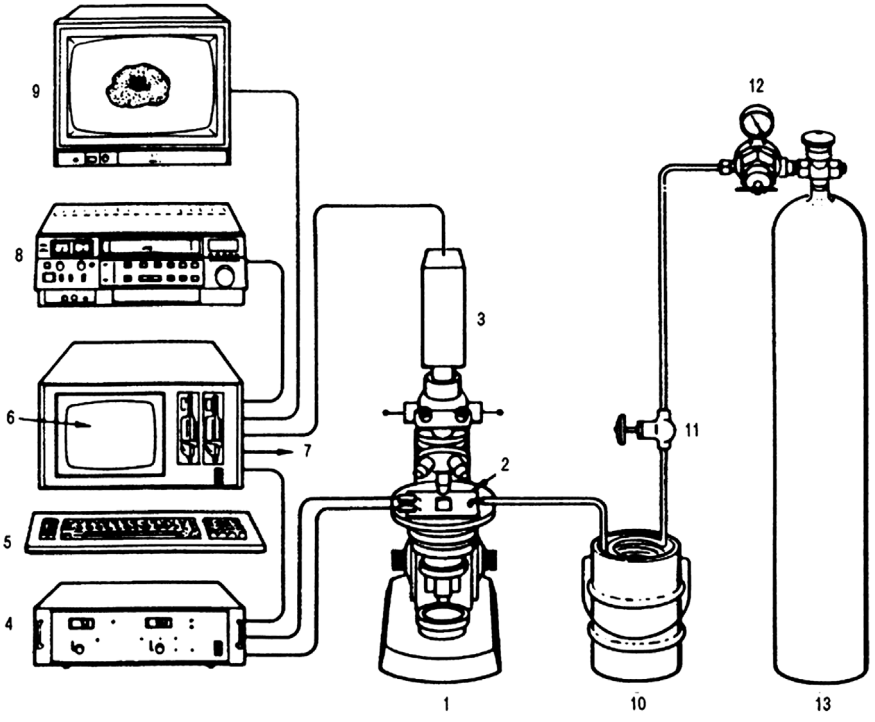

Figure 1.61 Scheme of a cryomicroscope research system. 1, microscope; 2, cryostat; 3, video camera; 4, temperate control; 5, keyboard; 6, menu display; 7, printer connection; 8, video recorder; 9, video monitor; 10, Dewar flask with LN_2; 11, metering valve; 12, pressure reducer; 13, N_2 cylinder. (See also Figure 1 from Ref. [49].)

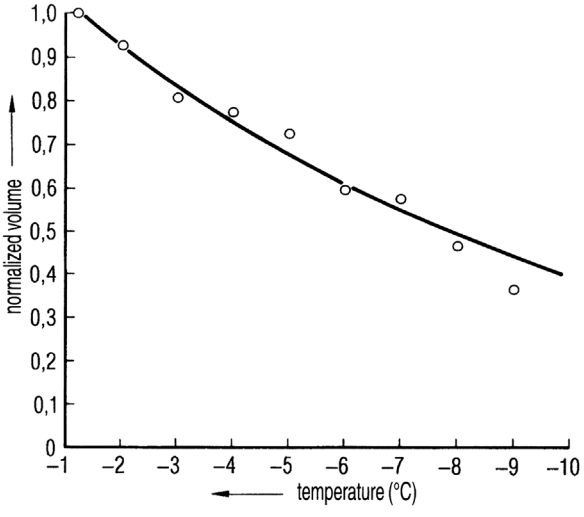

Figure 1.62 Volume change as a function of temperature of an insulated islet cell of a mouse. (See also Figure 4 from Ref. [49].)

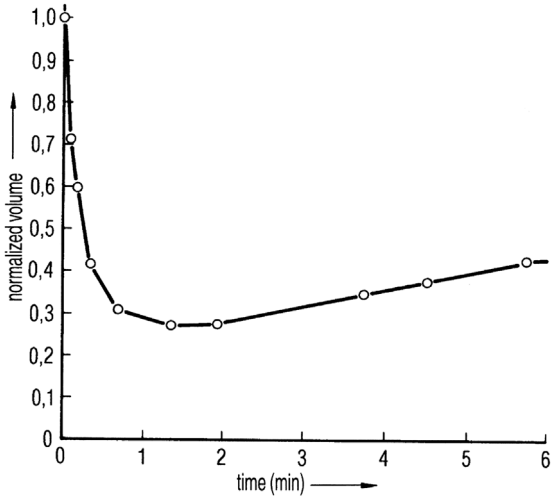

Figure 1.63 Volume changes of oocytes of rhesus monkeys as a function of the time elapsed after their exposure to 10% dimethyl sulfoxide solution. (See also Figure 6 from Ref. [49].)

different permeabilities of cell membranes for H_2O and CPAs are important for freezing of cells, as Figure 1.63 shows.

The volume of oocytes of a rhesus monkey placed in 10% v/v DMSO is reduced to almost one third, since the water can diffuse out of the cell into the surrounding, but the DMSO cannot enter the cell during the same time (measured at 23 °C).

The nucleation of ice in the cell is considered as the cause of cell damage. Figure 1.64 indicates in how many mouse oocytes intracellular ice is found as a

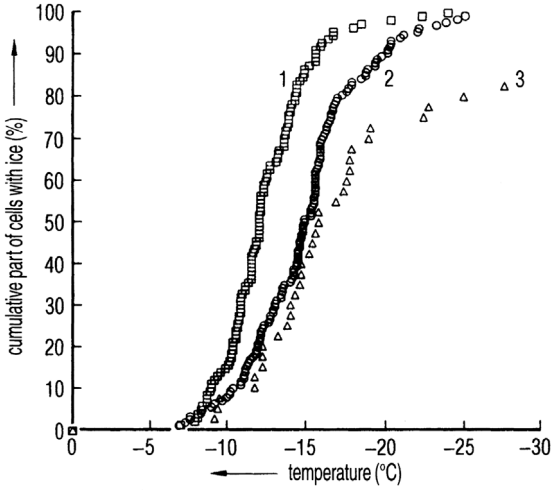

Figure 1.64 Cumulated abundance of intercellular ice forming in mice oocytes as a function of temperature with three different cooling rates: 1, 111 oocytes at 120 °C/min; 2, 132 oocytes at 5 °C/min; 3, 34 oocytes at 3.5 °C/min. (See also Figure 9 from Ref. [49].)

function of temperature at different cooling rates. In hepatocytes of rats, no ice could be detected during cooling to −21 °C up to a cooling rate of ∼40 °C/min, whereas at a rate of 140 °C/min practically all cells contained ice. The water did not have sufficient time to diffuse into the surrounding and froze in the cells. Figure 1.64 also demonstrates how the intracellular nucleation of ice depends on the absolute temperature and cooling rate: At ≃25 °C and a rate of 5 °C/min, practically all cells contain ice, whereas at 3.5 °C/min, ∼20% of the cells were without ice.

Dawson and Hockley [59] used scanning electron microscopy (SEM) to show the morphological differences between quick (150 °C/min) and slow (1 °C/min) freezing of trehalose and mannitol solutions. Figure 1.65 shows the surface of (a) a slowly and (b) a quickly frozen center part of a 1% trehalose solution. On the slowly frozen sample (c), a cracked surface can develop by concentrated solids, whereas the structure in the quickly frozen sample is amorphous and fibrous. Figure 1.66 shows the (a) coarse and (b) fine structure in the center part of

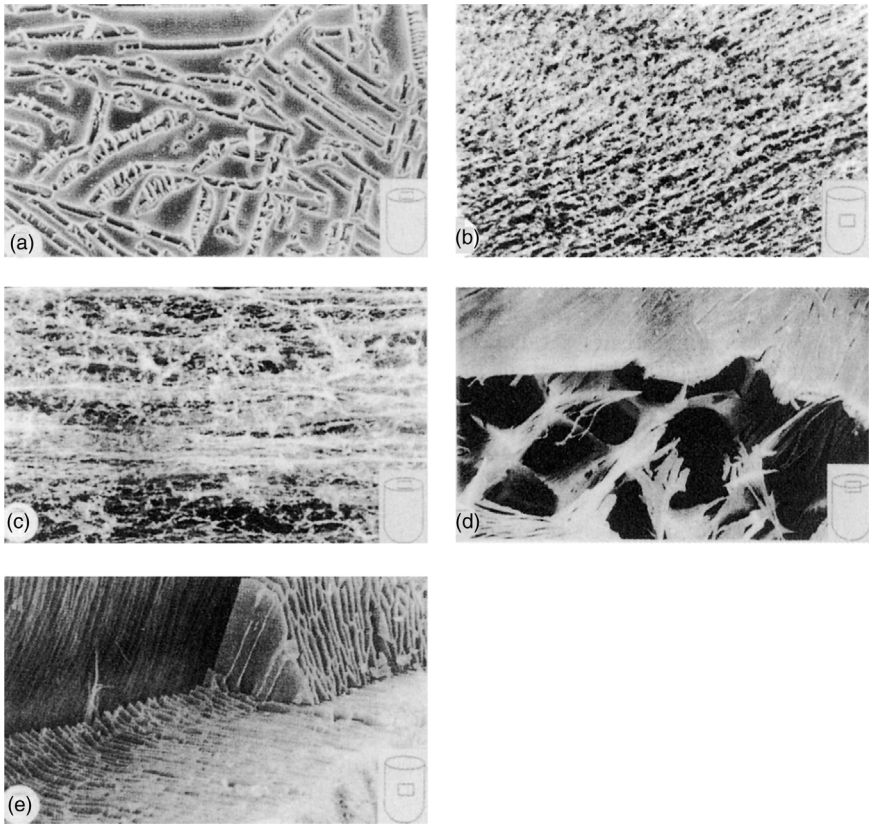

Figure 1.65 Photographs of different freeze-dried products obtained by scanning electron microscopy. (a) 1% trehalose solution, 1 °C/min, cut out of the surface. (b) 1% trehalose solution, 150 °C/min, cut out of the center. (c) 1% trehalose solution, 1 °C/min, cut out of the uppermost surface. (d) 1% mannitol solution, 1 °C/min, shows sugar crystallization. (e) Serum, 150 °C/min, morphology similar to plasma. (See also part of Figure 1 from Ref. [59].)

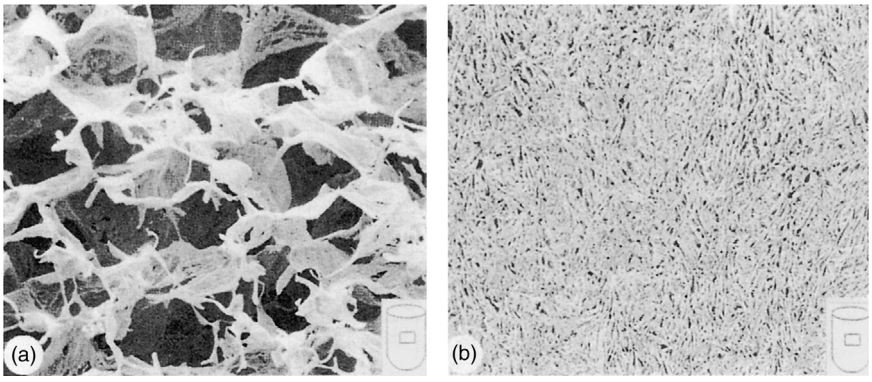

Figure 1.66 Photographs of a 1% lactose solution by scanning electron microscopy: (a) with 1 °C/min and (b) with 150 °C/min frozen. (See also Figure 3 from Ref. [59].)

(a) slowly and (b) quickly frozen 1% lactose. A collapsed part of a trehalose solution can be found in Figure 1.67a, while Figure 1.67b shows the dried product stored with too high a moisture content for 6 months. The pictures prove that different freezing rates will result in different structures and may concentrate solids on the surfaces, which reduces the drying speed or prohibits a low residual moisture content during drying.

1.1.5.4 Freeze-Dry Microscopy

Freeze-drying is still the method of choice to achieve improved stability of biopharmaceuticals when the product is not sufficiently stable in liquid formulation. Meister and Gieseler [60] used a freeze-drying microscope system consisting of a Zeiss Axio Imager.Al (Carl Zeiss MicroImaging, Goettingen, Germany) with a

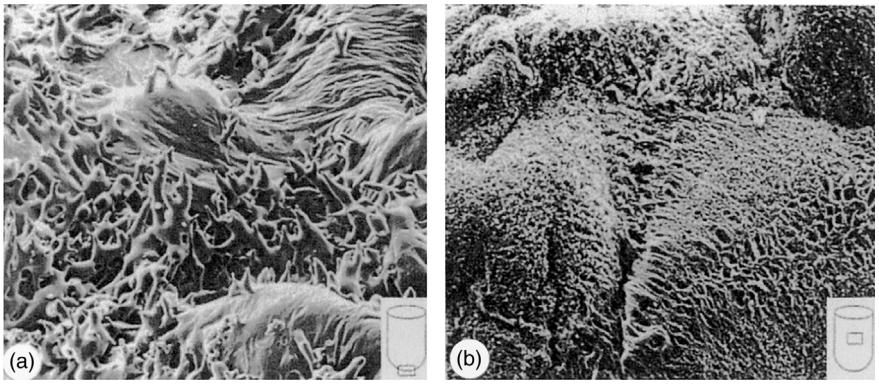

Figure 1.67 Photographs of trehalose solution freeze-dried in a vial, obtained by scanning electron microscopy. (a) Collapsed product from the bottom of the product. (b) Shrunk product after 6 months of storage at +20 °C with a too high RH and stored at too high a temperature. (See also Figure 6 from Ref. [59].)

lambda plate plus spectrum analyzer and an FDCS freeze-drying stage (Linkam Scientific Instrument, Surrey, UK) with a liquid nitrogen cooling system and a programmable temperature controller.

Abstract: The purpose of this study is to investigate the change of collapse appearance and temperature of protein/sugar mixtures as a function of nucleation temperature (T_a), sublimation velocity (V_{sub}), and the sugar/protein mole ratio when performing freeze-drying microscopy experiments.

HSA (human serum albumin) and BSA (bovine serum albumin) were used as samples, proteins were mixed with either sucrose or trehalose. Sucrose and trehalose are the most commonly used stabilizers for protein pharmaceuticals.

Differential scanning calorimetry (DSC) was used to determine the corresponding glass transition temperature (T'_g). To allow a more representative comparison between these analytical methods, a collapse midpoint temperature (T_c-50) was introduced. While there was no distinct correlation between T_a and the onset of collapse (T_{oc}) for either mixture, V_{sub} was found to correlate with the measured collapse temperature that is important for comparability of experiments. Application of the Gordon–Taylor equation failed to predict the critical temperature for any of the protein/sugar mixtures studied. (© 2008 Wiley-Liss, Inc. and the American Pharmacists Association, *J. Pharm. Sci. 98*, 3072–3087, 2009).

Applications: A well-designed freeze-drying cycle forms a glassy solid that can minimize degradation reactions of complex structures such as proteins or peptides and may provide acceptable shelf life for worldwide shipping and storage. It was estimated that more than 200 new antibody products are currently in development, many of them in a lyophilized form. However, formulation and cycle development become challenging if protein therapeutics require a large amount (>50 mg/mL) of active ingredients in the formulation to achieve the desired therapeutic effect.

Recent emphasis within the FDA on manufacturing sciences and practical analytical technology (PAT) encourages the pharmaceutical industry to further optimize and improve current freeze-drying processes and to design new cyc1es that are robust and economical.

1.1.5.5 Differential Scanning Calorimetry (DSC)

Differential scanning calorimetry measures the energy absorbed (endotherm) or produced (exotherm) as a function of time or temperature. It is used to characterize melting, crystallization, resin curing, loss of solvents, and other processes involving an energy change. Differential scanning calorimetry may also be applied to processes involving a change in heat capacity such as the glass transition, for example, glassmaking.

Meister and Gieseler [60] used DSC (Figures 1.68–1.70) to evaluate the critical temperature to characterize thermal transitions such as glass transitions (T_g), eutectic melting points (T_{eut}), and the glass transition temperature of the maximally freeze-concentrated product (T'_g). FDM is a better measure of collapse in a product that has been widely used in more recent years; here a user visually measures via microscopy the collapse temperature (T_c) of a given product during primary drying.

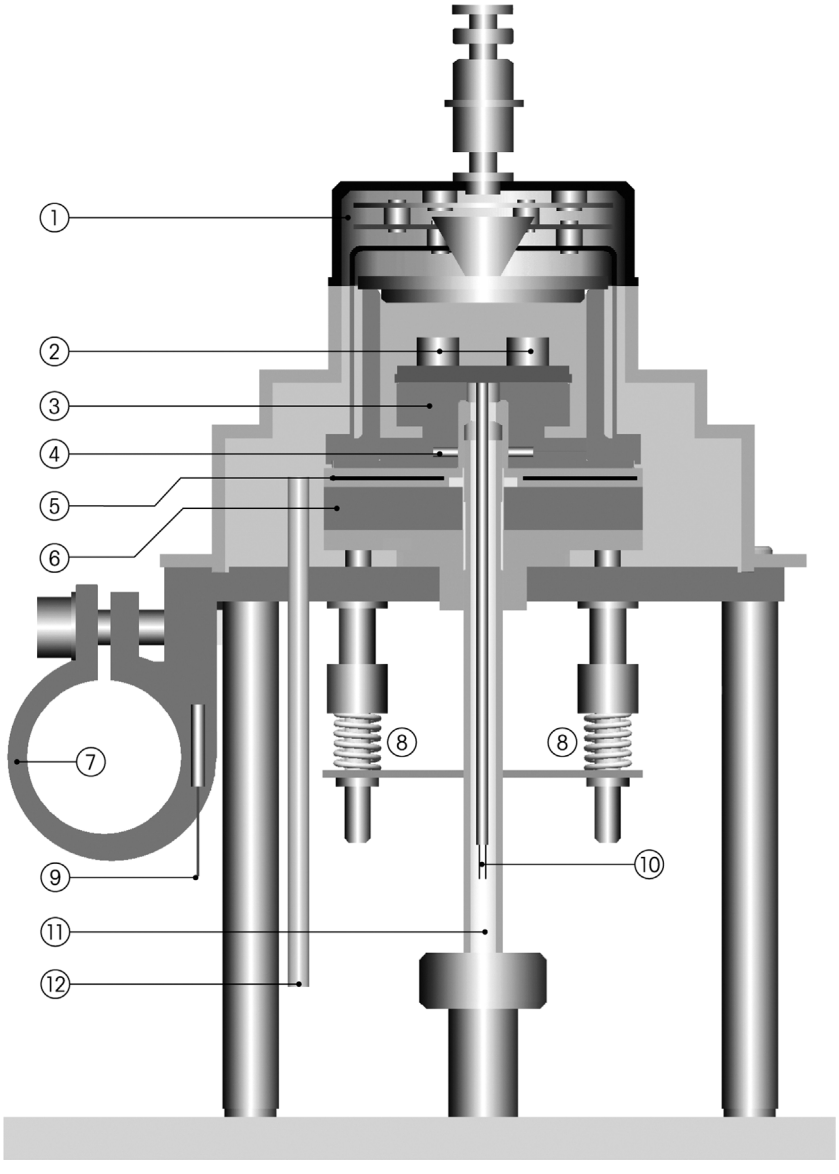

Figure 1.68 Schematic drawing of a DSC 3+ instrument: 1, furnace lid; 2, crucibles on the DSC sensor; 3, silver furnace; 4, PT100 of furnace; 5, flat heater between two insulating disks; 6, thermal resistance for cooler; 7, cooling flange; 8, compression spring construction; 9, cooling flange PT100; 10, DSC raw signal for amplifier; 11, purge gas inlet; 12, dry gas inlet. (Mettler-Toledo GmbH, Gießen, Germany.)

It is important to emphasize that the two technologies do not use the same experimental conditions to describe the physical property parameters, that is, the maximum allowable product temperature for primary drying. With DSC, it is an apparent glass transition temperature (T'_g) that is measured, which is commonly

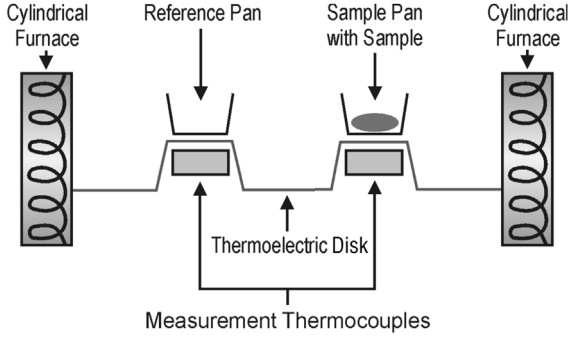

Figure 1.69 Scheme of a commercial apparatus for DSC measurements. The sample is placed in an aluminum pan. The sample pan and an empty reference pan are placed on small platforms within the DSC chamber. (See also Q100 DSC, TA Instruments, New Castle, DE, USA).

Figure 1.70 The DSC 3+ replaces the modulated DSC® apparatus, Model Q 1000, using the details of Figure 1.68. (Mettler-Toledo GmbH, Gießen, Germany.)

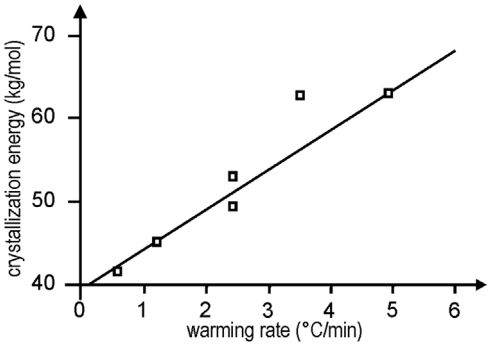

Figure 1.71 Crystallization energy of Na-cefazolin as function of the warming rate, measured by DSC.

described as the glass transition of a maximally freeze-concentrated solution. This transition appears as an endothermic shift in heat capacity that arises from a decrease of the viscosity of the glassy structure in a small temperature range, which in turn allows the system to access additional degrees.

Gatlin [61] measured not only T'_g for mannitol and Na-cefazolin by DSC, but also the dependence of the exothermic crystallization energy on the rewarming rate (Figure 1.71). The crystallization energy, extrapolated to a warming rate of zero, was calculated for mannitol (13.5 kJ/mol) and for Na-cefazolin (39.1 kJ/mol). These values agree with measurements by other methods. The activation energies were calculated with certain assumptions to be 335 kJ/mol for mannitol and 260 kJ/mol for Na–cefazolin. DeLuca [62] derived slightly different data: at a warming rate of 0.625 °C/min, he found 16.3 kJ/mol for mannitol and 41.8 kJ/mol for Na-cefazolin.

Na-cefazolin is unstable in its amorphous state. Takeda [63] described a method to ensure complete crystallization in which microcrystalline Na-cefazolin was added to supersaturated Na-cefazolin solution at 0 °C, frozen, and freeze-dried. The product did not contain amorphous or quasi-crystalline components.

Roos [64] measured T'_g of fructose and glucose by DSC and showed the influence of annealing/heat treatment. In Figure 1.72, DSC curves are shown for 60% solutions, cooled at 30 °C/min to −100 °C and rewarmed at a rate of 10 °C/min to −48 °C and cooled again to −100 °C at a rate of 10 °C/min. T_g of the nonannealed products were −85 and ≃88 °C, respectively. In the region of −50 °C, the crystallization of unfrozen water was seen as an exothermic event in both solutions (curves A). If rewarming was interrupted at ≃48 °C, the product remained at that temperature for ∼15 min (thermal treatment) and cooled again to −100 °C; the curves B were measured during warming: T'_g was increased to ≃57 °C, the exothermic of crystallization had disappeared, and all freezable water was frozen to ice. The temperature T_m is the onset temperature of the softening process in the product.

Talsma *et al.* [65] described the freezing behavior of certain liposomes by DSC measurements. Besides the expected influences of freezing and rewarming rates, and of the CPAs (mannitol and mannitol in tris buffer solutions), it was shown that heterogeneous and homogeneous crystallization in mannitol solutions exist and the nucleation of ice depends also on the liposome size: In small liposomes

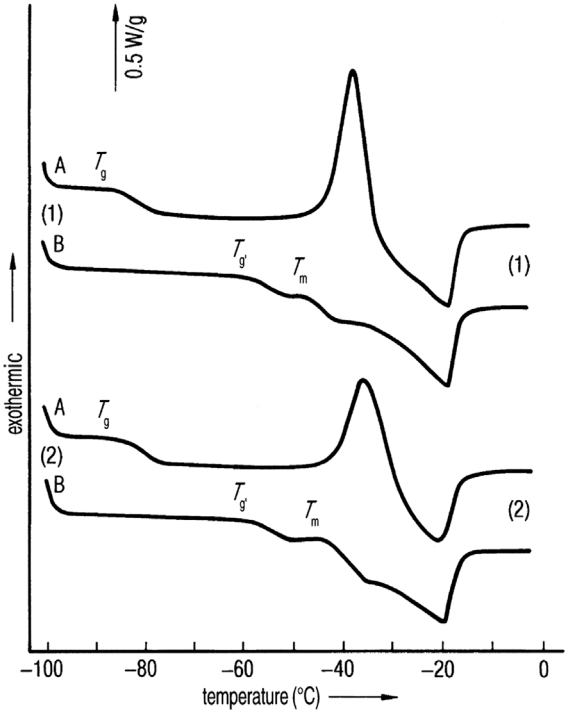

Figure 1.72 Results of annealing (thermal treatment) on the formation of ice in (1) 60% fructose and (2) 60% glucose solution. A: After cooling at 30 °C/min to −100 °C, the DSC plots were recorded during rewarming at 5 °C/min. $T_g \sim -85$ and −88 °C, respectively. At ≃48 and −44 °C, respectively, ice crystallization clearly starts, followed by the beginning of melting of ice (during freezing only part of the water has been crystallized). B: After cooling to −100 °C, the product was warmed at 10 °C/min to −48 °C, kept for 15 min at this temperature (thermal treatment), again cooled at 10 °C/min to −100 °C, and the DSC plot (B) was measured during rewarming. During the thermal treatment, all freezable water is crystallized, T'_g is increased to −58 and −57 °C, respectively. During rewarming, no crystallization can be detected. (See also Figure 2 from Ref. [64].)

(e.g., 0.14 μm), mannitol suppressed the heterogeneous crystallization more effectively than in large (0.87 μm) liposomes.

If in certain substances no crystallization or eutectic mixtures can be found by DSC (cephalosporin [66] with the experimental conditions used, one has to seek different conditions [63].

The development of DSC equipment with a low heat capacity and quick response times has made it possible to modulate the normal temperature ramp by a sinusoidal temperature oscillation, called modulated DSC (MDSC)®. By using Fourier transformation, the total heat flow can be separated into a reversing and a nonreversing »kinetic« component. The reversing heat flow will especially show glass transition events, which may be difficult to find in the total heat flow signal, or overlap with other nonreversing events. The reversing flow signal can be used to calculate heat capacity and its changes. The nonreversing component represents the kinetic events such as crystallization and enthalpic relaxation. Knopp

et al. [67] used temperature-modulated DSC (TMDSC) to define the collapse temperatures of sucrose solutions and compared the results with cryomicroscopy photographs. After substantial efforts at temperature calibration and reduction in temperature gradients in the sample, the collapse temperatures T_c of a 5 and 10% sucrose solution were determined: onset −37.7 °C. Earlier data for 10% sucrose solution (−32, −34 °C) were discussed as being too low for experimental reasons. Measurements of total heat flow, heat capacity, and kinetic heat flow for 5–80% sucrose solutions showed that below 20% w/w sucrose concentration, only one transition is observed, and for 40 and 60% a second transition is observed at a lower temperature. The kinetic heat flow signal for 60% sucrose shows a crystallization exotherm overlapping with the lower transition temperature range.

The authors considered that the higher transition temperature, as frequently accepted, does not indicate the collapse temperature T_c. They claimed T_c to be the midpoint between the end of the lower and the beginning of the higher transition, a reasonable average of −37 °C. They concluded that the structural relaxation time for water–sucrose glasses is short (<30 min) compared with the kinetics of ice crystallization. Kett and Craig [68] studied the glass transition region of 20, 30, and 40% sucrose solutions by modulated-temperature DSC (MTDSC). The heating rate was 2 °C/min with modulation of ±0.3 °C over 60 s. Before scanning, all samples were ›jump‹ cooled to −55 °C and then either annealed for 20–960 min at this temperature (isothermal) or annealed for 20 min at temperatures from −30 to −55 °C (isochronal). All transition temperatures were determined by the reversing and all enthalpies by the nonreversing signal. The glass transition region shows two transitions and one endotherm close to each transition.

Isothermal annealing shows an increase in the relaxation enthalpy with increasing annealing time and increasing sucrose concentration with a maximum at 400 min independent of the concentration. Figure 1.73 shows the effect of annealing temperature on the T_g onset. The authors recommended an optimum annealing temperature for 20–40% sucrose solutions between −38 and −42 °C and summarized that the onset temperature of glass transition and the accompanying endotherm relaxation signal increase with increasing annealing time up to ~7.5 h and then plateau. Chang *et al.* [69] performed modulated DSC (MDSC)

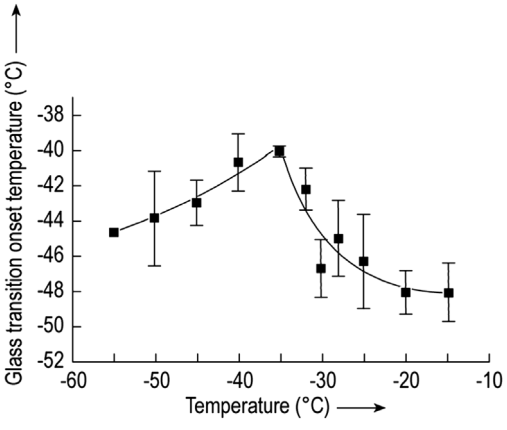

Figure 1.73 T_g onset of 40% sucrose solution as a function of annealing temperature. (See also Figure 4 from Ref. [68].)

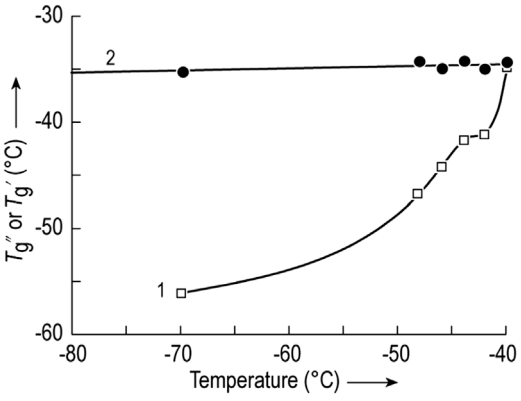

Figure 1.74 (1) T_g'' and (2) T_g' as function of annealing temperature for a 10% sucrose solution. (See also Figure 3 from Ref. [69].)

studies on 10% sucrose solutions that had been annealed between the two glass transition temperatures, T_g'' and T_g' (range −48.5 to −40.5 °C). The samples were treated in two ways: (1) quench cooled in LN_2, warmed to the selected annealing temperature and kept there for the annealing time (usually 1 h), modulated with an amplitude of 0.5 °C and a period of 100 s for 10 min to start from the steady state, beginning the linear scan at 1 °C/min; or (2) cooled at 1 °C/min to −68 °C, heated at 1 °C/min to the annealing temperature, and MDSC scan started after annealing as in (1). It was found that annealing shifts the reversing heat flow data for T_g'' to higher temperatures, close to the annealing temperature, and decreases the change in c_p. The authors concluded that T_g'' originates from a metastable condition, that is, excess water trapped in the sucrose phase, which crystallizes when $T > T_g''$, thereby raising T_g''. When the temperature reaches T_g', the product goes through a glass transition nearly coincident with reversible melting, both transitions being true glass transitions. Figure 1.74 shows T_g'' and T_g' as a function of the annealing temperature.

Craig *et al.* [70] assessed the behavior of amorphous lactose by MTDSC. The relaxation time of 10% freeze-dried amorphous lactose as a function of the difference between annealing (storage) temperature and T_g is given in Figure 1.75:

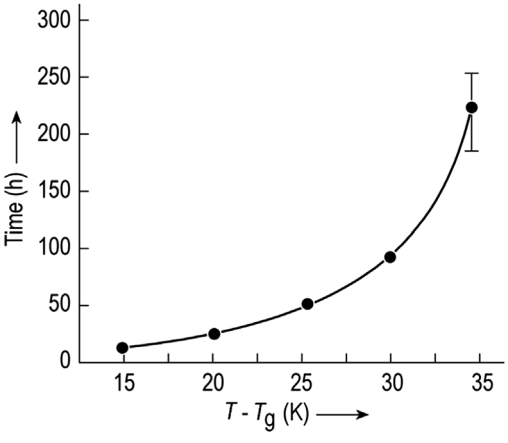

Figure 1.75 Relaxation time as a function of the difference between annealing temperature and T_g for a 10% amorphous freeze-dried lactose. (From Craig, 2000 [70]. Reproduced with permission of Springer.)

The relaxation time 15 K below T_g is ~10 h and 35 K below T_g is ~250 h. The authors discussed the difference between T_g measured with MTDSC and a ›fictive‹ T_g that would be measured by a linear heating signal. T_g is between 2.0 and 0.2 °C higher than the fictive value, decreasing with increased annealing time from 10 min to 16 h.

Another method to differentiate between reversible and the irreversible heat flow is StepScan® DSC [71]. The precondition for its use is a DSC system with ›power compensation‹: Sample and reference material are held in two separate calorimeters, each with its own heating elements. Both systems are maintained in equilibrium conditions. The amount of energy to keep the equilibrium is directly proportional to the energy change in the sample. The power compensation system measures heat flows, normal DSC systems measure temperatures. The StepScan method applies the heating (e.g., 10 °C/min) over a small temperature increment (e.g., 1.5–2 min), holds this temperature for a short time (e.g., 30 s), and calculates the heat capacity at that temperature. The irreversible or kinetic part of the total heat flow represents the ›slow‹ processes that take place during the scan: enthalpic relaxation, crystallization, and melting. With this method, a 5% sucrose solution was analyzed, as shown in Figure 1.76.

Van Winden *et al.* [72] used MTDSC in lyoprotected liposomes to detect the glass transition in samples in which it overlaps with the bilayer melting endotherm.

Kett *et al.* [73] studied T_g in freeze-dried formulations containing sucrose as a function of relative humidity and temperature during storage by TMDSC and thermogravimetric analysis. Craig *et al.* [74] found it helpful to assess the relaxation behavior of freeze-dried amorphous lactose by MTDSC. Relaxation times were calculated from measurements of T_g, c_p, and the magnitude of the relaxation endotherm. Scanning was performed at 2 °C/min with a modulation amplitude of ±0.3 °C and a period of 60 s.

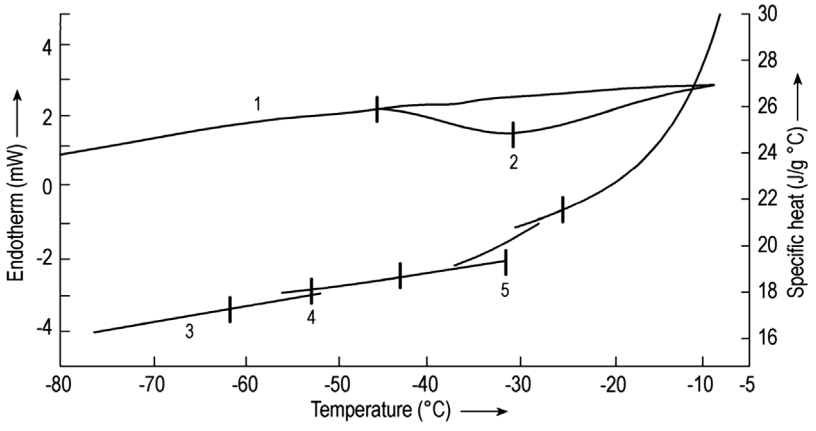

Figure 1.76 c_p and IsoK baseline data for 5% sucrose solution. 1, IsoK baseline; 2, recrystallization, −30.35 °C; 3, c_p; 4, T_g'' extrapolated to −52.38 °C, $dc_p = 4.08 \times 10^{-2}$ J/g °C; 5, T_g' extrapolated to −32.06 °C, $dc_p = 0.12$ J/g °C. (See also Figure 5 from Ref. [71].)

Figure 1.77 NMR analyzer, the ›Minispec‹ mq series, measurement range −100 to +200 °C. (See also Bruker Optik, Rheinstetten, Germany.)

1.1.5.6 Nuclear Magnetic Resonance

Nuclear magnetic resonance (NMR) is a highly sensitive analytical method. It can be used to study the way in which water behaves during freezing in aqueous saccharide and protein solutions and also in coffee extracts. Using NMR, it is possible to determine whether water is bound to other molecules (e.g., proteins) and cannot crystallize, how the collapse temperature T_c is influenced by unfrozen water and the changes in a glass of highly concentrated solutions during warming from low temperatures below and above T_g.

NMR spectroscopy (a commercial unit is shown in Figure 1.77) uses the fact that some atomic nuclei have a magnetic moment, for example, very distinct in a proton, the nucleus of hydrogen, but also in ^{13}C, ^{31}P, ^{14}N, and ^{33}S. In an external magnetic field, the energy levels split, as described in quantum mechanics. The size and extent of the split are given by Eq. (1.9):

$$\Delta E = \mu B g H_{\text{eff}} \tag{1.9}$$

where μB is the nuclear magneton, g is a constant (characteristic for the magnetic quality of a given nucleus), and H_{eff} is the effective strength of the magnetic field at the location of the nucleus.

The transition energy can also be described as a frequency of electromagnetic radiation:

$$\Delta E = hf \tag{1.10}$$

where h is Planck's constant and f is the frequency of radiation, or

$$\Delta E = h\, c/\Lambda$$

where c is the speed of light and Λ is the wavelength.

The energy difference between the levels depends on the field strength of the external magnetic field. To use 60, 100, or 270 MHz for NMR measurements with protons, the magnetic field strengths must be 14.1×10^3, 23.5×10^3, or 63.4×10^3 gauss (G). The last value is only possible with superconducting magnets. Since all other nuclei have a magnetic momentum that is small compared with that of the

proton, still higher magnetic field strengths are necessary. The magnetic momentum of a nucleus is, according to electrodynamic laws, the consequence of a rotating electric charge. This rotation is described in quantum mechanics as the spin (S) of the nucleus. Spin can only have discrete, defined energy levels parallel or vertical to the direction of the magnetic field ($S = \pm 1/2$). Transitions, for example, to higher levels (absorption) are only possible (they happen with a certain degree of probability) if S is not changed with the transition ($\Delta S = 0$) and the projection of the spin in the direction of the magnetic field changes by ± 1 ($\Delta S_z = \pm 1$). If a sample with a magnetic momentum is irradiated by ultrashort waves in an external magnetic field, only radiation of a defined wavelength and defined energy can be absorbed. This wavelength at a given external magnetic field is characteristic for the isolated nucleus.

In the nuclear (e.g., proton) part of a molecule, the external field is changed by factors that are characteristic for that molecule. The resonance frequency of isolated protons is shifted in a way typical of the chemical compound in which the proton is located. This shift is called the chemical shift of the resonance frequency (at a given external magnetic field).

The chemical shifts are small, for example, at a proton up to 30 ppm of the used frequency; if 100 MHz (10^8 Hz) is used, 10 ppm corresponds to 10^3 Hz. The shift is normally not measured absolutely, but compared with the known frequency of a reference substance, for example, for protons tetramethylsilane (TMS). The area of the resonance is proportional to the number of nuclei that give rise to it.

Besides the chemical shift of the resonance line, under certain conditions the lines split into two or more lines. This reflects the influence of the spin orientation of two or more neighboring nuclei on the magnetic field in the surrounding nuclei. The size of the splitting is called the coupling constant, *J*. *J* represents the quantity of influences between the nuclei, while the number of split lines and their intensity represent the number of influencing nuclei. The lines in an NMR spectrum are not infinitely small, but show certain linewidths, since the magnetic field at the location of a nucleus changes slightly, albeit constantly. After the high-frequency impulse is terminated, the earlier equilibrium is reinstated by magnetic noise and the system relaxes. Bloch connected the two possible relaxation processes with two characteristic times: t_{SGR}, the spin–lattice relaxation time, and t_{SSR}, the spin–spin relaxation time. The half-width of the resonance line measured at the half-height of the peak equals $1/t_{SSR}$. As shown in Figure 1.78, for very small molecular correlation times t_c, t_{SGR} and t_{SSR} are identical. The correlation time is the time that one molecule requires to travel the distance of its own diameter; it is a measure of the mobility of the molecules.

In aqueous solutions with small molecules, the relaxation is slow (0.1–0.5 s), while t_{SSR} of ice is very small (some 10^{-3} s) [76]. Close to the glass temperature of a substance, the relaxation time does not decrease exponentially and thus a different means of description must be used (Ref. [9] of Chapter 3).

Hanafusa [76] showed with this method how the amount of unfrozen water in a 0.57% solution of ovalbumin reaches practically zero at −20 °C, if 0.01 M sucrose is added (Figure 1.79). For globular proteins, Hanafusa described the freezing process as follows: between 0 and −20 °C, water molecules from the multilayer hydrate shell are decomposed. Below −45 °C, molecules from the monohydrate

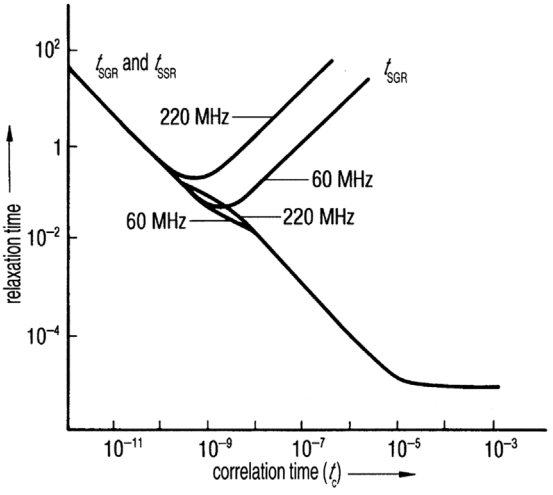

Figure 1.78 Relaxation time as a function of the molecular correlation time for two spectrometer frequencies, 60 and 220 MHz. t_{SGR}, spin–lattice-relaxation time; t_{SSR}, spin–spin relaxation time. (From Knowles, 1977 [75]. Reproduced with permission of John Wiley & Sons.)

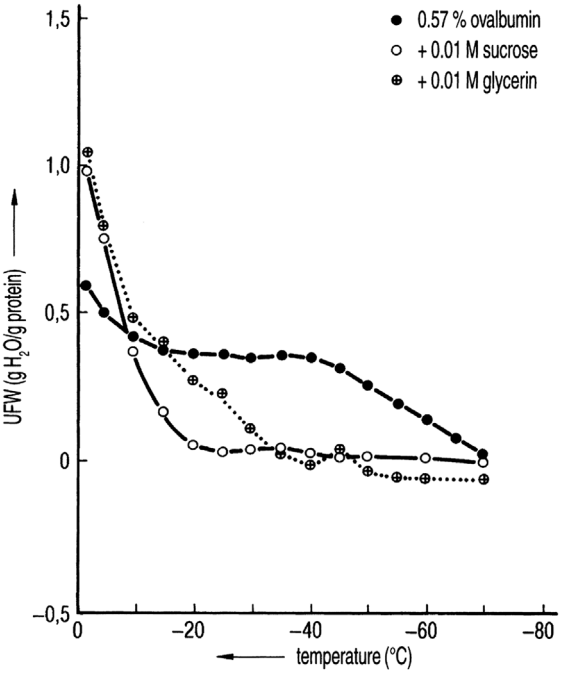

Figure 1.79 Unfreezable water (UFW) in a 0.57% ovalbumin solution as a function of the freezing temperature with different CPAs. (See also Figure 4 from Ref. [76].)

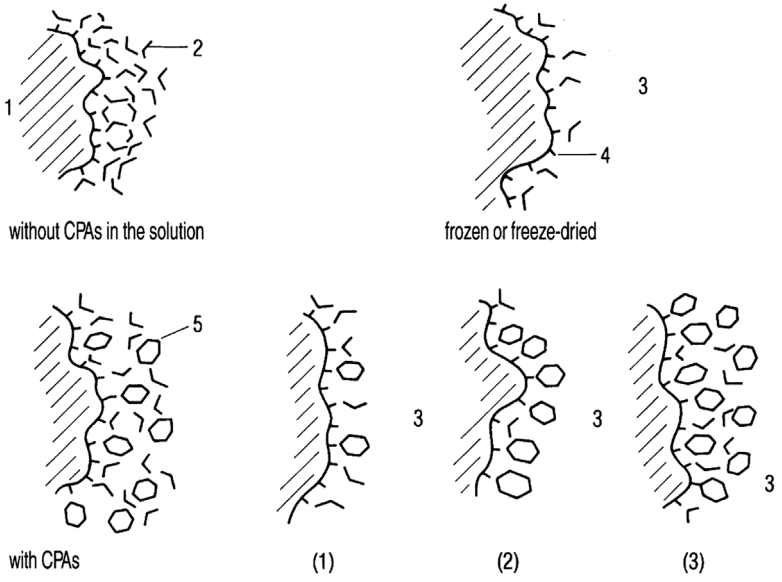

Figure 1.80 Schematic model of the action of CPAs in protein solutions during freezing and freeze-drying. (See also Figure 10 from Ref. [76].) *Top row:* Without CPA; the hydrate water of the ovalbumin has migrated into the ice and the freed valences are exposed to the influence of the environment. *Bottom row:* With CPA; part of the hydrate water of the proteins becomes replaced by CPA molecules. The molecules of the CPA, the remaining water molecules, and the protein molecule form a ›quasi‹ (replacement) hydrate layer. 1, protein; 2, water molecule; 3, ice or air; 4, exposed valence; 5, CPA molecule.

shell are removed, thereby destroying the shell; between −20 and −45 °C, an equilibrium exists between the hydrate bond to the protein molecule and the forces to insert additional water molecules into the ice crystals. By adding CPAs, the amount of bound water is much reduced. Water molecules are replaced by CPA molecules and form a ›quasi-hydrate‹ shell, which protects the protein during freezing and freeze-drying against denaturation. Hanafusa showed (Figure 1.80) a simplified, graphic picture of how, with rising concentration (1) to (3), the CPA molecules form a new shell for the protein. Some water molecules are so strongly incorporated that they can no longer diffuse to the ice crystals.

Nagashima and Suzuki [77] used NMR to show the interdependence of UFW, T_c, the cooling rate, and the concentration before freezing. The amount of UFW in g H_2O/g dry substance is measured, for example, of coffee extract with 25% solids (Figure 1.81), which at −20 °C has ~30% UFW (0.3 g/g) but is reduced at −50 °C to 0.1 g/g. Above −20 °C, the UFW rises rapidly. During freeze-drying above −20 °C, the structure will collapse. The authors demonstrated that after quick freezing (3–5 °C/min) of mannitol solution, crystallization of mannitol can be seen during rewarming. The UFW rose to ~50%, water then crystallized, and UFW was reduced to a few percent. The crystallization temperature measured agreed well with other reports (e.g., Ref. [54]) using DSC. During slow freezing, mannitol crystallizes and there is no hysteresis (Figure 1.82). Figure 1.83 shows the strong dependence of UFW for Japanese miso sauce. At −50 °C and a

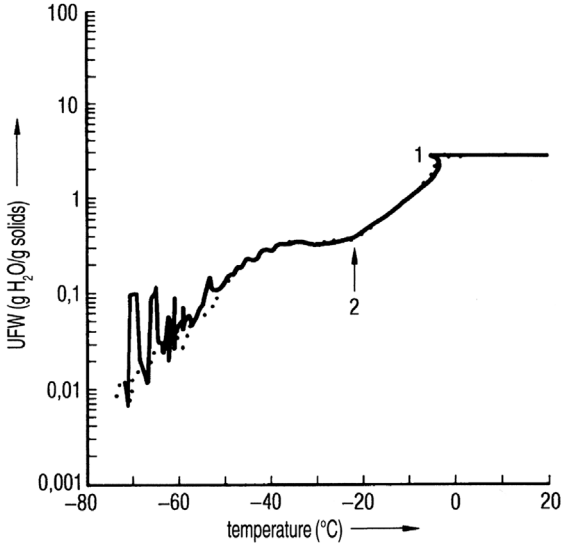

Figure 1.81 Freezing and thawing plot of coffee extract with 25% solids. UFW (g H_2O/g solids) as a function of temperature. 1, subcooling; 2, collapse temperature. (Figure 2 from Ref. [77].)

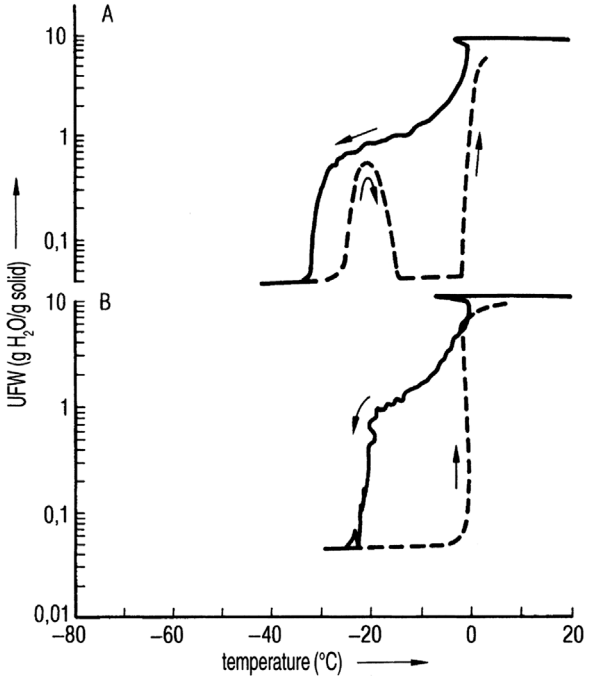

Figure 1.82 Freezing -and thawing plot of 9.1% D-mannitol solution. Freezing rate: (A) 5 and (B) 0.5 °C/min. (See also Figure 4 from Ref. [77].)

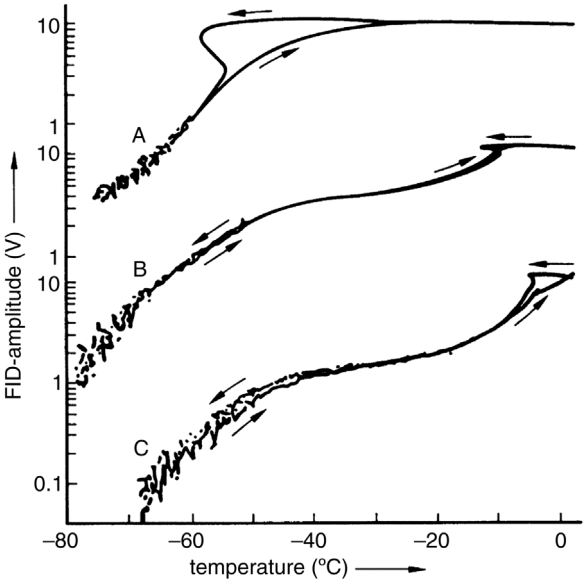

Figure 1.83 UFW content of miso sauce (A) and two dilutions (B and C) as a function of temperature. The solid content is (A) 52.7, (B) 26.4, and (C) 13.2%. (See also Figure 5 from Ref. [77].)

concentration of 52.7%, UFW is ~5 units, whereas at 26.4% solids in the original product, UFW remains at ~2 units and only at 13.2% solids ≈ 0.6 units UFW does not freeze.

Harz *et al.* [78] demonstrated by NMR spectroscopy that freezing of food (e.g., grapefruit juice) almost never followed the ideal expectation. The crystallization of carbohydrates is much hindered and further reduced by the high viscosity of the solutions. Water crystallizes much below the eutectic temperature, producing further increases in viscosity and leading to a glass phase during further cooling. Depending on the carbohydrates, this metastable phase at −18 °C can last for weeks or, on occasions up to 1 year.

Girlich [79] studied by NMR the molecular dynamics of aqueous saccharin solutions. At concentrations down to 30% solids, the saccharin molecules do not influence each other, while with decreasing temperature the existing H-bond bridges prevent a reorientation of the H_2O molecules. Dissolved saccharin molecules can destroy the H bonds, such that subcooling becomes possible. At >40% solids, associations of saccharin molecules are formed. H_2O is increasingly bound by H bridges and loses translational and rotational mobility. With increasing concentration of the solution, the saccharin molecules cross-link, and hydrate water becomes freed and can lead locally to low concentrations. T'_g of water becomes different from that of saccharin hydrates. Below 70% solids, the cross-linked system of saccharin molecules develops into a gel. During the observation time, no crystallization takes place and a metastable glass exists with a viscosity $>10^{12}$ Poise. The mechanical behavior is like that of solids.

Kanaori *et al.* [80] studied the mechanism of formation and association of human calcitonin (hCT) fibrils using NMR. hCT associates and precipitates during storage in aqueous solution. The freeze-dried hCT and its behavior were described.

Yoshioka *et al.* [81] studied the mobility of protons by NMR in freeze-dried bovine serum albumin (BSA) and γ-globulin (BGG) and its relation with aggregation susceptibility. The spin–spin relaxation time t_{SR} of protons in BSA and BGG was measured as a function of the water content in the range of 0.2–0.5 g/g (g water/g protein) in both products. The increase in t_{SR} and the increase in the aggregation susceptibility were strongly related.

1.1.5.7 Thermomechanical Analysis (TMA)

Carrington *et al.* [82] used thermomechanical analysis (TMA) to study the ice-crystallization temperature of 30% w/w fructose, sucrose, and glucose with and without sodium carboxymethylcellulose (CMC). TMA has been used to measure the expansion of the sample during freezing and rewarming. Parallel studies have been done using DSC. A typical result of TMA measurements during freezing is shown in Figure 1.84 for fructose with and without CMC during freezing with a rate of 5 °C/min. Figure 1.85 shows the plot of the warming profile of slowly frozen and annealed 30% sucrose solution, as determined by TMA. Figure 1.86 shows the warming DSC curve of 30% sucrose solution slowly frozen and annealed. On comparing the two temperatures T_{r1} and T_{r2} (as shown in Figures 1.85 and 1.86) by both methods for sucrose, $T_{r1} \approx -60$ °C (TMA) and −41.2 °C (DSC), $T_{r2} \approx -35$ °C (TMA) and −32.6 °C (DSC), it is obvious that several factors influence the resulting data, as discussed by the authors (onset data for DSC from a table in the publication, TMA estimated from the plot).

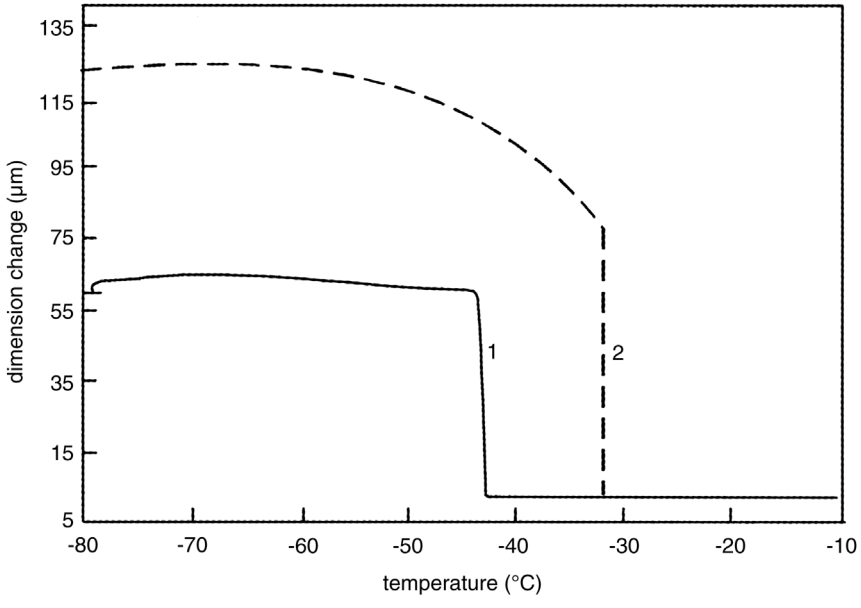

Figure 1.84 Dimension change as a function of temperature for 30% sucrose solution during freezing at 5 °C/min down to −80 °C. 1, fructose alone; 2, fructose plus 0.25% sodium carboxymethylcellulose (CMC) . (See also Ref. [82].)

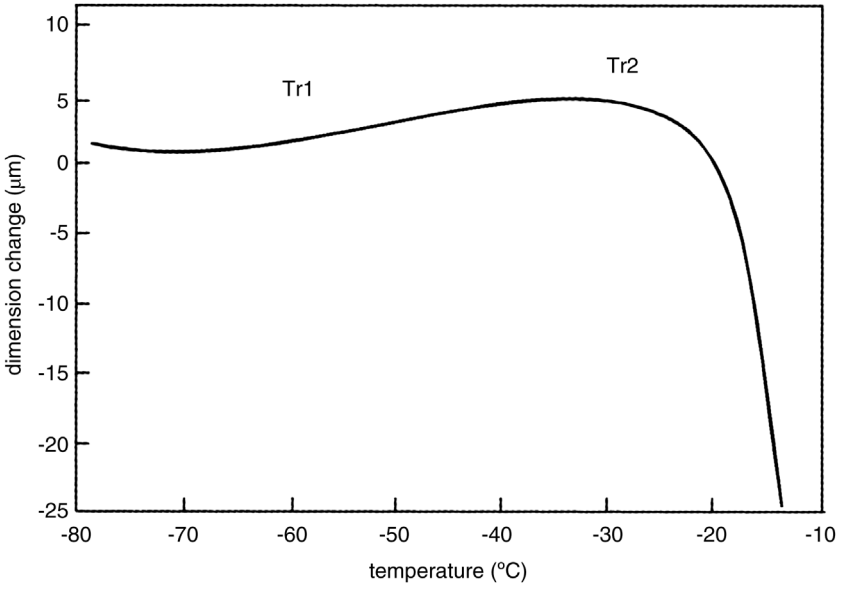

Figure 1.85 Dimension change as a function of temperature for 30% sucrose solution during warming at 2 °C/min after slow freezing to −80 °C and annealing up to −35 °C. (See also Ref. [82].)

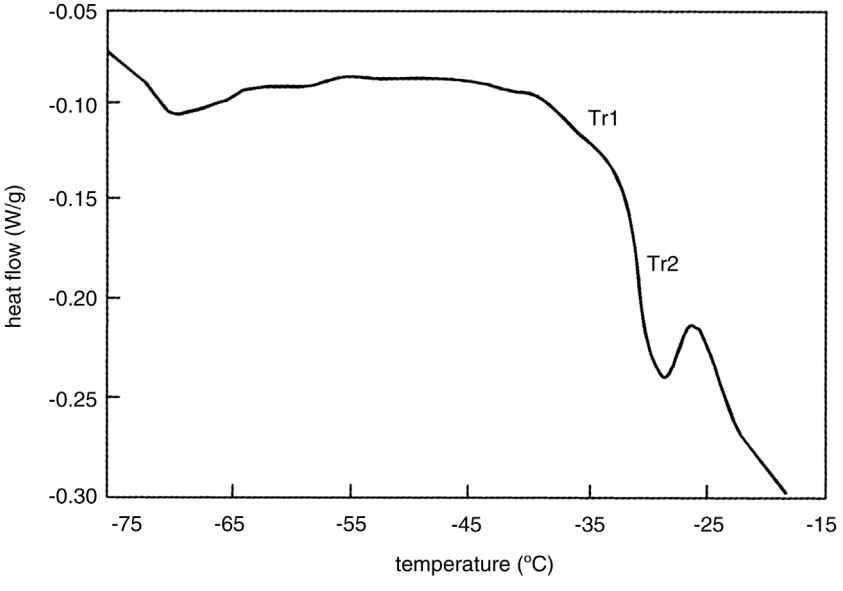

Figure 1.86 Heat flow as a function of temperature in the DSC thermogram of 30% sucrose solution frozen at 5 °C/min to −80 °C during warming (5 °C/min) after annealing up to −35 °C. (See also Ref. [82].)

TMA measurements have been helpful in explaining the breakage of vials during the warming of frozen solutions of mannitol and other stereoisomers [83]. For example, above −25 °C, mannitol expands 30 times more than standard type 1 flint glass. Depending on the filling volume and the concentration, 10–40% of the vials break when filled with 3% mannitol solution.

1.1.5.8 Dielectric Analysis (DEA)

Pearson and Smith [84] explained the advantages that DEA can provide to optimize freeze-drying processes by three examples. (i) The different relaxation behavior of bound water (two hydrogen bonds) and sorbed water (one hydrogen bond) can be used to determine the end of freeze-drying when the sorbed water is desorbed and the bond water still in place. (ii) The dielectric response of a material can be related to its crystal size and the level of hydration. (iii) The glass-forming property of excipients and their molecular mobility (viscosity) are strongly influenced by temperature and hydration. Dielectric studies have shown a non-Arrhenius behavior of glass-forming sugar solutions, resulting in a viscosity change of several orders of magnitude within small temperature or hydration changes.

Morris *et al.* [85] proposed the use of dielectric analysis to predict the collapse temperature of two-component systems. The background of DEA is explained and the ›take-off frequency‹ (TOF) is chosen as the best analytical method to identify the collapse temperature. Figure 1.87 shows the dielectric loss factor as a function of the frequency. The frequency at the minimum of this curve is called TOF by the authors. TOF varies with the temperature as shown in Figure 1.88. The extrapolated intersection of the two linear portions identifies the collapse temperature. The predicted T_c by TOF for 10% sucrose, 10% trehalose, 10% sorbitol, and 11% Azactam™ solution deviates from observations with a freeze-drying microscope (Table 1 in Ref. [85]) to slightly lower temperatures, the differences being −3, −1.4, 2.2, and 0.7 °C.

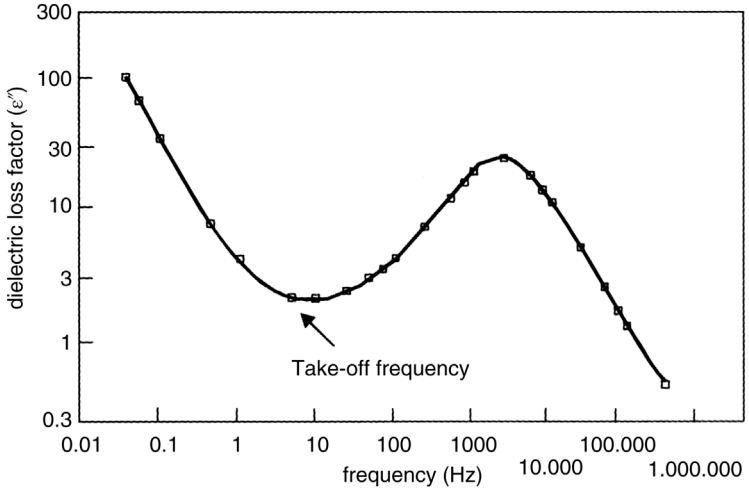

Figure 1.87 The take-off frequency, at a given temperature, occurs at the first minimum in the dielectric loss factor (ε'') versus frequency curve as frequency increases. (See also Figure 9 from Ref. [85].)

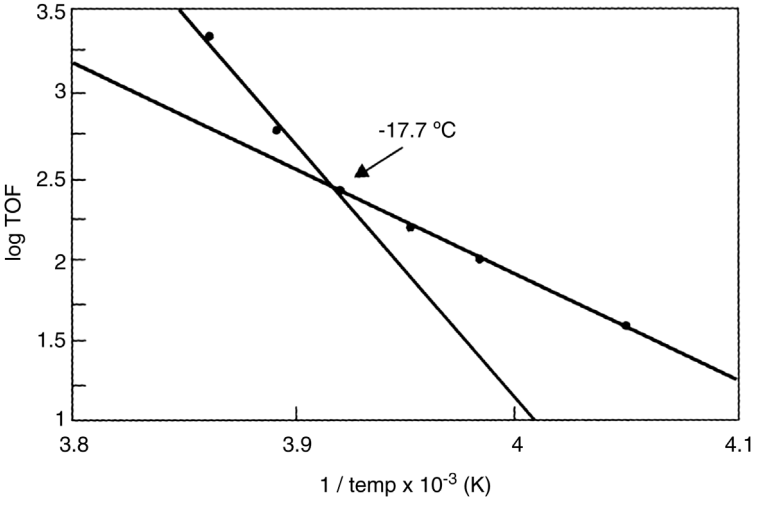

Figure 1.88 Collapse plot of log(TOF) versus 1/K. The extrapolated intersection of the two linear portions identifies the collapse temperature of the system. (See also Figure 10 from Ref. [85].)

Smith *et al.* [86] reviewed dielectric relaxation spectroscopy (DRS) as a method for the structural characterization of polymers and proteins providing, among others, information about the water content and states of water.

1.1.5.9 XRPD Diffractometer–Raman Spectroscopy

X-ray diffractometry on lyophilized products provide the following information:

- Crystalline samples can easily be distinguished from amorphous samples.
- Crystallinity (CI) can be determined in crystalline samples.
- Polymorphism (different modifications) of a substance can easily be identified.
- Hydrates (mannitolhydrate) are easily recognized.

The X-ray powder diffractometer (XRD) measurement is based on the diffraction of X-rays at the higher level structure of a crystalline substance. The wavelength of the X-ray is in the range of the lattice spacing in the crystal[1]. It is based on the Bragg law:

$n\lambda = 2d \times \sin\theta$
n = hole number
λ = wave length
d = distance
θ = angle

Cavatur and Suryanarayanan [87] have developed a low-temperature XRD technique to study the solid states of solutes in frozen aqueous solutions. In

1 Dr. Stefan Seyferth, Institute for Pharmaceutical Technology, University Nuerberg- Erlangen, Germany (2009).

frozen nafcillin sodium solution (22% w/w), no eutectic crystallization was observed. Annealing at −4 °C caused solute crystallization, which increased with annealing time. Two other products studied showed that XRD provides information about the degree of crystallinity without the interference of other events.

Raman spectroscopy was used by Sane *et al.* [88] to quantitate structural changes in proteins freeze-dried or spray dried. Monoclonal antibodies (e.g., RhuMAbVEGF) underwent secondary structural changes in the absence of a lyoprotectant. Increasing molar ratios of cryoprotectant could lead to complete structural preservation. The long-term stability of the dried proteins correlates with structural changes observed by Raman spectroscopy.

1.1.6 Changes of Structure in Freezing or Frozen Products

Independent of the growth of ice crystals (Section 1.1.2), which can be observed down to ≃100 °C, and possible recrystallization (Section 1.1.3), this section describes only such developments or changes of structures that can be influenced by additives. The addition of CPAs to albumins, cells, or bacteria influences the nucleation of ice – or at least its growth – in such a way that their natural structures are retained as much as possible. On the other hand, additives are introduced to crystallize dissolve substances. If this method does not help, for example, with antibiotics, the solution increasingly concentrates until a highly viscous, amorphous substance is included between ice crystals. This condition has disadvantages:

- The water is not crystallized to its maximum and can be removed during freeze-drying only with difficulty or not at all. The residual moisture content remains undesirably high.
- Drugs are often less stable in the amorphous state than as crystals [89–92].

The phase transition from amorphous to crystalline can sometimes be promoted by thermal treatment (annealing) (TT) [93]. It is recommended first to search for CPAs and process conditions that would lead to crystallization. The evaluation can be carried out using methods such as described in Section 1.1.5 (see also Yarwood and Phillips [94]. If this is not successful, the time and temperature for TT should be chosen in such a way that the tolerances for time and temperature are not too narrow, for example, -24.0 ± 0.5 °C and 18 ± 1 min are difficult to operate, while -30 ± 1.5 °C and 40 ± 2 min might be easier to control.

A suitable freezing rate, start-up concentration, and an amount of product per vial (e.g., for Na-ethacrynate) can be selected that result in a stable, crystalline phase. However, the addition of CPAs may provide another means of achieving crystallization, as seen for several pharmaceutical products [95].

De Luca *et al.* [96] showed that the addition of 5% *tert*-butyl alcohol (*t*BA) to aqueous sucrose and lactose solutions (up to 40%) resulted in a frozen matrix, which could be easily freeze-dried. They demonstrated by DSC that the melting point rose distinctly (with 60% solution to −10 °C), but the endotherm of melting returned to 25%, indicating that not much water had frozen. In solutions with 5%

*t*BA, the exotherm of crystallization became more visible and the melting of *t*BA could be recognized.

Kasraian and De Luca [97] developed a phase diagram by DSC for *t*BA. Two eutectics were observed at 20 and 90% *t*BA concentrations. Using a freeze-drying microscope, the change of ice crystals by *t*BA became visible, although 3% *t*BA was required to form large needle-shaped ice crystals. A solution with 10% *t*BA grew finer, needle-shaped ice crystals, and a 70% *t*BA solution formed very large hydrate crystals. The rate of sublimation of water and *t*BA depended on the concentration. The crystallization behavior of the water–*t*BA mixtures could explain the influence of *t*BA on the freeze-drying of sucrose and lactose, when used in certain concentrations. Oesterle *et al.*[98] showed that not only can *t*BA speed up the sublimation of ice from amorphous freeze-concentrated mixtures, but also similar effects can be achieved with volatile ammonium salts such as ammonium acetate, bicarbonate, and formate. In an 8.5% excipient solution, 0.1 M ammonium salt solutions and 5% *t*BA were studied. The onset temperatures of T'_g were determined by DSC as sucrose −33.6, PVP −21.1, and lactose −29.7 °C. The onset temperatures for *t*BA–ammonium mixtures were between 3 and 14 °C lower than without additives. Main drying (MD) was carried out 5 °C lower than the respective T'_g. The percentage weight losses during the first ~7 h of drying were the largest with 5% *t*BA in PVP and lactose solutions. In the sucrose solution, *t*BA and ammonium salts show approximately equal effects. The authors concluded that the sublimation rates can be enhanced by *t*BA and other additives, but the influence of these additives on the stability and activity of proteins is not clear.

Wittaya-areekul and Nail [99] studied the effect of formulation and process data on residual *t*BA. Sucrose and glycine were used as models for noncrystallizing and crystallizing solutes. The variables examined were initial *t*BA concentrations, cake thickness, freezing rates, temperature, and duration of SD. Freeze-dried glycine (crystallized) contained 0.01–0.03% *t*BA, regardless of freezing rate and initial *t*BA concentration. The level of *t*BA in freeze-dried sucrose was two orders of magnitude higher and effected by freezing rate (rapidly frozen contained twice as much *t*BA as slowly frozen) and initial *t*BA concentration (*t*BA concentrations above the threshold concentration for eutectic crystallization resulted in relatively low residual *t*BA, concentrations below contained significantly higher levels of *t*BA). Time and temperature of SD had a minimal influence on residual *t*BA in the dried product.

1.2 Drying

Drying is basically well understood and is governed by two transport mechanisms: (i) the energy transport to transform ice into water vapor (between −21 and −30 °C approximately 2805 kJ/kg) and (ii) the transport of the water vapor from the sublimation surface through the already dried product into the drying chamber to the condensation or absorbing system for the vapor. Figure 1.89 shows the process of the main drying (MD) observed with a cryomicroscope. A 10% aqueous solution of hydroxyethyl starch (HES) has been directionally frozen

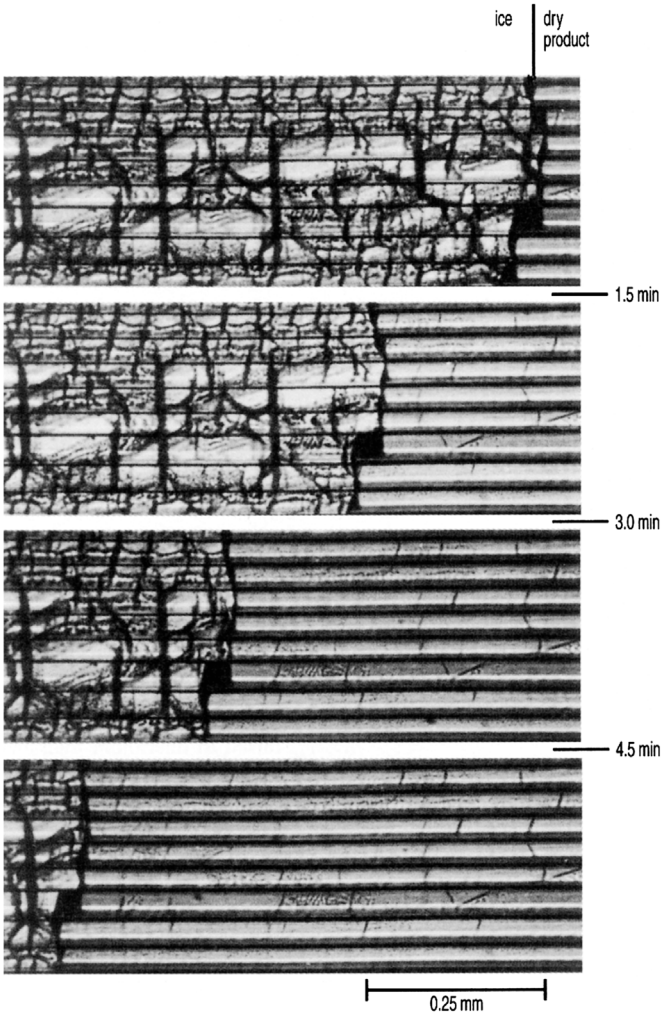

Figure 1.89 Main drying observed with a cryomicroscope. The HES solution was frozen under optimum conditions (see Figure 1.60). The solid, dark lines show the form of the sublimed ice crystals. (From Kochs, 1991[100]. Reproduced with permission of Elsevier.)

(see Figure 1.60). The ice dendrites are surrounded by the concentrated solid, which can be seen as a dark line after the ice is sublimed. In spite of optimal freezing, the sublimation speed is not uniform for all dendrites.

After the ice has been sublimed, the adsorbed water is desorbed from the solid. This process is governed by laws different from those of the main drying. This step is called secondary or desorption drying. During the secondary drying (SD), the energy transport does not play an important role, since the amount of water is normally less than 10% of the solids. Nevertheless, SD time-wise can be an important part of the total process and consume half or the same time as MD.

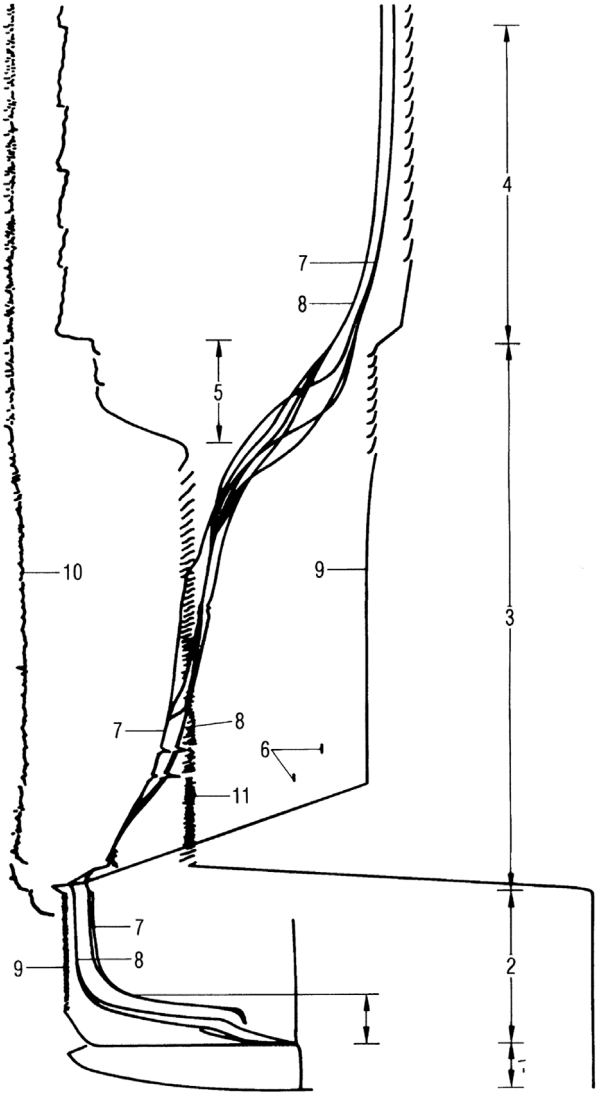

Figure 1.90 Course of a freeze-drying process. 1, precooling of the shelves; 2, freezing of the product; 3, evacuation and main drying (MD); 4, secondary drying (SD); 5, changeover from MD to SD; T_{sh} raised to maximum tolerable product temperature; 6, T_{ice} measurements by BTM; 7, temperature sensors RTD in the product; 8, temperature sensors Th in the product; 9, temperature of the shelves (T_{sh}); 10, ice condenser temperature; 11, pressure in the drying chamber (p_{ch}).

Figure 1.90 shows a typical run of a freeze-drying process, which can be divided into two parts: In MD, large amounts of water vapor (for example, 900% (w/w) of the solids) are sublimed and transported at an almost constant temperature at the sublimation front, (T_{ice}); in SD, the product temperature rises to the maximum tolerable temperature of the product and the water content is lowered, for example, by 9% (w/w) of the solids.

1.2.1 Main Drying (Sublimation Drying)

The amount of energy necessary for the sublimation depends on the sublimation temperature, but between −10 and −40 °C the energy varies by less than 2%. Furthermore, energy is consumed to heat the vapor during the transport through the already dried product or in contact with the warmer shelves. The specific heat of water vapor is 1.67 kJ/kg and the maximum increase in temperature is up to +20 or +40 °C. The energy consumption in this process can almost be neglected compared with the sublimation energy; heating the vapor from −30 to +30 °C results in ∼100 kJ/kg or ∼3.5% of the sublimation energy.

The necessary energy can be transduced to the ice in four different forms:

1) by radiation of heated surfaces;
2) by conduction from heated plates or gases;
3) by gas convection; or
4) by dielectric losses in the ice in a high-frequency field. The method is not discussed, since high-frequency fields with the necessary field strength in the pressure range of MD freeze-drying (1–0.01 mbar) start gas discharges.

(1) An infinite plate with a temperature K_{str1} and radiant efficiency ε_1 will transmit, independent of the distance, to a similar plate of frozen product with a temperature K_{str2} and a radiant efficiency ε_2 an amount of radiation energy. The surface heat flux q is

$$q = \delta(K_{Str1}^4 - K_{Str2}^4) \times 1/[(1/\epsilon_1) + (1/\epsilon_2) - 1) \tag{1.11}$$

where $\delta = 2.05 \times 10^{-7}$ kJ/m^2 h K^4.

This presentation is simplified. In practice, part of the energy, depending on the distance of the plates, will hit the walls of the chamber. This effect is small as long as the dimensions of the plates are large compared with their distance. For two plates of 1 × 1 m and a distance of 0.1 m, the effective radiation is ∼0.8q and with two plates of 0.5 × 0.5 m it is ∼0.7q [101].

The values of ε for products will normally be close to 1, which is also true for anodized aluminum and varnished steel. For polished steel, $\varepsilon = 0.12$. Figure 1.91 shows the energy transmission by radiation if both ε are 1.

At a shelf temperature of 100 °C, ∼2000–4000 kJ/h m^2 are transmitted, depending on the product temperature. At lower shelf temperatures, as is usual in freeze-drying plants for pharmaceutical products, q values between 500 and 1500 kJ/m^2 can be expected. However, for $\varepsilon = 0.12$, these data are reduced by a factor of 0.12.

At a shelf temperature of 100 °C and both $\varepsilon = 1$, at the beginning of a freeze-drying cycle (surface temperature −20 °C) ∼1.4 kg ice/h m^2 can be evaporated; at +30 and −30 °C, ∼0.4 kg/h m^2 remain. If $\varepsilon_1 = 0.12$, the sublimation rate is reduced to ∼200 and 50 g/h m^2, respectively.

In freeze-drying of pharmaceuticals in vials at 0.1 mbar, the contribution of radiation can be 20–30%, of gas conductivity 50–60% and of contact conductivity 10–30% of total energy transfer.

(2 and 3) An important part of the energy transfer is by conductivity, as well by direct contact of the product container with the shelf, as by the gas. Furthermore,

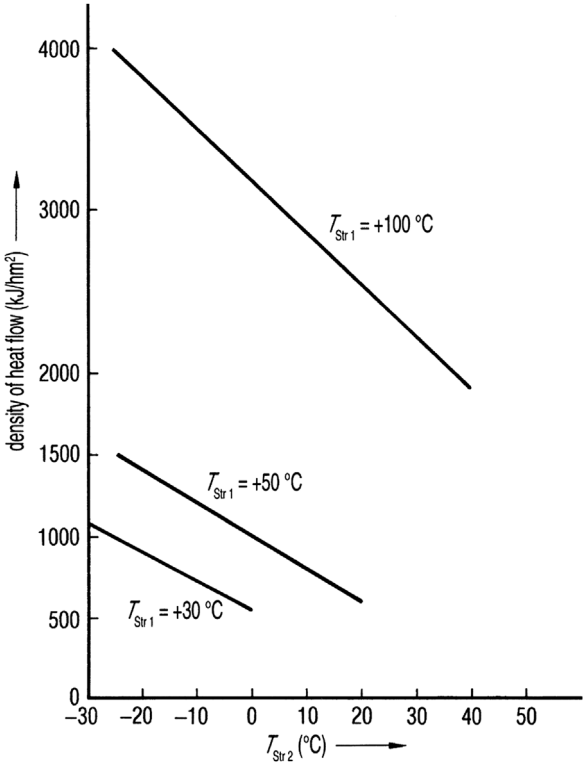

Figure 1.91 Heat transfer by radiation only. The figure shows only the order of magnitude. Density of heat flow (q) as a function of T_{Str2} (ice or product surface temperature) at three temperatures T_{Str1} of the radiation surface (+100, +50, +30 °C) as parameter.

the gas transports energy by convection, which becomes an essential factor, if the distance between the shelf and tray or vial becomes small. Figure 1.92 [5] shows that for distances larger than 10 mm, the energy transfer is independent of the pressure and becomes very small. However, for small distances, for example, 0.5 mm, the heat transfer coefficient rises between 0.13 and 1 mbar by a factor of 4.

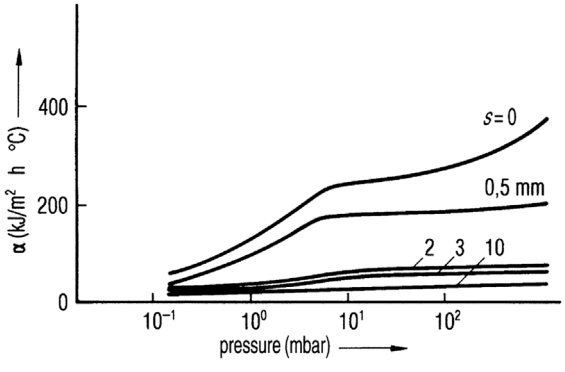

Figure 1.92 Heat transfer coefficient α as a function of pressure. Parameter s = distance between shelf and bottom of the product container (mm). Data measured in air. (Figure 4a from Ref. [5].)

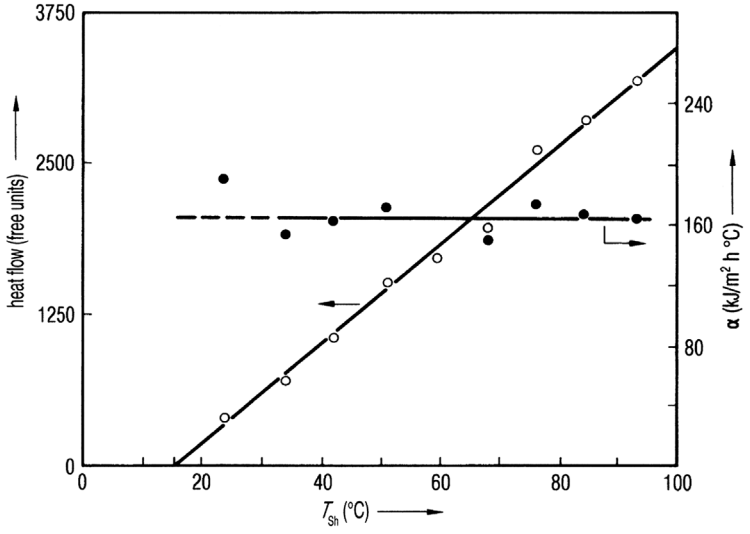

Figure 1.93 Heat transfer from a shelf with temperature T_{St} to the bottom of the product container with temperature T_{Bo} at pressure $p_{H_2O,ch} = 0.9$ mbar. (Adapted from Figure 4b in Ref. [5].)

If the shelf and the tray are as planar as technically possible, the plot marked $s = 0$ applies. At 0.2 mbar, a heat transfer coefficient of ~85 kJ/m^2 h °C can be achieved, rising by a factor of 2 at 1 mbar. In a well-designed freeze-drying plant with planar trays or vials, a heat transfer coefficient of 160 kJ/h m^2 °C at 0.9 mbar is possible (Figure 1.93), while at a pressure of 0.45 mbar, ~120 kJ/h m^2 °C (Table 1.14) is measured for the heat transfer coefficient K_{tot}. To sublime 1 kg of ice per hour and per m^2 with a coefficient of 120 kJ/h m^2 °C, the temperature difference between T_{ice} and T_{sh} (temperature of the shelf) must be an average of 23 °C.

Until now, only the heat transfer from the shelf to the tray or vial has been considered. The heat transfer to the sublimation front and the transport of the water vapor from the sublimation front into the chamber will now be included. Wolff *et al.* [102] described a model for a uniformly retreating ice front and experiments with milk and water to confirm the usefulness of the model. Three parameters were studied: the water diffusion in the dried layer, the external mass transfer, and the heat transfer from the shelf to the product. The last parameter was found to control the dehydration kinetics. Ybeme *et al.* [103] used a conductive paste on the shelves to reduce the heat transfer resistance between the shelf and the vials. The resistance toward mass transport was varied by using different restrictive capillaries. The conclusion of the experiments confirmed that the heat transfer to the vials limits the rate of sublimation. Chang and Fuscher [104] showed how and under which circumstances it was possible to use the T_{sh}, applied during secondary drying, already during the main drying. Recombinant human interleukin-1 receptor antagonist (rhIL-1ra) in various concentrations was studied in a solution of 2% (w/v) neutral glycine, 1% (w/v)

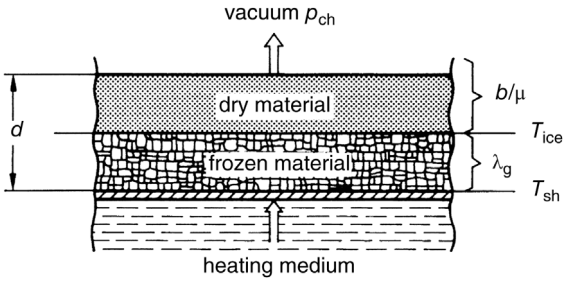

Figure 1.94 Scheme for the calculation of the drying time t_{MD} for the main drying. The product is frozen in plates. (see also Figure 6 from Ref. [105].)

sucrose, and 10 mM sodium citrate buffer at pH 6.5 (25 °C). At a 100 mg/mL rhIL-1ra concentration, no devitrification was seen to start at −37 °C and no recrystallization began at −27 °C as measured at lower concentrations (10–50 mg/mL). For this product, a temperature of −22 °C was considered low enough to avoid collapse. This temperature was controlled by pressure control as described in Table 1.15, its related text and Figures 2.115 and 2.116. The shortest drying time, keeping the temperature below −22 °C, was found to be at a shelf temperature of +40 °C, which was also used during SD. As the authors noted, this method cannot be applied to all formulations and is also dependent on the whole system, on the type of vial, heat transfer from the shelf to the sublimation front of the ice, water vapor transport, and so on. In Figure 2.116, an example is given in which the ice temperature range can be adjusted by pressure, valid for one product in one type of vial in one plant and with one shelf temperature.

The author has used a model and an equation developed by Steinbach [105] for many years and for many experiments in a wide field of applications. The model, shown in Figure 1.94, uses an infinitely expanded plate of the product with thickness d. Equation (1.12) describes the time of the main drying part of the freeze-drying cycle:

$$t_{md} = (\rho_g \xi_w LS \Delta m d)/T_{tot}[(1/K_{tot}) + (d/2\lambda_g) + (d/2LSb/\mu)] \qquad (1.12)$$

where

ρ_g = density of the frozen product (kg/m^2);
ξ_w = part of water (kg/kg);
LS = sublimation energy (2.805 kJ/kg);
T_{tot} = temperature difference ($T_{sh} - T_{ice}$);
K_{tot} = total heat transmission coefficient from the shelf to the sublimation front of the ice;
λ_g = thermal conductivity of the frozen product;
d = thickness of the layer (m);
Δm = content of frozen water = 0.9
b/μ = permeability (kg/m h mbar) for water vapor through the dried product.

In this equation the following simplifications are made:

- The layer is endless, energy is only transmitted from the shelf to one side of the layer.
- The vapor is only transported from the ice front through the porous dried layer.
- The frozen layer is not porous.
- The heat transport in the already dried layer is neglected.

The error resulting from the last assumption at $T_{tot} = 100\,°C$ is ~4% and at $T_{tot} = 50\,°C$ ~2% [105].

For the evaluation of the equation, four data are necessary in addition to those already known:

$$T_{tot} = T_{sh} - T_{ice}$$

K_{tot} heat transfer coefficient by conduction and by convection from the shelf to the sublimation front.
λ_g heat conductivity of the frozen product (ice), and
b/μ mass transport coefficient.

The equilibrium vapor pressure (p_s) can be measured by barometric temperature measurement (BTM) and be converted into temperature by the water vapor pressure diagram (see Section 1.2.3).

To develop an idea of how the various terms of Eq. (1.12) influence the drying time, some experimental date are used, described in this section.

m_{ice}	= mass of the frozen water	1.243 kg
F	= used surface area of the shelves	0.2193 m^2
d	= thickness of the product layer	7×10^{-3} m
T_{sh}	= temperature of the shelf during MD, maximum	+29 °C
T_{ice}	= temperature of the ice at the sublimation front	−22 °C
T_{tot}	= $T_{sh} - T_{ice}$, average temperature difference during main drying	43.88 °C
$p_{H2O,ch}$	= partial vapor pressure in the chamber during MD	0.245 mbar
p_s	= equilibrium vapor pressure at T_{ice}	0.85 mbar
Δp	= $p_s - p_{H20,ch}$	0.605 mbar
t_{MD}	= time of MD (frozen water is sublimed) (see Figure 1.116)	2.5 h
LS	= sublimation energy of ice	2.805 kJ/kg
ξ_w	= part of water in the initial product	0.931
ρ	= density of the frozen product, assumed as	900 kg/m^2
Δm	= part of freezable water, assumed as	0.9
λ_g	= heat conductivity in the frozen product	6.28 kJ/m h °C

With these data,

$$K_{tot} = (m_{ice} LS)/(t_{MD} F) \times 1/(T_{tot}) = 144.9\ \text{kJ/m}^2\,\text{h}\,°\text{C} \quad (1.12a)$$

$$b/\mu = (m_{ice}/(t_{MD} F)(d/2/\Delta p) = 1.3 \times 10^{-2}\ \text{kg/h m mbar} \quad (1.12b)$$

Using Eq. (1.12), t_{MD} is calculated::

$$\begin{aligned} t_{MD} &= \rho(\xi_w \Delta m L S d)/T_{tot}[(1/K_{tot}) + (d/2\lambda_g) + (d/2LSb/\mu)] \\ &\quad \text{term A} \quad \text{term B} \quad \text{term C} \quad \text{term D} \\ &\quad 374.5 \quad 6.9\times10^{-3} \quad 0.56\times10^{-3} \quad 0.096\times10^{-3} \\ t_{HT} &= 3744.5(6.9\times10^{-3} + 0.56\times10^{-3} + 0.096\times10^{-3}) \\ t_{HT} &= 2.8\ \text{h(calculated)} \end{aligned} \tag{1.12c}$$

Equation (1.12) describes the main drying reasonably well if some experimental data are used.

The influence of different parameters on the MD is now discussed.

Term A: A variation of d changes this term proportionally; the T_{tot} influence is the inverse ratio. *Term B:* This is approximately 12 times larger than term C, and 70 times larger than term D. In both terms, d enters a second time, but as the absolute numbers are much smaller than term A, the influence of d in these terms is reduced.

If term A is constant, term B, the influence of the heat transfer term on t_{MD}, is in the example 91%. Term C, the influence of the heat conductivity, is 10 orders of magnitude smaller than term B. The heat conductivity depends on the characteristics of the product. In Ref. [5], an average value of 6.28 kJ/m h °C is used at −30 °C; in Ref. [3], a value of 5.9 kJ/m h °C is reported. However, even if λ_g varies by ±50%, term C would vary approximately between 0.37×10^{-3} and 1.1×10^{-3} and the influence on drying time is hardly noticeable (±5%).

Term D, also linear with d, shows the influence of the water vapor transport from the sublimation surface through the dried product into the vial or tray on t_{MD}. b/μ (kg/m h mbar) has often been measured: Steinbach [106] measured 1.3×10^{-2}, Gehrke and Deckwer [107] found for different groups of bacteria an order of magnitude of 4×10^{-2}, Sharon and Berk [6] demonstrated how b/μ decreases for tomato pulp from 3×10^{-2} to 0.8×10^{-2} when the solid concentration rose by a factor of 4, while Oetjen and Eilenberg [5] used 1.3×10^{-2} as an average value. Kasraian and DeLuca [108] measured the resistance of the vapor transport through the dried cake of a 5% (w/w) sucrose solution with and without 3–5% *tert*-butyl alcohol (*t*BA) and obtained the following results: In the absence of *t*BA, and with a skin on the surface, $b/\mu = 0.13\times10^{-2}$ kg/m h mbar. After the skin had cracked, $b/\mu = 0.77\times10^{-2}$ and with BTA, b/μ is in the range of 15.4×10^{-2}–2.5×10^{-2} kg/m h mbar. By using the two extreme data for b/μ 0.13×10^{-2} and 15.4×10^{-2} kg/m h mbar, t_{MD} rises to ~2.8 h or remains at ~2.5 h. The influence of b/μ becomes measurable in the example given only at very small values of b/μ resulting from a skin on the surface. With the normal variation of b/μ, its influence remains in the region of a few percent.

As long as the sublimation energy is not to be transported through the already dried layer of product (see Figure 1.94), the heat transfer (term B) is the decisive factor. For a layer thickness of 25 mm (for freeze-drying a large thickness), term $A = 1.205\times10^{3}$, term B remains (heat transfer is not modified) at 6.9×10^{-3}, term $C = 1.99\times10^{-3}$, and term $D = 0.34\times10^{-3}$. t_{MD} then becomes 11.1 h. The drying

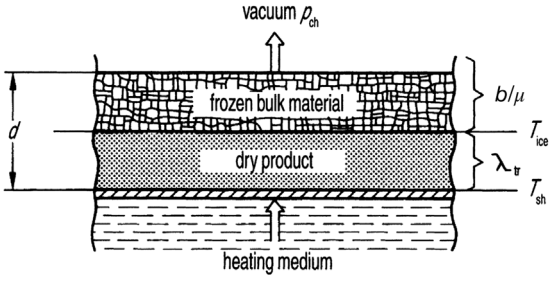

Figure 1.95 Scheme for the calculation of the drying time t_{MD} for the main drying of granulated product. (See also Figure 4 from Ref. [105].)

time is not extended by a factor of 25/7 = 3.6, but by a factor of 4.4, owing to the increase mainly in term C and slightly in term D.

If the material is granulated, for example, frozen and granulated coffee extract, having a solid content perhaps of 40% and a density of 0.6 g/cm^3 (Figure 1.95), Eq. (1.12) is still applicable, but the product data are different. The heat transfer through the dried product is $\lambda_{tr} = 8.37 \times 10^{-2}$ kJ/m h °C. To make the results more comparable, $d = 0.7$ cm and T_{tot} have been retained from the earlier example, even though T_{tot} were normally higher, for example, 100 °C:

$$t_{MD} = (\rho \xi_w LSd)/T_{tot}(1/K_{tot} + d/2\lambda_{tr} + d/2LSb/\mu)$$

$$t_{MD} = (0.6\times10^3\times0.6\times 2805\times7\times10^{-3}\ )/51\times(6.9\times10^{-3}+41.8\times10^{-3}+0.096\times10^{-3})$$

term A	term B	term C	term D
138.6	6.9×10^{-3}	41.8×10^{-3}	0.096×10^{-3}

$$t_{MD} \approx 6.8\ \text{h} \qquad (1.13)$$

In this example of the granulate, the main drying time (term A is assumed constant) depends largely on term C, while the vapor transport has virtually no influence.

λ_{tr} is given in Ref. [5] as 8.4×10^{-2}–16.8×10^{-2} kJ/m h °C, while Magnussen [7] uses for freeze-dried beef at 0.4 mbar a value of 15.5×10^{-2} and at 1.1 mbar a value of 17.2×10^{-2}. Sharon and Berk [6] found for concentrated tomato pulp with 28% solids $\lambda_{tr} = 28.5\times10^{-2}$ kJ/m h °C at 0.5 mbar and 31.8×10^{-2} at 1 mbar. If the concentration of solids is only 6%, the values were 12.6×10^{-2} and 15.9×10^{-2} kJ/m h °C, respectively. Steinbach used 16.7×10^{-2} and Gunn *et al.* [8] found 5.9 and 9.2×10^{-2} kJ/m h °C for turkey meat at 0.5 and 1 mbar, respectively.

With the two extreme values 5.9×10^{-2} and 31.8×10^{-2} kJ/m h °C, term C becomes 59.3×10^{-3} or 11×10^{-3} and $t_{MD\ (5.9)} \approx 9.1$ h and $t_{MD(31.8)} \approx 2.5$ h. The heat conductivity in the product becomes the decisive value. It is a function of the chamber pressure, but changes in the interesting pressure range 0.5–1 mbar by only 15%. However, it varies with the solid content by a factor of 2 and is dependent on the structure. The λ_{tr} of turkey meat parallel to the fiber structure is three times larger than given above.

In Figures 1.96–1.98, three runs of freeze-drying in two different plants are shown. Figure 1.99 gives the scheme of the plant for the run in Figure 1.96 and Figure 1.100 gives the scheme of the runs plotted in Figures 1.97 and 1.98.

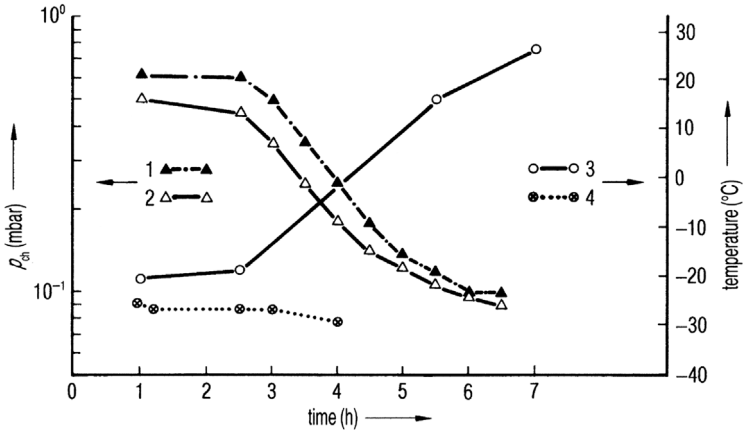

Figure 1.96 Course of a freeze-drying process in a plant as shown in Figure 1.99. Pressure control during MD not activated. 1.0 kg of product in four aluminum trays with machined bottom, T_{St} after evacuation controlled at +29 °C, $d = 0.6$ cm. 1, p_{ch} heat conductivity gauge (TM); 2, p_{ch} capacitive gauge (CA); 3, T_{Pr} resistance thermometer (RTD); 4, T_{ice} by barometric temperature measurement (BTM); end of MD: 3.5 h.

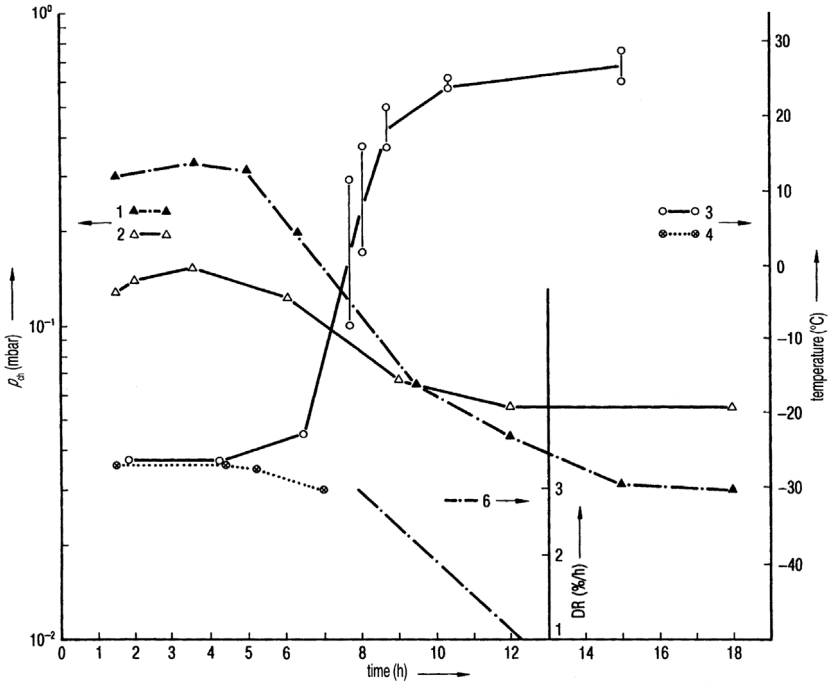

Figure 1.97 Course of a freeze-drying process in a plant as shown in Figure 1.100. Pressure control not activated. 2.4 kg of product in three welded stainless steel trays with flattened bottom. T_{sh} after evacuation controlled at +29 °C, $d = 0.6$ cm. 1–4, as in Figure 1.96; 6, desorption rate (DR), desorbable water in % of solids (see Section 1.2.2); end of MD: 5 h.

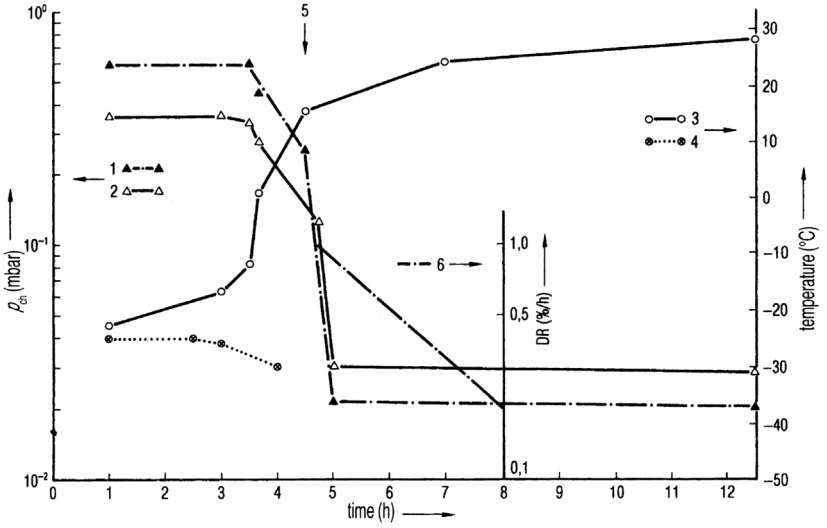

Figure 1.98 Course of a freeze-drying process in a plant as shown in Figure 1.100. Pressure control during MD 0.36 mbar (CA). 0.678 kg of product in 404 vials. T_{sh} controlled up to +29 °C in such a way that $p_{ch} = 0.36$ mbar was not exceeded during MD. $d = 0.64$ cm. 1–4, as in Figure 1.96; 5, end of pressure control; 6, DR (see Section 1.2.2); end of MD: 3.0 h.

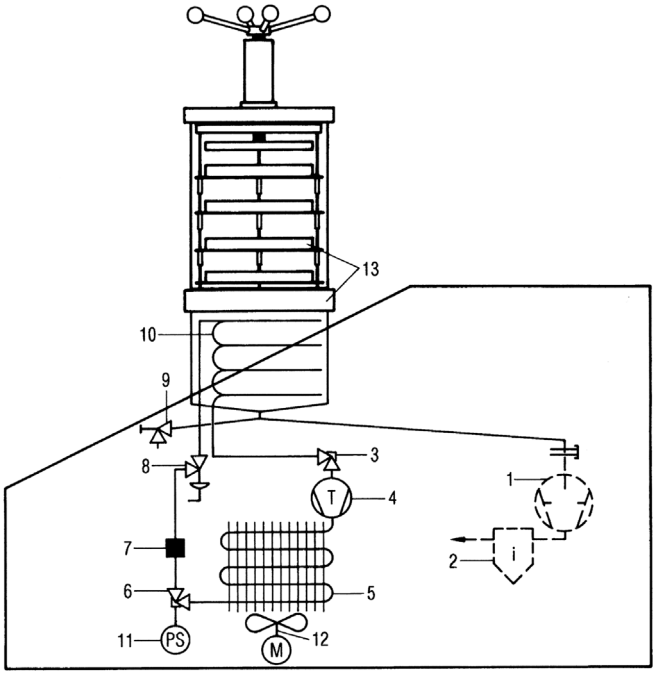

Figure 1.99 Scheme of the freeze-drying plant in which the tests shown in Figure 1.96 were carried out. 1, vacuum pump; 2, exhaust filter; 3, valve; 4, refrigeration machine; 5, liquefier; 6, valve; 7, filter; 8, expansion valve; 9, drain valve; 10, ice condenser; 11, pressure switch; 12, ventilator; 13, drying chamber with heated shelves. (Lyovac® GT 2, Steris GmbH, Hürth, Germany.)

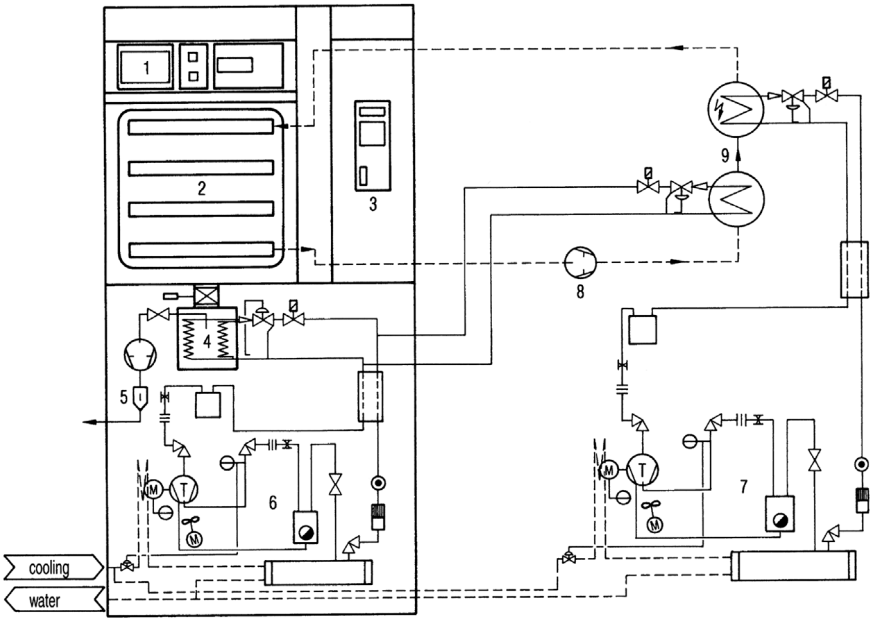

Figure 1.100 Scheme of the freeze-drying plant in which the runs in Figures 1.97 and 1.98 were carried out. 1, process documentation; 2, drying chamber with shelves; 3, operation control; 4, ice condenser; 5, vacuum pump with exhaust filter; 6, refrigeration machine for the ice condenser; 7, refrigeration machine for the shelves; 8, circulation pump for the brine; 9, heat exchanger (Lyovac® GT 6, Steris GmbH, Hürth, Germany.)

Table 1.14 summarizes the plant, the experimental data, and the relevant results. From these data, the values to calculate t_{MD} in Eq. (1.12) can be deduced when they are unknown.

Data for the three test runs:

ρ	density	0.9×10^3 kg/m^3
ζ_w	part of water	0.931 kg/kg
Δm	part of frozen water	0.9 kg/kg
LS	sublimation energy	2805 kJ/kg
λ_g	heat conductivity in the frozen product	6.3 kJ/m h °C

Data for test run in Figure 1.96:

d	thickness	6×10^{-3} m
T_{tot}		38.6 °C
t_{MD}	time of main drying	3.5 h

Data for test run in Figure 1.97:

d	7×10^{-3} m
T_{tot}	56 °C
t_{MD}	5.0 h

Data for test run Figure 1.98:

d 7×10^{-3} m
T_{tot} 51 °C
t_{MD} 3.0 h

With the help of these data, K_{tot} and b/μ can be calculated, if the water pressure at the sublimation front (p_s) and the partial vapor pressure in the chamber, measured by a hygrometer, are taken from the respective curves.

The results are summarized in Table 1.14: The K_{tot} values show the dependence on pressure (see results in Table 1.15), rising from ~62.4 kJ/m h °C at 0.15 mbar to ~119.3 kJ/m h °C at 0.45 mbar. The accuracy of the measurements to determine K_{tot} can be estimated in the two runs 1.62 and 1.62/W (Table 1.15) as ~±5%. Jennings [109, p. 612] claims that means of increasing K_{tot} to vials by a factor of 5–10 have been obtained. Nowhere in the literature studied were such data found. In Section 2.5.3, a continuous freeze-drying plant for granulated food

Table 1.14 Summary of the conditions during test runs and their results derived from Figures 1.96–1.98; $P_{H_2O,ch}$ was measured with a hygrometer during MD.

Parameter	Test run, Figure 1.96	Test run, Figure 1.97	Test run, Figure 1.98
Shelf area used (m^2)	0.166	0.343	0.172
Heating of shelf	Electrical resistance	Circulated brine	Circulated brine
T_{co} (°C)	Down to −45	Down to −53	Down to −53
Product	Skimmed milk, 9.67% solids		
Freezing method	Freezer down to −30 °C	Precooled shelves	−45 °C
T_{ice} (°C)	−22.3	−27	−21
p_s of T_{ice} (mbar)	0.83	0.51	0.94
Average p_{ch} during MD (mbar)	0.45	0.15	0.36
K_{ges} (kJ/m^2 h °C)	119.3	65.7	90.4
b/m (kg/h m^2 mbar)	0.010	0.011	0.011
t_{MD} taken from run, approx. (h)[a)]	3.5	5.0	3.0
t_{MD} calculated Eq. (1.14) (h)	3.0	4.3	3.4
Pressure control (mbar)	No	No	0.36

a) MD assumed terminated if T_{ice} is approximately 1–1.5 °C smaller than the average of all T_{ice} measured during MD. The amount of sublimed ice during MD is assumed to be 90% of the freezable water.

Table 1.15 Comparison of four test runs in the same plant (type as in Figure 1.99) with the same product and the same product thickness as in the run of Figure 1.96 in Table 1.14.

Parameter	Test run, Figure 1.96	Test run, Figure 1.96/W	Test run, Figure 1.96/ 0.36 mbar	Test run, Figure 1.69/ 0.20 mbar
T_{ice} (°C)	−22.3	−22.5	−26.8	−30.5
p_s (mbar)	0.83	0.81	0.53	0.36
p_{ch} (mbar)	0.45	0.50	0.36	0.21
p_{H2O} (mbar)	0.31	0.31	0.23	0.19
K_{tot} (kJ/m^2 h °C)	119.3	114.5	79.1	62.4
b/μ (kg/m^2 h mbar)	0.01	0.009	0.011	0.014
$t_{MD,}$ taken from run (h)	3.5	3.5	4.5	6.0
t_{MD} calculated (Eq (1.14)	3.0	3.1	4.4	5.8
$T_{Sh} - T_{ice}$ (°C)	38.6	39.1	38.1	36.3

Test run Figure 1.96/W: best possible repeat of test run Figure 1.96, both runs not pressure controlled. Test run Figure 1.96/0.36 mbar and 1.62/0.21 mbar differ from 1.62 and 1.62/W by pressure control 0.36 and 0.21 mbar, respectively. The results show:

1) The deviation between the two repeated runs is smaller than 5%, (the higher p_{ch} could indicate a larger content of permanent gases in the product).
2) T_{ice} can be controlled by pressure in a temperature range of 8–10 °C (with otherwise equal conditions).
3) K_{ges} decreases with decreasing p_{ch} (from 0.5 to 0.21 mbar) by approximately 50%.
4) t_{MD} decreases with increasing pressure to approximately 50%, since the decisive data in Eq. (14) is K_{tot}. T_{sh}–T_{ice} changes only slightly, the control avoids exceeding the controlled pressure. T_{sh} increased more slowly, which means that MD T_{sh}–T_{ice} is smaller than without pressure control.
5) Pressure control does not always shorten the MD, as can be read frequently. The pressure control adjusts a desired T_{ice}. If T_{ice} without pressure control is larger than with pressure control (as in this example), MD would only decrease when the run would have been operated at 0.7 mbar (if the product tolerates the increased T_{ice}.

is described (Ref. [17] of Chapter 2) in which the sublimation rate (kg/m^2 h) is 5–10 times higher than in standard plants. In the described plants, the granulated product is in direct contact with the heated shelf, which vibrates at 50 Hz for product transportation. By this vibration, the granulates are constantly and thoroughly mixed; each particle comes in contact with the heated shelf between 5 and 10 times per second (see Figure 2.108).

The permeability (kg/m h mbar) for water vapor through the dried product fluctuates by a larger margin, which can be estimated from all six test runs (Tables 1.14 and 1.15) as $1.1 \times 10^{-2} \pm 25\%$. However, the measurement of these data is of interest to judge whether the b/μ will influence the process time, as can be the case with products that have a high solid content and are dried with a large thickness. Small b/μ can also result from a skin on the surface of the

product (see Ref. [108]). Overcashier *et al.* [110] investigated the relationship between resistance to water vapor flow through the dried layer and the microstructure of the dried cake. Recombinant humanized antibody HER2 (rhuMAb HER2) formulated in trehalose and protein-free formulations containing trehalose and sucrose were studied. The mass transfer resistance decreased with increase in temperature for all materials, and the resistance also decreased from rhuMAb Her2 to trehalose to sucrose. The dry cake was porous with a denser layer at the top. The formulated trehalose and sucrose possessed 2–20 μm holes in a plate-like structure. Material dried at higher temperatures or with lower T_c showed more holes and a lower resistance to water vapor flow. The authors concluded that a lower resistance to water vapor flow may be due to small-scale product collapse.

Schellenz *et al.* [111] confirmed that the assumption of an infinite plate in Eq. (1.12) is a reasonable approximation, even for drying of products in vials. They show by the measurement of temperature profiles and by X-ray photographs during drying of a 5% mannitol solution, 23 mm filling height that the sublimation front retreats mostly from the top parallel to the bottom. The heat transfer from glass vials deforms the flat surface only to some extent close to the wall.

Drummond and Day [112] studied the influence of different vials, molded glass, glass tubing, and molded resin on the freeze-drying of 5% solutions of maltose and mannitol with arginine added. The freeze-drying performances, the inter- and intravial uniformity, and the morphology were compared. The lyophilization performance was best for glass tubing vials, with molded vials only marginally lower but better than resin vials. Intravial uniformity was found to be best for the resin vials. However, during drying this depends on the cycle parameters used. Intervial uniformity differences were measured both by the time at which nucleation of ice occurred and by temperatures during the drying process, but the differences for the three types of vial were in the same range. The morphology of mannitol in resin vials was found to be similar to the morphology in both types of glass vials. The authors concluded that the temperature distribution in a vial indicates a greater degree of uniformity in the cake, the temperatures from vial to vial are more consistent with resin vials, and the morphology in resin, molded, and tubing vials was not significantly different.

Pikal [113] compared the heat transfer mechanisms for three types of vials at a pressure of 0.13 mbar (T_{sh}, T_{ice} not specified):

Gas conduction	50–60% of total heat transfer
Radiation	20–30% of total heat transfer
Contact conduction	10–30% of total heat transfer

He gave for seven types of vials the part for the contact heat transfer coefficient between 0.2×10^{-4} and 1.7×10^{-4} cal/s cm^2 $K = 3$–25.7 kJ/h m^2 °C. At an average of 20%, K_{tot} can vary between 15 and ~130 kJ/h m^2 °C.

In Table 1.14, $K_{tot} = 65.7$ kJ/h m^2 °C was measured at 0.15 mbar and in Table 1.15, $K_{tot} = 62.4$ kJ/h m^2 °C was found at 0.21 mbar. In Eq. (1.12a), 144.9 kJ/h m^2 °C at ~0.3 mbar is calculated.

Table 1.16 Freezing and subcooling.

	5% mannitol (6R design)		10% sucrose (10 R design)	
	Freezing rate (+10 °C/ – 30 °C) (°C/min)	Subcooling (°C)	Freezing rate (+10 °C/ – 30 °C) (°C/min)	Subcooling (°C)
s-vial	0.92	−10	1.06	−7
qc-vial	1.07	−7	1.11	−8
p-vial	0.79	−10	0.67	−12

s-vial, tubing glass vial; qc-vial, quartz-coated tubing glass vial; p-vial, resin vials, 6R-design.
Source: Data from Ref. [114].

Summarizing, the selection of vials could influence the main drying time theoretically by a factor of 10 (see Eq. (1.12)), but the difference can easily be a factor of 2, and sometimes a factor of 4.

Willemer *et al.* [114] studied the influence of tubing glass, coated tubing glass, and resin as vial materials on the freezing and freeze-drying of 1 and 5% mannitol and 10% sucrose solution. During freezing, the different forces between the walls and liquid influence the structure of the freezing product and its subcooling, as shown in Table 1.16. The freezing speed in the coated vials was up to 16% greater than in standard vials, but in the resin vials the freezing speed was 14% lower. As shown in Table 1.17, the main drying is ∼20% longer in resin vials than in glass vials. The weight loss in the quartz-coated vials during sublimation is faster than in the other vials; also, the standard deviation of weight loss in the quartz-coated vials is by far the lowest, indicating high intercontainer homogeneity of the product. The secondary drying time is almost the same for glass and polymer vials and partially reduces the difference in the total drying time.

The discussions so far about main drying have assumed that trays or vials are exposed to uniform temperatures on the shelves.

Table 1.17 Weight loss during main drying of a 5% mannitol solution in R6 vials.

Drying time (h)	3.5	4.5	6.0	6.5	3.5	4.5	6.0	6.5
	Weight loss (% of initial weight)				Standard deviation of 12 vials			
s-vial	91.85	94.40	94.81		2.89	0.8	0.7	
qc-vial	90.24	95.05	94.47		1.59	0.35	0.63	
p-vial	71.87	87.68		95.22	2.53	3.0		0.41

Source: Data from Ref. [114].

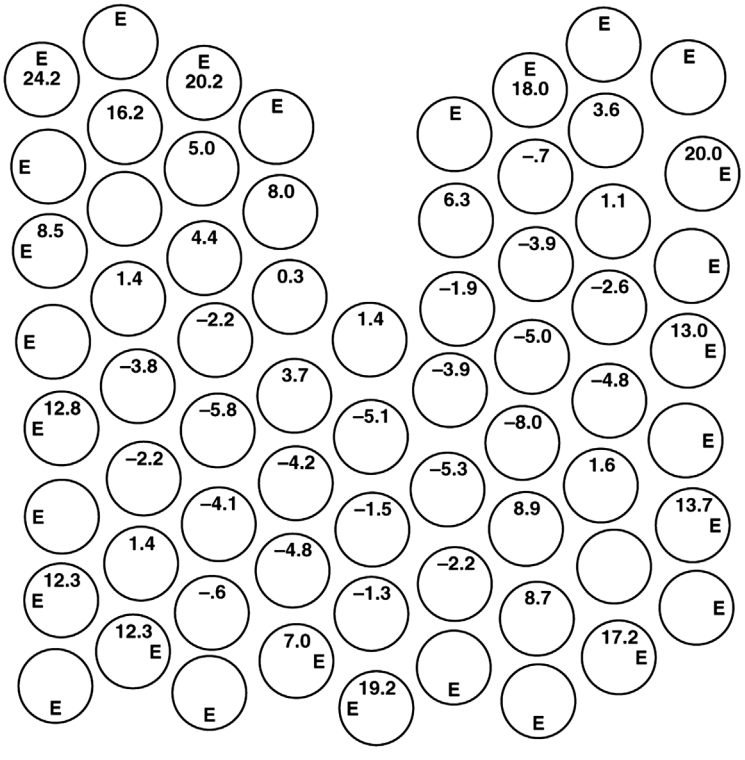

Figure 1.101 Vials on the shelf of a freeze-drying plant. Vials on the edge marked E, figures indicate the % deviation of the sublimed water in the vial from the average amount of water sublimed from all nonedge vials. The average deviation of all E vials is 15% and the average deviation of all non-E vials is 0.11%. (See also Figure 35 from Ref. [113].)

Pikal *et al.* [115] freeze-dried pure water in vials at 0.25 mbar and $T_{sh} = 5\,°C$ until ~25% of the water had sublimed. Then the vials were weighed and the loss of water was determined for each vial. The results are shown in Figure 1.101. All edge vials are marked E. The figure in the circle is the percentage deviation from the average sublimation rate for all nonedge (nE) vials. The average deviation for all nE vials is 0.83%, SD 5.13%. The average deviation of all E vials is 15.0%, SA 5.3%. The E vials receive additional energy from the walls (~15 °C) and ~15% more ice sublimes in the same time.

Kobayashi [116] has shown that this condition exists in some freeze-drying plants, as the walls and doors of chambers can have temperatures different from those of the shelves. During freezing, this could lead to slower freezing at the edges of the shelves.

During main drying, the influence of the wall temperatures can be small, as long as the shelves are only heated to +15 or +25 °C. If the shelf temperature during main drying is, for example, −10 °C, the vials at the edge will receive more energy than planned, which could lead to collapse or melting of the product in these vials. In contrast, during secondary drying, the vials at the edge will be warmed up more slowly than those in the center if the shelf temperature is, for example, +35 °C.

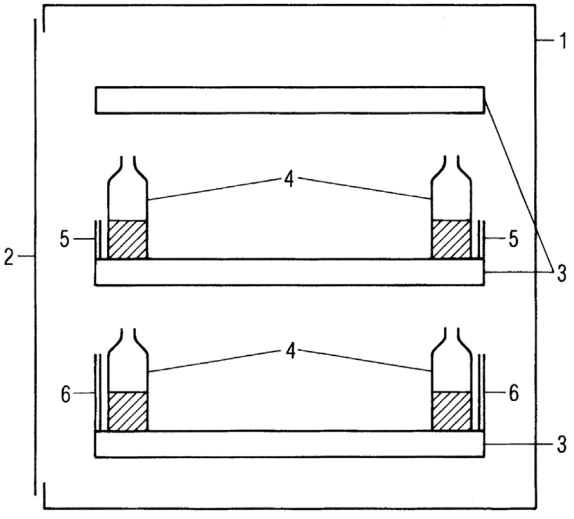

Figure 1.102 Scheme related to the plots in Figure 1.103. 1, chamber wall; 2, chamber door; 3, shelves; 4, vials with product; 5, radiation shield, height ≥ filling level of the vials; 6, radiation shield, height ≈ cylinder length of the vials.

Kobayashi proposed that all walls and the door are operated at the same temperatures as the shelves, although this is not always necessary if the shelves are shielded from the walls and the door, as shown schematically in Figure 1.102. The curves in Figure 1.103 indicate that this shielding is sufficient in some cases: During freezing, the vials at the edges of the shelves are exposed practically to the shelf temperature, whereas during secondary drying, the influences of the walls and the door are reduced.

Wall and door influences exist mainly by radiation or by the small heat conductivity of the gas. It can be seen from Figure 1.103 that the shielding in the temperature range between −40 and 0 °C is effective. However, the shielding becomes more important with an increasing temperature difference between the shelves and surrounding and it is especially necessary if the vials contain only a small amount of product.

In Figure 1.104 the influence of shielding the product in vials from the walls and doors is summarized. For each run (a), (b) and (c), six groups of vials (168 vials each) filled with 2.8 cm^3 (9 mm thickness) of human albumin product, containing 6% solids, were used. Rows 4, 5, and 6 were close to the door and 1, 2, and 3 close to the back wall; the condenser connection was at the bottom of the chamber. The RM were determined by the Karl Fischer method. Figure 1.105 shows the program of the tests.

In run (a) no shield was used, in run (b) a shield as sketched in Figure 1.102 was used, and in run (c) a temperature-controlled shielding as shown in Figure 2.66. The results are summarized in Table 1.18. The results should be considered as an example; they are influenced by the following factors: the product temperature at the end of freezing, T_{ice} during MD, the amount of product per vial, the cake thickness, and the geometric design of the chamber and the room temperature. As

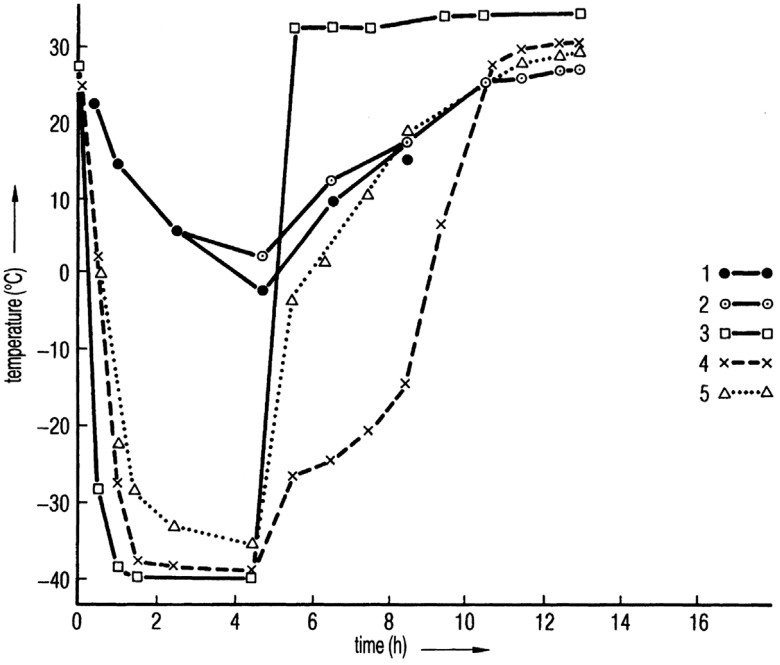

Figure 1.103 Temperature distribution during freezing (4.5 h) and freeze-drying (8 h). Each shelf carries a frame for radiation shielding. The design can be different depending on the kind of vials and the loading and unloading system. 1, internal temperature of wall of the chamber; 2, internal temperature of the door; 3, T_{sh}; 4, T_{pr}; 5, temperature on the inner side of the radiation shield.

can be seen from Figures 1.103 and 1.105, the main influence is a low shelf temperature during freezing and MD. If the amount of product is small, the influence of wall temperatures is relatively large (radiation and gas conductivity depend on the wall and vial surfaces and on the temperatures; if the amount of product is small, their relative importance increases).

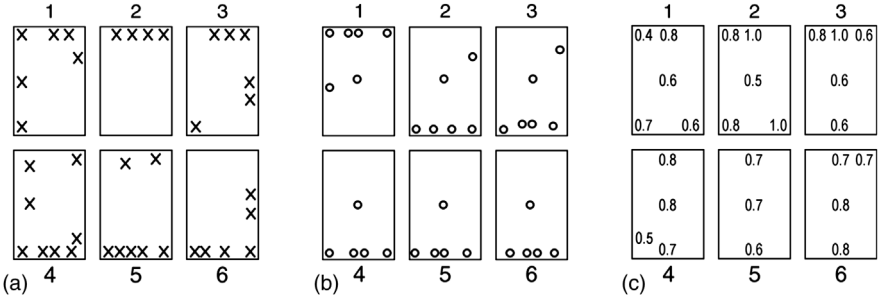

Figure 1.104 Residual moisture content in three identical runs with different shielding between vials and walls and door(s). In each run, six groups of vials were formed (168 vials each). Rows 4–6 were close to the door and rows 1–3 to the back wall. (a) No shielding. (b) Shielding as shown in Figure 1.102. (c) Shielding as described in Section 2.3.2, Figures 2.66–2.68.

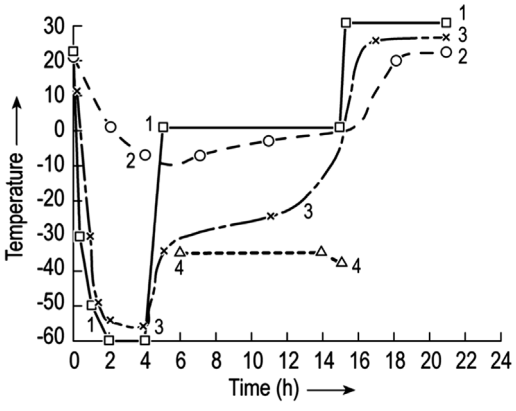

Figure 1.105 Temperature as a function of time in a pilot plant of ~170 L chamber volume, loaded with 1008 vials, containing ~2.8 kg of product with 169 g of solids, $d = 9$ mm. 1, T_{sh}; 2, wall temperature; 3, T_{pr}; 4, T_{ice}.

In Table 1.14 two different plants and three different types of container were used; in Table 1.15 it was always the same plant. During main drying, different pressures were applied.

The control of a desired constant total pressure is called pressure control (p_c) and can be operated by two methods:

- A dry inert gas, for example, nitrogen, is fed into the chamber by a needle-valve in such a way that the desired total pressure is built up.
- The valve between the condenser and vacuum pump set (Figures 1.99 and 1.100) is closed until the desired total pressure is built up. If the controlled pressure is exceeded, the valve opens.

Table 1.18 Residual moisture content distribution in three runs with and without shielding between walls and product.

	Run a	Run b	Run c
Shrunk product			
Row 1–3	10	0	0
Row 4–6	13	0	0
RM			
In shrunk product	7/21%	–	–
	av. 15%, SD 6.2%		
Product in center vials	0.9/1.1%	0.6%/1.0%	–
	av. 1%, SD 1%	av. 0.85, SD 0.15	
Product row 1–6	–	0.9%/4.5%	–
		av. 1.9%, SD 1.6%	
All vials	–	–	0.4%/1.0%
			av. 0.72%, SD 0.15%

Run a, no shielding. Run b, shielding as sketched in Figure 1.102. Run c, shielding as shown 2.3.2 Figure 2.58.

In the second case, the gas included in the product is released during sublimation of the ice and used for pressure control. In every liquid product, some gas is dissolved. Indeed, liquids [117] may contain gas contents from 5×10^{-5} up to 1×10^{-3} kg/kg, often very close to the upper value, although the actual content depends very much on the history of the product.

The test run in Figure 1.98 contained 1.535 kg of product having a water content of 1.39 kg and containing 0.7 g of air. The total pressure of 0.37 mbar, including 0.25 mbar water vapor pressure, was to be controlled. The air had to be pumped off at a partial pressure of air of 0.12 mbar; 0.7 g of air at 0 °C and 0.12 mbar represents a volume of ~7.3 m^3. During the main drying time of 3.0 h, 2.4 m^3/h must be removed. If the vacuum pump has an effective pumping speed for air of, for example, 4.8 m^3/h, the pump would operate on average for 50% of MD. If the dissolved amount of gas is 10-fold larger, this must to be considered in the layout of the vacuum pump.

The second method has two advantages:

- Only gas of the product is used and no additional inert gas supply is needed.
- At the end of MD, when less and less dissolved gas is freed, the chamber pressure drops automatically, as is necessary for secondary drying.

The advantage of pressure control is the improved heat transfer leading to shorter drying times or possibly lower shelf temperatures. On the other hand, which is equally important, the ice temperature can be accurately controlled by the controlled pressure: In Table 1.15, the ice temperature at the sublimation front is −26.8 °C at a pressure of 0.36 mbar and −30.5 °C at 0.21 mbar (see column 3 or 4). In the test run in Figure 1.98, 0.36 mbar results in $T_{ice} = -21$ °C, since K_{tot} is larger between vials and shelves at the same shelf temperature of +29 °C. Should the total pressure exceed the desired value, the shelf temperature must be reduced accordingly. Figure 1.106 illustrates how T_{ice} is reduced in 4 h from −26.8 to −28 °C. The shelf temperature should have been raised slightly or the controlled pressure of 0.36 mbar increased. The change in shelf temperature is usually much too slow for such small changes; however, the change in pressure is quick and can easily be performed in small steps. The method of pressure control can only be applied as long as the partial vapor pressure is large compared with the pressure of permanent gases. If the pressure of permanent gases is of the same magnitude as or larger than the vapor pressure, the water vapor transport is hindered and the ice temperature is no longer a well-defined function of the control pressure.

To summarize, main drying is controlled by only two variables:

- the controlled operation pressure p_c;
- the selected shelf temperature T_{sh}.

These two data result in a temperature of the ice at the sublimation front T_{ice} in a given plant and a given product.

The uniformity of the drying rate for all vials in a charge depends on

- the shielding of the vials at the border of each shelf from influences of the walls and door(s);
- the uniformity of freezing and thermal treatment (annealing) in all vials.

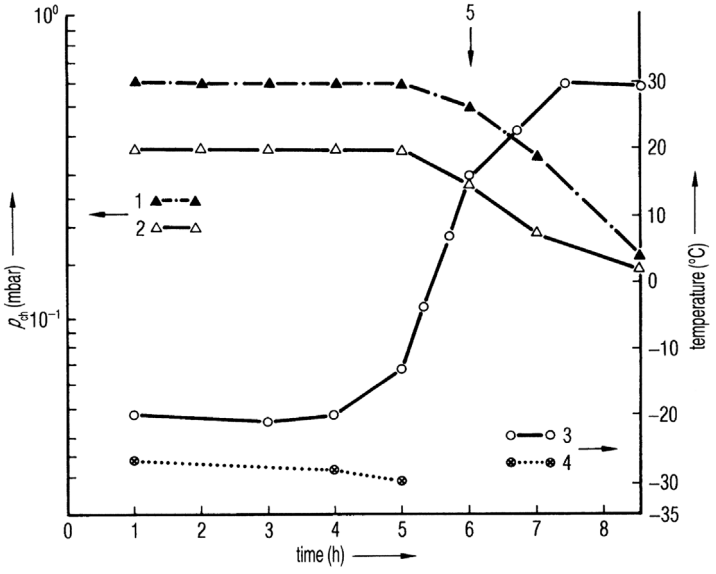

Figure 1.106 Course of a freeze-drying process during which T_{ice} was not kept constant at −26.8 °C. To avoid a decline in temperature, either T_{sh} could have been increased after 2 h (difficult to control as the inertia of the heating system is substantial) or p_c increased until T_{ice} is constant at −26.8 °C. 1, p_{ch} (TM); 2, p_{ch} (CA; 3, T_{pr} (RTD; 4, T_{ice} (BTM; 5, end of pressure control.

Two notes can be raised regarding the last point: Searles *et al.* [118] stress the influence of the ice nucleation temperature T_n on the primary drying rate and its uniformity. T_n (see Section 1.1.2) is stochastic, cannot be directly controlled, and depends on, among others, the particulate content, vial surface, and the time and temperature history of the product before freezing. The same authors [119] underline the importance of annealing up to T'_g to reduce the heterogeneity of sublimation rates. They found an increase in the drying rates of hydroxyethyl starch after annealing of up to 3.5-fold.

1.2.2 Secondary Drying (Desorption Drying)

During secondary drying (SD), the water will be removed that interacts with the solids such that the water cannot crystallize. The water can be bound to the surface of crystals in a crystallized product or can be included in amorphous product.

Fakes *et al.* [27] described the moisture sorption behavior of mannitol, anhydrolactase, sucrose, D-(+)-trehalose, dextran 40, and providone (PVP K24) before and after freeze-drying in a 10% solution. All products were frozen at 0.50 °C/min to −40 °C and freeze-dried at 0.13 mbar and $T_{sh} = -15$ °C for 28 h. SD lasted for 14 h at $T_{sh} = 25$ °C. Table 1.19 shows the moisture contents before and after freeze-drying. Figure 1.107 present the weight change in % of sucrose, trehalose, mannitol, and lactose in an atmosphere with increasing relative

Table 1.19 Moisture contents of bulking agents.

Bulking agent	Before lyophilization (% w/w)	After lyophilization (% w/w)
Mannitol	0.12	0.15
Lactose, anhydrous	0.86	1.63
Sucrose	0.15	2.51
Trehalose	9.2	1.17
Dextran 40	5.8	0.24
Povidone K24	8.6	0.37

Table 1 from Ref. [27].

humidity (RH) with time, before (top) and after (bottom) freeze-drying. In Figure 1.108, the same data are shown for providone and dextran. The results can be summarized with simplifications: Lyophilized mannitol is practically nonhygroscopic. Lactose gains ~10% up to 55% RH, followed by rapid desorption thereafter. DSC and X-ray diffraction (not shown) confirmed that the amorphous freeze-dried lactose was converted to the crystalline state at 55% RH and 25 °C. Sucrose behaves in a similar manner, but the uptake at RH 55% is ~4%, followed by desorption with increasing RH, being converted into the crystalline state, which is also possible by heat only. Lyophilized trehalose adsorbs an additional 10% up to 45% RH and is converted to the crystalline state at more than 50% RH. Dextran and providone absorbed up to 18 and 30% moisture, respectively, at 70% RH and remained amorphous. Under the experimental conditions of this study, all products were freeze-dried under the same freezing and drying conditions, and all moisture sorption measurements were at 25 °C and for a relatively short time. The authors considered this study as a useful guideline for the selection of optimal bulking agents.

In addition to substantial differences in the sorption behavior of products, the moisture distribution in each vial of one charge must be considered when the SD process is developed. Pikal and Shaw [120] studied this distribution in dextran 40, human serum albumin (HSA), bovin somatotropin (BST), and glycine. Thirty vials where filled with 10 or 20 mm cake thickness, loaded on shelves at 5 °C, cooled to −40 °C, and frozen in 30–45 min. T_c was determined for all products as >−12 °C. In Table 1.20, the water content of four products is shown in four different positions in the vials after 6 and 8 h of SD. With one exception, the water content in the core is twice as high as in the total vial, which is close to the content near the wall. Figure 1.109 shows the mean water content and the ratio of the content near the wall/mean content of a 1 cm BST cake. The error of the mean content decreases with time and the error of the ratio increases.

Pikal [121] described three possibilities for defining the change from main to secondary drying:

- an increase in product temperature;
- a decrease in the partial water vapor pressure;
- a pressure rise dp/dt (dt time) measurement.

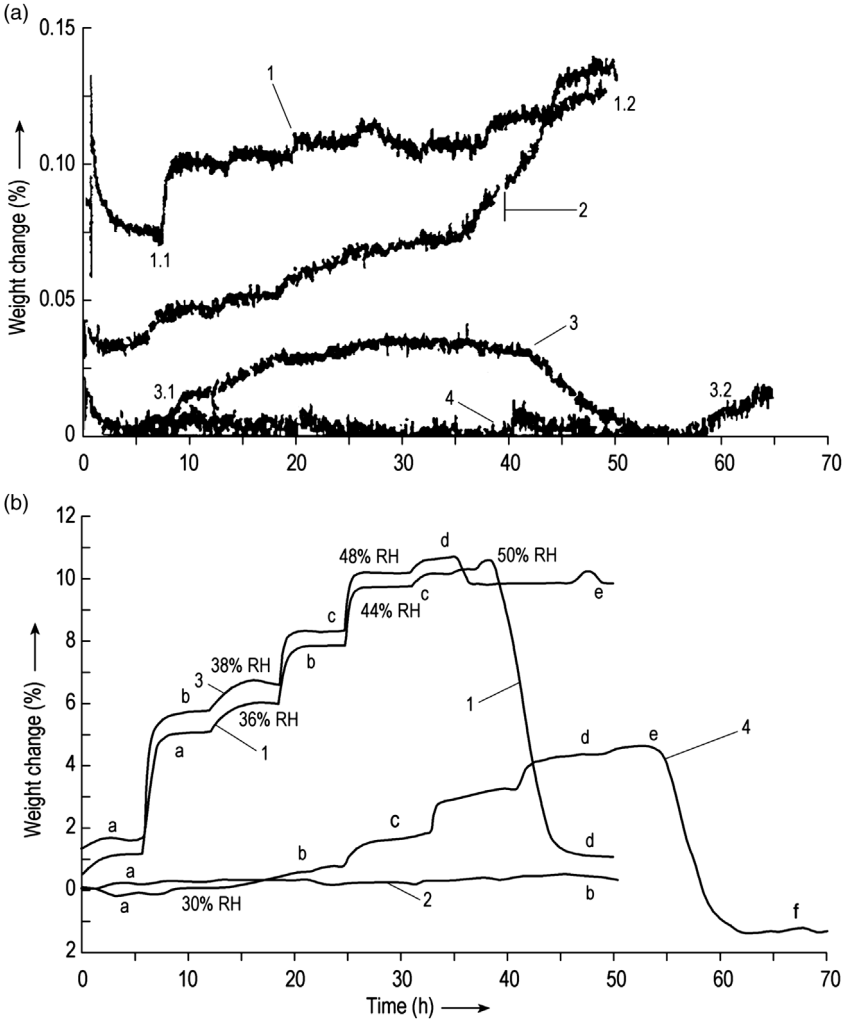

Figure 1.107 Moisture sorption profiles of anhydrous lactose (1), mannitol (2), trehalose (3), and sucrose (4). Before (a) and after (b) lyophilization (% weight change from the data in Table 1.18) at different relative humidity (RH) changes over 50–60 h. Before lyophilization: 1, lactose – 1.1 RH 10%, 1.2 RH 60%; 2, mannitol; 3, trehalose – 3.1 RH 10%, 3.2 RH 60%; 4, sucrose. After lyophilization: 1, lactose – 1a RH 30%, 1b RH 40%, 1c RH 50%, 1d RH 80%; 2, mannitol – 2a RH 10%, 2b RH 80%; 3, trehalose – 3a RH 10%, 3b RH 30%, 3c RH 40%, 3d RH 50%, 3e RH 80%; 4, sucrose – 4a RH 10%, 4b RH 30%, 4c RH 40%, 4d RH 50%, 4e RH 60%, 4f RH 80%. (see also Figure 1 from Ref. [27].)

As shown in Figures 1.96 and 1.97, the product temperature increases at the end of main drying; the measurements made by temperature sensors vary widely and are therefore a relatively uncertain indicator for the end of the main drying. The partial water vapor pressure changes during the transition from main drying to secondary drying over a period of several hours depend on the process

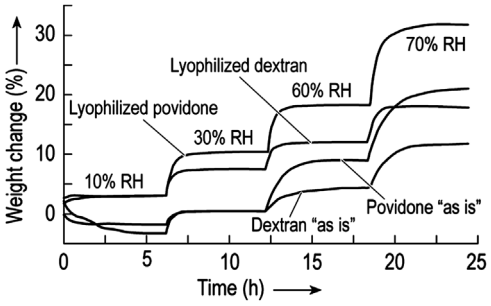

Figure 1.108 Moisture sorption profiles of dextran and povidone: % weight change from the data in Table 1.18. (Figure 2 from Ref. [27].)

Table 1.20 Water distribution given in % (w/w) (standard error) after 6 or 8 h of secondary drying in a 2 cm cake.

	Dextran	has	BST (6 h)	BST (8 h)
Whole vial	2.4 (0.2)	2.4 (0.8)	3.0 (1.0)	2.0 (0.4)
Position				
Core top	5.0 (0.3)	3.5 (0.3)	5.0 (0.2)	4.5 (0.3)
Core middle	5.0 (0.3)	4.5 (1.0)	5.2 (0.3)	4.2 (0.2)
Core bottom	4.9 (0.3)	3.8 (0.6)	15.0 (3.0)	4.5 (0.3)
Near vial wall	2.0 (0.1)	2.6 (0.6)	3.2 (1.0)	2.0 (0.4)

From Figure 4 in Ref. [120].

conditions (e.g., 2–3 h in Figures 1.96 and 1.97). In practice, one may have to wait several hours before the higher temperature for the secondary drying can be applied in order to avoid partial collapse. It is well known that the third possibility, pressure rise measurements for a given time, can be used to determine the changeover. The method can be applied more generally if the amount of water desorbed per unit time is measured and related to the solid content. This can be

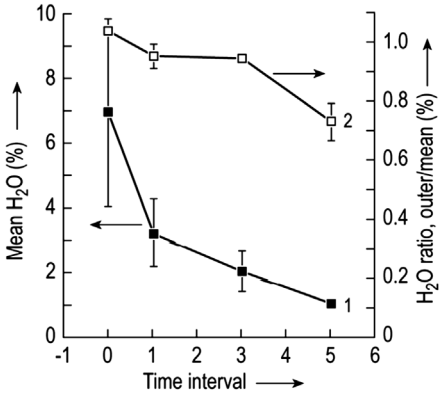

Figure 1.109 Mean water content (1) and ratio of water content (2) near the wall/mean water content in 1 cm cake of BST as a function of drying time. 0 h, start of SD. (Figure 5 from Ref. [120].)

defined as desorption rate (DR):

$$\mathrm{DR} = \frac{\text{amount of water desorbed} \times 100}{\text{time} \times \text{mass of solid}} (\%/\mathrm{h}) \tag{1.14}$$

The amount of water desorbed can be calculated by the pressure rise after the valve between the chamber and condenser has been closed, divided by the time of closure and the chamber volume (see Section 1.2.3, Eq. (1.16a)).

Calculation of the desorption rate:

$$\mathrm{DR} = 2.89 \times 100 \times \frac{V_{\mathrm{ch}}}{mf} \times \frac{\mathrm{d}p}{\mathrm{d}t} \tag{1.14a}$$

V_{ch} = chamber volume in liter (L)
m_{f} = mass of product solids (kg)
$d_{\mathrm{p}}/d_{\mathrm{t}}$ = pressure rise in time (mbar/s)
G = weight
V_{N} = nominal volume of water (= 22.4 L/mol). This corresponds to 22 400 L at 1 mbar and neglects the temperature change. From this, a linear dependence formulated as follows:
1 mol water (H_2O) has a volume of 22 400 L at a pressure of 1 mbar.
Converted to g (with $M_{H2O} = 18$ g/mol) results to
1 mol × 18 g/mol = 18 g

With these assumptions, the molar volume at 1 bar (1000 mbar) can be calculated as follows:

$$V1_{\text{mol } H_2O} = 22.400 \text{ L mbar}/1000 \text{ mbar} = 22.4 \text{ L/mol(nominal volume)}$$

What happens during the pressure rise?

There is an increase of H_2O molecules. To calculate the increase of mass, a comparison between state 1 and state 2 must be determined. For this purpose, the fixed chamber volume is taken as a reference and $p1 = 0.02$ mbar and $p2 = 0.1$ mbar selected. Thus, one can define the number of moles in the chamber as follows:

state 1: $V1_{\mathrm{H2O}}$ (L/mol) = 22 400 L mbar/0.02 mbar mol = 1 120 000 L/mol
state 2: $V2_{\mathrm{H2O}}$ (L/mol) = 22 400 L mbar/0.10 mbar mol = 224 000 L/mol.

$V1$ and $V2$ are the volumes that take up 1 mol under the given pressure.

With these values, the number of moles (with reference to the chamber volume) and thus the mass of water vapor (which is inside chamber) can be determined:

$$V_{\mathrm{N1}} = \frac{160\,l}{1,120,000 \text{ L/mol}} 1.429 \times 10^{-4} \text{ mol} \Rightarrow V_{\mathrm{N1}} \times 18 \text{ g/mol} = 0.0025722 \text{ g} = \mathbf{m1}$$

$$\mathrm{V_{N2}} = \frac{160\,l}{224,000 \text{ L/mol}} = 7.143 \times 10^{-4} \text{ mol} \Rightarrow V_{\mathrm{N2}} \times 18 \text{ g/mol} = 0.0128574 \text{ g} = \mathbf{m2}$$

The increase of mass is therefore $m2 - m1 = 0.102\,858$. This increase on mass refers to 30 s measuring time, converted to 1 h:

$$\Delta m = \frac{0.102852 \times 3600}{30} = 1.234224\,\mathrm{g/h}\left(\frac{\mathrm{g \times s}}{\mathrm{s \times h}}\right)$$

Thus, the desorption rate is

$$100 \times \frac{1.234224}{500} = 0.025\,\mathrm{g/h} \quad \left(\frac{\mathrm{g \times s}}{\mathrm{s \times h}}\right) = \left(\frac{\mathrm{g}}{\mathrm{h}}\right)$$

For confirmation: The same results calculated using the equation:

$$2.89 \times 100 \times \frac{160\,\mathrm{l}}{500\,\mathrm{g}} \times \frac{0.08\,\mathrm{mbar}}{30\,\mathrm{s}} = 0.025\,\mathrm{g/h}$$

Both calculation methods yield the same result. Herewith the constant 2.89×10^2 in the above equation is nothing but a constant that includes the following conversion:

- conversion to standard nominal volume;
- conversion to gram (mass);
- conversion to hour.

To understand the calculation steps here,

$$\left\{ \left[\frac{22400 \frac{1}{\mathrm{mol}}}{p_2 - p_1} \right]^{-1} \cdot V_k \right\} \cdot 18 \frac{\mathrm{g}}{\mathrm{mol}} \left(\frac{3600 \frac{s}{h}}{\mathrm{d}t} \right) \cdot \frac{100}{m_\mathrm{f}}$$

$$p_2 - p_1 = \mathrm{d}p$$

This makes

$$\frac{V_\mathrm{k}}{m_\mathrm{f}} \cdot \frac{\mathrm{d}p}{\mathrm{d}t} \cdot \left[\frac{3600 \frac{s}{h}}{22400 \frac{1}{\mathrm{mol}}} \times 100 \times 18 \frac{\mathrm{g}}{\mathrm{mol}} \right] = \underline{\underline{2.89 \times 10}}$$

This confirms the previous equation:

$$\mathrm{DR} = 2.89 \times 100 \times \frac{V_\mathrm{ch}}{m_\mathrm{f}} \times \frac{\mathrm{d}p}{\mathrm{d}t}$$

Figure 1.110 shows the three times repeated measurement of desorption rates, without pressure control, to demonstrate the reproducibility and two measurements where the main drying was pressure controlled at 0.36 and 0.21 mbar. The process conditions for these five measurements correspond to those in Table 1.15.

By barometric temperature measurements (BTM) and the measurements of the desorption rate (DR), the influence of varied drying conditions can be seen and analyzed. Figure 1.111 compares four different test runs:

1) *Test run (see Figure 1.97 and Table 1.14):* Without pressure control, in this installation – with the given shelf area, condenser temperature, the dimensions of the connection between chamber and condenser – a total pressure of

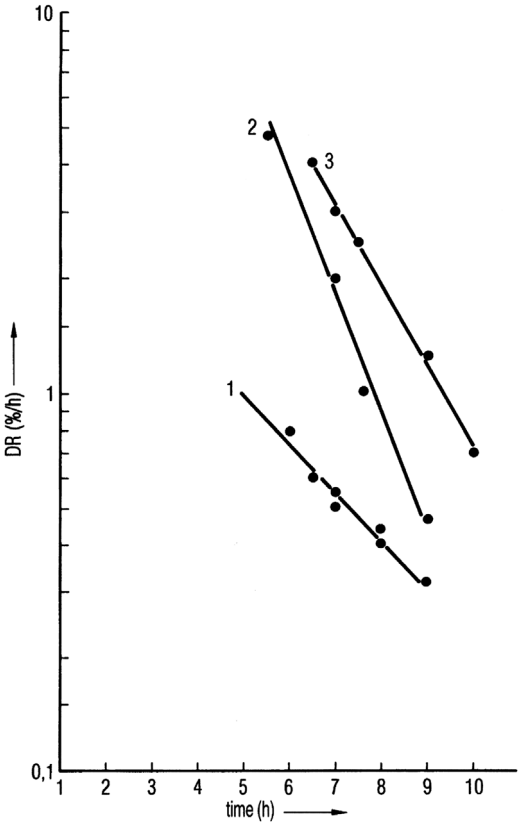

Figure 1.110 Desorption rate (DR) data as a function of drying time. 1, three repeated tests, pressure control not activated, process data as in the two left columns in Table 1.15; 2, process data as in Table 1.15, pressure control activated at 0.36 mbar; 3, process data as in Table 1.15, pressure control activated at 0.20 mbar.

0.15 mbar exists for ~5 h. The gas in the chamber is always pure water vapor. The ice temperature during this time is almost constant at ≃27 °C. The heat transfer coefficient at this pressure is small at ~65.7 kJ/m^2 h °C. The product temperature (resistance thermometer) increases only after these 5 h above the ice temperature. After 11.5 h, the desorption rate (DR) is ~0.8%/h. The total drying time, depending on the desired residual moisture content, is between 13 and 15 h.

2) *Test run:* Curves 2 in Figure 1.111 are taken from the test run, as shown in Figure 1.97, but with pressure control 0.36 mbar (total pressure measured with Capacitron). The ice temperature was −22 °C (constant) for 3 h and DR reached 0.5%/h after 10 h. Secondary drying could have been started much earlier, thus shortening the drying process.
3) *Test run:* The results of this run are only shown in Figure 1.111 in curves 3. In this run the shelf with the tray was inclined in such a way that a uniform thickness of 7 mm was varied from 5 to 9 mm. Otherwise, the conditions were the same as those in the second test (Figure 1.98). The ice temperature during main drying was similar but the DR value of 5.5%/h at ~9 h shows the variation of thickness of the layer. A DR of 0.5%/h was reached not in 10 h, but in 13 h. The test also showed (not in the figure) that the product temperature (T_{pr}) varied at 9 h from 0 to +22 °C.

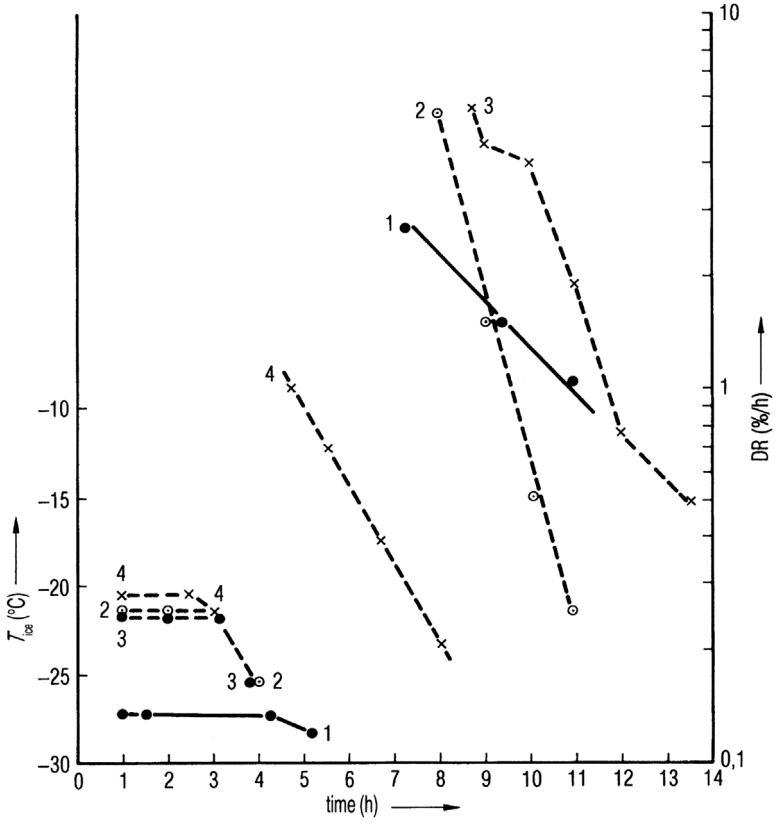

Figure 1.111 Synopsis of T_{ice} and desorption rate of the two tests in Figure 1.97 (1) and Figure 1.98 (4) and comparison with two other tests: (2) carried out as (1) but with activated pressure control at 0.36 mbar and (3) only one tray used (instead of three trays in Figure 1.97), which was placed at such a slope that the thickness of the product was 0.5 cm on one side and 0.9 cm on the other. The DR data measures, in spite of the chosen process data, the amount of desorbed water per hour in % of solid content. It can be seen that a DR value of 0.5%/h in test 4 is reached in 6.2 h, in test 2 in 10.2 h, and in test 1 in 13.5 h, but in test 3 the time cannot be estimated. Because of the unequal product thickness, the DR values can change (9.5 h), and the desorption process is not uniform for such a product.

4) *Test run (see Figure 1.98 and Table 1.14):* The analysis of the run shows that the relatively high heat transfer coefficient of 90.4 kJ/m^2 h °C at a controlled pressure of 0.36 mbar resulted in a constant ice temperature of −22 °C for 2.5 h. Secondary drying was started after 3.5 h and a DR of 0.5%/h was reached at ∼6 h.

The measuring of desorption rates can be used, as the above examples show, to determine the amount of desorbable water if the following prerequisites are fulfilled:

- The product shows a reproducible desorption isotherm, meaning that it is not measurably changed at the applied temperature.

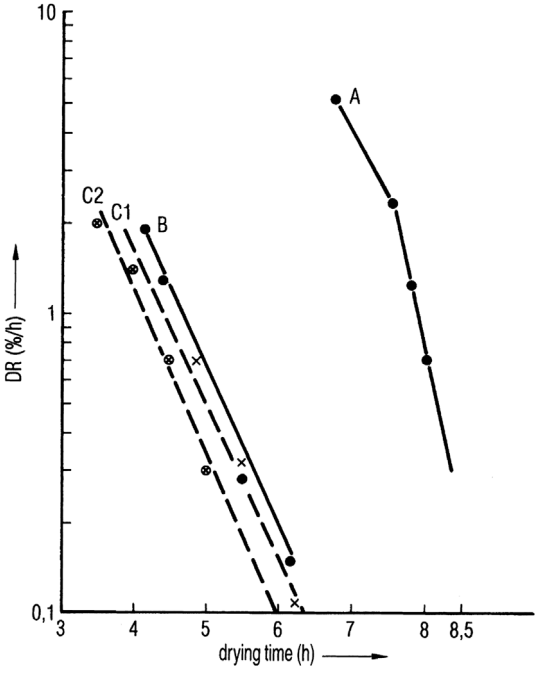

Figure 1.112 Desorption rate (DR) as a function of time for three different foodstuffs: A, B, and C. C1 and C2 differ in the product temperature, +42 and +47 °C, respectively. Product A contains ~85% water, whereas B and C contain only ~60% water. The slope change in A at 7.5 h indicates that the final product temperature was reached at around that time. (The plots are based on measurements by Dr. Otto Suwelack, Billerbeck, Germany.)

- The final temperature must be applied for some time, depending on the layer thickness, in order to reduce the temperature gradient in the product.

The DR values on a semilogarithmic scale plotted as a function of time (Figure 1.112) can be straight lines as long as the temperature of the product is approximately constant and the DR values are not less than 0.1%/h (sometimes 0.05%/h). In Figure 1.112, the change in inclination in plot A at 7.5 h indicates that the final temperature was only reached at ~7.5 h. After a drying time of ~8 h at a temperature of ~50 °C, product A showed a DR of 0.7%/h and after 8.5 h a DR of ~0.3%/h. Product B has, at 42.5 °C shortly before 6 h, a DR of 0.25%/h and at 6.3 h a DR of 0.14%/h. The desorption rate of product C1 at 42 °C was reached at 6.3 h, whereas at 47 °C (C2) already after 5.8 h only 0.1%/h are desorbed.

By integrating the DR values over time, it is possible to calculate the residual moisture content (RM) . The integral is calculated from the last measurement of DR over time up to any other measured DR. The integral is the RM at the time up to which the integral was calculated. The RM calculated in this way is too small by the amount of water that would have been desorbed after the measured DR. Thus, a method of calculation can be deduced: The straight line of the DR values is extrapolated until the still desorbable RM is small compared with the RM to be measured.

Example: By integrating the DR value for product C1 from 0.1 up to 2%/h, the line C1 in Figure 1.113 is obtained; at 3.6 h, the RM was 2.5%. The RM at 3.6 h is too small by the amount of water that would have been desorbed after 6.2 h. Between 6.2 and 7 h, 0.08%/h would have been desorbed. The RM at 3.6 h would not have been 2.5% but 2.56%. This example shows that it is always possible to extrapolate the desorption rates, as long as the error introduced by the integration can be made small compared with the RM to be calculated.

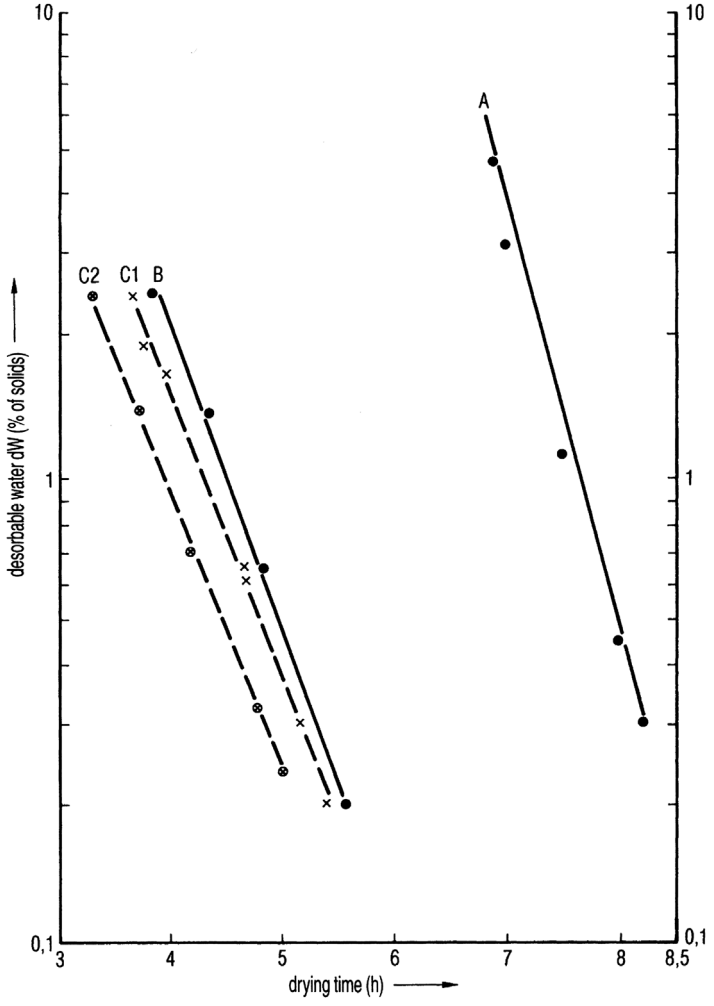

Figure 1.113 Desorbable water in % of solids (dW) as function of the drying time. The dW values were calculated from the data in Figure 1.112. In plot A, after 7.5 h only, 1% (of solids) water can be removed by further drying at this temperature. If, for example, 0.3% is required, the drying can be terminated at 8.3 h.

It should be clear that the RM calculated in this way, for example, 0.1%, must not be identical with residual moisture contents measured using other methods (see Section 1.3.1) because there will always be some water that cannot be desorbed at the end temperature of the drying. This content of bound water for one product and one temperature is a stable value that can be taken from the measurements of absorption isotherms.

The residual moisture content measured by desorption is therefore called desorbable water (dW) and it indicates how much water can still be desorbed at that temperature – or put other way – how much water could be desorbed by further drying, for example, a product having dW = 0.5% can only be further dried by a maximum of 0.5% at the chosen $T_{sh,SD}$. This is of interest for products in which the water content should not be lower than a predetermined value. Pikal [121] missed the exact proof that overdrying (removal of a certain amount of bound water) is detrimental to the product. Hsu *et al.* [122] have shown that freeze-drying of tissue-type plasminogen activator (tPA) below 7.6% RM denatures the product, as 7.6% RM corresponds to a monolayer of water molecules on the tPA molecule. However, the dried product having 7.6% RM at a temperature of 50 °C during storage for 50 days loses more of its activity than a product with a lower water content. Hsu *et al.* recommended examining the optimum water content that cannot be reached on the basis "the lowest residual moisture is the best."

Secondary drying is dominated by the sorption behavior and the structure of the product. Therefore, the DR plots are not always as straightforward as shown so far. Figure 1.114 gives the DR plots of a 10% mannitol solution frozen in 300

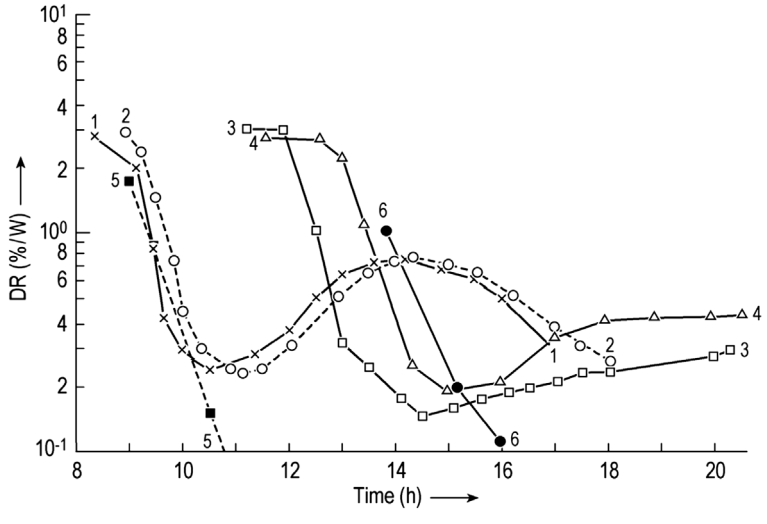

Figure 1.114 DR as a function of drying time of 10% mannitol solution frozen in 300 vials on a shelf with a freezing rate of 0.3–0.6 °C/min, $d = 10$ mm. Process data during MD: In plots 1 and 2, $T_{sh} = 20$ °C, $p_c = 0.3$ mbar, and $T_{ice} = -22.50$ and -22.53 °C, respectively; in plots 3 and 4, $T_{sh} = 5$ °C, $p_c = 0.3$ mbar, and $T_{ice} = -24.92$ and -25.26 °C, respectively. For comparison, plot 5, 10% egg albumin, 400 vials, 10 mm, 0 °C, 0.3 mbar; plot 6, 10% saccharose, 400 vials, 10 mm, 0 °C, 0.15 mbar. (From Ref. [123].)

vials on a shelf with a freezing rate of 0.3–0.6 °C/min, $d = 10$ mm. The process data during MD were as follows:

Plots 1 and 2: $T_{sh} = 20$ °C, $p_c = 0.3$ mbar, $T_{ice} = -22.50$ and -22.53 °C
Plots 3 and 4: $T_{sh} = 5$ °C, $p_c = 0.3$ mbar, $T_{ice} = -24.92$ and -25.26 °C

and for comparison:

Plot 5: 10% egg albumin, 400 vials, 10 mm, 0 °C, 0.3 mbar
Plot 6: 10% saccharose, 400 vials, 10 mm, 0 °C, 0.15 mbar

The drying at a lower T_{sh} did not change the desorption behavior. In the product there exists a combination of two or more structures. Slow freezing produces in a 10% mannitol solution a mixture of α- and β-polymorphs, and fast freezing the δ form (Ref. [124], see also Ref. [23]). If the mannitol solution is frozen in LN_2 at a rate of ~30–60 °C/min, Figure 1.115, a single structure exists. The product in plot 1 is collapsed. The DR plot 3 turns flatter at 0.3%/h. After annealing (plot 2) or MD at a lower p_c (0.08 mbar) and a lower T_{ice} (5 °C) (plot 4), the flatter part disappears into a straight line (see caption of Figure 1.115).

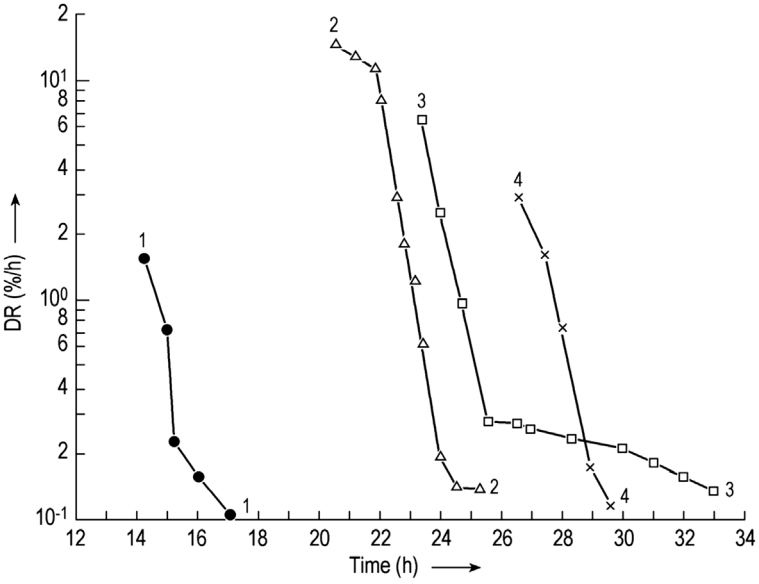

Figure 1.115 DR as a function of drying time of 10% mannitol solution frozen in LN_2 in 130 vials. Plot 1: Product is collapsed because 380 vials have been loaded (also confirmed by visual inspection of the dry product); after a short time of SD, the water evaporates with difficulty from the highly viscous concentrates. Plot 3: In liquid, nitrogen frozen at a rate of 30–60 °C/min, below DR = 0.3%/h the unfrozen water in viscous inclusions is difficult to remove. Plot 2: As plot 3, but the product is annealed after freezing before drying, the unfrozen water is crystallized. Plot 4: As plot 3, but dried at T_{ice} 5 °C lower than in plot 3 (−41 °C); at this temperature, the viscosity is about two decades higher. The product can be successfully dried, but the drying time is ~5 h longer. E: indicates the error in the range of 0.2%/h (From Meister, 2009 [60]. Reproduced with permission of Elsevier.)

Desorption rates not only document the progress of SD and permit the calculation of dW, they also reflect the history of the product during freezing and main drying. For technical details, see Section 1.2.3.

1.2.3 Temperature and Pressure Measurement

Temperature and pressure measurements during freeze-drying are difficult tasks. Thermal elements (Th) and temperature-depended electrical resistance (RTD) systems measure only their own temperature and that of their surroundings only if they are in very close contact with them. Furthermore, they heat themselves and their surroundings by the current flow through the sensors. Also, they influence the crystallization of the product in their surroundings:

- by the energy they produce;
- by inducing heterogeneous crystallization, which can be different in the product without sensors [125]; and
- by different subcooling, which can be smaller around the sensor and result in a coarser structure.

These structure changes and the heat input by the sensors also influence the main drying of vials with sensors. In addition to these problems of principle, there are also practical ones: Ths and RTDs have to be inserted into the product and connected with vacuum-tight lead-throughs to the measuring system. During freezing, the type of sensors used can have the influence shown in Figure 1.116 [126]. The position of the sensors during freezing has a limited influence [127], as shown in Figure 1.117. During freezing, temperature sensors provide a reasonably accurate temperature picture, even if the product with sensors reacts differently to the way it does without sensors.

During main drying, the situation is very different: The condition of a close contact with the product is only true at the beginning of MD; thereafter, the measured temperature depends on circumstances that are difficult to analyze.

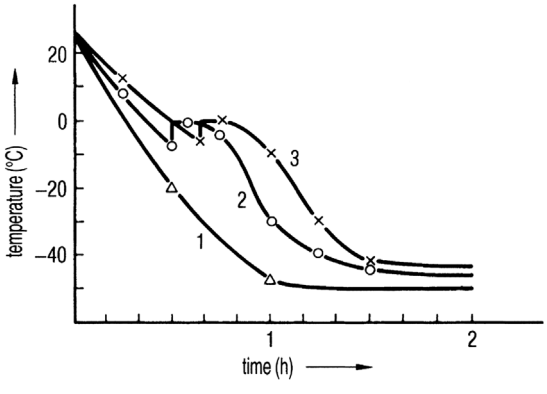

Figure 1.116 Temperature in the product as a function of freezing time, measured by one RTD and one Th each in three vials. The vials had been distributed diagonally on one shelf (the differences between the three vials are within the accuracy of the drawing). 1, T_{sh}; 2, T_{pr} measured by RTD; 3, T_{pr} measured by Th. (See also Figure 3 from Ref. [126].)

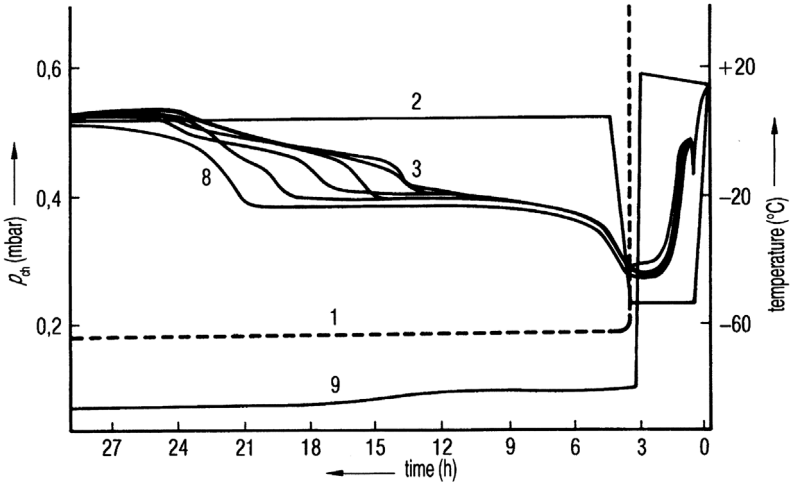

Figure 1.117 Temperature and pressure as a function of the process time. During freezing, the data measured by six temperature sensors are reasonably close together. The split-up after 12 h shows that the progress of MD has reached a level at which the different locations of the sensors become relevant. 1, p_{ch}; 2, T_{sh}; 3–8 temperature sensors; 9, T_{co}. (See also Figure 3 from Ref. [127].)

The position of the sensor, on top, in the center, or near the bottom contact with the vial wall, decides the measured data, as shown in Figure 1.118. If the filling volume of vials is small (a few millimeters layer thickness) or if the product is granular, it is especially difficult to obtain useful data. Also, in homogeneous layers with a thickness of 6–10 mm, temperature differences during main drying can be 10–20 °C when measured with three RTDs, as shown in Figure 1.97. Such differences can also be found between two vials in the same charge during main drying.

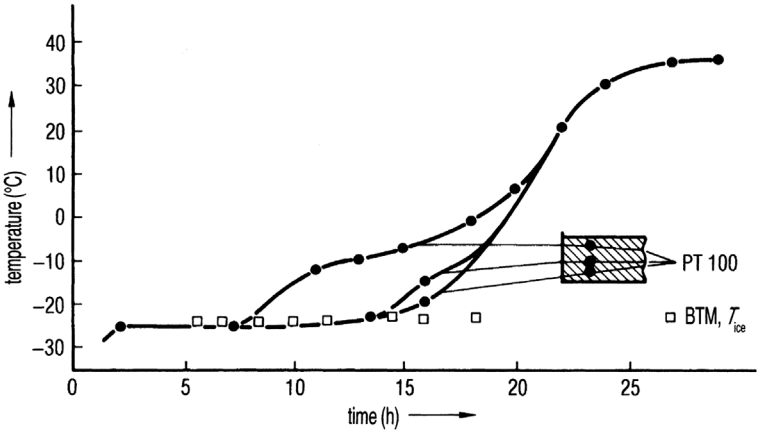

Figure 1.118 Product temperature measured in three different locations in the product as function of the drying time. T_{ice} is measured simultaneously by BTM. (See also Figure 3 from Ref. [128].)

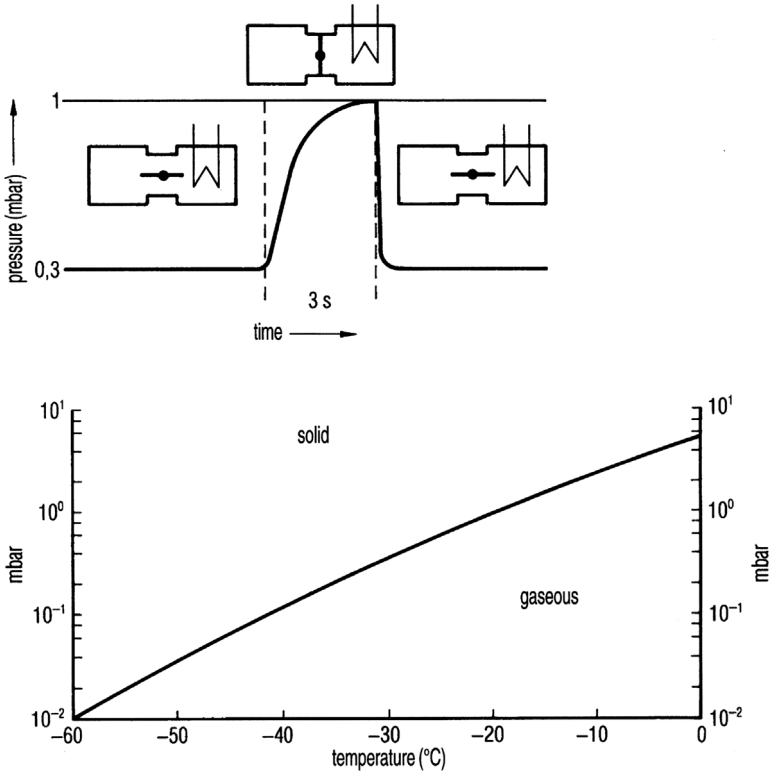

Figure 1.119 Scheme of the "barometric temperature measurement" (BTM) and plot of the water vapor pressure of ice. (Figure 4 from Ref. [130].)

The most important parameter during main drying is the temperature at the moving sublimation front, which cannot be measured by Ths or RTDs. In 1958, Neumann and Oetjen [129] showed that the barometric temperature measurement (BTM) measures exactly this value. This is shown schematically in Figure 1.119: If the drying chamber is separated from the condenser by a valve for a short time, the pressure in the chamber rises to the saturation vapor pressure (p_s) corresponding to the temperature of the sublimation front. p_s can be converted into the ice temperature by the water vapor–temperature diagram (e.g., 0.3 mbar = −30 °C). Data for accurate conversion are given in Table 1.21 for temperatures between −100 and −1 °C.

Milton *et al.* [131] used this method and referred to it as manometric temperature measurement. They used times of pressure rise of up to 30 s. During this time, the ice temperature will increase, mainly owing to continued heat flow. Therefore, an equation has been developed to transform the experimental pressure data, including three other corrections, into the true vapor pressure of the ice. If the valve is closed for only a very short time, <5 s, and the pressure is measured and recorded 60–100 times/s, these data can be recorded as shown in Figure 1.120. The automatic pressure rise measurements (1) can then be plotted and the computer calculates the first derivative (2). The peak time represents the

Table 1.21 Equilibrium water vapor pressure of ice and the related specific density of the vapor.

t °C	p_s mbar	ρ_D g/m^3	t °C	p_s mbar	ρ_D g/m^3
−100	$1.403 \cdot 10^{-5}$	$1.756 \cdot 10^{-5}$	−50	39.35	38.21
−99	1.719	2.139	−49	44.49	43.01
−98	2.101	2.599	−48	50.26	48.37
−97	2.561	3.150	−47	56.71	54.33
−96	3.117	3.812	−46	63.93	60.98
−95	3.784	4.602	−45	71.98	68.36
−94	4.584	5.544	−44	80.97	76.56
−93	5.542	6.665	−43	90.98	85.65
−92	6.685	7.996	−42	102.1	95.70
−91	8.049	9.574	−41	$114.5 \cdot 10^{-3}$	106.9
−90	9.672	11.44	−40	0.1283	0.1192
−89	11.60	13.65	−39	0.1436	0.1329
−88	13.88	16.24	−38	0.1606	0.1480
−87	16.58	19.30	−37	0.1794	0.1646
−86	19.77	22.89	−36	0.2002	0.1829
−85	23.53	27.10	−35	0.2233	0.2032
−84	27.96	32.03	−34	0.2488	0.2254
−83	33.16	37.78	−33	0.2769	0.2498
−82	39.25	44.49	−32	0.3079	0.2767
−81	46.38	52.30	−31	0.3421	0.3061
−80	$0.5473 \cdot 10^{-3}$	$0.6138 \cdot 10^{-3}$	−30	0.3798	0.3385
−79	0.6444	0.7191	−29	0.4213	0.3739
−78	0.7577	0.8413	−28	0.4669	0.4127
−77	0.8894	0.9824	−27	0.5170	0.4551
−76	1.042	1.145	−26	0.5720	0.5015
−75	1.220	1.334	−25	0.6323	0.5521
−74	1.425	1.550	−24	0.6985	0.6075
−73	1.662	1.799	−23	0.7709	0.6678
−72	1.936	2.085	−22	0.8502	0.7336
−71	2.252	2.414	−21	0.9370	0.8053
−70	$2.615 \cdot 10^{-3}$	$2.789 \cdot 10^{-3}$	−20	1.032	0.8835
−69	3.032	3.218	−19	1.135	0.9678
−68	3.511	3.708	−18	1.248	1.060
−67	4.060	4.267	−17	1.371	1.160
−66	4.688	4.903	−16	1.506	1.269
−65	5.406	5.627	−15	1.652	1.387

Table 1.21 (*Continued*)

t °C	p_s mbar	ρ_D g/m^3	t °C	p_s mbar	ρ_D g/m^3
−64	6.225	6.449	−14	1.811	1.515
−63	7.159	7.381	−13	1.984	1.653
−62	8.223	8.438	−12	2.172	1.803
−61	9.432	9.633	−11	2.376	1.964
−60	$10.80 \cdot 10^{-3}$	10.98	−10	2.597	2.139
−59	12.36	12.51	−9	2.837	2.328
−58	14.13	14.23	−8	3.097	2.532
−57	16.12	16.16	−7	3.379	2.752
−56	18.38	18.34	−6	3.685	2.990
−55	20.92	20.78	−5	4.015	3.246
−54	23.80	23.53	−4	4.372	3.521
−53	27.03	26.60	−3	4.757	3.817
−52	30.67	30.05	−2	5.173	4.136
−51	34.76	33.90	−1	5.623	4.479

Source: From Smithsonian Metrological Tables, 6th edn, 1971 and VDI-Wasserdampftafeln, 6. Ausgabe (1963).

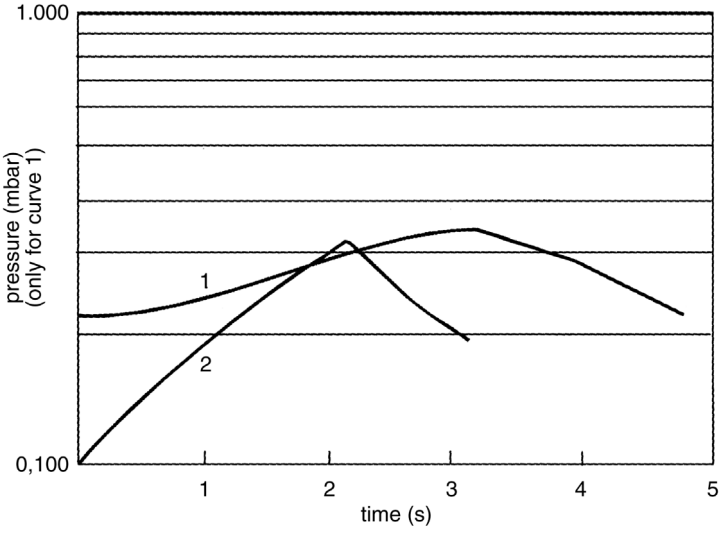

Figure 1.120 Pressure rise as a function of time. 1, pressure rise in the chamber after the valve is closed; 2, first derivative of 1. A maximum of 2 is reached at 2.14 s, the related equilibrium vapor pressure is $p_s = 0.286$ mbar corresponding to $T_{ice} = -32.7$ °C. (Figure 2 from Ref. [132].)

Table 1.22 Protocol of T_{ice} during main drying.

t_{MD} (h)	T_{ice} (°C)	$T_{ice/n}$ (°C)	t_{MD} (h)	T_{ice} (°C)	$T_{ice/n}$ (°C)
02.0	−23.5	−23.5	02.3	−23.3	−23.4
02.5	−23.5	−23.5	02.8	−23.6	−23.5
03.0	−23.3	−23.4	03.3	−23.4	−23.4
03.5	−23.4	−23.4	03.8	−23.4	−23.4
04.0	−23.7	−23.5	04.3	−24.1	−23.5
04.5	−24.4	−23.6	04.8	−24.3	−23.7
05.0	−25.1	−23.8	05.3	−25.9	−23.9

$T_{ice/n}$: sum of all n T_{ice} measurements divided by n, after thermal equilibrium has been reached (in this run after 2 h). The main drying in this run could have been terminated after 5 h, but it is useful to wait for the next data, so that the decision is not dependent on one measurement.

time when p_s has been reached. In the example this time was 2.14 s after the valve had been closed. The related equilibrium pressure is $p_s = 0.286$ mbar corresponding to $T_{ice} = -32.7$ °C. Table 1.22 shows the results of such measurements. The average temperature from 2.0 to 4.8 h is −23.66 °C, the standard deviation being 0.39 °C.

In a production plant, the valve between the chamber and condenser could have a diameter of 1 m or more, and it cannot be closed in 5 s or less, 6–7 s may also work. However, the method can be applied with some changes in the software: The movement of the valve is controlled for its reproducibility and accuracy and the pressure rise is used for the calculation of T_{ice} after the valve has reached a certain position. Table 1.23 shows such measurements for a valve with a diameter of 1.1 m.

T_{ice} data depend on the number of vials in the chamber. T_{ice} is the temperature at the sublimation front of the ice at which the heat transfer from the shelf to the

Table 1.23 Extracts of T_{ice} data measured in a plant with a valve of 1.1 m diameter between the chamber and condenser (Measurement Steris GmbH).

t_{MD} (h)	T_{ice} (°C)	t_{MD} (h)	T_{ice} (°C)
01.65	−42.0	05.17	−41.7
02.10	−41.9	05.23	−41.8
02.80	−41.8	05.38	−42.0
AV	−41.9 SA 0.1 °C	AV	−41.8 SA 0.15 °C
04.45	−42.0		
04.70	−41.9		
04.95	−41.6		
AV	−41.8 SA 0.21 °C		

AV= average value of all measurements −41.85 °C SA 0.14 °C.
SA = Standard deviation.

Table 1.24 Comparison of runs with different numbers of vials.

No. of vials	Average T_{ice} (°C)	Saturation vapor pressure p_s (mbar)	Standard deviation of T_{ice} (°C)	Main drying time t_{MD} (h)
50	−35.75	0.206	0.192	9.9
100	−34.33	0.230	0.162	10.7
400	−32.38	0.296	0.228	11.4

T_{ice} data are the average of four runs with each number of vials. All vials with the same product and filling height.

ice front is in equilibrium with the energy consumption at this front by the sublimation of ice. The heat transfer coefficient is constant; with more or fewer vials the heat transfer surface increases or decreases, producing more or less vapor. The vapor passes the same geometric dimensions of the plant. For more vapor transport a higher and for less vapor transport a smaller pressure difference is needed. T_{ice} increases with more vials, as shown in Table 1.24. $p_{co} \ll p_c$, therefore dp for 400 vials is ~50% larger than for 50 vials. If, for example, −35 °C is not to be exceeded, p_c for 400 vials has to be lowered (see Figure 2.116 and text).

T_{ice} data not only show the ice temperature of the sublimation but also provide some information about the composition of the cake. In Figure 1.121, the

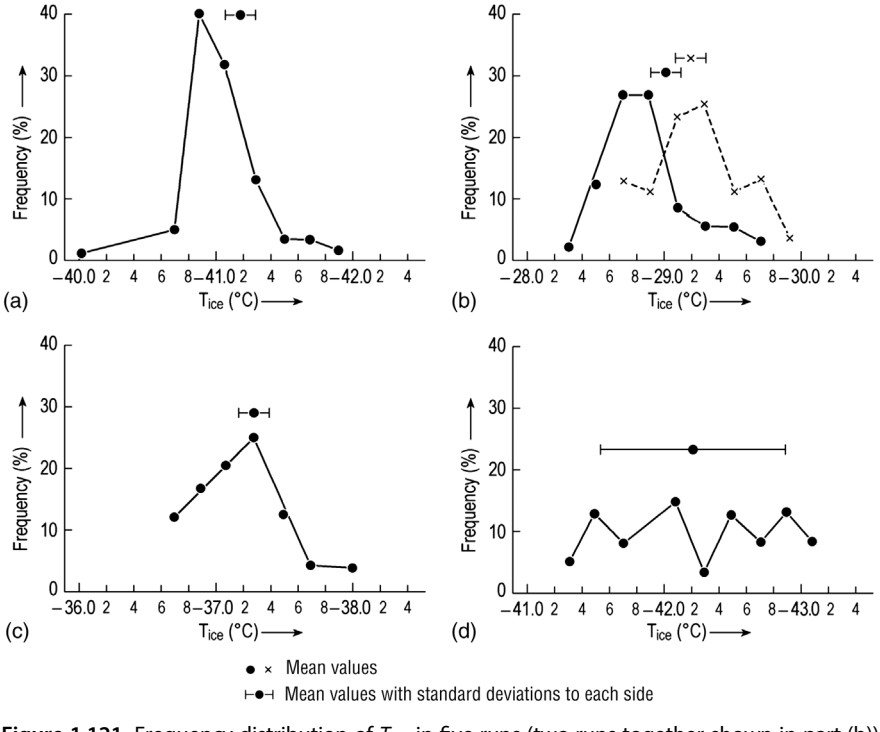

Figure 1.121 Frequency distribution of T_{ice} in five runs (two runs together shown in part (b)). Data in Table 1.25.

Table 1.25 Data for the four runs in Figure 1.122.

	Product egg albumin (ea)	ea	ea + 0.9% NaCl	Pharmaceutical
Code in Figure 1.121	(a)	(b)	(c)	(d)
Cake thickness (mm)	20	20	20	20
Freezing method	Shelf (sh)	LN_2	LN_2	sh
T_{sh} (°C)	−5	20	20	0
p_c (mbar)	0.1	0.3	0.1	0.07
Mean T_{ice} (°C)	−41.1	−29.2	−37.3	−42.2
SA (°C)	0.18	0.3	0.3	0.6

frequency of T_{ice} data for runs a–d is shown. Table 1.25 provides the process conditions for these runs.

a) The albumin is freeze-dried at low p_c and T_{sh}, resulting in a very stable, uniform cake; 70% of all T_{ice} data are between −40.9 and 41.1 °C with SA <0.2 °C.
b) The albumin in two runs is frozen in LN_2, not annealed; the two mean T_{ice} are within the SDs, but the frequency analysis shows that freezing without annealing produces slightly different cakes.
c) The addition of 0.9% NaCl made the frequency analysis broader than in (a); the SA is as in (b).
d) In spite of the low p_c (0.07 mbar) and the low T_{ice} (−42.2 °C), the frequency distribution of T_{ice} indicates an incompletely frozen product with high concentrated inclusions, which pass through the sublimation front at irregular intervals. ER measurements (not shown) confirm that the product should theoretically be frozen down to −65 °C and dried at $T_{ice} \leq 50$ °C. The product manufactured with the data shown was not unacceptable. This example shows that a compromise is sometimes necessary, if it can be carefully monitored. A process operated at T_{ice} −40 °C resulted in an unacceptable shrinkage.

Table 1.22 shows also T_{ice}/n, which is the sum of all measurements divided by the number of measurements. After 4.3 h, T_{ice} drops in 1 h by 2.5 °C below the highest T_{ice}/n (−23.4 °C). As shown in Figure 1.122, this decrease in ice temperature marks the end of main drying and can be used to switch over manually or automatically to secondary drying.

As a disadvantage of the BTM method, Bardat *et al.* [127] described the danger of collapse or melting of the product during the pressure rise measurement. This can only happen if T_{ice} and thereby p_s are larger than the maximum tolerable T_{ice}. The measurement is not the reason for the collapse, it is the too high T_{ice} shown by the measurement. Bouldoires [133] pointed out that the BTM method can only be used for discontinuous installations having a valve between the drying chamber and condenser.

For the use of BTM, two conditions have to be fulfilled.

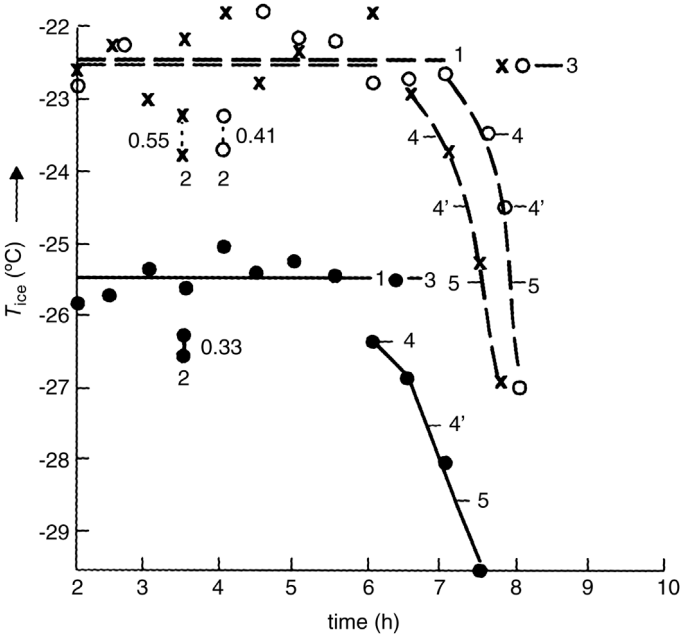

Figure 1.122 T_{ice} as a function of drying time. (○), (×): measurements and repetition with the same product and the same process data; (●) another product with other process data. 1, average T_{ice}; 2, standard deviation of T_{ice}; 3, maximum $T_{ice/n}$ for (○) and (×) identical −22.53 °C; 4, maximum $T_{ice/n}$ −1 °C; 4′, maximum $T_{ice/n}$ −2 °C; 5, maximum $T_{ice/n}$ −3 °C. (Figure 6 from Ref. [132].)

The first condition is that the leak rate of the chamber has to be so small that the pressure rise in the chamber during the time of valve closure due to leak rate is small compared with the pressure rise due to the water vapor.

Example: The pressure in the chamber rises in 3 s from 0.28 to 0.41 mbar. With a chamber volume of 200 L, this is 8.7 mbar L/s of water vapor. This vacuum chamber should have a leak rate not larger than 0.08–0.09 mbar L/s (1% of 8.7 mbar L/s). Such a leak rate has no measurable consequences. Even if it were 10 times larger (0.8–0.9 mbar L/s), the pressure in the chamber would rise in 3 s to 0.42 mbar. Converted into temperature, this would be an error of 0.1 °C. A leak rate of 0.8–0.9 mbar L/s is already larger than could be pumped off by a reasonable pumpset in this size of freeze-drying plant. The partial pressure of air, p_{air}, must be small compared with the water vapor pressure. At 0.28 mbar, total pressure p_{air} should be 0.03–0.04 mbar. A vacuum pump that can pump 0.8–0.9 mbar L/s at 0.03–0.04 mbar must have a pumping speed of ∼100 m^3/h, which is unusually large for a 200 L chamber. A vacuum pump with a 40 m^3/h pumping speed will theoretically evacuate a chamber and condenser (total 500 L) in ∼6 min down to 0.1 mbar. Even if it takes 10 min with the loaded chamber, the pumping speed of the pump is sufficient. With this pump, the leak rate of the plant should not exceed 0.4 mbar L/s, which would be pumped at ∼0.04 mbar.

The necessary leak tightness of a plant can be summarized as follows.

To ensure an undisturbed water vapor transport (see Section 1.2.4), the leak rate of a freeze-drying plant must allow BTM with sufficient accuracy. This applies for vapor pressures with ice temperatures ranging between −50 and −10 °C corresponding to 0.04–2.5 mbar. The pressure range for DR measurements is normally one decade below the above data and this has to be considered in the specification of the plant. All measurements discussed above have to be carried out with a capacitance vacuum gauge, because these instruments measure pressure independently of the type of gas. All vacuum gauges based on the change of heat conductivity as a function of pressure show a result that depends not only on the pressure of the gas mixture but also on the type of gas. Leybold AG [134], a company based in Cologne, Germany, indicates that for instruments based on heat conductivity such as the Thermovac in the pressure range from 10^{-3} to 1 mbar, with measurements in pure water vapor (carried out with an instrument calibrated in air), the reading value must be multiplied by 0.5 to give the correct water vapor pressure. If the mixture of water vapor and air changes, the reading value of, for example, 0.28 mbar water vapor pressure in pure water vapor corresponds to 0.14 mbar. At 80% water vapor, the reading value must be corrected to 0.17 mbar. In freeze-drying plants during main drying, the water vapor content can vary between 60 and 95%. An average correction factor of 0.65 can be used, as can be seen in Figure 1.97: Here 0.34 mbar with a Thermovac corresponds to 0.16 mbar, showing a correction factor of ∼0.5, with the progress of drying after 8 h, 0.11 mbar with the Thermovac corresponding to 0.08 mbar measured with a Capacitron with a correction factor of 0.73. Given that the reproducibility of the heat conductivity manometer in the pressure range of 10^{-2}–1 mbar is ∼10% of the reading [134] while capacitance gauges are rated at 0.5% of the reading [135], the advantages of the capacitance method are clear. The difference in price for the two types of instruments is small compared with the investment cost, even for a pilot freeze-drier. BTM should therefore always be carried out with a capacitance instrument.

The second condition for a reliable BTM is that, in the tolerable measuring time, so much ice can sublime as to fill the chamber with saturated water vapor. The measuring must be chosen in such a way that the temperature of the ice during closing of the valve between the chamber and condenser does not rise to a disturbing degree. Assuming extreme conditions, one can estimate that the temperature of the ice increases by ∼0.25 °C/s under the following stipulations:

- K_{tot} is high, for example, 84 kJ/m^2 h °C;
- ΔT is large, for example, 50 °C;
- the product with 10% solids has been dried so that only 15% of the water is ice and the layer thickness is 0.7 cm.

The measuring time should be <3 s; this is possible, as can be seen from Tables 1.22 and 1.23 and Figure 1.120.

The chamber volume and the amount of ice to be sublimed during MD must satisfy the following conditions:

$$V_{ch} \mathrm{d}p/\mathrm{d}t \ll m_{H2O}/t_{MD} \tag{1.15}$$

where

V_{ch}	=	chamber volume (L);
dp	=	$p_s - p_{H2O,ch}$ (mbar), pressure rise during measuring time;
dt	=	time (s) until p_s is reached;
m_{H_2O}	=	mass of water to be sublimed during the time of MD;
t_{MD}	=	time of MD (s), secondary drying not included.

An example of Figure 1.98:

V_{ch}	=	160 L
dp	=	0.51 − 0.13 mbar = 0.38 mbar
dt	=	3 s
M	=	2.24 kg water, 85% to be sublimed = 1.90 kg
t_{MD}	=	5 h = 18 × 10 × s
		(1 g H_2O is converted into 1.24×10^3 mbar L)

results in

$$\frac{160 \times 0.38}{3} \ll \frac{1.9 \times 10^3}{18} \times \frac{1.24 \times 10^3}{10^3} \qquad (1.15a)$$

$$20.27 \ll 131$$

With the data of the example condition (1.15) is satisfied, BTM can be applied.

If in this example a chamber of 1000 L were used, the left side of the equation would become 126.7; in this case, the chamber is too large or the amount of water to be sublimed too small. Thus, 2–4 kg of product in a 160 L chamber or 30–80 kg in a 1000 L chamber will satisfy Eq. (1.15).

If these conditions are met, the curves as shown in Figure 1.120 are measured.

Figure 1.122 shows one measurement and one repetition of this measurement and a third measurement with another product and other process data. Toward the end of main drying, the data on T_{ice} will systematically decrease; this effect can be used for an automatic change from main to secondary drying (see Section 2.6.2.2).

The temperature measurement during secondary drying with Th or RTD is possible, as shown in Figure 1.97, with an accuracy of ~±3 °C.

The change from main drying to secondary drying is difficult to determine by the product temperature, as shown in Figure 1.123. This can also be seen in Figures 1.124 and 1.125 [126]. Nail and Johnson [125] compared (see Figure 1.126) the pressure measured by a heat conductivity vacuum gauge (TM) with pressure rise measurements during secondary drying and indicated the related RM. In Figure 1.127, the pressure measured by TM is compared with the p_{H2O} measured by a mass spectrometer. The signal of the mass spectrometer is reduced during the first two time units, but changes very little between the third and seventh time units. Connelly and Welch [136] also used a mass

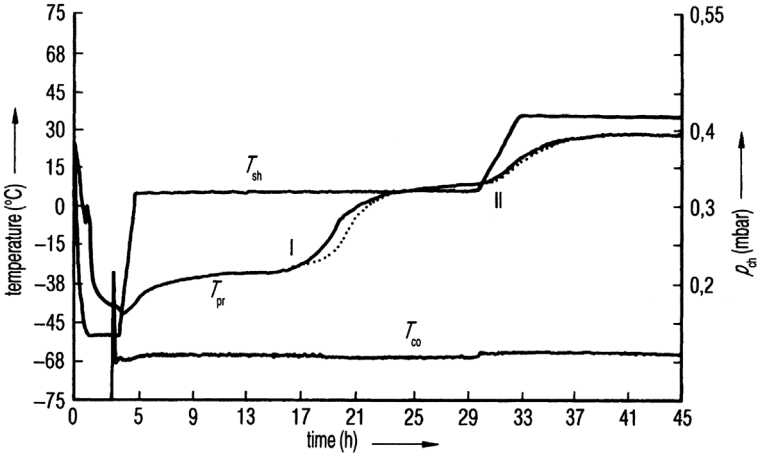

Figure 1.123 Increase in the product temperature T_{pr} as a function of process time. The increase (I) starts at ~16 h and reaches T_{sh} at ~22 h. Secondary drying (SD) started (II) at ~30 h. Between 16 and 22 h, there is no measurable indicator of when to start SD. Also, the safety margin between 22 and 30 h cannot be connected with the measured product temperature. (See also Figure 2 from Ref. [127].)

spectrometer to determine the end of main drying and of secondary drying. They also found that the change in output signal changed by 10: 1 between main drying and the end of secondary drying. It is suggested that one should not use the water vapor pressure measured by the mass spectrometer directly, but divide this data by the total pressure measured by the mass spectrometer. As shown in Figure 1.128, these normalized values show a plateau during the first ~7 h of main drying for 5% bovine serum albumin and afterward a decay between 7 and 23 h. A further suggestion is not to plot these normalized values, but their natural logarithms. By this method, the shape of the plot is meaningful, whereas the absolute value of the *y*-axis is more difficult to interpret. The authors concluded that the main drying is terminated at about 7 h of the cycle. However, there was no measurable indicator of whether to use the exact end of the plateau or 1–2 h later. For example, the decline of the curve in Figure 1.129 changes again at ~12 h (this can also be found in the curve in Figure 1.128). The end of secondary drying is suggested to be established by the following procedure:

1) Taking a baseline measurement of the partial pressure of the ice on the condenser in the empty plant.
2) Measuring the partial pressure during the run and terminating the secondary drying if the two values are close together. In certain cases, this might be too insensitive; in this case, it is suggested to close the valve between the chamber and condenser and measure the increase in water vapor pressure in a certain time. (*Note:* It is surprising that the water vapor pressure at the beginning of main drying is only 40% of the total pressure during the sublimation of distilled water and 30% during the sublimation of bovine serum albumin.)

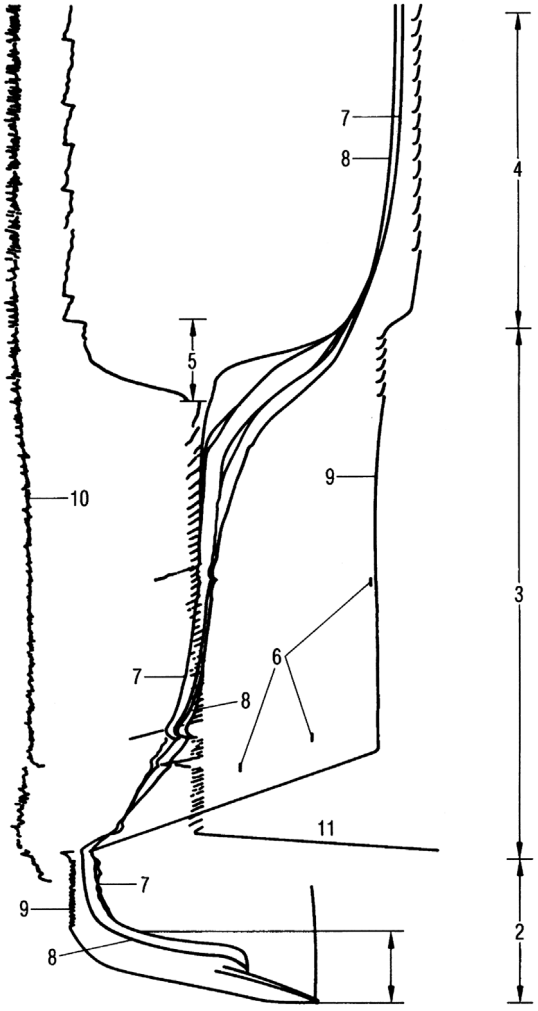

Figure 1.124 Course of the freeze-drying after the product has been frozen at 0.6 °C/min to −50 °C. 2, Freezing; 3, MD; 4, SD; 5, DR measurements to define the end of MD; 6, some BTM; 7–9, as in Figure 1.124; 10, T_{co}; 11, p_{ch}. At the beginning of DR measurements, the pressure control in this example is deactivated. When the DR value has reached a predetermined number, T_{sh} (in this case) is increased to the maximum tolerable temperature. The optimum time frame for the change from MD to SD cannot be estimated from the T_{pr} plot. (See also Figure 6 from Ref. [126].)

The pressure rise measurements in Figure 1.126 change during the final hours from 0.26 to 0.05 mbar, showing that this method is more sensitive than p_{H2O} measurements with the mass spectrometer alone.

Figure 1.130 shows a comparison between measurements made with TM, CA, and a hygrometer and demonstrates that the hygrometer data are not much more sensitive to the change in vapor pressure than the data with the other two instruments. The end of main drying can be between 2.5 and 5 h, depending on

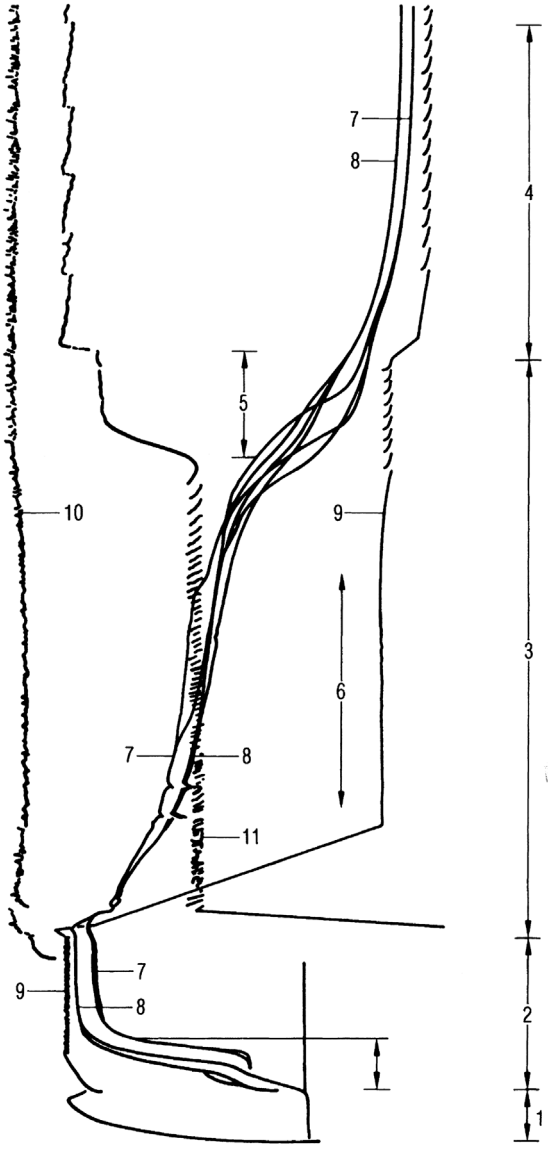

Figure 1.125 Course of the freeze-drying after the product has been frozen on precooled shelves at ~−50 °C at ~1 °C/min. Nomenclature as in Figures. 1.124 and 1.125. The rise of T_{pr} is different. The optimum time frame for the change from MD to SD cannot be estimated from the T_{pr} plot. (See also Figure 7 from Ref. [126].)

which change of inclination is chosen. From the BTM measurements, one can conclude (see Figure 1.122) that the main drying is terminated at ~3.5 h.

Figure 1.131 [138] summarizes the measurements of three runs of the product temperatures with RTD, T_{ice} with BTM, and of the pressures by CA. The plots show that the difference in pressures during main and secondary drying is largest

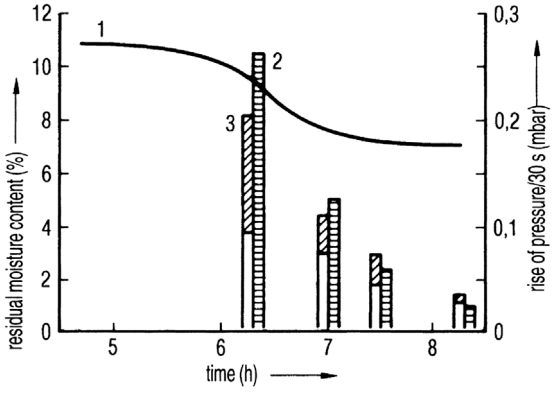

Figure 1.126 Plot of the pressure measured by heat conductivity vacuum gauge (TM) during SD. In addition pressure rises in 30 s and related RM data are shown. 1, p_{ch} measured by TM; 2, pressure rise in 30 s; 3, RM in % of solids. (See also Figure 5 from Ref. [125].)

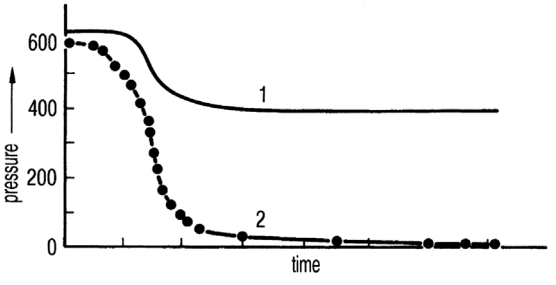

Figure 1.127 Comparison of p_{ch} data: TM measurements and signals of mass spectrometer for mass 18 during freeze-drying. 1, p_{ch} by MT; 2, mass spectrometer signal at mass 18. (See also Figure 10 from Ref. [125].)

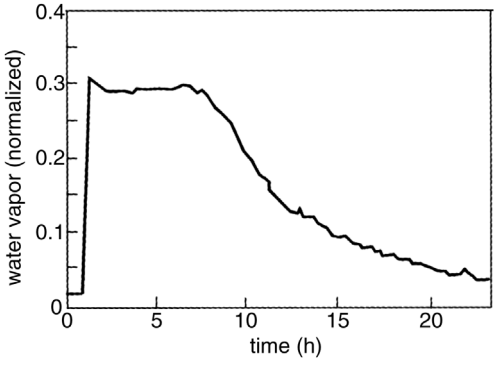

Figure 1.128 Water vapor partial pressure divided by total pressure as a function of time of 5% bovine serum albumin solution. (See also Figure 3 from Ref. [136].)

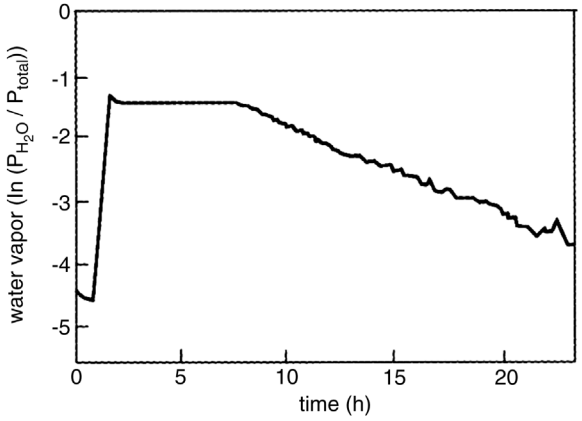

Figure 1.129 Natural logarithm of water vapor partial pressure divided by total pressure as a function of time for 5% bovine serum albumin solution. (See also Figure 5 from Ref. [136].)

with no pressure control and still clearly recognized with p_c at 0.2 mbar in relation to an ice temperature of ≃30 °C.

The water vapor desorption can be measured as shown in the scheme in Figure 1.132 and be calculated by

$$D = \frac{\mathrm{d}pV_{\mathrm{ch}}}{\mathrm{d}t}(\mathrm{mbar\,L/s}) \tag{1.16}$$

where

V_{ch}	=	chamber volume (L);
$\mathrm{d}p$	=	pressure increase (mbar);
$\mathrm{d}t$	=	measuring time for pressure increase (s).

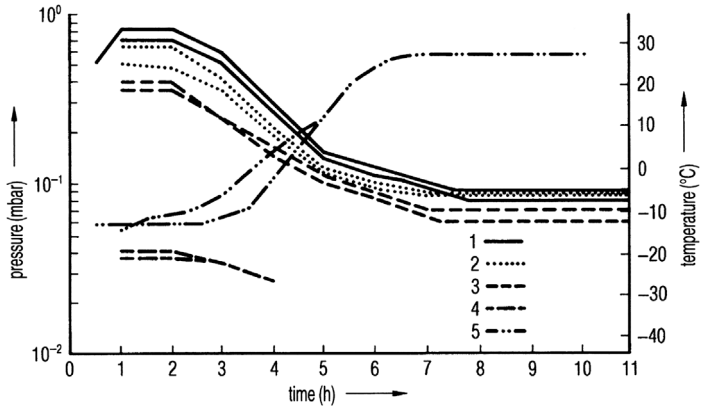

Figure 1.130 Course of two tests with identical products and identical process conditions, also using a hygrometer. The pressure drop at the end of MD, measured by the hygrometer, is not more informative than the data provided by CA. Below a certain pressure (in this case, below ~0.09 mbar), the hygrometer had to be recalibrated for the lower pressures. 1, p_{ch} (mbar) TM; 2, p_{ch} (mbar) CA; 3, hygrometer (System 3A, Panametrics, Hofheim, Germany); 4, T_{ice} (BTM) (°C); 5, T_{pr} (°C) RTD. (See also Figure 7 from Ref. [137].)

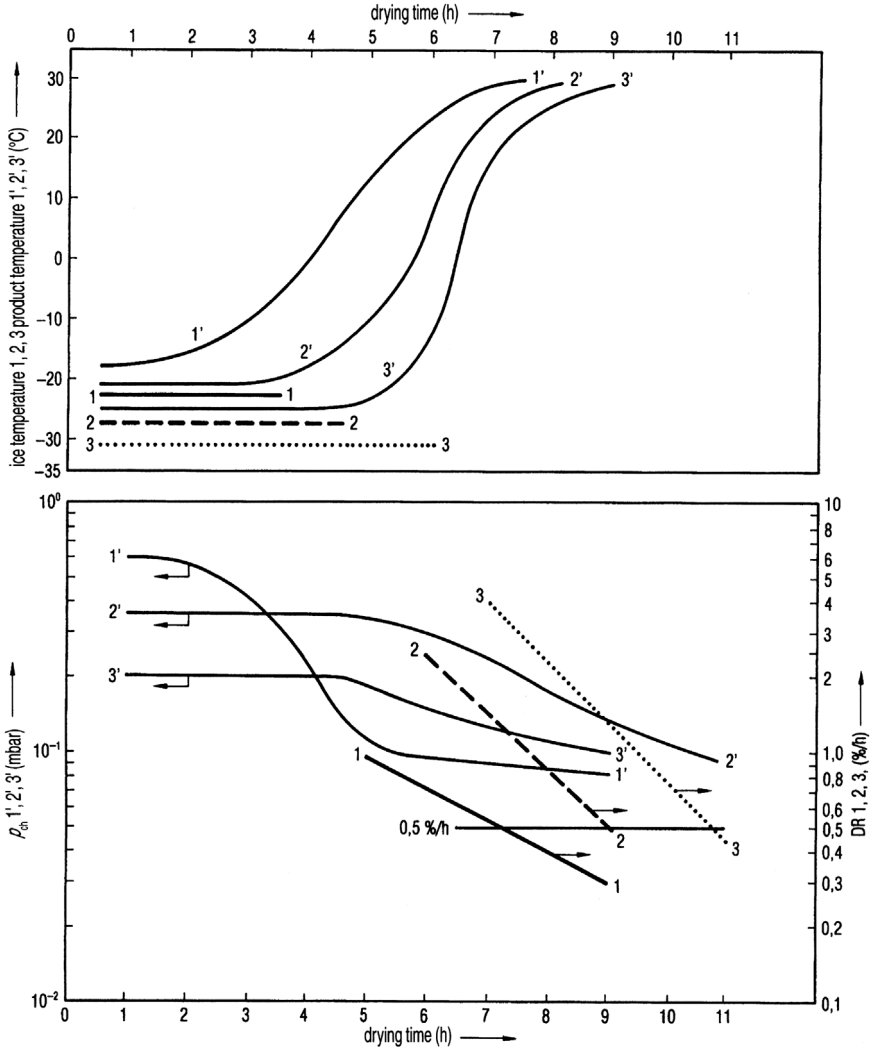

Figure 1.131 Summary of the results of three runs, which are differentiated by the control pressure: 1, no pressure control; 2, pressure controlled at 0.36 mbar; 3, pressure controlled at 0.20 mbar. The graphs show T_{Ice} marked as 1, 2, 3 and T_{pr} marked as 1′, 2′, 3′ in the upper drawing. In the lower drawing, the DR are marked as 1, 2, 3 and the p_{ch} as 1′, 2′, 3′. The increase in the product temperature (T_{pr}) and decrease of chamber pressure (p_{ch}) depend on the chamber pressure, because K_{tot} is pressure-dependent and T_{sh} has been programmed up to +30 °C in such a way that the control pressure has never been exceeded. In the test 1, T_{sh} has been raised to +30 °C as quickly as technically possible. The end of MD and SD are difficult to define by T_{pr} and/or by p_{ch}. The DR values measure the amount of water desorped from the product per hour in % of solids. The end of drying has been determined by DR: 1, after 7 h, DR = 0.55%/h; 2, after 8.5 h, DR = 0.65%/h; 3, after 11 h, DR = 0.45%/h. As shown in Figure 1.113, dW (RM) can be calculated from DR data and the end of drying can be expressed as residual moisture content in % of solids. (Based on Figure 1 from Ref. [138].)

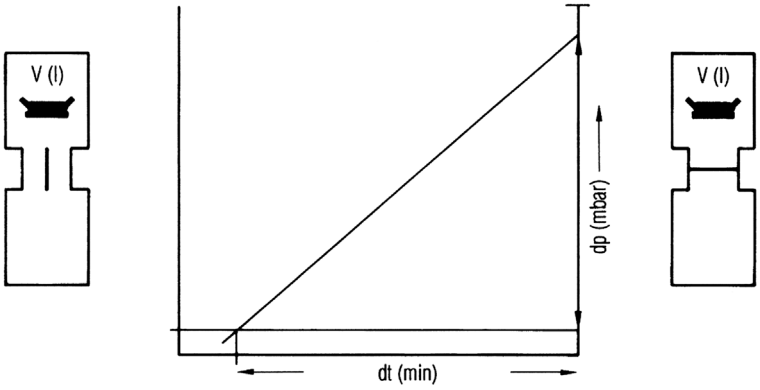

Figure 1.132 Scheme of the measurement of the desorption rate (DR).

By using $22.4 \times 10 \times$ L mbar, corresponding to 18 g H_2O, the units mbar L can be converted into g. This relationship is accurate enough as the temperature of the water vapor depends on several factors and will also be modified by a change of T_{sh}. The desorption process can be best illustrated by using the desorption rate (DR), which measures the desorbed amount of water in % of solids of the product per hour:

$$DR = 2.89 \times 10^2 (V_{ch}/m_{solid})(dp/dt) \tag{1.16a}$$

(desorption of water vapor in % of solids per h), where V_{ch}, dp, and dt are as in Eq. (1.16) and

$$m_{solid} = \text{mass of solids (g)}.$$

Measurements of the desorption rate (DR) require three conditions:

- For a product, a reproducible desorption isotherm exists and the product does not change at the end temperature during secondary drying.
- The end temperature has to be applied for some time depending on the cake thickness in order to minimize the temperature gradients in the product.
- The leak rate of the plant must be so small that a pressure rise due to the leak rate is also small compared with the pressure rise resulting from the desorbed water.

To measure DR values, one has to use measuring times of ~30 s. A prolonged time (compared with BTM) can be used, since the product temperature during this time is almost constant. On the other hand, the absolute pressures are approximately one decade smaller than during BTM (Figure 1.98, $p_{MD} =$ 0.36 mbar, $p_{SD} = 0.03$ mbar). To measure, for example, 1%/h in the run in Figure 1.98, one must calculate 65.5 g solids in a chamber volume of 160 L by Eq. (1.16b):

$$dp/dt = DR/V_{ch} = 1.4 \times 10^{-3} \text{ mbar/s} \tag{1.16b}$$

This pressure range can be measured by a CA if $dt > 15$ s. Manufacturers of CAs give the reproducibility of such instruments as ±0.005 mbar. With a few years of

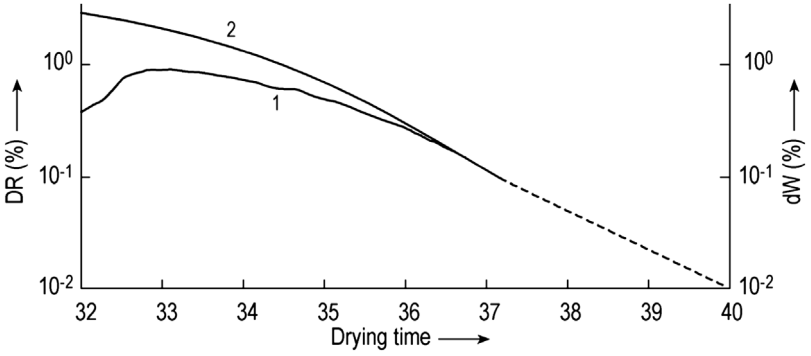

Figure 1.133 DR as a function of drying time. Plot 1, DR; plot 2, integration of plot 1 over time to calculate dW.

experience, the authors found a reproducibility of better than ±0.003 mbar between the calibration intervals of 3–4 months. If a long time, 120 s, is taken and the error should be smaller than ±10%, dp has to be a minimum of 0.034 (±0.003) mbar in 120 s. If the chamber volume is 160 L and $m_{solid} = 65.5$ g (or 160 g), DR = 0.2%/h (or 0.08%/h) can be measured within ±10%. The necessary accuracy of the DR measurement depends on the order of magnitude of dW to be achieved and its desired accuracy. If, for example, 1% RM ± 10% is required, DR measurements down to 0.1%/h are sufficient as shown in Figure 1.133: Plot 1 extrapolated to 0.01%/h is reached in 40 h; the integration of DR over time from 37.2 h until the change from MD to SD results in dW = 2.60% at 32 h. DW 1% is reached in 34.0 h. If the DR data from 37.2 to 40 h were to be included in the extrapolation, the time would have been 34.2 h as shown in the graph. For the two plots in Figure 1.134, the ratio of solids to the chamber volume was too small for plot 1 for data <0.05%/h and for plot 2 for data <0.3%/h. Plot 1 could be used to calculate ~1% dW; the ratio in plot 2 is too small.

Figure 1.135 shows the influence of the filling height on DR data: plot 1, two runs with 300 vials and identical process data; plot 2, 10% of 300 vials were overfilled by 10%; plot 3, 50% of 300 vials were overfilled by 10%. These data demonstrate that it is not possible to freeze-dry vials with the same product, but different filling heights in one charge. The plots indicate that in plot 1 the final $T_{sh,SD}$ is reached at ~8.1 h, in plot 2 at ~8.2 h, and in plot 3 the change from MD to SD was not finished at 7 h and it took 8.5 h before $T_{sh,SD}$ was reached. The desorption behavior of the product in all four runs is identical; when the temperature is reached, all plots are parallel.

As a rule of thumb, the following can be used: 1 g of solid in a chamber volume of 1 L is sufficient to measure dW at 1% with an error of ±10%. If the ratio m_{solid}/V_{ch} becomes smaller than 1, the error in dW increases. It is possible to prolong dt, for example, to 180 or 320 s, and improve the accuracy, but 90–120 s has been shown to be a practical range.

The leak rate (qL, mbar L/s) has to be small compared with the pressure rise to be measured in the chamber volume. For the example [Eq. (1.16b)] above, $qL \ll 1.4 \times 10^{-3} \times 160 \ll 0.22$ mbar L/s or the maximum qL, $qL_{max} = 2.2. \times 10^{-2}$ mbar L/

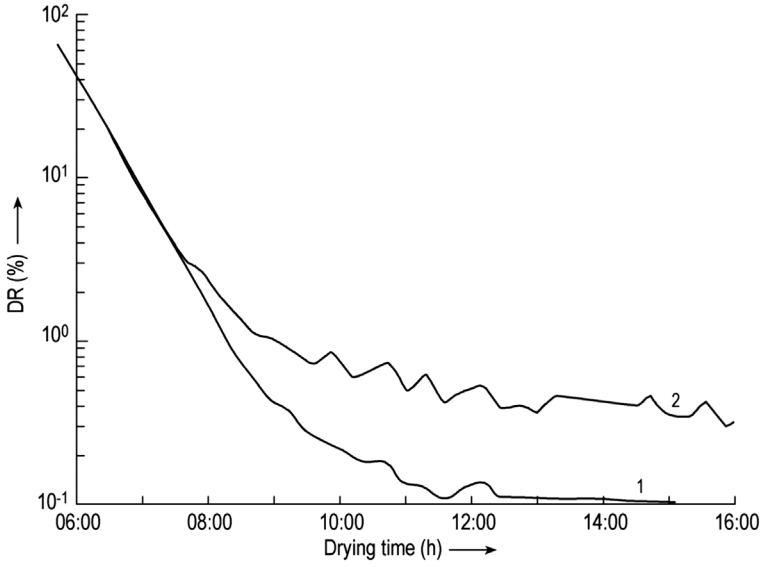

Figure 1.134 DR as a function of drying time. The ratio m_{solid}:V_{ch} is too small in plot 1 for DR data <0.05%/h and for plot 2 for data <0.3%/h. The ratio in plot 2 is too small for reproducible measurements.

s. With this qL_{max}, the "true" DR is measured as 0.24 mbar L/s or ~10% too large, DR = 1%/h is calculated as 1.1%/h or a DR 0.1%/h is calculated as 0.2%/h. For many freeze-drying plants, one can expect that the leak rate will be in the region of 10^{-3} mbar L/s. If the leak rate of a plant is stable and known, it can be accounted for in the DR value. In normal operation, one would expect that a 100 L chamber

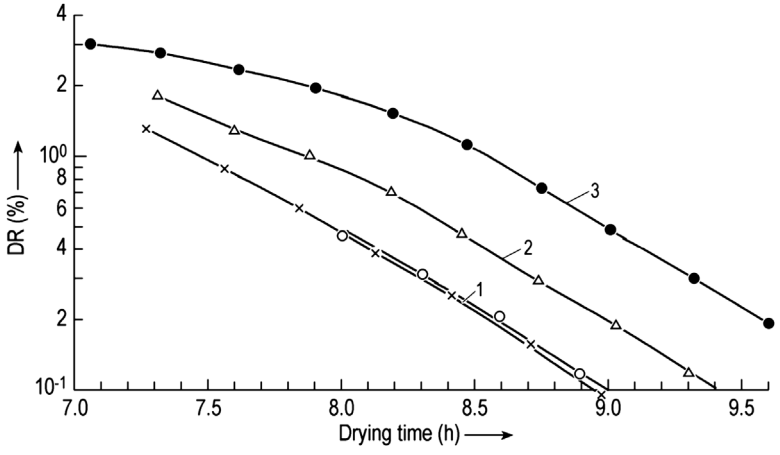

Figure 1.135 Four DR plots as function of drying time in the same plant, with the same product and process conditions, 300 vials per run. Plot 1, two runs on two different days; plot 2, one run, 270 vials normally filled, 30 vials 10% overfilled; plot 3, 1 run, 150 vials normally filled, 150 vials 10% overfilled.

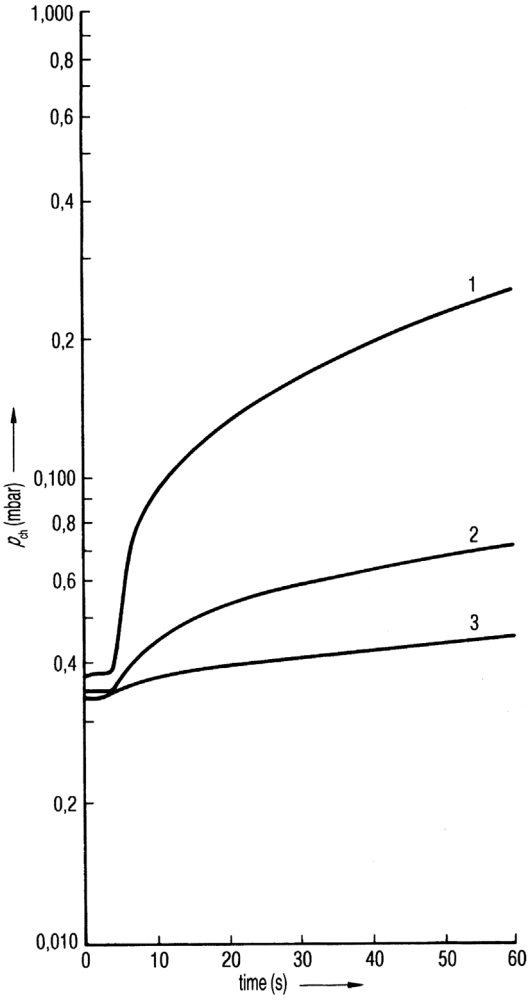

Figure 1.136 Automatically measured and recorded pressure rise as a function of time after the valve between the chamber and the condenser has been closed. Three measurements were selected: 1, shortly after the valve has been closed; 2, 2.5 h later; 3, 5.75 h later. A computer can calculate dp/s from the measured $p_t - p_0/t$; p_0, pressure after closing the valve; p_t, pressure after the measuring time t. (Based on measurements of Steris GmbH, Hürth, Germany.)

is loaded with 2.5 kg of liquid product, containing 250 g of solids, and the leak rate could then be fourfold larger, as mentioned above.

The pressure rise measurement can be made automatically, as shown in Figure 1.136.

The leak rate becomes critical if the solid content is small, for example, 1%, then qL_{max} has to be $\sim 2 \times 10^{-3}$ mbar L/s, all other conditions being equal. In such cases, the leak rate of the chamber should be measured before charging the product.

The secondary drying step depends on only one factor: the sorption behavior of the product and its temperature dependence that is shown for one product in Figure 1.137. Table 1.26 illustrates the consequences. RM data can only be achieved as quickly as possible if the water vapor pressure in the chamber is small compared with p_{eq} (e.g., 10% of p_{eq}); this parameter is called $p_{eq,0.1}$ in the table and the pressure of the permanent gases p_p is small compared with $p_{eq,0.1}$, as also

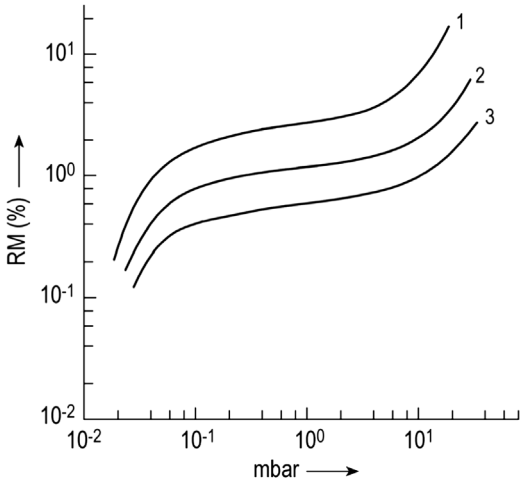

Figure 1.137 Desorption isotherms of the residual moisture content (% w/w) as a function of water vapor pressure: (1) 20; (2) 40; (3) 60 °C.

shown in Table 1.26. One may argue that the chosen factor of 10 is too large and a factor of 8 might have a similar effect. The answer can only be given for a given geometry of the plant and the absolute pressure in question. Therefore, a factor of 10 has been chosen for simplicity. To operate SD at $p_{eq,0.1}$, the condenser temperature T_{co} has to be smaller than given in the table as $T_{co}<$ (how much smaller depends on the condenser configuration, that is, to condense the vapor on the surface with a minimum of flow resistance and interference with permanent gas and water molecules). For $T_{co}<$ in the table, it is assumed that the equilibrium pressure of the ice on the condenser surface needs to be only 10% below $p_{eq,0.1}$.

The main consequences of Table 1.26 are as follows:

At a product temperature of 20 °C, it is difficult to achieve an RM of <0.5%; ~2% can be realized if the pumpset consists of, for example, one roots pump and a two-stage gas ballast main pump.

At 40 °C 1% RM is possible with a more standard pumpset: a large two-stage gas ballast pump or for production plants better 1 roots pump plus a small gas ballast pump.

Table 1.26 RM (%) in a matrix of product temperature T_{pr} and water vapor equilibrium pressure p_{eq}, together with data for $p_{eq,0.1} = 0.1 p_{eq}$ and p_p = pressure of permanent gas.

$p_{eq}/p_{eq,0.1}/p_p$	$T_{co}<$	T_{pr} (°C)		
(mbar)	(°C)	20	40	60
0.02/0.002/2 10^{-4}	≃73	0.2	0.1	0.06
0.04/0.004/4 10^{-4}	≃68	0.9	0.4	0.2
0.1/0.01/0.001	≃61	1.9	0.8	0.4
1.0/0.1/0.01	≃43	3.0	1.4	0.6
10/1.0/0.1	≃20	6.0	2.0	1.0

If the product can be brought to, for example, 50 °C during SD, 0.6–1% can be achieved and the product could be cooled before unloading to, for example, 25 °C. This type of program shortens the SD and the RM can be reached more easily.

If RM, for example, <3% is the goal, two possibilities can be used: 20 °C and $p_p \approx 0.01$ mbar or roughly estimated ~30 °C and $p_p \approx 0.03$ mbar.

1.2.3.1 Wireless Temperature Measurement

In Section 1.2.3 is described how difficult and questionable it is to measure a temperature in the product. It is irrelevant whether thin wire thermocouples (Tc) or electrical resistance (RTD, PT-100) are used [129]. Apart from the described negative effects at the measuring points, it is practically impossible to position the sensor (PT-100) in the center of the vial. The wire (cable) always exerts a leverage effect on the sensor, thereby preventing a precise positioning. A new wireless and battery-free temperature measurement system (TEMPRIS – Temperature Remote Interrogation System) makes it possible. The temperature is an important physical parameter to measure the product temperature during a freeze-drying process. In particular, to measure and record temperature as accurate as possible, as genuine as possible, as reproducible, in real-time as possible, in a wide measurement range as possible and over an adequate period of time.

The advantage of this technology is that process parameters can be acquired in real-time, wireless, and battery-free sensor technology.

Principle: The TEMPRIS wireless temperature system (iQ mobil solution GmbH, Wolfratshausen, Germany) [139,140] uses 8–16 sensors, the interrogation unit (IRU), including transmitter and a computer system with associated software installed to record the data to file. The battery-free sensors receive their power by excitation of the passive transponder by means of an amplitude-modulated electromagnetic signal in the internationally available 2.4 GHz ISM band, with evaluation of the backscatter response. The signal is demodulated in the transponder by means of a diode detector and used to stimulate a quartz-based circuit. This way the resonator itself is used as an energy storage device. The maximum possible storage time is defined by the quality factor Q of the resonator. In the second step, the amplitude modulation is deactivated and only the continuous-wave (CW) carrier is radiated. The stimulated resonance circuit continues to oscillate at its characteristic frequency that depends on its temperature. This free oscillation is mixed with the CW carrier and then retransmitted to the IRU. The IRU measures the modulation frequency of the response and the exponential drop in amplitude. In combination with the statistical parameters of several consecutive responses, the key variable is derived. In order to avoid interferences, the system changes automatically to a new carrier frequency within the ISM band after each interrogation cycle. As a result, the duration of the usable oscillations depends directly on the resonant frequency and the quality factor of the resonant circuit used.

One of the most important features of TEMPRIS is that literally the same sensors can be used during laboratory-scale development and subsequent routine manufacturing [141]. The use of TEMPRIS therefore eliminates the obstacle of interpreting temperature profiles obtained from different temperature sensors

Figure 1.138 TEMPRIS Wireless temperature system for precise measurement of product temperature in lyophilization. (IQ-mobil solutions GmbH, Holzkirchen, Germany.)

during scale-up, thermocouples in the laboratory, and RTDs that are typically used in production (Figure 1.138).

An integral benefit of the wireless sensors is their application as a complementary PAT (practical analytical technology) tool to monitor product temperature profiles during cycle development and optimization [142,143].

1.2.4 Water Vapor Transport during Drying

The water vapor transport in a freeze-drying plant can be described schematically with the aid of Figure 1.139. The ice (1) is transformed into vapor and has to flow out of the container (2) into the chamber (4). Between the chamber wall or any

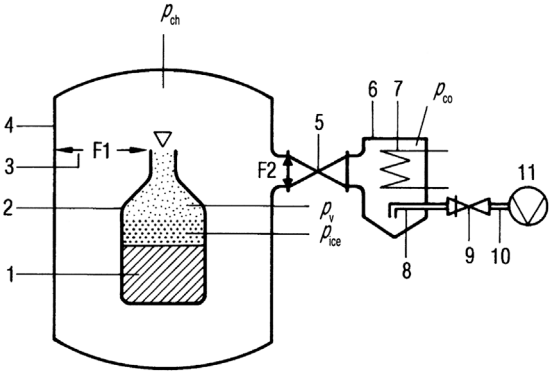

Figure 1.139 Scheme for the estimation of the water vapor transport in a freeze-drying plant. 1, Frozen product; 2, vial or the end of a shelf; 3, open surface (F1) for the water vapor flow between 2 and 4; 4, chamber wall; 5, valve with an open area F2; 6, condenser chamber; 7, cooling and condensing surface in the condenser chamber having a surface F3; 8, vacuum pipe with diameter *d*; 9, stop valve; 10, vacuum pipe with length *l* (from 8 to 11); 11, vacuum pump; p_{ice}, water vapor pressure at the sublimation front of the ice; p_v, pressure in the vial; p_{co}, pressure in the condenser.

other limitation, an area (3, F1) is necessary. The vapor then flows through the area F2 into the condenser (7), having a surface of F3 on which the water vapor will mostly condense. A mixture of remaining water vapor and permanent gas is pumped through (8)–(10) by a vacuum pump (11).

Example: p_{ice} at the sublimation front is 0.937 mbar (−21 °C) (see example in Table 1.14), in the chamber a $p_{H_2O} = 0.36$ mbar has been measured, resulting in a pressure difference of ~0.6 mbar. With these data, the water vapor permeability $b/\mu = 1.1 \times 10^{-2}$ kg/h m mbar is calculated. With these data known, it is possible to calculate dp for different conditions, if the mass of frozen water m_{ice}, the time t_{MD}, the thickness (d), and the surface (F) are known. This dp depends on the amount of vapor transported (Tables 1.14 and 1.15). In the examples given, it changes between 0.15 mbar in a slow drying process (6 h) to 0.6 mbar for a shorter drying time ~3 h.

Transport out of the container (2) into the drying chamber produces no measurable pressure drop if the product surface is equal to the opening of the container (e.g., with trays). Vials without stoppers in the vial neck do not produce a measurable pressure drop if, for example, 1 g/h water at a T_{ice} of −20 °C and a pressure difference of 0.6 mbar are transported. In this example, the velocity of water vapor is a few m/s.

If stoppers are in the vials, in the freeze-drying position, the situation is different: Depending on the type of stopper (Figure 1.140), the drying

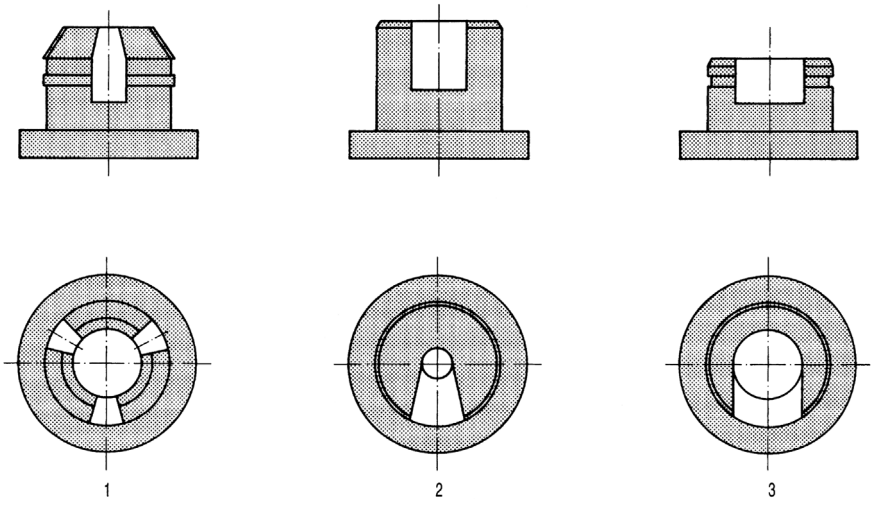

Figure 1.140 Influence of different forms of stoppers on the water vapor transport out of the vials into the chamber. At a pressure of 1 mbar in the vial the following relative amounts of water vapor are transported into the chamber in 3 h:

Stopper:	None	1	2	3
	100%	77%	75%	66%

performance can be reduced to 66 or 77%, or generally 60–80%. To achieve the same performance, the temperature would have to be increased from −20 to −17 °C, resulting in a 30% higher pressure. If the temperature increase is not tolerable, the pressure in the drying chamber must be reduced and a slower drying process could result.

If the main drying time is long (e.g., 33 h), the vapor flow through the stopper openings is small, t_{MD} can be identical within measuring limits, but t_{SD} can be prolonged by the increased flow resistance at low pressures (e.g., 4×10^{-3} mbar). During SD[2] without stoppers, dW = 0.4% was reached in ~1.5 h, with a type 1 stopper in ~2.5 h, and with type 2 in ~3.5 h. An optimum stopper form for a given product cannot be calculated; its influence should be measured when the process data are finalized.

Vapor transport into the condenser depends strongly on the geometric design of the plant. Under favorable conditions and including a valve between the chamber and condenser, a vapor speed of 60–90 m/s can be expected, resulting in a pressure drop between the chamber and condenser of a factor of 2, as an order of magnitude.

With these estimated conditions and a condenser at, for example, −45 °C = 0.07 mbar, the following pressures can be assumed:

- p_{co} times 2 = 0.144 mbar (p_{ch})
- p_{ch} times 1.5 = 0.216 mbar (p_{F1})
- p_{Fl} + 0.2–0.6 mbar = 0.4 to 0.8 mbar

This results in $p_s \approx -29.5$ to ≈ -22.5 °C.

At this condenser temperature and in this plant, products could be dried at ice temperatures between −29 and −23 °C. As shown in Table 1.14, an ice temperature of −22.3 °C (test run in Figure 1.96) has been successfully operated at a condenser temperature of −45 °C and a pressure difference $p_{ch} - p_{co}$ ~0.4 mbar.

If the freeze-drying conditions are extreme, namely, small solid content and low sublimation temperature, for example,

- solid content 1.7%,
- T_{ice} during MD −40 °C,
- layer thickness 3.8 mm, and
- vials with stoppers,

one has to consider that the water vapor permeability b/μ will be larger as in the earlier example. If $b/\mu = 6.9 \times 10^{-2}$ kg/m h mbar and ice temperature −41 °C = 0.115 mbar are measured, the water vapor pressure in the chamber will be 0.065 mbar. The condenser temperature should therefore represent a pressure of ~0.035 mbar, which would require a condenser temperature of ≃51 °C.

If stoppers with more favorable channels are used, the vapor pressure in the vials could have been 0.09 mbar, leaving a $\Delta p = p_{ice} - p_{F1} = 0.025$ mbar, which is in agreement with $b/\mu = 6.9 \times 10^{-2}$ kg/h m mbar in this test.

2 Measurements by Steris GmbH, 50354 Hürth, Germany.

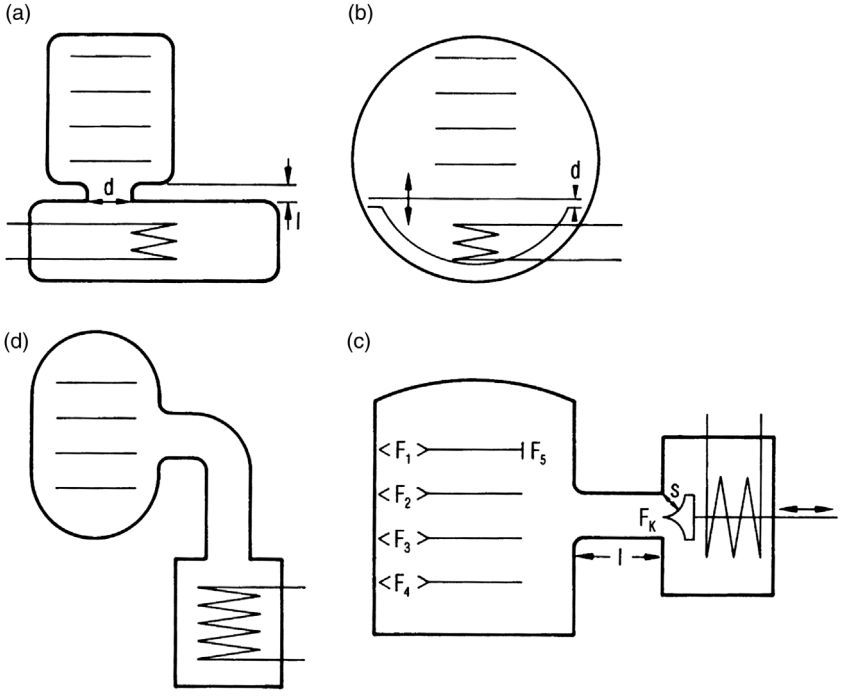

Figure 1.141 Four different geometric layouts of condenser and drying chamber. (a) Chamber and condenser in a housing not divided by a valve, water vapor transport into the condenser through an opening *d* with the length *l* (*d*, maximum approximate condenser or chamber diameter). (b) Chamber and condenser located in the same housing; the condenser compartment can be separated from the drying chamber by a lid. In the open position, the water vapor flows through a clearance with height *d*. (c) Drying chamber with four shelves, a connecting pipe to the condenser with the cross section *d* (area F_K) and a length *l*. In the open position of the valve, a circular clearance *s* can be an additional bottleneck after F_K. (d) Layout similar to part (c), but the chamber and condenser are connected by a 90° bend.

The water vapor transport from the chamber to the condenser depends largely on the geometric design of the installation. Assuming that only one bottleneck exists between the chamber and condenser having a diameter (d), which is large compared with the length (l) of the connection (Figure 1.141a), one could expect a jet flow that follows Eq. (1.3.9) in Ref. [144], For this case, the connection must have the shape of a jet with no obstacle in it (e.g., a valve lid). Technically, this case is not possible. Even in a plant as shown in Figure 2.93, the water vapor has to pass through a ring-type jet and is then deflected toward the condenser surface. To estimate the influence of p_{ch}, d, and l, the Günther–Jaeckel–Oetjen equation, Eq. (1.3.11) in Ref. [144], or its graphical plots, Figures 1.3.4 or 1.3.6 in Ref. [144], can be used. Figure 1.142 is an evaluation of the quoted equation and plot for the area of interest for freeze-drying. It shows the specific flow of water vapor through tubes with a ratio of $l/d = 1$, 1.6, 2.5, and 5 as a function of pressure at the inlet of the tube.

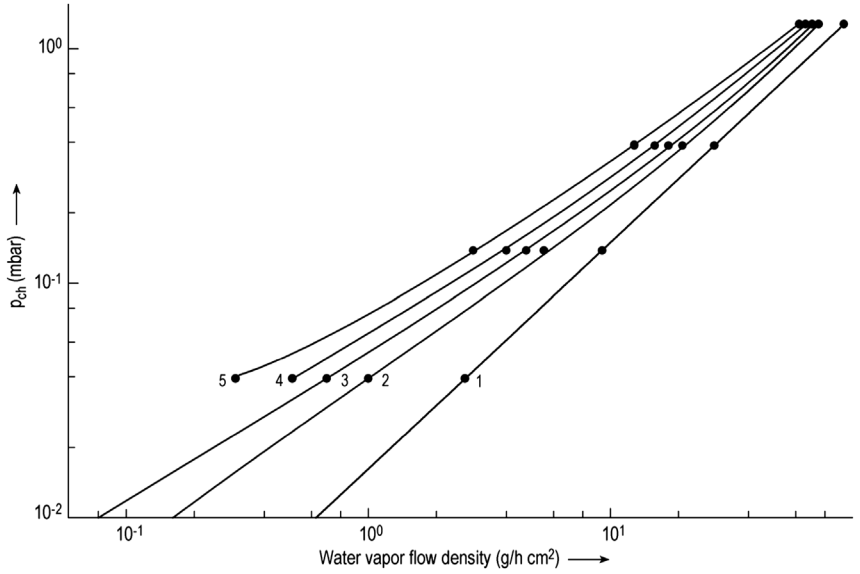

Figure 1.142 Density of water vapor flow (g/cm^2 h) as function of p_{ch} with jet flow (1) and $l/d = 1$ (2), 1.6 (3), 2.5 (4), and 5 (5) as parameter; (4) and (5) are not plotted below 4×10^{-2} mbar, these data depend very much on the design details of the plant. They should be measured if needed.

In the pressure region of 1 mbar, the expected specific flow of water vapor is reduced for the mentioned ratio to ~60% of that passing through an ideal jet. At 0.04 mbar pressure in the chamber, the specific throughput is reduced to 25 or 10%. This becomes even more drastic if the velocity of the water vapor is plotted as a function of p_{ch} (Figure 1.143). In an ideal jet, the velocity of the vapor flow under the conditions chosen is approximately the velocity of sound. However, even with $l/d = 1$, the velocity is strongly reduced as a function of pressure and reaches 0.04 mbar at only approximately one-third of this maximum speed for $l/d = 1$ and 10% for $l/d = 5$.

To summarize, one can say that in the pressure range 0.1–0.3 mbar and $l/d = 5$, a vapor velocity between 50 and 100 m/s can be expected. The graphs and figures are given to underline the influence of the pressure in the chamber and the geometry of the plant. General guidelines for the design of a plant can be as follows:

- All cross sections, through which the vapor has to flow, ahead of the smallest one must be large compared with the smallest, for example, F_k in Figure 1.141c $> F_1$ to F_5.
- If a valve is installed in F_k, its cap should influence the vapor flow as little as possible (see, for example, Figures 2.20 and 2.88).
- The path of the vapor should be deflected as little as possible; a deflection of 90° (Figure 1.141d) not only prolongs l, but it also transpires that l has been increased by a multiple of l.

To predict the vapor flow in a plant from Figure 1.142 is difficult since not only is the flow influenced by the design of the valve, the method of connecting the

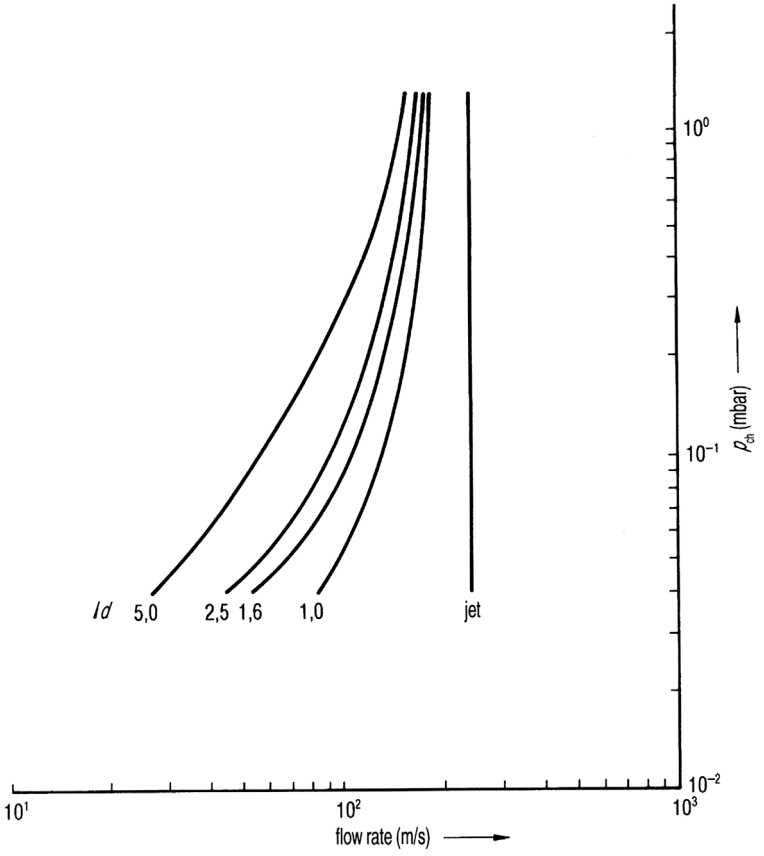

Figure 1.143 Rate of water vapor flow (m/s) as a function of p_{ch} through a jet and different *l*/*d* pipe dimensions as parameter.

chamber wall and condenser, and the location of the condenser surfaces, but also each factor depends differently on the chamber pressure. Since the vapor flow in a plant is a very important characteristic quality of a plant, it should be measured and taken into account for processes at different pressures in one plant or if a given process is to be transferred to another plant. The recommended 2–3 flow measurements can be carried out with distilled water filled into the maximum possible number of vials in the plant to be studied. The vials are filled to a uniform level, for example, 15 mm. The amount of water in all vials and the total weight of all bottles and stoppers are determined. The vials are loaded on the shelves, cooled to $\leq$45 °C, and freeze-dried until 50–60% of the water has sublimed. Depending on the pressure range for which the plant is designed, 2–3 runs should be carried out with approximately the following data for pharmaceutical freeze-drying:

Run 1: $T_{sh} = 20$ °C, controlled operation pressure $p_c = 0.2$ mbar, T_{ice} measured, for example, −32 °C. In this test three things can happen: (1) the test runs as planned; (2) a p_c of 0.2 mbar cannot be maintained and the pressure rises to, for

example, 0.4 mbar; the amount of water vapor produced under these conditions cannot be transported to the condenser, as 0.4 mbar is needed (the reason could also be the condenser capacity, which can be identified by a rising condenser temperature); (3) $p_c = 0.2$ mbar cannot be reached; the surface of the shelves or the heat transfer from the brine to the sublimation front is not large enough to produce the amount of water vapor that could be transported from the sublimation front to the condenser. At the equilibrium pressure (after 1–2 h from start), for example, 0.1 mbar, the plant is capable of transporting XX kg/h. With the vials used and $T_{tot} = 52$ °C, only XX kg/h of water can be sublimed. With this information, K_{tot} can be calculated. By a few additional tests (not discussed here), one can decide whether the heat transfer from the brine to the shelf surface or the heat transfer from the shelf to the vial is the reason (or both). Run 1 gives either the kg/h transported at 0.2 mbar or the maximum kg/h evaporated under these conditions and transported at, for example, 0.1 mbar.

Run 2: $T_{sh} = 0$ °C, controlled operation pressure $p_c = 0.08$ mbar, T_{ice} measured, for example, −40 °C. In this test, three things can happen: (1) the test runs as planned; (2) a p_c of 0.08 mbar cannot be maintained and the pressure rises to, for example, 0.1 mbar. The amount of water vapor produced under these conditions cannot be transported to the condenser as 0.1 mbar is needed (the reason could also be the condenser capacity, which can be identified by a rising condenser temperature); (3) $p_c = 0.08$ mbar cannot be reached; this case cannot be imagined with the data given in run 2. $T_{tot} = 40$ °C must transfer enough energy for a sublimation at 0.08 mbar, which may exceed the possible flow (point 2 above).

Run 3: This run is only necessary if the plant has to freeze-dry products at very low p_c, for example, 0.03 mbar corresponding to $T_{ice} \approx -48$ °C. At 0.03 mbar, the mean free path is ∼15 mm and the calculation of the flow depends on design details of the plant, which cannot be expressed in an equation, but the flow can be measured as in runs 1 and 2. *Data for run 3:* $T_{sh} = -10$ °C, $p_c = 0.03$ mbar, T_{ice} measured = −50.2 °C. Before the test one can guess what might happen: Assuming that the plant is expected to sublime 1 kg/h of ice at $T_{ice} = -50$ °C, from Figure 1.142 the extrapolated flow in a well-designed plant is ∼0.3 g/cm^2 h, and the valve between the chamber and condenser has to have a diameter of 65 cm or more. These figures limit the size of a plant for these low pressures: a valve diameter of 1.1 m may be technically the maximum. At 0.03 mbar and 0.3 g/h cm^2, a flow of 2850 g/h is possible. If the main drying time is, for example, 30 h, the maximum amount of water in the plant can be 85 kg if each vial is filled with 4 cm^3 of water, and ∼20.000 vials per charge are the technical limit for this pressure range. The consequence of these estimates is the limitation of T_{ice} in production plants to ≃50 °C with the techniques used today. The data on size and temperature limitations are examples and not absolute values: If one accepts a longer t_{MD} than optimally possible, for example, 90 h instead of 30 h used above, the 20.000 vials can theoretically be increased to 60.000 if T_{tot} is reduced from ∼40 to ∼13 °C. T_{sh} will not be 0 °C but has to be −27 °C. This will raise some problems during the last part of MD mainly depending on the cake thickness. They have to be evaluated and will likely lead to a compromise between an acceptable t_{MD} and a useful T_{tot}.

Table 1.27 Water vapor flows in two production plants (Pr 1 and Pr 2) and two pilot plants (Pl 1 and Pl 2).

	Pr 1[a)]	Pr 2[b)]	Pl 1[c)]	Pl 2[d)]
Shelf area (m^2)	30	40	0.04	0.04
p_c (mbar)	0.3/0.4	0.06	0.3/0.16/0.07	0.06
g/h cm^2	4.7	1.4	12.0/4.2/1.1	1.5
Valve diameter (cm)	80	110	12.5	10
Ratio l/d	>>5	1.6	~3	~1.5

a) Pr 1 Connection between chamber and condenser approximately 500 cm with a 90° bend.
b) Pr 2 Designed as shown in Figure 1.141, chamber and condenser directly connected.
c) Pl 1 Designed as shown in Figure 1.144.
d) Pl 2 Designed as in Figure 1.145.

In Table 1.27 measured l/d data are presented for two production and two pilot plants. With a valve and a chamber/condenser design as shown in Figure 2.20, the effective l/d can be 1.6 or slightly smaller. Figure 1.144 is a sketch of the chamber/condenser design in Pl 1, characterized by $l/d = 3$. After the chamber/condenser configuration has been changed to the principle in Figure 1.145, the data for Pl 2 were measured.

In an expediently designed plant, one can expect to reach in the pressure range above 8×10^{-2} mbar a vapor velocity in the cross section F_k of between 50 and 80 m/s ($l/d = 2.5$–5). However, 90 m/s will be reached only if the design uses special features, for example, a funnel-like connection between the chamber wall and the location of the valve, slow changes in the outline, and smooth surfaces

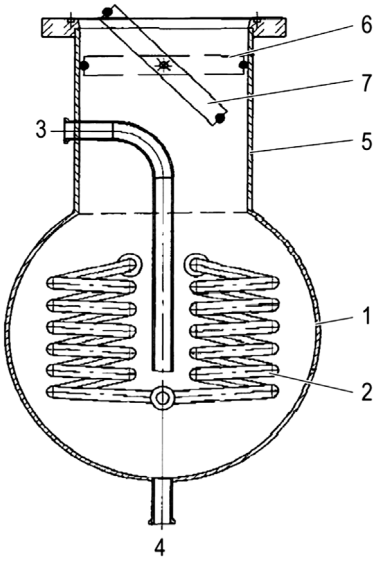

Figure 1.144 Scheme of the condenser design in plant Pl 1 in Table 1.27. 1, condenser wall; 2, condenser coil; 3, suction tube of vacuum pump; 4, water drain; 5, connection to drying chamber; 6, valve with seal in closed position; 7 valve in open position.

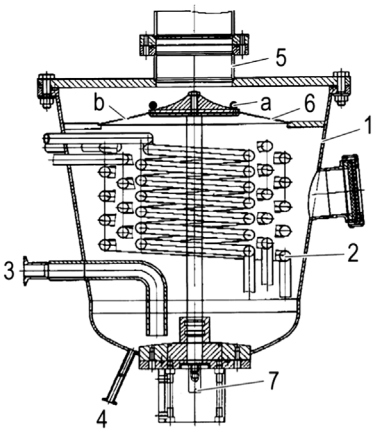

Figure 1.145 Scheme of the condenser design in plant Pl 2 in Table 1.27. 1, condenser wall; 2, condenser coils; 3, suction tube of vacuum pump; 4, water drain; 5, connection to drying chamber; 6, valve with seal (a) in open position and temperature shield (b); 7, hydraulic for valve operation.

without sharp edges or holes. It is also recommendable to clarify the maximum amount of vapor transportable at several pressures in a plant specification; examples and data are given above and in Figure 2.20 and the related text.

1.2.4.1 Endpoint Determination of Main and Secondary Drying

The known methods are described in Section 1.2.3. Neumann and Oetjen [129] have made BTM and PRM familiar and developed to reliable and valuable measuring methods (see Figure 1.119).

The change from main drying to secondary drying is difficult to be determined by product temperature sensors (see Figures 1.123 and 1.124). Nail and Johnson [125] used mass spectrometry to determine the end point of MD and SD. Also, Connelly and Welch [136] report about this method. The vacuum gauges (common TM) were compared with the p_{H2O} measured by a mass spectrometer. Deviations were visible.

TDLAS (tunable diode laser absorption spectroscopy) is a technique for measuring the concentration of certain species such as water vapor and many other gases, in a gaseous mixture using TDLAS. The advantage of TDLAS compared to other techniques for concentration measurement is the ability to achieve very low detection limits. Apart from concentration, it is also possible to determine the temperature, pressure, velocity, and mass flux of the gas under observation. TDLAS is one of the common laser-based absorption technique[3]. The principles are gas molecules absorb energy at specific wavelengths in the electromagnetic spectrum. By transmitting a beam of light through a gas mixture sample containing a quantity of the target gas (water vapor), and tuning the beams wavelength to the target gas – water vapor – absorption lines, and accurately measuring the absorption of that beam, one can deduce the concentration of the target gas molecules integrated over the beams pathway length. This measurement is usually expressed in units of ppm-m. Dealing with TDLAS requires some experience with this technique. The detection limit for water vapor is 1 ppm-m.

3 TDLAS, Add. No. 38 RD; Huanghe, Dongying; Shandong-China.

Another method is the use of a mass spectrometer. Mass spectrometers are highly sensitive measuring instruments that determine the composition (mixture) of gases. The device operates with a turbo-molecular pump in a high vacuum range[4,5]. A mass spectrometer decomposes the molecules of a gas in atoms and ionizes them. In a mass filter, the mass/charge ratio of the atoms is measured. The deflection depends on the field strength and the molecule mass/weight. The measuring limit is 10 ppm.

With TDLAS and mass spectrometry, the drying progress is primarily measured via the gas humidity. Both methods are partly suitable to determine the switchover point from MD to SD. However, the residual moisture in the product cannot be measured.

The freeze-drying process cannot be controlled by this technique.

1.2.5 Collapse and Recrystallization

A possible collapse of the product during main drying and recrystallization during the drying can have a significant influence on the quality of the final product. Therefore, these two events will be discussed again with regard to the drying process.

If, during freezing, not all freezable water has been frozen, the collapse temperature depends strongly on the amount of unfrozen water present. The highly concentrated, highly viscous, amorphous substance does not show at a temperature of, for example, −85 °C any measurable mobility. The water molecules can no longer migrate to the existing crystals and the unfrozen water is solidified. If the temperature is increased, the viscosity of, for example, 10^{14} P does not decrease with temperature, but with the difference in the temperatures $T - T'_g$. T'_g represents the highest possible T_g if all freezable water is frozen. Incompletely frozen products have an unnecessarily low T_g, for example, −85 °C, while T'_g for this product is only −58 °C. If such an incompletely frozen product is freeze-dried above −85 °C, the structure will soften and at T_c will collapse.

T'_g, T_c, and T_r can be close together or are approximately in a 10% range, as shown in Table 1.28. For sorbitol, T'_g is shown at a higher temperature (−43 °C) than T_c (−57 °C), a fact that cannot be explained.

All temperatures mentioned are influenced by the methods of their measurement [146], for example, very thin samples in a cryomicroscope, very small amounts of product (mg range) in an installation for differential scanning calorimetry, and some temperature gradients in the sample during the measurement of the electrical resistance (ER). T'_g, T_c, and T_r measured with pure substances can supply helpful information about the temperature range to be expected. For products containing two or more ingredients, the data must be measured for the specific mix since traces of additives or residues can change the data substantially; see, for example, Figures 3.9 and 3.10.

The question of aroma retention was of special interest between 1968 and 1975 for the freeze-drying of food. Thijssen and Rulkens [147,148] are of the opinion that slow freezing and quick freeze-drying provide good retention of the test

4 Oerlicon Leybold Vacuum GmbH, Cologne; Bonner Str. 498/Germany.
5 Pfeiffer Vacuum GmbH, Berliner Str. 43: 35614 Asslar/Germany.

Table 1.28 T'_g data, related UFW (unfreezable water), and T_r and T_c data.

Substance	T'_g (°C)	UFW (%)	T_r (°C)	T_c (°C)
Dextran	−9		−10	−9
Fructose	−42	49.0	−48	−48
Glucose	−43	29.1	−41	−40
Glycerin	−65	45.9	−60/−65	
Lactose	−28	40.8		−31
Trehalose	−30	16.7		
Maltose	−30	20.0		−30/−35
Ovalbumin	−10		−10	−10
Polyethyleneglycol	−13		−65	−13
Polyvinylpyrrolidone	−19.5		−24	−23
Sorbitol	−43	18.7		−57
Sucrose	−32	35.9	−32	−32

T'_g and UFW data from Ref. [6] of Chapter 3; T_r and T_c data from Ref. [145].

substance, 0.1% acetone in a dextrin solution, because the slow freezing produces large ice crystals, which include highly concentrated solutions between them. The pore size in a solution of 20% dextrin frozen at 0.5 °C/min is ∼3 μm, whereas at a freezing speed of 20 °C/min, it is only 1.8 μm. The freeze-drying speed with 3 and 1.8 μm pores has a ratio of 0.17:0.07. Furthermore, the retention increases with increasing solid content: In a 10% solution, retention is practically nil, but between 20 and 30% solids, it increases to 45–60%. Flink and Karel [149] showed (Table 1.29) that the loss of volatile substance, 1-butanol in a maltose solution, occurred in the first 6 h of the MD; during SD from 6 to 24 h, the volatile content remains practically unchanged.

Voilley *et al.* [150] confirmed the increasing retention with decreasing freezing speed and with the increasing number of carbon molecules of the alcohol (Figure 1.146).

Table 1.29 Loss of 1-butanol during the freeze-drying of a maltose solution.

Drying time (h)	Average water content (g/100 g solid)	Average content of 1-butanol (g/100 g solid)
0	430	4
3	178	3.30
6	36	2.20
12	11	2.45
24	0.7	2.50

Table IV in Ref. [149].

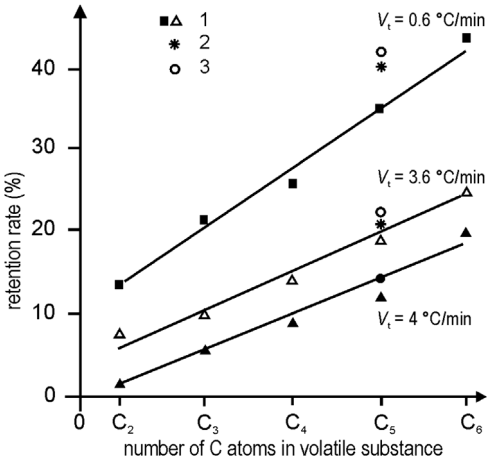

Figure 1.146 Percentage of alcohol retained as a function of the number of carbon molecules in the alcohol molecule with three freezing speeds as parameter. The solution consists of 30 g of saccharose, 15 g of glucose, 15 g of fructose, 15 g of citric acid, 5 g of $CaCl_2$, 15 g of pectin, 5 g of freeze-dried albumin, 900 g of water, and 100 ppm of volatile substance. 1, Homologous series; 2, 3-methyl-1-butanol; 3, cyclopentanol.

During MD, the retention is unchanged with time, but decreases with increasing temperature during SD. Flink [151] proved, by additional tests, his model about the retention of volatiles, called "microregion entrapment." A product frozen and ground up does not lose more volatiles than when frozen in a block. The microregions are smaller, as can be achieved by grinding, and there is no concentration of volatiles in the surfaces. If the microstructure is destroyed, for example, by collapse, the retention decreases. Maltose, sucrose, and lactose each have a better retention for volatiles than either glucose or dextran (Table 1 in Ref. [151]).

Gero and Smyrl [152] showed the retention from formic acid to butyric acid as a function of the dextran concentration and a special behavior of the acid (Figure 1.147), while Seger *et al.* [153] demonstrated that organic solvents

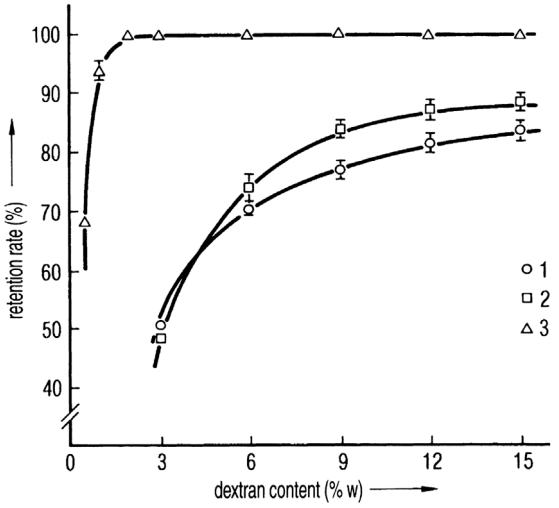

Figure 1.147 Retention of acid as a percentage of the initial concentration (0.05 M) as a function of dextran concentration. Three retained acids: 1, *n*-butyric acid; 2, isobutyric acid; 3, lactic acid. (From Gero, 1982 [152]. Reproduced with permission of John Wiley & Sons.)

used during the production of a formulation, for example, methanol, ethanol and *n*-butanol, cannot be completely removed by freeze-drying as they influence the freezing structure and freeze-drying process. During freezing, methanol and ethanol often form films on the surface, which makes drying difficult or impossible. The residues are pushed to the surface by the crystallizing ice and dry by evaporation from the liquid phase, thus forming skins. (*Note*: It is also possible that the mixture under the chosen conditions does not freeze completely and cannot be dried at all.)

1.2.6 Drying Processes without Vacuum

From time to time, drying at low temperatures at atmospheric pressure has been discussed and tried experimentally, because vacuum installations are high-cost investments and expensive to operate. There are three basic problems that must be solved in such a low-temperature drying process:

1) 1 kg of ice, when sublimed at 0.6 mbar, has a volume of $\sim 2000\ m^3$. Since the atmospheric pressure is ~1700 times larger, $\sim 3.4 \times 10^6\ m^3$ of air must be transported to carry the water vapor (the vapor content is <1/1000).
2) If only the diffusion of vapor in resting air is used to transport the vapor from the sublimation front to the condenser (or vapor absorber), only $4 \times 10^{-2}\ g/m^2\ h$ can be transported over a distance of 100 cm. Even if the condenser could be positioned at a distance of 1 cm, the result is only $4\ g/m^2\ h$. Transport of vapor by diffusion cannot be used practically.
3) By mixing an absorbing granulate or powder with the product to be dried, the distance of the diffusion can become very small or the water molecules may move by surface diffusion. In both cases, the problem is the same: first to find an acceptable drying agent (absorber) and then to separate it quantitatively from the dried product.

In recent years, several publications have tackled these problems. Kahn-Wyler [154] lists four reasons that prove that fluidized-bed drying (solving problem 2 above) is not suitable:

- The structure of the frozen product is difficult to control.
- The abrasion of the already-dried product is too large.
- The separation of the carrier-substrate (glass spheres) from the dried product is not complete enough.
- Abrasion of the installation results in product contamination.

Labrude and Rasolomana [155] reported an atomizer–spray-drying system for oxyhemoglobin in a 0.25 M sucrose solution at temperatures between +80 and +100 °C, which resulted in an unchanged dry product if the relative humidity was kept below 3%. When this dry product was compared with a freeze-dried product, in both cases a met-oxyhemoglobin (met-HBO) content of ~3% was found. By ESM (electron scanning microscopy) and spectrometric measurement, it was shown that the structure of the dried molecules had not changed measurably.

However, with this process described, two problems remain: at +80 °C, water has a vapor pressure of ~470 mbar; 3% of this value is ~14 mbar. Depending on the efficiency of the heat exchanger and water condenser, ~100 times more transport gas must be cooled than water vapor can be condensed. If the partial pressure of the vapor in the transport gas were to be, for example, 3–4 mbar (to allow an increase to 14 mbar during drying), condensation of the vapor must occur at ≃5 °C. The transport gas must be cooled to that temperature and reheated to +80 °C. Absorption systems to remove water vapor are technically feasible, but the temperature of +80 °C would still very likely have to be lowered and the dust produced by abrasion becomes a problem (see problems 1 and 3).

Wolff and Gibert [156] described the freeze-drying of small pieces (maximum 5 mm) in a fluidized bed process at −5 to −15 °C. The absorber was granulated corn starch added to the product in an amount 10 times the amount of water to be absorbed. The operating pressure was 0.5 mbar. Whether the enumerated advantages, including low investments, 35% saving of energy, and shorter drying time, outweigh the disadvantages of the above-mentioned point 3 was not discussed by the authors.

Mumenthaler [157] discovered similar problems, as already mentioned: freezing in a fluidized bed with CO_2 clogs the filters, reducing the yield to only 80–90%, with an additional loss of 10% fines.

1.2.7 Microwave Freeze-Drying

The limitations on heat transfer rates in conventionally conducted freeze-drying operations have led to attempts to provide internal heat generation by the use of microwave power. Basically, a faster drying can be achieved with microwaves because they generate the heat directly inside the product.

Principle: A microwave freeze-drier in simple terms is a conventional freeze-drier, with the added capability of allowing microwaves to be applied in the drying chamber. The whole drying process proceeds under vacuum environment of 0.5–2.5 mbar by sublimation. The quality of microwave freeze-dried products differs from conventional freeze-dried products substantially and not only in the texture. Compared to conventional freeze-drying where drying starts from the outside to the inside of the product, the microwave system generates heat within the product itself so that sublimation takes place within the complete product volume. And here is the uncertainty of this technology. There is too much and too fast water vapor generated that cannot be removed, leading to partial melting.

However, this drying technique was never successful in the conversation of food or pharmaceutical products. The damages to the product are too big. A microwave freeze-drying in the pharmaceutical industry is almost impossible, because products in vials are not suitable for microwaves.

Definition and regularities: Microwaves are electromagnetic waves within a frequency band of 300 MHz to 300 GHz. Within the electromagnetic spectrum, they are embedded between the radio frequency range at lower frequencies and infrared and visible light at higher frequencies.

Due to international regulations for industrial microwaves applications, mainly the frequencies 2450 and 915 MHz are being used.

1.2.8 Spray Freeze-Drying

The method consists of two steps: spray-freezing into a cryogenic gas or spray-freezing into vapor over liquid. Freeze-drying mostly is a fluidized bed process. Malecki (1970) dried an egg–albumin solution (10% solids) and apple juice (14% solids) after spraying in liquid nitrogen frozen droplets in a fluid-bed process. The droplet sizes ranged between 250 and 600 μm. The droplets were dried at −20 and −34 °C, respectively. It is mentioned that spray drying of products is possible that do not tend to agglomerate. However, longer drying times were found, compared to conventional freeze-drying.

Wolff (1990) talks about his work in the field of food technology, the drying of potato cubes in a fluidized-bed process at different temperatures, with minimum success, the mechanical stress on the product due to the turbulences is high.

Kahn (1987) dried pharmaceutical granulates for the first time. Freeze-drying is recommended for temperature-sensitive API (active pharmaceutical ingredients). However, this technology (spray freeze-drying) was not followed.

Only in early 2002, Webb [158] reports an application for recombinant interferon-γ-lyophilized and spray-lyophilized formulations. Other authors report on the use of spray drying, but the use in the pharmaceutical industry is limited, because of elaborate time and batch process, complicated handling of cryogenic liquids, possible protein instability during spraying, complicated scale-up[6], and sterile work (production) almost impossible.

1.3 Storage

The storage of a freeze-dried product starts with the end of the secondary drying and its transfer into a suitable packing. In the drying plant, a certain residual moisture content (RM) is achieved as a function of the product temperature and the drying time (Section 1.2.2).

The desorption isotherm describes, under equilibrium conditions, the amount of water absorbed on the product at a given temperature as a function of water vapor pressure, as shown in Figure 1.148. To approximate the equilibrium at a given temperature in a short time, the pressure during SD should be small compared with the equilibrium vapor pressure, for example, at +40 °C and a desired RM <1%, p_{ch} should be several times 10^{-2} mbar. If the product (blood plasma) is to be exposed only to +20 °C, the pressure has to be small compared with 10^{-2} mbar. As shown in Section 1.2.2, a prolonged drying time does not result in a lower RM – only a higher temperature will achieve this. To maintain a low RM, a hygroscopic product has to be protected against the reintroduction of moisture already in the drying chamber. If vials are used, they can be sealed in the chamber, as shown in Section 2.3.3. If bulk material or food has been dried, the chamber has to be vented with dry air or inert gas. At +20 °C and 70% relative humidity, air contains $\sim 1.3 \times 10^{-2}$ g H_2O/L. During the venting of a 200 L chamber with this air, 2.6 g of water vapor are introduced. If the chamber is

6 Schiffter, Heiko A.-Institute of Biomedical Engineering; University of Oxford, UK, 2002.

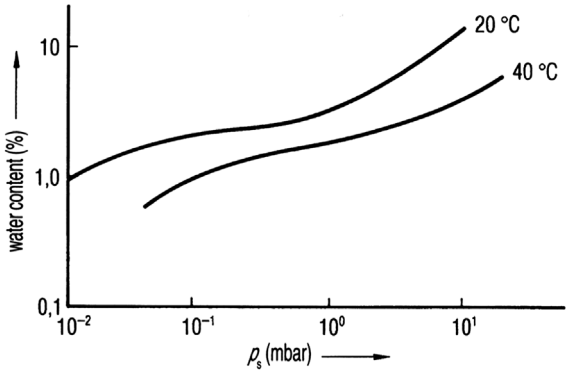

Figure 1.148 Desorption isotherm of blood plasma. (See also Figure 9 from Ref. [126].)

filled with 300 vials each containing 1 cm^3 with a solid content of 10%, the RM will be increased by ~9%. If the solid content is only 1%, the RM rises to ~90%. The dew point of the venting gas should correspond to the end pressure of SD in the chamber, for example, if the end pressure is 2×10^{-2} mbar, the dew point of the gas should be −55 °C, minimum −50 °C.

1.3.1 Measurement of the Residual Moisture Content (RM)

For all measurements of RM, the product must be handled in such a way as to exclude water absorption from the surroundings. Filling a freeze-dried product into another container and/or weighing it should only be done in boxes or isolators filled with dry gas (see above).

The boxes can contain, for example, P_2O_5 or be rinsed with dry gas. Handling in the isolator should be done wearing rubber gloves fixed to the isolator. Balances used in such a dry gas need some modifications to avoid electrostatic charges, which could lead to substantial errors.

1.3.1.1 Gravimetric Method

Until a few years ago, this method had been obligatory, as shown in Title 21 of the *Code of Federal Regulations for Food and Drugs*, Section 610.13 [159]. The weighed sample is stored at temperatures between +20 and +30 °C in a chamber, together with P_2O_5 and repeatedly weighed until the weight becomes constant. The smallest sample should be larger than 100 mg, if necessary taken from several vials. Higher temperatures lead to shorter times before the weight is constant, but they may desorb more strongly any bound water or even change the product. With this method, at 20–30 °C, water can be detected that is weakly bound to the solid.

1.3.1.2 Karl Fischer (KF) Method

By this method, the weighed dry product is dissolved in methanol and titrated with Karl Fischer solution until the color changes from brown to yellow. The visual observation can be replaced by an ammeter, which shows a steep increase in

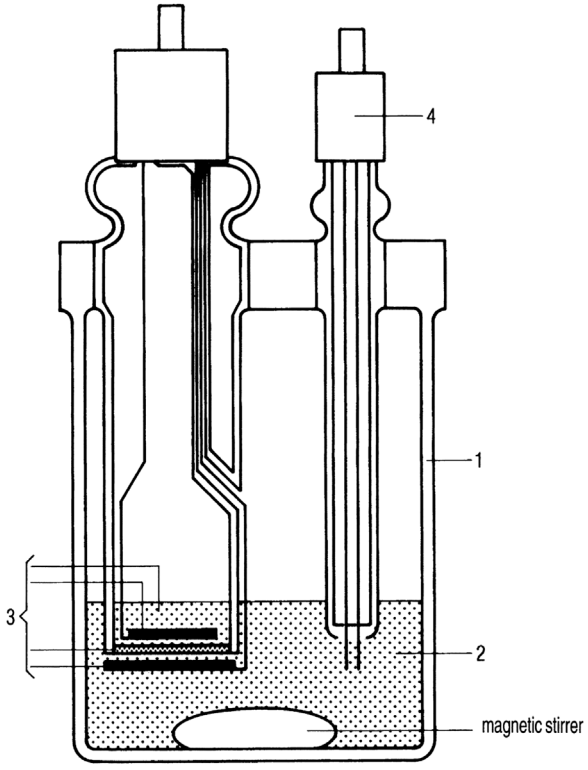

Figure 1.149 Scheme of the Messzelle DL 36 coulometer for measurement of residual moisture content (RM) after Karl Fischer. In the titration cell (1), iodine is electrolytically produced (3) from an iodine-containing analyte (2). Water in the titration cell reacts with the iodine. When the water is used up, a small excess of iodine is produced, which is detected by special electrodes, which leads to iodine production being stopped. The amount of water in the cell can be calculated from the reading of the coulometer and the amount of electrical charge needed. The solids are either introduced into the cell by a lock or the water is desorbed in an oven and carried by a gas stream into the cell. In a sample 10 μg can be detected with an accuracy of reading of 0.1 μg. (KF Coulometer DL36, Mettler-Toledo, Schwerzenbach, Switzerland.)

current when the end point of the titration is reached (dead-stop titration). The samples can be two to four times smaller than for the gravimetric method. To avoid the visual observation completely, iodine can be produced by electrolysis and the water content is calculated using Coulomb's law. Such an apparatus (e.g., Figure 1.149) is available commercially. The smallest amount of water to be detected by such instruments is 10 μg. Wekx and De Kleijn [160] showed how the Karl Fischer method can be used directly in the vial with the dried product. The Karl Fischer titration cannot be used if the product reacts with iodine in the Karl Fischer reagent or does not dissolve in methanol or the moisture cannot be extracted by the methanol. A Karl Fischer apparatus in a glove-box is shown in Figure 1.150.

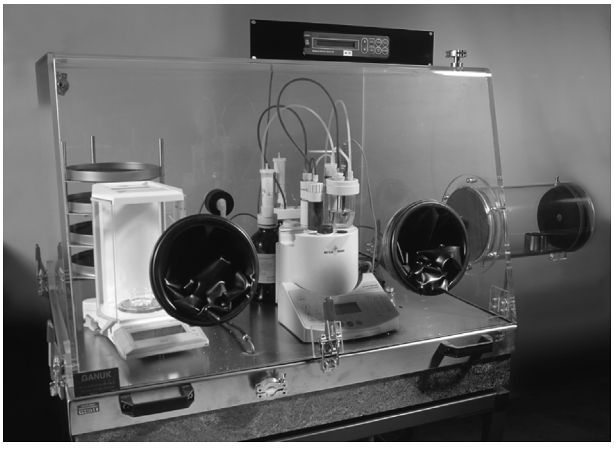

Figure 1.150 Mettler-Toledo DL 38 Karl Fischer apparatus in a glove-box with Mettler-Toledo AG 135 balance (left), drying agent (left, behind), and air lock on the right (Steris, Hürth, Germany).

1.3.1.3 Thermogravimetry (TG, TG/MS)

The weight loss of the product is measured by an electrical balance at constant temperature or at a given temperature–time profile. For the balance and handling of the product, the rules given in Section 1.3.1 should be carefully observed, as the sample with such a balance can be as small as 2 mg. A thermogravimetric analyzer in a glove-box is shown in Figure 1.151. May *et al.* of the Center for Biologic

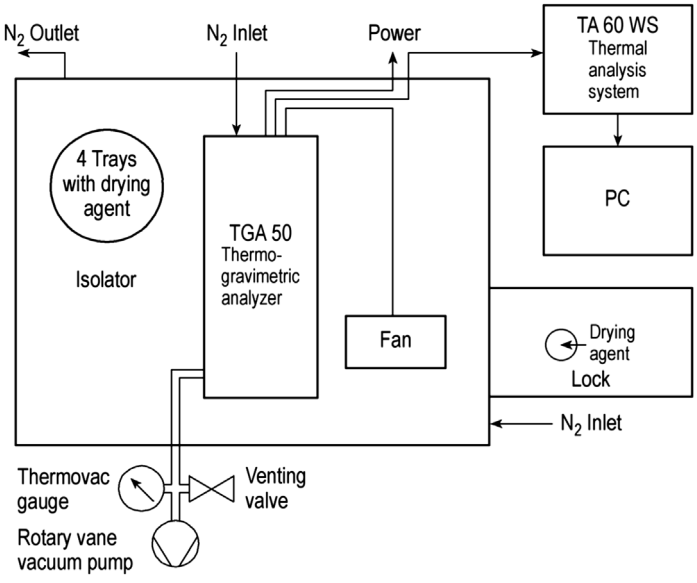

Figure 1.151 Scheme of a thermogravimetric analyzer (Shimadzu TGA 50). (Steris, Hürth, Germany.)

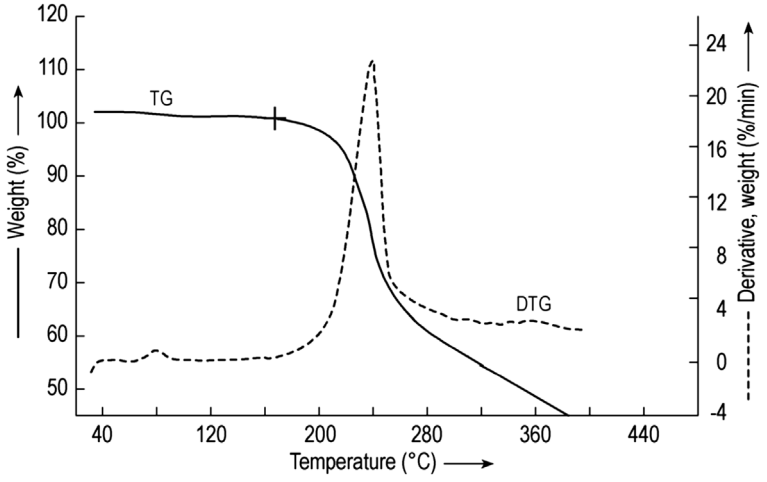

Figure 1.152 Weight (%) as a function of temperature of freeze-dried ×-interferon measured by the thermogravimetric (TG) method and the derivative of weight over time (DTG) (%/min). The assumed end point of water desorption is marked (+). RM by TG, 0.98–1.28%; RM by Karl Fischer, 1.28%. (See also Figure 1 from Ref. [161].)

Evaluation and Research, Food and Drug Administration [159] described the reading of a mass spectrometer (MS) during weighing to differentiate between desorbed water and volatile products, which might come from residual solvents or decomposed parts of the product.

May *et al.* [161] studied the residual moisture (RM) of ×-interferon and US Standard Pertussis Vaccine (Lot 8 and 9) by TG, TG/MS, the KF method, and a new method called "vapor pressure moisture methodology" (VPM). VPM measures the vapor pressure of water in the space above the cake in the closed vial. Light from an infrared diode passes through the vial to a photodetector. The vial temperature is lowered from room temperature to −55 °C at a constant rate. When the water vapor condenses, the light beam is obscured by the condensate, changing the signal to the photodetector. The temperature at the condensation is converted into pressure and the micrograms of water in the headspace volume are calculated. Figure 1.152 shows the TG data for ×-interferon. the mean RM in three different lots was found to be $1.15 \pm 0.15\%$. The RM by the KF method was found in one lot to be 1.28%. Figure 1.153 shows the corresponding data for Pertussis Vaccine Lot 9. The end temperature of water desorption and the beginning of decomposition was decided with the plot of the derivative of weight over time (%/min); the end of water desorption is assumed when the derivative leaves the horizontal line. Table 1.30 summarizes the results obtained by different methods. VMP does not supply information about the RM of the product. It permits repeated measurements over a period of time on the same vial to quantify changes of the water content in the space above the product.

1.3.1.4 Infrared Spectroscopy

Lin and Hsu [162] described the determination of residual moisture in protein pharmaceuticals in sealed glass vials by near-infrared (NIR) spectroscopy. Five

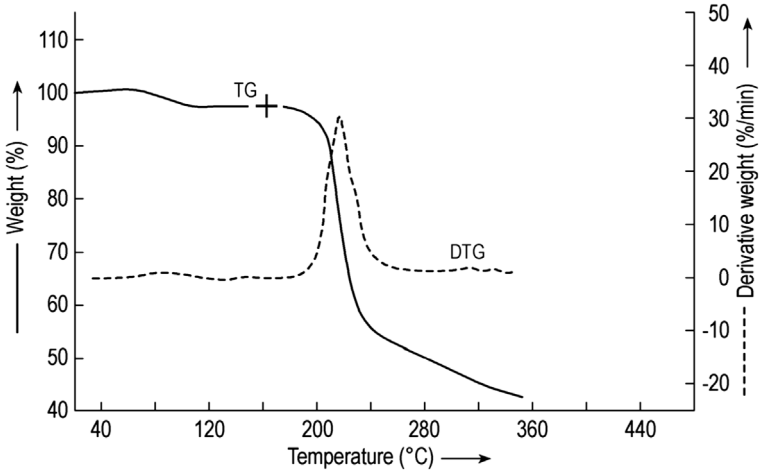

Figure 1.153 Weight (%) as a function of temperature of freeze-dried US Standard Pertussis Vaccine Lot 9 measured by the thermogravimetric (TG) method and the derivative of weight over time (DTG) (%/min). The end point of water desorption is marked (+). RM by TG, 4.75%. (See also Figure 3 from Ref. [161].)

proteins were studied: recombinant humanized monoclonal antibody (rhuMAb) E25, rhuMAb HER2, rhuMAb CD11a, TNKase, and rt-PA. Higher moisture contents (RM) were obtained by adding appropriate amounts of MilliQ water to the wall of the vial in a horizontal position and letting the water vapor diffuse to the dried product. Generally, in 1–2 days an equilibrium state was reached. Three common mathematical tools were used to quantify complex spectra (overlapping peaks from different components or their chemical interaction). The effects of the following influences on the IR calibration were studied: concentration of each

Table 1.30 Comparison of RM data measured by KF, TG, and VPM methods for α-interferon and US Standard Pertussis Vaccines.

Product	RM by KF (%)	RM by TG (%)	Content of water in vial space (mg/vial)
α-Interferon			
Lot A		1.19	2.05
Lot B		0.98	6.67
Lot C	1.28	1.28	4.76
Pertussi vaccine			
Lot 8		2.44	9.50
Lot 9		4.75	26.00

Table 2 from Ref. [161].

excipient, product cake porosity, cake height and diameter, and excipient-to-protein ratio. Karl Fischer titration data (called RF) were used as standards for comparison with the NIR data.

Figure 1.154a–e shows the relationship between RF and RNIF for the five products. The Karl Fischer titration results can fluctuate up to ±0.5% with day-to-day and operator variations. Therefore, a difference between RF and RNIR of ≤0.5% is accepted as good. The porosity change from 30 to 100 mg/mL was ≤0.5%. The cake dimensions must exceed the NIR penetration depth, otherwise the RNIR measured will be too small.

Small changes in the formulation compositions can be accommodated, whereas substantial changes, for example, sucrose from 42.5 to 170 mM, show an increase in absorbance with increasing concentration (Figure 1.155). The RNIR calibration for 85 mM therefore cannot be used for a product with lower (42.5 mM) or higher (>120 mM) concentrations of sucrose; the water signal at 5200 cm^{-1} is changed by the changing product signal at 5200 cm^{-1}. Generally, RNIR calibration is specific for a given formulation and product dimensions. Changes are only tolerated as long as the NIR measurement has an optical path long enough for sufficient reflected radiation and the spectrum of the calibrated product is not changed by modified concentrations of the ingredients.

Summary of Section 1.3.1

Water in the dried product can be bound in many different forms: as surface water, as water bound more or less to the dry substance, or as water of crystallization. Therefore, each method can lead to different results for different substances. There are products for which the RM values by gravimetry and by Karl Fischer titration show very little difference. May *et al.* [159] presented four examples of such substances but, as shown in Table 1.31, the RM obtained by gravimetry can be 0.3–0.6% smaller than by Karl Fischer titration, whereas the thermogravimetric data, within the given errors, are close to the Karl Fischer data. In Figure 1.156, the RM data measured by the KF method are compared with the dW data calculated from DR data during the secondary drying. The vials for KF measurements were closed at the time indicated in the upper graph by the mean points and the error beams. Three runs were carried out with the same pharmaceutical product, the same process data (given in Figure 1.156), and the same load in the same plant. The RM data by the KF method vary after the change from MD to SD by ±1%, which is reduced after ~21 h to ±0.5%. The dW data for all three runs vary after the start of SD by ±0.5% and by less than 0.05% after 21 h. The top and lower plots show that at the end temperature the RM of 0.5% will not be lowered significantly by further drying. The same information is given by dW: After 21 h, the possible desorption of water can be neglected, as it will be less than 0.02%/h. In this product and under the process conditions chosen, the moisture content of 1.5% as found by the KF method cannot be removed by desorption at this temperature in an acceptable time.

1.3.2 Influence of Vial Stoppers on the Residual Moisture Content

The stoppers for vials contain a certain amount of water, which depends on the composition of the stoppers. De Grazio and Flynn [163] showed that the selection

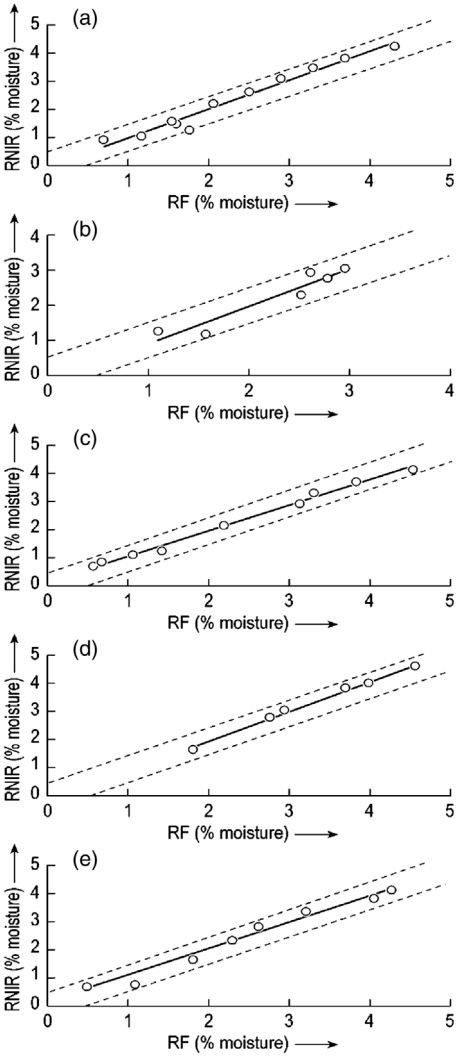

Figure 1.154 Relation between RNIR and RF for (a) rhuMAb E25, (b) rhuMAb HER2, (c) rhuMAb CD11a, (d) TNKase, and (e) rt-PA. Dotted lines represent ±0.5% moisture of solid lines. (See also Figure 1 from Ref. [162].) Data for the plots:

Plot	Equation	R^2 a)	RMSEC b)
(a)	$y = 1.05x - 0.08$	0.97	0.210
(b)	$y = 0.97x + 0.07$	0.97	0.243
(c)	$y = 0.93x + 0.14$	0.99	0.154
(d)	$y = 1.09x - 0.20$	0.99	0.135
(e)	$y = 0.99x + 0.12$	0.98	0.212

a) Coefficient of determination (linearity of calibration).
b) Root mean square error (uncertainty of calibration).

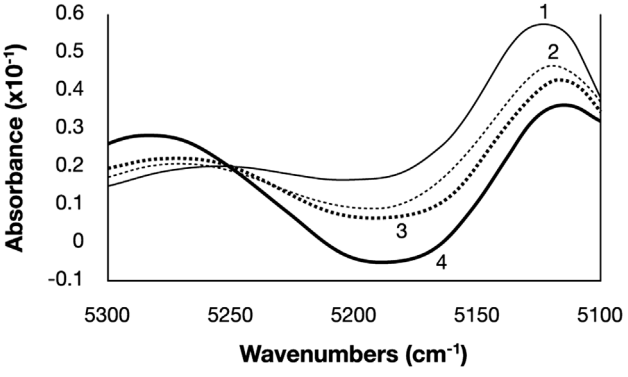

Figure 1.155 Second-derivative spectra of lyophilized rhuMAb containing RF 0.8%. All formulations contained 40 mg/mL rhuMAb E25, 5 mM histidine and 0.01% polysorbate 20. Sucrose concentration: (1) 42.5; (2) 85; (3) 120; (4) 170 mM. (See also Figure 6 from Ref. [162].)

of the polymer, the additives for the vulcanization, and the filler influence the adsorption and desorption of water. However, even the best possible mixture increases the RM in 215 mg of sucrose from 1.95 to 2.65% during 3 months of storage at room temperature. Other stopper mixtures show an increase of up to 1.7%. Pikal and Shah [164] demonstrated that the desorption of water from the stopper and the absorption of water by the product depend, in the equilibrium state, on the mass and water content of the stopper and the water content and sorption behavior of the dry product.

If the stopper is as small as technically possible and its material optimized, the water content of the stopper depends on its prehistory: Steam-sterilized stoppers take up water (e.g., 1.1% of their weight), which can only be removed by 8 h of

Table 1.31 Residual moisture content (RM) of different vaccines measured by four different measurement methods.

Test method	% RM ± standard deviation of the vaccines			
	Rubella virus	Mumps virus	Rubella and mumps virus	Measles, mumps, and rubella virus
Gravimetric[a)]	0.42 ± 0.18	1.10 ± 0.40	0.41 ± 0.26	0.18 ± 0.14
Karl Fischer[b)]	1.03 ± 0.14	1.54 ± 0.20	0.72 +/− 0.16	0.80 ± 0.14
TG-profile[b)]	1.26 ± 0.16	1.54 +/− 0.15	0.76 ± 0.12	0.76 ± 0.11
TG–60 °C hold[b)]	1.17 ± 0.20	1.53 ± 0.17	0.74 ± 0.13	0.70 ± 0.08

a) Average of 5–12 determinations.
b) Average.
TG-profile: thermogravimetric profile by a given course of temperatures.
TG–60 °C hold: by a constant temperature of +60 °C.
Part of Table 1 from Ref. [159].

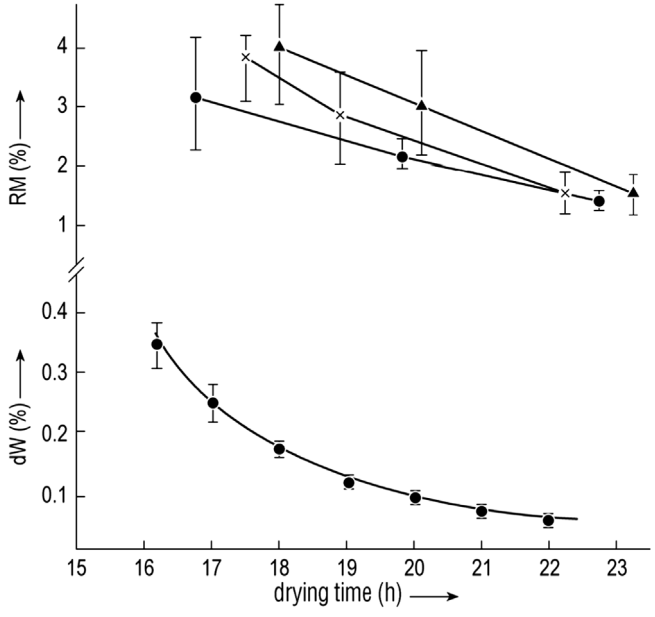

Figure 1.156 *Top:* RM measured by KF as a function of drying time. Ten vials were each closed at the time indicated by mean RM data. The cake from 5–7 vials out of each 10 vials closed was analyzed with 3–5 samples from each vial. The average data shown in the top graph are the mean values of 15 or more measurements. The bars are not standard deviations; they mark the minimum and the maximum of all measured data. (●) Run 1, mean $T_{ice} = -38.56\,°C$, SA = 0.38 °C. (+) Run 2, mean $T_{ice} = -38.59\,°C$, SA = 0.36 °C. [Mean T_{ice} of all runs −38.58 °C, SA = 0.02 °C] (▲) Run 3, mean $T_{ice} = -38.52\,°C$, SA = 0.39 °C. Process data for all three runs: freezing rate ~0.9 °C/min, final temperature −50 °C, $d = 10$ mm, $T_{sh,MD} = 0\,°C$, $p_c = 0.08$ mbar, $T_{sh,SD} = 40\,°C$. Below: dW data calculated from DR measurements during secondary drying as a function of drying time. (●) Mean dW of all three runs; bars, minimum and maximum of all calculated dW.

vacuum drying [164] or by 8 h of recirculated hot air (110 °C) drying down to 0.1% [165]. Figure 1.157 [164] shows that a steam-sterilized stopper, vacuum dried for 8 h, releases slightly less water to lactose than does an untreated stopper. A stopper dried for only 1 h increases the RM in 6 months of storage at 25 °C by a factor of 2.4. Figure 1.157 [164] also shows that an equilibrium is reached that, practically, does not change later. The time to reach the equilibrium depends strongly on the temperature. For a given product, the time to reach half-maximum increases from 4 days at +40 °C to 10 months at +5 °C. It is surprising that the absorption isotherms for lactose are found to be independent of temperature at +25 and +60 °C; this applies also to vancomycin at +25 and +40 °C. Figure 1.158 shows the equilibrium water content as a function of stopper treatment and amount of dry product independent of the storage temperatures of +25 and +40 °C for two different products; vancomycin is clearly more hygroscopic than lactose.

Earle *et al.* [166] showed that the RM in the product Pedvax HIB TM did not change during storage at 2–8 °C for 24 months if the stoppers were

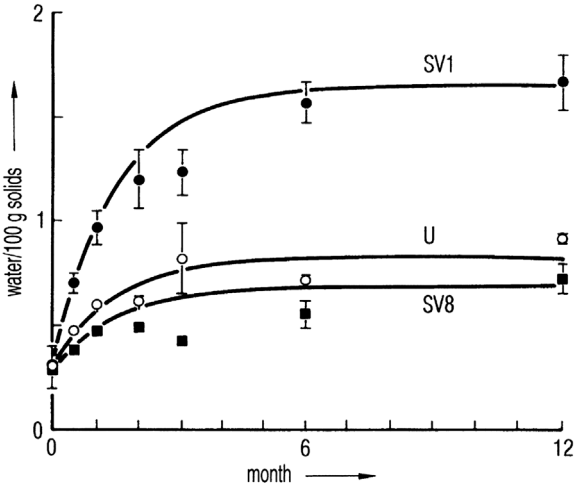

Figure 1.157 Water content of 100 mg of lactose at +25 °C as a function of time. The vials were closed with 13 mm stoppers subjected to different pretreatment: SV1, steam-sterilized; U, untreated; SV8, steam-sterilized followed by vacuum-drying for a minimum of 8 h. The lines were calculated by a model system. (See also Figure 4 from Ref. [164].)

steam-sterilized, vacuum-dried for 6 h, and finally dried at +143 °C for 4 h. If the vials were closed with stoppers that had not been dried, the RM increased in 12 months to ~5.3%. Danielson [167] warned against toxic components that could diffuse or migrate from the stopper to the product. A protective coating does not prevent the extraction of these substances, but a Teflon coating is better

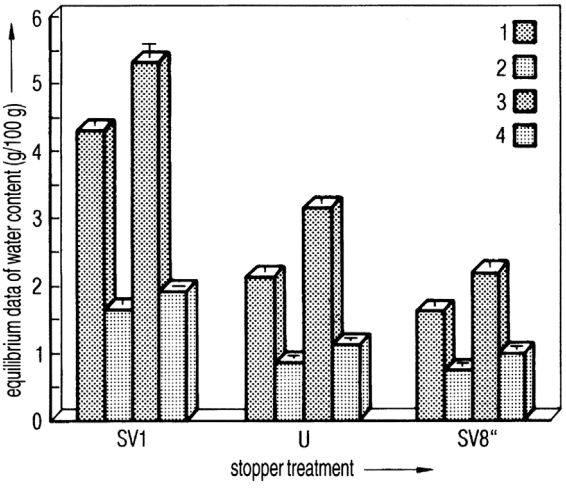

Figure 1.158 Equilibrium water content in two different freeze-dried products, each with two different amounts of product per vial. The equilibrium data are extrapolated from the +25 and +40 °C values. SV1, U, and SV8 as in Figure 1.158; 1, 25 mg of lactose; 2, 100 mg of lactose; 3, 25 mg of vancomycin; 4, 100 mg of vancomycin. (See also Figure 7 from Ref. [164].)

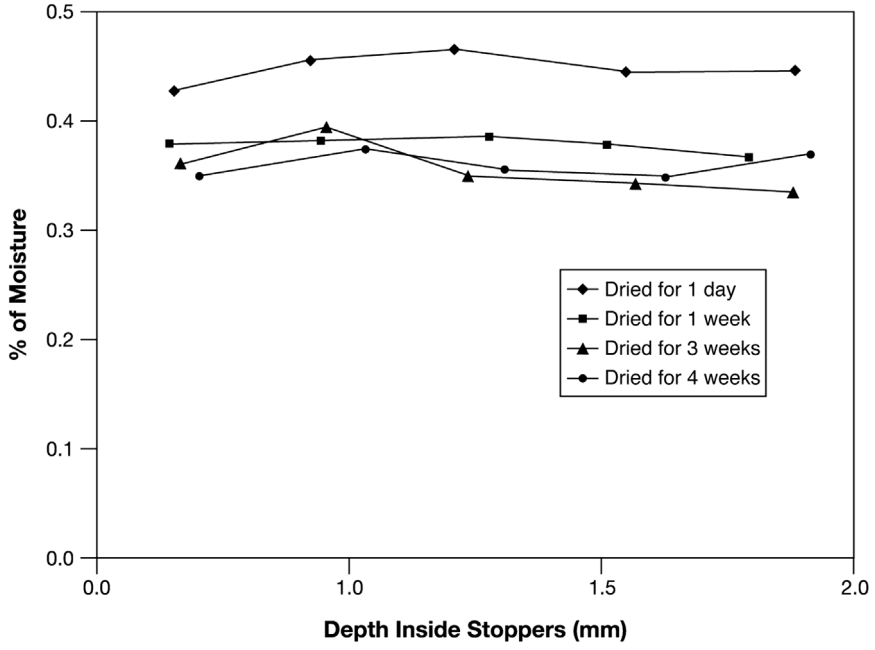

Figure 1.159 Moisture distribution inside the described rubber stoppers that were autoclaved at 121 °C for 30 min and then dried at 100 °C for different times. (See also Figure 7 from Ref. [169].)

than none. Corveleyn *et al.* [168] determined the water content of five chlorobutyl and three bromobutyl stoppers in the range of 0.85–1.49 and 1.71–1.99%, respectively, after they had been stored for 85 days at 95% RH. During sterilization, the moisture uptake was 0.82–0.9% for the chlorobutyl and 0.41–0.57% for the bromobutyl stoppers. Wang *et al.* [169] differentiated between free and bound water in stoppers. In Figure 1.159, the moisture distribution in stoppers (FM257/2, V9032, Helvoet Pharma, Pennsauken, NJ, USA) is shown after autoclaving at 121 °C for 30 min and drying at 100 °C for different times. The moisture distribution in Figure 1.159 no longer changes after 1 week of drying. The remaining amount of ~0.35%, bound to the stopper material, cannot be removed at 100 °C. The authors concluded that water that cannot be removed at 100 °C is bound in such a way that it cannot jeopardize the pharmaceutical product. Only the free water can diffuse from the stopper to the product. The moisture content is measured by the Karl Fischer method with different temperatures in the oven, 100 °C to determine the free water content and up to 300 °C to measure the free and bound water. The authors suggested developing a similar program for other stoppers, since the time for such measurements is relatively short (1 week) instead of observing the RM in a product over long times. Table 1.32 summarizes the results with the stoppers described above. Table 1.33 lists the limits of the free moisture content in two types of stoppers and for different cake weights under the assumption that a maximum RM increase of 0.5% in the product is acceptable.

Table 1.32 Moisture analysis of FM257/2, V9032 stoppers (Helvoet Pharma, Pennsauken, NJ, USA).

Oven dry	Moisture content (%) ± SA	Free moisture content (%)
No	0.52 ± 0.02	0.21
16 h	0.34 ± 0.02	0.03
1 week	0.31 ± 0.02	–

All stoppers were autoclaved for 16 min, vacuum dried for 30 min, and oven dried at 100 °C for the specified time. Table 4 from Ref. [169].

Table 1.33 Maximum moisture content of stoppers for a hypothetical product with a 0.5% moisture increase limit.

Stopper weight (g)	Cakes weight (g)	Limit for free moisture (%)
2.5	0.4	0.13
2.5	0.2	0.07
2.5	0.1	0.03
2.5	0.05	0.02
0.6	0.4	0.56
0.6	0.2	0.28
0.6	0.1	0.14
0.6	0.05	0.07

Table 3 from Ref. [169].

1.3.3 Qualities of the Dry Substances and Their Changes

During the storage of a freeze-dried product, its qualities can change under the influence of at least three conditions: residual moisture content, storage temperature, and gas mix in the packing, assuming that the freeze-drying itself has been carried out under optimum conditions and the product had the intended qualities at the end of the freeze-drying process. The changes that can be related to one or mostly to a combination of the three conditions can be divided into four groups:

1) Changes in the reconstitution with water and/or the solubility.
2) Chemical reactions in the dried product.
3) Deterioration of the biological–medical activity of the product.
4) Changes of the physical structure of the product, for example, from an amorphous to a partially or totally crystalline form.

Often changes occur that have to be accounted for as a combination of several of the four categories. In this section some typical examples are given, although some special changes are also mentioned in Chapters 3 and 4.

Liu and Langer [170] showed that BSA, ovalbumin, glucose oxidase, and β-lactoglobulin rapidly lost their solubility at 37 °C and, within 24 h, 97% became insoluble if 30% (w/w) of a buffered, physiological NaCl solution was added to the dried product. The aggregation induced by the moisture was attributed to intermolecular S–S binding. This aggregation can be minimized if the RM is optimized for a given albumin.

Zhang *et al.* [171] studied the effect of the reconstitution medium on aggregate formation in recombinant keratonocyte growth factor (KGF). Several additives reduced aggregation substantially, but similar effects were observed by adjusting the ionic strength of the reconstitution medium. Optimization of the reconstitution conditions increased the recovery of soluble active proteins; for KGF, the recovery of the soluble active proteins corresponds to the native, monomeric form. Furthermore, Zhang *et al.* [172] demonstrated that interleukin-2 (I) and RNase (II) show significant aggregation upon storage at +45 °C when pure water is used for reconstitution. The extent of aggregation can be substantially reduced if, for example, heparin or phosphates are added to the reconstitution water. Shalaev *et al.* [173] studied the acid-catalyzed inversion of amorphous sucrose to glucose and fructose at RM <0.1%. Sucrose colyophilized with, for example, citric acid undergoes acid-catalyzed inversions at 50 °C even at RH = 0.1%. The authors concluded that colyophilization of acidic substances with sucrose can produce substances capable of further reaction with other ingredients even at very low RM.

Yoshika *et al.* [174] studied the inactivation of β-galactosidase (I) during storage in relation to the water mobility by ^{17}O NMR spectroscopy. An increase in water content also produced an increase of the spin–lattice relaxation time, T_1, the inactivation being more dependent on T_1 than on the pH value. It was assumed that the water increased the mobility of the water around the enzyme, thus enhancing enzyme inactivation. The freeze-dried samples with little water also showed a greater inactivation rate than was expected from details of pH value and water mobility, this inactivation being induced by the salts used as additives for freeze-drying. Yoshika *et al.* [175] also used NMR spectroscopy but with the ^{1}H spin–spin relaxation time T_2. T_2 was measured on BSA and γ-globulin (BGG) as a function of hydration level. Freeze-dried BSA and BGG became sensitive to aggregation if the water content exceeded ~0.2 g/g protein. T_2 of the protein protons began to increase at low water contents and followed the increase in aggregation in time with increasing water content. For freeze-dried BGG, both the aggregation and the T_2 of the protein proton decreased at water contents >0.5 g/g protein.

The stability of moisture-sensitive drugs was studied by Vromans and Schalks [176] using amorphous vecuronium bromide. Its decomposition in a formulation depends more on the water activity a_w than on the water content. Glass-forming excipients may not only be cryoprotective but also stabilizing. Cleland *et al.* [177] found that an appropriate molar ratio of sugar to protein stabilized recombinant humanized monoclonal antibody (rhuMAb HER2) for 33 months at 40 °C. A 360: 1 molar ratio was successful in stabilizing the protein. This three- to fourfold below the normally used iso-osmotic concentrations in formulations. Souillac *et al.* [178] compared the enthalpies of freeze-dried and

physical mixtures of Rh-DNase, rh-GH, and rH-IGF-1 with mannitol, sucrose, trehalose, and dextran. For the physical mixtures, a linear relationship between the enthalpies and the percentage of protein was observed; for freeze-dried mixtures, this relationship was nonlinear. The authors concluded that direct interactions take place between the proteins and the carbohydrates in lyophilized mixtures.

Hsu *et al.* [179] demonstrated that decomposition can take place in a packaged product. It was assumed that the freeze-drying had ended with a monomolecular layer of water, which may not have been evenly distributed, but could be attached as clusters to certain locations of the molecule. This water provided optimum protection against denaturation during both drying and storage. This was demonstrated with two very different products, made by gene technology: too little water, less than one monolayer, makes *t*PA and methemoglobin physically unstable, whereas a higher water content leads to biological instability during storage.

Examples of the fourth type of changes were described by To and Flink [180] and Van Scoik and Carstensen [181]: According to To and Flink, the change from an amorphous to a crystalline phase is induced either by high storage temperatures T ($T > T_c$) or by water absorption. (*Note:* More water increases the mobility of the amorphous solid, promoting nucleation of crystals and their subsequent growth.)

Van Scoik and Carstensen [181] with their experiments differentiated between nucleation of sucrose crystals and their growth. The nucleation parameters of temperature and residual moisture were discussed and additives suggested to stop nucleation or to delay or speed it up. The influence of gases used for venting the chamber with vials or filled into the packaged bulk product is difficult to summarize. Only O_2 should be excluded in most cases. Spiess [182] suggested dry air for the storage of cauliflower and blueberry, while carrots and paprika should be stored in a gas with <0.1 mg O_2/g dry substance. Less sensitive products such as peas, green beans, and mushrooms tolerate 0.2–0.5 mg O_2/g dry substance. For drugs, viruses. or bacteria, no general recommendation can be given, since the influence of CPAs, structural additives, buffer, and so on, have to be taken into account.

The purity of gases used should also be specified, as certain impurities can have a decisive effect on storage behavior, for example, gas desorption from stoppers. Greiff and Rightsel [183] showed that influenza viruses without CPAs keep their infectivity best when stored with 1.6% RM in helium. In argon, the infectivity decreases ~10 times and in O_2 20 times faster if the average of the storage temperatures is used. Corveleyn and Remon [184] freeze-dried two different tablet formulations containing 25 mg of hydrochlorothiazide. Tablets where packed in PVC/aluminum blister packs, in PVC–poly(vinylidene chloride) (PVDC)/aluminum blister packs, closed containers with a desiccant tablet, and open containers and stored at three RHs, 45, 60, and 85%, at 60 °C. After 1 month at RH 85%, all tablets except those packed in PVDC/aluminum blister packs showed an increase from RM 2.7 to 6.8%. At a moisture content of 7.2%, one of the formulations collapsed. The increase in moisture content and decrease in mechanical strength for the PVDC/aluminum blistered tablets was much slower.

None of the packaged material used for freeze-dried tablets offered protection against moisture uptake and structural collapse.

References

1 Duckworth, R.B. (1971) Differential thermal analysis of frozen food systems: I. The determination of unfreezable water. *J. Food Technol.*, **6**, 317–327.

2 Riedel, L. (1972) Enthalpy–water content diagram for lean beef (also valid for other meats with fat content below 4%), in *Recommendations for the Processing and Handling of Frozen Foods*, 2nd edn, International Institute of Refrigeration, Paris, pp. 28–29.

3 Riedel, L. (1972), in *Recommendations for the Processing and Handling of Frozen Foods*, 2nd edn, International Institute of Refrigeration, Paris, pp. 32 and 34.

4 Steinbach, G. (1994) *Die Bedeutung des Einfriervorganges, Berechnung des Gefriervorganges, Verein Deutscher Ingenieure*, VDI-Bildungswerk, RW 1570, p. 3.

5 Oetjen, G.W. and Eilenberg, H.J. (1969) Heat transfer during freeze-drying with moved particles. International Institute of Refrigeration (Comm. X, Lausanne), pp. 19–35.

6 Sharon, Z. and Berk, Z. (1969) Freeze-drying of tomato juice and concentrate, studies of heat and mass transfer. International Institute of Refrigeration (Comm. X, Lausanne), pp. 115–122.

7 Magnussen, O.M. (1969) Measurements of heat and mass transfer during freeze-drying. International Institute of Refrigeration (Comm. X, Lausanne), pp. 65–74.

8 Gunn, R.D., Clark, J.P., and King, C.J. (1969) Mass transport in freeze-drying, basic studies and processing implications. International Institute of Refrigeration (Comm. X, Lausanne), pp. 79–98.

9 Oetjen, G.W. (1999) Industrial freeze-drying for pharmaceutical applications, in *Freeze-Drying/Lyophilization of Pharmaceuticals and Biological Products* (eds L. Rey and J.C. May), Marcel Dekker, New York, pp. 267–335 (Table 3 and Fig. 10, Pharmaceutical freeze-drying).

10 Umrath, W. (1974) Cooling bath for rapid freezing in electron microscopy. *J. Microsc.*, **101** (1), 103–105.

11 Riehle, U. (1986) Schnelleinfrieren organischer Präparate für die Elektronenmikroskopie. (Die Vitrifizierung verdünnter wässeriger Lösungen). *Chem. Ing. Tech.*, **40**, 213–218.

12 de Quervain, M.R. (1975) Crystallization of water, a review, in *Freeze-Drying and Advanced Food Technology* (eds S.A. Goldblith, L. Rey, and W.W. Rothmayr), Academic Press, New York, pp. 3–15.

13 Oetjen, G.W. (1949) Absorptionsmessungen an Lösungen von Neodymsalzen. Dissertation, Universität Göttingen, 1947. Z. Naturforsch. 4a, No. 1.

14 Dowell, L.G. and Rinfret, A.P. (1960) Low temperature forms of ice as studied by X-ray diffraction. *Nature*, **188**, 1144–1148.

15 Luyet, B. (1960) On various phase transitions occurring in aqueous solutions at low temperatures. *Ann. N. Y. Acad. Sci.*, **568**, 549–569 (Fig. 14).

16 Luyet, B. (1969) On the amount of water remaining amorphous in frozen aqueous solutions. *Biodynamica*, **10**, 277–291.

17 Shamblin, Sh.L. and Zografi, G. (1999) The effect of absorbed water on the properties of amorphous mixtures containing sucrose. *Pharm. Res.*, **16**, 1119–1124.

18 Zeng, X.M., Martin, G.P., and Marriott, C. (2001) Effects of molecular weight of polyvinylpyrrolidone on the glass transition and crystallization of co-lyophilized sucrose. *Int. J. Pharm.*, **218**, 63–73.

19 Shalaev, E.Y., Lu, Q., Shalaev, M., and Zografi, G. (2000) Acid-catalyzed inversion of sucrose in the amorphous state at very low levels. *Pharm. Res.*, **17**, 366–370.

20 Kouassi, K. and Roos, Y.H. (2001) Glass transition and water effects on sucrose version in non-crystalline carbohydrate food systems. *Food Res. Int.*, **34**, 895–901.

21 Saleki-Gerhardt, A. and Zografi, G. (1994) Non-isothermal and isothermal crystallization of sucrose from the amorphous state. *Pharm. Res.*, **11**, 1166–1173.

22 Yu, L., Milton, N., Groleau, E.G., Mishra, D.S., and Vansickle, R.E. (1999) Existence of a mannitol hydrate during freeze-drying and practical implications. *J. Pharm. Sci.*, **88**, 196–198.

23 Cannon, A. and Trappler, E.H. (2000) The influence of lyophilization on the polymorphic behavior of mannitol. *PDA J. Pharm. Sci. Technol.*, **54**, 13–22.

24 Pyne, A. and Suryanarayanan, R. (2001) Phase transitions of glycine in frozen aqueous solutions and during freeze-drying. *Pharm. Res.*, **18** (10), 1448–1454.

25 Hinrichs, W.L.J., Prinsen, M.G., and Frijlink, H.W. (2001) Inulin glasses for the stabilization of therapeutic proteins. *Int. J. Pharm.*, **215**, 163–174.

26 Davidson, P. and Sun, W.Q. (2001) Effects of sucrose/raffinose mass ratios on the stability of co-lyophilized protein during storage above T_g. *Pharm. Res.*, **18**, 474–479.

27 Fakes, M.G., Dali, M.V., Haby, Th.A., Morris, K.R., Varia, S.A., and Serajuddin, A.T.M. (2000) Moisture sorption behavior of selected bulking agents used in lyophilized products. *PDA J. Pharm. Sci. Technol.*, **54**, 144–149.

28 Thijssen, H.A.C. and Rulkens, W.H. (1969) Effect of freezing rate on rate of sublimation and flavour retention in freeze-drying. International Institute of Refrigeration (Comm. X, Lausanne), pp. 99–114.

29 Godward, J., Gunning, P., and Hills, B.P. (1999) An NMR protocol for determining ice crystal size distribution during freezing and pore size distribution during freeze-drying. *Appl. Magn. Reson.*, **17**, 537–556.

30 Reid, D.S., Lim, M.H., and McEvoy, H.M. (1983) Studies on the freezing processes in aqueous model systems. Paper 354, International Institute of Refrigeration (Comm. C1, Paris).

31 Burke, M. and Lindow, S.E. (1990) Surface properties and size of the ice nucleation of active bacteria: theoretical considerations. *Cryobiology*, **27**, 80–84.

32 Rasmussen, D. and Luyet, B. (1970) Contribution to the establishment of the temperature concentration curves of homogeneous nucleation in solutions of some cryoprotective agents. *Biodynamica*, **11** (225), 33–44.

33 Sutton, R.L. (1991) Critical cooling rates to avoid ice crystallisation in solutions of cryoprotective agents. *J. Chem. Soc., Faraday Trans.*, **87**, 101–106.

34 Correleyn, S. and Remon, J.P. (1995) The use of maltodextrin in the lyophilization of a model protein, LHD (lactate dehydrogenase). *Pharm. Res.*, **13**, 146.

35 Sutton, R.B. (1992) Critical cooling rates for aqueous cryoprotectants in the presence of sugars and polysaccharides. *Cryobiology*, **29**, 585–598.

36 Levine, H. and Slade, L. (1988) Principles of 'cryostabilisation' technology from structure/property relationship of carbohydrate/water system: a review. *Cryo Letters*, **9**, 21–63.

37 Shalaev, E.Yu. and Kaney, A.N. (1994) Study of the solid–liquid state diagram of the water– glycine–sucrose system. *Cryobiology*, **31**, 374–382.

38 Jang, J.W., Kitamura, S., and Guillory, J.K. (1995) The effect of excipients on the glass transition temperatures for FK 906 in the frozen and lyophilized state. *PDA J. Pharm. Sci. Technol.*, **49**, 166–174.

39 Gordon, M. and Taylor, J.S. (1952) Ideal copolymers and the second-order transitions of synthetic rubbers in non-crystalline copolymers. *J. Appl. Chem.*, **493**, 493–500.

40 Nicolajsen, H. and Hvidt, A. (1994) Phase behavior of the system trehalose–NaCl–water. *Cryobiology*, **31**, 199–205.

41 Carpenter, J.F., Arakawa, T., and Crowe, J.H. (1992) Interactions of stabilizing additives with proteins during freeze-thawing and freeze-drying, in *Developments in Biological Standardization*, vol. 74 (eds J.C. May and F. Brown), Karger, Basel, pp. 225–239.

42 Timasheff, S.N., Lee, J.G., Pittz, E.P., and Tweedy, N. (1976) The interaction of tubulin and other proteins with structure stabilizing solvents. *J. Colloid Interface Sci.*, **55**, 658–663.

43 Prestrelski, S.J., Arakawa, T., and Carpenter, J.F. (1993) Separation of freezing- and drying-induced denaturation of lyophilized proteins using stress-specific stabilization: II. Structural studies using infrared spectroscopy. *Arch. Biochem. Biophys.*, **303**, 465–473.

44 Carpenter, J.F., Prestrelski, S.J., Anchordogy, T.J., and Arakawa, T. (1994) Interaction of stabilizers with proteins during freezing and drying. *Formulation and Delivery of Proteins and Peptides*, ACS Symposium Series 567, American Chemical Society, pp. 134–147.

45 Rey, L. (2020) Glimpses into the realm of freeze-drying: classical issues and new ventures, in *Freeze-Drying/Lyophilization of Pharmaceutical and Biological Products* (eds L. Rey and J.C. May), Marcel Dekker, New York, pp. 1–30.

46 Meryman, H.T. (1968) The 'minimum cell volume' modes of freezing injury. *Nature*, **218**, 333 (International Institute of Refrigeration (IIR) (Comm. X), pp. 897–900, Washington, DC, 1971).

47 Pushkar, P.S. and Itkin, U.A. (1971) The study of the intercellular and extracellular crystallization of the biological objects on freezing. International Institute of Refrigeration (Comm. X, Washington, DC), pp. 861–868.

48 Nei, T. (1983) Ice particles formed in various cells. International Institute of Refrigeration (Comm. 1, Paris), pp. 429–430.

49 Cosman, M.D., Toner, M., Kandel, J., and Cravalho, E.G. (1989) An integrated cryomicroscopy system. *Cryo Letters*, **10**, 17–38.

50 De Antoni, G.L., Perez, P., Abraham, A., and Anon, M.C. (1989) Trehalose, a cryoprotectant for *Lactobacillus bulgaricus*. *Cryobiology*, **26**, 149–153.

51 Rey, L. (1962) Influence of the preliminary freezing period and adsorption phenomena in freeze-drying. Vortrag auf der 5, Gefriertrockentagung Leybold, Köln, pp. 3–19.

52 Willemer, H. (2002) Comparison between measurements of electrical resistance and cryomicroscope visualization of pharmaceutical products to be freeze-dried. ISL–FD, Lyophilization Conference, Amsterdam, October 2002.

53 MacKenzie, A.P. (1985) A current understanding of the freeze-drying of representative aqueous solutions. *Fundamentals and Applications of Freeze-Drying to Biological Materials, Drugs and Foodstuffs*, International Institute of Refrigeration, pp. 21–34.

54 Hatley, R.H.M. (1992) The effective use of differential scanning calorimetry in the optimisation of freeze-drying processes and formulations, in *Developments in Biological Standardization*, vol. 74 (eds J.C. May and F. Brown), Karger, Basel, pp. 105–122.

55 Luyet, B. and Rasmussen, D. (1968) Study by differential thermal analysis (DTA) of the temperatures of instability of rapidly cooled solutions of glycerol, ethylene glycol, sucrose and glucose. *Biodynamica*, **10** (211), 167–191.

56 Rasmussen, D. and Luyet, B. (1969) Complementary study of some non-equilibrium phase transitions in frozen solutions of glycerol, ethylene, glycol, glucose and sucrose. *Biodynamica*, **10**, 319–331.

57 Hsu, C.C., Walsh, A.J., Nguyen, H.M., Overcashier, E.D., Koning-Bastiaan, H., Bailey, R., and Nail, S.L. (1996) Design and application of a low-temperature Peltier-cooling microscope stage. *J. Pharm. Sci.*, **85**, 70–71.

58 Nunner, B. (1993) Gerichtete Erstarrung wässriger Lösungen and Zellsuspensionen. Dissertation, Rheinisch-Westfälische Technische Hochschule Aachen.

59 Dawson, P.J. and Hockley, D.J. (1992) Scanning electron microscopy (SEM) of freeze-dried preparations: relationship of morphology to freeze-drying parameters, in *Developments in Biological Standardization*, vol. 74 (eds J.C. May and F. Brown), Karger, Basel, pp. 185–192.

60 Meister, E. and Gieseler, H. (2009) Freeze-dry microscopy of protein/sugar mixtures: drying behaviour, interpretation of collapse temperature and a comparison to corresponding glass transition data. *J. Pharm. Sci.*, **98** (9), 3072–3087.

61 Gatlin, L.A. (1992) Kinetics of a phase transition in a frozen solution, in *Developments in Biological Standardization*, vol. 74 (eds J.C. May and F. Brown), Karger, Basel, pp. 93–104.

62 DeLuca, P.P. (1985) Phase transitions in frozen antibiotic solutions. International Institute of Refrigeration (Comm. C1, Tokyo), pp. 87–92.
63 Takeda, T. (1989) Crystallization and subsequent freeze-drying of cephalothin sodium by seeding method. *Yakugaku Zasshi*, **109**, 395–401.
64 Roos, Y.K.M. (1991) Thermal history and properties of frozen carbohydrate solutions. Paper 350, International Institute of Refrigeration (XVIII Congress, Montreal).
65 Talsma, H., van Steenbergen, M.J., Salemink, P.J.M., and Crommelin, D.J.A. (1991) The cryopreservation of liposomes: 1. A differential scanning calorimetry study of the thermal behavior of a liposome dispersion containing mannitol during freezing/thawing. *Pharm. Res.*, **8**, 1021–1026.
66 Williams, N.A. (1988) Differential scanning calorimetric studies on frozen cephalosporin I solutions. *Int. J. Pharm.*, **44**, 205–212.
67 Knopp, S.A., Chongprasert, S., and Nail, S.L. (1998) The relationship between the TMDSC curve of frozen sucrose solutions and collapse during freeze-drying. *J. Thermal Anal. Calorim.*, **54**, 659–672.
68 Kett, V.L. and Craig, D.Q.M. (2000) The effect of annealing on the glass transition region of sucrose solutions. Proceedings of the 28th NATAS Annual Conference on Thermal Analytical Applications, pp. 653–658.
69 Chang, L.-Q., Tang, X.-L., Pikal, M.J., Milton, N., and Thomas, L. (1999) The origin of multiple glass transitions in frozen aqueous solutions. Proceedings of the 27th NATAS Annual Conference on Thermal Analytical Applications, pp. 624–628.
70 Craig, D.C.M., Barnews, M., Royall, P.G., and Kett, V.L. (2000) An evaluation of use of modulated DSC as a means of assessing the relaxation behavior of amorphous lactose. *Pharm. Res.*, **17**, 696–700.
71 Sichina, W.J. (2000) Utilization de StepScan DSC pour l'optimisation des procedes de lyophlisation. *Spectral Analyse*, **29** (216), 35–37.
72 van Winden, E.C.A., Talsma, H., and Crommelin, D.J.A. (1998) Thermal analysis of freeze-dried liposomes–carbohydrate mixtures with modulated temperature differential scanning calorimetry (MTD-SC). *J. Pharm. Sci.*, **87**, 231–237.
73 Kett, V.L., Craig, D.Q.M., and Deutsch, D. (1999) Thermal analysis of freeze-dried formulations. Proceedings of the 27th NATAS Annual Conference on Thermal Analytical Applications, pp. 618–623.
74 Craig, D.Q.M., Barsner, M., Royall, P.G., and Kett, V.L. (2000) An evaluation of the use of modulated temperature DSC as a means of assessing the relaxation behavior of amorphous lactose. *Pharm. Res.*, **17**, 696–700.
75 Knowles, P.F., Marsh, D., and Rattle, H.W.E. (1976) *Magnetic Resonance of Biomolecules*, John Wiley & Sons, Inc., Chichester.
76 Hanafusa, N. (1992) The behavior of hydration water of protein with the protectant in the view of HNMR, in *Developments in Biological Standardization*, vol. 74 (eds J.C. May and F. Brown), Karger, Basel, pp. 241–253.
77 Nagashima, N. and Suzuki, E. (1985) Freezing curve by broad-line pulsed NMR and freeze-drying. International Institute of Refrigeration (Comm. C1, Tokyo), pp. 65–70.

78 Harz, H-.P., Weisser, H., and Liebenspacher, F. (1989) Bestimmung des Fest-Flüssiggleichgewichtes in gefrorenen Lebensmitteln mit der gepulsten Kernresonanzspektroskopie. DKV-Tagungsbericht, Hannover, pp. 741–752.

79 Girlich, D. (1992) Multikernresonanzuntersuchungen zur molekularen Dynamik wässeriger Saccharidlösungen. Dissertation, Naturwissenschaftliche Fakultät III, Biologie and vorklinische Medizin der Universität Regensburg, 1991, S. Roderer Verlag, Regensburg.

80 Kanaori, A.J. and Nosaka, A.J. (1995) Studies on human calcitinin fibrillation by proton nuclear magnetic resonance spectroscopy: characterization of the lyophilized fibril. Proceedings of the International Society of Magnetic Resonance, XIIth Meeting, Part 1, pp. 274–275 (*Bull. Magn. Reson.* 17, 1–4.

81 Yoshioka, S., Aso, Y., and Kojima, S. (1996) Determination of molecular mobility of lyophilized bovine serum albumin and gamma-globulin by solid-state 1H NMR and relation to aggregation-susceptibility. *Pharm. Res.*, **13**, 926–930.

82 Carrington, A.K., Sahagian, M.E., Goff, H.D., and Stanley, D.W. (1994) Ice crystallization temperatures of sugar/polysaccharide solutions and their relationship to thermal events during warming. *Cryo Letters*, **15**, 235–244.

83 Williams, N.A. and Gugliemo, J. (1993) Thermal mechanical analysis of frozen solutions of mannitol and some related stereoisomers: evidence of expansion during warming and correlation with vial breakage during lyophilization. *J. Parenter. Sci. Technol.*, **47**, 119–123.

84 Pearson, D.S. and Smith, G. (1998) Dielectric analysis as a tool for investigating the lyophilization of proteins. *Pharm. Sci. Technol. Today*, **1** (3), 108–117.

85 Morris, K.R., Evans, S.A., Mackenzie, A.P., Scheule, C., and Lordi, N.G. (1994) Prediction of lyophile collapse temperatures by dielectric analysis. *PDA J. Pharm. Sci. Technol.*, **48**, 318–329.

86 Smith, G., Duffy, A.P., Shen, J., and Ollliff, C.J. (1995) Dielectric relaxation spectroscopy and some applications in the pharmaceutical science. *J. Pharm. Sci.*, **84**, 1029–1044.

87 Cavatur, R.K. and Suryanarayanan, R. (1989) Characterization of frozen aqueous solutions by low temperature X-ray powder diffractometry. *Pharm. Res.*, **15**, 194–199.

88 Sane, S., Mulkerrin, M., and Hsu, Ch. (2000) Raman spectroscopic characterization of drying-induced structural changes in proteins: correlating the structural changes with long-term stability. Book of Abstracts, 219th ACS National Meeting, San Francisco, CA, March 26–30, 2000, BIOT–380. American Chemical Society, Washington, DC.

89 MacKenzie, A.P. (1992) The physico-chemical basis for the freeze-drying process, in *Developments in Biological Standardization*, vol. 74 (eds J.C. May and F. Brown), Karger, Basel, pp. 51–67.

90 Pikal, M.J. (1977) Thermal decomposition of amorphous beta-lactam antibacterials. *J. Pharm. Sci.*, **66**, 1312.

91 Pikal, M.J. *et al.* (1978) Quantitative crystallinity determinations for beta-lactam antibiotics by solution calorimetry: correlations with stability. *J. Pharm. Sci.*, **67**, 767.

92 Kovalcik, T.R. and Guillory, J.K. (1988) The stability of cyclophosphamide in lyophilized cakes: Part I. Mannitol, lactose, and sodium bicarbonate as excipients. *J. Parenter. Sci. Technol.*, **42**, 29.

93 Gatlin, L.A. (1992) Kinetics of a phase transition in a frozen solution, in *Developments in Biological Standardization*, vol. 74 (eds J.C. May and F. Brown), Karger, Basel, pp. 93–104.

94 Yarwood, R.J. and Phillips, A.J. (1989) Processing factors influencing the stability of freeze-dried sodium ethacrinate, in *Pharmaceutical Technology: Drug Stabilization* (ed. M. Rubinstein), Ellis Horwood, Chichester, pp. 40–48.

95 Koray, D.J. and Schwartz, J.B. (1989) Effects of excipients on the crystallisation of pharmaceutical compounds during lyophilization. *J. Parenter. Sci. Technol.*, **43**, 80–83.

96 De Luca, P.P., Klamat, M.S., and Koida, C. (1989) Acceleration of freeze-drying cycles of aqueous solutions of lactose and sucrose with tertiary butyl alcohol (*t*BA). *Congr. Int. Technol. Pharm.*, **1**, 439–447.

97 Kasraian, K. and De Luca, P.P. (1995) Thermal analysis of tertiary butyl alcohol–water system and its implication on freeze-drying. *Pharm. Res.*, **12**, 484–490.

98 Oesterle, J., Franks, F., and Auffret, T. (1998) The influence of tertiary butyl alcohol and volatile salts on the sublimation of ice from frozen sucrose solutions: implications for freeze drying. *Pharm. Dev. Technol.*, **3**, 175–183.

99 Wittaya-areekul, S. and Nail, S.L. (1998) Freeze-drying of *tert*-butyl alcohol/water cosolvent systems: effects of formulation and process variables on residual solvents. *J. Pharm. Sci.*, **87**, 491–495.

100 Kochs, M., Körber, Ch., Nunner, B., and Heschel, I. (1991) The influence of the freezing process on vapor transport during sublimation in vacuum-freeze-drying. *J. Heat Mass Transfer*, **34**, 2395–2408.

101 Vdi e.v. (1988) *VDI-Wärmeatlas*, 5. Auflage, p. Kb 5, VDI-Verlag, Düsseldorf.

102 Wolff, E., Gibert, H., and Rudolf, F. (1989) Vacuum freeze-drying kinetics and modeling of a liquid in a vial. *Chem. Eng. Process.*, **25**, 153–158.

103 Ybema, H., Kolkmann-Roodbeen, L., te Booy, M.P.W.M., and Vromans, H. (1995) Vial lyophilization: calculation on the rate limitation during primary drying. *Pharm. Res.*, **12**, 1260–1263.

104 Chang, B.S. and Fuscher, N.L. (1995) The development of an efficient single-step freeze-drying cycle for interleukin-1 receptor antagonist formulation. *Pharm. Res.*, **12**, 831–837.

105 Steinbach, G. (1974) Wärmeübertragung and Stofftransport bei der Gefriertrocknung. Berechnung von Gefriertrocknungsprozessen, VDI-Bildungswerk, BW 1610.

106 Steinbach, G. (1971) Equations for the heat and mass transfer in freeze-drying of porous and nonporous layers and bodies. International Institute of Refrigeration (Comm. XIII, Washington, DC), pp. 674–683.

107 Gehrke, H.-H. and Deckwer, W.-D. (1990) Gefriertrocknung von Mikroorganismen. II. Mathematische Beschreibung des Sublimationsvorganges. *Chem. Ing. Tech.*, **62** (9), 770–771.

108 Kasraian, K. and DeLuca, P.P. (1995) The effect of tertiary butyl alcohol on the resistance of the dry product layer during primary drying. *Pharm. Res.*, **12**, 491–495.

109 Jennings, T.A. (1999) *Lyophilization: Introduction and Basic Principles*, Interpharm Press, Englewood, CO, p. 314.

110 Overcashier, D.E., Patapoff, T.W., and Hsu, Ch.C. (1999) Lyophilization of protein formulations in vials: investigation of the relationship between resistance to vapor flow during primary drying and small-scale product collapse. *J. Pharm. Sci.*, **88**, 688–695.

111 Schellenz, G., Engel, J., and Rupprecht, H. (1995) Sublimation during lyophilization detected by temperature profile and X-ray technique. *Int. J. Pharm.*, **113**, 133–140.

112 Drummond, J.N. and Day, L.A. (1997) Influence of vial construction and material on performance, uniformity and morphology during freezing and freeze drying. PDA Proceedings of International Congress, Osaka, pp. 401–427.

113 Pikal, M.J. (2000) Heat and mass transfer in low pressure gases: application to freeze-drying, in *Transport Processes in Pharmaceutical Systems* (eds G.L. Amidon, P.I. Lee, and E.M. Topp), Marcel Dekker, New York, pp. 611–686.

114 Willemer, H., Spallek, M., Auchter-Krummel, P., and Heinz, J. (1998) Freezing and freeze drying of pharmaceuticals in tubing, vials with quartz-coated surfaces and resin vials. PDA Proceedings of International Congress, Basel, pp. 99–108.

115 Pikal, M.J., Roy, M.L., and Shah, S. (1984) Mass and heat transfer in vial freeze-drying pharmaceuticals: role of vial. *J. Pharm. Sci.*, **73**, 1224–1237.

116 Kobayashi, M. (1991) Vial variance of the sublimation rate in shelf freeze-drying. Paper 312, International Institute of Refrigeration, Montreal.

117 Oetjen, G.W. (1973) Vakuumtechnik, in *Ullmanns Enzyklopädie der technischen Chemie*, 4. Auflage, Band 3, Verlag Chemie, Weinheim, p. 104.

118 Searles, J.A., Carpenter, J.F., and Randolph, T.W. (2001) The ice nucleation temperature determines the primary drying rate of lyophilization for samples frozen on a temperature-controlled shelf. *PDA J. Pharm. Sci. Technol.*, **90**, 860–871.

119 Searles, J.A., Carpenter, J.F., and Randolph, T.W. (2001) Annealing to optimize the primary drying rate, reduce freezing-induced drying heterogeneity, and determine $T_{g'}$ in pharmaceutical lyophilization. *J. Pharm. Sci.*, **90**, 872–887.

120 Pikal, M.J. and Shaw, S. (1997) Intravial distribution of moisture during the secondary drying stage of freeze drying. *PDA J. Pharm. Sci. Technol.*, **51**, 17–24.

121 Pikal, M. (1991) Freeze-drying of proteins. Part I: process design. *Pharm. Technol. Int.*, **3**, 37–43.

122 Hsu, C.C., Ward, C.A., Pearlman, R., Nguyen, H.M., Yeung, D.A., and Curley, J.G. (1992) Determining the optimum residual moisture in lyophilized protein pharmaceuticals, in *Development in Biological Standardization*, vol. 74 (eds J.C. May and F. Brown), Karger, Basel, pp. 255–271.

123 Haseley, P. and Oetjen, G.W. (1999) The influence of the freezing speed on mannitol solutions during main- and desorption drying. Paper 608, International Institute of Refrigeration, XX. International Congress of Refrigeration, Sydney.

124 Kim, A.I., Akers, M.J., and Nail, S.L. (1998) The physical state of mannitol after freeze-dying: effects of mannitol concentration, freezing rate and a noncrystallizing cosolute. *J. Pharm. Sci.*, **87**, 931–935.

125 Nail, St.L. and Johnson, W. (1992) Methodology for in-process determination of residual water in freeze-dried products, in *Developments in Biological Standardization*, vol. 74 (eds J.C. May and F. Brown), Karger, Basel, pp. 137–152.

126 Willemer, H. (1992) Measurements of temperature, ice evaporation rates and residual moisture content in freeze-drying, in *Developments in Biological Standardization*, vol. 74 (eds J.C. May and F. Brown), Karger, Basel, pp. 123–136.

127 Bardat, A., Biguet, J., Chatenet, E., and Courteille, F. (1993) Moisture measurement: a new method for monitoring freeze-drying cycles. *J. Parenter. Sci. Technol.*, **47**, 293–299.

128 Willemer, H. (1993) Moderne Anlagen, in *Lyophilisation*, vol. 35 (eds D. Essig and R. Oschmann), Wissenschaftliche Verlagsgesellschaft, Stuttgart.

129 Neumann, K.H. and Oetjen, G.W. (1958) Messund Regelprobleme bei der Gefriertrocknung. First International Congress on Vacuum Technology, Namur.

130 Lentges, G., Oetjen, G.W., Willemer, H., and Wilmanns, J. (1971) Problems of measurement and control in freeze-drying down to −180°C. International Institute of Refrigeration (XIII Congress, Washington, DC), pp. 707–715.

131 Milton, N., Pikal, M.J., Roy, M.L., and Nail, S.L. (1997) Evaluation of manometric temperature measurement as a method of monitoring product temperature during lyophilization. *J. Parenter. Sci. Technol.*, **51**, 7–16.

132 Haseley, P. and Oetjen, G.W. (1998) Equipment data, thermodynamic measurements, and in-process control quality control during freeze-drying. PDA International Congress, Basel, pp. 139–150.

133 Bouldoires, J.P. (1969) Experimental study of heat and mass transfer during freeze-drying through dielectric and vapour pressure measurements, International Institute of Refrigeration (Comm. X, Lausanne), pp. 189–206.

134 Leybold, AG (1987) Vacuum Technology: Its Foundations, Formulae and Tables, Köln, 9th edn, p. 52.

135 Welch, J. (1993) Vacuum measurement in steam sterilizable lyophilizers. *J. Parenter. Sci. Technol.*, **47** (1), 29–34.

136 Connelly, J.P. and Welch, J.V. (1993) Monitor lyophilization with mass spectrometer gas analysis. *J. Parenter. Sci. Technol.*, **47**, 70–75.

137 Willemer, H. (1994) Influence of product temperature and gas composition on the lyophilisation process. International Congress, Basel, pp. 63–77.

138 Willemer, H. (1994) Water vapour pressure, its influence on the freeze-drying process and its control. 40th Annual Congress of the International Association for Pharmaceutical Technology, Abstracts, Medpharm, Stuttgart, pp. 1–67.

139 Mangold, A. (2009) Drahtlose Temperatur-Messung in der Lyophilisation: "TEMPRIS Praxisbericht in Produktionsanlagen". Das Erlangen-Seminar, March 19–20th.

140 Mangold, A. (2009) TEMPRIS, precise measurement of Tp I freeze-drying. Bologna.

141 Schneid, S. and Gieseler, H. (2008) Evaluation of a new wireless temperature remote interrogation system (TEMPRIS) to measure product temperature during freeze-drying. *AAPS PharmSciTech*. doi: 10,1208/s12249-008-9099-8

142 Hammerer, K.H. (2007) Wireless temperature-measurement as an innovative PAT- method. 2nd European Congress of Live Science Process Technology, Nuernberg, Germany, March 28.

143 Wilbur, B. (2012) Pfizer: Process Development of a Dual Syringe. Presented at CHI PepTalk Gilyos GmbH (www.gilyos.com).

144 Diels, K. and Jaeckel, R. (1962) *Vakuum Taschenbuch*, 2nd edn, Springer, Berlin, pp. 22–24.

145 MacKenzie, A.P. (1974) Collapse during freeze-drying, qualitative and quantitative aspects. *Freeze-Drying and Advanced Food Technology*, Academic Press, New York, p. 282.

146 Pikal, M.J. and Shah, S. (1990) The collapse temperature in freeze-drying: dependence on measurement methodology and rate of water removal from the glassy phase. *Int. J. Pharm.*, **62**, 165–186.

147 Thijssen, H.A.C. and Rulkens, W.H. (1969) Effect of freezing rate on rate of sublimation and flavour retention in freeze-drying. International Institute of Refrigeration (Comm. X, Lausanne), pp. 99–114.

148 Thijssen, H.A.C. and Rulkens, W.H. (1968) Retention on aromas in drying food liquids. *De Ingenieur, Chemische Techniek (Niederlande)*, **80**, 45–56.

149 Flink, J. and Karel, M. (1970) Retention of organic volatiles in freeze-dried solutions of carbohydrates. *J. Agric. Food Chem.*, **18**, 295.

150 Voilley, A., Sauvageot, F., and Simatos, D. (1971) Coefficients de volatilité rélative et retention au cours de la lyophilisation de quelques alcools, International Institute of Refrigeration, Washington, DC, pp. 639–647.

151 Flink, J. (1975) The retention of volatile components during freeze-drying: a structurally based mechanism, in *Freeze-Drying and Advanced Food Technology* (eds S.A. Goldblith, L. Rey, and W.W. Rothmayr), Academic Press, pp. 351–372.

152 Gero, L. and Smyrl, T.G. (1982) Behavior of low molecular weight organic acids during freeze-drying. *J. Food Sci.*, **47**, 954–957.

153 Seager, H., Taskis, C.B., Syrop, M., and Lee, T.J. (1985) Structures of products prepared by freeze-drying solutions containing organic solvents. *J. Parenter. Sci. Technol.*, **39**, 161–179.

154 Kahn-Wyler, A. (1987) Kaltlufttrocknung von pharmazeutischen Präparaten and gefrorenen Lösungen in der Wirbelschicht. Dissertation, Philosoph.-Nat. Fakultät der Universität Basel.

155 Labrude, P. and Rasolomana, M. (1988) Atomization of oxyhemoglobin in the presence of sucrose. Study by circular dichroism and electronic paramagnetic resonance, comparison with freeze-drying. *STP Pharma Sci.*, **4** (6), 472–480.

156 Wolff, E. and Gibert, H. (1991) La lyophilization en lit fluidise d'adsorbant, optimisation et applications. Paper 313, International Institute of Refrigeration, Montreal.

157 Mumenthaler, M. (1990) Sprühgefriertrocknung bei Atm.-Druck: Möglichkeiten and Grenzen in der pharmazeutischen Technologie and der Lebensmitteltechnologie. Dissertation, Universität Basel.

158 Webb, S. *et al.* (2002) Surface adsorption of recombinant human interferon-γ interferon lyophilized and spray-lyophilized formulations. *J. Pharm. Sci.*, **91** (6), 1474–1487.
159 May, J.C., Wheeler, R.M., Etz, N., and Del Grosso, A. (1992) Measurement of final container residual moisture in freeze-dried biological products, in *Developments in Biological Standardization*, vol. 74 (eds J.C. May and F. Brown), Karger, Basel, pp. 153–164.
160 Wekx, J.P.H. and De Kleijn, J.P. (1990) The determination of water in freeze-dried pharmaceutical products by performing the Karl Fischer titration in the glass container itself. *Drug Dev. Ind. Pharm.*, **16**, 1465–1472.
161 May, J.C., Rey, L., Del Grosso, A., Etz, N., and Wheeler, R. (2000) TG, TG/MS: applications to determination of residual moisture in pertussis vaccine and other freeze-dried biological products. Proceedings of the 28th NATAS Annual Conference on Thermal Analytical Applications, pp. 67–74.
162 Lin, T.P. and Hsu, Ch.C. (2002) Determination of residual moisture in lyophilized protein pharmaceuticals using a rapid and non-invasive method: near-infrared spectroscopy. *PDA J. Pharm. Sci. Technol.*, **56**, 196–205.
163 De Grazio, F. and Flynn, K. (1992) Lyophilization closures for protein based drugs. *J. Parenter. Sci. Technol.*, **46**, 54–61.
164 Pikal, M.J. and Shah, S. (1992) Moisture transfer from stopper to product and resulting stability implications, in *Developments in Biological Standardization*, vol. 74 (eds J.C. May and F. Brown), Karger, Basel, pp. 165–179.
165 Brinkhoff, O. (1993) Primärpackmittel für Lyophilisate, in *Lyophilisation*, vol. 35 (eds D. Essig and R. Oschmann), Wissenschaftliche Verlagsgesellschaft, Stuttgart, p. 145.
166 Earle, J.P., Bennett, P.S., Larson, K.A., and Shaw, R. (1992) The effects of stopper drying on moisture levels of haemophilus influenzae conjugate vaccine, in *Developments in Biological Standardization*, vol. 74 (eds J.C. May and F. Brown), Karger, Basel, pp. 203–210.
167 Danielson, J.W. (1992) Toxicity potential of compounds found in parenreral solutions with rubber stoppers. *J. Parenter. Sci. Technol.*, **46**, 43–47.
168 Corveleyn, S., De Smedt, S., and Remon, J.P. (1997) Moisture absorption and desorption of different rubber lyophilization closures. *Int. J. Pharm.*, **159**, 57–65.
169 Wang, Z., Frankel, B.A., and Lambert, W. (2001) Determination of moisture in rubber stoppers: effect of Karl Fischer oven temperatures. *PDA J. Pharm. Sci. Technol.*, **55**, 162–170.
170 Liu, W.R. and Langer, R. (1991) Moisture induced aggregation of lyophilized proteins in the solid state. *Biotechnol. Bioeng.*, **37**, 177–184.
171 Zhang, M.Z., Wen, J., Arakawa, T., and Orestrelsky, S.J. (1995) A new strategy for enhancing the stability of lyophilized protein: the effect of the reconstitution medium on the keratinocyte growth factor. *Pharm. Res.*, **12**, 1447–1452.
172 Zhang, M.Z., Pikal, K., Nguyen, T., Arakawa, T., and Prestrelski, S.J. (1996) The effect of reconstitution medium on the aggregation of lyophilized recombinant interleukin-2 and ribonuclease A. *Pharm. Res.*, **13**, 643–646.

173 Shalaev, E.Y., Lu, Q., Shalaeva, M., and Zografi, G. (2000) Acid-catalyzed inversion of sucrose in the amorphous state at very low levels of residual water. *Pharm. Res.*, **17**, 366–370.

174 Yoshika, S., Aso, Y., Izuutsu, K., and Terao, T. (1993) Stability of beta-galactosidase, a model protein drug, is related to water mobility as measured by oxygen-17 nuclear magnetic resonance (NMR). *Pharm. Res.*, **10**, 103–108.

175 Yoshika, S., Asu, Y., and Kojima, Sh. (1996) Determination of molecular mobility of lyophilized bovine serum albumin and gamma-globulin by solid-state 1H NMR and relation to aggregation-susceptibility. *Pharm. Res.*, **13**, 926–930.

176 Vromans, H. and Schalks, E.J.M. (1994) Comparative and predictive evaluation of the stability of different freeze dried formulations containing an amorphous, moisture-sensitive ingredient. *Drug Dev. Ind. Pharm.*, **20**, 757–768.

177 Cleland, J.L., Lam, X., Kendrick, B., Yang, J., Yang, T.H., Overcashier, D., Brooks, D., Hsu, C., and Carpenter, J.F. (2001) A specific molar ratio of stabilizer to protein is required for storage stability of a lyophilized monoclonal antibody. *J. Pharm. Sci.*, **90**, 310–321.

178 Souillac, P.O., Costantino, H.R., Middaugh, C.R., and Rytting, J.H. (2002) Investigation of protein/carbohydrate interactions in the dried state: 1. Calorimetric studies. *J. Pharm. Sci.*, **91**, 206–216.

179 Hsu, C.C., Ward, C.A., Pearlman, R., Nguyen, H.M., Yeung, D.A., and Curley, G. (1992) Determining the optimum residual moisture in lyophilized protein pharmaceuticals, in *Developments in Biological Standardization*, vol. 74 (eds J.C. May and F. Brown), Karger, Basel, pp. 255–271.

180 To, E.C. and Flink, J.M. (1978) 'Collapse', a structural transition in freeze-dried carbohydrates. *J. Food Technol.*, **13**, 583–594.

181 Van Scoik, K.G. and Carstensen, J.T. (1990) Nucleation phenomena in amorphous sucrose systems. *Int. J. Pharm.*, **58**, 185–196.

182 Spiess, W. (1974) *Verfahrensgrundlagen der Trocknung bei niedrigen Temperaturen*. VDI-Bildungswerk, BW 2229, p. 5.

183 Greiff, D. and Rightsel, W.A. (1969) Stabilities of dried suspensions of influenza virus sealed in vacuum or under different gases. *Appl. Microbiol.*, **17**, 830–835 (Table 3).

184 Corveleyn, S. and Remon, J.P. (1999) Stability of freeze-dried tablets at different relative humidities. *Drug Dev. Ind. Pharm.*, **25**, 1005–1013.

2

Installation and Equipment Technique

2.1 Freezing Installation

2.1.1 Cooling by Liquids: Shell-Freezing and Spin-Freezing

The freezing of liquids in vials, bottles, or flasks in a liquid bath is the most common freezing method used in laboratories. As the liquid must have a low melting point, alcohol (ethanol, melting point −114 °C) cooled by CO_2 (boiling point −80 °C at 1 atm) is frequently used. The bath can also be cooled by refrigerated coils.

In the cooled bath the container can be rotated slowly (shell-freezing) or quickly (spin-freezing), as shown in Figure 2.1. The aim of both methods is to reduce the thickness of the liquid product before freezing, to, for example, 15–20 mm. For production purposes, this cannot be used since, first, the sterility of pharmaceutical products cannot be assured and the liquid must be removed from the surfaces before loading the vacuum plant. This can be done by hand for a limited number of containers, but not on a production scale.

If the contents of vials have to be frozen in a production process as quickly as possible in liquids, LN_2 must be used. Figures 2.2 and 2.3 show an automatic freezing plant for vials, which are subsequently cooled in LN_2. The product can be filled into vials with high filling level. Depending on the size of the vials and the amount of product filled, freezing rates up to >10 °C/min can be achieved. Such freezing rates minimize freeze concentration and separation effects, but lead to very small crystals. They will dry more slowly and can contain unfrozen (not crystallized) water. The disadvantages of the unfrozen water are described in Section 1.2.5. By a thermal treatment of the product (see in Ref. [45] of Chapter 1 and Section 1.1.6), these problems can be overcome, but the procedure on a production scale is complex. It is necessary to warm the product for a given time at a given temperature, recool it to low temperatures, and then begin the drying process. Temperature and time must be kept within small tolerances. The data can be developed, for example, by studies with a cryomicroscope or by DSC measurements.

Freeze-Drying, Third Edition. Peter Haseley and Georg-Wilhelm Oetjen.

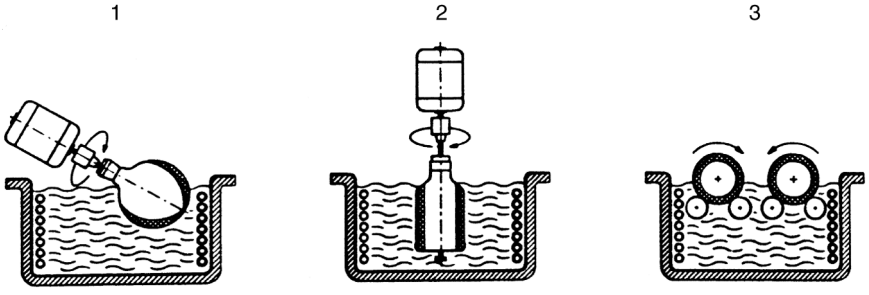

Figure 2.1 Freezing methods. 1, *shell-freezing*: a flask is placed in cold bath in such a way that the neck of the flask is covered by the liquid. A motor turns the flask and the product freezes on the wall. 2, *spin-freezing*: one or more bottles are fixed to a jig and immersed in the bath. The jig turns the bottle(s) so fast around its (their) axle(s) that the liquid is distributed evenly on the wall(s). 3, *shell-freezing*: the bottles are placed on cylinders in the bath, the cylinders turn in the bath. The bottles are turned by the cylinders around their axles. (See also Figure 3 from Martin Christ Gefriertrocknungsanlagen GmbH, D-37507 Osterode, Germany.)

2.1.2 Cooled Surfaces

In most laboratory, pilot and production plants, in which the content of vials and trays are freeze-dried, the shelves can be cooled to −40 to −50 °C, and in special plants −60 °C or slightly lower can be reached. The containers can be loaded on to precooled or room temperature shelves. The possible freezing rates can be estimated using Eq. (1.3) and by methods described in Section 1.1.1. If the shelves are precooled, the loading must be done quickly to minimize the condensation of water vapor from the air on the shelves. For production plants

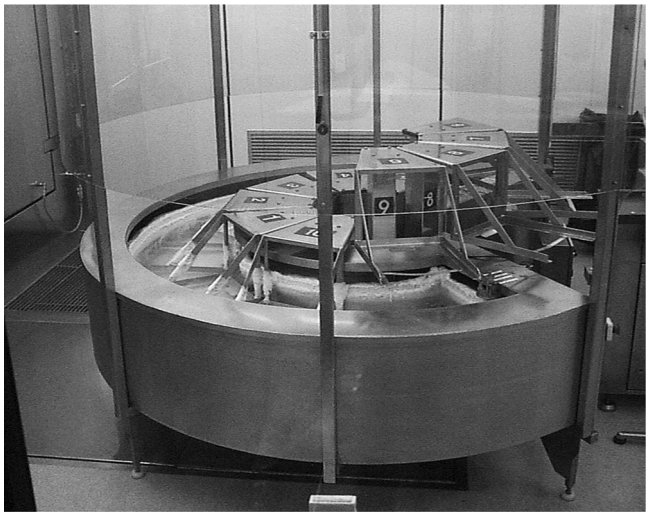

Figure 2.2 This figure shows an LN_2 freezing device in which 50 mL vials with a high (approximately 30 mm) product filling are frozen quickly. The freezing speed is >10 °C/min. The LN_2 freezing system is designed as a rotary system. (Baxter SA, Lessines, Belgium).

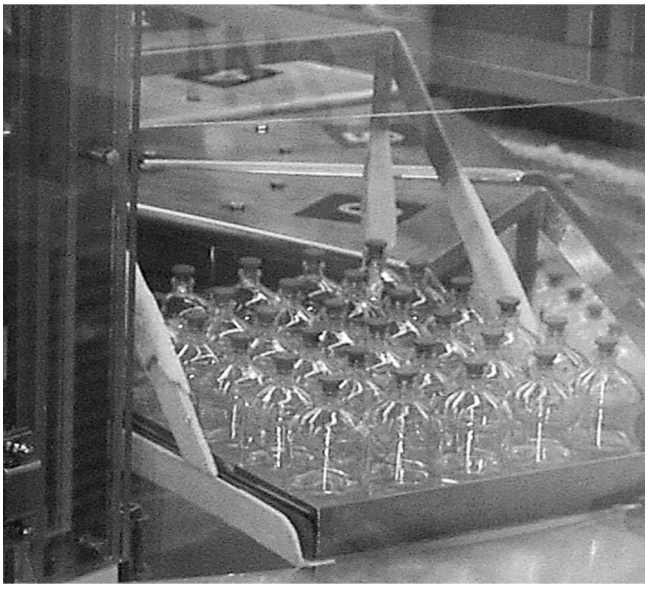

Figure 2.3 The vials filled with product are placed in baskets and taken to the infeed station of the freezing system. The basket is lowered automatically into the LN_2 bath and is transported step by step through the system. At the exit station, the basket is lifted automatically out of the LN_2 bath and manually loaded on to the shelves of the freeze-dryer that have been precooled to <−60 °C. The product temperature when taken out of the freezing bath is approximately −80 °C. (Baxter SA, B-7860 Lessines, Belgium.)

with tens or hundreds of thousands of vials, special loading installations (see Section 2.4.1) are necessary to minimize this problem.

For the freezing of food, stainless steel belt conveyors are used, which are cooled with a spray of cold heat transfer fluid. The design of such conveyors is difficult, since sealing of the moving belt between the heat transfer fluid and food can cause leaks and abrasion.

2.1.3 Product in the Flow of Cold Air, Foaming, and Freezing of Extracts and Pulps

The freezing of pharmaceutical products is almost always done in vials, bottles, ampoules, syringes, or sometimes trays. Food or similar products can be frozen in a flow of cold air in a fluidized bed freezer, if the product is granulated or in small pieces. These conveyor belt or fluidized bed freezers are available commercially in various forms. Figures 2.2 and 2.3 show a plant in which vials with product are cooled and frozen in LN_2. Whether and when such a process provides enough advantages of quality to justify the cost can only be decided from case to case. Two advantages are (i) freezing in a sterile gas with little O_2 and (ii) very rapid freezing.

Figure 2.4 illustrates a process in which the outer layer of a product is quickly frozen as a congealed crust. These CRUSToFREEZE™ plants have a capacity between 1500 and 5000 kg/h and require 0.5–0.8 kg LN_2 per kg of product, which has to be frozen totally on a conveyor belt. Figure 2.5 shows the product exit of the

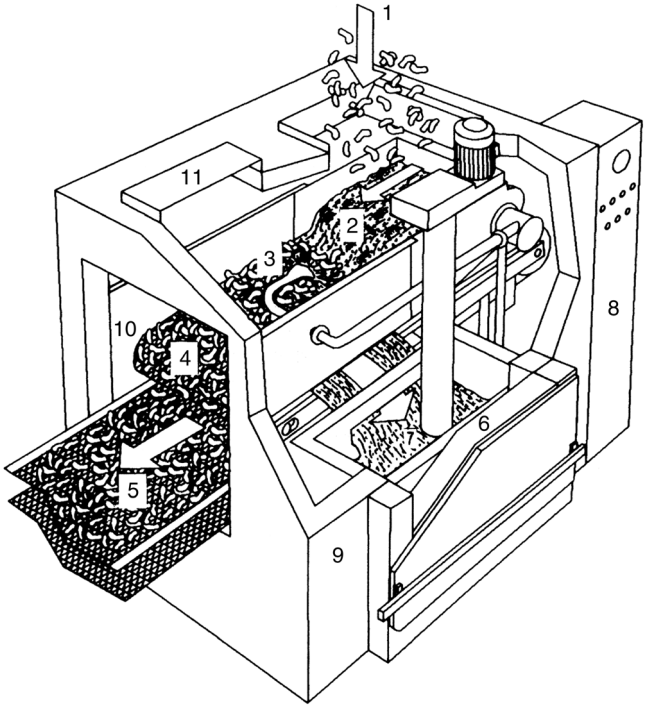

Figure 2.4 Schematic drawing of the IQF-freezing process CRUSToFREEZE® (AGA AB, Frigoscandia Equipment AB, S-25109 Helsingborg, Sweden). 1, Product entry; 2, IQF mixer; 3, injection of LN_2; 4, conveyor belt; 5, belt for frozen product; 6, LN_2 pump; 7, storage container; 8, control unit; 9, insulated housing; 10 and 11, access openings.

plant in Figure 2.4. The freeze-drying of coffee and tea extracts, fruit pulps, or small pieces of meat requires a multistage pretreatment. The granulated end product from coffee and tea extracts should have a defined grain size, a desired color, and a predetermined density. Fruit pulps should become granulated, with the appearance of fruit pieces, while meat pieces should not stick together like a small meat ball but be recognized as single pieces when presented in a meal.

Coffee and tea extracts are therefore foamed by N_2 or CO_2 during cooling and partially freezing (e.g., to −5 °C) in a type of ice-cream machine. This foam must have a desired density, with the inclusion of certain amount of small ice crystals. The foam is cooled on a conveyor belt not to −18 °C, but to −40 °C or colder, as this product must pass a grinding and sieving system to achieve a desired grain size and density.

A typical grinding and sieving system produces dust, which has to be collected. If in addition a CIP (Clean in Place) installation is installed, the total preparation equipment becomes a major part of the whole freezing and freeze-drying installation.

The color of the end product is influenced by the freezing rate (fine crystals show a lighter color). Furthermore, the color is influenced by the structure of the foam and the surface of the dried product. To freeze meat in single pieces, special temperatures have to be used during cutting and preparation of each type of meat.

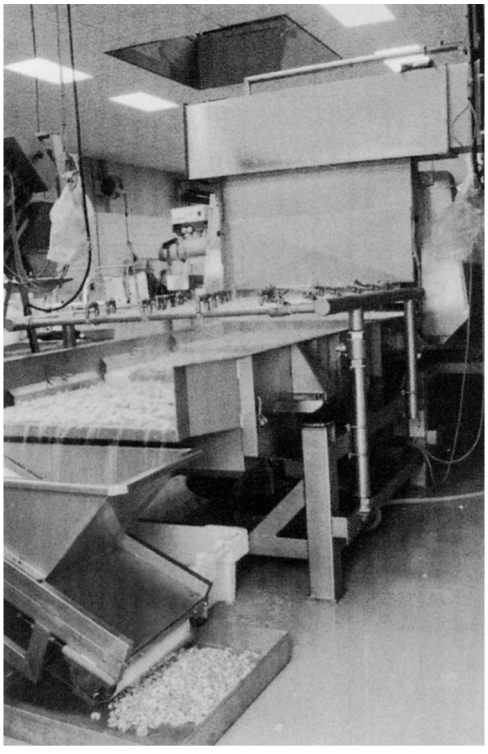

Figure 2.5 Exit lock of the CRUSToFREEZE® as shown in Figure 2.4.

2.1.4 Droplet Freezing in Cold Liquids

The process sounds simple, but becomes difficult if droplets of uniform size are to be produced. The other problem is the formation of a gas veil, which is produced if the liquid, for example, LN_2, evaporates (see Table 1.8 and Figure 1.8).

Figure 2.6 shows the schematic drawing of a process for freezing pellets for freeze-drying and Figure 2.7 illustrates the details of the freezing chamber. Such

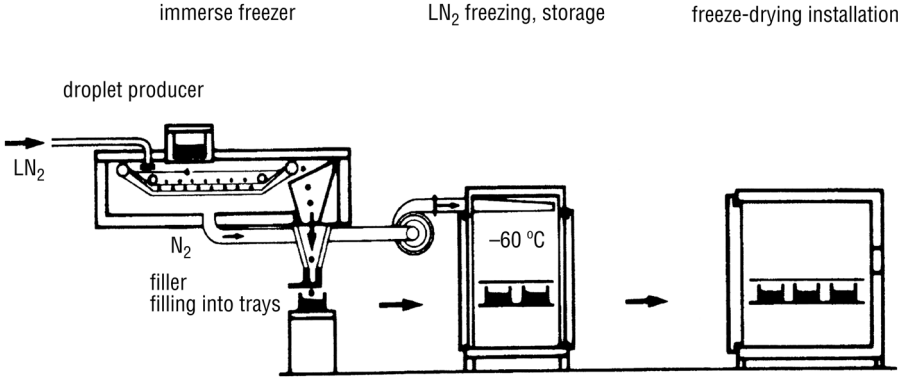

Figure 2.6 Course of processes in a freezing plant, in which the liquid product is frozen dropwise in LN_2. (Based on Cryopel, Messer Group GmbH, D-47803 Krefeld, Germany.)

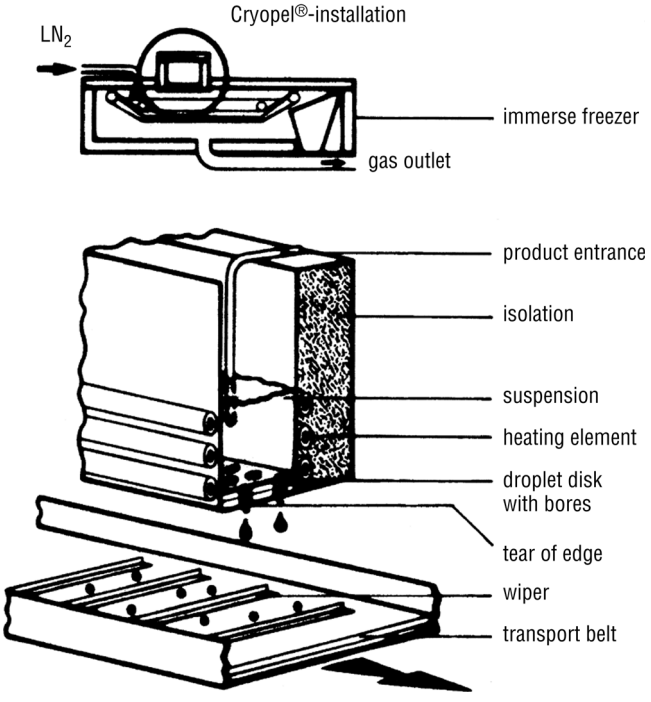

Figure 2.7 Details of the freezer shown in Figure 2.6.

installations are offered under the trade name Cryopel™, with throughputs between 10 and 250 kg/h.

An alternative would be the Cryobreak™ process. Liquid nitrogen is introduced into a pipe-shaped reaction vessel and transported by means of a propeller screw. The product to be frozen is led into the rapidly streaming liquid nitrogen through nozzles. When making contact with the liquid nitrogen, the product is torn into small parts, which immediately freeze. A pump conveys the frozen granulate and the liquid nitrogen to a separating device. The granulate is separated and any remaining liquid nitrogen is returned to the reaction vessel. The granulate does not have a uniform shape; a certain amount of fines is unavoidable.

The Cryopel and Cryobreak processes are suitable for industrial production only in a limited way. The attainable throughput is 300 kg/h at the most.

A new process – Cryogen® Rapid Pelletizer (Figure 2.8a) – avoids such disadvantages. Pellets of uniform quality and size can be produced in large quantities. This process combines the advantages of very rapid freezing in liquid nitrogen with economical utilization of the cold gas energy. The nitrogen consumption can be decreased by roughly 30% in comparison with the processes applied up to now.

The Cryogen Rapid Pelletizer has a modular construction. Its nominal freezing capacity is approximately 250 kg/h per module. Up to a maximum of six modules can be combined to form one unit (Figure 2.8b).

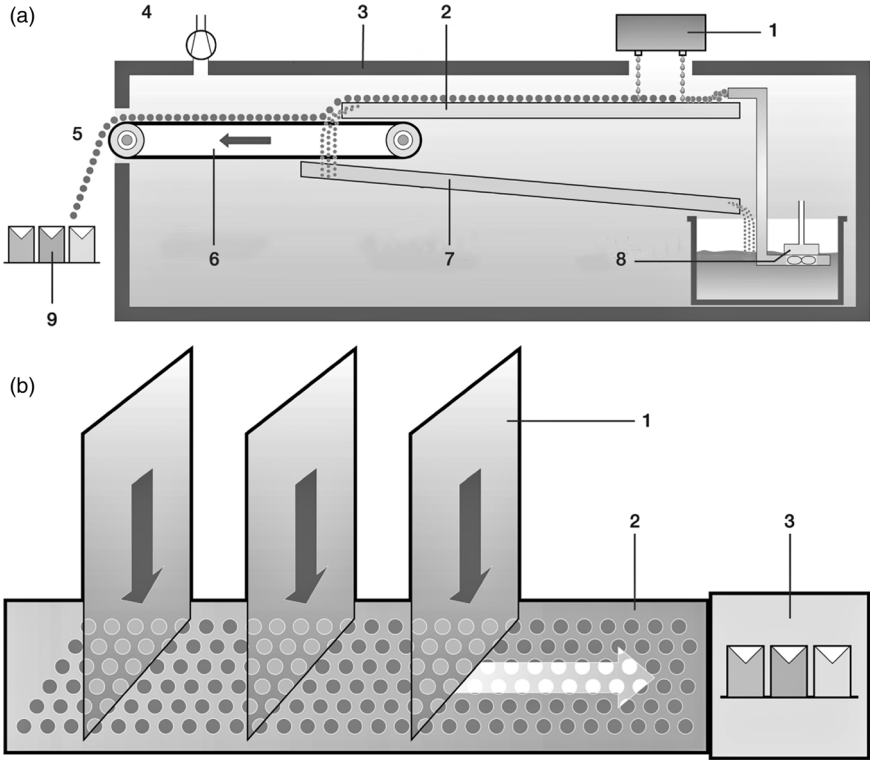

Figure 2.8 Schematic drawings of a Cryogen Rapid Pelletizer. (a) Pellet production. 1, dropper unit; 2, pelletizing channel; 3, insulation; 4, ventilator; 5, product; 6, conveyor belt; 7, return channel for liquid nitrogen; 8, liquid nitrogen pump; 9, weighing and packaging. (b) Principle of a pelletizer with several modules and one conveyor belt. 1, pelletizing modules; 2, conveyor belt; 3, weighing and packaging. (Messer Group GmbH, 47803 Krefeld, Germany.)

Figure 2.8 shows a schematic drawing of a Cryogen Rapid Pelletizer. This process is of special interest if a product has to be frozen more quickly than is possible on belts or in trays: A pellet of 2 mm diameter is cooled from 0 to −50 °C in ∼10 s or at a rate of ∼300 °C/min. The advantages are minimum freeze concentration, free-flow product, and small ice crystals (which are acceptable in this case of small transport distances for energy and water vapor). It is likely that some pellets (those too large or too small) will need to be removed by sieving.

Such freezing processes are more suitable for a production of foods and clean operations than for use in the pharmaceutical industry. It is extremely difficult to attain sterile conditions.

Yokota [1,2] sprayed the liquid to be frozen in a film of cold *n*-hexane, which flows down the inner wall of a conical vessel. The frozen particles are sieved off. With this method, two problems need to be solved: (i) the droplet size cannot be influenced, product parts can be extracted, and the product and *n*-hexane must be completely separated, and (ii) the process must be sterile.

2.1.5 Freezing by Evaporation of Product Water

This method (see Section 1.1.1) is only mentioned in order to highlight the problems associated with it; no applications are given. The withdrawal of water from an aqueous product under vacuum is a vacuum-drying process with known consequences, namely, structure changes and shrinkage. Depending on the viscosity of the product, it is difficult to dissolve skin surfaces or sticking lumps are formed. The remaining water may no longer be freezable. This method cannot be recommended as a freezing step for products that are to be freeze-dried.

2.1.6 Nucleation-on-Demand Technology – ControLyo™

The importance of nucleation temperature is well known (Gieseler/Meister). Many scientific papers are published by renowned scientists [2,3]. Freezing is the most important step in the whole freeze-drying process. If this process is not well understood and done, no one can expect a high-quality end product, and an error at this stage cannot be corrected later in the drying process.

In the context of optimizing the freezing step, it is helpful to understand the basic of nucleation and supercooling. These physical behaviors are as follows:

- Nucleation temperature is the temperature at which freezing or ice crystal formation begins to take place.
- Nucleation rarely occurs at the equilibrium or the thermodynamic freezing point of the solution. In a laboratory or development freeze-dryer, it is common for nucleation to occur between 10 and 20 °C below the thermodynamic freezing point.
- The degree of supercooling can have a dramatic impact on the drying behavior. High degree of supercooling → small ice crystals → smaller pores during sublimation → increases resistance to mass transfer → increased primary drying time.
- Low degree of supercooling → larger ice crystals → larger pores during drying → reduced resistance to mass transfer → decreased primary drying time.
- This effect can be significant. Studies have shown that for every 1 °C increase in the nucleation temperature, main drying (MD) time can be reduced by as much as 3–4%.

A new technique, known as "ControLyo" or "Nucleation-on-Demand Technology",[1] can help to improve the nucleation process. Exemplary freezing process and technical requirements on the lyophilizer: The chamber must be built for overpressure (TUEV or ASME rating).

The products (vials) are loaded on precooled shelves, precooled to 4 °C. After loading, the temperature is reduced to −4 °C or whatever temperature is desired – cooling rate, for example, of 0.5 °C/min. After −4 °C has been reached, pressurize the chamber with an inert gas (argon or nitrogen) to approximately 1.7 bar. The gas dissolves in the still liquid product. This temperature (insistence temperature) is kept for as long as necessary to achieve vial to vial temperature homogeneity

1 Praxair, Inc., 39 Old Ridgebury Rd., Danbury, CT 06810 USA.

(e.g., 25–35 min.). Depending on the product, continue to lower the shelf temperature, for example, to −6 °C. After equilibrium temperature distribution is reached, rapidly depressurize the chamber pressure. What happens is similar to the foaming of a soda bottle on quick opening. The gas inside the product escapes, resulting in the formation of microscopic gas bubbles. Relatively large ice crystals are formed. This provides the best conditions for a shorter main drying time. Reductions of main drying time up to 30% are possible.

The freezing process continues up to the selected temperature. *Conclusion:* By using "Nucleation-on-Demand-Technology," controlled nucleation can be reached. Negative side effects can be minimized, as, for example, the edge effect (Ref. [57] of Chapter 1) unequally freezing (see Section 1.2.1 and Figure 1.101).

2.2 Components of a Freeze-Drying Plant

2.2.1 Installations for Flasks and Manifolds

Figure 2.9 shows an installation for flasks and other containers in which the product is to be dried. For this type of plant, a condenser temperature of −55 °C is sufficient as this temperature corresponds with a water vapor pressure of $\sim 2 \times 10^{-2}$ mbar, allowing a secondary drying down to $\sim 3 \times 10^{-2}$ mbar. This is acceptable for a laboratory plant, in which the limitations are not the condenser temperature but the variation of heat transfer to the various containers, the

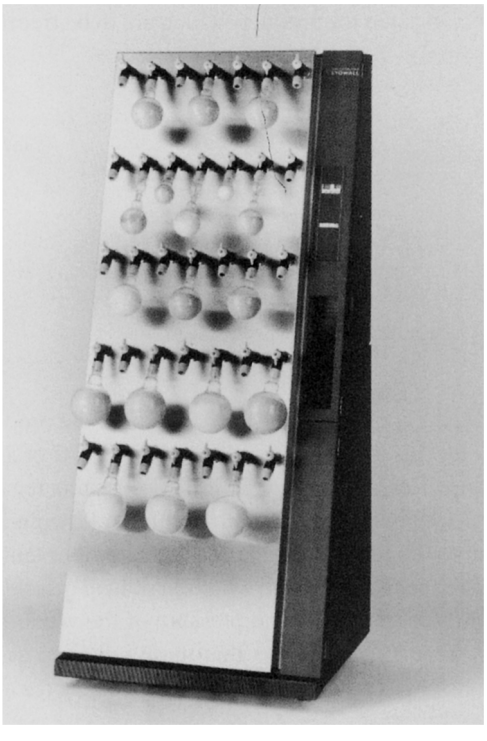

Figure 2.9 Freeze-drying plant for flasks or bottles, 35 connections NS 29/32, maximum 7.5 kg ice in 24 h, T_{co} down to −53 °C. (Lyowall®, Steris GmbH, D-50354 Hürth, Germany.)

rubber tube connections, and the end pressure of the vacuum pump (two-stage pump, $\sim 2 \times 10^{-2}$ mbar). Figure 2.9 shows that these units are designed for very different needs. The ice condenser in this plant can take up 7.5 kg of ice at temperatures down to −53 °C.

These installations are relatively easy to handle, their disadvantage being the control of T_{ice}. The heat transfer from the air is difficult to adjust, since it depends on the geometry of the containers and their location at the plant. If, for example, −30 °C has to be the ice temperature, then the containers have to be cooled by a bath of $\simeq$ 10 °C. It is preferable to dry such products in a chamber with shelves, which can be cooled and heated.

2.2.2 Drying Chambers and Forms of Trays

Drying chambers for freeze-drying are built in three basic configurations (Figure 2.10):

- Bell with baseplate
- Rectangular or cylindrical chamber
- Tunnel with round cross section

Bells with baseplate are used for laboratory plants; they are cost-effective, but cannot be sterilized by steam. Figure 2.11 shows a typical bell installation in which the shelves are usually heated, but cooling can be provided in addition to a closing mechanism for vials.

In Figure 2.12, a drying chamber is shown with a Plexiglas™ door and a hydraulic closing system for the vials (not to be sterilized by steam). Figure 2.13 represents a rectangular production chamber, sterilizable by steam, designed for automatic loading and unloading (see Section 2.4.1). The shelves are loaded with vials through a small door (see Section 2.4) that can be closed by a hydraulic system (see Section 2.4.1). Figure 2.14 shows a rectangular chamber (CIP/SIP) with a small loading door and main service door on the right-hand side of the chamber.

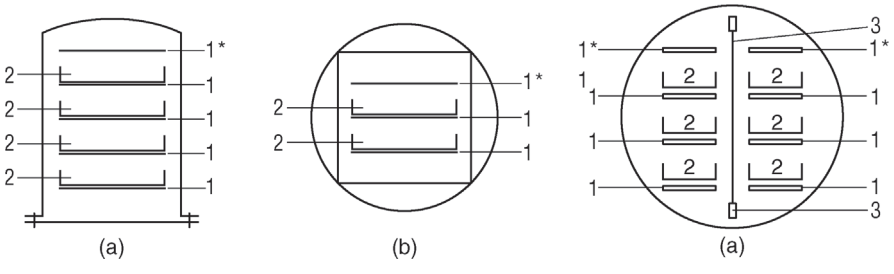

Figure 2.10 Basic types of freeze-drying chambers. (a) Belljar or vertical cylinder. (b) Rectangular or cylindrical chamber with one (or two) door(s). (c) tunnel dryer, in which the trays are transported in and out by a system (shown as a carrier on a monorail). 1, temperature-controlled shelves; 1∗, temperature-controlled plate, to expose the product on the upper shelf to the same conditions as on the other shelves; 2, trays or vials; 3, transport system for trays.

Figure 2.11 Freeze-drying plant of the type in Figure 2.10a. 1600 cm^2 temperature-controlled shelf area stoppering device for vials on four shelves, valve between chamber and condenser, for BTM and DR measurements, freezing is possible between the condenser coils or in the shelves if they are cooled and heated by brine from a thermostat, T_{co} down to −55 °C. (LYOVAC® GT 2, Steris GmbH, D-50354 Hürth, Germany.)

Figure 2.12 R&D freeze-drying plant for cycle development with 0.54 m^2 shelf area, T_{sh} from −50 to +70 °C; stoppering device for vials; T_{co} down to −70 °C; ice storage capacity 10 kg. (AFD 0.5; Austar Group P.R. China.)

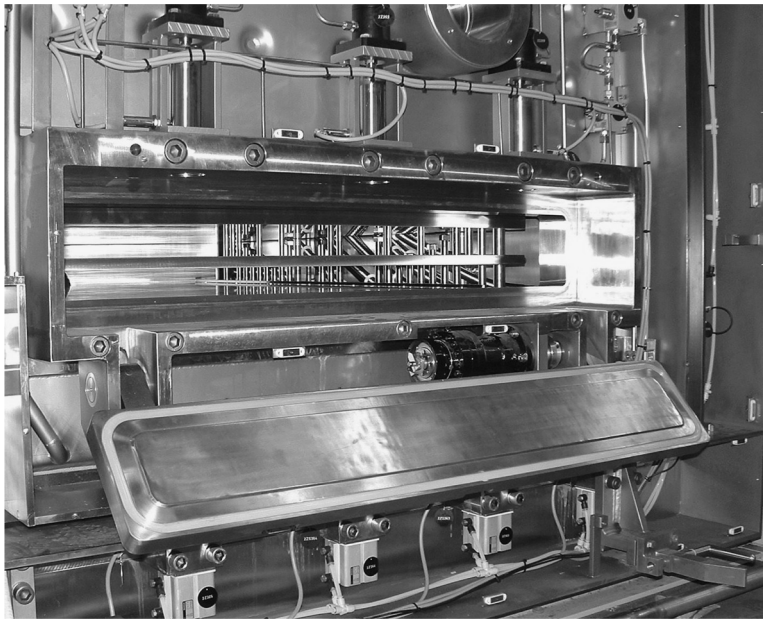

Figure 2.13 Rectangular chamber, steam-sterilized, with a small loading door in the main door, which can be designed to open either upward or downward (in this example, the loading door opens downward). (Steris GmbH, D-50354 Hürth, Germany.)

Figure 2.14 Rectangular chamber (CIP/SIP) with a small loading door and main service door on the right-hand side of the chamber (AUSTAR Group, P.R. China).

Tunnels as drying chambers are used for luxury and food products or other products prepared on a large scale, for example, collagen. The rapid loading and unloading of, for example, 500 kg of product in 15 min is a typical requirement. The product, in trays, is placed on cars hanging on an overhead rail. The cars can either be quickly moved between the heated shelves and later unloaded the same way or they can be continuously moved through the tunnel. In the other method (Figure 2.13), larger trays are pushed through the free distances between the heating plates (see Section 2.5.2). All chambers must be easy to clean (see Section 2.3.4), that is, the surfaces must be smooth and all corners rounded, leak tight, and with no measurable resistance to the flow of water vapor. If the water evaporation rate is high (e.g., up to 3 kg/h m^2 in food freeze-drying) or the operating pressure is low [p_c 0.08 mbar during MD for pharmaceuticals], the transport path for water vapor has to be carefully calculated (see Section 1.2.4). If at all possible, bottles or vials should be placed directly on the shelves, as the heat transfer is more effective when there are no trays between the vials and shelves. For pilot and small production plants, trays can be used with a bottom that may be removed before evacuation. If trays are used, they should have a machined bottom, as can be seen from Table 1.14; the heat transfer coefficient for machined bottoms can be up to twice that of trays with uneven bottoms.

For granulated luxury products and food, two basic forms of tray are used (Figure 2.15): (a) large, rectangular or square trays with low walls (e.g., 400 × 500 × 30 mm) or (b) ribbed trays (e.g., 500 × 160 × 50 mm). Trays of type (a) are pushed

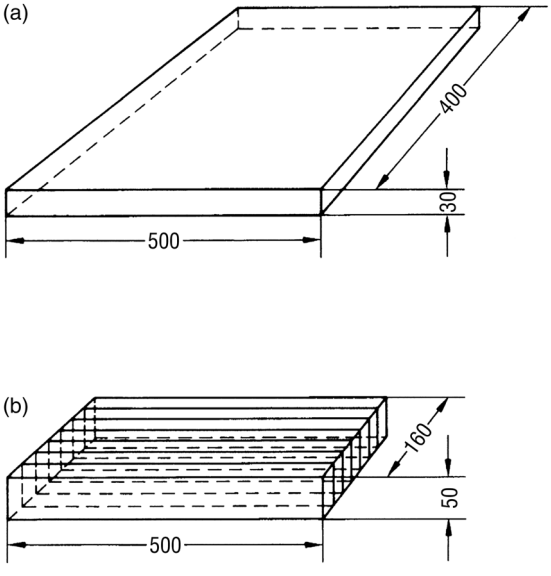

Figure 2.15 Type of tray for freeze-drying small cubes or granules of food. Tray (a) 400 × 500 mm, 30 mm height; tray (b), for example, 500 × 160 mm, 50 mm height.

through the plant between the heated shelves without contact (System Atlas Industries, Ballerup, Denmark). The ribbed trays (b) are made from extrusion-molded aluminum with a machined bottom (Figure 2.15). During the drying process they are placed on the heated shelves, but for transport they are elevated slightly and lowered onto the shelves again in the new position (System Leybold; now ALD Vacuum Technologies, Erlensee, Germany). The distances between the ribs can be modified to meet the dimensions of the granulate. For certain products with small granulates (mm range) ribbed trays are used with inserts to facilitate vapor flow from the product into the chamber. This is especially important if the water evaporation rate is high, for example, 2–3 kg water/m^2 h.

Rolfgaard [4] compared the types of trays and heating systems: The ribbed trays are said to have an uneven temperature distribution, because the distances between shelf and tray vary between 0.1 and 1 mm. The ribs could compensate for this only partially. The variation in distances is correct, but Rolfgaard overlooked that the thermal conductivity in the bottom of the tray is so effective that practically no temperature differences are established in the bottom. Even with an evaporation of 3 kg ice/m^2 h and the assumption that all heat is transmitted only in the center of the tray (8 cm from the border of the tray), the temperature difference between border and center is ~5 °C. During the drying under actual conditions, no measurable temperature differences can exist.

However, there is a major difference between the two forms of trays and heating systems. As shown in Figure 1.91, ~1.3 kg ice/h m^2 can be sublimed by radiation heat, if the shelves have a temperature of +100 °C and the product temperature is −20 °C. The main difference is the method of heat transfer: With a flat tray and mostly radiation energy, the density of the heat flow is limited and it can be substantially larger with ribbed trays standing on the heated shelf. Using the temperatures as above and an average value $K_{tot} = 100$ kJ/h m^2 °C from Tables 1.14 and 1.15, ~4.3 kg ice/h m^2 can be sublimed.

Figure 2.16 (Suwelack, O., Billerbeck, Germany, unpublished data) shows the ice evaporation/m^2 h for different flat and ribbed trays. The difference in sublimation rates is a factor of ~4 or 400%. The ribbed trays are more expensive than flat trays, as Rolfgaard states. However, as shown in Figure 2.16, the ice sublimation rate of ribbed trays is ~3.5 times larger than that of flat trays. This is understandable from Eq. (1.15), in which the layer thickness d is decisive for the drying time (if the maximum possible T_{ice} during MD and the maximum T_{pr} during SD are applied). If the rib distance is chosen similar to the layer thickness in a flat tray, the drying time becomes similar, but the ribbed tray has a load per m^2, which is three to four times higher than a flat tray and the necessary heat transfer is possible by contact and convection.

Trays for Special Applications

Nearly all pharmaceutical products must be processed under strict aseptic conditions and be protected from outside contamination. In addition, as is the case for antimitotic drugs used in cancer therapy, some products are toxic, such as cytostatica, and should not be released into the environment. Bulk freeze-drying

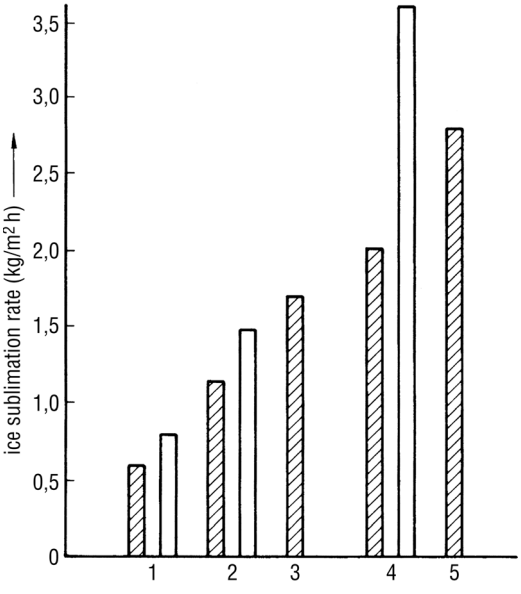

Figure 2.16 Ice sublimation rate (kg/m^2 h) for five different types of tray. 1, flat tray as in Figure 2.15a, with 20 mm filling height; 2, flat tray with one rib of 20 mm height; 3, ribbed tray; 4, ribbed tray; 5, ribbed tray for cubes or granules of food. (Designed by Dr Otto Suwelack, D-48723 Billerbeck.) All tests were carried out with the same granulate. *Hatched columns:* Heating plates or shelves were heated for ~30 min to 100 °C; when the tray bottom reached +40 °C, the temperature was reduced in such a way that the +40 °C was kept constant. *White columns:* Heating plate or shelves were heated to +140 °C for ~2 h and the temperature reduced after +40 °C was reached as above. Measurements by Dr Otto Suwelack, D-48723 Billerbeck, Germany.)

is best done within a controlled, confined container that in turn does not hinder processing.

W. L. Gore & Associates (Figure 2.17) has developed a type of tray from which product particles cannot escape during the drying process – the Lyoguard™ tray. Rey [5] has carried out several studies with the Lyoguard™ freeze-drying trays.

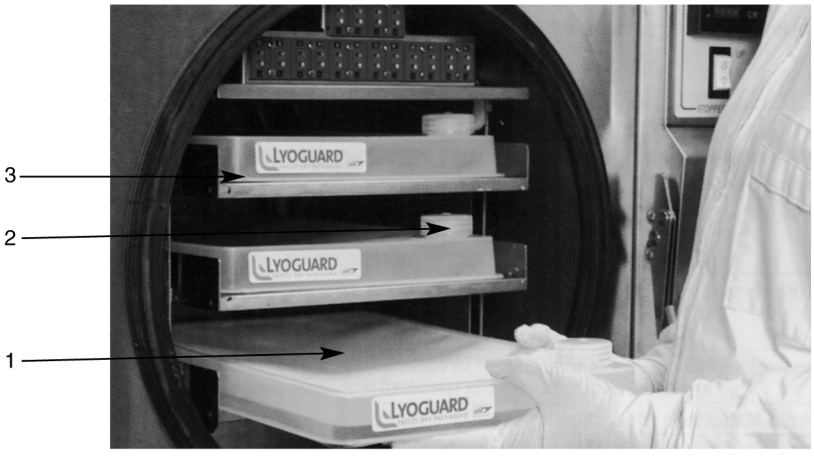

Figure 2.17 Lyoguard™ tray for special applications. 1, Gore-Tex© membrane barrier; 2, fill cap, allows thermocouple attachment; 3, flexible, transparent thin-film bottom. (Based on W. L. Gore, D-85636 Putzbrunn, Germany.)

2.2.3 Shelves and Their Cooling and Heating

As shown in Section 1.2.1, heat transfer from the shelves to the container depends largely on planar shelves and trays. Stainless steel shelves in pharmaceutical plants are polished until the roughness height is R_a 1.5 (corresponding to ~1.0–1.5 µm). The deflection should be smaller than 1 mm/m. The small roughness height also improves the cleaning and sterilization. In food installations using ribbed trays, the shelves are made from deep-drawn plates with tolerances of 0.1 mm. With radiation heating, the roughness is not important for the heat transfer.

Shelves in plants for pharmaceuticals are mostly cooled and heated with heat transfer fluid. The amount of heat transfer fluid per unit time and its distribution in the shelf have to be guided in such a way that the temperature difference between the inlet and outlet of the shelf is <1.5 °C during the maximum sublimation rate in MD. This maximum temperature difference and the maximum heat to be supplied at this difference should be written into a plant specification. It is recommended to use two cooling systems for the cooling of the heat transfer fluid and the condenser, otherwise the temperature control of the condenser and of the heat transfer fluid can influence each other. In large continuous plants, which need no cooled plates because the product is frozen outside and temperatures below +30 °C are normally not needed, the plates are heated by vacuum or pressurized steam or by a heat carrier.

2.2.4 Water Vapor Condensers

Calculation of the Sublimation Performance and, as a Result, the Size of the Valve between Chamber and Condenser (see Figure 2.18)

The volumes of water vapor are too large to be pumped by mechanical vacuum pumps in the pressure range of freeze-drying: 1 kg of ice at 0.4 mbar represents a volume of ~2800 m^3 or at 0.04 mbar ~25 000 m^3 (see Figure 1.2). Only steam ejectors could do this, but these need large quantities of cooling water and steam, in addition to large areas for the multistage systems. In today's plants, water vapor is therefore condensed on cold surfaces, consisting of plates or mostly of tube coils (see Figure 2.19a and b).

This section deals with the calculation of the flow path in a lyophilizer, in particular the connection between chamber and condenser.

The course of sublimation is not linear. A rule of thumb says that 50% of the ice amount will sublimate in the first quarter of the primary drying time. This rule has been proven in practice.

Of course, the physical rules for free vapor flow must be considered. Vapor transport into the condenser depends strongly on the geometric design of the plant (Figure 1.2.4). Under favorable conditions between the chamber and the condenser, a vapor speed of 60–90 m/s can be expected.

The connection between the chamber and the condenser should be straight and if the installation had been designed with $l/d = 1.6$, it would likely be the best possible technical solution (see Figures 2.20–2.22). Of course, the flow paths in the chamber have to ensure a free flow. These are the areas between the shelves,

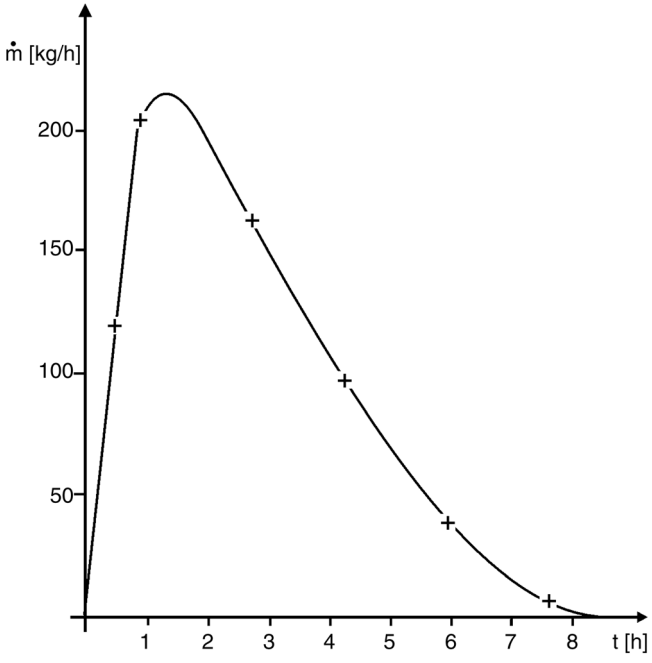

Figure 2.18 Sublimation performance of a food lyophilizer, loaded with 818 kg of celery. Drying time 8 h. (Vakutec Trocknungsanlagenbau, Heidenau, Germany, 12/2003; Dieter Rudolph.)

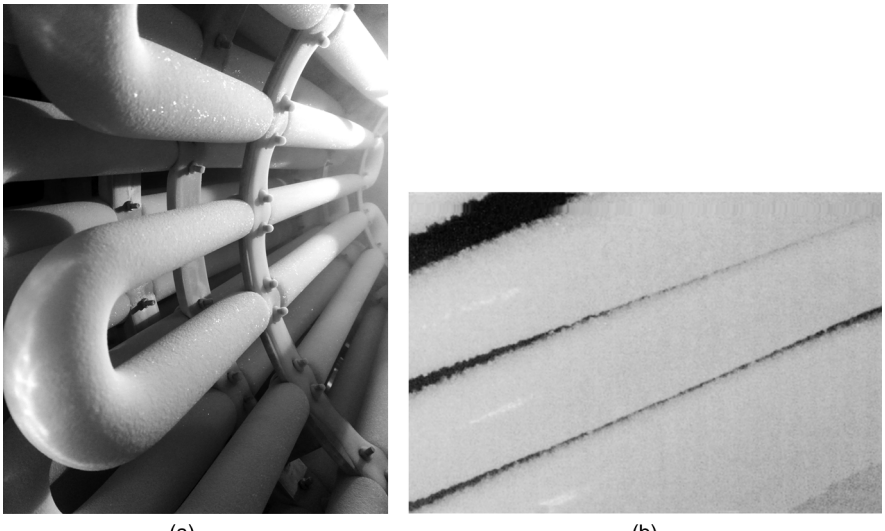

(a) (b)

Figure 2.19 Coils in a condenser covered by ice, observed through a window during two freeze-drying processes. (a) Smooth, solid surface. (Photograph by Austar Group, P. R. China.) (b) Porous, snow-like surface, which occurs typically, if the pressure of permanent gases during MD is high. (Photograph by Dr Otto Suwelack, D-48727 Billerbeck, Germany.)

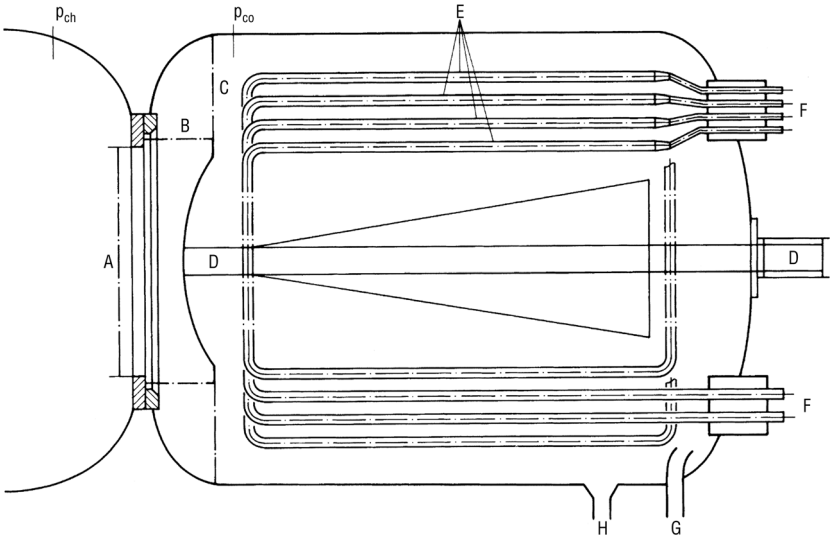

Figure 2.20 Schematic drawing of a water vapor condenser for a freeze-drying plant. A, free diameter of the connection to the chamber; B, cylindrical opening by the movement of D; C, opening between condenser wall and valve plate; D, valve plate, hydraulic valve drive; E, condensation surface of the refrigerated coils; F, inlet and outlet of the refrigerant; G, tube connection to the vacuum pump; H, water drain during defrosting of the condenser; p_{ch} and p_{co} pressure in the chamber and in the condenser, respectively.

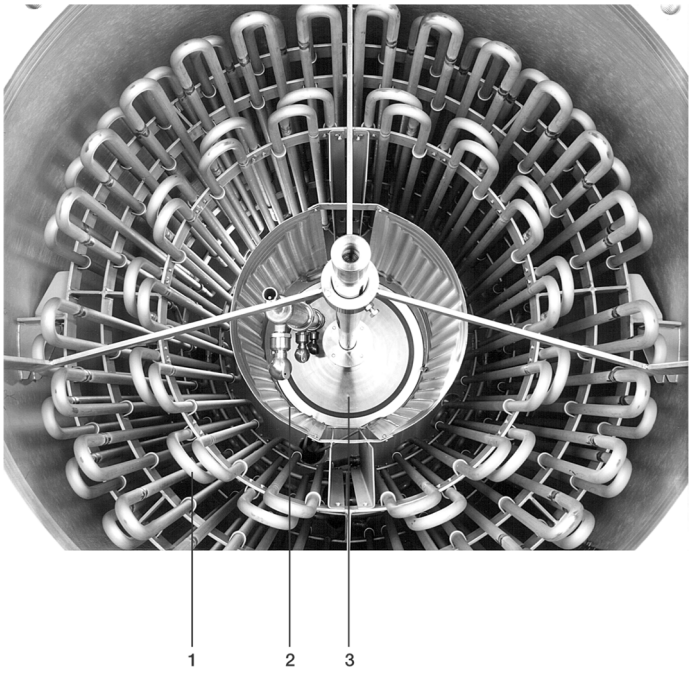

Figure 2.21 Inside view of a condenser showing two evaporators. 1, Tube condenser cooled by direct expansion of refrigerant, for example, R404A (see Table 2.3); 2, plate evaporator cooled by direct expansion of LN_2; 3, valve plate of the mushroom valve. (Steris GmbH, D-50354 Hürth, Germany.)

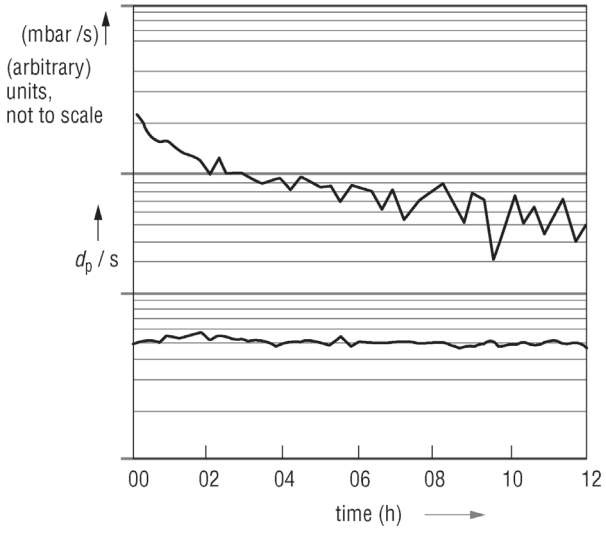

Figure 2.22 Comparison of valve D (Figure 2.20) functions. *Upper plot:* The valve does not operate reproducibly. *Lower plot:* Measurements of the pressure that rise per second (d*p*/s) are on the order of magnitude of 1.2×10^{-4} mbar/s, standard deviation (SA) $\sim 0.04 \times 10^{-4}$ mbar/s. (Measurements by Steris GmbH, D-50354 Hürth, Germany.)

the shelf package, and the side walls. In the first quarter of the primary drying, large vapor volumes have to be transported from the chamber into the condenser.

Example: 1 kg of ice at 0.5 mbar turns into a vapor volume of approximately 2.740 m^3.

Calculation example: 100 kg of ice amount shall be sublimed (primary drying) in 18 h at a vapor pressure of 0.5 mbar (corresponding to −27.1 °C T_{ice})

q = max. sublimation amount (kg/h)
G = Ice amount (kg) (batch load)
h = primary drying time

$$q = \frac{G}{2} \times \frac{1}{0.25 \times h} = \frac{2 \times G}{h} \left(\frac{kg}{h}\right) \tag{2.1a}$$

$$q = \frac{2 \times 100}{18} = 11.11 \frac{kg}{h} \tag{2.1b}$$

corresponds to approximately 304 400 m^3 of water vapor.

In order to carry this volume of water vapor into the condenser (at 80 m/s vapor speed), a pathway of 450 mm diameter is necessary. One can see that the engineering and the design of this part has a decisive impact of the plant performance.

Consequently, the maximum cooling capacity for the condensation of the water vapor emitted is calculated from q (maximum sublimation amount kg/h). For the condensation of 1 kg ice, approximately 0.9 kW cooling capacity is needed.

Q_{total}	=	$Q_{ice1} + Q_{crystallization} + Q_{water} + Q_{evaporation}$
Q_{ice1}	=	$(m \times c_1 \times \text{delta } T_1) = (1 \times 0.5 \times 40) = 20$ kcal ($= 0.022$ kW)
$Q_{crystallization}$	=	$(m \times 80) = 80$ kcal ($= 0.09$ kW)
Q_{water}	=	$(m \times c_2 \times T_2) = 1 \times 1 \times 100 = 100$ kcal ($= 0.12$ kW)
$Q_{evaporation}$	=	$(m \times 567) = 567$ kcal ($= 0.67$ kW)
m	=	mass (amount of water/ice in kg)
c_1	=	specific heat of ice (0,5 kcal/kg °C)
delta T_1	=	40 °C (−40 °C to 0 °C – to warm up the ice)
crystallization heat	=	80 kcal/kg °C
c_2	=	specific heat of water (1 kcal/kg°C)
T_2	=	100 °C (to warm up the ice from 0 °C to 100 °C)
evaporation heat	=	567 kcal/kg are needed to convert 1 kg water into vapor.

Condensers must fulfill five essential requirements:

1) The surface area has to be large enough to condense the ice at a maximum thickness, which does not reduce the heat transfer from the tube surface to the condensing surface of the ice. The heat conductivity of ice depends on its structure. If this structure is solid and smooth, one can calculate 6.3 kJ/m h °C; if the structure is more like snow, the heat conductivity is much lower, for example, one decade; this happens typically if the air pressure is too high (see Figure 2.19). To condense 1 kg of water in 1 h on 1 m^2 surface on top of an existing ice layer of 1 cm, the temperature difference between tube surface temperature and the ice surface temperature is ~4.5 °C. To reduce this temperature difference to 2 °C, the condenser would have to be defrosted every 30 min. Therefore, it is practical to design the condensing surface large enough to take up the total amount of ice of one charge in a layer of ~1 cm, for example, if the total amount of ice to be condensed is 10 kg, the surface should be 1 m^2 to form a layer of 1 cm; if the main drying time is long with a small amount of water per hour, then half the size (0.5 m^2) may be sufficient. In this example, the temperature difference during a main drying cycle of 5 h is limited to 1–2 °C (see Figure 2.23).
2) The geometry of the connection between the chamber and condenser must be designed for the transportation of large volumes of water vapor. The volumes of water vapor to be transported at different sublimation pressures are shown in Figures 2.24–2.26.
3) The temperature difference between inlet and outlet temperature at the coil(s) of the refrigerant should be small, to ensure a uniform condensation on the total coil. On warmer areas no ice will condense until the temperature at the ice surface has increased to the warmer temperature on the coil. For large surfaces, it is necessary to use several coils or plates in parallel, each of which must be separately temperature controlled. If the condenser is operated in an

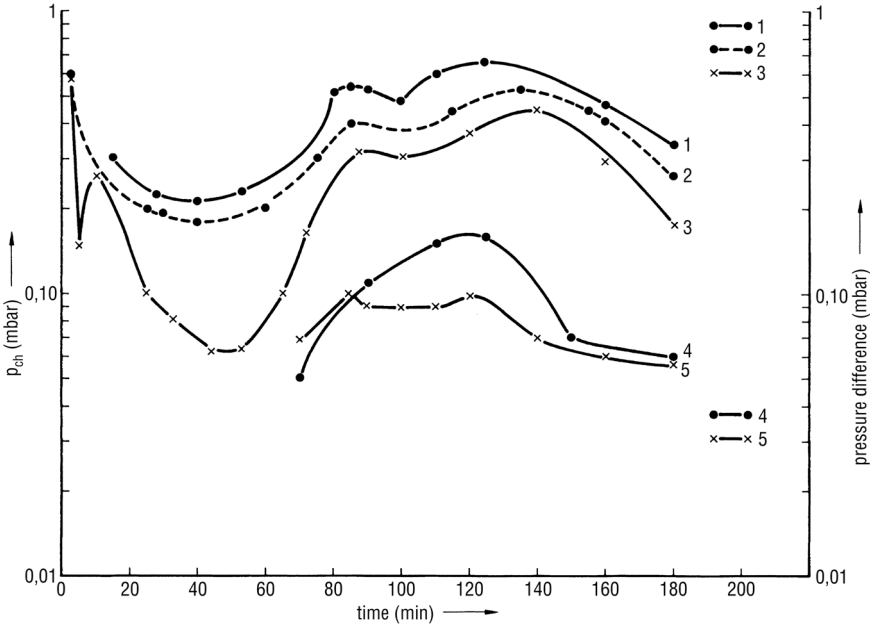

Figure 2.23 Plots of a test to determine the specific water vapor flow or the water vapor speed in a production freeze-drying plant with ~30 m^2 shelf area. For the tests 300 kg of distilled water were filled into ribbed trays, which were placed on the shelves. Six RTD were placed in different trays and frozen with the water. The RTD temperatures and BTM measurements were practically identical, because the RTD were always immersed in the ice and during the test only 25% of the ice was sublimed. 1, p_s, calculated from T_{ice} by Table 1.21; 2, p_{ch}; 3, p_{co}; 4, pressure difference ($p_s - p_{ch}$); 5, pressure difference ($p_{ch} - p_{co}$). (*Note:* The temperature of the shelves was hand controlled, because automatic control of the large plant would have been too slow for the short test time.)

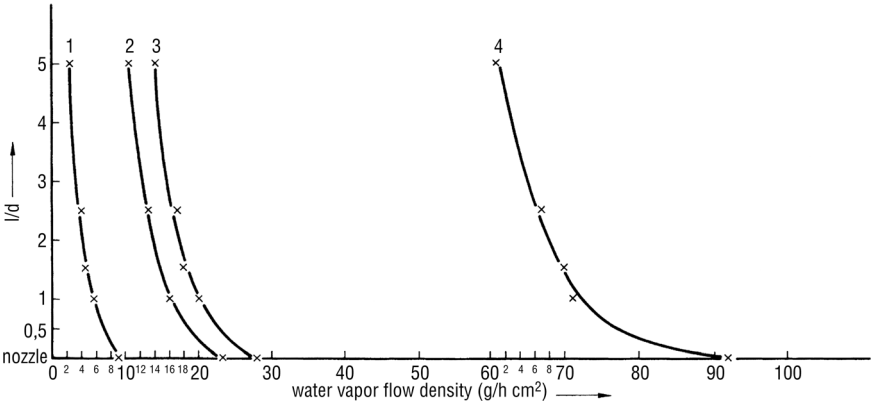

Figure 2.24 Water vapor flow density (g/cm^2 h) as a function of the ratio *l/d* of the connecting tube from the chamber to the condenser at four different pressures p_{ch} as parameters (*l* length, *d* diameter of the tube): 1, 0.1 mbar; 2, 0.32 mbar; 3, 0.4 mbar; 4, 1.3 mbar.

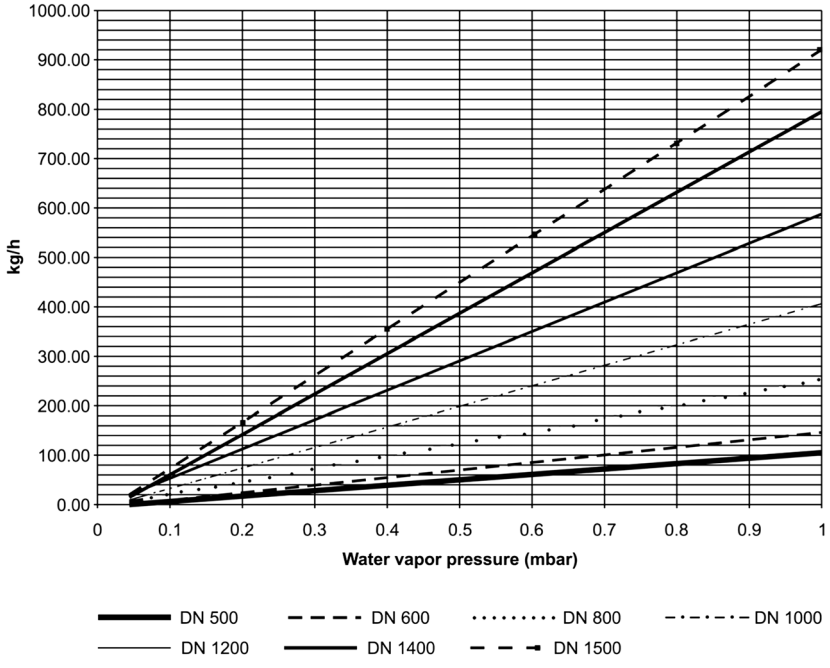

Figure 2.25 The diagram shows the water vapor transportation rate (kg of H_2O per hour) at different pressures and different valve sizes. See Figure 1.142 for sizes and pressures below 0.1 mbar. The values shown apply to $l/d = 1.6$ and a straight connection between chamber and condenser.

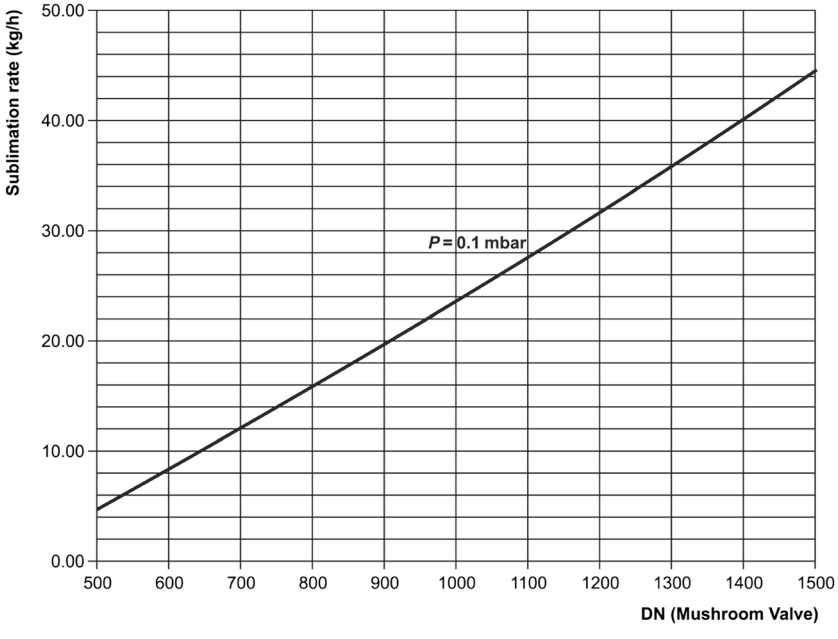

Figure 2.26 The diagram shows the water vapor throughput at different cross sections ($l/d = 1.6$) at a given sublimation pressure of 0.1 mbar. A precondition is that the connection between the chamber and condenser must be straight.

overflow mode (this applies to condensers that are operated with ammonia), the weight of the liquid column should not change the boiling temperature of the liquid at the bottom of the column measurably.

4) The flow of water vapor should deviate as little as possible before the first condenser surface. The condenser design has to ensure that the water vapor is completely frozen and the remaining water vapor pressure is practically equal to the vapor pressure at the ice surface. This can only be achieved if the vapor passes over several condenser surfaces in series.
5) The permanent gases must be pumped off at the lowest position in the condenser. They are denser than water vapor, concentrate at the bottom of the condenser, and fill up the condenser housing in time. This permanent gas reduces the vapor transport to the cold surfaces and forms a 'snow ice' as can be seen in Figure 2.19. A condenser (Figure 2.20) meets these requirements in general, but other designs are possible (see Figure 2.105).

The qualities of a condenser can be judged in general terms as follows:

- It is important to know the leak rate of the valve D (Figure 2.20) not only against the atmosphere but also between the chamber and condenser for the pressure rise measurements for BTM and DR data. The leak rate can be measured as follows: pressure rise measurement in the chamber and condenser with valve D open and valve G closed; the same measurement with valve D closed and G open and with valve D closed, but atmospheric pressure in the condenser. There should be no measurable difference between the three data and the absolute value should correspond to the criteria given in Section 1.2.3. The effect of the closing time and closing characteristics on the BTM and DR measurements can be checked by the following procedure. The shelves of the chamber and the condenser are at operating temperatures (e.g., +30 and −55 °C) and the chamber and condenser are evacuated by the pumping system. Air is injected through a needle valve until the pressure becomes similar to the operation pressure during SD, for example, 0.04 mbar. Valve D is closed for 60 s as during DR measurements, the pressure rise recorded, and valve D opened at the end of 60 s. This is done over several hours to test the reproducibility of the valve operation. Figure 2.22 shows the result: in the upper plot, the valve does not close correctly; in the lower plot, the valve operates reproducibly. During the first 4 h, the pressure rise per second (dp/s) has been an average 1.263×10^{-4} mbar/s, SA 0.06×10^{-4} mbar/s; in the second 4 h, 1.203×10^{-4} mbar/s, SA 0.04×10^{-4} mbar/s, and from 8 to 12 h, 1.160×10^{-4} mbar/s, SA 0.04×10^{-4} mbar/s. dp/s changes in the first 4 h by ∼5%, in the following 4 h by ∼3% and the next 4 h by ∼2% and ∼1% thereafter. This small effect is due to the decrease of water desorbed from the chamber surfaces. The BTM measurements during MD do not show this effect since they are made under almost equilibrium conditions. However, it is helpful to be aware of such an effect, which can vary with the design of the plant.

  Maximum ice condensation per unit time is attained by the following tests: shelves of the chamber are loaded with ice, the chamber and condenser are evacuated, and the shelves' temperature is raised until T_{ice} has reached the value

to be tested. The difference between the inlet and outlet temperatures of the refrigerant should remain unchanged or should not exceed 1–2 °C. After a rise of shelf temperature, it is important to wait ~30–60 min to allow for an equilibrium status, before the temperature difference becomes meaningful. In this way, the maximum p_{ch} can be determined, at which the condenser operates as specified.

- To measure the absolute amount of water vapor transported per unit time at a certain pressure, the test described above can be carried out with a weighed amount of ice on the shelves, either as plates directly on the shelves or with water in trays frozen on the shelves (Figure 2.23). Sublimation at the desired pressure should be continued for 5–6 h. A shorter time results in problems, since the time to reach approximately equilibrium conditions is 1 h or more, depending on the size and the design of the plant. If the chamber pressure rises with increasing shelf temperature, but the condenser temperature changes only very little, the condensation on the condenser surface is not the bottleneck, but the water vapor transport between chamber and condenser is the controlling part of the process. In this case, the pressure difference between chamber and condenser should be measured, preferably with a capacitance gauge designed to measure pressure differences. The pressure difference is expected to be small (e.g., 0.01–0.05 mbar). The pressure difference gauge avoids the inaccuracy of two instruments. From the difference and the absolute pressure p_{ch}, the amount of water vapor transported can be estimated by the principles discussed in Section 1.2.4.

For production plants, the loading of the plant with the required amount of ice (which should correspond to a full charge) is time consuming and several tests should be avoided. For a sufficient estimation of the water vapor transport and the bottle necks of it, one test can be carried out as follows.

A plant having a shelf area of ~30 m^2 has been loaded with 300 kg of water in trays and frozen on the shelves. Water vapor transport and condenser temperatures have been measured in this case between 0.4 and 0.6 mbar, which is about two to three times higher than the normally expected operating pressure of the plant (to obtain a measurable quantity of ice sublimed in a reasonable test time). The data for the test are shown in Figure 2.23. Three Pt100 resistance thermometers have been frozen in the ice. One CA each has been connected to the chamber and to the condenser at the places marked p_{ch} and p_{co} in Figure 2.20. Furthermore, the surface temperatures of the condenser coils are measured. Approximately 50 min after the start of heating and evacuation, the equilibrium conditions start to become visible, and after ~90 min they are effective. The pressure difference between T_{ice} (converted into pressure) and the chamber pressure depends on the absolute pressure, which corresponds to the amount of water vapor transported per unit time, but the difference $(p_{ice} - p_{ch}) < p_{ice}$. In the first 50 min, T_{ice} (or p_s) and the pressure in the condenser drop, because ice is only sublimed after the shelf temperature has started to rise from the −30 °C seen at the start. After 2.25 h, the shelf temperature has been lowered to pass the pressure range of 0.3 mbar a second time in order to avoid possible distortion by the nonequilibrium conditions at the beginning.

The following conclusions can be drawn from this experiment for the water vapor transport and the working of the condenser:

- The water vapor flows from the sublimation front into the chamber and to the connection between chamber and condenser with a favorable small pressure drop; there are no measurable flow resistances, for example, between the shelves or the shelves and the chamber walls.
- The pressure losses between chamber and condenser are surprisingly small (only 25–30% of the chamber pressure). The reason for this becomes understandable from the last conclusion.
- The condenser design and surface can handle the vapor flow during main drying of this test. The possible low temperatures could be needed during secondary drying.
- The visual observation of the condenser coils shows, in the visible zone, a compact solid, glassy structure. Inclusions of permanent gasses resulting in 'snow-like' surfaces were not seen.
- If the sublimed amount of water is calculated per unit surface area of diameter A (Figure 2.20) and time, as shown in Figure 2.24 for different l/d ratios of the connection between chamber and condenser, the average value for this test is 4.7 g/h cm^2. With $l/d = 5$, the vapor flow density should be 10–14 g/h cm^2 in the pressure range between 0.3 and 0.4 mbar. Figure 2.24 shows that 4.7 g/h cm^2 can only be expected in the pressure range between 0.32 and 0.4 mbar, if l/d is much larger than 5. A rough extrapolation indicates that the l/d value in this test had to be ~20. If one or two 90° bends are part of the connection, the actual length can be smaller, since each 90° bend does not contribute to the resistance by its physical length, but by a multiple of it. The actual flow resistance of a bend depends more on its design and surface structure than on its physical length. Therefore, it is difficult to estimate the resistance, and one has to measure it by tests as described above. In this test, the average vapor speed has been calculated as ~50 m/s. From Figure 1.143, one can see that at $l/d = 5$, a vapor speed of ~100 m/s should be expected in the measured pressure range, if the connection between chamber and condenser is straight. If the installation had been designed with $l/d = 1.6$, which would likely be the best possible technical solution, the same water vapor flow density can still be achieved at a pressure one decade lower, at 0.04 mbar. The design of the connection between chamber and condenser is one of the most critical parts of a freeze-drying plant. It should clearly be straight and as short as possible. As Figures 1.142 and 1.143 show, this becomes especially important for pressures below a few times 10^{-1} mbar.

2.2.5 Refrigerating Systems and Refrigerants

The special requirement of refrigerating machines for freeze-drying plant is the capability to run with small load near the end temperature of the compressors. This can reduce the necessary cooling of the motor and the circulation of the lubricant. A safe solution is to limit the minimum suction pressure of the compressor, for example, by a bypass, which guarantees a minimum flow of refrigerant.

Instead of controlling the refrigerant temperature in each group of coils or plates with its own sensor and injection valve, a centralized electronic injection valve can be used. The compressor capacity is subject to capacity fluctuations, summoned by changing liquifaction and evaporation pressures and temperatures. This also varies the available cooling capacity. The object of the electronic control is to adapt the cooling capability of the compressor precisely to the particular need of cooling capacity.

All of these must be well tuned with each other. The refrigerant for the condenser is normally injected directly into the coils or plates, while the shelves are mostly cooled and heated by a heat transfer fluid. Therefore, the condenser temperatures are normally lower than that of the shelves.

In the new global warming potential, according to the new regulation, the previous emphasis on refrigerant filling quantity in kilogram is replaced by a new emphasis on its global warming potential (GWP). Consequently, going forward refrigerants causing higher CO_2 emissions will face stricter scrutiny. This measure shall play its part in the EU's goal to reduce emissions of fluorinated greenhouse gases from industry to 70% below 1990 levels by 2030. (EG no.842/2006)

The scheduled countdown to 2030, the year in which the most complete relinquishment of the use of climate damaging, fluorinate-containing cooling agents becomes effective, is dominating the European as well as US legislation governing refrigeration and air-conditioning technology. Consequently, within the European Union, stricter laws and regulations take effect. In concrete terms, beginning with 2005, many existing refrigeration systems may no longer be maintained (see Figure 2.27 and 2.28).

The current regulation mainly affects the so-called hydrofluoroclorocarbons (HCFCs), for example, in particular the refrigerant R22 and all mixtures containing this substances.

With the newest version of what is known as "F-gas Regulation" beginning January 1, 2015, the ban of this group of substances now also includes existing systems.

Directly banned new systems:

Effective date of ban	System	Maximum allowed GWP	Refrigerant
1.1.2000	Hermetically sealed compressors for commercial use	2500	R404A
1.1.2022	Hermetically sealed compressors	150	R404A + R134A
1.1.2000	Stationary cooling systems; unless operating temperatures are below −50 °C	2500	R404A + R507

Year	2016–2017	2018–2020	2021–2023	2024–2026	2027–2029	2030
Reduction to	93%	63%	45%	31%	24%	21%

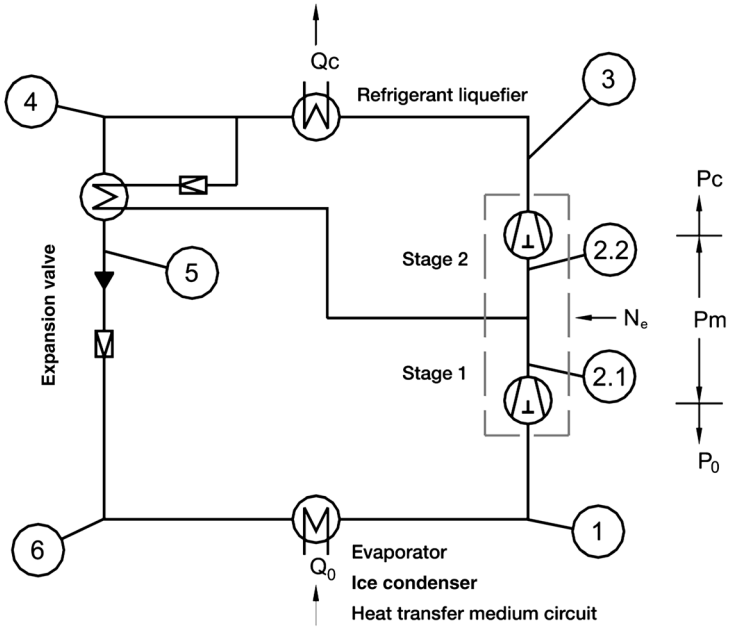

Figure 2.27 Function diagram of the operating principle of a compressor cooling system. N_e, power input of the compressor; Q_0, evaporator cooling capacity; Q_c, liquefier capacity; P_c, liquefying pressure; P_m, middle pressure; P_0, evaporating pressure. 1, Evaporator suctioning condition, stage 1; 2.1, compressor pressure gas, low-pressure stage; 2.2, compressor suctioning condition, stage 2; 3, pressure gas, high-pressure stage; 4, refrigerant liquid downstream of liquefier; 5, subcooled refrigerant; 6, unstressed refrigerant upstream of evaporator.

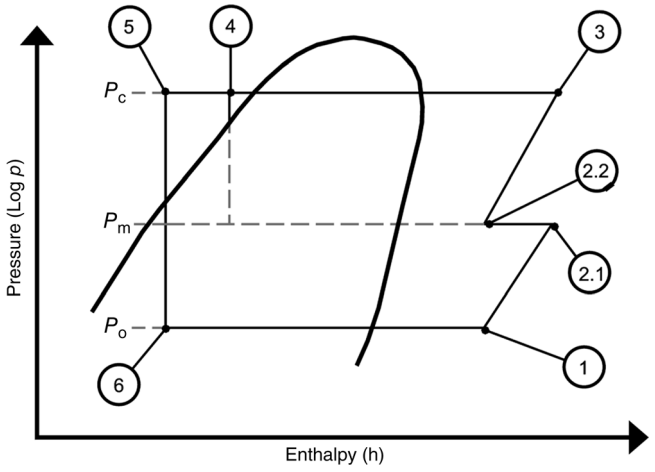

Figure 2.28 Representation of a cooling process in Mollier-h; log *P* diagram (operation with subcooler). P_c, liquefying pressure; P_m, middle pressure; P_0, evaporating pressure. 1, evaporator suctioning condition, stage 1; 2.1, compressor pressure gas, low-pressure stage; 2.2, compressor suctioning condition, stage 2; 3, pressure gas, high-pressure stage; 4, refrigerant liquid downstream of liquefier; 5, subcooled refrigerant; 6, unstressed refrigerant upstream of evaporator. (See also Spelzhaus, L. (1998) *TAR Betriebsseminar – Kaelteanlagentechnik, Wartung, Instandsetzung, Messtechnik*, TUEV-Akademie Rheinland GmbH, Koeln, Germany, pp. 28–35.)

Table 2.1 Long-term refrigerant alternatives.

Type	Manufacturer	Mixture	ODP[a)]	GWP[b)]	Availability	Oil
HP 62 (R404A)	Diverse	R125/R134a R143a	0	3750	Unlimited	Polyol ester
Genetron AZ 50 (R507A)	Allied signal	R125/R143a	0	3800	Unlimited	Polyol ester
R507A	Diverse	R125/R143a	0	3800	Unlimited	Polyol ester
FX 70 (R404A)	Elf Atochem	R125/R134a R143a	0	3750	Unlimited	Polyol ester
KLEA 60 (R407A)	ICI	R32/R125 R134a	0	1920	Unlimited	Polyol ester
R410A	Solvay	R32/R125	0	1890	Unlimited	Polyol ester

a) ODP = ozone depletion potential.
b) GWP = global warming potential.

Because of the problems caused by ozone depletion and the hothouse effect and in accordance with the ›Montreal Protocol 1986‹ international agreement, refrigerants that contribute to ozone depletion may no longer be produced. The refrigerants mostly affected by the CFC/ozone problem are fully halogenated refrigerants containing fluorine, chlorine, and hydrocarbons. In the meantime, there is scientific agreement that compounds containing chlorine or bromine are the substances responsible for the depletion of the ozone layer. The long life of these compounds and the resulting enriching effect in the atmosphere are also responsible for global warming of the atmosphere (hothouse potential). The low temperatures required in freeze-drying processes used to be reached with refrigerants containing CFCs.

When changing over to another refrigerant, as shown in Table 2.1, it is important to carry out the following:

- After exchanging the refrigerant, change the oil.
- All system components related to the refrigerant such as thermostatic expansion valves, control manometers, and the installed filter dryer must be replaced.

Heldner *et al.* [6] show the temperatures that should be reached on the shelves and in the condenser and what can be attained with the different refrigerants (Tables 2.2 and 2.3).

Table 2.2 Phase down scenario for refrigerants

Year	2016–17	2018–20	2021–23	2024–26	2027–29	2030
Reduction to	93%	63%	45%	31%	24%	21%

A phase down scenario affects all refrigerants. Whereby total quantity of F-gases marketed in the EU (in tons CO_2-equivalent) will be gradually reduced to 21% of its current level by 2030.

Table 2.3 Temperature ranges in freeze-drying units when using different refrigerants.

Part in the system	Required process temperature	Refrigerant (°C)			
		R507	R402A	R404A	R410A
Shelves	<−55 °C	<−55	<−55	<−55	<−60
Ice Condenser	<−75 °C	<−75	<−75	<−75	<−80

Cooling of the shelf heat transfer system and of the condenser is effected by compressor cooling systems. Nowadays cooling with liquid nitrogen (LN_2) is being carried out more and more.

A compressor cooling system mainly consists of the following:

1) A two-stage compressor (Figure 2.29)
   In this, the refrigerant vapor is compressed mechanically. Two-stage motor compressors are used mostly in freeze-drying systems. This compressor is installed in a screwed-on housing together with an electric motor.
2) A liquefier
   In this unit, refrigerant in the gas phase is liquefied through the removal of heat.
3) A throttling valve (expansion valve)
   This is a regulating element for expansion of the liquid refrigerant from liquefying pressure to compressing pressure.
4) An evaporator
   In this unit, liquid refrigerant is evaporated by supplying heat.

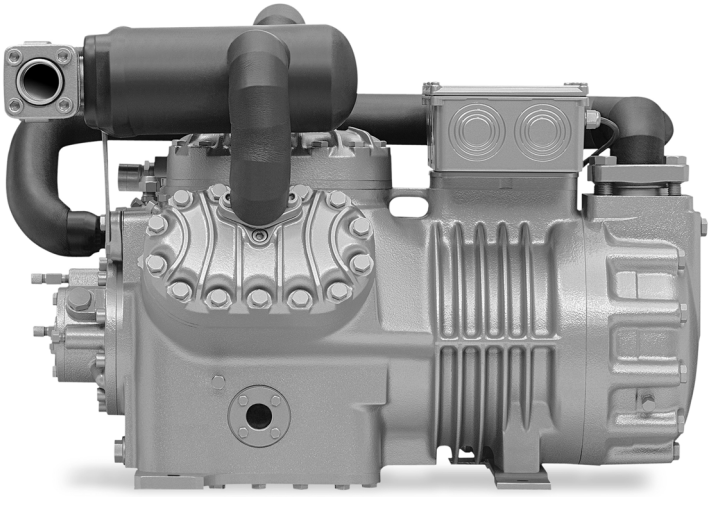

Figure 2.29 Two-stage piston compressor. (Bitzer, Kühlmaschinenbau GmbH, D-72065 Sindelfingen, Germany).

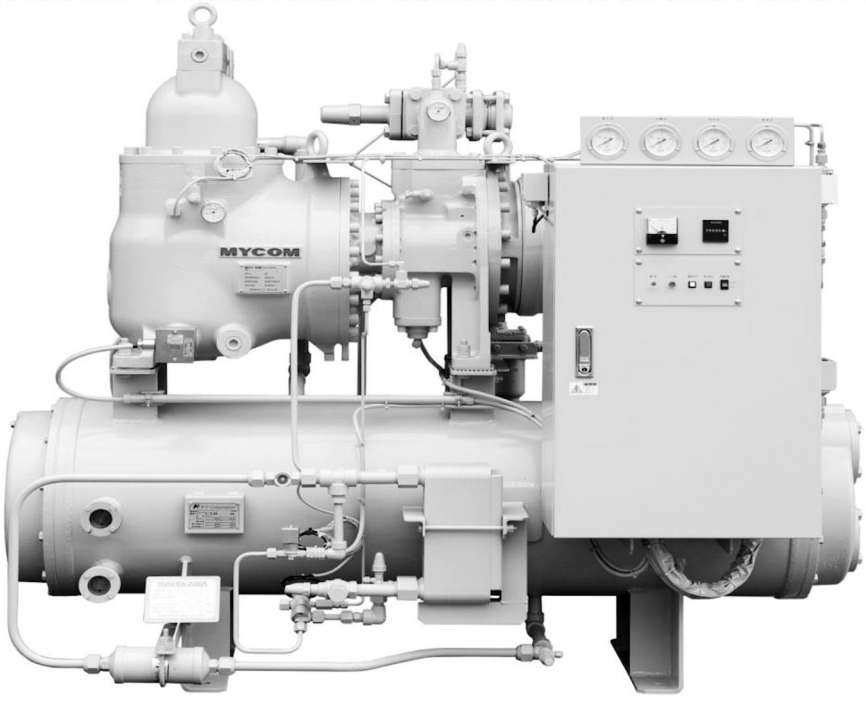

Figure 2.30 Two-stage semihermetic compound screw compressor, MHS series. (Mayekawa Europe, B-1930 Zaventem, Belgium.)

To be able to meet the cooling requirements of a freeze-drying system, two-stage piston compressors are mostly used. These machines are robust and their technical properties have been proved. More recently, two-stage screw compressors (Figures 2.30 and 2.31) are being used to increase cooling capacity (Figure 2.32), to reduce the noise level down to below 75 dBA and to reduce maintenance [6].

Comparison of the Cooling Capacity

The different volumetric capacities and the cooling efficiencies of both compressor types are compared in Figure 2.32.

The greater cooling capacity of the screw compressors with the same motor drive as the piston compressors is due to their greater volumetric displacement and their greater volumetric efficiency at a high compression ratio. The higher rotation rate of the screw compressors and the larger rotation angle result in a higher cooling capacity above −55 °C. The screw compressor has a rotation angle of 360° (320° can be utilized); the piston compressor has a rotation angle of only 180°. For users of refrigerating systems, the cooling efficiency is an important parameter to evaluate the operating costs of both systems as a function of temperature (Figure 2.33).

The new generation of Mycom screw compressors – MHS series – offers high efficient cooling capacity because of a new rotor profile. With the water-cooled

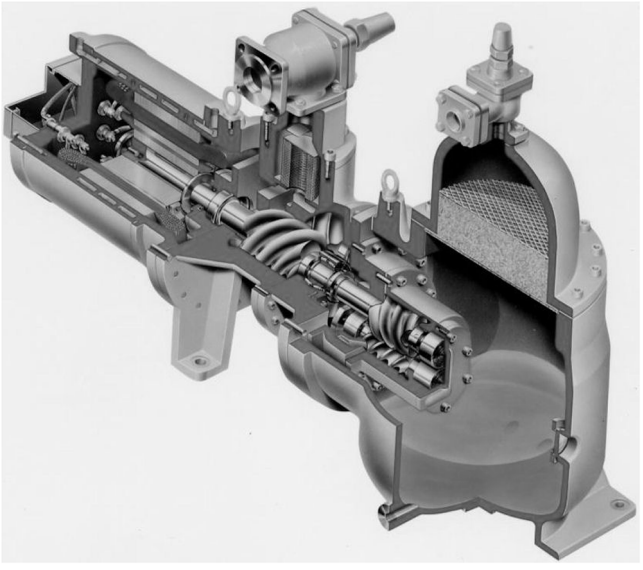

Figure 2.31 Cut model of Mayekawa Mycom two-stage screw compressor. (Mayekawa Europe, B-1930 Zaventem, Belgium).

semihermetic motor, there is no loss in refrigerating capacity, related to the motor cooling.

Calculation of the Cooling Efficiency by Eq. (2.2)

$$E_c = C_c / P_{kw} \tag{2.2}$$

where E_c = cooling capacity with reference to the electrical power consumption, C_c = compressor capacity, and P_{kw} = electrical power consumption.

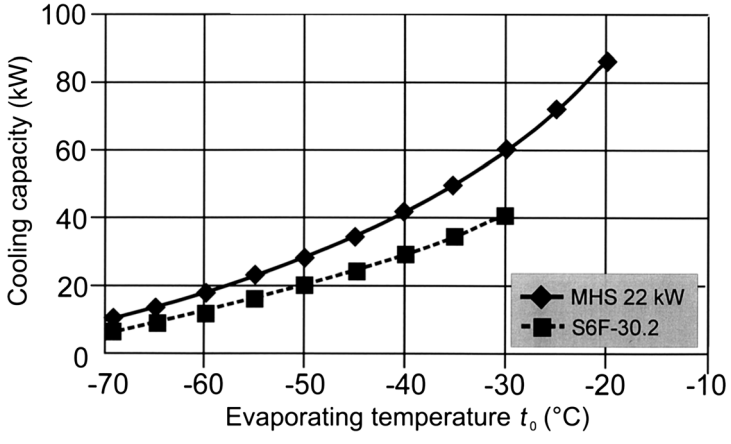

Figure 2.32 Cooling capacity of both compressors operating with R404A at a liquefying temperature of 30 °C. The curves show the cooling capacity for both compressor types at different evaporating temperatures.

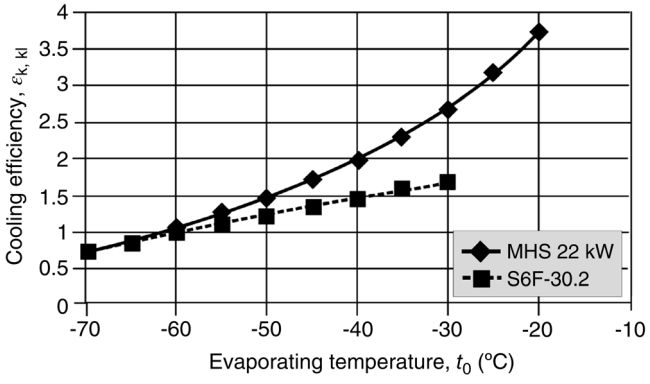

Figure 2.33 Cooling efficiency figure of a screw and a piston compressor operating with R404A at a liquefying temperature of 30 °C. The curves show the cooling efficiency for both compressor types at different evaporating temperatures.

At evaporating temperatures between −30 and −45 °C, the screw compressor is more economical. At temperatures of −55 °C and lower, the piston and screw compressors are equally efficient. The reason for this lies in the lower power input of the piston compressor at low evaporating temperatures. Another advantage of the screw compressor is the low noise level. The disadvantage might be the price, but this must be evaluated in each individual case. Another alternative should be mentioned to complete the picture: this alternative to screw compressors would be the use of cooling cascades.

Liquid Nitrogen: An Alternative to Conventional Compressor Cooling Systems

Nitrogen is a colorless, odorless, and tasteless gas. Roughly 78 vol% of the atmosphere consists of nitrogen. Nitrogen cannot burn and is nontoxic, but the concentration of O_2 in closed areas must be monitored.

At a pressure of 1013 mbar, the temperature of nitrogen is 77.3 K or −196 °C. About 199 kJ of heat is required as evaporating heat, that is, the amount of heat required to change 1 kg of liquid nitrogen from the liquid to the gas phase under the given conditions (Figure 2.34). In addition to this evaporating enthalpy, a further 240 kJ of additional heat can be used to heat the nitrogen to an ambient temperature of 20 °C.

Figure 2.35 shows the design principle of such a system. Heating and cooling of the shelves are effected indirectly over a heat transfer medium, while the condenser evaporator is cooled directly. Contrary to conventional condenser evaporators, which are equipped with evaporator coils, plate evaporators are preferred for LN_2-cooled evaporators (Figures 2.35 and 2.36). Figure 2.37 shows a schematic drawing of an evaporation construction with plates.

Briefly stated, the following are advantages of cooling freeze-dryers with LN_2 over conventional cooling systems:

- Reduced electrical power requirements.
- No cooling water required.
- Savings on capital costs.

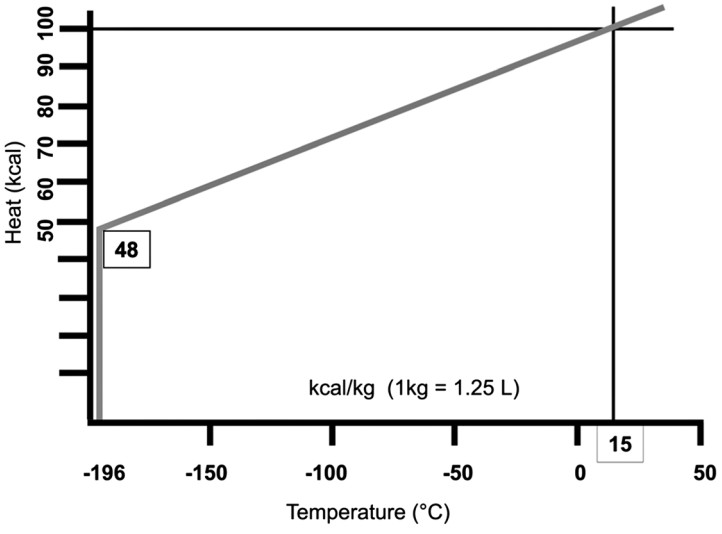

Figure 2.34 Refrigerating capacity of liquid nitrogen at different temperatures.

- High cooling capacity:
  - fast shelf cooling;
  - controllable condenser temperature (not recommended if cooled by compressors and direct refrigerant expansion).
- Product protection for a limited time if there is a power failure.
- Shortening of the secondary drying time and low residual moisture if the product requires condenser temperatures below −80 °C.
- Useful for solvents, depending on their melting temperature and vapor pressure.

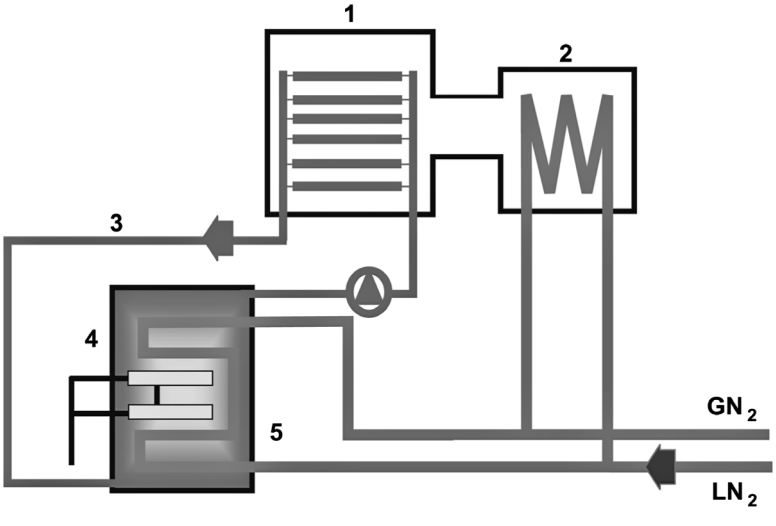

Figure 2.35 Simplified P&I diagram of liquid nitrogen. 1, chamber and shelves; 2, condenser; 3, silicone oil circuit; 4, heater; 5, heat exchanger.

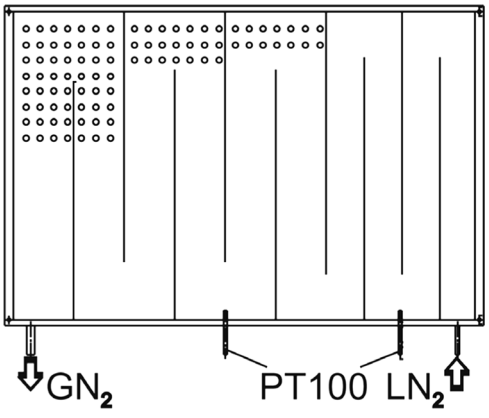

Figure 2.36 LN_2 evaporator plate – cross section. The cross sections of the channels from the liquid nitrogen inlet to the gaseous nitrogen outlet are increasing considering the expansion of the gas.

- Reduced noise level.
- Smaller footprint.
- No compressor required and thus no maintenance needed.
- Occasionally, a use can be found for the gaseous N_2 by-product.

Using LN_2 to cool freeze-dryers is a new application, but not a new technology. The benefits and disadvantages need to be considered in each individual case. As a

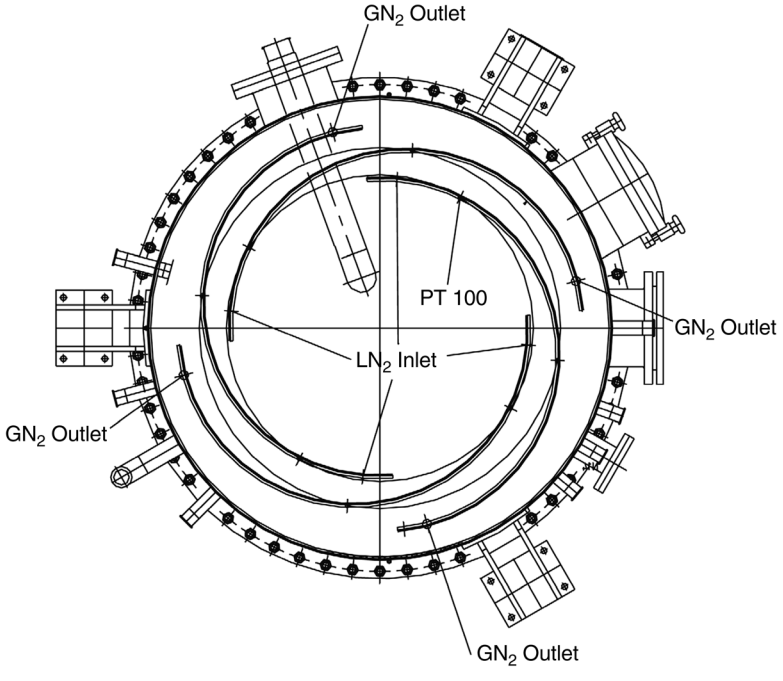

Figure 2.37 LN_2 condenser – cross section. The arrangement of the evaporator plates ensures a uniform ice distribution.

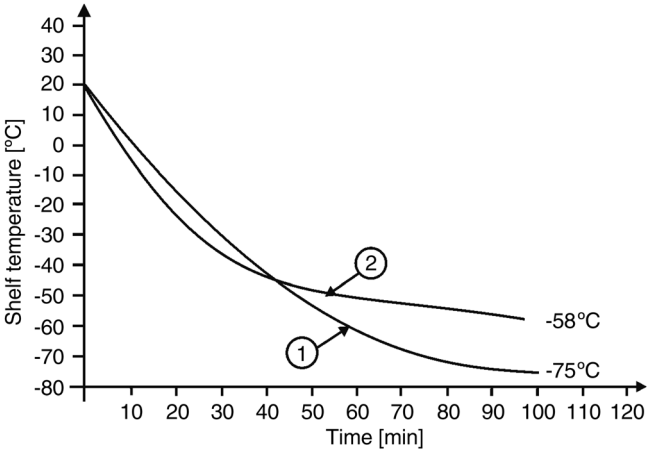

Figure 2.38 Temperature of the shelves in a freeze-drying plant as a function of cooling time, calculated for two different refrigerants. 1, LN_2 heat exchanger with a capacity of 60 kW; 2, compressor cooling system using R404A.

rule of thumb, the following can be assumed: To freeze and sublime 1 kg of water, ~19.5 kg of LN_2 is needed.

Willemer [7] showed (Figure 2.38) the cooling time of a 31 m^2 shelf area in a freeze-drying plant by a two-stage compressor system operated with R404A, where −55 °C is reached in ~85 min. With LN_2 cooling, −70 °C is reached in ~85 min. At −40 °C, the time difference is only ~20 min. Whether and how the use of LN_2 is technically advisable and economically justified has been studied by several authors. Snowman [8] sees the following advantages: no compressors, condenser temperatures between −70 and −120 °C, and a reserve of cooling medium during technical problems (the product can be kept cold with LN_2 in a tank). The disadvantages are that LN_2 is more expensive per kW cooling output than the electrical energy needed for the same cooling effect and the installation has to be designed for LN_2; a change in an existing plant to LN_2 cannot be justified. Snowman described a method to save LN_2 and to control the desired condenser temperature.

Figure 2.39 [8] demonstrates the application of a cooling circuit with recirculated flow: an injector pump operated with just evaporated LN_2 aspirates the warmer GN_2 coming from the condenser and feeds the mixture back into the condenser. The desired condenser temperature can be controlled by a throttle valve. To achieve a uniform temperature distribution, the gas mixture is alternately fed to one or the other end of the condenser. No results of such a system were given.

Cully [9] estimated for a freeze-drying plant with 30 m^2 shelf area that, starting with the third year of operation, LN_2 cooling is more economic than cooling with compressors. The main saving, in his opinion, comes from avoiding high maintenance costs of the compressors. The investment costs for compressor or LN_2 plants are assumed to be equal in this calculation. A modification of an

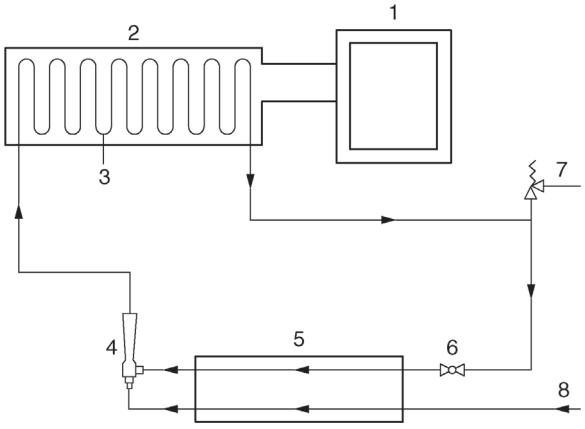

Figure 2.39 Cycle cooled by LN_2 of a condenser in a freeze-drying plant. A part of the GN_2 is cooled in a heat exchanger and pumped back in the cycle by a jet pump. 1, drying chamber; 2, condenser; 3, condenser coil; 4, jet pump; 5, heat exchanger; 6, throttle valve; 7, pressure-controlled GN_2 outlet; 8, LN_2 inlet. (See also Ref. [8], p. 342.)

existing plant is also, in the opinion of Cully, uneconomical, the payback time being ~9 years.

Steris GmbH[2] showed a different possibility of saving LN_2 and yet retaining some of the advantages. In the condenser housing, besides the conventional coils, a LN_2-cooled plate is installed, which will be operated only under two conditions:

- During secondary drying, if an operating pressure below, for example, 10^{-2} mbar should be reached quickly. The conventionally cooled condenser remains in operation at its end temperature. In this operation, some ice sublimes from the condenser to the LN_2-cooled surface. However, the surfaces of the LN_2 plate can be controlled between −80 and −100 °C, which corresponds to a water vapor pressure of $\sim 5 \times 10^{-4}$ to 2×10^{-5} mbar.
- Should the compressors fail temporarily, the LN_2 condenser can maintain a low pressure, for example, 0.1 mbar for 2 h, depending on the LN_2 on hand. This would allow a product temperature of $\simeq 40$ °C to be kept in the chamber. This is supported by a heat exchanger in the heat transfer fluid circuit, which can also be cooled by LN_2.

It is possible that the maintenance problems with multistage screw compressors are substantially smaller than with piston compressors, but so far only one publication has been found [10] comparing the technical data and operating costs of piston and screw compressors for two brands. The maintenance costs of both systems are not discussed.

In large freeze-drying plants for food and other mass products, it is economical to use ammonia absorption plants for cooling, which can be heated by steam or directly fired by oil or gas. If the required capacity is on the order of

2 GEA Group, Germany.

Table 2.4 Comparison of technical data and cost estimates of absorption and compressor refrigeration plants. (Data provided by Deutsche Babcock-Borsig AG, D-13500 Berlin, Germany.)

		Absorption refrigeration plant			Compressor refrigeration plant		
Refrigerating capacity tot.	kW	1000	500	250	1000	500	250
Evaporation temp.	°C	−55	−55	−55	−55	−55	−55
Heat demand	kW	3681	1840	920	na	na	na
Steam	kg/h	6700	3350	1675			
Use of heat							
Condenser	kW	1645	823	411	1552	776	388
Absorber	kW	2180	1090	545			
Solution cooler	kW	856	428	214			
Cooling tower	kW	4681	2341	1170	1870	935	467
Cooling water	m^3/h	410	205	102	165	83	41
Fresh water demand	m^3/h	8.5	4.3	2.1	3.4	1.7	0.8
Current demand							
Engines	kW	35	18	9	900	450	225
Cost estimate	T€	1950	1350	1200	1250	625	315

500 kW at −55 °C or larger, the low operating and maintenance costs of the absorption plant should be studied and evaluated. The investment costs are shown in Table 2.4 and the total cost per year for 1000 kW at −55 °C shows a substantial advantage for the absorption plant. In an NH_3 absorption plant (see schematic drawing in Figure 2.40), a water–ammonia mixture is evaporated in a steam-heated or oil-fired boiler (1), the vapor is separated in a rectifier column (2) into NH_3 vapor and a residual solution. The ammonia vapor is liquefied in a condenser (3) and pumped (4) into the water vapor condenser (5) (which is the NH_3 evaporator). In this schematic drawing, NH_3 is not injected into the water condenser but is pumped (4) through the condenser. In this case, only part of the ammonia (10–20%) evaporates by the heat transmitted from the frozen ice on the surface of the condenser coils. The mixture of liquid and gaseous ammonia is conducted into a separator (8) and the NH_3 vapor flows into an absorber (9), where it mixes with the remaining solution from the rectifier column and returns to the boiler (1).

As shown in Table 2.5, in large plants the absorption system is more economical than compressor installations, independent of the price of steam or electricity. The low maintenance costs are reflected in the calculation, but the high uptime and reduced production interruption should also be accounted for in an evaluation; the absence of large, heavy, moving machine parts is the reason for this advantage.

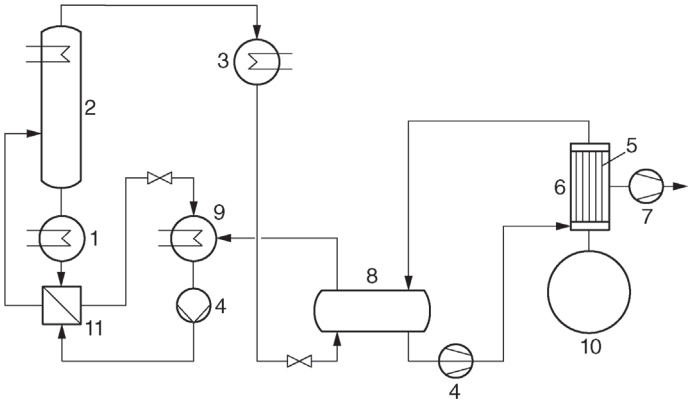

Figure 2.40 Schematic drawing of an absorption refrigeration plant. (Based on information from Deutsche Babcock-Borsig AG, D-13500 Berlin and ALD Vacuum Technologies GmbH, D-63526 Erlensee, Germany.) 1, expulsion of NH_3 from the water–NH_3 solution; 2, rectification column for NH_3; 3, NH_3 condenser; 4, NH_3 pump; 5, condenser coils for water vapor; 6, condenser housing; 7, vacuum pump; 8, separation of the gaseous NH_3 from liquid NH_3; 9, absorption of the gaseous NH_3 in the water from the expulsion; 10, drying chamber; 11, heat exchanger.

Table 2.5 Total annual cost of a refrigeration plant with a capacity of 500 kW at −55 °C and 8000 annual operating hours and for an absorption and a compressor plant. $Kk = A[(q-1)q^n/q^{n-1}]$. (Data provided by Deutsche Babcock-Borsig AG, D-13500 Berlin, Germany.)

		Absorption refrigeration plant				**Compressor refrigeration plant**	
Capital costs yearly							
A investment		T€	1950			A T€	1250
p interest rate		%	6			p %	8
n amortization time		ano	25			n ano	10
q = q+ p/100			1.06				1.08
		T€/ano	155.55	155.55	155.55	T€/a	186.3
Energy costs		heating cost	€4/MWh	€7.5/MWh	€15/MWh		
Steam		T€/a	58.9	110.4	220.8	T€/a	0.0
Fresh water	€1/m^3	T€/a	17.2	17.2	17.2	T€/a	6.8
Current	€150/MWh	T€/a	10.8	10.8	10.8	T€/a	270.0
Operation and maintenance							
% of the first investment		T€/a (1%)	19.5	19.5	19.5	T€/a (6%)	75.0
Staff costs		T€/a	10.0	10.0	10.0	T€/a	30.0
Total costs per year		T€/a	271.95	323.45	433.85	T€/a	568.10

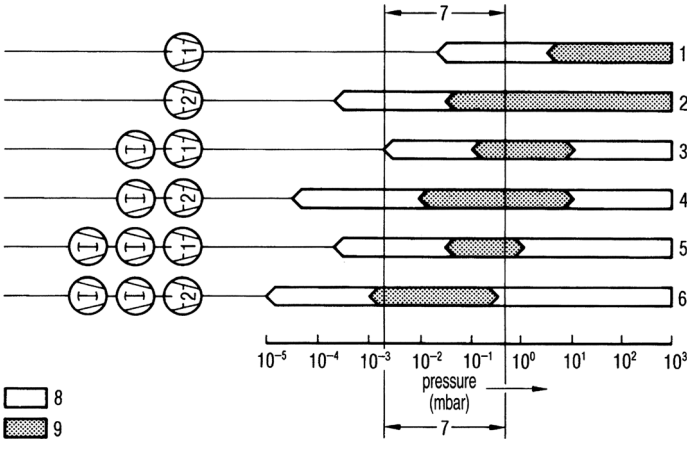

Figure 2.41 Working range of vacuum pumps and multistage pump sets. 1, single-stage pumps; 2, two-stage pumps; 3, two-stage pump sets with single-stage backing pump; 4, three-stage pump set with two-stage backing pump; 5, three-stage pump set with single-stage backing pump; 6, four-stage pump set with two-stage backing pump; 7, working range of pump sets (2×10^{-3} to 5×10^{-1}) in a freeze-drying plant depending on T_{co} and p_{ch} during NT; 8, start-up range of the pump set; 9, working range of the pump set. (Part of Figure 2 from Leybold AG, D-50968 Cologne, Catalogue HV 300, Part A 7.)

2.2.6 Vacuum Pumps

The vacuum pumping system in a freeze-drying plant has to fulfill two tasks:

- To reduce the air pressure in the chamber and condenser to the necessary partial pressure of air (mostly 0.01–0.1 mbar).
- To pump off the gases from the product and the air entering the plant through leaks at a partial pressure of the permanent gases which has to be small compared with the water vapor pressure.

Figure 2.41 gives a review of the working range of different vacuum pumps and pump combinations. The pressure range of interest for freeze-drying is 5×10^{-1} to 2×10^{-3} mbar, for which single-stage vacuum pumps are not suitable. Two-stage pumps reach $\sim 10^{-2}$ mbar with gas ballast, which makes them applicable in the upper part of the pressure range. This type of pump is only available with a maximum pumping speed of 300 m^3/h. In a freeze-drying plant, the pumps have permanently to pump some water vapor with the permanent gases and therefore should always be operated with gas ballast to avoid condensation of water in the pumps.

During the operation with gas ballast, such an amount of air will enter the pump house (after the pump house is separated from the vacuum chamber) that the water vapor at the operating temperature of the pump cannot condense during the compression phase of the pump. Consider an example: water vapor is pumped at a partial pressure of 0.5 mbar and the temperature of the pump is +70 °C. Under these conditions, the water vapor will condense if the compression

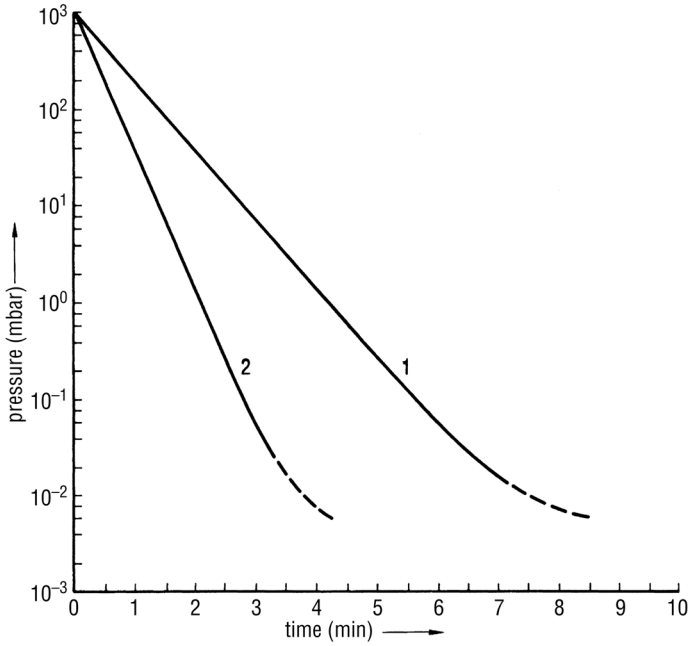

Figure 2.42 Pressure as a function of the evacuation time of a 1000 L volume with 1, a two-stage vacuum pump with a pumping capacity of 100 m^3/h, operated with gas ballast; 2, a two-stage vacuum pump with a pumping capacity of 200 m^3/h, operated with gas ballast. (See also Leybold AG, D-50968 Cologne, Germany, Catalogue HV 300, Part A 2, p. 29.)

exceeds ~310 mbar. If the pressure in the pump house is increased by air from 0.5 mbar to, for example, 50 mbar, the compression needs only to be 1000/50 = 20. The original water vapor at 0.5 mbar is compressed by a factor of 20, and the water vapor pressure reaches only $0.5 \times 20 = 10$ mbar. No condensation can take place at 70 °C in the pump house.

Figure 2.42 shows that a volume of 1000 L (chamber and condenser) will be evacuated to 0.01 mbar in ~8 min by a pump with the capacity of 100 m^3/h. For a volume of 100 L, a pump with a capacity of 10 m^3/h is sufficient. The pump for evacuation only can be relatively small. A pump with 100 m^3/h has this capacity also at a pressure of 0.05 mbar; however, at this low pressure, 100 m^3/h represents only 1.4 mbar L/s or 1.1×10^{-3} g/s. This pumping capacity is more than sufficient if the leak rate is smaller than 0.01 mbar L/s, which can be expected for most plants. The critical dimension for the pump size can be the gas from the product. In a chamber of 700 L (plus 300 L condenser volume), there may be, for example, 10 kg of product, which may have a minimum of 10 g (but often 100 g) of air dissolved within, which may become free during the main drying for, for example, 8 h, which is 1.2 or up to 12 g/h or 0.3×10^{-3} to 3×10^{-3} g/s. Therefore, a pumping speed of 1.1 g/s might be sufficient, but it would be preferable to use a pump with a threefold higher pumping speed. Two-stage pumps with such a capacity are expensive or are not available.

The following equation can be applied to calculate the pumping speed of a vacuum pump set for a given unit size:

$$S_{\text{eff}} = \left(\frac{2.3V}{T} \times \frac{\log P_{\text{a}}}{P_{\text{MD}}}\right) + \left(\frac{S_{\text{w}} \times P_{\text{RS}} \times 3600}{P_{\text{SD}}}\right) + \left(\frac{Q_{\text{L}} \times 3600}{P_{\text{SD}}}\right) + \left(\frac{M \times 10^{-3}}{t_{\text{MD}}}\right)\left[\frac{\text{m}^3}{\text{h}}\right] \tag{2.3}$$

where

V = volume of the system (m^3)
T = evacuation time from P_A (atmospheric pressure) to P_{SUB} (sublimation pressure (h)
P_A = atmospheric pressure (mbar)
P_{MD} = main drying pressure (mbar)
S_W = surface of the chamber walls; door; shelves; condenser walls; evaporator (m^2)
P_{RS} = water vapor released from the metal surfaces (e.g., 1×10^{-4}) (mbar L/s m^2)
Q_L = leak rate of the system (mbar L/s)
P_{SD} = secondary drying pressure (mbar)
M = maximum amount of product (L)
t_{MD} = main drying time (h)

As shown in Figure 2.41, it is more efficient to use a backing pump combined with one or two roots blowers (Figure 2.43). The backing pump requires only 40 m^3/h capacity, combined with a roots pump of 200 m^3/h. This system evacuates 1000 L also in 8 min down to 0.01 mbar, but below 0.1 mbar, the system has a capacity of 200 m^3/h or 2.2×10^{-3} g/s at 0.05 mbar. Such a pumping system is preferable for freeze-drying compared with a large two-stage pump alone.

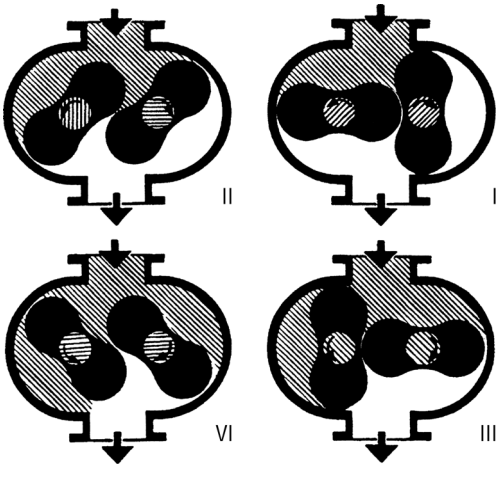

Figure 2.43 Working principle of a one-stage roots pump (pumping direction vertical). (See also Leybold AG, D-50968 Cologne, Germany, Catalogue HV 300, Part A 6, p. 4.)

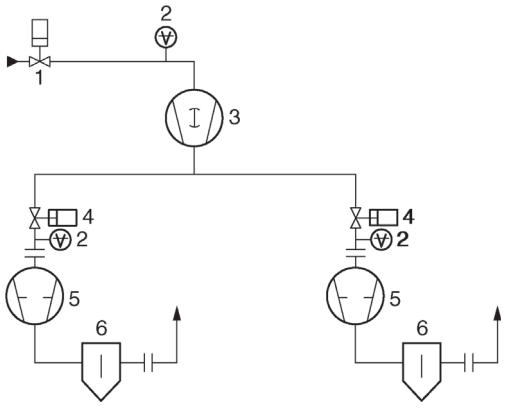

Figure 2.44 Schematic drawing of a vacuum pump set, designed for a production freeze-drying plant. 1, vacuum valve behind the condenser; 2, vacuum gauge; 3, roots pump; 4, vacuum valve between roots and backing pumps; 5, backing pump; 6, exhaust filter.

If a high pumping capacity is required in production freeze-drying plants, a single backing pump with two blowers in parallel (Figure 2.41) is an effective solution.

Figure 2.44 shows the complete pumping system for a freeze-drying plant. Two backing pumps are used for two reasons:

- during evacuation, both pumps run parallel, while during freeze-drying, one pump can be sufficient;
- the second pump can be shut off to save electricity and acts as a standby.

A small amount of oil vapor diffuses back from all oil-sealed vacuum pumps in spite of the air flow to the pump. This amount is greatest if the air flow becomes small and the pump is running close to its final pressure. If a small amount of air is fed via a needle valve into the pump, so that the pump always runs at a pressure 5–10 times larger than its end pressure, 98% of the back streaming can be avoided. It is possible to stop 99% of the back streaming by using a trap filled with activated aluminum oxide. However, this method is not recommended for practical reasons: The aluminum oxide has to be exchanged from time to time and it is difficult to decide the correct time for the exchange since some gases from the drying chamber can also be absorbed.

If the back streaming of oil has to be completely excluded, pumps without oil seals must be used, as known in the semiconductor industry. In these pumps, two to four stages (depending on the manufacturer) of claw pumps (see schematic drawing in Figure 2.45) are used. Figure 2.46 shows the gas path through the pump. Figure 2.47 shows the working diagram of a four-stage claw pump, built up to 400 m^3/h. For larger pumping capacities, an oil-free roots pump can be added in series.

Such pump sets have to be adapted for freeze-drying conditions: Between the third and fourth stages a water-cooled condenser must be installed to prevent condensation of water vapor during compression. Depending on the operating pressure in the condenser of the freeze-drying plant, a second condenser may have to be installed between the second and third stages.

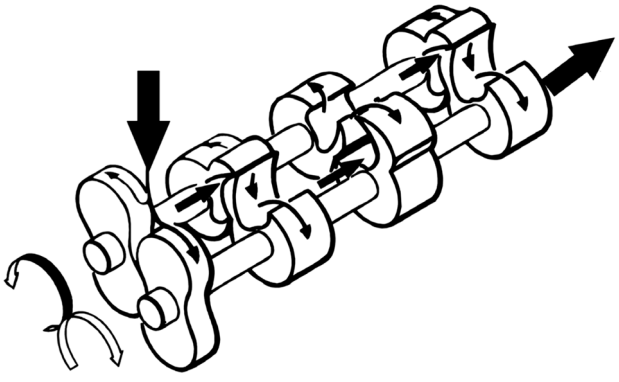

Figure 2.45 Working schematic of a dry vacuum pump operating on the so-called claw principle. The short gas path through the pump prevents condensation from forming between the stages (BOC Edwards GmbH, D-85551 Kirchheim/Munich, Germany).

In production units, vacuum pump set combinations are almost always used (Figures 2.44 and 2.48). Some of the reasons for this are as follows:

- quick pump-out times at the beginning of a process;
- high pumping speed;
- low ultimate pressure in the secondary drying phase;
- high operating reliability.

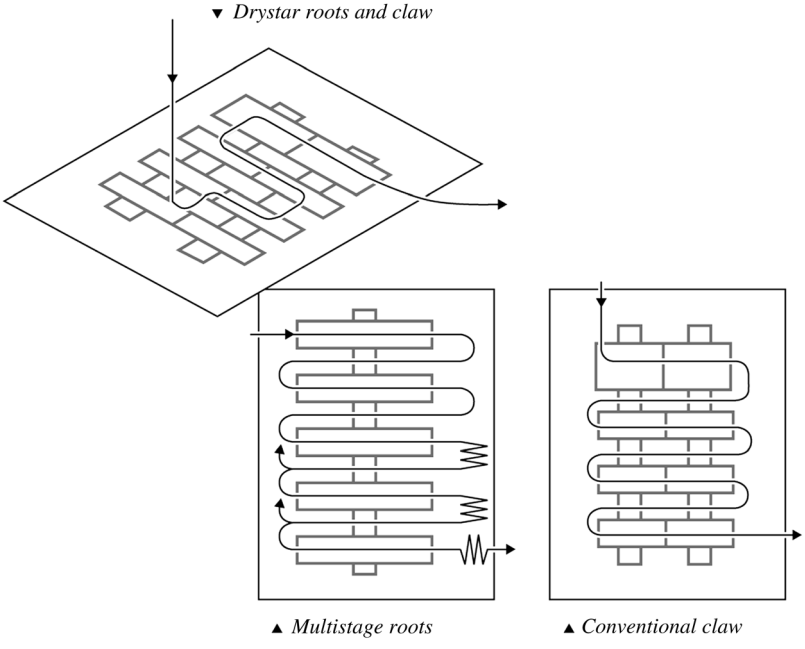

Figure 2.46 Schematic drawing of the gas path in a BOC Edwards Drystar GV pump (BOC Edwards GmbH, D-85551 Kirchheim/Munich, Germany). The path of the gas through the pump is the shortest connection between the claw stages.

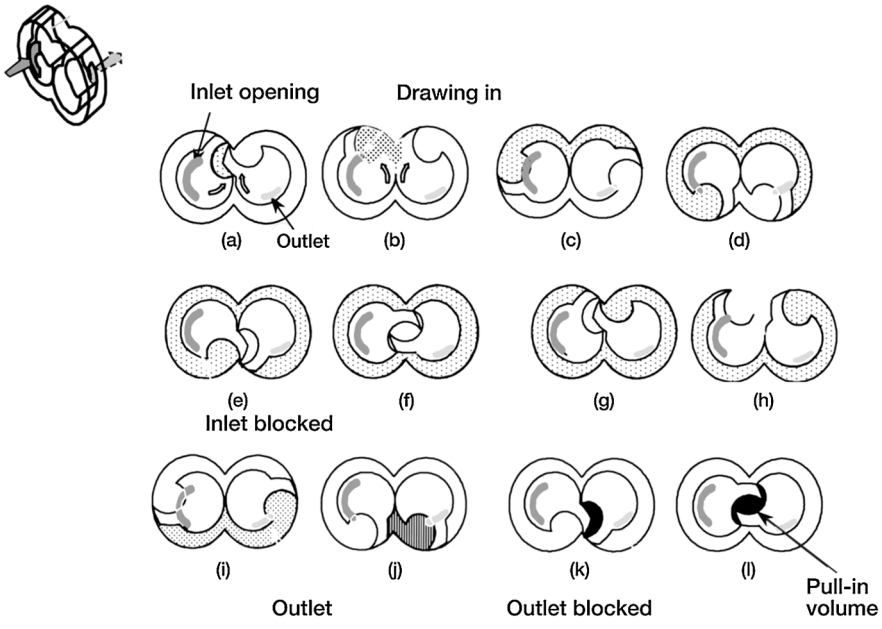

Figure 2.47 Working schematic of a four-stage dry vacuum pump, type BOC Edwards Drystar GV. Pump sequence inside one claw. (See also BOC Edwards GmbH, D-85551 Kirchheim/Munich, Germany.)

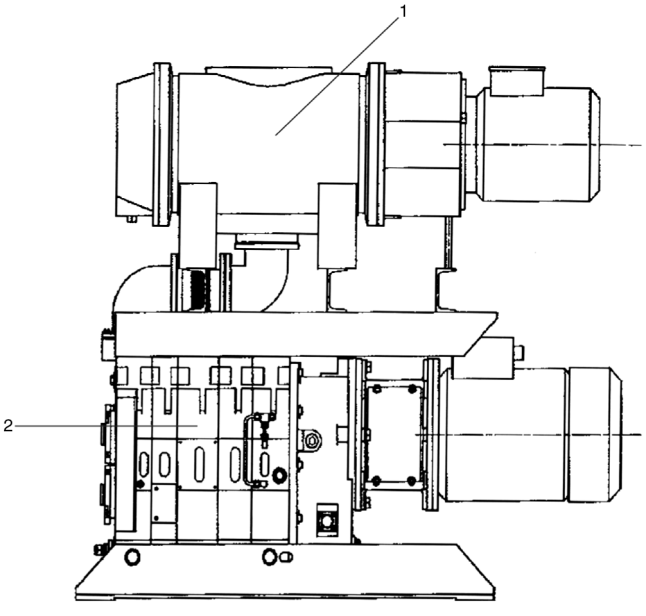

Figure 2.48 Dry vacuum pump combination with a dry roots pump for fast evacuation, a high pumping speed, and a low ultimate vacuum. Such combinations are available for pumping speeds from 250 to 4000 m^3/h. (See also BOC Edwards GmbH, D-85551 Kirchheim/Munich, Germany.)

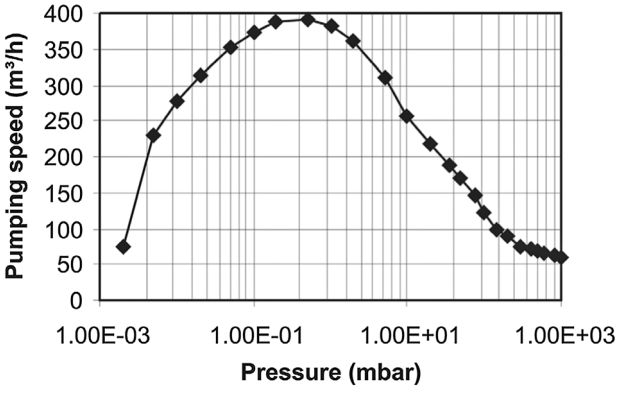

Figure 2.49 The diagram shows the pumping speed for a pump set combination consisting of an EH 500 roots pump and a GV80 dry vacuum pump (BOC Edwards). The advantage of such a combination is the high pumping speed in the range of 10–0.1 mbar. The end vacuum that can be reached is 0.005 mbar. (See also BOC Edwards GmbH, D-85551 Kirchheim/Munich, Germany.)

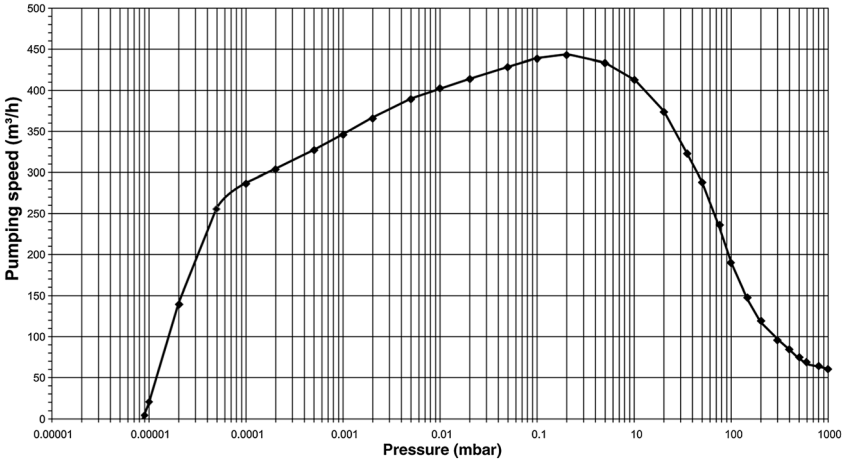

Figure 2.50 The diagram shows the pumping speed for a pump set combination consisting of an EH 500 Roots pump, an additional EH 250 roots pump, and a GV80 dry vacuum pump (BOC Edwards). The advantage of such a combination is the high pumping speed in the range of 10–0.001 mbar. The end vacuum that can be reached is 0.0001 mbar.

In Figures 2.49 and 2.50, the pumping speed curve of an EH 500/GV 80 (BOC Edwards) pump combination is shown.[3]

2.2.7 Inlet Venting Filters

All the gases that enter the chamber during the freeze-drying process of a parenteral product must be sterile [11]. This is attained by using hydrophobic

3 BOC Edwards GmbH, D-85551 Kirchheim/Munich, Germany.

inlet filters, which are an integral part of the system and that are routinely sterilized together with the entire freeze-drying system before every new batch is processed. This can be effected either with one filter or with two filters installed one after the other.

Gas inlet is effected to regulate the pressure during the main drying phases for partial venting for the stoppering of vials and for the final venting after the vials have been stoppered. Product contamination through the gas that has been introduced is thus impossible. As with all critical sterilization grade filters used in the manufacture of parenteral products, it is important that the sterilizing efficiency of the filter(s) is assured by regular integrity tests. Regulatory authorities expect all critical filters to be integrity tested.

All the filters used must comply with the demands made by regulatory authorities. In sterilizable systems, hydrophobic diaphragm filters made of either polyvinylidene fluoride (PVDF) or polytetrafluoroethylene (PTFE) with a diaphragm pore width of 0.2 µm may be used. The filter elements are encased in stainless steel casings, which are resistant to pressure and temperature.

During a sterilization process, sterile steam is led through the filter and the entire piping. The piping must be laid out in such a way that condensate and the liquid testing medium can flow off without hindrance. During the sterilization process, the temperatures of all the critical points, that is, all the points where the coldest temperatures are expected, are measured and controlled. Some installations have a steam bypass around the filter housing to allow the temperature on the downstream side of the filter to rise before allowing steam into the filter, thus ensuring an acceptable pressure drop across the filter membrane. This is done to minimize the stress experienced by the filter during sterilization, reducing the risk of integrity failure or filter collapse.

The Parenteral Society [12] recommends the following criteria for integrity testing:

1) The test should be reproducible. Testing a filter under the same conditions should give the same results within the error margins inherent in the test.
2) The test should have been correlated with a bacterial challenge test (BDT). The FDA considers a sterilizing grade filter as one that produces a sterile filtrate when challenged with 10 *Pseudomonas diminuta* per cm^2 of filter surface.
3) The limit set for a filter must have a sufficient safety margin with respect to the data derived in the challenge testing, taking into account the errors associated with the system, without regularly failing integral filters.
4) The test should be acceptable to the regulatory authorities.
5) The tests should not be destructive or contaminating.
6) The filter should be dry after testing.
7) The test should be practical and easy to perform.
8) The test should not present any major safety hazards.
9) The test should preferably be able to be performed without removing the filter or housing from the system.
10) It is desirable that the test be performed after steam sterilization but before freeze-drying the next batch, without risking the integrity of the freeze-dryer.

Water-based tests [water intrusion tests (WITs)] [13] were developed a few years ago, but it is only recently that they have been promoted as a reliable alternative to the diffusion flow test.

The difference lies in the fact that the hydrophobic filter cartridge in the filter housing is flooded with sterile water at the inlet side. After applying the test pressure, the decrease in pressure is measured. This pressure decrease is caused by the penetration of the water in the membrane matrix.

Contrary to the diffusion test, where the air diffused through the wet membrane causes a pressure drop at the inlet side, in the WIT, the pressure drop is caused through the lowering of the water level at the upstream side of the housing.

With an intact membrane, the penetration of water is very small. It will be correspondingly higher with a damaged membrane and this can even lead to a water breakthrough.

The WIT is based on the capillary depression of nonwetting liquids at the membrane surfaces. To overcome these negative capillary forces, a certain pressure gradient is required. This pressure gradient depends among other things on the pore size. This is generally known as the water penetration point (WPP). The WPP depends on the hydrophobicity of the filter material and on the pore size. It can be compared to the bubble point process.

The basic preconditions for a WIT are as follows:

- Determination of the net volume of the filter housing. This can be done, for example, by filling it with water and then weighing the water.
- Use of WFI at a temperature of 22 ± 3 °C. The same temperature applies to the compressed air streaming in. WFI is heated or cooled in a separate container.
- Avoidance of temperature fluctuations during the test.
- Use of a completely hydrophobic filter cartridge.
- Use of a drying device for the filter housing – a water ring pump, for example – for optimum drying of the housing after a steam sterilization process.

Course of a WIT of a 0.22 µm PTFE filter membrane [14] is as follows:

- The filter housing is filled completely with WFI at the inlet side.
- The inlet valve is closed.
- Pressure builds up at the inlet side of the filter housing until a test pressure of 3500 mbar is reached.
- After the test pressure has been reached, a stabilization time of 10 minutes begins in order to saturate the water column, to distribute the water bubble-free over the entire membrane surface and to ensure complete compaction.
- The subsequent test time lasts 10 min. It is not advisable to shorten either the stabilization time or the test time because this could cause increased intrusion values due to insufficient thorough water distribution on the membrane surface.

The tests have to show that they are reproducible, providing comprehensive validation documents showing a good correlation between the tests and the HIMA bacterial challenge test. These provide practical limits with acceptable levels of assurance with limited risk of failing.

The test can be performed *in situ* and after sterilization (Figure 2.51). The test requires a drying phase to remove all traces of the test liquid.

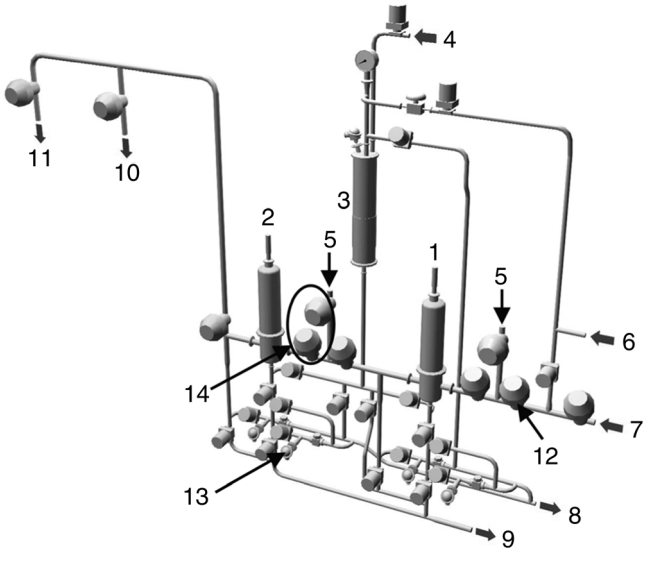

Figure 2.51 Basic principle of a venting filter for *in situ* integrity tests. Arrangement of the sterile venting filters for in-line sterilization and integrity tests (I tests). The integrity tests are carried out following the water intrusion method (WIT). In this figure, WIT is carried out only at the primary filter. The secondary filter is installed as a backup filter (police filter). 1, primary filter with a 0.22 μm cartridge; 2, secondary filter with a 0.22 μm cartridge; the secondary filter can be sterilized independent of the primary filter; 3, test liquid reservoir (WFI) with jacket heater; 4, inlet valve for the test liquid (WFI); 5, pure steam inlet valves; 6, inlet valve for filtered air (5 bar absolute); 7, inlet valve for venting gas (1060 mbar); 8, drain line with valves; 9, connection to the water ring pump (WRP); 10, connection to the condenser; 11, connection to the chamber; 12, sanitary valves; 13, temperature sensors; 14, separate sterilization for secondary filter.

In modern freeze-drying systems, the filter integrity test is carried out automatically. All the relevant process parameters are documented by the control system of the unit. The important thing is to make sure that after every integrity test, the filter and the entire piping system are perfectly dry. This is effected by means of the installed liquid ring pump.

Validation has to be carried out by the user on the basis of the data supplied by the filter manufacturer. The supporting documentation supplied by the manufacturer, showing correlation with the HIMA BCT, should be included in the validation protocol.

2.2.8 Vacuum Measuring Systems

The total pressure during freeze-drying may be measured by several methods, although only two are mostly used: heat conductivity and the membrane pressure difference gauge. Their operating principles and their advantages and disadvantages are described below.

The principle of design of a heat conductivity gauge (TM) is shown in Figure 2.52. Electrical energy is fed into the wire (2) in such a way that the

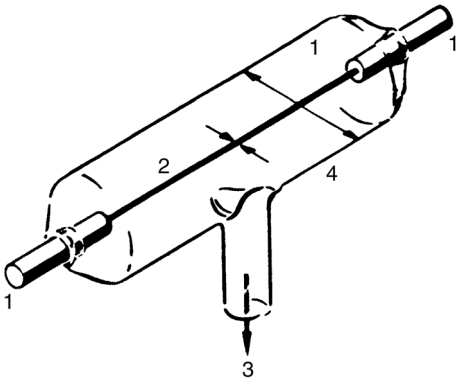

Figure 2.52 Schematic drawing of a vacuum gauge on the principle of heat conductivity (TM). 1, wire support; 2, wire, $d = 5–20\,\mu m$; 3, connection; 4, housing. (From Wutz, 1982 [15]. Reproduced with permission of Springer.)

temperature of the wire is kept constant. This amount of heat per unit time is in the area 2 of Figure 2.53 and is approximately proportional to the pressure. This range is between area 1, pressure independent, and area 3, practically no heat conductivity. The measuring range of such a measuring tube is between 10^{-2} and ~3 mbar. The position of area 2 depends on design details; it can be moved within certain limits, for example, the lower end can be moved below 10^{-2} mbar, but the upper limit is also reduced. The reproducibility of such an instrument is given, for example, by Leybold AG as less than 20% of the observed value between 10^{-3} and 10^{-2} mbar and less than 15% of the observed value between 10^{-2} and 1 mbar; an observed value of, for example, 0.1 mbar can be 0.085 or 0.115 mbar.

For barometric temperature measurement (BTM) (see Section 1.2.3), the conversion of p_s into ice temperatures (T_{ice}) with the data used above would lead to p_s 0.115 mbar = −41.0 °C, p_s 0.100 mbar = −42.2 °C, $p_s = 0.085$ mbar = −43.5 °C. An inaccuracy of more than ±1 °C is not acceptable. In addition, this measurement depends on the type of gas, as shown in Figure 2.54. If the reading of a TM, calibrated in air, is 0.1 mbar, it would be 0.05 mbar partial pressure in pure water vapor. During the main drying, a rough correction factor of 0.65 can be used to establish the order of magnitude of pressure, for example, if the instrument reads 0.1 mbar in a freeze-dryer during MD, the total pressure can be expected to be on the order of 0.065 mbar. Because of these disadvantages, TMs are being replaced by membrane differential gauges (CA) as described in Ref. [16].

The sensor consists of a metal casing that is divided into two chambers by a welded metal diaphragm (Figure 2.55). Only an impact or protective plate is on one side of the diaphragm, which protects it from mechanical damage. At the other side of the diaphragm, ring-shaped palladium electrodes are coated on to a ceramic disk (Figure 2.56), which, together with the diaphragm, form two condensers. If the differential pressure between the two sides of the diaphragm changes, the diaphragm is deformed and the distances between the diaphragm and the two electrodes change. This means a change in capacity, which can then be very accurately measured with an electronic bridge circuit. With the appropriate electronic equipment, the changes in capacity caused by the absolute pressure differences on both sides of the diaphragm are converted into a linear

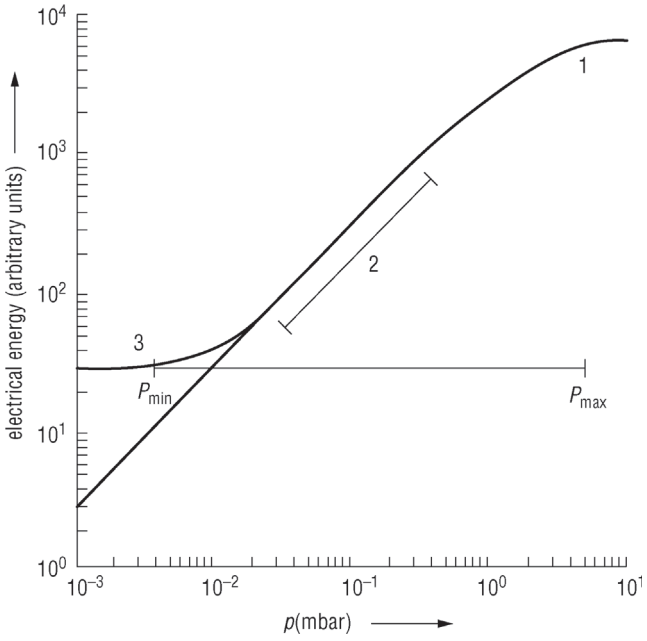

Figure 2.53 Electrical energy fed to the wire (to keep it at constant temperature) as a function of pressure in the TM housing. 1, range of pressure independent conductivity; 2, range of pressure proportional conductivity; 3, range in which the heat conductivity through the gas is negligible; p_{min} to p_{max} useful measuring range. (From Wutz, 1982 [15]. Reproduced with permission of Springer.)

constant voltage signal. Thus, a process is available that directly measures the pressure.

The sensors are manufactured as differential or absolute pressure sensors. The differential pressure sensors are connected on both sides to absolute pressure sensors, of which the difference between the two pressures is to be measured. They are then evacuated down to a pressure lower than 1×10^{-7} mbar on one side (a chemical getter protects the vacuum of 10^{-7} mbar from residual degassing).

The resolution of a capacitive sensor is determined by the changes in capacity that can still be measured. With the sensor dimensions used by MKS Instruments, a minimum deflection of $y = 10^{-10}$/m can be measured, resulting in a low measurable pressure of $\sim 1.10^{-6}$ mbar.

The effective measuring range of the individual pressure sensor types[4] is limited by its different zero point stability (0.02%) given at 2×10^{-3} mbar.

The accuracy of a measuring system is expressed by giving the measuring uncertainty. The measuring uncertainty is the sum of all the errors caused by linearity, hysteresis, reproducibility, and the temperature effect. The linearity error is the difference between the pressure sensor outlet and the ideal straight line from the zero point to the final value. Hysteresis is the deviation of the two

4 MKS Instruments Deutschland GmbH, D-81829 Munich, Baratron Series Catalogue.

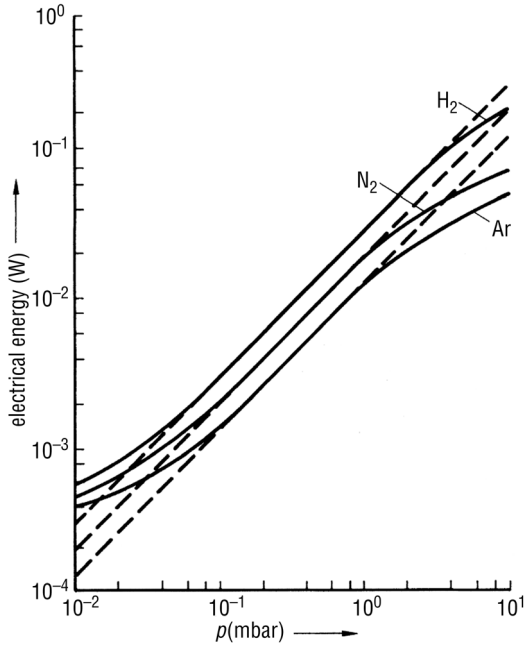

Figure 2.54 Electrical energy to keep the wire temperature constant as function of pressure for different gases as parameter. (From Wutz, 1982 [15]. Reproduced with permission of Springer.)

measuring curves to each other that is obtained on moving from the zero value of the measuring system toward the final value and then from the final value back to the zero point. The reproducibility error describes the deviation of measurements carried out one after the other under identical conditions. The total uncertainty of

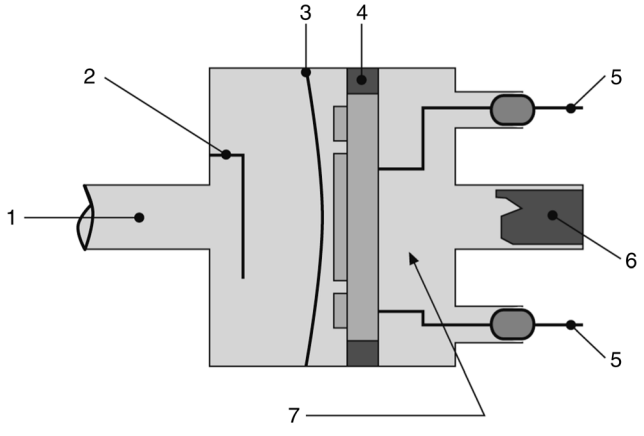

Figure 2.55 Schematic drawing of a sensor. (See also MKS Instruments Deutschland GmbH, D-81829 Munich, Baratron Series Catalogue.) 1, measuring side; 2, deflector/protective shield; 3, welded diaphragm; 4, electrodes; 5, electrode lead-throughs; 6, getter pump to maintain a low reference pressure; 7, reference side of very high vacuum (1×10^{-7} mbar).

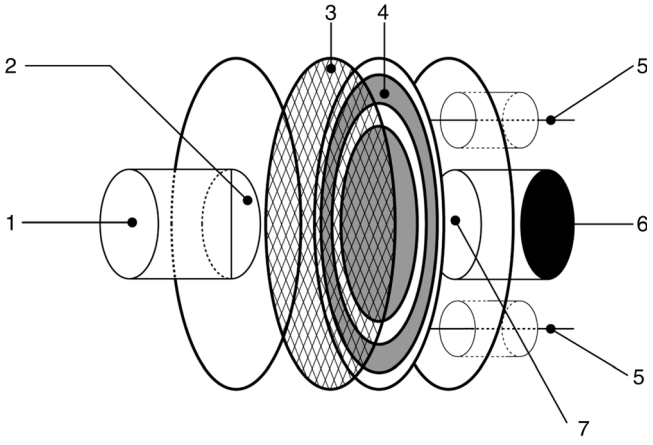

Figure 2.56 Arrangement of electrodes. (See also MKS Instruments Deutschland GmbH, D-81829 Munich, Baratron Series Catalogue.) 1, measuring side; 2, deflector/protective shield; 3, welded diaphragm; 4, electrodes; 5, electrode lead-throughs; 6, getter pump to maintain a low reference pressure; 7, reference side of very high vacuum (1×10^{-7} mbar).

a system also includes inaccuracies that originate from changes in temperature. Since these changes in temperature depend on the environment in which the system is being operated, it is necessary to give the temperature coefficients separately. The temperature effect plays a role only in the lower measuring range (0.1 mbar) of a pressure sensor (thermal transpiration [16]).

The measuring inaccuracy is given as a percentage of the corresponding measured value plus the corresponding temperature coefficients. This is the most important characteristic of every pressure sensor.

Manufacturers such as MKS Instruments encapsulate the sensor in a temperature-regulated environment.

The pressure measured in this way is independent of the type of gas and, since a capacitance can be measured very accurately, the instruments have a high resolution and reproducibility. For freeze-drying, the CAs should have a measuring range either of 10^{-4}–1 or 10^{-3}–10 mbar. The resolution with these instruments is 1×10^{-4} and 1×10^{-3} mbar, respectively, and the reproducibility at 0.1 mbar is better than ±0.005 mbar. In the temperature region of 40 °C, the vapor pressure changes by ~0.0014 mbar per 0.1 °C. Theoretically, temperature differences of ±0.3 or ±0.4 °C should be measurable. In the explanation of Table 1.22, a standard deviation of 0.38 °C has been calculated.

The diaphragm or capacity gauges are more expensive than TMs, but the difference can be neglected even in the cost of a pilot plant. Sensors for such gauges are available for sterilization by steam.

Partial gas or vapor pressures during freeze-drying can also be measured by a mass spectrometer and water vapor pressures by hygrometers, sensitive only for water vapor. Both systems are necessary for development and analytical work, but in production plants they need only to be used to check or identify process data.

2.2.9 Leak Rate Detection

The leak rates of a freeze-drying plant can be measured at the empty plant with the condenser cooled and the shelves heated by measuring the pressure rise per unit time multiplied by the installation volume in the dimensions mbar L/s. It should be noted that the plant has to be evacuated for several hours, for example, down to 10^{-2} mbar, before the pressure rise measurements, to avoid the influence of small amounts of ice and the desorption of gas from the surfaces. Furthermore, the pressure rise should be measured up to 0.2–0.4 mbar to detect possible gas desorption. Only if the pressure rise has been for some time proportional to time (Figure 2.57) does it represent a leak rate (LR), which is defined as

$$\mathrm{LR} = (\mathrm{d}p/\mathrm{d}t) \times V(\mathrm{mbar\,L/s}) \tag{2.4}$$

If the chamber and condenser have a volume of 1000 L, the leak rate can be calculated with the data from plot 1 in Figure 2.57:

$$\mathrm{LR} = [(0.13 - 0.10)/7200] \times 1000 = 0.0042 = 4.2 \times 10^{-3}\ \mathrm{mbar\,L/s} \tag{2.4a}$$

If the pressure rise of plot 3 is used during the first 3 h, the leak rate would appear to be $\sim 1.2 \times 10^{-2}$ mbar L/s.

Figure 2.58 shows two pressure rise measurements of the same plant: plot 1 measured by TM and plot 2 by CA. During the first 20 h, the ratio plot 1/plot $2 \approx 0.6$, indicating that the gas desorbed is mostly water, as can be expected at 30 °C. Other gases such as CO_2 desorb only at much higher temperatures. The pressure in the first hour and also in the first 3 h (not shown) was 8×10^{-2} mbar/h

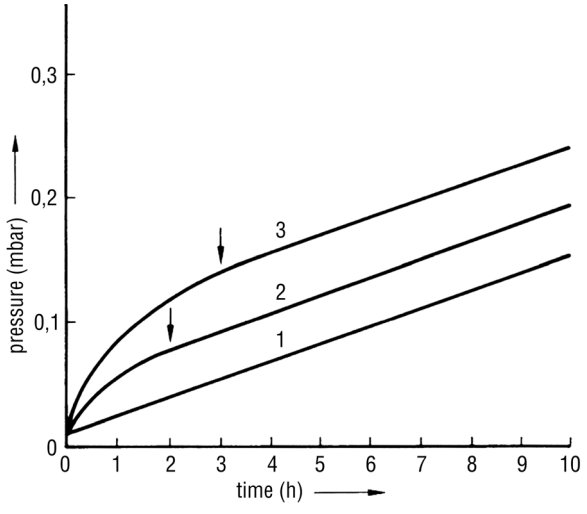

Figure 2.57 Pressure in the chamber and condenser as a function of time after both have been shut off from the pump set. 1, plot of pressure if no measurable gas is desorbed from the walls; 2, plot of pressure if desorption of gas stops after 2 h at a pressure of 0.08 mbar; 3, plot of pressure if desorption of gas stops after 3 h at a pressure of 0.14 mbar.

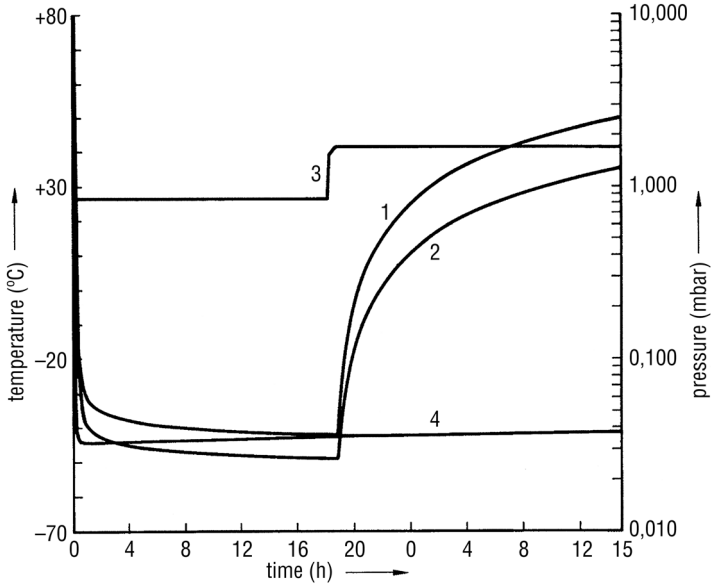

Figure 2.58 Pressure rise measurement as in Figure 2.38 in a plant evacuated for 18 h with heated shelves. T_{sh} should not have been changed before measurement of the rise, because the temperature-dependent desorption has to be adapted to the new temperature level, as discussed in the text in the remarks about 'history'. 1, p_{ch} measured by TM; 2, p_{ch} measured by CA; 3, T_{sh}; 4, T_{co}.

and this falls during the next 4 h to 7×10^{-2} mbar/h and during the last 10 h to 4×10^{-2} mbar/h.

This example is to show that the water desorption during applicable measuring times becomes less and less. If the pressure rise of 8×10^{-2} mbar/h in this installation is converted into leak rate, LR = 3.6×10^{-3} mbar L/s, or after 10 h it drops to 1.8×10^{-3} mbar L/s. In the LR range of 10^{-3} mbar L/s, one has to expect such variations between different measurements, since desorption depends on the history of the plant before measurements start and variations of this size disturb neither the BTM nor DR measurements.

If the leak rate disturbs the drying process, measurement of the ice temperature, or desorption rate, the leak has to be located and closed. Leak 'hunting' at a completely installed freeze-drying plant can only be done with a helium leak tester, as shown schematically in Figure 2.59. The installation (1) is evacuated by a vacuum pump (4). With a pistol (5), helium from a pressure bottle (3) is sprayed on the components of the plant most likely to leak: door seals, valves, windows, lead-through, and other flanges. Together with the air, helium diffuses into the plant and is detected by a mass spectrometer (2) specially adjusted to the mass 4 of He and connected to the vacuum pumping line. A freeze-drying plant cannot be evacuated by the small pumping system of a mass spectrometer (1.6 m^3/h backing and 33 L/s diffusion vacuum pump); therefore, the mass spectrometer is operated parallel to the pumping system of the freeze-dryer. Only part of the total gas flow passes through the mass spectrometer, as shown in Figure 2.60. If the throttle *L*

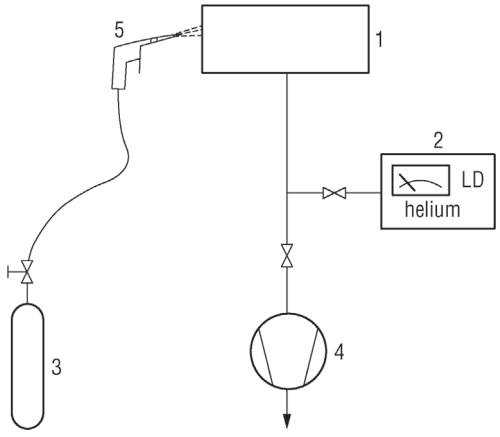

Figure 2.59 Detection of a leak by a helium leak detector. 1, chamber with a leak; 2, helium leak detector; 3, pressure bottle with helium; 4, vacuum pump system, evacuating the chamber; 5, helium spray pistol. (See also Leybold AG, D-50968 Cologne, Germany, Catalogue HV 300, Part B 10, p. 4.)

has a conductance, which is small compared with the pumping speeds of S and S_{LS}, $Q_{LS} = (L/S)Q_{to}$. If L and S are known and constant, the part flow measured by the mass spectrometer is only the L/S part of the total He flow. If, for example, $S = 360\ m^3/h = 100\ L/s$ at 0.1 mbar and $L = 0.1$ L/s, the leak detector will measure 1/1000 of the total He that has entered through the leak. Thereby, the smallest leak detectable increases by a factor of 1000, but this is not detrimental, as the sensitivity of the mass spectrometer is, for example, 2×10^{-10} mbar L/s and if the sensitivity becomes 1000 times smaller, it is still 2×10^{-7} mbar L/s. For a freeze-dryer it is sufficient to locate leaks larger than 2×10^{-4} mbar L/s. L/S could become 1/100 000 and leak detection is still possible at a pressure of 10 mbar. Helium leak testers are available in a transportable box of ~50 L with automated measurements.

Leaks and loss of power are the most unwanted events during freeze-drying (see the end of this chapter about defects). Therefore, it is recommended to make a leak test before each freeze-drying run, although this routine test does not have to follow the procedure described above. If the leak rate is measured once, the pressure as a function of time during the evacuation period can be recorded and compared with the evacuation plot of the actual run. If these plots do not deviate from each other, one can conclude that no additional leak has developed. This routine test should only be applied if the cleaning and sterilization of the plant

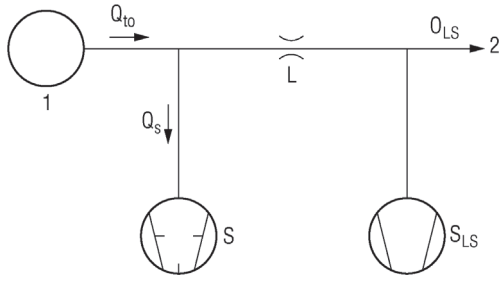

Figure 2.60 Leak hunting with the part stream method. 1, object to be tested; 2, helium leak detector; L, slit with a fixed conductivity. (See also Leybold AG, D-50968 Cologne, Germany, Catalogue HV 300, Part B 10, p. 7.)

have been the same as before the last run, to keep the desorption qualities of the surfaces as identical as possible.

2.2.10 Process Control Systems

The control system of the freeze-drying unit provides control, monitoring, and documentation of the process. Such a system must be reliable and comply with GMP and GAMP (Good Automation Manufacturing Practice) demands with respect to computer validation. It should be SCADA (Supervisory Control and Data Acquisition) compatible. A possible hardware architecture is shown in Figure 2.61.

The hardware architecture must be flexible with respect to bus technology, expansions, network integration, and modem access. The use of standard components and software and also a maintenance-friendly design will simplify qualification and validation for both the manufacturer and the user. It is advisable to design the machine control separately from the data management (i.e., recipe and data administration) to ensure that if there is a failure, loss of data does not result in losing a batch. Programmable Logic Controllers (PLCs)

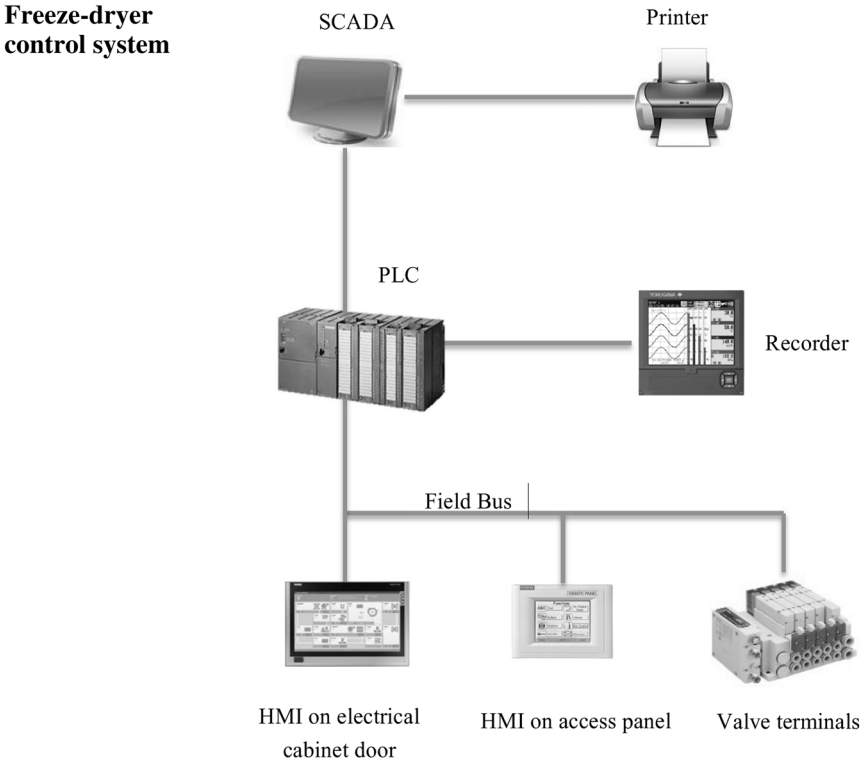

Figure 2.61 (1) SCADA PC. (2) Color printer. (3) PLC. (4) Recorder. (5) HMI installed on electrical cabinet door. (6) HMI installed on access panel. (7) Valve terminals. (Austar Group, China.)

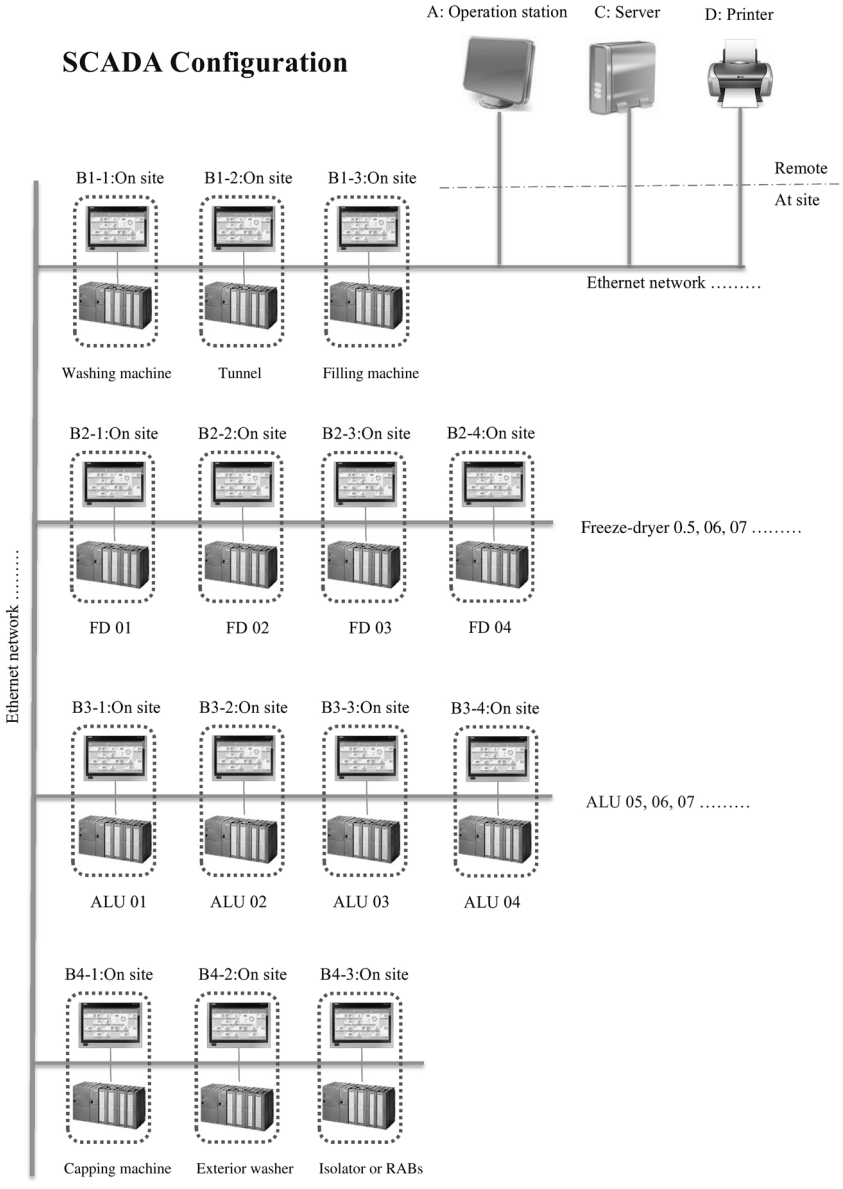

Figure 2.62 SCADA (Supervision, Control, and Data Acquisition). Example of a SCADA solution for several freeze-dryers (No. 1, No. 2, . . . , *X*) and an automatic loading and unloading system (ALUS) built into an isolator. In addition, a central CIP system for cleaning the freeze-dryers is monitored and controlled. (Austar Group, P.R. China)

can be used for the machine hardware. The operator administrates the data at the PC level (Figure 2.62).

At the PC level, the freeze-drying process and all secondary processes are visualized, controlled, and documented. Such secondary processes include

condenser defrosting, CIP/SIP, plant tests, failure statistics, calibration values, counter of operating hours, plant schematic, table of valves, actual temperature and pressure values, recipes, start parameters, and machine parameters.

The control system must also be SCADA compatible as shown in Figure 2.62.

A freeze-drying plant should have as a minimum the following measuring capabilities:

1) During freezing:
   - inlet and outlet temperatures of the shelves, if there are different blocks of shelves, each block should be measured, if temperature sensors in the product are used at least three should be applied.
2) During main and secondary drying:
   - shelf temperatures and product temperatures as above;
   - condenser temperature(s), in a multiple coil condenser at each separately injected block of coils;
   - temperature of the ice at the sublimation front (see Section 1.2.3);
   - total pressure in the chamber by a diaphragm gauge (CA);
   - total pressure in the condenser by CA, close to the vacuum pump connection (see Section 2.2.4);
   - total pressure by CA between the shut-off valve and the vacuum pump (the last two CAs can have the same data processing system, since no fast changes have to be measured);
   - software to record DR data and calculate the residual water content (dW) (see Section 1.2.3);
   - vacuum gauge up to atmospheric pressure during the venting of the plant.

Figure 2.63 shows the visualization of a freeze-drying plant at the PC level. For production plants, the following data of machines should be supervised:

- temperatures of the cooling and heating medium after the circulation pump(s) and after the heat exchanger(s);
- temperature of the refrigerant at each injection valve;
- operating temperature of all electric motors;
- open or closed position of all valves (without injection valves).

The control system of a freeze-drying plant should allow programming the following data independent of each other during manual operation:

Start of the cooling of the shelves:

- cooling speed of the shelves down to a specified end temperature; the plant manufacturer has to specify the possible maximum and minimum speed for a temperature interval, for example, 1 °C/min from 0 to −40 °C, 2 °C from 0 to −20 °C, 0.3 °C from −35 °C to −45 °C;
- thermal treatment during freezing or annealing;
- nucleation-on-demand freezing technology (2.1.6);
- start of evacuation after a preset shelf temperature has been reached;
- selection of shelf temperature as a function of time;
- start of the heating after a preset chamber pressure has been reached, for example, with a delay of 0.5 or 15 min;

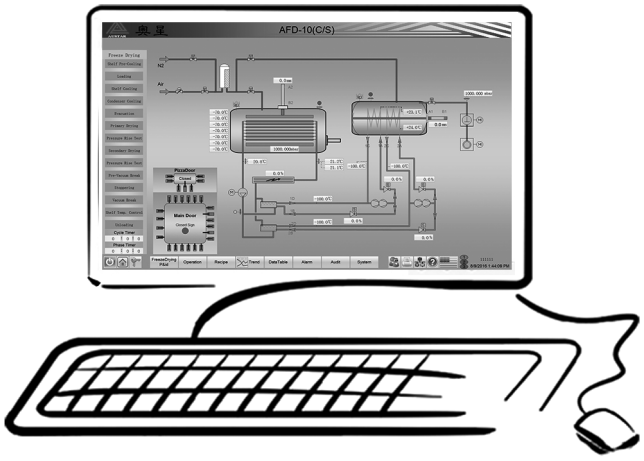

Figure 2.63 Visualization at the PC level designed as follows:

- Man–machine interface in Windows
- Intouch or i-Fix visualization package
- Database management (recipes and history filing)
- Compatibility of network integration

(Austar Group, P.R. China.)

- preset the time between two BTMs, for example, 15 or 30 min; if MD is long, for example, 20 h, the time can be increased to 60 min or decreased to 10 min for a very short MD;
- the shelf temperature can be changed during hand operation;
- the operation pressure can be preset and changed, for example, if T_{ice} is too low, the p_c can be raised or vice versa.

Chase [17] presents an alternative method to monitor and control the freeze-drying process by measuring the flow of nitrogen to keep the operation control pressure, p_c, constant. The mass flow controller (FMC) consists of a proportional valve, an integral flow meter, and a capacitance manometer (CA). The CA measures the total pressure in the plant, the valve opens if the pressure drops below the preset value and vice versa. The flow of nitrogen necessary to keep the pressure constant is measured by the flow meter. Figure 2.64 shows the high N_2 flow at the start of the drying, because the product is heated up and the water vapor pressure is still low; after ~2 h, the water vapor pressure rises and the N_2 flow can be reduced to keep the total pressure constant. After 34 h, the water vapor flow decreases and the N_2 flow increases until the water vapor flow becomes very small at ~49 h and the N_2 flow almost constant.

2.2.11 Problems, Failures, and Deviations

Possible problems during the operation of freeze-drying plants can mostly be assigned to four categories:

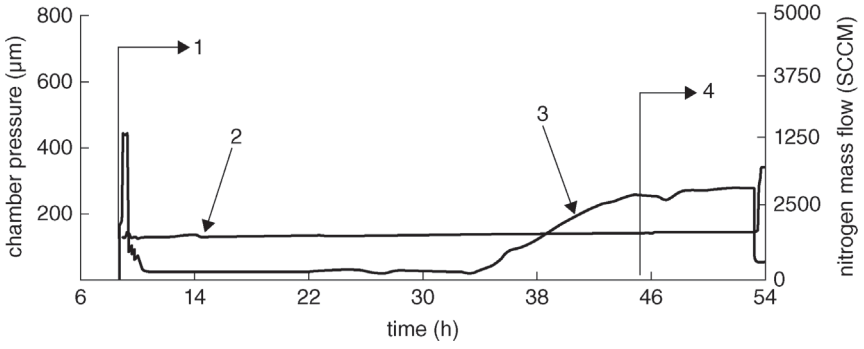

Figure 2.64 Chamber pressure and nitrogen flow-rate as a function of drying time. 1, main drying; 2, chamber pressure; 3, nitrogen flow; 4, secondary drying. (Figure 4 from Ref. [17].)

- those occurring before the evacuation starts;
- those requiring immediate, preferably automatic, action;
- those to be corrected automatically or by hand within few minutes;
- deviations that must be documented.

The analysis of problems and the required counteractions will depend on the operation principles of the operator, the value of a lyophilization charge, the sensitivity of the product to deviations from the set values, and several other factors. Nevertheless, an analysis of possible problems and a guideline for counteractions should be established for every freeze-drying plant as part of the instruction manual, even if it has to be adjusted for new products.

The following summary cannot be a complete list, and reflects only the more likely events causing trouble (in Section 6.1 several problems are discussed related to product structure, stoppers, traces of volatile components, etc.).

Trouble before the evacuation starts:

These events can be avoided in most cases, if the following start-up rules are used: (1) the plant is evacuated down to the lowest operation pressure; if this pressure is reached, possible water or ice from the cleaning or sterilization is evaporated; (2) the condenser is cooled to the operating temperature and the shelf heated to the maximum temperature during SD; (3) if the lowest operation pressure is reached again, the leak test can be done (see Section 2.2.6); (4) the shelves are cooled back to the loading temperature and the plant is vented with a gas as specified (see end of Section 1.2.3 and Figures 2.57–2.59).

With this start-up, the most critical machine data are to be checked: no remaining ice, cooling and heating working, and leak rate acceptable. The procedure takes some time, but minimizes problems occurring during the freeze-drying process.

Trouble requiring immediate action:

The most undesirable event is a power failure. In that case, the valve between vacuum pump and the condenser has to close automatically. If the power failure lasts only a few minutes, the condenser has a certain heat capacity to maintain the sublimation of ice. The tolerable time of power failure depends on the plant design.

A power failure exceeding the time limit is most critical during MD. In this case, a standby power generator with a start-up time of, for example, 1 min either for the operation of the whole plant or at least for the critical components is the only answer. The sequence of importance for the components can be as follows:

- operation of a part of the pumping set to maintain the vacuum in the chamber and the condenser;
- operation of a part of the refrigerant compressors or the injection of LN_2, if the condenser has a separate evaporator for it (see Section 2.2.5);
- operation of a part of the cooling system for the shelves.
- another undesirable event is air pressure due to a leak in the plant which reduces or stops the sublimation. The counteractions could be:
- reduction of the shelf heating temperature to the minimum possible value;
- using the full pumping capacity or adding an auxiliary pump set.

If the loss of the product can be avoided by these steps, hunting for the leak could become possible (depending on the arrangement of the plant in the building). With experience it is possible to predict that leaks will not be generated through porous steel, but by seals in flanges or doors. The probability of newly developed leaks after the suggested start-up procedure has been used is 10–100 times smaller than without this test, but it cannot be fully excluded.

Trouble to be corrected automatically or manually in minutes:

The failure of the condenser compressors can be bearable for some time (see above). For production plants, two smaller compressors are recommended rather than one large unit, as this permits the process to be continued with a prolonged drying time. On failure of the refrigerant compressors for the heat transfer fluid in the shelves, the shelf temperature will rise slowly, if the temperature is below room temperature. Stopping the heat transfer fluid pump(s) will slow this temperature rise during the main drying and the sublimation of ice will withdraw energy from the shelves. A failure of other components, for example, valves or gauges, could be compensated by replacements or standby units. For these types of failures, the plant must be operable and controllable completely manually.

With freeze-dryers used in production and also with pilot plants, all the critical plant components should be supplied redundant to make sure that the process can be continued if there is a mechanical or electrical failure. Redundancy is particularly advisable in the following cases:

- vacuum pumps;
- circulation pumps;
- cooling system.

Deviations to be documented:

All deviations from the preset data must be documented, even if they are within the given tolerances. For the important process data, not only is a comparison of the actual with the preset data recommended, but also a trend analysis should be installed. This permits the recognition of systematic deviations long before the tolerances are exceeded.

Example: The heat transfer fluid temperature is set at $-30 \pm 1\,^{\circ}C$. The heat transfer fluid temperature has been for some time between -31 and $-30.5\,^{\circ}C$, and

it rises, for example, in 2 h from this range to −30 and −29.5 °C. Warning of this trend is helpful. Either the pumping speed of the heat transfer fluid pump is reduced or the injection valve of the refrigerant has shifted or the refrigerant compressor has changed its capacity.

Analyze: The inspection system on the motor of the heat transfer fluid pump shows no warning; the temperature of the refrigerant before the injection valve is constant. It follows that the injection valve has shifted and should be adjusted.

2.3 Installations Up to 10 kg Ice Capacity

2.3.1 Universal Laboratory Plants

As indicated by the title of this subsection, the manufacturers of such plants attempt to make them flexible for different applications by using a modular concept. Often, the basic unit consists of a condenser, a vacuum pump, and a vacuum gauge, to which various drying systems can be added, for example, manifolds for flasks, ampoules or vials, baseplates with belljars, or small chambers with temperature-controlled shelves. A schematic drawing of such a plant is given as an example in Figure 1.99. A plant equipped with a manifold is shown in Figure 2.65, and the same basic system with a belljar is presented in Figure 2.11.

The following qualities could be important in selecting the most suitable laboratory plant:

- Ice condenser:
  - Maximum ice capacity at an ice thickness of 1–1.5 cm
  - Can the condenser surface be observed visually?
  - Method of ice defrosting (e.g., electric heating, warm water, warm vapor from the compressor). If the ice must be examined for certain components carried over with the ice (aroma, volatile components), hot air or water may be not applicable.
- Refrigerant compressor:
  - Air or water cooling
  - Lowest operating temperature
  - Cooling capacity at 5 and 10 °C above lowest temperature
- Vacuum pump:
  - Two stages (recommended) with gas ballast (necessary)
  - Valve between the vacuum pump and condenser, which closes automatically if the electric power is disrupted
- Vacuum gauge:
  - If a heat conductivity gauge (TM) is offered, the additional price for a capacitance gauge, which is strongly recommended, should be requested.
- Shelves:
  - Range of controlled temperature
  - Speed of cooling and heating from xx to yy °C for cooling and from zz to ww °C for heating
  - Recommended method of freezing, if the shelves cannot be cooled

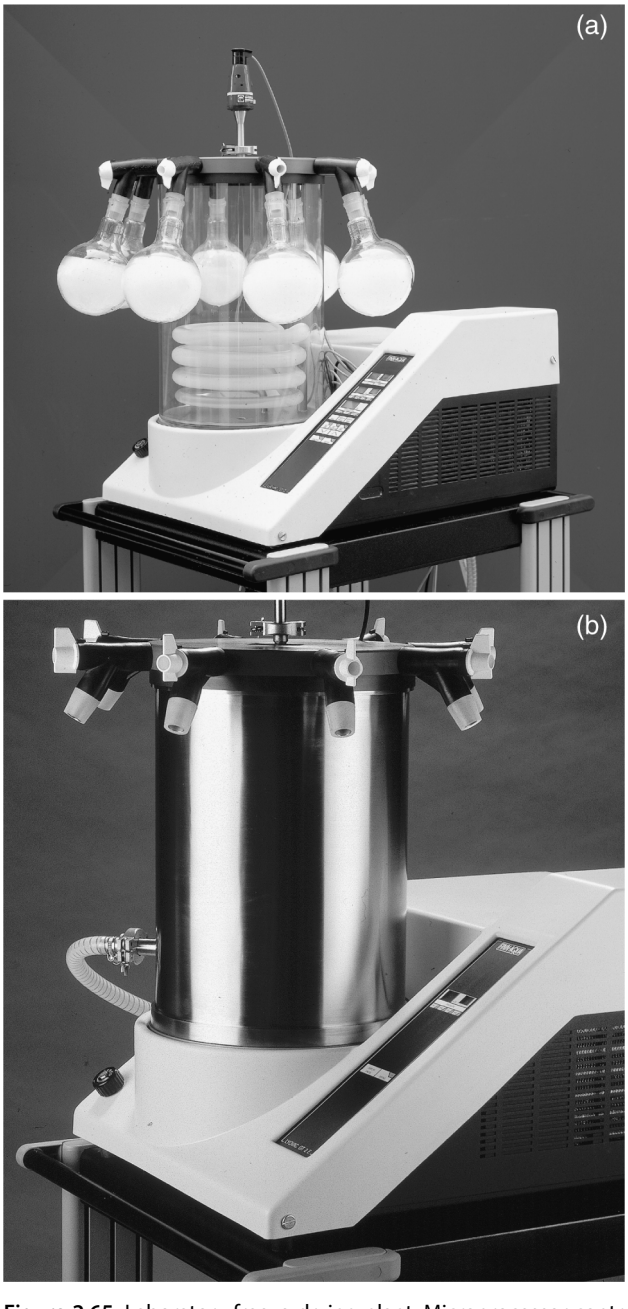

Figure 2.65 Laboratory freeze-drying plant. Microprocessor controlled, air-cooled compressor, condenser end temperature −53 °C, ~3 kg of ice sublimed in 24 h. (a) Unit with eight valve connections for eight containers, condenser in an acrylic glass cylinder. (b) Same unit with a stainless steel cylinder, containers not shown. (LYOVAC® GT 2, Steris GmbH, D-50354 Hürth, Germany.)

  - Uniformity of temperature for all shelves, for example, ±1 °C during main drying
  - Levelness and smoothness of the shelves
  - Temperature measurement in the product
- Valve and its free diameter between chamber and condenser:
  - Without this valve no pressure rise measurements can be carried out for BTM (T_{ice}) or DR data for the calculation of the residual moisture.

The process data from manifold installations can hardly be transferred to chamber-type plants. This applies, practically, also to the process transfer from belljar-type installations to chamber plants. Results obtained in laboratory plants of the chamber type must be analyzed carefully, if they are to be transferred to another plant. If the product, the layer thickness of the product, and the vials or trays are identical, then the following conditions should be observed and compared:

- Freezing method and freezing rate must be the same.
- Evenness, smoothness, and temperature uniformity of the shelves must be comparable.
- The temperature shielding of the product against wall and door influences have to be comparable.
- The shelf temperature and the controlled operation pressure must be controlled in such a way that T_{ice} in the laboratory plant is stable and measured with a standard deviation less than ~0.5 °C.
- The conditions of water vapor transport between the chamber and condenser, the condenser surface, the capacity of the refrigerant compressors, and the vacuum pumping capacity must all be the same (pro rata) for the product dried in the laboratory as in the plant to which the process will be transferred.

It is likely asking too much of most laboratory plants if used as pilot plants for production process development. The best application of laboratory plants is the freeze-drying of preparations and products that do not require to be operated within small tolerances, but can be dried under noncritical process data.

2.3.2 Pilot Plants

In the plants described in this section, the process data can be developed, verified, and – in a measurable and reproducible way – modified to achieve the specified quality of the product in the most economical process.

All these plants are of the chamber type with cooled and heated shelves and a condenser that can be separated from the drying chamber by a valve. Refrigeration and vacuum systems should be laid out for temperatures and pressures that can be expected under extreme experimental conditions, even if these extreme data may not be used in the production process. Pilot plants for pharmaceutical or medical products should be laid out differently than those used for food.

The following proposal for a pilot plant specification is given in general terms and will have to be supplemented by specific requirements:

	Pharmaceuticals	Food
Size of chamber	Approximately cubic[a], 100–200 L[b] or ~50 L[b]	$1 \times 0.5 \times 0.5$ m[c]
Condenser surface	4–6 kg of ice at a layer thickness of 1.5 cm[d] or >2 kg for 50 L chamber	10–15 kg of ice at a layer thickness of 1 cm[e]
Condenser temperature	Minimum −55 °C, Preferably −65 °C	Minimum −45 °C, Preferably −50 °C
Refrigeration capacity of the compressors at 10 °C higher than the above minimum temperatures	Specification of manufacturer	
Type of valve between chamber and condenser	As shown in Figure 1.145 (6) or Figure 2.20 (D), preferably no butterfly valve as in Figure 1.144 (7)	
Water vapor transport from chamber to condenser[f]	Water vapor g/h at p_{ch} 0.06 and 0.3 mbar, measured by CA	Water vapor g/h at p_{ch} 0.2 and 1.0 mbar measured by CA
Vacuum pumping set	Two stages, with gas ballast, in maximum 15 min	Two stages, with gas ballast in maximum 10 min >0.1 mbar[g] down to 0.02 mbar[g]
Leak rate of chamber and condenser[h]	$<2 \times 10^{-3}$ mbar L/s	$<2 \times 10^{-2}$ mbar L/s
Shelves	One shield on top, two to four for product	One shield on top, two for product
Shelf temperature	Minimum −55 °C, Preferably −80 °C, Maximum +60 °C	Minimum −10 °C, Preferably −40 °C Maximum +120 °C
Amount of heat transfer fluid circulated through the shelves and specific heat capacity of the heat transfer fluid[i]	Specification of manufacturer	
Method of product shielding from influences of wall temperature[j]	Specification of manufacturer	
Method of condenser defrosting, cycle time	Specification of manufacturer	

a) Depth of chamber should be limited for cleaning and loading.
b) To measure DR data, the ratio of chamber volume (L) to mass of solids (g) should be ~1 or (depending on the desired accuracy of DR) maximum 2. If only small amounts of the test product are available, it is recommended to use a smaller chamber, for example, 50 L, otherwise the free volume of the chamber has to be reduced by glass or aluminum bars.
c) Chamber should be large enough for two production trays on one shelf and or one each on two shelves, one on top of the other.

d) With pharmaceuticals, the vapor flow (kg/h) during MD is usually smaller than for food; therefore, the ice layer produces a relatively smaller temperature difference between coil and ice surfaces, and the ice layer can be thicker than for food plants.
e) See note d.
f) Flow of water vapor with pure ice in trays (see Section 1.2.4).
g) Measurements with chamber and condenser at room temperature.
h) Details in Section 2.2.6. For maximum tolerable leak rates see Section 1.2.3 as referred for BTM and DR measurements.
i) With this information, the maximum flow of energy can be estimated, which can be transported during freezing and main drying at a desired temperature difference between inlet and outlet temperature of the heat transfer fluid at the shelves, for example, 2000 kJ/h at a temperature difference of 3 °C. With this amount of energy, ~0.7 kg of ice could be sublimed per hour (this estimate gives only the maximum possible sublimation rate; whether it can be achieved or not depends on heat and mass transfer conditions in the process [see Section 1.2.1 and Eq. (1.14)]).
j) Depending on the shelf temperature during freezing, thermal treatment, MD, and the uniformity of the product temperature during SD, the shielding requires the technical optimum at low temperatures, rapid changes of temperatures and a high degree of product temperature uniformity (for details, see Figures 1.104 and 1.105).

The requirements on the measure, control, and safety installations are described in Sections 2.2.8 and 2.4. The degree of automation of pilot plants will depend on the expected operating conditions. However, it is recommended to automate the pilot plant in the same way as the production plant, to simulate the same operation. Details of automation are given in Section 2.6. At least BTM and DR measurements should be automatic, this being far more accurate and less tedious than manual operation and visual reading.

The pilot plant, shown schematically in Figure 2.66, permits the product to

1) be frozen down to −80 °C, at freezing rates of 1–2 °C/min (depending on the cake thickness), for example, ~2 °C/min at 15 mm;
2) be dried during MD at T_{ice} down to −50 °C;
3) be dried during SD at pressures down to $<1 \times 10^{-3}$ mbar (see end of Section 1.2.3 and Table 1.24).

The specifications of the plant are given in the caption of Figure 2.66. As can be seen from the tables in the caption, the main drying time depends on the heat transfer and the vapor flow rate. To optimize a freeze-drying cycle, it is helpful to calculate a table as shown in Figure 2.66 for runs 1–7, which can be commented upon as follows:

Run 1: If the product layer is small (e.g., 15 mm) with a small temperature gradient in the frozen product and the dry product on the surface tolerates 30 °C and $T_{ice} = -35$ °C is low enough (see Section 2.6.2.4), the conditions of run 1 are an optimum.

Runs 2 and 3: If T_{ice} is correctly chosen, but the temperature gradient in the product or the surface temperature is too high, the conditions of run 2 or 3 can be used, accepting a prolonged t_{MD}.

Runs 4–6: If T_{ice} in runs 1–3 is too high, a lower p_c has to be used. This does not necessarily increase t_{MD}, as seen in runs 5 and 6 compared with run 3. However, the conditions in run 6 may not work: the flow rate seems too large. The only possible remedy is to reduce T_{tot} correspondingly as in run 7 or 8.

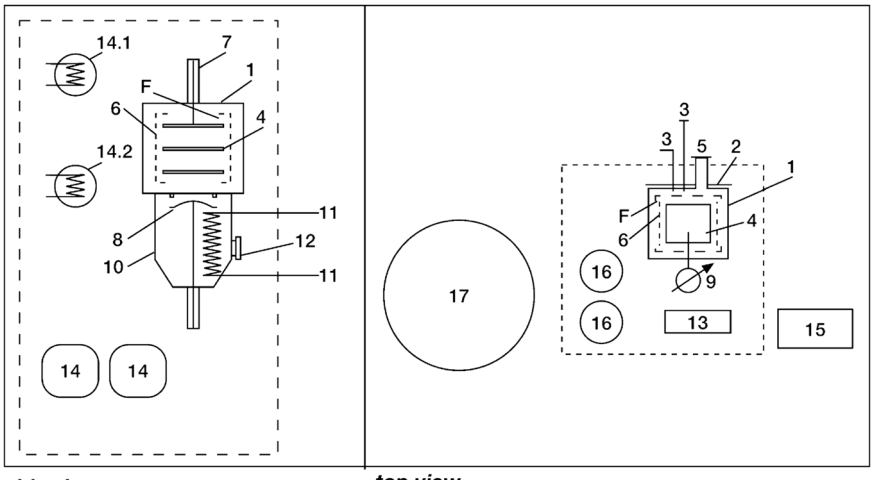

Figure 2.66 Dimensional schematic drawing of a pilot plant (LYOVAC® FCM 2, Steris GmbH, D-50354 Hürth, Germany). 1, 50 L chamber, requiring 25–50 g solids per run; 2, door with a temperature-controlled shield; 3, manipulator to close the stoppers of certain vials during drying, swiveling cover if not in use; 4, temperature-controlled shelves (range optional), −80 to +80 °C; 2 shelves for ~120 vials, 30 mm outer diameter (temperature up to +80 °C is, for example, only required if the product is to be virus inactivated in the plant by heat treatment); cooling rate (d ~15 mm, 20 to −50 °C), ~2 °C/min; heating rate (empty, −50 to 0 °C), ~3 °C/min; 5, window for camera (optional); 6, overlapping temperature-controlled shields (not on top and bottom, see Figures 1.100 and 1.101); 7, hydraulic for pressing the stoppers into the vials; 8, valve, water vapor flow in the table below, 150 mm diameter; 9, capacitive vacuum gauge, 10, condenser housing; 11, condenser surfaces, not dimensional, 150 g/h between −50 and −70 °C, capacity >2 kg; 12, view port for condenser surface; 13, vacuum pump set: roots and two-stage rotary pump, end pressure 1×10^{-3} mbar, time from 1000 to 0.02 mbar in loaded plant ~12 min; 14, Flexcons (volume changes of brine with temperature); 15, control panel; 16, heat exchangers for the brine in shelves and condenser; 17, LN_2 storage tank, movable; 18, operation panel; F, space for water vapor flow; leak rate $<2 \times 10^{-3}$ mbar L/s.

Table: Maximum water vapor flow-rates given by the hydrodynamic data of the plant. The maximum sublimation rates depend also on the heat transfer from the brine to the sublimation front of the ice (see Eq. (1.12)). The main drying time will generally be governed above 0.06 mbar by the heat transfer and below 0.06 mbar by the water vapor transport, as shown in the example below:

p_c (mbar)	Flow-rate (g/h)[a)]	T_{ice} (°C)[b)]
0.3	1600	−28
0.1	350	−37
0.06	125	−41
0.04	60	−44
0.02	25	−49

a) Data are measured with a given configuration and dimensions of vials, especially the data <0.04 mbar should be verified for the actual situation.

b) T_{ice} depends besides on the pressure on other process data (see Section 1.2.3). Data given are for orientation, and should not be used for process development.

Example with the above data: 120 vials filled with 1.488 cm^3 of solution of 20 mm layer thickness containing 10% solids can be main dried if $K_{tot} = 60$ kJ/h °C m^2 under the following conditions [Eq. (1.12)]:

Run	p_c (mbar)	T_{sh} (°C)	T_{ice} (°C)	T_{tot} (°C)	t_{MD} (h)	Flow–rate (g/h)
1	0.1	30	−35	65	10.4	129
2	0.1	20	−36	56	12.1	111
3	0.1	0	−37	37	18.6	72
4	0.06	20	−39	59	11.5	117
5	0.06	0	−41	41	16.6	81
6	0.04	0	−44	44	15.5	86
7	0.04	−10	−45	35	19.5	69
8	0.04	−15	−46	31	22.0	61

The data and the discussion above should be taken as guide for a process development, not as absolute. The data are from one specific project and rounded for simplicity, for example, at a given p_c, T_{ice} will vary with T_{sh}, but the result will not be round figures as shown; the t_{MD} has been calculated with a constant $K_{tot} = 60$ kJ/°C h m^2; as shown in Figure 1.92 and Table 1.15, K_{tot} decreases with decreasing pressure. The dependence of T_{ice} on p_c can be very different as used in the example (see Section 2.6).

Figure 2.67 shows the front view of the plant with the door and the shielding door open and the manipulator behind the swiveling cover. Figure 2.68 is the plant with the shielding door closed and the manipulator ready for use.

2.3.3 Manipulators and Stoppering Systems for Vials

In the operation of pilot plants, it may be important to close some vials during secondary drying without interruption of the drying process. Vials closed at certain moments can provide various information: The residual moisture content can be determined not only by measuring the DR during SD, but also by other methods (see Section 1.3.1) and compared with data calculated from DR measurements. Furthermore, it can be investigated whether and how much the chemical structure and/or the activity of the product changes at certain times and temperatures during drying. During main drying it is recommended that closed vials are not removed as this may change the drying conditions for the product in vials close to those removed.

By using manipulators, as shown schematically in Figure 2.69, certain vials can be closed and left in their position or be removed from the plant by a lock. In a plant without a manipulator it is not possible to close vials after venting the plant for a short time, because during MD the product will collapse or melt and during SD the continuation of the drying will be different (gas has been absorbed by the solids). Figure 2.70 shows a pilot plant with a manipulator.

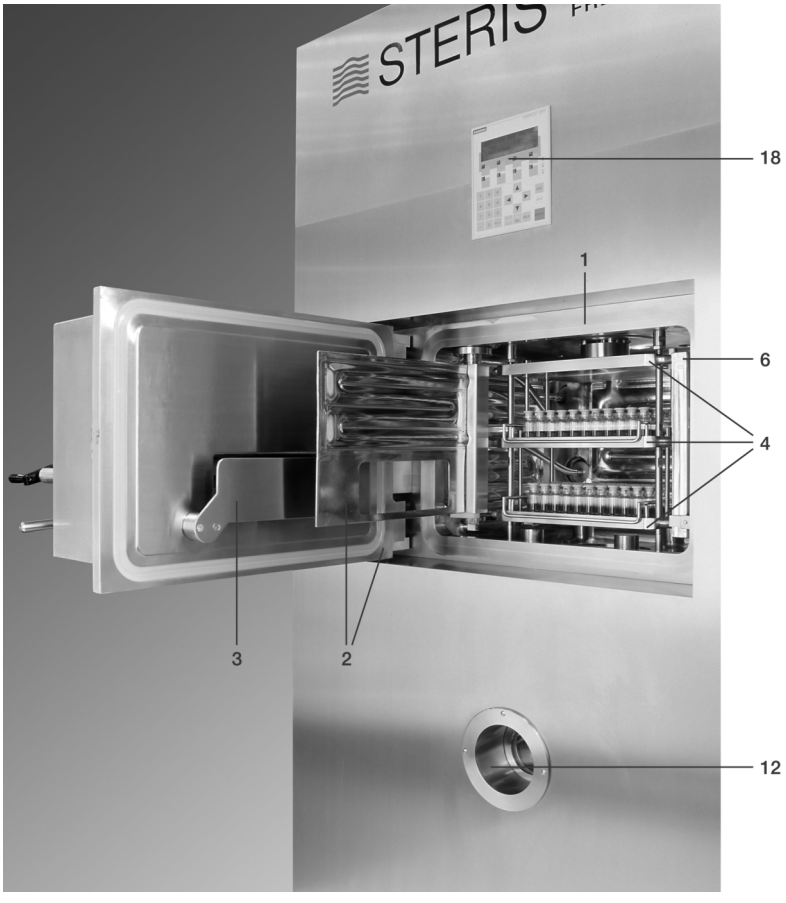

Figure 2.67 Partial view of the plant shown in the schematic drawing in Figure 2.66. 1, chamber; 2, door and temperature-controlled shield; 3, swiveling cover, if manipulator is not in use; 4, temperature-controlled shelves; 6, temperature-controlled shields; 12, view port for condenser surface; 18, operation panel. Numbers are identical with Figure 2.66, specifications are given there.

An important step in the freeze-drying process with vials is the stoppering or closing of the vials either at the end pressure of SD or at a chosen partial pressure of a specific gas. This avoids handling of open vials, which can lead to contamination and adsorption of water vapor from the atmosphere.

This step is so important that some laboratory plants and usually all pilot and production plants are equipped with respective mechanisms. Figure 2.71 shows a production freeze-dryer which is equipped with a stoppering system. The principle is simple: The shelves are connected flexibly with inlet and outlet of the heat transfer fluid. The shelves are pressed together, one after the other, by a plate, which is moved by an external force; in this way the stoppers are pushed into the closed position. If the pressure necessary for this stopper movement is 1 kg per stopper, the resulting total force for 100 vials per shelf is 100 kg, but if

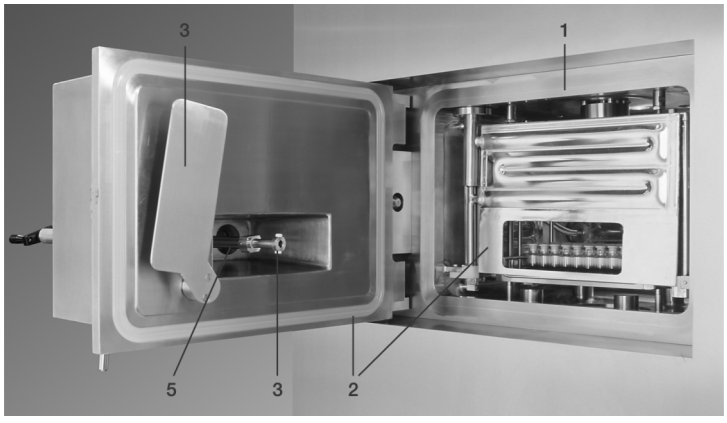

Figure 2.68 Partial view of the plant shown in the schematic drawing in Figure 2.66. 1, chamber; 3, manipulator swiveling cover open; 5, window for camera. Numbers are identical with Figure 2.66, specifications are given there. (LYOVAC® FCM 2, Steris GmbH, D-50354 Hürth, Germany.)

10 000 vials are loaded per shelf, the total force is 10 tons, which has to be applied evenly in order to avoid vials breakage.

The technical problems to be solved are twofold: All parts must be steam-sterilized and no abrasion can be tolerated in the chamber. For this the manufacturers offer various solutions, in that the pressure plate is:

- operated by several motor driven spindles; or
- drawn by motor powered ropes; or
- moved by a centralized hydraulic system, as shown in Figure 2.72.

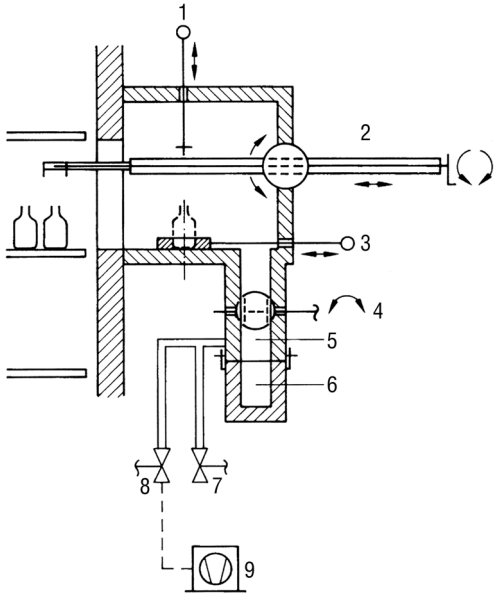

Figure 2.69 Schematic drawing of a manipulator including a vacuum lock. 1, tool to close vials; 2, arm of the manipulator; 3, rod to push vials; 4, ball cock; 5, exit channel; 6, exit container for vials; 7, venting valve; 8, vacuum valve; 9, vacuum pump.

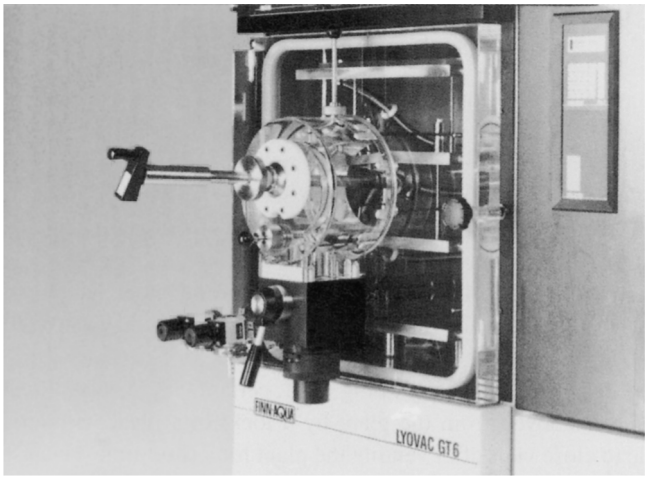

Figure 2.70 Manipulator as shown in Figure 2.69, connected to a LYOVAC® GT6. (Photograph Steris GmbH, D-50354 Hürth, Germany.)

The shaft (2) is surrounded by a chamber (3), which is evacuated and steam-sterilized. The chamber and the shaft are sealed from the drying chamber by a special sealing system. The advantages are that the slick cylinder is easy to clean and to sterilize, with no possible abrasion. The disadvantage is the greater height, as the cylinder chamber must be as long as the lift of the pressure plate. Another solution to avoid the greater height is to use a bellows as shown in Figure 2.73.

Figure 2.71 Production freeze-dryer AFD 10-C/S with 10 m^2 shelf area and 150 kg ice condenser storage capacity. (Austar Group, P.R. China.)

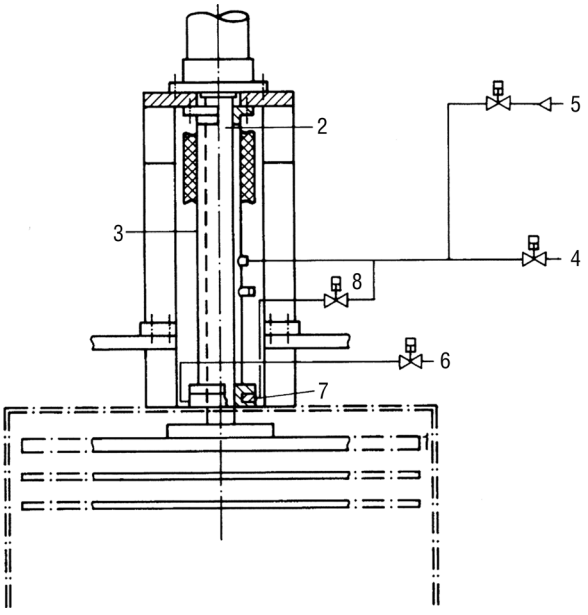

Figure 2.72 Schematic drawing of a steam-sterilizable closing mechanism for vials. The pressure plate (1), by which the stoppers are pushed into the vials, is sterilized jointly with the chamber. The shaft (2), to which the pressure plate is connected, moves into the chamber during stoppering. It is not sterilized with the chamber. Therefore, the shaft is sterilized in a separate chamber (3). This chamber can also be connected to the vacuum pumping system (4) as to the steam supply (5). Water condensing during the sterilization can be drained by (6). A special seal (7) can (by (8)) also be connected to steam or vacuum and be sterilized. (Schematic drawing from Product Information by Steris GmbH, D-50354 Hürth, Germany.)

2.3.4 Cleaning Installations, Sterilization by Steam, and Vaporized Hydrogen Peroxide (VHP®)

Clean in Place (CIP)

Cleaning and sterilization of freeze-dryers are two process steps with the highest priority in aseptic production systems. The rule 'CIP is followed by SIP' is applied here. In Standard DIN 11 438, cleaning in place is defined as follows: 'CIP is the cleaning of systems without taking them apart and without major modification with regard to the operating status'. The FDA states: 'The FDA regulations for cleaning validation of production systems can be fulfilled by automated plants and processes in so far as these systems are suitable for CIP cleaning'. A CIP system is always custom-tailored and is designed according to the size and design of the freeze-dryer (see Figure 2.74), the group of products to be manufactured, and the cleaning agents and detergents to be used. Cleaning is one of the main quality factors for freeze-dryers. Cleaning is the first and the last step in the production of medicinal products.

The goals of a CIP system are as follows:

- Improvement of the hygienic status because of permanently maintained cleaning parameters without the need to rely on the skills and care of an operator and without the disadvantages of physical labor.

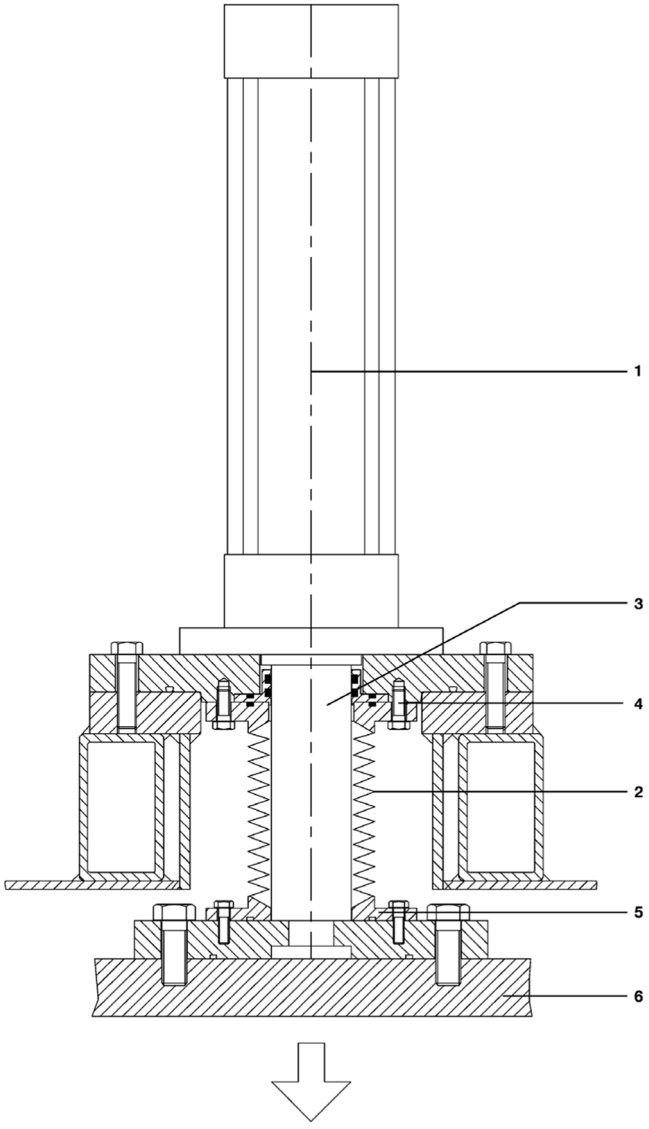

Figure 2.73 Stoppering with bellows. 1, hydraulic cylinder; 2, stainless steel bellow; 3, hydraulic ram; 4, seal package; 5, gasket; 6, pressure plate. (LYOVAC® freeze-drying plant, Steris GmbH, D-50354 Hürth, Germany.)

- Economic benefits due to shorter downtimes, reduction of labor costs, and better control of the cleaning results and efficiency.
- Reduction of accidents because the system is not open during cleaning and there is no need of handling dangerous substances.
- Reproducibility and qualification assured by the automatic control system.

Automatic cleaning systems have been used for several years for the cleaning of freeze-dryers operating in the aseptic production of pharmaceutical products, thus

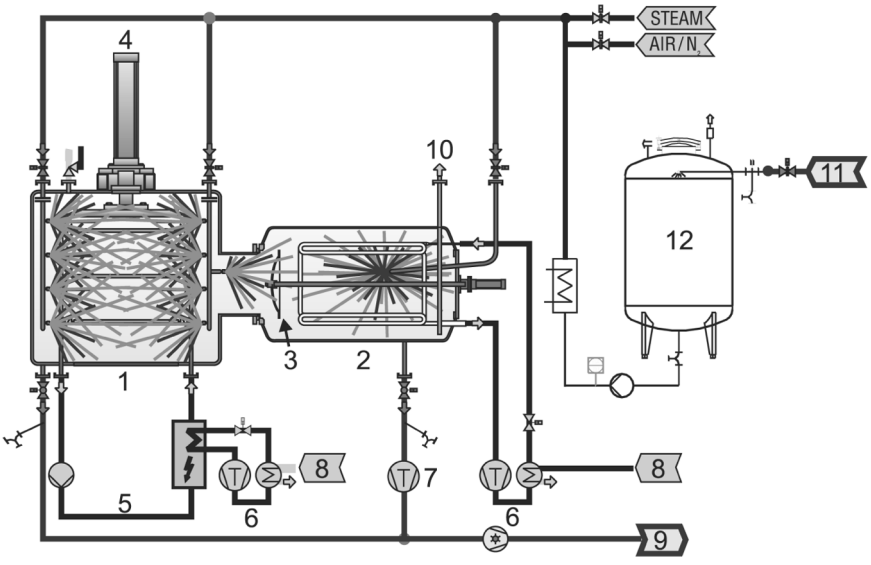

Figure 2.74 CIP principle. 1, chamber; 2, condenser; 3, chamber–condenser valve; 4, hydraulic stoppering system; 5, silicone oil circuit; 6, cooling system; 7, vacuum system; 8, cooling water; 9, drain water; 10, exhaust vacuum pump; 11, CIP fluid inlet; 12, CIP fluid tank. (Schematic drawing from 'Fundamentals of Freeze-drying' by Steris GmbH, D-50354 Hürth, Germany.)

complying with cGMP guidelines that require the avoidance of cross-contamination in the handling and production of different products. During a cleaning process, optimum accessibility to all the surfaces is ensured. The shelf assembly, hydraulic stoppering device, and evaporator in the ice condenser make this task difficult. Ports and so-called dead ends must also be cleaned. It is important that the cleaning water runs off unhindered at the lowest points of the chamber and condenser. For ports, the rule of thumb is $I = 6 \times d$; even better is $I = 2 \times d$ (I = depth of port; d = diameter). In general, ports may not be smaller than DN 40.

To attain a high degree of cleaning, the four T Principles (Wolpers, Frank: Cleanin-Place Systems for the Pharmaceutical Industry; VDMA Seminar, Interphex 2001, Philadelphia) must be taken into account:

Temperature:	→	Thermal effect: An increase in temperature of 1 °C increases the cleaning efficiency by 5% (over 30 °C). *Caution:* With proteins, too hot a cleaning medium will cause the dirt particles to burn on to the surfaces of the shelves and walls. Precleaning at 40 °C is, therefore, advisable.
Turbulence	→	Mechanical effect: Turbulence, as defined by the Reynolds number (*Re*), is basically a function of flow velocity and viscosity. For successful CIP cleaning, the flow velocity in the pipes should be a minimum of 2 m/s (or *Re*>8000).
Time	→	Effect of the cleaning time.
Titration	→	Chemical effect: This is the influence of the chemicals in the detergents, cleaning agents, or acids used. The concentration of these chemicals depends on the degree of equipment contamination.

To attain a high degree of cleaning, flat spray jets are used for cleaning the chamber. The pressure at the jet outlet should be in the region of 6 bar.

The rotation of a spray head is the best method to clean condensers because of their complex geometric design. The rotation of the spray heads, however, must be monitored to control the cleaning effect. A degree of cleaning of ≥99% is considered the optimum. Such a figure was reported by Steris GmbH, Huerth, Germany.

The cleaning agents used are mostly demineralized water (DE) and water for injections (WFI). The use of cleaning media and detergents will depend on the components of the product.

A typical cleaning process consists of the following phases:

- preliminary rinse with DE or WFI water;
- cleaning process either with a cleaning solution or with a detergent;
- final rinse preferably with WFI.

The process must be carried out in such a way that it can be validated. The following parameters are documented:

- water temperature;
- time;
- pressure;
- conductivity in the drain.

Usually, a process is run using a 'single-use solution', that is, the cleaning water, usually mixed with a cleaning agent or detergent, runs into the drain after use. In a few special cases, after the preliminary cleaning in the main cleaning process, the cleaning solution used is recirculated. The final rinse, however, is always single-use water and exits to a drain.

The qualification of a cleaning process is effected in the process steps described below. The cleaning process must be reproducible.

- Contamination of the surfaces to be cleaned with a 0.1% riboflavin solution or another placebo solution.
- After the door has been closed, the shelves are heated to a temperature between 55 and 60 °C to dry the riboflavin solution.
- Start of the cleaning process following the given parameters.
- Drying of the system with a liquid ring pump.
- Opening of the chamber door and inspection of the inner areas using a UV lamp. Riboflavin residuals show up under phosphorescent light. The cleaning process can be considered successful if no phosphorescent visible residuals can be detected.

For validation, this process must be repeated under the same conditions three times in a row and must attain the same results.

A suitably designed CIP system, consisting of a storage tank or tanks, piping, pump, and control system, is required for today's freeze-dryers. Such a CIP system must be designed to withstand sterilization processes. As a rule, CIP systems are sterilized with pure steam so that usually one speaks of a CIP/SIP system. The design and construction must be carried out following cGMP rules.

Three different CIP processes are common today:

1) single-use CIP;
2) single-use and recirculation CIP;
3) CIP with short-time intermediate storage of the cleaning solution.

Cleaning systems must be designed in such a way that cross-contamination of the effective medicinal contents of the products is precluded. For this reason, CIP systems of types 2 and 3 are recommended.

A CIP system consists mainly of the following hardware (for example of a CIP Skid installation, see Figure 2.75):

- centrifugal pump;
- dosing pump to control the dosage of the detergent (optional);
- heat exchanger to heat or cool the cleaning solution (water);
- tank to mix the cleaning solution (if required).

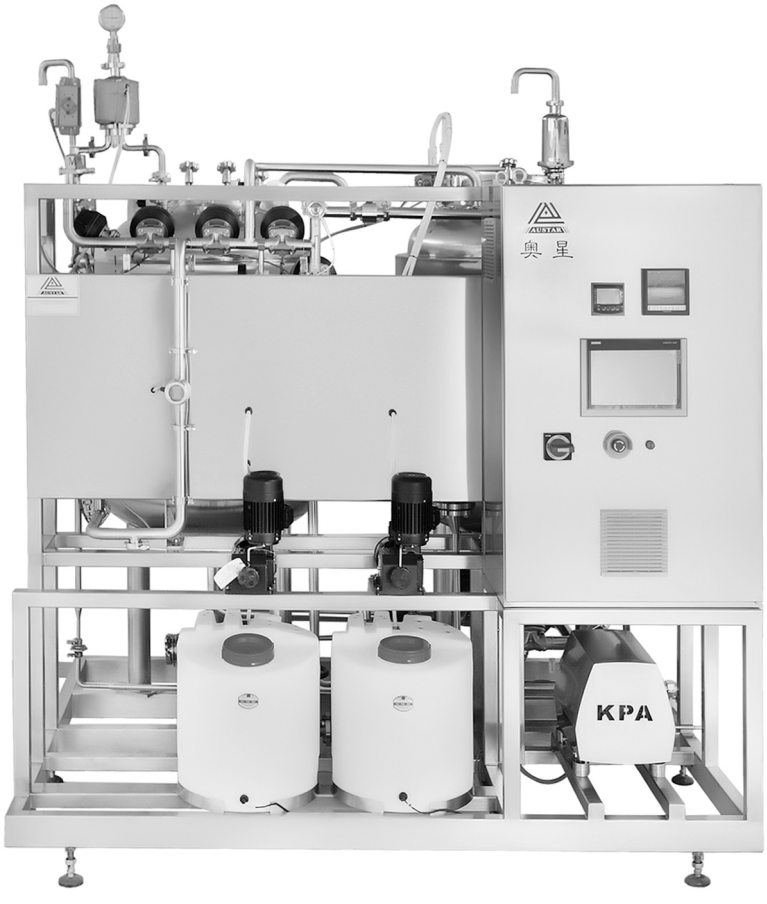

Figure 2.75 CIP Skid Installation. (Austar Group, P.R. China.)

The flow volume and the pressure of the CIP system must be designed in accordance with the requirements of the freeze-dryer. The freeze-dryer must basically be capable of being cleaned with a CIP system.

The qualification of CIP systems requires documentation during the design and manufacturing phases.

DQ	*Design qualification* After receipt of the order, the DQ establishes an exact procedure or a detailed specification that forms the basis of all further qualification steps.
IQ	*Installation qualification* The IQ verifies that all the quoted items are delivered and installed as specified in the DQ. This is sometimes called the ›as built‹ check.
OQ	*Operational qualification* The OQ verifies that the system performs in compliance with the requirements and functions described in the DQ.
PQ	*Performance qualification* The PQ verifies that the entire system, including the CIP system, works properly and in a way that can be reproduced.

Validation of CIP Procedures

CIP processes can be validated by the following:

- sampling;
- a swab test;
- the rinsing water or steam condensate method.

The FDA notes the following:

›There are two general types of sampling that have been found acceptable. The most desirable is the direct method of sampling the surface of the equipment. Other methods are the use of rinse solutions and measuring of conductivity.

›The FDA does not intend to set acceptance specifications or methods for determining whether a cleaning process is validated. . . . The user's rationale for the residue limits established should be logical, based on the manufacturer's knowledge of the materials and the practical, achievable and verifiable data. The objective of the inspection is to ensure that the basis for any limits is scientifically justifiable. However, unlike product residues, it is expected that no (or for ultra-sensitive analytical test methods, very low) detergent levels remain after cleaning.

Summary

- The CIP cleaning of freeze-dryers requires extensive planning.
- A CIP system is always custom designed.
- Computer-controlled cleaning sequences with interlocks prevent unauthorized route switching due to operator errors.
- CIP processes can be sufficiently qualified and, therefore, fulfill cGMP requirements for validation.

Table 2.6 Time to achieve equivalent microbial lethality at different exposure temperatures.

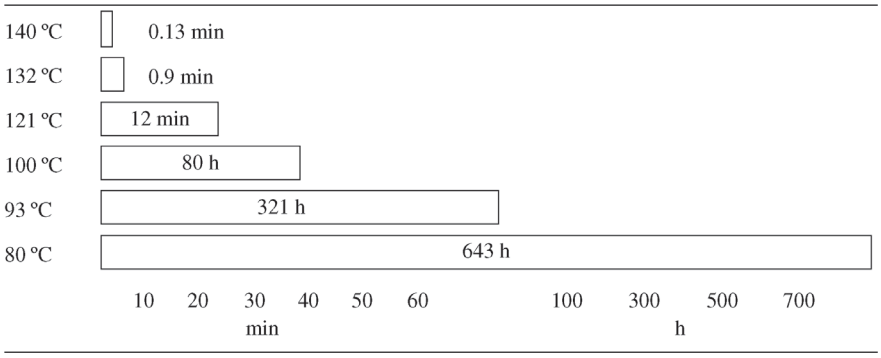

- The user develops a validation plan giving the highest and lowest limits for the verification of successful cleaning.
- The user and the manufacturer determine the required CIP process.
- Verification of the correlation between the amount of product residuals in the last rinse water.
- Optimization of the CIP process parameters until the desired level of cleanness is reached.

Sterilization in Place (SIP)

Steam sterilization is the method mostly used to sterilize freeze-dryers. High-quality, ultrapure steam (water for injection standard: USP XXII or PhEur equivalent) is used to achieve a minimum exposure of 121 °C for 30 min or the equivalent temperature–time combination for effective sterilization (Table 2.6). This method is easy to validate and is recommended by regulatory authorities as being reliable. The definition of sterilization is a validated process used to render a product surface free of all forms of viable micro-organisms (EN 556-1:2001). According to the authorities, a product or surface is only sterile when a validated sterilization process has been applied (EN 550, EN 552, EN 554, EN ISO 14160, and EN ISO 14937). To meet these regulations, Pure Water and Pure Steam Generators are installed (see Figures 2.76 and 2.77).

Steam sterilization is a highly effective and reliable method to kill microbiological populations by using saturated steam (Table 2.7). Microorganisms are eliminated by the denaturation of cell albumin (EN 566-1:2001).

Three factors are critical to ensure successful sterilization:

- time;
- temperature;
- moisture.

The FDA tends to prefer a sterilization process before each batch. This demands a high degree of reliability, safety, and tightness of the system. The sterilization process should not reduce the life span of the plant.

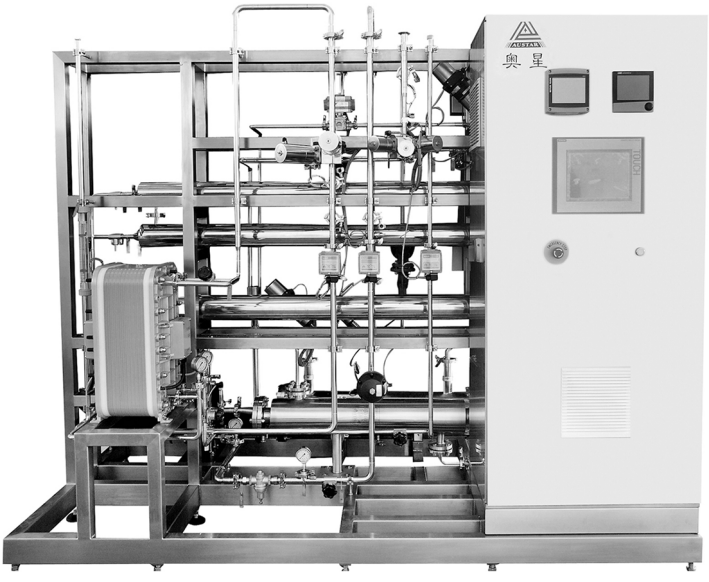

Figure 2.76 Pure Water Generator PWG2-0550 with FDA cGMP compliance. (Austar Group, P.R. China.)

Figure 2.77 Pure Steam Generator T/TC-PSG 450 (Brand Finn-Aqua/Austar) with a capacity of up to 445 kg (calculated with 8 bar plant steam and 3 bar pure steam). (Austar Group, P.R. China.)

Table 2.7 Example of inactivation of bacterial populations during steam sterilization processes (logarithmic processes).

Exposure time	Bacteria living at beginning of time period	Bacteria killed in 1 min	Bacteria surviving at end of time period	Logarithm of survivors (end of minute)
1	1.000.000	900.000	100.000	5
2	100.000	90.000	10.000	4
3	10.000	9.000	1.000	3
4	1.000	900	100	2
5	100	90	10	1
6	10	9	1	0
7	1	0.9	0.1	–1
8	0.1	0.09	0.01	–2
9	0.01	0.009	0.001	–3
10	0.001	0.0009	0.0001	–4
11	0.0001	0.00 009	0.00 001	–5
12	0.00 001	0.000 009	0.000 001	–6
13	0.000 001	0.0 000 009	0.0 000 001	–7

Design Criteria

- Engineering of the pressure vessels (chamber and condenser) in accordance with the valid regulations covering pressure vessels in the country of the user.
- Selection of the most suitable materials, preferably stainless steel of a quality corresponding to AISI 316 L (DIN 1.44044, DIN 1.4435).
- Free flow of the condensate from the vessels. An accumulation of condensate in the chamber, condenser, and/or piping must be precluded.
- Avoidance or minimation of ›dead ended‹ piping. The ratio of the piping diameter to piping length should be from 2 to a maximum of 6 ($l{:}d = 2–6$).
- Piping that comes in contact with operating media must also be sterilized. Such piping must be laid out inclined toward the chamber or condenser. The steam supply also takes place in the CIP installation in chamber and condenser (see Figures 2.78–2.80).
- Valves free of dead ends (sanitary valves) should be used exclusively. Diaphragm valves are recommended as the most appropriate valves.
- It must be possible to sterilize gauge heads. Particular care must be taken in choosing temperature-resistant gauges. Drifting of calibrated values at high sterilization temperatures must be precluded (see Section 2.2.8).
- A certified sealing material that is FDA compliant (21CFR-177-2600 and 21CFR 178.3570) should be used, for example, PTFE or silicone.
- Drain ports must be provided with steam traps to prevent recontamination from the drain lines. Bypass lines should be provided to ensure the rapid outflow of large amounts of condensate.

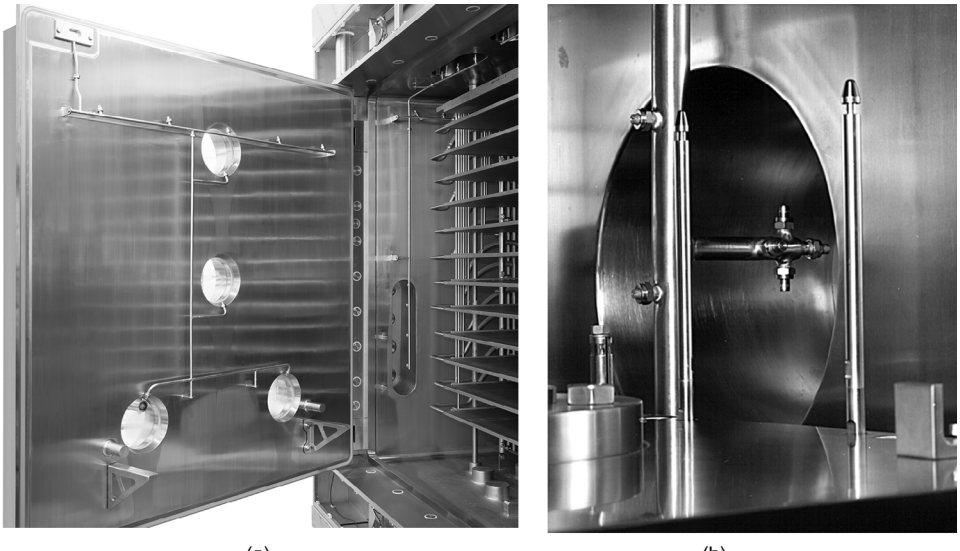

(a) (b)

Figure 2.78 CIP spray rod in the drying chamber for cleaning of the shelves and chamber walls. (a) Spray nozzles are installed on the service door for dedicated cleaning of sight glasses and ports in the chamber. (Photograph GEA Group, Germany.) (b) The 90° flat spray jets are placed at different positions and heights on these rodes. The connecting pipe between the chamber and the condenser as well as the valve is cleaned. The positioning of the jets is determined over computer animation to achieve the highest possible degree of cleaning: >99%. (Photograph Steris GmbH, D-50354 Hürth, Germany.)

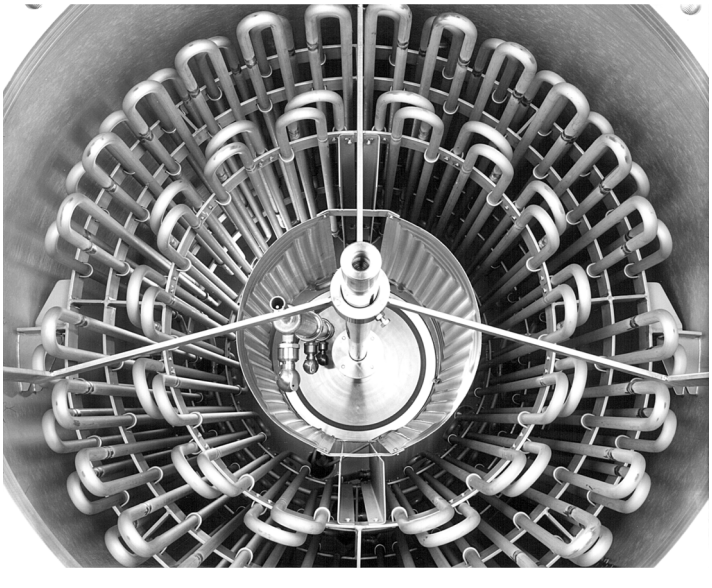

Figure 2.79 Rotating spray head in the condenser. In addition to 90° flat spray jets, rotating spray balls are also used, as can be seen in the middle of this picture. (Photograph Steris GmbH, D-50354 Hürth, Germany.)

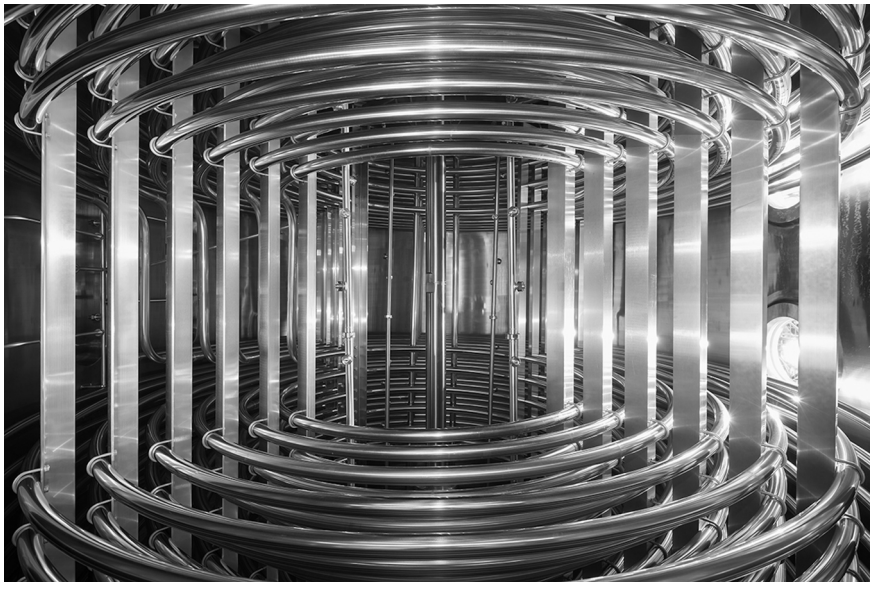

Figure 2.80 Evaporator coils inside of an ice condenser. CIP spray rod for cleaning of the interior of the condenser after defrosting. The coils are separated in two sections for better access for cleaning validation. (Copyright courtesy of GEA Group, Germany.)

- The temperature measuring points should be the coldest points in the system: all drain ports, dead ends, the bottom of the chamber, gas inlet filters.
- Safety valves should be chosen that exclude any type of contamination of the vessels or piping when opened, for example, valves with a bioseal. These are valves in which the valve seat returns to the closed position after pressure has been released. Contrary to this are rupture disks that must always be replaced. In such cases, the process must be repeated.
- Door seals: If the door is equipped with a seal that provides tightness both in the vacuum and overpressure ranges, the door locking system must ensure that there is no gap between the door and the door flange at the lower areas of the door. This danger must be reckoned with if double seals are used, for example, inflatable seals. Condensate collects at the lower area of the door and chamber flange so that the sterilization temperature cannot be reached.
- Temperature validation ports for positioning temperature sensors in freeze-dryers are required for validation.
- Orbital welding of the piping should be preferred wherever possible to avoid bioburden growth.

To illustrate the topics in this list, please see Figures 2.81–2.83.

Only pure steam should be used to meet pharmacopeia specifications. Filtered ›plant steam‹ should be excluded since it contains a high level of noncondensable gases, mainly air. Pure steam should have less than 3.5% of noncondensable gases per unit volume and a dryness value between 0.9 and 1.05 (demanded by regulation BS 3970). The large chamber and condenser must be sterilized in a short time. The dimensions of the steam piping and the pressure reduction station

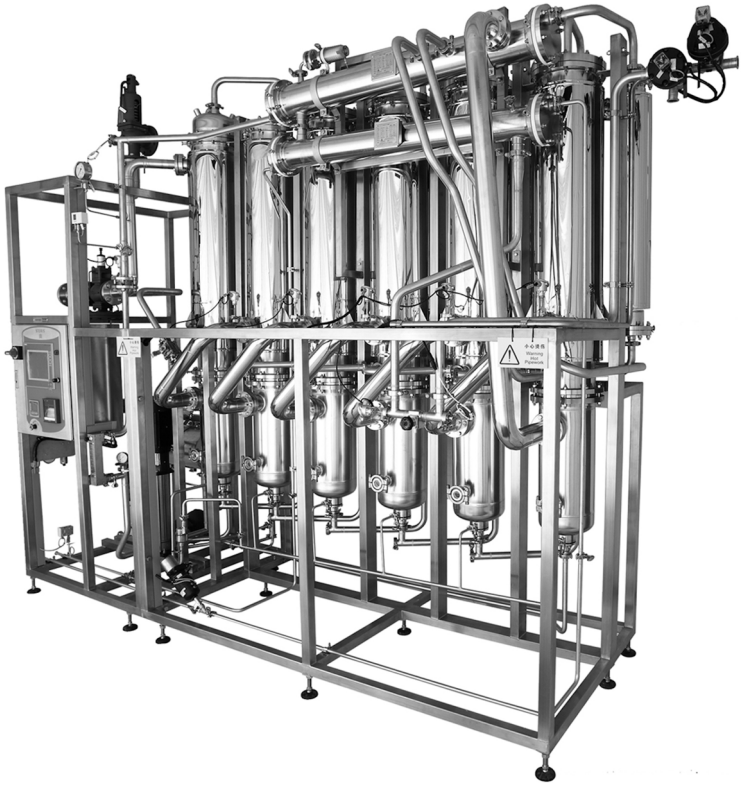

Figure 2.81 Distiller for WFI (Water for injection) T/TC-MWS 450 (Brand Finn-Aqua/Austar) with FDA compliance and a capacity of up to 890 L/h (at 8 bar). (Austar Group, P.R. China.)

Figure 2.82 CIP system with two tanks for cleaning with detergent and WFI. (Copyright courtesy of GEA Group, Germany.)

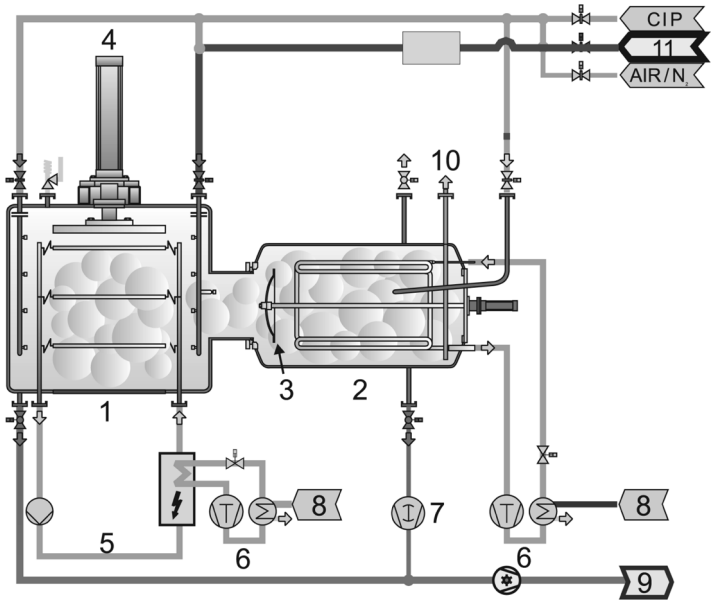

Figure 2.83 SIP principle. 1, chamber; 2, condenser; 3, chamber–condenser valve; 4, hydraulic stoppering system; 5, silicone oil circuit; 6, cooling system; 7, vacuum system; 8, cooling water; 9, drain water; 10, exhaust; 11, steam inlet. (Schematic drawing from ›Fundamentals of Freeze-Drying‹ by Steris GmbH, D-50354 Hürth, Germany.)

must reflect this requirement. To avoid superheated steam, pressure reduction through the reducing valve in the pure steam inlet port should be less than 2:1. At all times, pressure reduction should be kept to the minimum possible. The drying chamber and condenser as well as all the piping are evacuated to remove noncondensable gases by using a liquid ring pump with injector.

Repeated pulsing can be used to provide efficient removal of noncondensable gases. The system is evacuated to a pressure lower than 50 mbar. Steam is then injected to return the system to atmospheric pressure. The system is then reevacuated prior to injecting the steam for sterilization. This pulsing can be repeated several times to achieve improved air removal.

After the final pulsing stage, steam is injected until the sterilization pressure and temperature are reached.

The sterilization phase begins when the temperature in the system reaches the set sterilization temperature. The set sterilization temperature is normally measured by controlling the temperature in the expected coldest spots. These spots are mainly the drain ports of the chamber and condenser as well as the gas inlet filters. The sterilization phase begins when all the measuring points have reached the set temperature value. This sterilization temperature must be maintained uninterrupted at all the measuring points for the time set. If the temperature at one of the measuring points should fall below the set value, the timer is returned to zero and the sterilization phase must begin again. As soon as the sterilization phase has been completed, the overpressure in the system is released over a special pressure release valve. At this time, the drain valves are

closed. After the overpressure has been released and the pressure release valve closed, the drying and recooling processes start. Drying of the chamber, condenser, piping, and venting filter is effected by a liquid ring pump. This pump is connected to the drain piping. Any residual condensate that might still be present is pumped off. Such drying is effective because any residual condensate will evaporate quickly owing to the high temperature prevalent in the system. Because of the great material mass, it is state-of-the-art technology today to provide the chamber and its door with a double jacket. Cold water can be used to cool the chamber and the chamber door. It is also possible to connect the chamber walls and door to the heat transfer system of the shelves. To accelerate the cooling process, the shelves are cooled over the heat transfer circuit.

Sterilization could cause leaks. A leak test, therefore, should be carried out on the entire system after the sterilization cycle (see Section 2.2.9).

In the freeze-dryers of today, the entire sterilization process is carried out automatically, controlled, and documented by the freeze-dryer control system. This includes a leak test. Depending on the size of the freeze-dryer, the time needed for CIP cleaning and sterilization is between 8 and 12 h.

Sterilization by steam is a standard procedure, but can be replaced by the VHP® (Vaporized Hydrogen Peroxides) process, which works at ambient temperature and without pressure. For example of a Pilot freeze-drying plant sterilizable with VHP, see Figure 2.84. Nakahira [18] described the development of applicable sterilization cycles, the necessary changes in the freeze-drying plant, and the

(a)

Figure 2.84 (a) Pilot freeze-dryer LYOVAC™ FCM 10-P (0.6 m^2 shelf area), with full size door for manual loading and unloading. Design pressure −1 to 0.5 bar (+50 °C), design temperature from −80 °C to +50 °C. (b) Details of the plant with closed acrylic door. (Copyright courtesy of GEA Group, Germany.)

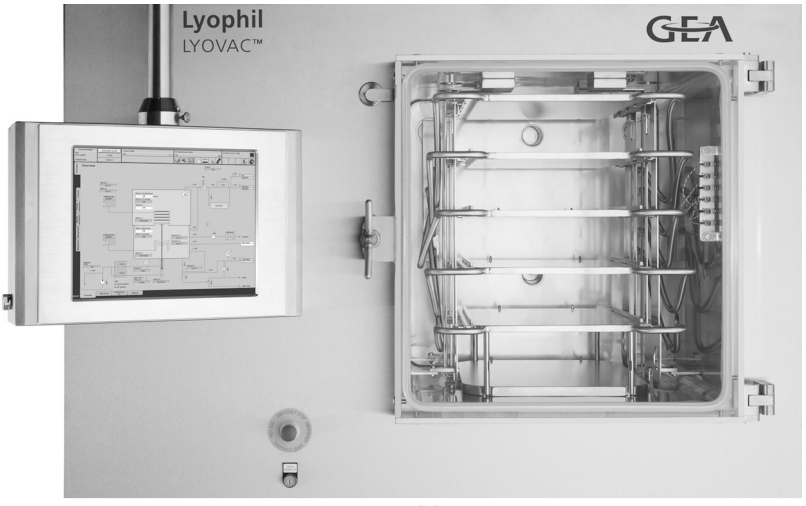

(b)

Figure 2.84 (*Continued*)

sterility test necessary to validate the process. Sterilization by VHP requires certain conditions that result from the nature of the H_2O_2 vapor:

- The plant must be dry, otherwise the H_2O_2 will dissolve in the water.
- The installation must be evacuated to ~1 mbar to ensure that the vapor reaches all parts and corners of the plant. H_2O_2 can still be applied at +5 °C, but at higher temperatures, for example, +25 °C, the time to effect the sterilization is shorter. At higher temperatures, for example, +50 °C, the time required is still shorter, but H_2O_2 decomposes more readily and higher concentrations of H_2O_2 have to be used. Table 2.8 shows the results with the resistant *Bacillus stearothermophilus* [19].

Table 2.8 shows a typical set of *D* values (time in which the number of bacteria is reduced by one decade) for *Bacillus stearothermophilus* for different surface temperatures of the parts to be sterilized and the necessary concentrations of H_2O_2.

Table 2.8 Typical *D* values (exposure time in which the number of bacteria is reduced by one decade) for *Bacillus stearothermophilus* for different exposure times and the necessary H_2O_2 concentrations.

Temperature of the surfaces to be sterilized (°C)	Approx. H_2O_2 concentration (mg/L)	Typical *D* value (min)
+4	0.3–0.5	8–12
+25	1–2	1–2
+37	3–4	0.5–1
+55	10–12	0.02

Source: From Ref. [19].

Furthermore, some technical prerequisites must be fulfilled:

- Not all materials are resistant to H_2O_2,as shown, for example, in the following list:

Resistant	Stainless steel
	Aluminum
	Silicon, viton
	Teflon™
Not resistant in all compositions	Polyurethane
	Plexiglas™
	EPDM
Not resistant	Nylon

- The pump set must be laid out to pump water that may be in the plant, but also to be resistant against H_2O_2. In smaller plants, it is possible to place a catalyst to decompose the H_2O_2 in front of the oil-filled vacuum pump. In larger plants, it is recommended to use a liquid-ring pump combined with an air injector for drying of plant and venting of the H_2O_2.
- In Ref. [19], the following example is given: to a drying chamber of 4.5 m^3, a tube of 120 cm length and 1 cm internal diameter is attached. On a stainless steel foil of 120 cm length, 10^6 *Bacillus stearothermophilus* spores are placed at a distance of 10 cm and the foil is placed in the tube. Plant and tube are evacuated to 1 mbar at 25 °C. On four occasions 28–56 g of H_2O_2 are injected into the chamber. All spores up to a depth of 80 cm in the tube were killed (22 tests). At a depth of 90 cm, 1 of 22 tests was positive, while at 120 cm, 14 of 22 tests were positive and surviving spores were found.

The sterilization process consists of three phases, as shown in Figure 2.85:

- The installation is evacuated for drying to 1 mbar, minimum below 10 mbar. The almost horizontal plot at A is most likely related to some evaporation of water. For the documentation of the process, the leak rate of the plant must be measured to prove that no outside air, perhaps contaminated, can enter the plant during phase 3. This test (see Section 2.2.8) is best done at the end of phase 1.
- For the sterilization phase (2), a certain amount of H_2O_2 is injected into the plant and pumped off after some time. This procedure is performed once or may be repeated several times.
- Removal of the H_2O_2: The vapor is pumped off by the vacuum pump set, the plant vented with sterile air up to 500 mbar, again evacuated, and so on. At the end of this procedure, the remaining H_2O_2 concentration is checked, for example, by the Dräger H_2O_2 test tube,[5] which indicates H_2O_2 concentrations down to 0.1 ppm.

5 Dräger Tubes for H_2O_2, Drägerwerk AG, D-23542, Lübeck.

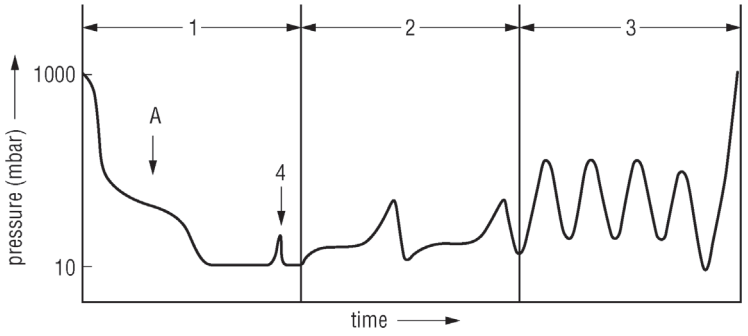

Figure 2.85 Typical course of pressure during a sterilization by the VHP-process®. 1, drying of the plant to be sterilized by evacuation down to 1 or 10 mbar; 2, several injections of H_2O_2 each followed by an evacuation; 3, several times venting of the plant with sterile air; 4, leak test of the plant before the start of 2. (VHP is a process of Steris Corp., Mentor, OH; see also Ref. [19].)

Steris Corp[6] offers complete installations for VHP sterilization of freeze-drying plants, which are programmable and automatic: 4–400 g H_2O_2 per injection can be preset, as well as the parameter of the drying, sterilization, and venting phases. The process is documented.

Nakahira [18] described, on the basis of his experience with VHP, the advantages of this process: a short sterilization time at room temperature; the possibility of updating existing plants; and VHP does not, in contrast to ethylene oxide and formaldehyde, affect the health of the operators and can be decomposed to water and O_2 without contaminating the atmosphere.

2.4 Production Plants

For a production freeze-drying plant, no general guidelines for a specification can be given as for pilot plants. The specification must follow the intended production process, but it is important to adhere to certain design criteria (see Figure 2.86):

- The surfaces should have a surface quality in the range between $R_a = 0.5$ and 0.8 µm to permit effective cleaning and sterilization.
- With cube-shaped chambers, the chamber floor should be inclined toward the drain ports to permit the unhindered outflow of cleaning solutions and condensate. The corners of the chamber should be rounded off (minimum radius: 15 mm).
- If possible, there should be no welded seams at the corners.
- Sufficiently large distances between the shelf assembly and the walls of the chamber should be planned as well as a sufficiently large clearance between the shelves to ensure the unhindered flow of water vapor.
- A door locking system that corresponds to sterile room conditions and that also fulfills all safety requirements should be taken into account. A steam-

6 Steris Corporation, Erie, PA 16506, USA.

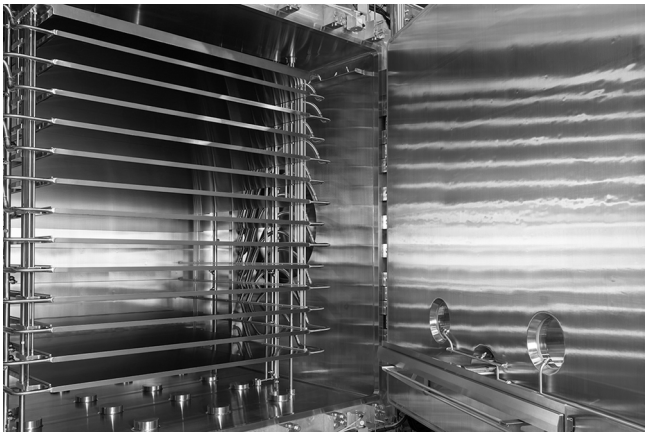

Figure 2.86 Freeze-dryer chamber with shelves. Pusher for unloading of vials is installed on the full size door with dedicated CIP system. (Copyright courtesy of GEA Group, Germany.)

sterilizable stainless steel bellows separates the valve shaft from the chamber-condenser valve (see Figure 2.87).

- The chamber wall and door insulation must be free of asbestos and must be water vapor tight; the insulation must correspond to sterile room conditions. The entire insulation must comply with all safety regulations.
- The shortest possible connection between chamber and condenser and its internal diameter as shown in Figure 2.88 is increasingly important with decreasing operating pressures (e.g., below 8×10^{-2} mbar).

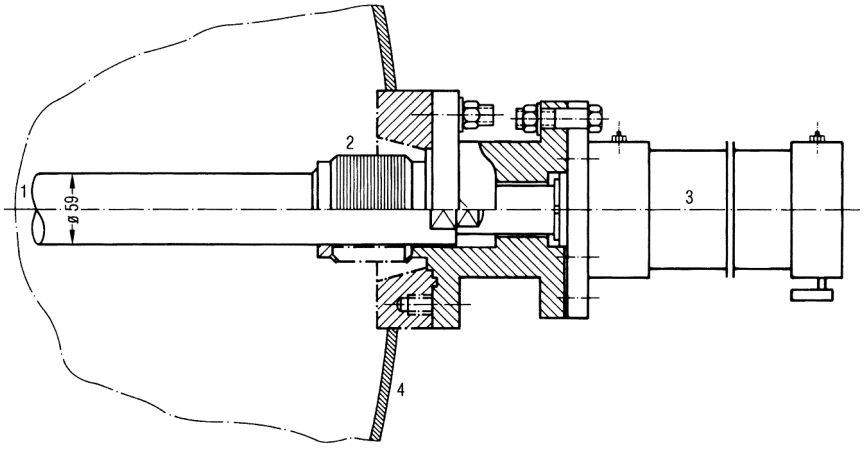

Figure 2.87 Schematic drawing of a steam-sterilizable stainless steel bellows, which separates the valve shaft from the chamber–condenser valve. 1, to the valve plate; 2, bellows; 3, valve drive; 4, condenser wall. (Schematic drawing from source material by Steris GmbH, D-50354 Hürth, Germany.)

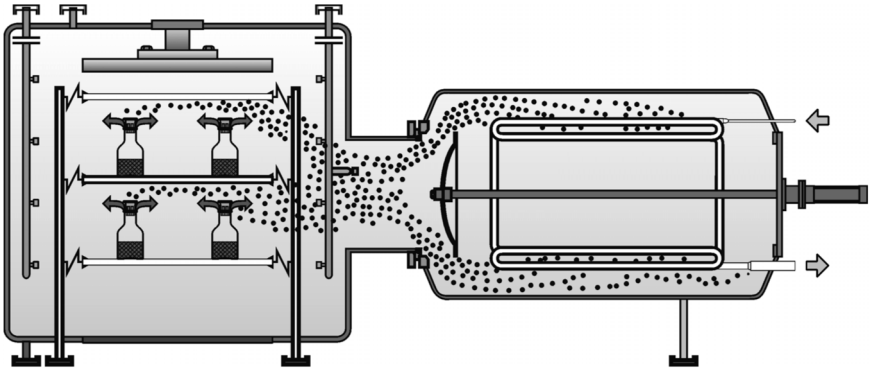

Figure 2.88 Water vapor flow from the drying chamber (*left*) to the condenser. (Schematic drawing from source material by Steris GmbH, D-50354 Hürth, Germany.)

As shown in Figures 1.142 and 1.143, the specific water vapor flow ($g/cm^2\,h$) drops at 0.1 by a factor of almost 2 if l/d (length/diameter) for the connection goes from 1 to 5, and at 0.04 mbar the factor is ~3.

Figure 2.89 shows a freeze-drying plant in which each chamber and the related condenser are flanged together. The plant drawn schematically in Figure 2.90

Figure 2.89 Steam sterilizable-production plant with two LYOVAC® GT 500-D. The condensers are directly flanged to the chambers and have an ice capacity of 500 kg each. (Steris GmbH, D-50354 Hürth, Germany.)

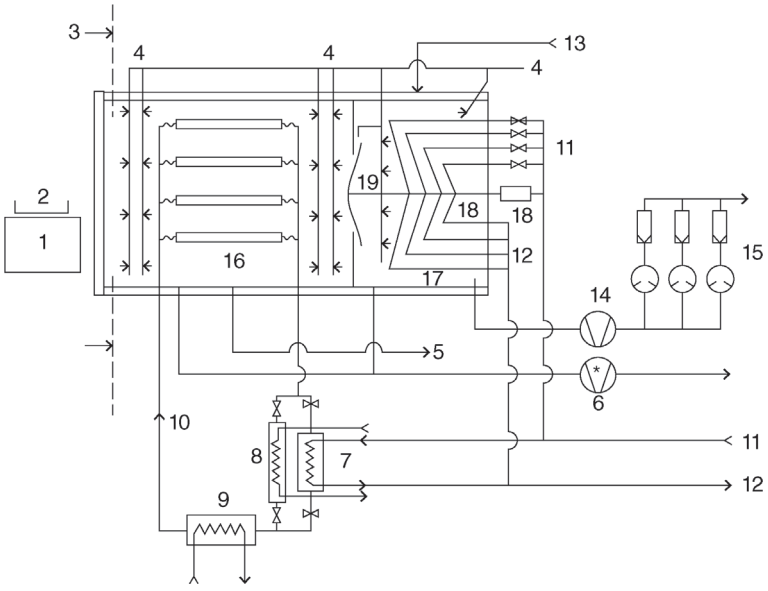

Figure 2.90 Scheme of a freeze-drying production plant with ~20 m^2 shelf area. The chamber and condenser are in the same vacuum chamber, separated by a wall in which the valve is built, providing the shortest possible path for the water vapor. The condenser and the heat exchanger are cooled by LN_2. The condenser surface consists of plates (Figure 2.91); its temperature can be controlled between −110 and −60 °C. The shelves can be controlled by the circulated brine between −70 and +50 °C. The trays with product can be automatically loaded and unloaded by a trolley. The shelves can be pressed together in one block and the trays are loaded on to the shelves by pushing one shelf after another in front of the trolley. 1, trolley for loading and unloading; 2, product in trays; 3, sterile room; 4, CIP system; 5, water drain; 6, liquid ring pump; 7, heat exchanger for the brine cooled by LN_2; 8, heat exchanger for the heat transfer fluid, cooled by water (+20 °C); 9, heat exchanger for the heat transfer fluid, electrically heated; 10, heat transfer fluid circuit; 11, LN_2 inlet; 12, N_2 gas outlet; 13, water for defrosting; 14, roots vacuum pump; 15, three two-stage pump sets; 16, chamber; 17, condenser; 18, condenser plates; 19, hydraulically operated valve between chamber and condenser. (Steris GmbH, D-50354 Hürth, Germany.)

goes one step further, the chamber and condenser being in one housing, separated internally by a plate. The plant is cooled by LN_2. The directly cooled condenser consists of plates, as can be seen in Figure 2.91. Figure 2.92 is a view in another production plant from the chamber into the condenser, in which the seal of the valve can be exchanged without dismantling the condenser.

Both installations have full-size doors that are opened during loading and unloading. The loading of 50 000 or 100 000 vials takes some time and the shelves should therefore be at room temperature to avoid condensation of ice from the humidity of the atmosphere.

If the loading of vials has to be done on cold shelves, a smaller loading door as shown in Figure 2.93 should be built in to reduce the amount of air diffusing into the chamber. In addition, a small overpressure of sterile air or N_2 in the chamber reduces the condensation of ice. If N_2 is used, the O_2 content near the loading door should be monitored.

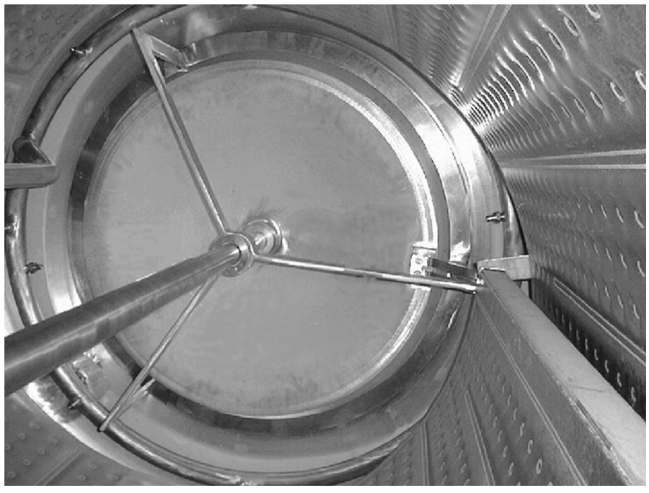

Figure 2.91 Condenser with evaporator plates (18) as shown in Figure 2.90. See also Figure 2.37. (Steris GmbH, D-50354 Hürth, Germany.)

The process control and the monitoring and documentation of all relevant data and a hierarchic warning and alarm system can be planned and installed as suggested in Sections 2.2.10, 6.2.4, and 6.2.5. Some of the suggestions may appear overdone, for example, inlet and outlet temperatures of each shelf or shelf package. However, these data can prove that the freezing of the product on

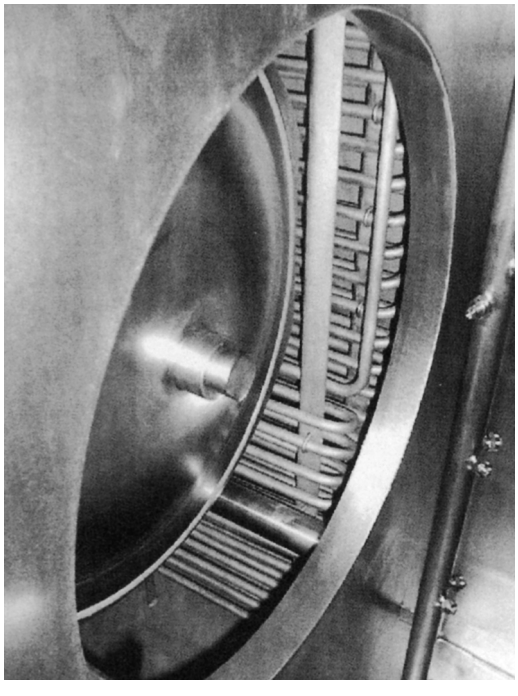

Figure 2.92 View of a valve inside the condenser. The condenser coils are seen in the background. In front to the right is a part of the CIP system. The seal of the valve can be replaced in the position shown. (Steris GmbH, D-50354 Hürth, Germany.)

Figure 2.93 Automatic loading system in front of a freeze-drying plant with loading door (slot door). (Copyright courtesy of GEA Group, Germany.)

all shelves has been uniform or a deviation can be seen on shelf ›XX‹. Similar analysis can be made for MD. Another example is the temperature at all injection valves for the refrigerant. If one valve (of several) malfunctions, the time of MD may be prolonged (no condensation of ice on one coil) or the final end pressure during SD is reached much later than usual (ice sublimes from the coil warmer than the others). Production freeze-drying plants are like airplanes: they carry a very precious load. The earlier a deviation from the normal or preset data can be analyzed, the more likely the load will be safely brought home.

2.4.1 Loading and Unloading Systems

The increasing demands made in recent years by national and international health and regulatory authorities with respect to sterilization and safety against contamination require a rethinking of freeze-drying processes.

The following are preconditions for aseptic production:

- ensuring Class (A) conditions during the entire handling of the product;
- reduction of personnel in the sterile area – humans are the largest source of contamination;
- automatic loading and unloading systems that function largely without operators;
- loading and unloading systems that comply with cGMP guidelines.

Different demands made on production processes, the local conditions, and the desired degree of automation lead to different solutions. Industry offers proven concepts that can be validated, for example, a concept in which trays filled with bulk product or vials are introduced into a drying chamber semi- or fully automatically. However, loading and unloading systems that operate without trays are preferred: the vials are loaded into the drying chamber or chambers fully automatically from the filling machine, as shown in Figures 2.94 and 2.95.

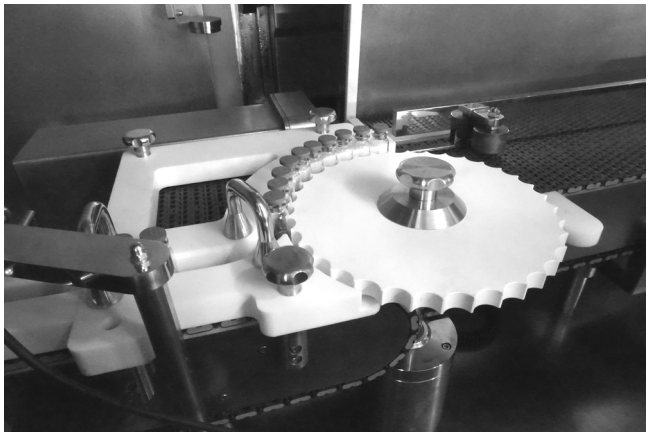

Figure 2.94 Turning table of a freeze-dryer loading system. (Austar Group, P.R. China.)

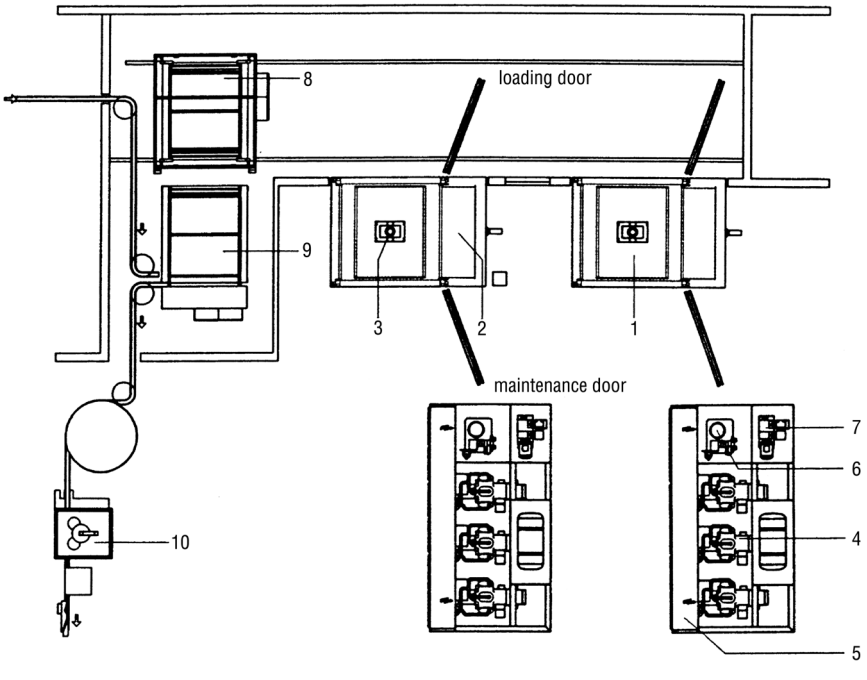

Figure 2.95 Schematic drawing of an automatic loading and unloading system (ALUS) for two freeze-drying plants. 1, drying chamber; 2, ice condenser; 3, stoppering device for closing the vials; 4, refrigerant compressors; 5, power supply; 6, hydraulic system; 7, vacuum system; 8, loading and unloading carrier, which is loaded in the position shown from the formatting table and moved to one of the chambers; during unloading the closed vials are loaded from each chamber on to the same carrier; it will be moved to the position shown and the vials are transported via the unloading table to the capping machine; 9, unloading table; 10, capping machine. Both chambers have a small loading and unloading door (similarly to Figure 2.97) and a large door for maintenance. (Steris GmbH, D-50354 Hürth, Germany.)

Figure 2.96 Production system comprising of three production freeze-dryer LYOVAC™ FCM 600-D (40.8 m^2 shelf area each) with cross-movable transfer cart system (open RABS) for automatic loading and unloading. Loading speed 600 vials/min (two rows) and unloading speed 600 vials/min. The inductive power supply system includes independent circuits to fulfill requirements regarding flexibility, independent and parallel operation of transfer carts on the same circuit. (Copyright courtesy of GEA Group, Germany.)

Three concepts represent an acceptable standard:

- Automated guided vehicle (AGV)
  The vials are transported between the filling machine and the drying chamber or between the drying chamber and the capping machine by means of an AGV (Figures 2.96 and 2.97).
- Push and pull system
  The vials are taken from the filling machine directly in front of the freeze-dryer by means of conveyors and pushed onto a shelf in the drying chamber (Figure 2.93). Unloading of the drying chamber is effected over a pulling system: the vials are pulled out of the drying chamber and placed on a conveyor belt, which transports them to the capping machine (Figures 2.93 and 2.99).
- Push/push system, similar to push and pull systems for the loading operation. Unloading of the drying chamber is effected from the rear side of the chamber. The vials are pushed by a telescope push bar back on the conveyor belt, which transports them to the inspection and capping machine. The advantage of such a push/push system is less mechanical installations on the sterile Class A area, the inner space of the isolator system, and no mechanism moving above the vials.

The push and pull system has proved useful for automatic loading and unloading systems that operate under an isolator (Figure 2.98). Such systems are also available as AGV systems.

Another concept is the automatic loading and unloading system for freeze-drying chambers that have been designed as push-through chambers. In such

Figure 2.97 Transfer cart (open RABS) for automatic loading and unloading using one track and guide rail system with floor rails providing power. The transfer cart is docked to the unloading table in the back. (Copyright courtesy of GEA Group, Germany.)

cases, the sterile loading side (unprocessed product) is separated from the sterile unloading side (freeze-dried product).

Materials used must be cleaned and disinfected with the usual cleaning and disinfecting agents. Friction in the transport system must not cause particles. Electric motors without ventilators must be used and the sensors installed must be resistant to the cleaning and disinfecting agents. In general, every process must be reproducible, documented, and validated.

Design Criteria

In addition, the following should be considered:

- The objects must be transported smoothly without jarring to prevent the liquid in the vials or ampoules from sloshing.
- The vials or ampoules transported must not be damaged, for example, through scratches at the outer surfaces.
- It must be easy to adapt the system to different sizes of vials or ampoules.
- It must be possible to adapt the loading and unloading system to the filling speed of the filling line and to the speed of the capping machine.
- The entire transportation area must be fully covered by laminar flow units.
- All the motor drives must be placed below the transportation level.
- It must be possible to reject and remove fallen vials or ampoules automatically.
- It must be possible to count the vials or ampoules before being loaded into the freeze-dryer.
- With AGV systems, data transfer between the AGV and the control system must be effected without the use of cables, for example, through infrared data transfer.
- The system must be equipped with a PLC control system with markers in case there is an interruption in operation. This marker system ensures that the

Figure 2.98 Automatic loading and unloading system for two freeze-dryers installed in open RABS system. Gloves in the glass doors allow access during operation. Hinged conveyor under LF allow operator to cross line. (Copyright courtesy of GEA Group, Germany.)

loading or unloading process is continued in the correct sequence when operation is resumed.

For product safety, such systems have proved to be suitable for freeze-dryers in which the drying chamber is loaded and unloaded shelf by shelf. Loading and unloading are effected at the same constant height. An automatic journeymeter integrated in the cylinder of the hydraulic stoppering device of the drying chamber positions the shelves accordingly. It should be possible to load a drying chamber partially.

Isolator technology is required especially when processing toxic or anticancer products and where the operator and his environment must be protected. An automatic loading and unloading system installed in an isolator system can be CIP cleaned and can be sterilized with vaporized hydrogen peroxide (VHP) (Figure 2.98).

Figure 2.99 Automatic loading and unloading system for vials fix installed in front of a freeze-dryer. Vials are nested for maximum loading capacity. Loading and unloading through a slot door (pizza door) opens 180° upward. (Copyright courtesy of GEA Group, Germany.)

The filling temperature is critical for some pharmaceutical products. It is therefore decisive for the subsequent freeze-drying process that the filled vials pass through a known and reproducible course of temperature and time when the vials are pushed on to the cold shelves, as shown in Figure 2.93.

When the vials are pushed on to the cold shelves, for example, −40 °C, the product will start freezing, for example, with a freezing rate of 1 °C/min between +10 and −35 °C. The product in the first vials will be frozen down to −35 °C in 45 min and approach −38 °C in the time thereafter. If the loading time is, for example, 5 h, the freezing of the last vials to −35 °C will take 5 h 45 min. The first vials have been kept for 5 h at $\simeq$ 35 °C. It must be tested whether the structure of frozen product in the vials is uniform enough to obtain the specified quality of the dried product within the specified drying time. The ice crystals will grow in 5 h at $\simeq$ 40 °C. Theoretically, the ice crystals in the first vials will be larger than in the last ones and therefore will, in general, dry faster, which could lead to an overdrying of product in the first vials before the last ones are dried. The opposite is also possible, if the growing ice crystals push well-distributed small enclosures of concentrated solids into larger areas with unfrozen water. These areas may take longer to dry or require a lower T_{ice} during MD. Whether the crystal growth has a measurable influence on the product or the process can be estimated by tests with methods described in Sections 1.1.5 and 1.1.6, for example, by ER measurements and observation of the drying process in a cryomicroscope.

There will be some differences and it is a quantitative question whether they can be tolerated or not. For a final decision, test runs in a pilot plant should be carried out with freshly frozen product and product that has been resting for 5 h before drying. These tests are recommended because the methods mentioned above use different sized samples in different configurations than are used in production. The amount of product and its geometric dimensions will also influence the structure as well as the number of crystallization nuclei in the product, which can be very different in a normal laboratory and in a clean production area.

2.4.2 What Is an Isolator?

An isolator system is typically a glass and stainless steel enclosure that creates a closed environment around the product processing environment (Figure 2.100). The isolator system and associated equipment is subject to a validated biodecontamination cycle rendering the product processing environment sterile. Operator access to the product processing environment is via glove ports, and equipment, components, and materials are connected to the isolator system via transfer systems allowing the sterility of the product processing environment to be maintained. In EudraLex Annex 1,

"Manufacture of Sterile Medical Products",[7] the minimum recommended background environment classification for an isolator system used in aseptic manufacture is ISO 8.

7 EudraLex: European Commission, Directorate General for Health and Food: "Manufacturing of Sterile Medical Products".

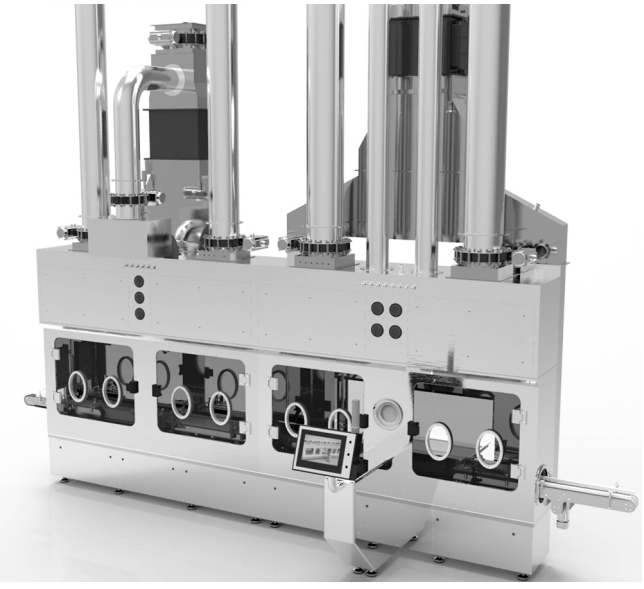

Figure 2.100 Isolator module with air handling system (Austar Co.LTD, Beijing, P.R. China.)

An isolator has many elements associated with creating and maintaining the product processing environment, including the following:

Air handling system: The isolator air handling system provides the appropriate environmental cleanliness (ISO 5 environment) and manages pressure, temperature, and humidity within the isolator system to allow product processing.

The biodecontamination system (2.4.3): The isolator biodecontamination system is the most important part of the isolator and is used to render the isolator system and enclosed equipment sterile to allow the product process to be undertaken while minimizing the risk of contamination.

The most common biodecontamination medium is hydrogen peroxide (H_2O_2). The purpose of biodecontamination of the isolator is to define boundaries, typically to supply and exhaust HEPA filters and all parts of the isolator and enclosed equipment within these boundaries. The biodecontamination cycle typically has five phases:

- leak test (to ensure the system is suitable for H_2O_2 exposure);
- dehumidification (where excess humidity is removed from the environment and the correct pressure, temperature, and humidity conditions are set);
- conditioning (where the H_2O_2 concentration is established);
- biodecontamination (the exposure phase where the H_2O_2 concentration is maintained for the validated time period to ensure complete biodecontamination); and
- aeration (where the H_2O_2 is removed from the isolator after biodecontamination).

For biodecontamination systems partially integrated with the isolator air handling system (where the air handling system is used in the aeration phase

of the biodecontamination cycle), typical cycle times are 8–12 h (depending on the isolator complexity and materials of construction) with H_2O_2 residual of ≤1 ppm at the completion of aeration.

Shorter biodecontamination cycles and lower residuals of H_2O_2 can be achieved by fully integrating the biodecontamination system into the isolator air handling system (where the air handling is used in all phases of the biodecontamination cycle), however, increasing cost and complexity of the isolator system.

Environmental monitoring system: Viable solution and total particulate monitoring systems are integrated into the isolator to ensure that the product processing environment is maintained.

Transfer system(s): Transfer systems allow product pathway connections to be made to the isolator and allow equipment, components, and materials to be introduced or removed from the isolator. The most common type of transfer systems is alpha/beta as it allows two sterile environments to be connected securely together and transfer from one sterile environment to another with a low-level risk.

The following are key advantages of an isolator system:

- Isolator systems remove the operator from the direct contact with the critical product process (i.e., open parts of the process where potential contamination could be introduced to the product being processed).
- Isolators minimize the ISO 5 environment required for the critical product process reducing HVAC and cleaning requirements when compared to an ISO 5 clean room environment.
- Isolator systems allow a validated biodecontamination process to be undertaken rendering the critical environment sterile, exposing the product.
- Isolators can be located in an ISO 8 environment, reducing transition airlocks and operator gowning required to support an ISO 5 clean room environment.
- Isolators allow a reduction in long-term operating costs.
- Isolators allow enhanced operator safety when handling potent/toxic products.
- Isolators allow special processing environments to be created, for example, anaerobic environments.

Besides advantages, there are also disadvantages:

- Integration of isolators as part of a system is complex, a high level of details has to be established for the baseline process and the operator interface with the process so that the equipment and operator ergonomics including process set up process operation and process decontamination and cleaning.
- There is a significant amount of work required to integrate the isolator with the facility and other equipment. This work can be reduced by engaging a single supplier.
- When a process deviation occurs, error recovery in an isolator can be complex.
- Changes are difficult.[8]

8 Austin McDonald Sterile Technology LLC (www.steriletechllc.com).

ALUS/Isolator design considerations

Isolator systems and the enclosed equipment fundamentals impact the quality of the product being processed. Therefore, before design and manufacture of the isolator system and enclosed equipment commences, the process must be clearly defined, the potential product risks understood, and the necessary design features incorporated to mitigate the potential risks. Considering this, all product process steps should be defined in detail, including operator interface requirements, transfer requirements, and environmental monitoring requirements for each of the product phases:

- Process setup
- Process operation
- Process decontamination and cleaning

Lyophilizer/ALUS design considerations

Lyophilizer and ALUS should have the following design features to allow integration with an isolator system:

Loading door: The lyophilizer should be provided with a loading/unloading door (sometimes referred to as a slot or pizza door) to integrate the lyophilizer with the isolator. Indeed, the loading/unloading door is the only element of the lyophilizer that is required to be integrated with the isolator.

Indexing shelf system: As the access to the lyophilizer is via a loading/unloading door, the shelf stack must move to allow each shelf to be presented in turn for the loading process. This requires that all shelves be stored below the loading level at the beginning of the process and as the process progresses, the shelves index up. Error recovery is a critical consideration for the shelf stack as it is possible for the shelf position to be "lost" during product processing with product on the shelves preventing the stack from returning to its starting position below the loading level. Therefore, for error recovery, the shelf stack should index fully up for home position.

Loading systems: There are a number of automatic loading configurations (2.4.1). For compact loading systems it is important to provide sufficient accumulation upstream of the loading mechanism to ensure that the filling equipment is not stopped during the loading operation (as frequent stop/starts significantly affect equipment reliability). The accumulation should also consider vial check weight frequency. If the vial check weight frequency is every 5 min, then 6 min of vial accumulation will be required before the vial enters the loading mechanism. This will ensure that vials with potential weight issues have not entered the shelf stack.

Unloading system: The unloading process is the reverse of that to the loading process. Also, here error recovery is critical for the shelf stack.

Sterility interlocks: The lyophilizer and the isolator are sterilized/biodecontaminated using independent systems. Therefore, it is important for the lyophilizer and the isolator control system to incorporate flags and interlocks to prevent a nonsterile environment being exposed to the sterile environment.

Pressure equalization: Pressure equalization between the lyophilizer chamber and the isolator is typically not an issue as seal disengagement and door movement is quite slow.

Solution (liquid products) and lyophilized product mix: If a product process is required to process both solution and lyophilized, products separating the lyophilization process from the solution process should be considered.

Figure 2.101 Vial with installed antenna is placed on the ALUS conveyor belt. (Tempris Sensor Technology, IQ Mobil Solutions GmbH, D-83607 Holzkirchen, Germany.)

Product thermocouple placement (Figure 2.101)[9]: An isolator system with an integrated loading and unloading system makes it extremely difficult to place wired control thermocouples into the product vials and then enter the vials into the lyophilizer. While wireless thermocouples are available, those should be considered (1.2.3.1). Alternative to wireless thermocouples or in addition BTM (Barometric Temperature Measurement 1.2.3) is a reliable process control method.

Isolator design considerations:

The isolator should have the following design features to allow integration with lyophilizers and associated loading/unloading systems.

Operator safety: As the operator can interface with the isolator via glove ports, it is important that safety is considered (Figure 2.102). Light curtains are typically

Figure 2.102 Automatic loading and unloading system for two freeze-dryers installed in open RABS system. Gloves in the doors allow access during operation. Hinged conveyor under LF allow operator to cross line. (Copyright courtesy of GEA Group, Germany.)

9 iQ-mobil solutions GmbH, D-83607 Holzkirchen, Germany; www.tempris.com.

used to stop the operating mechanism if an operator attempts access to the isolator and enclosed equipment during processing. The significant disadvantage of light curtains is that they are often activated inadvertently with hard emergency stops requiring error recovery of the loading/unloading system, the slot door, and possibly the shelf stack. To avoid these light curtain issues, glove port covers that stop the machine if removed can be used instead.

Equipment design for isolators: The equipment enclosed within the isolator must be laid out to ensure access via glove ports for adjustment, fault clearance, and if necessary repairs during product processing. To support this, the format parts should allow installation without tools, hand screws should be oversized to allow manipulation via gloves, and all parts should be sufficiently sized to allow pick up and manipulation via gloves. As the loading and unloading system will be contained in an ISO 5 environment, the vial handling mechanism should be a minimum of 300 mm above the base plate of the isolator to allow undirectional airflow over the vials and all the equipment enclosed within the isolator system and should be easy to clean. The equipment should be constructed and built of materials that are nonparticulate generating, resistant to cleaning solutions, H_2O_2, and should minimize the absorption of H_2O_2 to ensure impact on the length of the aeration phase. Finally, equipment within the product environment must be "dry cycled" during the biodecontamination process to ensure all surfaces are exposed to the H_2O_2.

Mock-up: It is recommended to build an isolator mock-up system to ensure that all the design features are matching with the specification.

Isolator system leak tightness: It is important to ensure that the isolator system and enclosed equipment has a low leak rate to prevent entrainment of contamination into the isolator environment and to protect the operator environment during H_2O_2 biodecontamination. It is also important that the leak rate of the isolator system is consistent as the leak rate is tested automatically in the first phase of the validated biodecontamination process. The leak rate specification can vary depending on the product process requirements (i.e., potent products require a lower leak rate than nonpotent products) and detailed leak rate guidance for isolator systems and enclosed equipment is provided in ISO 14644-7: 2004 and ISO 106-2: 1994. To meet even the least stringent leak rate specification, there must be no open path (in the machine plate) between the equipment mechanical space and the product environment. Additionally, all shafts (rotating and reciprocation) penetrating the machine plate should be fully sealed to prevent a potential open path. It is important that the seals are durable and designed not to be replaced, as replacement would require significant downtime.

Vision panels/access: The isolator system must be provided with sufficient vision panels to allow the product process to be observed and access panels to allow format part changes.

Transfer system(s): Two 150 mm diameter alpha/beta transfer systems would be required to support the transfers typically with a loading and unloading system isolator, one each for environmental monitoring material introduction/removal and cleaning material introduction/removal. The potential of removing vials between failed check weight cycle should also be considered.

Environmental monitoring: A viable and total particulate monitoring system should be provided in close proximity to the lyophilizer slot door.

Lighting: Sufficient lighting should be provided in the isolator to allow the product process to be observed, allow effective line clearance, and inspect the isolator system and the enclosed equipment surfaces postcleaning.

Wash-in-place system: Some isolator systems include wash-in-place systems. However, enclosed equipment is typically quite complex and prevents effective cleaning with such systems. Additionally, no matter how effective the isolator air handling system is, it is not possible to fully dry the isolator and enclosed equipment. The ability to completely dry the isolator system is critical as residual moisture will impact the validation biodecontamination system. Consequently, wash-in-place systems are typically used to wet the surfaces of isolators and enclosed equipment after processing of potent products. The isolator is then fully cleaned and dried via the opened vision/access panels.

Isolator documentation considerations: As the isolator system and the enclosed equipment fundamentally impact the quality of the product being processed, the appropriate documentation must be generated to demonstrate traceability from the design process through validation and operation. Based on the GAMP format, the following are the documentation required:

- Process description
- GMP risk assessment
- Qualification strategy document
- User requirements specification
- Functional specification
- Hardware design specification
- Software design specification
- Requirement traceability matrix
- Functional risk assessment
- Vendor internal testing procedures
- Factory acceptance testing
- Site acceptance testing procedures
- Installation/operation qualification
- Performance qualification
- Process validation
- Standard operation procedures

2.4.3 Isolators: Validation of Decontamination Processes

Pharmaceutical isolators are to be equipped with a mobile or an integrated decontamination system.

The decontamination should be carried out preferably with H_2O_2 (hydrogen peroxide).

Biodecontamination with hydrogen peroxide is state of the art worldwide, approved by the FDA, and recommended as biodecontamination. In comparison with other antibacterial gases, hydrogen peroxide is virtually an ideal gas. It achieves effective results even at room temperature and in a dry atmosphere and

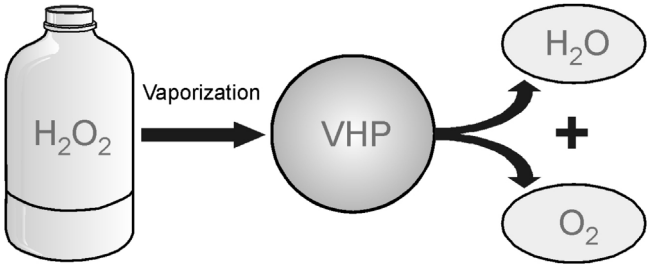

Figure 2.103 VHP is degraded into nontoxic by-products during the aeration process leaving behind water and oxygen. (Steris Corp., Mentor, Ohio, USA).

at the end of the process, breaks down into water and oxygen ($H_2O + O_2$) (see Figure 2.103).

The decontamination cycle depends on various process parameters as well as the ambient conditions such as pressure, temperature, and the relative humidity of the interior area.

The cycle development usually occurs between the completed operation qualification (OQ) and the performance qualification (PQ). It is used to determine the process parameters for an effective, reproducible, documented, and successful decontamination that complies with the requirements of the authorities (e.g., FDA) and the customer.

The PIC/S-1 recommendation stipulates a minimum spore reduction of 6 log. For safety reasons, however, spore reduction ranging from 10 to 12 log is recommended (for isolators and airlocks) in the production of pharmaceuticals (see Figure 2.104).

Figure 2.104 In research labs, **V**aporized **H**ydrogen **P**eroxide-VHP is widely used to decontaminate rooms and filters with no condensation for better material compatibility and shorter cycle time. (Steris GmbH, D-50933 Cologne, Germany.)

The cycle development at an isolator occurs according to a structured process, which is summarized in a plan that determines and defines the positions of the BIs (biological indicators). In addition, the maximum possible H_2O_2 injection rate quantity (grams per minute) is determined.

At the beginning of the cycle development, the isolator temperature and humidity levels are recorded, since these variables have an impact on the sporicidal process. During production, there should be as little fluctuation as possible in temperatures of the surfaces. With these findings regarding the temperature distribution, critical zones are identified in order to possibly reposition or additionally position the biological indicators (BI). By measuring the surface temperatures, what are known as hot and cold spots are detected that prevent effective decontamination.

The next important step in the cycle development is the preliminary investigation of the lethality. For this purpose, a number of BIs are placed together with an appropriate amount of nutrient in an easily accessible location in the isolator.

The Procedure

1) At the beginning of the injection phase, the BIs are placed in the nutrient solution within a specified time interval. The *D* value is thus subsequently determined in accordance with ISO 11138 2 using the LSKM method.
2) The *D* value describes the time in minutes required to kill 90% of the test organisms under the prespecified conditions. The start time of exposure for the subsequent worst-case lethality test is determined with the help of these tests.
3) BIs and chemical indicators (CI) are used for the worst-case lethality test. While chemical indicators merely indicate the quality of the kill rate at geometric locations in the isolator based on their changes in color, the average system *D* value can be determined for each position with the help of BIs.
4) FDA Guidance 3 recommends positioning BIs in critical areas of the isolator.
5) All BI positions are to be typed according to the following rationale:
   - *Geometry:* Selection according to the geometry of the isolator.
   - *Difficulty:* Difficult to decontaminate with H_2O_2 because the area might be shaded.
   - *Critical:* Critical because contact with the product or operator intervention is necessary.
   - *Worst case:* A worst case is the position where killing of the BIs takes the longest.

The first cycle is run using the parameters determined in the preliminary lethality test. All BI and CI positions are tested during this cycle. For all further tests, the H_2O_2 injection time is lengthened according to the selected interval until all BIs no longer exhibit any growth at all positions.

The position at which growth is indicated last is considered the worst-case position in terms of lethality. Using the LSKM method, a minimum spore reduction of 6 log is indicated for this position.

The average system D value of this position can be used as the basis for determining the total decontamination time. This is usually 10 or 12 times (for the correspondingly desired 10- or 12-log spore reduction) as long as that of the average system D value of the worst-case position.

The conclusion of the cycle development involves inspection of the ventilation to determine the ventilation period. This test should ensure that the required maximum residual H_2O_2 concentration is below the limit. Thanks to catalyst technology, low residual concentrations can be reached in the isolator after a short ventilation period. The residual H_2O_2 concentration should be less than 0.5 ppm.

A plan for process validation is created based on a successful cycle development. This plan includes validation of the decontamination process and ventilation with three validation runs each. Revalidation is required at yearly intervals.

2.5 Production Plants for Food

2.5.1 Discontinuous Plants

Basically, the chamber plants described in Section 2.4 can be used for foodstuffs and other products, as described in Sections 5.1 and 5.2. Freeze-drying plants for food and similar products have to handle large quantities of product. The cleaning requirements remain, but no sterilization is necessary. The product can be transported in trays as described in Section 2.2.2 and dried in cylindrical tunnels. Figure 2.105 shows the two systems most commonly used today. Their characteristic features are as follows:

	A	B
Drying chamber	Tunnel	Tunnel
Condenser	Flanged to the tunnel	In the lower part of the tunnel
Connection between chamber and condenser	Vacuum-tight valve	Barrier plate
Trays	Ribbed trays[a)]	Flat trays[a)]
Shelves – heated by	Steam or heat transfer fluid	Heat transfer fluid
Tray transport	In carriers on an overhead rail	Pushed over rails
Heat input	Trays lowered on the shelves	Mostly radiation during drying
Defrosting of the condenser	Steam	Warm water
Loading and unloading	Carrier with trays is moved in and out	Trays are moved to each shelf level by a lift
BTM/DR measurement	Possible, vacuum-tight valve not tight enough	Not possible, barrier plate

a) See Section 2.2.2.

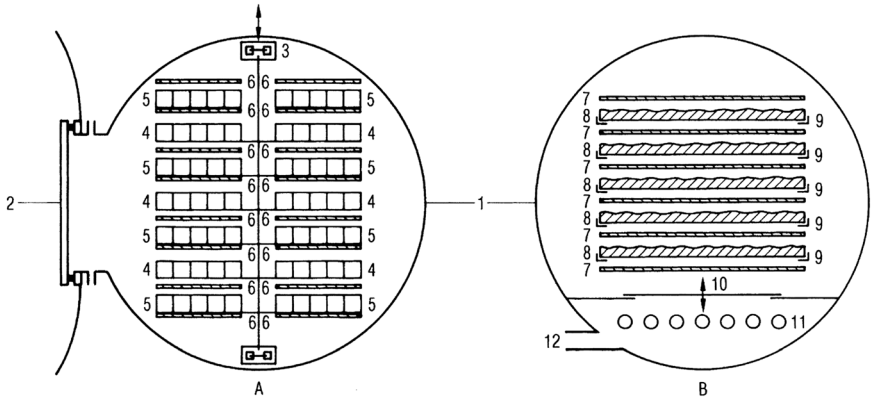

Figure 2.105 Schematic comparison of two commonly used tunnel freeze-drying systems for the freeze-drying of food and luxury food. 1, drying tunnel; in A: 2, valve before the condenser; 3, lift and transport device; 4, trays in transport position; 5, trays on the shelves during drying; 6, heated shelves; in B: 7, radiation plates; 8, trays; 9, guide rails for the tray transport; 10, separation plate between tunnel and condenser; 11, condenser; 12, vacuum connection.

2.5.2 Continuous Plants with Tray Transport

Both systems A and B can be used for continuous operation with vacuum locks. In system A (Figure 2.106), one or two carriers are moved into a lock (4) in front of several connected tunnels (8). The lock is evacuated and the carrier(s) are moved into the tunnels. At the same time, the equal number of carriers is moved from the tunnels into an exit lock (10). Both locks can be separated from the tunnels by two large slide valves (7). In system B (Figure 2.107), each tray (1) passes through an entrance lock (2) into a paternoster lift (3), which moves the tray to a certain level and pushes it into the drying zone. The last tray is pushed by the entering tray into the exit paternoster lift (6), which moves the tray into the exit lock (7).

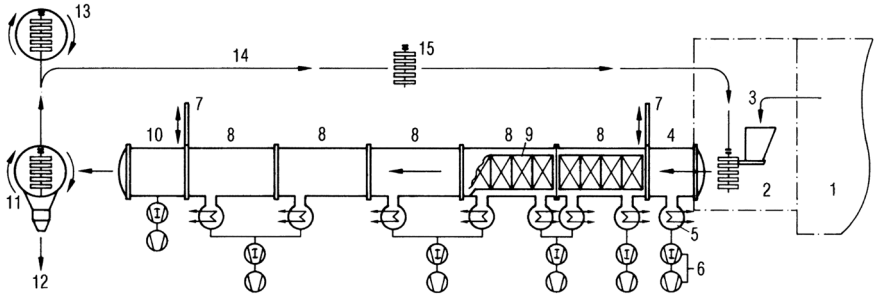

Figure 2.106 Schematic drawing of a CQC freeze-drying plant. 1, preparation room, for example, freezing, grinding, sieving; 2, loading area; 3, loading of trays and carriers; 4, entrance lock; 5, ice condenser; 6, two-stage vacuum pump set; 7, sliding gate valve between tunnel and lock; 8, four drying tunnels; 9, transport carrier with trays; 10, exit lock; 11, unloading of trays; 12, exit of dry product; 13, washing of carriers and trays; 14, return of trays; 15, carrier with empty trays. (Based on ALD Vacuum Technologies GmbH, D-63526 Erlensee, Germany.)

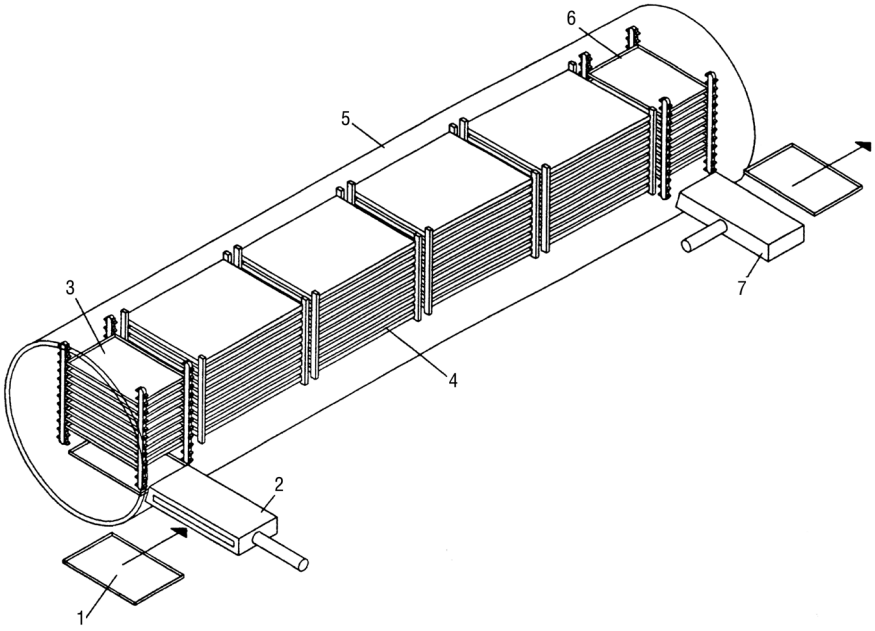

Figure 2.107 Schematic drawing of a CONRAD® freeze-drying plant. 1, tray; 2, entrance lock; 3, lift for the trays; 4, heating zones; 5, tunnel wall; 6, lift for the trays; 7, exit lock. (Based on Atlas Industries A/S, DK-2750 Ballerup, Denmark.)

2.5.3 Continuous Plants with Product Transport by Wipers or by Vibration

Oetjen and Eilenberg [20] have shown that granulated products (which do not stick together) can be freeze-dried with a 5–10 times higher ice sublimation rate if the product is rolled over on the heating surface, compared with a static layer. Figure 2.108 shows the drying time of granulated product for different layer thicknesses as a function of the mixing frequency. In the disk dryer (Figure 2.109), the product passes through a vacuum lock on to the first disk. Wiper blades distribute the granulates on the disk and push it over the edge of the first disk to the second one, and so on. The product is brought back to atmosphere through an exit lock. This form of transport works with a mechanically stable product, but with foamed granulated coffee extract a substantial amount of fines is produced, because the wiper blades not only push the product but also partially abrade or mill the granulate. The particles produced with a size smaller than 0.5 mm can be 20% of the throughput or more. Certain products, for example, those which roll or have too soft a surface, cannot be dried in such a plant. As shown by Oetjen [21], the abrasion can be kept as low as by the filling of trays (1.5% of the throughput) if the product is transported on a vibrating bed. Figure 2.110 shows a schematic drawing of a vibration freeze-dryer. Figure 2.111 illustrates this type of plant: the vacuum chamber and the entrance lock are shown at the top and assembly of the vibrated and heated shelves at the bottom.

The output of such high-speed dryers is limited by the increasing density of the water vapor flow. The grains of the product are floating in the vapor stream as in a

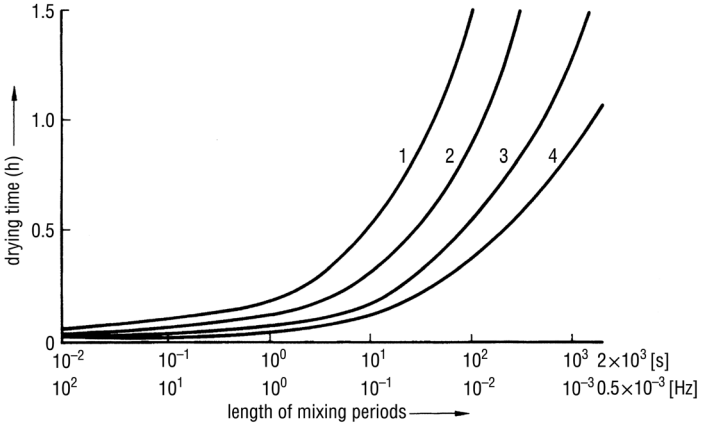

Figure 2.108 Drying time as a function of a periodic, thorough mixing of a granulated product. Layer thickness: 1, 20 mm; 2, 12 mm; 3, 8 mm; 4, 5 mm. (See also Ref. [20].)

fluidized bed and the smallest particles are carried along with the vapor to the condenser. Even if only 1% of the dried product is carried away, it sums up to 10 kg per day if the throughput is 1000 kg per day. In 4 weeks, this totals to 280 kg or 1 m^3 of coffee powder. To remove this from the vapor stream, very large filters have to be used in order to minimize the pressure drop in the filters.

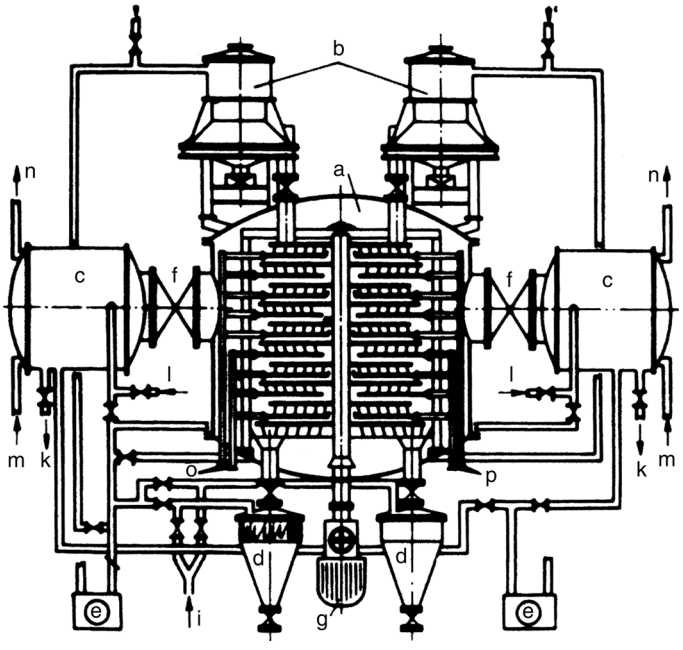

Figure 2.109 Schematic drawing of a disk dryer, heated disk surface 95 m^2. a, dryer housing; b, alternating locks with product storage; c, ice condenser; d, alternating locks for product removal; e, vacuum pumps; f, shut-off valve for the condenser; g, drive of product wipers; i, venting of product locks (N_2); k, drain of water after defrosting; l, evacuation of the condensers; m, refrigerant to the condenser; n, refrigerant outlet; o, heating medium to the disks; p, heating medium outlet. (See also Ref. (Suwelack, unpublished, 2003).)

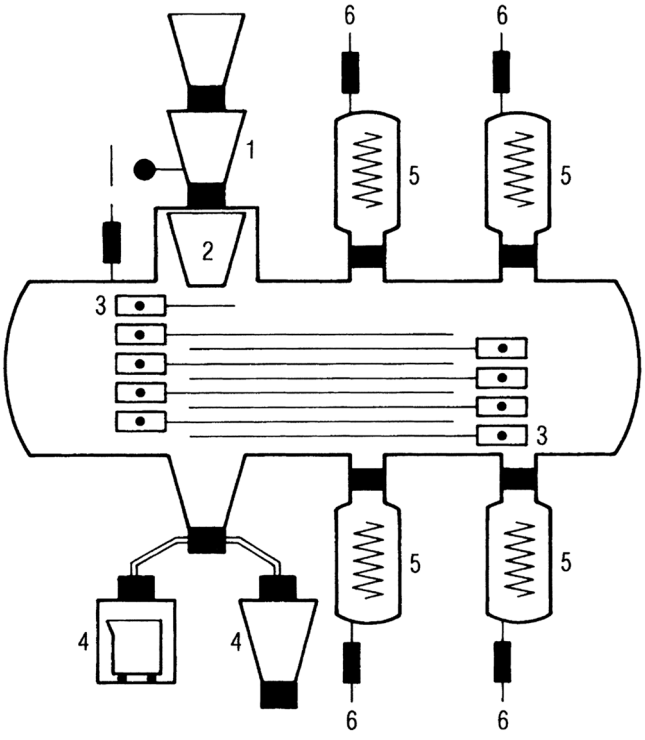

Figure 2.110 Schematic drawing of a horizontal vibration dryer with 10 m^2 drying surface. 1, entrance lock for the product; 2, storage and dosage unit; 3, heated shelves vibrated at 50 Hz; 4, alternating locks for product removal; 5, condensers; 6, connection to the vacuum system. (See also Ref. [21].)

2.6 Process Automation

This section describes the automation of freeze-drying processes. The automatic loading and unloading a freeze-drying plant can be found in Section 2.4.1.

2.6.1 Prerequisites for Process and Related Plant Automation

The automation of a process requires the knowledge of the process data, their acceptable tolerances, and sensors to measure the data with a specified reproducibility. During the product and process development, later automation should be kept permanently in mind, since not all sensors or methods of measurement can be used in an automated operation, for example, the type of sensor in the product during freezing influences the freezing rate (Figure 2.112) and the structure of the product. In a production plant with automatic loading and unloading, no sensor with wire connections can be used, and other methods of freezing documentation are required. Laboratory conditions of process development may be different from the production area with a strictly limited number of particles/m^3. If a process developed with sensors and method A has to be changed to B, it could require a completely new development phase.

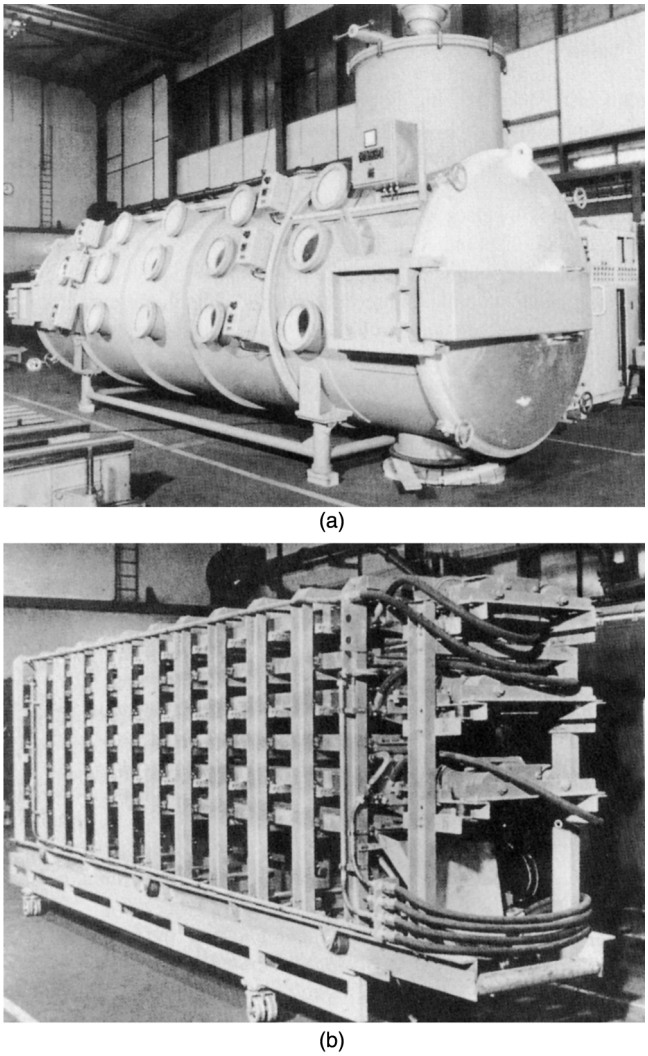

(a)

(b)

Figure 2.111 Photograph of a vibration dryer with 10 m^2 surface vibrated with a frequency of 50 Hz. (a) Freeze-dryer with the product feeding system in front. (b) Heated vibration shelves removed from the chamber. (Slides 21 and 22 from Ref. [22].)

Process automation is more safely and economically possible if the required data, for example, temperature or pressure, are not at the far end of technical possibilities. As shown in Figure 3.10, a factor VIII solution can require $T_{ice} \sim -55$ °C or ~ -35 °C with different excipients. As shown in Section 1.2.4, it will be very difficult or impossible to design a large production plant for $T_{ice} < -45$ °C. If $T_{ice} < -40$ °C is required, one should try to change the route of product development. In addition to the qualification and validation of the plant, it is recommended to perform a preventive failure analysis for all equipment involved in the automated system. The possible failures are listed, their consequences analyzed,

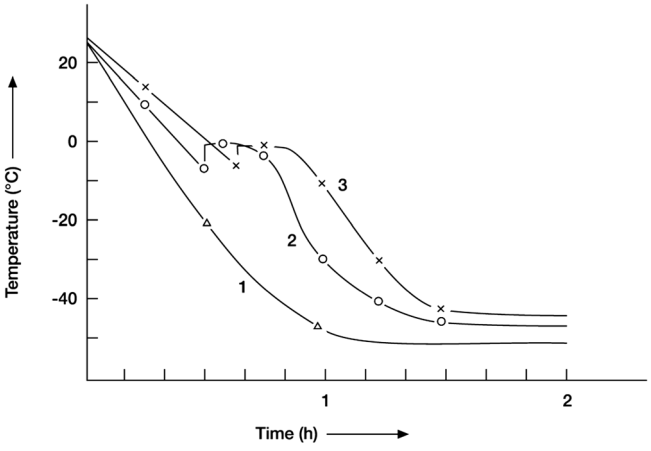

Figure 2.112 Influence of the sensor type on temperature measurements. 1, T_{sh}; 2, T_{pr} by RTD; 3, T_{pr} by Th. (Measurements by Steris GmbH, D-50354 Hürth, Germany.)

preventive steps installed where possible, and actions documented for actual failures. In Section 2.2.11, failures are classified in four groups of declining importance and in Section 6.1 seven unexpected events and their possible origins are studied. For electronic boards or electronic equipment the 'mean time between failures' can be calculated from the components used in the electronic system and components with too short an average lifespan can be identified.

2.6.2 Control of the Process and Related Plant Data by Thermodynamic Data Measured during the Process: Thermodynamic Lyophilization Control (TLC)

Today, most freeze-drying processes are operated by data developed in a pilot plant and qualified in the production plant. The process supervision is based on time-controlled temperatures and pressures. TLC uses data measured during the process to control and document its progress as given in Table 2.9.

2.6.2.1 Control of the Process without Temperature Sensors in the Product

There are two reasons for not using temperature sensors in the product. First, as mentioned in Section 2.6.2 and Figure 2.112, the temperature measured will depend on the type of sensors and their place in the product (e.g., near the bottom). Furthermore, any sensor will influence the beginning and the rate of freezing and thereby the structure of the product. Second, sensors with wire connections cannot be used in plants that are automatically loaded and unloaded.

The freezing process is not time and location wise a uniform event, as shown in Section 1.1.5 and Figure 2.113. Independent of the two reasons above, it is of interest to find an integral method to document the freezing section. The inlet and outlet temperatures of the heat transfer fluid circulated in the shelves offer a solution for such a measurement, as presented in Figure 2.114. All four curves are

Table 2.9 Program for a thermodynamic lyophilization control (TLC) process.

Section	Step	Start[a)]	End[b)]	T^a_{co}/T^e_{co}[c)] (°C)	T^a_{sh}/T^e_{sh} (°C)	p^a_c/p^e_c (mbar)	T_{ice} (°C)	SA (°C)	$T_{ice,max}$[d)] (°C)
01 Freezing	01		T^e_{sh} −40 °C	–	20/≤ 40	–	–	–	–
	02	T_{sh} −40 °C	A[e)]	–	≤40	–	–	–	–
	03	A[e)]	A[f)]	–	≤40	–	–	–	–
	04	A[f)]	T_{co} ≤ 60 °C	20/≤60	≤40	–	–	–	–
	05	T_{co} ≤60 °C	p<0.1 mbar	≤60	≤40	1000/0.1	–	–	–
02 MD	01	p_c<0.1 mbar	T_{sh} 5 °C	≤60	−40/5	0.1			
	02	T_{sh} 5 °C	$+X$[g)] = D[h)]	≤60	5	0.1	−25.1	–	–
	03	D	$D+Y$[i)]	≤60	5	0.1	−25.5	0.3	−25.0
	04	(−25.0–1.5 °C)[j)]	(−25.0–3.0 °C)[k)]	≤60	5/30	0.1	−26.5	0.7	−25.0
	05	−28 °C[k)]	0.05 mbar	−60/−70	30	0.1/0.05	DR (%/h)		dW (%)
03 SD	01	0.05 mbar	0.05 mbar	≤70	30	<0.05	1.2		2.2
	02	0.04 mbar	0.04 mbar	≤75	30	0.04	0.5		1.0
	03	0.04 mbar	0.03 mbar	≤75	30	0.03	0.2		0.5
	04	0.03 mbar	<0.03 mbar	≤75	30	0.03	0.05		<0.5
	05	End of SD, dW <0.5%							
04 vial closing	01	0.03 mbar	400 mbar N_2		20	–	–		–
05 vial unloading	01	400 mbar	atm N_2			–	–		–

a) Start criterion for the start of a step.
b) End criterion for the end of a step.
c) T^a_{co}/T^e_{co}, T^a_{sh}/T^e_{sh}, p^a_c/p^e_c data at the beginning[a]/and at the end[e] of one step.
d) $T_{ice,max}$ highest av. T_{ice} during one run.
e) A time at which dT between heat transfer fluid inlet and outlet <for example, 0.2 °C.
f) A rest time at T_{sh}, which depends d and K_{su}.
g) X time at which T_{ice} measurements start after T_{sh} = 5 °C; this time depends on d, K_{tot} and T_{tot}.
h) D time of first T_{ice} data.
i) Y time at which $T_{ice,max}$ is measured.
j) (−25.0 °C – 1.5 °C) time at which $T_{ice} = T_{ice,max}$ minus 1.5 °C.
k) Time at which $T_{ice,max}$ minus 3 °C is reached.

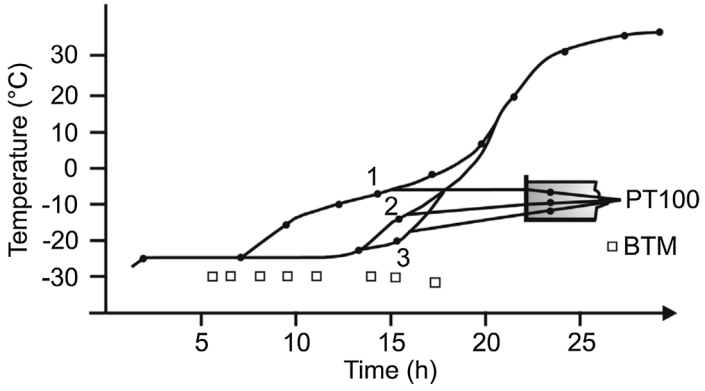

Figure 2.113 Temperature measurements as a function of drying time. Three RTDs are placed in the product: 1, near the top; 2, in the center; 3, near the bottom. T_{ice} was measured by BTM, marked as ●. (Measurements by Steris GmbH, D-50354 Hürth, Germany.)

the averages of two runs. Figure 2.114 permits the following conclusions to be drawn from these tests:

- In this installation and with this load, the beginning and end of the crystallization can be followed. At 20 min ~8%, at 50 min ~60%, and at 70 min ~90% of

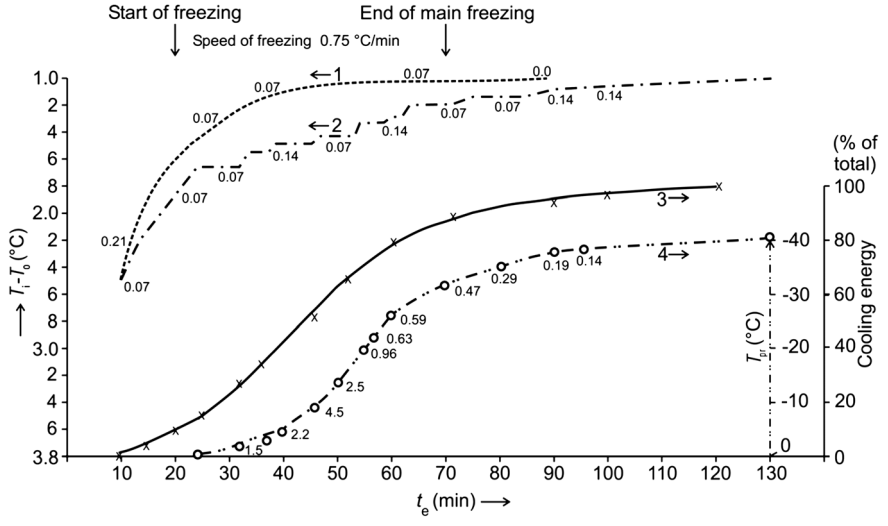

Figure 2.114 Thermodynamic data during freezing. All four curves are the average of two runs. 1, the difference between inlet (T_i) and outlet (T_o) temperatures of the shelves of the plant with empty vials; 2, the same temperature difference during cooling with filled vials; the standard deviations between these two runs are given as figures on curves 1 and 2; 3, energy used for cooling and freezing the product as percentage of the total energy used; 4, temperature in the product measured by sensors, two sensors in two vials during each run. The curve is the average of these four temperatures, the numbers are the standard deviations of these four measurements. (See also Ref. [23].)

the total energy are removed from the product. The period from 20 to 70 min is called here the main freezing time.
- The degree of subcooling has not been uniform in all vials, as can be seen from the steps in plot 2. This is confirmed by the large standard deviations of the four sensors plot 5: at the beginning, between 30 and 60 min, the SA goes from 1.5 to 4.5 °C, then back to 0.5 °C and at the end 0.14 °C.
- The prerequisites and limitations of this method are discussed in Section 2.6.2.5.

2.6.2.2 Measurement of the Ice Temperature at the Sublimation Front and the Desorption Rate as Process Guides

The decisive data during MD is the temperature of the ice at the sublimation front, T_{ice}, which can only be measured by BTM. Figure 1.119 shows the principle: the valve between the chamber and condenser is closed for less than 3 s, to fill the chamber with water vapor of saturation pressure p_s corresponding to T_{ice} as shown in Table 1.21. The two conditions for the use of BTM, a leak rate of the chamber below a certain limit and enough ice subliming during the time the valve is closed, are described in detail in Section 1.2.1.

This section concentrates on the T_{ice} data used for automation and process control, which requires two more conditions: a high frequency of pressure data recorded after the valve is closed, for example, 50–100 data per second (see Figure 1.120 and related text) and precision control of the valve movement, if the valve is large and does not close in times ~1 s (see Table 1.16 and related text).

T_{ice} changes very rapidly if p_c is changed as shown in Figure 2.115. The change of p_c therefore is the best tool to lower or raise T_{ice}, should it become close to the tolerances. The control of p_c permits accurate control of T_{ice}. Figure 2.116 shows T_{ice} as a function of p_c. The rapid changes of T_{ice} by changes of p_c are understandable since T_{ice} is the temperature at the sublimation front of the ice at which the heat transfer from the shelf to the ice front is in equilibrium with the energy consumption at this front by the sublimation of ice. The heat transfer is governed by Eq. (1.12), the sublimation by the transport of vapor from the sublimation front to the condenser, see Section 1.2.4. A decrease in pressure reduces the density of water vapor flow ($s^{\#}$) more than proportional with a practically immediate reaction. At a given geometry of the plant, $s^{\#}$ depends only on the pressure in the chamber. The plot in Figure 2.116 depends also on the other facts influencing the equilibrium: K_{tot}, T_{tot}, and d in Eq. (1.12), the structure of the product reflected in T_{ice} (see Figure 1.122) during MD, and the number of vials per run influencing the vapor flow (see Table 1.24), if all not mentioned factors are constant. The function $T_{ice} = f(p_c)$ is correct only if the factors K_{tot}, T_{tot}, d, product structure, and number of vials are constant, but for plants with identical $s^{\#}$ data, the influence of the other factors may be small enough to do some extrapolation. For all T_{ice} plots as a function of p_c it is typical that the difference between p_s and p_c increases with decreasing pressure: for example, at −30 °C, 0.38 and 0.22 mbar (58%); and at −50 °C, 0.039 and 0.016 mbar (41%).

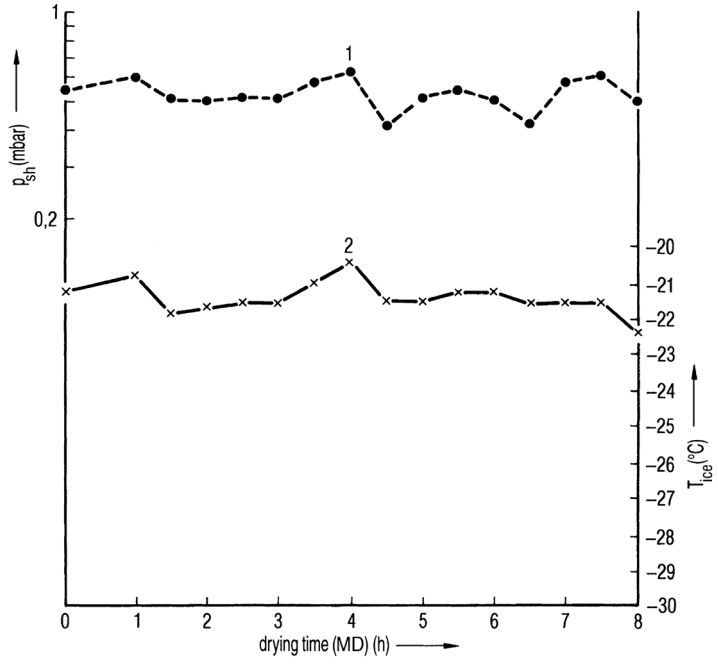

Figure 2.115 Temperature at the sublimation front of the ice, T_{ice}, as a function of the varied operating pressure, p_c. 1, pperating pressure; 2, temperature at the sublimation front, T_{ice}. After 5 h drying time, the T_{ice} follows the operation pressure more slowly, because the main drying is reaching finalization. (Measurements by Steris GmbH, D-50354 Hürth, Germany.)

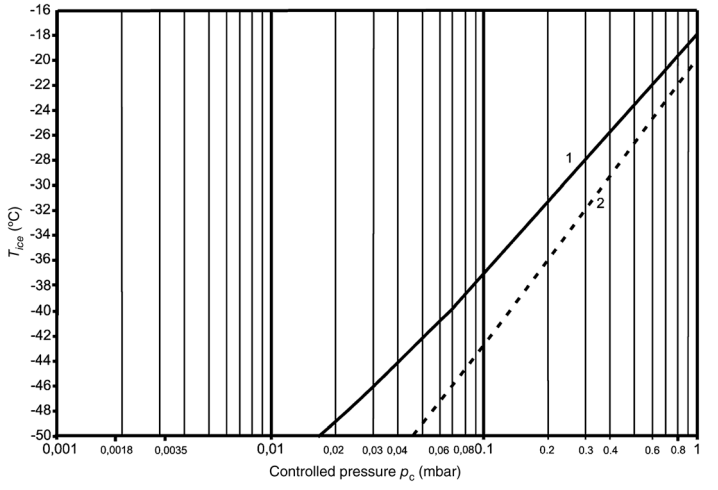

Figure 2.116 T_{ice} as a function of p_c. The plot shown is only valid under certain conditions (see text). 1, T_{ice} as function of p_c; 2, saturation vapor pressure of ice. (Measurements by Steris GmbH, D-50354 Hürth, Germany.)

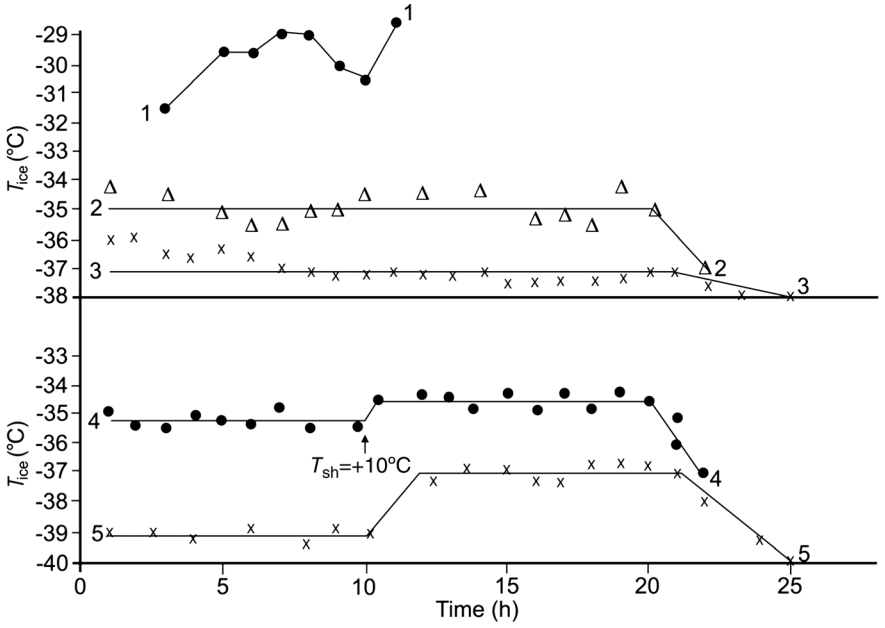

Figure 2.117 T_{ice} as indicator of the frozen structure of a 10% mannitol solution, $d = 10$ mm.

Runs 1–3	Product frozen in vials on the shelves down to <−45 °C
Run 1	Sublimation rate too high for the possible water vapor transportation, T_{ice} rises, product collapses, T_{ice} is irregular
Run 2	T_{sh} 0 °C, p_c 0.15 mbar, av. T_{ice} −34.9 °C, SA 0.65 °C, product contains highly concentrated inclusions between ice crystals, depending on the position of the sublimation front; T_{ice} changes abruptly with the amount of concentrates being dried
Run 3	T_{sh} −5 °C, p_c 0.08 mbar, av. T_{ice} −37.2 °C, SA 0.7 °C, due to lower T_{sh} and p_c the mobility of water molecules in the concentrate is reduced. In the first ~6 h, T_{ice} is a little higher than av., inclusions near the surface from freeze concentration are dried, thereafter the structure becomes more uniform represented by a lower temperature of the ice
Runs 4 and 5	Product frozen in LN_2 and loaded on shelves at −45 °C, T_{sh} is raised to +10 °C and kept for 10 h
Run 4	T_{sh} and p_c as in run 2, av. T_{ice} −35.1 °C, SA 0.50 °C, after 11 h −34.5 °C, SA 0.6 °C
Run 5	T_{sh} and p_c as in run 3, av. T_{ice} −39.1 °C, SA 0.22 °C, after 12 h −37.0 °C, SA 0.33 °C

(Measurements by Steris GmbH, D-50354 Hürth, Germany.)

Figure 2.117 shows how T_{ice} measurements can be an indicator of the frozen structure of a 10% mannitol solution:

- The sublimation rate in run 1 is too large for the possible vapor transportation, T_{ice} rises, the product collapses, T_{ice} becomes irregular.
- Quick freezing distributes the inclusions between the crystals more uniformly (runs 4 and 5), SD values of T_{ice} are small: 0.39 and 0.33 °C.

- Lower T_{ice} (run 3, −37.2 °C, SA 0.65 °C; run 2, −34.9 °C, SA 0.7 °C) decreases molecule mobility, the structure is more stable during main drying, at the beginning of MD the changes in T_{ice} are more pronounced, the top layer of the product is the last frozen and contains more concentrated inclusions than the middle and lower part.

As mentioned in Section 1.2.3, the measurement of T_{ice} can also be used as a quantitatively measurable criterion to terminate MD and change to SD. Figure 2.118 summarizes the T_{ice} data for six different runs with 10% saccharose solution, $d = 10$ mm, $p_c = 0.15$ mbar. The different parameters are number of vials, freezing rate, T_{sh}, time elapsed between end of freezing and start of drying.

Plot 1: No stable T_{ice} is found, the product is collapsed, T_{sh} 30 °C leads to a T_{tot} producing a sublimation rate larger than can be transported to the condenser.

Plot 2: T_{sh} is lowered to −5 °C, a stable T_{ice} is observed.

Plots 3 and 4: These represent the two runs in which the product has been frozen by LN_2. The process data are identical, but the time between the end of freezing and the beginning of MD is ∼2 h longer for run 3, resulting in somewhat grown ice crystals and a faster MD.

Plot 5: T_{ice} is ∼1.4 °C lower than in plot 2. The lower vapor flow, resulting from a smaller number of vials, is more important than the higher T_{sh}. The shorter t_{MD} results from a larger T_{tot}: 34.5 °C in plot 5 and 28 °C in plot 2.

Plot 6: The larger number of vials has increased T_{ice}, but T_{tot} is larger (32 °C) than in run 2 (28 °C), that is, ∼14%; the decrease in t_{MD} is only 8%; part of the T_{tot} advantage is lost in the higher T_{ice} owing to the increased vapor flow. It is interesting to note that the standard deviation (SA) of T_{ice} data of the LN_2 frozen products are on average 0.51 °C for the slowly frozen product 0.31 °C. The LN_2 frozen product has not been thermally treated, and it will contain partially unfrozen water included in relatively uniform distributed enclosures between the ice crystals.

In all five runs (except 1) the criteria to change from MD to SD proposed in Figure 1.122 can be used: The maximum of all measured average T_{ice} is written as (max. T_{ice}/n). Different steps to change from MD to SD can be related to max. T_{ice}/n, for example,

(max. T_{ice}/n) −1 °C = raise T_{sh} from $T_{sh,MD}$ to $T_{sh,SD}$;
(max. T_{ice}/n) −2 °C = terminate BTM and start DR measurements.

Depending on the slope of the T_{ice} plot, the change can be connected to −1.5 and 3 °C or both steps can be connected, for example, at −1.5 °C. The consequences of an earlier or later change are discussed below.

The secondary drying is governed by two factors: the temperature of the product and the binding energy of the water to the solid. The desorption rate DR is the tool to monitor its progress (see Section 1.2.3):

$$D = \mathrm{d}p \times V_{ch}/\mathrm{d}t \ (\mathrm{mbar\ L/s}) \tag{1.16}$$

where

V_{ch} = chamber volume (L)
$\mathrm{d}p$ = pressure increase (mbar)
$\mathrm{d}t$ = measuring time for pressure increase (s)

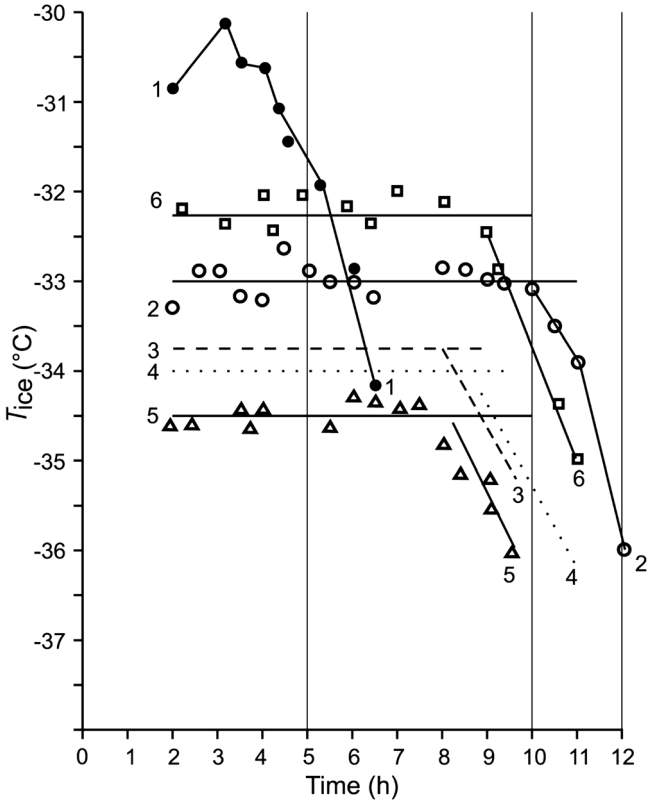

Figure 2.118 T_{ice} of a 10% saccharose solution as a function of MD time with different number of vials, freezing methods, and different T_{sh}, $d = 10$ mm, $p_c = 0.15$ mbar.

Run	Vials (No.)	Freezing method[a)]	T_{sh}[b)] (°C)	p_c[c)] (mbar)	T_{ice}[d)] (°C)	SA[e)] (°C)	t_{MD}[f)] (h)
1	300	W	+30	0.15	–	–	–
2	300	W	−5	0.15	−3.18	0.30	11.1
3	100	LN_2	0	0.15	−33.79	0.44	9.1
4	100	LN_2	0	0.15	−34.10	0.58	9.3
5	100	W	0	0.15	−34.54	0.36	9.15
6	400	W	0	0.15	−32.26	0.33	10.15

a) Freezing method: W, loaded on the shelf at room temperature, product cooled with the shelf; LN_2, frozen in liquid nitrogen.
b) T_{sh}, shelf temperature during MD.
c) p_c, controlled operation pressure.
d) T_{ice}, average.
e) SA, standard deviation of T_{ice}.
f) t_{MD}, drying time at which T_{ice} has reached (max. T_{ice}/n) − 1 °C; (max. T_{ice}/n) = maximum of all measured average T_{ice}. (Figure 1 from Ref. [24].)

$$DR = 2.89 \times 10^2 (V_{ch}/m_{solids})(dp/dt) \quad (1.16a)$$

(desorption of water vapor in % of solids per h)

with V_{ch}, dp, dt as in Eq. (1.16) and m_{solids} = mass of solids (g).

DR can be calculated from automatic pressure rise measurements similar to T_{ice}. During SD no time limit for the pressure rise exists, the product has to warm up close to T_{sh} anyway. The accuracy of the DR measurement depends on the reproducibility of the vacuum gauge and the amount of solids per chamber volume (see Eq. (1.16a)). As a rule of thumb, 1 g solid/L of chamber volume results in DR 0.1%/h ± 10%, if $dt = 60\,°C$. For the pressure rise time, 60–120 s is recommended depending on the product temperature and how well the rule 1 g/L is met (longer measuring time for ratios <1).

It has been shown in Figures 1.114, 1.115, and 1.133–1.135 how DR data not only document the desorption process but also reflect the product structure after freezing and during MD. Furthermore, the limits of DR measurements by the reproducibility of the capacitive vacuum gauge (CA) were discussed with those figures.

In Figure 2.118, T_{ice} of a 10% saccharose solution is shown. In Figure 2.119, DR data for the same runs are given. The data for run 1 are not connected by a line since they are from the partially collapsed product, which does not represent a desorption process but is a mixture of vacuum drying of water and some desorption of the collapsed product. This can be seen not only from the T_{ice} plot in Figure 2.118 but also from the fact that the water removal in run 1 of Figure 2.119 seems to be fast until 4%/h and rapidly becomes difficult thereafter. The runs in the table below Figure 2.119 are listed with increasing drying time, here defined as the time in which 1% residual moisture (dW) is reached. It can be seen that the sequence in Figure 2.119 does not immediately show the drying time for a desired dW. Only the integration of DR over time leads to dW, defined as water which could still be desorbed by further drying. dW is discussed later. The reasons for the sequence as shown by increasing total drying time have been chosen to show the different influences during MD and SD:

• MD:	T_{tot} (Eq. (1.12)) is smallest in runs 2 and 6: $1/T_{tot}$ ratio 1:0.9, ratio t_{MD} 1:0.9, governed by the heat transfer, in this example the vapor flow to the condenser was not a bottleneck.
• SD:	The heat conductivity in the dry material is the governing factor: in the fine structure produced by quick freezing in LN_2 the heat conductivity is a factor of ~2 smaller than in the slowly frozen product.
• Run 6:	The smaller T_{tot} and the larger temperature span for warming (from −5 °C instead of 0 °C to 20 °C at the beginning of SD) prolong the total drying time by 2–3 h.

This summary can also be seen in the graph: the DR data for the slowly frozen product in runs 5 and 6 are parallel as well as the LN_2 frozen products in runs 3 and 4; the plot of run 2 is closer to runs 5 and 6 but is a little delayed at the beginning as explained above.

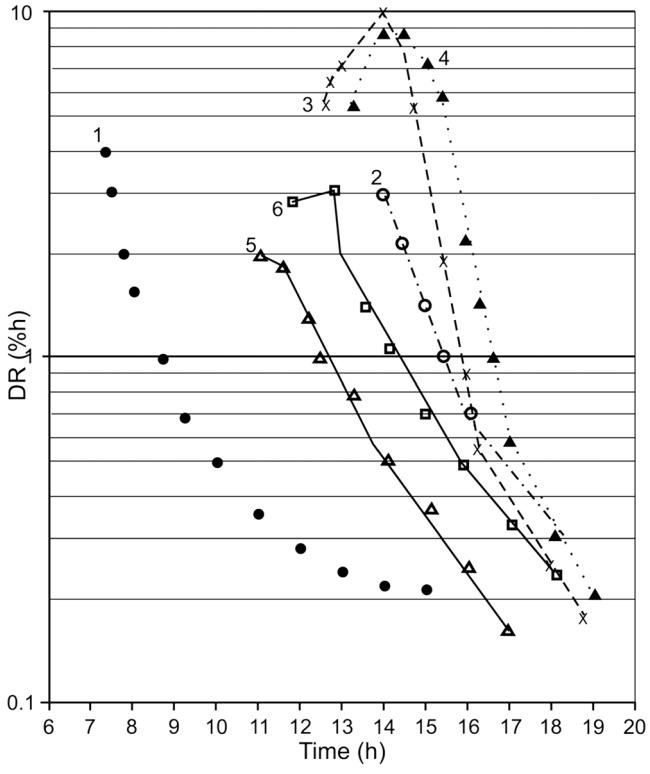

Figure 2.119 DR as a function of time for the same runs as in Figure 2.118. Some data for the runs are repeated below with additional new data.

Plot No.[a)]	Vials (No)	FM[b)]	T_{sh}[c)] (°C)	t_{MD}[d)] (h)	DR (%/h)[e)]		dW (%)[f)] 1	t_{+20}[g)] (h)	$v_{Tsh/20}$[h)] (°C/min)	t_{SD}[i)] (h)
					1.0	0.3				
6	400	W	0	10.15	14.3	17.6	14.6	12.9	0.12	4.45
5	100	W	0	9.15	12.5	13.9	15.0	12.4	0.10	5.85
3	100	LN_2	0	9.1	15.9	17.6	15.6	14.8	0.06	6.5
4	100	LN_2	0	9.3	16.4	18.2	16.1	15.8	0.07	6.8
2	300	W	−5	11.1	15.6	18.8	18.0	14.4	0.10	6.9

a) In Figure 2.118.
b) FM, freezing method: W, vials charged on shelves of room temperature and cooled with the shelf; LN_2, product frozen in vials cooled by LN_2.
c) T_{sh}, shelf temperature during main drying.
d) t_{MD}, as in Figure 2.118.
e) DR (%/h), time (h) in which 1.0 or 0.3%/h has been reached.
f) dW (%), time (h) in which the desorbable water content has reached 1%.
g) t_{+20}, time (h) in which T_{pr} has reached 20 °C.
h) $v_{Tsh/20}$, heating rate (°C/min) up to 20 °C.
i) t_{SD}, time (h) for SD.
(Figure 2 from Ref. [24].)

The increase in DR values during ~2 h after the change from MD to SD indicates that some ice was still present and sublimed during the increase in T_{sh}. Run 5 was switched over at about the optimum time, run 6 could have been changed from MD to SD 1–1.5 h and run 2~3 h earlier. To optimize the change, the recommendations given above regarding the decrease in T_{ice} at the end of MD compared with max. T_{ice}/n can be used.

Table 2.10 is a survey of 17 runs with 10% pure albumin or albumin + 0.9% NaCl solutions. The data show the following:

1) The operating pressure (p_c) influences T_{ice} mostly for the reason given above; it increases from $\simeq 38\,°C$ to $\simeq 25\,°C$ between 0.1 and 0.5 mbar. The standard deviations are between ~0.3 and ~ 0.6 °C. The average of all standard deviations is 0.45 °C.
2) The influence of the freezing method: the loading of the vials on C or W shelves influences the freezing rate (not shown) marginally: on precooled shelves (C), the rate was between 0.65 and 0.40 °C/min and on warm shelves (W) between 0.25 and 0.40 °C/min; with LN_2 30–65 °C/min have been reached. T_{ice} during MD is only measurably different for the product frozen in LN_2 (~1 °C higher than frozen on the shelves).
3) The influence of NaCl: the addition of 0.9% NaCl lowered T_{ice} by ~0.7 °C, standard deviation ~0.4 °C.
4) The differences between 100 and 400 vials per run: average T_{ice} for 100 vials is always lower than that for 400 vials. The amount of water vapor transported per unit time with 100 vials is smaller than with 400 vials, which requires a lower vapor pressure as shown by T_{ice}. The influence of the number of vials on T_{ice}, that is, the pressure necessary to transport the vapor is small provided that $s^{\#}$ is small compared with max. $s^{\#}$ (see Figure 1.142). This has two effects: (1) if T_{ice} has to be, for example, below −29 °C, 100 vials can be dried with the process data used, but with 400 vials p_c has to be lower, for example, by 0.1 mbar; (2) quickly frozen albumin (1604) needs a higher T_{ice} to transport the water vapor sublimed by the same heat transfer. The difference in T_{ice} can be adjusted by adjusting T_{ice}, that is, changing p_c accordingly.
5) The relative small differences in T_{ice} for this product by layer thickness, load, freezing methods, and additional ions should not be overlooked because of their consequences. The drying time proportional to d in the range between 8 and 20 mm and the influence of p_c is decisive for the freeze-drying process, but also the other factors are important as can be seen more clearly from the DR measurements during SD.

In Figure 2.120, six DR data are plotted from runs marked in Table 2.10. Plot 1 has the shortest t_{MD} since K_{tot} is highest at 0.5 mbar and T_{tot} is larger than in 2001. In plots 2 and 3 all data are very close, no difference due to C or W is found. Plot 4 is $d = 10$ mm, LN_2 frozen, plot 5 is (W) but $d = 20$ mm and plot 6 is LN_2 frozen and $d = 20$ mm. If the DR data are extrapolated to 0.02 mbar and integrated as described in Section 1.2.3 in connection with Eqs. (1.16) and (1.16a), the dW data can be calculated as shown in Figure 2.121; for clarity, plots 2 and 3 have been omitted.

Table 2.10 Survey of runs with 10% albumin and with albumin +0.9% NaCl solutions, filling height 10 mm, except those with italic numbers: 20 mm.

	p_c (mbar)(X)					
	0.1(C)	**0.1(W)**	**0.3 (C)**	**0.3 (W)**	**0.3(LN_2)**	**0.5(W)**
400 vials with albumin solution						
Run No.		0912	1612	1512		2001
T_{sh} (°C)[a)]		0	20.0	20.0		20.0
T_{ice} (°C)[b)]		−35.58	−28.90	−28.71		−24.86
SA (°C)[c)]		0.35	0.45	0.47		0.55
t (h)[d)]		10.3	5.5	5.8		5.3
400 vials with albumin + 0.9% NaCl solution						
	3001	2901		1401		
	20.0	20.0		20.0		
	−37.27	−36.73		−29.23		
	0.31	0.50		0.43		
	7.5	7.8		5.8		
100 vials with albumin						
			1712	0901/*0202*	1604/*2404*	1301
			20.0	20.0/20.0	20.0/20.0	20.0
			−29.49	−29.29/−29.96	−28.83/−28.87	−25.74
			0.64	0.59/0.32	0.51/0.30	0.45
			5.5	5.5/10.8	5.5/9.5	4.7
Plot No. in Figure 2.120		3	2/5	4/6	1	
100 vials with albumin + 0.9% NaCl solution						
	2301	2101		1901/*0302*		
	20.0	20.0		20.0/20.0		
	−37.96	−37.73		−30.01/−30.27		
	0.47	0.47		0.51/0.36		
	7.6	8.4		5.3/10.5		

p_c, operating pressure; (X) in parentheses indicates the method of freezing: (C) vials with product loaded on precooled shelves ($\simeq 50$ °C), (W) vials with product loaded on shelves of room temperature and cooled with the shelves, (LN_2) vials with product cooled by LN_2.

Source: Table 1 from Ref. [24].

a) T_{sh} (°C) shelf temperature during MD.
b) T_{ice} av. T_{ice} during t.
c) SA standard deviation during t.
d) t drying time after which T_{ice} has reached (max. T_{ice}/n) −1 °C.

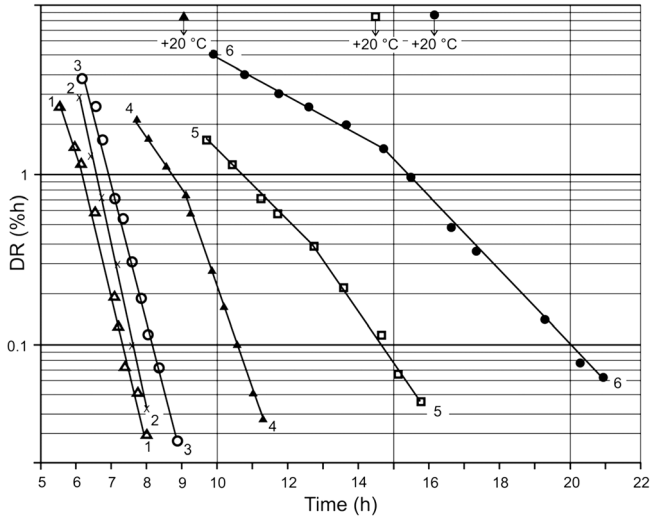

Figure 2.120 Desorption rates (DR) as a function of total drying time. Hundred vials filled with 10% albumin solution, with different freezing methods and different p_c and product thickness. Parameter: 1, 0.5 mbar (W); 2, 0.3 mbar (W); 3, 0.3 mbar (C); 4, 0.3 mbar (LN_2); 5, 0.3 mbar (W), 20 mm; 6, 0.3 mbar (LN_2), 20 mm. (From Ref. [25].)

From the plots one can draw the following conclusions for the drying processes:

1) In all studied processes with this product, dW = 0.1% can be reached.
2) The drying times (hours) at which the given dW data are achieved are as follows:

	Plot 1	Plot 4	Plot 5	Plot 6
At dW 2%	5.3	7.7	10.6	15.4
At dW 1%	5.6	8.4	11.6	16.9
At dW 0.4%	6.3	9.5	14.5	19.0
At dW 0.1%	6.9	11.0	15.1	22.0

The times double from plots 4 to 6 (10/20 mm) and more than double from plots 1 to 5 below dW 1% (influence of finer structure in plot 5 during desorption since 1 was dried at $T_{ice} = -25.7\,°C$ and 5 at $-30.0\,°C$).

Savage *et al.* [26] showed that an RM of <0.7% is necessary for a virus reduction on the order of 10^4 for hepatitis A virus, porcine parvovirus, and pseudorabies virus in freeze-dried factor VIII using dry heat for 72 h at 80 °C. In their opinion, the handling of a sample to determine RM by the Karl Fischer or the gravimetric method involves such a substantial risk of error that they developed a method to measure RM by near-infrared (NIR) spectroscopy (see Figures 1.155 and 1.156

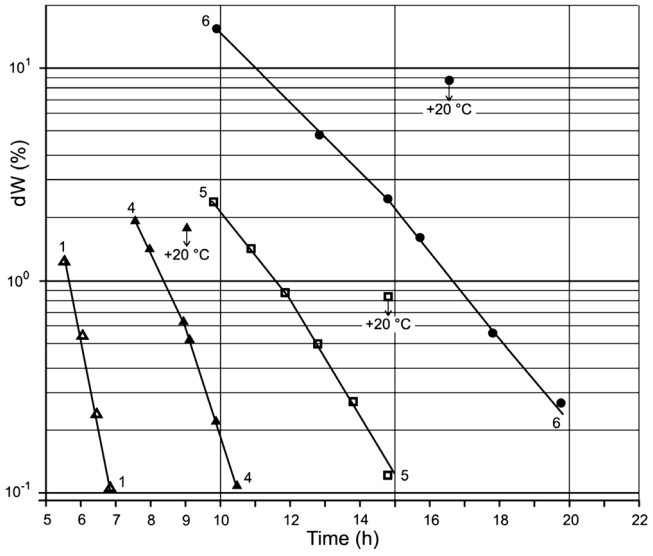

Figure 2.121 Residual moisture content (dW) as a function of time. Hundred vials with 10% albumin solution, with different p_c, different freezing methods and layer thickness as parameter. 1, 0.5 mbar (W); 4, 0.3 mbar (LN_2); 5, 0.3 mbar (W), 20 mm; 6, 0.3 mbar (LN_2), 20 mm. (Figure 5 from Ref. [25].)

and related text). The infrared beam penetrates the bottom of the vial and the reflected light is analyzed. The advantage of NIR is that theoretically the product in all vials manufactured can be measured and samples can be stored and checked again later. The main disadvantage of all the methods remain: the measurement has to be done after the freeze-drying process is terminated and the product unloaded. With TLC, the required RM determination can be done during SD. As shown in Figure 2.121, the RM in the product changes from 1.2 to 0.6% in 0.5–1.7 h. In general, short drying times make it difficult to achieve the desired RM range. Quick freezing (with thermal treatment), a low T_{ice} during MD (maintaining a fine structure), a reduced rate of temperature increase at the beginning of SD, a larger layer thickness, and short intervals between DR measurements (e.g., 6 min instead of 15 min) can increase the predictability of the dW data. The other prerequisite for such a process is the uniformity of RM in the vials as discussed in Section 1.2.1, Figure 1.104.

2.6.2.3 Measurement of the Residual Moisture Content (RM) during the Process

In Section 1.3.1, the various methods to determine the residual moisture content are described. In this section, the methods are analyzed to see how they can be applied in an automated process. In principle, three approaches can be used to determine RM:

1) With a stoppering device vials are closed during SD at certain intervals and analyzed for RM after the end of freeze-drying.

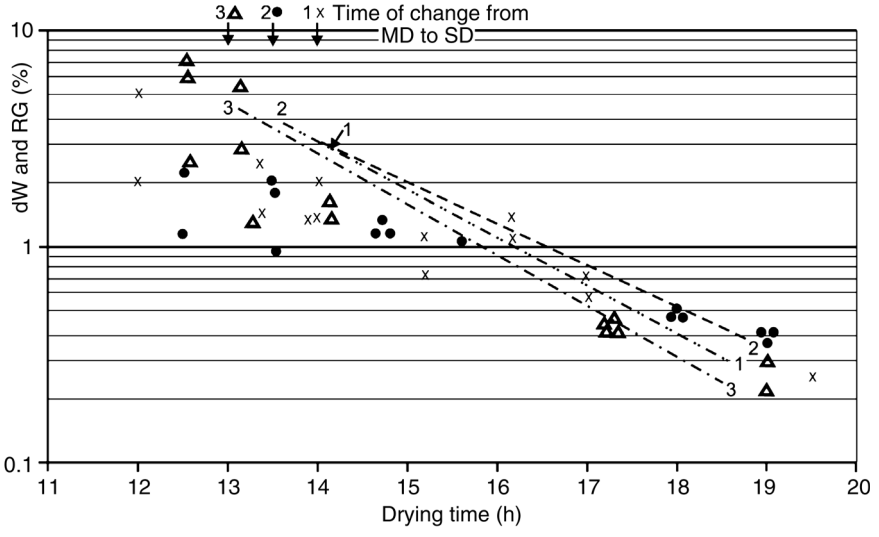

Figure 2.122 dW data calculated from DR measurement: runs 1, 2, and 3 dotted lines; compared with data from gravimetric measurements (RG): run 1, ×; run 2, •; run 3, ▲. For RG measurements, 10 vials were closed at the shown time and measured after the end of SD [25].

2) At the expected end of SD, pressure rise measurements are carried out; if dp/dt becomes $<X$ mbar/90 s, SD is terminated.
3) During SD, the desorption rates (DR) are repeatedly measured and the RMs are calculated by integrating DR over time.

Method 1 is carried out in a pilot plant and the result has to be transferred to the production unit. This transfer is complicated by the fact that RM data vary substantially from vial to vial during SD, as shown in Figure 2.122 for gravimetric measurements and published in Ref. [59] of Chapter 1 for the Karl Fischer method (Table 2.11). Method 2 provides an average value of the whole charge, but the time of the required dp/dt (dW) cannot be calculated, because dp/dt depends on the chamber volume and the solid content of the charge and the data cannot be extrapolated. It seems possible, of course, to relate a dp/dt value at a known product temperature to a measured RM value but the problem can be seen from Fig. 1.122. The three runs are carried out with the best possible identical data, presented in Figure 2.123.

Table 2.11 Mean water content (RF) in a 1 cm cake thickness of bovine somatotropin (BST) varies substantially at the end of MD and at the beginning of SD.

RF at 7.0% varies from 4 to 10%	(±3%)
RF at 3.2% varies from 2.2 to 4.2%	(±1%)
RF at 2.0% varies from 1.5 to 2.5%	(±0.5%)
RF at 1% the standard error is within drawing accuracy	(<0.1%)

Source: Data from Ref. [59] of Chapter 1.

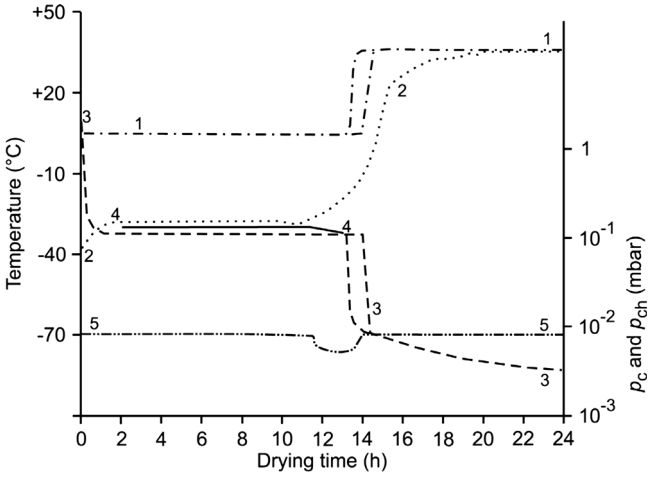

Figure 2.123 Process data for the three freeze-drying runs in Figure 2.122. 1, shelf temperature T_{sh}; 2, product temperature by sensors; 3, chamber pressure; 4, T_{ice} by BTM; 5, condenser temperature. Double lines for the same data indicate the maximum and minimum values measured. T_{ice} for the three runs, −34.99, −35.02, and −34.81 °C; average T_{ice} for the three runs: −34.94 °C, SD 0.11 °C. Freezing rates: run 1, 0.7; run 2, 0.65; run 3, 0.75 °C/min. (Figures 4 and 5 from Ref. [25].)

At 1% dW, the time difference between runs 3 and 1 is 45 min, at 0.5% 55 min; expressed differently: if run 3 had been terminated at 16.5 h, the time at which run 1 had RM 1%, run 3 is at 0.7%.

These data are from pilot plants with several hundred vials; in automated production plants with several tens of thousands of vials, one has to accept larger variations between charges: slightly different loading times resulting in different structures, larger differences in subcooling and freezing rates because of the larger number of vials involved and for the same reasons larger variations of drying rates. Method 3 documents and analyzes each run and provides the individual dW data for each run. The limit of all integral methods is the number of individuals required to change the result measurably or the number of 'error' vials that pass undetected.

For BTM and DR data, the undetected number of 'error' vials cannot be given as a percentage of the total number as it depends on the accuracy of T_{ice} and DR, on the ratio of chamber volume to solid content of the charge, and the individual magnitude of deviation from the average (see Section 1.2.3 and Figures 1.133 and 1.134). If the required dW is specified as, for example, <1.5%, the probability of 'error' vials is extremely small; if the specification requests, for example, 1.2%>dW>0.6%, the probability has to be evaluated; a ratio between solids (g) and chamber volume (V_{ch})>1,7 min intervals between DR measurements, 90 s pressure rise time, a relatively flat DR plot with time and shielding of the vials/product from wall and door influences can reduce the probability of undetected errors by a factor of 100 or more.

2.6.2.4 The Transfer of a Freeze-Drying Process from a Pilot to a Production Plant

The transfer of a freeze-drying process from a pilot to a production plant or from one production plant to another requires two sets of data: (1) the qualities of the

product before drying and of the dried product and (2) the performance of the pilot or the used plant and of the future production plant.

1) The critical qualities of the product and its packing discussed in this book are as follows:
   1.1. Type of vials and stoppers (Sections 1.3.2 and 1.2.4) to be used for the product, K_{tot} of these vials (Table 1.14 and Ref. [168] of Chapter 1 Section 1.2.1).
   1.2. Maximum temperature of the liquid product and maximum holding (loading) time at this temperature.
   1.3. Filling height of the vials [d in Eq. (1.12)].
   1.4. Required cooling rate and end temperature of freezing [28] of Chapter 1 in Section 1.1.4).
   1.5. Time and temperature of thermal treatment (Section 1.1.5, e.g., 1.1.5.3 and 1.1.5.4).
   1.6. $T_{g'}$, $T_{c,}$ proposed maximum T_{ice} should be, for example, ~3 °C below $T_{g'}$ or T_c. 3 °C results from 1 °C for accuracy of T_{ice}, 1 °C for accuracy of T_{sh}, and 1 °C as safety margin.
   1.7. Steps of change from MD to SD (maximum average T_{ice}/n) −1 °C; (maximum average T_{ice}/n) −2 °C (this section).
   1.8. Maximum tolerable temperature during SD, under vacuum (e.g., 50 °C) and at the end of SD before unloading (e.g., 25 °C).
   1.9. Operating pressure required during SD (Section 1.2.3).
   1.10. Range of dW in the dried product (e.g., <1.5% or 0.6–1.2%).
   1.11. Gas type and pressure during closing of vials by stoppers (e.g., N_2, dew point ≤50 °C; 400 mbar).
2) Performance data of the pilot plant or used one and the future production plant. The data used are examples selected from different actual operations to support some of the conclusions.

	Pilot plant	Production plant 1	Production plant 2
2.1. Chamber volume (L)	170	2000	14 000
2.2. Number of vials per charge	500	9000	70 000
2.3. Solid content per charge [Eq. (1.16b) and text thereafter] (g)	125	2250	17 500
2.4. Cooling and warming rate of the empty shelves (°C/min)	4	4	1.8
2.5. Lowest/highest shelf temperature (°C)	–60/60	–75/50	–75/50
2.6. Leak rate with cold condenser and warm shelves (Section 2.2.8) (mbar L/s)	2×10^{-4}	6×10^{-4}	6×10^{-3}
2.7. End temperature of condenser (°C) (Table 1.26, Section 1.2.3)	−70	≤90	≤90
	0.001	0.001	2×10^{-4}

(*continued*)

(*Continued*)

	Pilot plant	Production plant 1	Production plant 2
2.8. Total end pressure of vacuum pump set without condenser (mbar)			
2.9. Total end pressure of total plant (mbar) (see Table 1.26)	0.002	0.003	2×10^{-4}
2.10. Type of product shielding from walls, temperature of shielding at 2.5 data	as Figure 1.103 ±3 °C of 2.5 data		
2.11. Density of water vapor flow ($s^{\#}$) (g/h cm^2) at 0.2 mbar and at 0.06 mbar	7 0.8	9 1	9 1
2.12. Type of vacuum gauge		Capacitive	
2.13. Type of temperature measurement	BTM/ RTD	BTM/RTD	BTM/RTD

3) The transfer of the freeze-drying process of a product as per 1 from the pilot plant (PP) to production plant 1 (P1) or from production plant 1 (P1) to plant 2 (P2) is commented on as follows (the transfer from PP or P1 to P2 is called T1 and from PP or P1 to P2 is called T2):
   3.1. Vials and stoppers are identical, K_{tot} is measured in PP as 80 kJ/m^2 h °C at 0.1 mbar and 40 kJ/m^2 h °C at 0.06 mbar, no problem for T1 and T2.
   3.2. The loading time in PP is 10 min, in P1 ~1 h, in P2 7–8 h. If room temperature is acceptable for 10 h, no problem for transfer; if not so, the product has to be cooled, for example, to +5 °C.
   3.3. With identical d no problem for T1 and T2.
   3.4. The cooling rate in PP is 1 °C/min from 0 to −35 °C and the end temperature −55 °C. In P1 the cooling rates of the shelves (Section 2.6.2.4, point 2.4) are identical with PP, with identical vials and shelf surfaces in both plants T1 is possible. This does not apply to T2: In P2 the cooling rate is only 45% of PP. If 4 °C/min of shelves lead to 1 °C/min in the product, one has to expect a freezing rate of ~0.4–0.5 °C/min in P2. Besides the prolonged freezing time, the critical problem is the likely structural changes in the frozen product. If the cycle development in PP has not shown that the freezing rate can be 0.7 °C/min ± 0.3, but has to be 1 °C/min +0.2/−0, T2 is not possible. The reason for the slow cooling rate in P2 has to be analyzed and corrected or P2 cannot in the present form be used for the developed freeze-drying process.
   3.5. The heat treatment transferred from PP or P1 to P2 will most likely produce a product that behaves like an untreated one, may be more like a wrongly treated one: rewarming too slowly, end temperature of treatment not reached, cooling too slowly providing time for uncontrolled freeze concentration. For the further comments, it is assumed that the cooling rate of P2 shelves is adjusted.

3.6. Maximum T_{ice} is determined by methods as described in Section 1.1.5 and in 1.6 of this section as −40 °C, p_c in PP was 0.06 mbar and T_{sh} 0 °C. With $d = 14$ mm, t_{md} can be calculated by Eq. (1.12): $t_{MD} \sim 20$ h.

3.7. Load of the three plants:	PP	P1	P2
Number of vials	500	9000	70 000
Water content (kg)	3.8	68.4	532
Water/h (g/h)	190	3420	26 600
Maximum s (g/h cm^2)	0.8	1.0	1.0
Valve diameter (cm)	17	66	182
Solid content (g)	200	3600	28 000
Chamber volume (L)	170	2000	14 000

Consequences from 3.7:

1) T1 is possible if the valve in P1 has a diameter of ~70 cm or larger.
2) P2 would need a valve with a diameter of 1.8 m, which is technically not possible, even two valves of 1.2 m would not be sufficient, T2 is not possible (ratio g/L >1).
3) BTM and DR measurements are possible in PP and P1 (and also in P2).
4) In a plant with a valve diameter of 1.2 m, ~30 000 vials could be dried.
5) It is possible to place 60 000 vials in a plant called P3 with a valve diameter of 1.2 m if MD is prolonged from 20 to 40 h by reducing T_{sh} from 0 °C to −20 °C for most of MD. In this case T_{sh} has to be increased by an intermediate step of 0 °C. With $T_{sh} = -20$ °C, the temperature in the dried product cannot exceed −22 °C and it would take an unacceptable time to remove the rest of the ice under these conditions. During the change from MD to SD, T_{pr} should be $\simeq 5$ °C.

3.8. The difference of $s^{\#}$ in (2.11) indicates that the water vapor flow in P1 and P2 is more favorable than in PP. To operate at the same T_{ice} in P1 and P2 as in PP, the operating pressure p_c in P1 and P2 could be raised a little. This is not recommendable since the lower T_{ice} has two advantages: The product is dried at a lower T_{ice} (less molecule mobility) and MD is shorter: T_{ice} is lower, for example, −43 °C, T_{tot} rises from 40 to 43 °C, t_{MD} can be 7% shorter. If $s^{\#}$ in P1 and P2 were smaller, p_c has to be lowered, for example, to 4×10^{-2} mbar, and the maximum possible water vapor transportation through the valves has to be checked.

3.9. The change from MD to SD has been automatic in PP in one step: stop p_c and start $T_{sh,SD}$ at (max. av. T_{ice}/n) −1.5 °C. This can be transferred to P1 (and P2 or P3).

3.10. DR measurements with this product are possible down to 0.1%/h as shown in PP, which has a leak rate (LR) of 2×10^{-4} mbar L/s. DR = 0.1%/h corresponds in this example to $dp/dt = 3 \times 10^{-3}$ in 60 s. LR

corresponds to a dp/dt 1.6×10^{-3} mbar in 60 s. LR contributes in the same time 7×10^{-3} mbar. The pressure rise measured under these conditions (DR′) represents 2/3 DR and 1/3 LR or DR is 1/3 smaller than DR′. This error is reduced to 10% at DR ~0.5%/h. If these DR data are inserted in Figure 1.133, one can see that dW <1.5% can be well determined with these data. If 0.6–1.2% is required, LR should be $\sim 0.5 \times 10^{-4}$ mbar L/s or the LR influence has to be deducted from the measured DR′. For P1 dp/dt due to LR in 60 s is only 15% of PP data, whereas dp/dt due to DR in 60 s is ~10 times larger. Therefore, the DR will theoretically be measurable well below 0.01%/h, theoretically because other influences may limit the accuracy, for example, partially unfrozen water and or freeze-concentrated inclusions (see, for example, Figure 1.115). T1 is possible with no problems, T2 is possible with changes of the cooling rates of the shelves.

3.11. dW calculation in P1 is possible for the reasons given for DR.

3.12. The total end pressure (point 2.9 above) of the plants PP, P1, and/or P2 is low and both condensers cold enough to achieve RM ~1% at T_{pr} 20 °C and <0.5% at 40 °C, if the product has adsorption isotherms as shown in Figure 1.137. The vapor transportation during SD is no problem, the amount of vapor is less than 1% of the vapor transported during MD at a pressure of 10% of MD.

The transfer of process data from the pilot plant to the production plant 1 is possible, if the remarks above are taken into account, the transfer to production plant 2 is not possible: The possible vapor flow is not sufficient at the necessary pressure for the amount of ice sublimed under the conditions operated in the pilot plant. Theoretically, a plant with two valves of 1.2 m diameter each could handle 60 000 vials in the process developed by the pilot plant or a plant with one valve and double MD is feasible.

2.6.2.5 Summary of Prerequisites, Limits, and Suggestions for Automated Thermodynamic Lyophilization Control

1) An adjustable rate of brine circulation in the shelves could be necessary (especially for smaller plants) to obtain a measurable temperature difference (dT) between inlet and outlet during freezing; dt should not be too large (uniform freezing), a maximum of 3–4 °C (see Figure 2.114) is a practical range.
2) A valve between chamber and condenser that closes reproducibly and seals the condenser from the chamber with a leak rate that is small compared with LR of the total chamber.
3) A limited and measured leak rate of the chamber.
4) A minimum amount of solids per chamber volume.
5) Pressure measurements by capacitive vacuum gauges.
6) A water vapor flow from the chamber to the condenser larger than the vapor sublimed from the ice.
7) Single-valued desorption rates.
8) Thermal stable products at $T_{sh,SD}$.

9) A minimum product temperature and a maximum pressure to obtain a desired residual moisture content at the end of secondary drying.

Critical data measured by two or more independent sensors, for example,

- Inlet and outlet temperature of the heat transfer fluid on each shelf (or group of shelves) and on all shelves in total.
- Pressure in the chamber, in the condenser after the last condenser surface and before the pump set.
- Outlet temperature of the condenser refrigerant of each group of coils or plates and temperatures on the surface of coils or plates near the inlet of the refrigerant.

References

1 Yokota, T. (1989) A continuous method for freezing droplets by a wetted-wall column in freeze-drying. *Kagaku Kogaku Ronbashi*, **15**, 877–880.
2 Rhambahatla, S., Ramot, R., Bhugra, C., and Pikal, MJ. (2004) Heat and mass transfer scale-up issues during freeze-drying: II. Control and characterization of the degree of super-cooling. *AAPS Pharm. Sci. Technol.*, **5** (4), e58.
3 Gieseler, H. (2007) PAT for freeze-drying cycle optimization in the laboratory. *Euro. Pharm. Review*, **1**, 62–67.
4 Rolfgaard, J. (1987) *Industrial Freeze-Drying for the Food and Coffee Industry*, Atlas Industries, Ballerup, Denmark.
5 Rey, L. (2002) Optimizing lyophilization of biopharmaceuticals. *Genet. Eng. Use*, **22** (1), 1–6.
6 Heldner, M., Steinkamp, H., and Spreckelmeyer, J. (2000) Einsatz von neuen Kältemitteln und der LN_2-Technik bei Lyophilisationsanlagen. APV-Symposium, Bonn, September 2000.
7 Willemer, H. (1995) Freeze-drying plants with modern refrigerants including liquid nitrogen. 1st World Meeting of APGI/APV Arbeitsgemeinschaft für Pharmazeutische Verfahrenstechnik, Budapest, May 1995.
8 Snowman, J.W. (1994) Replacement of conventional refrigeration systems in freeze-drying by liquid nitrogen cooled systems. PDA Asian Symposium, Tokyo, pp. 329–345.
9 Cully, R. (1994) *Refrigerants, the Environment and the Liquid Nitrogen Option*, International Society of Pharmaceutical Engineering (ISPE), Antwerp.
10 Haseley, P., Spreckelmeyer, J., and Steinkamp, H. (1997) Betriebsbedingungen in Gefriertrocknungsanlagen bei Einsatz von Schrauben- und Hubkolbenverdichtern. DKV, pp. 155–170.
11 Guide to Inspections of Lyophilization of Parenterals. US Food and Drug Administration, Washington, DC, July 1993.
12 The Parenteral Society (2006) Integrity Testing of Freeze-Dryer Inlet Filters. Technical Monograph No. 8.
13 Jaenchen, R. and Malsy, J. (1992) Analysis of water penetration through hydrophobic filters as a method of integrity testing. Pall Corporation, Dreieich.
14 Bracht, K. and Troger, H. (1991) The water intrusion test – a new method for integrity testing hydrophobic filter elements. Sartorius, Göttingen.

15 Wutz, M., Adam, H., and Walcher, W. (1982) *Theorie und Praxis der Vakuumtechnik*, vol. 2, Vieweg, Wiesbaden.
16 (a) Poulter, K.F. *et al.* (1983) Thermal transpiration with thermostatic capacitive manometers *Vacuum*, **33**, 311. (b) Jitschin, W. and Röhl, P.I. (1987) Thermal transpiration with thermostatic capacitive manometers. *Vac. Sci. Technol.*, **5** (3).
17 Chase, D.R. (1998) Monitoring and control of the lyophilization process using a mass flow controller. *Pharm. Eng.*, **1998**, 92–98.
18 Nakahira, K. (1994) Validation of deep vacuum vapor phase hydrogen peroxide sterilizer retrofit to a production lyophilizer. PDA Asian Symposium, Tokyo, pp. 1/6–6/6.
19 Steiner, R. (1994) VHP(sterilisation of freeze-dryers. International Society of Pharmaceutical Engineering (ISPE) Seminar on Lyophilisation, Antwerp, November 1994.
20 Oetjen, G.W. and Eilenberg, H.J. (1969) Heat transfer during freeze-drying with moved particles. International Institute of Refrigeration (Comm. X, Lausanne), pp. 19–35.
21 Oetjen, G.W. (1971) Continuous freeze-drying of granulates with drying time in the 5–10 minutes range, International Institute of Refrigeration (XIII Congress, Washington, DC), pp. 697–706.
22 Oetjen, G.W. (1969) Freeze-drying processes and equipment. XVIII Congresso Nationale del Freddo, Padua, June 1969.
23 Haseley, P. and Oetjen, G.W. (1998) Equipment data, thermodynamic measurements and in-process quality control during freeze drying. PDA International Congress, Basel, pp. 139–150.
24 Haseley, P. and Oetjen, G.W. (1998) Some influences on the thermodynamic data during freezing and freeze drying of a model substance. 10th Annual A3P Congress, Bordeaux, October 1998.
25 Haseley, P. and Oetjen, G.W. (1998) Opportunities and limitations of control of freeze drying by thermodynamic data from the process: freeze drying of pharmaceuticals and biologicals. Center for Pharmaceutical Processing Research in cooperation with Purdue University and the University of Connecticut, USA.
26 Savage, M., Torres, J., Franks, L., Masecar, B., and Hotta, J. (1998) Determination of adequate moisture content for efficient dryheat viral inactivation in lyophilized factor VIII by loss on drying and by near infrared spectroscopy. *Biologicals*, **26** (2), 119–124.

Further Reading

Austar Co. LTD., Beijing P.R. China; www.austar.com.hk.
EU Regulation (EG) No. 842/2006.
EU Regulation No. 517/2014 from January 2015.
GAMP Registered Trade Mark ISPE.
Gaster, A.J. (1994) In place cleaning systems for freeze dryers. PDA Asian Symposium, Tokyo, pp. 289–293.

GEA Lyophil GmbH, D-50354 Huerth, Germany; www.geapharmasystems.com.
Gieseler, H. (2009) The freezing stage in freeze-drying: fundamentals concepts. SP Scientific LyoLeam Webinar.
Haseley, P. (1994) New cooling and sterilization technology in freeze-dryers and a comparison of operating costs. PDA Asian Symposium, Tokyo, pp. 305–317.
Haseley, P., Spreckelmeyer, J., and Steinkamp, H. (1997) Operating conditions in freeze-dryers when using screw and piston compressors. Deutsche Kälte-Klima-Tagung, Hamburg.
Haseley, P. and Oetjen, G.W. (1998) Equipment data, thermodynamic measurements, and in-process control quality control during freeze-drying (Fig. 4). PDA International Congress, Basel, pp. 139–150.
ISO Standards – International Organization for Standardization (EN/ISO).
ISPE – GAMP, Good Automated Manufacturing Practice.
Leybold AG, D-50968 Cologne, Catalogue HV 300, Part A 11, p. 29.
Metall+Plastik GmbH, Cleanroom Technology, D-78315 Radolfzell, Germany.
Searles, JA., Carpenter, T., and Randolph, TW. (2001) The nucleation temperature determines the primary drying rate of lyophilization for samples frozen on a temperature controlled shelf. *J. Pharm. Sci.*, **90**, 860–871.
Sever, R. (2010) Controlling nucleation in lyophilization: effects of process and product. CPRR Freeze-Drying of Pharmaceuticals and Biological Conference, October 2010.
STERIS Corp., Mentor, OH.
STERIS GmbH, D-50933 Cologne, Germany.
The Parenteral Society (1994) Sterilization of Freeze-Dryers. Technical Monograph No. 5, Swindon (European Standards EN 556-1; EN 1441; EN 550; EN 552; EN 554).

3

Pharmaceutical, Biological, and Medical Products

The freeze-drying of pharmaceutical, biological, and medical products has been performed for one or more of the following reasons: the ingredients of the formulation are not stable in the liquid state and other methods of water removal destroy or reduce the active ingredient; the amount of the active ingredient is very small; the dosing of liquids is safer to control than that of a powder; sterilization of the vials before filling and filling into the final container minimizes handling and reduces possible contamination; and the desired structure of the product can only be achieved by solidifying it and removing the solvent in this phase.

3.1 Proteins and Hormones

Schiffter [1] deals with the importance of proteins and peptides for the human organism. Proteins and peptides are the drugs of the future. During the freeze-drying process, there are critical steps that must be followed. During the precooling and freezing phase, the "cold denaturation" (hydration) and thus the solubility of nonpolar groups within the protein structure increase with decreasing temperature. The weakening of the hydrophobic interaction leads to denaturation and increase of the concentration and viscosity of dissolved constituents of the formulation during the crystallization of ice → "ph-shift" by the crystallization of buffer components; that is: phase separation (liquid–liquid) within the unfrozen phases (very frequently observed in PEG:Dextrose; PVP: Dextrose, or PVP:Ficoll formulations) → formation of ice–water interfaces and thereby surface-induced denaturation.

Critical process steps during primary drying (Figure 3.1)*:* A large portion of the water is already separated during freezing from the protein base. In aqueous solution, proteins are fully hydrated, so the surface of the protein is coated with a monolayer of water (approximately 0.25–0.35 g/g protein).

Jiang and Nail [2] studied the effect of process conditions on the recovery of protein activity in the absence of protective agents after freezing and freeze-drying. Catalase, β-galactosidase (GS), and lactate dehydrogenase (LDH) showed a loss of activity after freezing with a higher recovery at higher concentrations. Sodium phosphate buffer and cooling in LN_2 resulted in the lowest recovery. Only

Freeze-Drying, Third Edition. Peter Haseley and Georg-Wilhelm Oetjen.

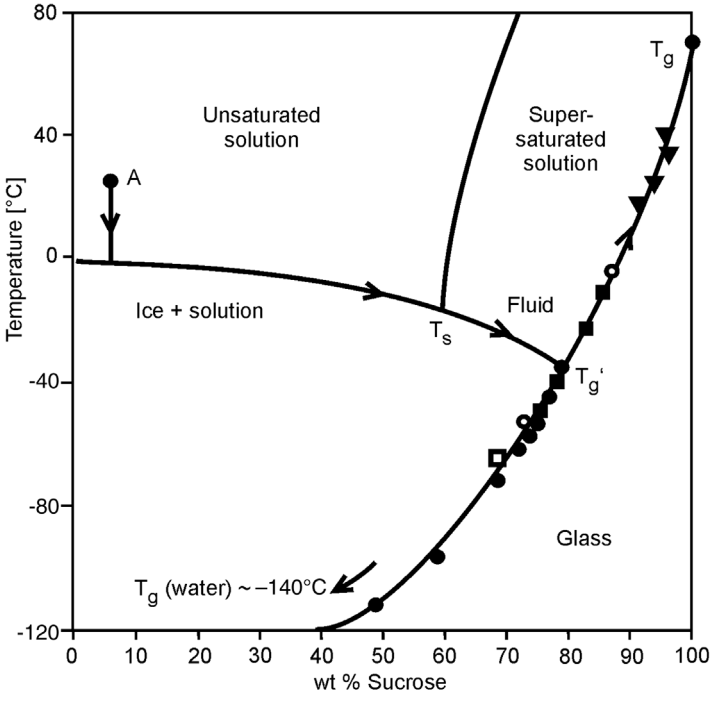

Figure 3.1 The stability of proteins during the freezing and primary drying phase.

for GS was T'_g observed as indicative for T_c, otherwise the apparent glass transition did not correlate with T_c (cryomicroscope). Freeze-drying was carried out under conditions with retention or collapse of the structure. Recovery of activity decreased continuously during MD without a sharp drop at T_c. The recovery dropped at RM >10%.

With the exception of Ref. [3], all products described in this chapter make use of lyoprotectants. Carpenter *et al.* [4] showed that the protection of the native structure of proteins requires two different mechanisms during freezing and freeze-drying. Phosphofructokinase (PFK) was chosen as a model substance, because it is irreversible denatured during freezing and thawing. During freezing, the best substances to minimize denaturation have higher repellent than attractive forces between the protein and excipient. A 3 M NaCl solution destabilizes the activity of PFK by 80%, whereas a 1 M polyethylene glycol (molecular weight 600) solution protects the activity completely. During freeze-drying and in the dry state, only such carbohydrates that can be bound to the protein molecule by replacing water molecules and thereby forming hydrogen bonds with the protein prevent a loss of activity. This basic understanding has been studied and discussed in recent years in many publications: the influence of amorphous or crystalline structure, the consequences of it on storage stability, and many details for specific products.

Craig *et al.* [5] define ›frozen into the glassy state‹ when the bonding between molecules remains essentially the same as that of a liquid, but the translational

and rotational motion of the molecules practically disappear below the transition temperature T_g, leaving only vibrational motion. This event changes the heat capacity c_p without heat transfer during the process. This is called a second-order phase transition, while, for example, crystallization is of first order. As a second-order transition, it should be independent of the cooling rate used. This is not the case, making the argument incomplete. The authors explain how the inclusion of the ›configurational entropy‹ and the consideration of the relaxation times of the cooling process can explain the cooling rate dependence of T_g. The viscosity η at T_g can be in the range of 10^{12}–10^{14} Pa s. The viscosity of glass-forming systems and the relaxation time can be calculated (Eqs. (1) and (3) in Ref. [5]), allowing some prediction of their behavior as a function of time. The methods to measure T_g are described in Section 1.1.5. The remark of the authors that T_c can be expected, for most cases, to be ~20 °C above T'_g is misleading, as shown in Section 1.1.5 (Ref. [156] of Chapter 1) and the same applies to the ›ideal secondary drying protocol to follow the T_g increase in the sample‹ (see Section 1.2.2).

Hatley and Blair [6] presented mean T_g data for anhydrous carbohydrates (Table 3.1), which vary in the literature owing to measurement and interpretation differences. Small amounts of water may depress the data substantially. The physical stability of amorphous formulations below T_g is generally accepted, and a collapse can be avoided. This does not always apply to the chemical stability. If the temperature is reduced below T_g, the configurational entropy diminishes until it reaches zero. This T_0 (also shown in Table 3.1) is called the zero mobility temperature at which the molecular motion stops. The authors define three areas of chemical reactions: above T_g, chemical reactions are generally possible; at T_g, reactions such as aggregation, which require substantial molecular motion, stop; and between T_g and T_0, reactions involving only small molecules, for example, oxidation and hydrolysis, may proceed at low rates. Below T_0, no reactions are possible.

Table 3.1 T_g values for glass-forming anhydrous carbohydrates (they vary in the literature owing to measurement and interpretation differences) (part of Table 1 in Ref. [6]).

Glass former	T_g (°C)	T_0 (°C)
Trehalose	120	44
Dextran	83	
Sucrose	77	3.5
Lactose	70	
Maltose	44	
Glucose	30	
Fructose	13	
Sorbitol	−2	
Glycerol	−93	

T_0 Zero mobility temperature (see text).

To summarize, the development of a maximum storage time and temperature for an amorphous product by accelerated temperature tests is very complex; even with the actual temperatures several conditions have to be considered, as follows: Crystallization above T_g is an event depending on time, $T–T_g$, heating rate, and RM; 2–3% RM may, for example, reduce T_g of sucrose to a range from 28 to 40 °C; the influence of $T - T_g$ is not linear, but follows an equation similar to Eq. (3) in Ref. [5]; the heating rate during storage may not be 1 °C/min but a few °C per day or week (almost equilibrium conditions), resulting in crystallization close to T_g.

Remmele *et al.* [7] studied with infrared spectroscopy the structure–hydration behavior of a 49.4 mg/mL lysozyme D_2O solution with and without 10% sucrose. The sample was cooled in the measuring chamber to −100 °C and then connected to a freeze-drying installation, after which the temperature of the sample was raised to +40 °C. Table 3.2 summarizes the freeze-drying process and the observations made.

From the form and the peak location of the O–D stretch band in the spectra, it is concluded that the main drying is completed at −10 °C; between −13 and −10 °C a combination of main and secondary drying has occurred. T'_g for sucrose is reported as −40 °C [8] and as −32 °C [9] and T_c as −37.7 °C (Ref. [156] of Chapter 1). All three temperatures were exceeded long before the main drying was completed and the product collapsed, as confirmed by the appearance of the product and the very slow secondary drying. During a second test, the temperature was kept below T'_g. The residual moisture of the second run was 4% instead of 7% in the first test. From the changes in the protein band, it was concluded that sucrose had substituted for water by hydrogen bonding.

Pikal [10] also suggested that the mechanism of protection of proteins is different during freezing and drying. For the selection of CPAs, Pikal recommends that three points be observed:

- CPAs should, at least partially, solidify in the amorphous state. However, an amorphous state alone does not ensure protection. Izutsu *et al.* [11] showed for

Table 3.2 Freeze-drying of a 49.5 mg/mL lysozyme D_2O solution.

Time (h)	Duration (h)	Temperature (°C)	Observation
0–2.4		−100 to −45	
2.4–3.9	1.5	−45	D_2O crystal growth
3.9–4.9	1.0	−45 to −24	Sublimation of ice
4.9–5.2	0.3	−24 to −13	Decreasing sublimation of ice, remaining structure: amorphous
5.2–10.5	5.3	−13 to −10	Substantial loss of water
10.5–17.5	7.0	−10 to +18	Ice completely removed
17.5–18.4	0.9	+18 to +20	Noticeable loss of water
18.4–26.6	8.2	+20 to +27	Noticeable loss of water
26.6–46.0	9.4	+27 to +40	End of drying

β-galactosidase by X-ray diffraction that only additives that do not crystallize avoid denaturation. Dilution of protein in the solidified protective agent reduces the chance of reactions between the protein molecules. Amorphous substances dry more slowly, which makes it easier to avoid overdrying.
- T_g should be chosen as high as possible and RM should be small, since high RM reduces T_g.
- Buffer substances or other salts should be used at the lowest possible concentrations, since they may partially crystallize (changes of pH value) and they will mostly reduce T_g.

De Luca [12] recommends, furthermore, the addition of, for example, *tert*-butyl alcohol (TBA) to increase the transport of water vapor out of the product and to avoid collapse in sucrose, lactose, and sorbitol solutions. Thus, higher temperatures during drying (e.g., for hemoglobin in sucrose solution) can be applied.

Skrabanja *et al.* [9] do not accept a combination of 12 different excipients, for example, for erythropoietin, as the efficacy of each component cannot be proven. The mostly frequently used excipients are listed in five groups:

1) *Protein:* human serum albumin, gelatin
2) *Amino acids:* glycine, arginine, alanine
3) *Alcohols:* mannitol, PEG (polyethylene glycol)
4) *Carbohydrates:*
   - monosaccharides: glucose, fructose
   - disaccharides: lactose, maltose, sucrose, trehalose
   - polysaccharides: dextran, HP-β-CD.
5) *Other:*
   - metals
   - surfactants
   - polymers
   - buffer salts.

Quick cooling is often advantageous, for example, for recombinant DANN-proteins, in order to avoid crystallization of salts and to obtain the best possible, homogeneous cake.

Figure 3.2 shows the influence of different freezing methods on the activity of a recombinant DNA protein. However, in the case of other macromolecules, for example, a monoclonal antibody, there may be exceptions from the rule and different factors (e.g., pH value) play an important role.

Jiang and Nail [13] showed in a detailed study the various influences during freezing and freeze-drying on the recovery of activities of catalase (CA), β-galactosidase (GS), and lactate dehydrogenase (LDH): concentration of the protein, freezing method, type of buffer, event of collapse, and, most important, residual moisture content (RM). In Table 3.3, T'_g and T_c are compared for the three solutions and the recovery of protein activity after freeze-drying is given. In Figure 3.3, the activity recovery versus LDH concentration with three buffer systems as parameter is plotted after freezing in a freezer down to −40 °C. No loss of protein due to adsorption on the container walls was found for all three products. The dependence of recovery on concentration and the buffer selection is most pronounced in LDH.

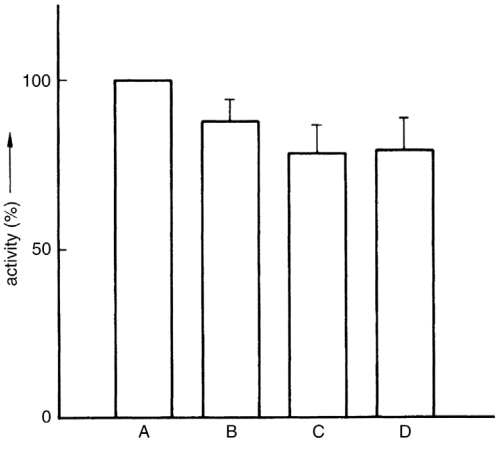

Figure 3.2 Influence of different freezing processes on the activity of recombinant DNA protein. A: solution before freezing; B: freeze-dried after quick freezing; C: freeze-dried after freezing on precooled shelves; D: freeze-dried after cooling shelves and product simultaneously. (Figure 1 from Ref. [9].)

Figure 3.4 shows the dependence of the recovery of activity on the freezing method and the protein concentration for LDH in phosphate buffer. The highest LDH concentration and freezing in a freezer preserve the activity best. The activity recovery of LDH after freeze-drying versus LDH concentration is plotted in Figure 3.5. The freeze-drying cycle was 6 h freezing at −45 °C, drying for 24 h at −30 °C and at 25 °C for 4 h, and pressure throughout the total cycle $\sim 9 \times 10^{-2}$ mbar. The data represent the loss during drying only (freezing effect is deducted). Figure 3.6 presents the loss of LDH activity during freeze-drying with a shelf

Table 3.3 Comparison of T'_g and T_c for three protein solutions (Table 1 from Ref. [13]) and recovery of protein activity after freeze-drying (%) (Table 2 from Ref. [13]).

Protein	T'_g (°C)	T_c (°C)	Structure retention (%)[a)]	Collapse (%)[b)]
CA	−29	−15	92	88
GS	−28	−29	95	85
LDH	None detected	−28	95	50

a) Freeze-drying conditions resulting in retention of microstructure.
b) Freeze-drying conditions produce collapse: T_{sh} −10 °C, p_c high enough to produce total collapse.

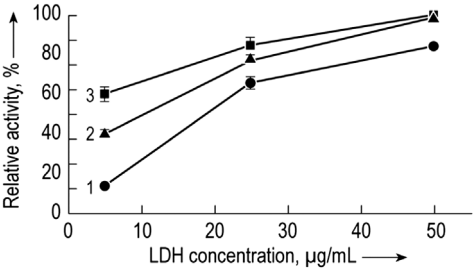

Figure 3.3 Activity recovery versus concentration of LDH after freezing in a freezer at −40 °C for 20 h and thawing at room temperature in different buffer solutions: (1) 0.05 M sodium phosphate, pH 7.4; (2) 0.050 M citrate, pH 7.4; (3) 0.05 M Tris, pH 7.4. (From Jiang, 1998 [13]. Reproduced with permission of Elsevier.)

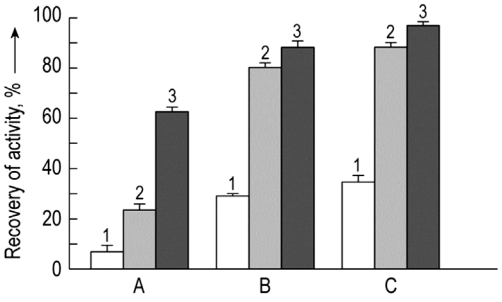

Figure 3.4 Activity recovery of LDH after freezing by three methods: A, cooled in LN_2 and transferred to a −40 °C freezer; B, frozen on the shelves of the freeze-drier ramped from 25 to −40 °C at 0.5 °C/min; C, placed in a freezer at −40 °C. LDH concentration: (1) 5; (2) 25; (3) 50 µg/mL. (From Jiang, 1998 [13]. Reproduced with permission of Elsevier.)

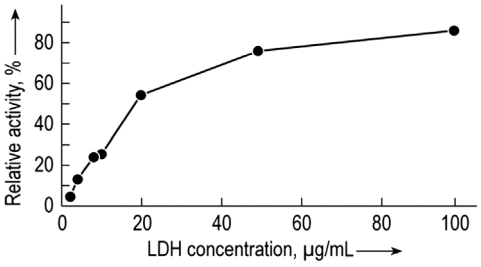

Figure 3.5 Activity recovery of LDH after freeze-drying versus LDH concentration. (From Jiang, 1998 [13]. Reproduced with permission of Elsevier.)

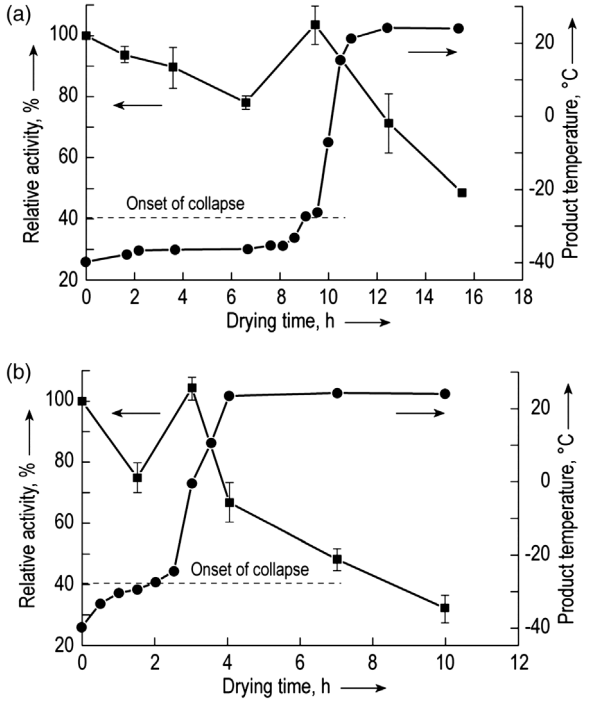

Figure 3.6 (a) Activity loss during freeze-drying versus drying time with $T_{sh} = -30$ °C. (b) As part (a), but $T_{sh} = 25$ °C. (From Jiang, 1998 [13]. Reproduced with permission of Elsevier.)

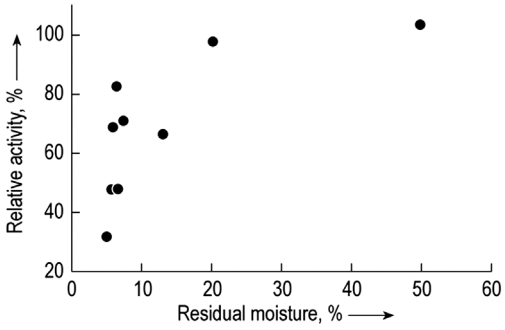

Figure 3.7 Activity recovery of LDH versus residual moisture content. (From Jiang, 1998 [13]. Reproduced with permission of Elsevier.)

temperature of (a) −30 and (b) 25 °C. The activity loss in Figure 3.6a at 6 h and in Figure 3.6b at 1 h is attributed by the authors to the interruption of the drying process at that time to remove vials for analysis. The final recovery at the end of drying is ~50 and 30%, respectively, with a decrease from 100% during secondary drying. Table 3.3 shows a similar result for LDH but not for the other two enzymes. Figure 3.7 shows the recovery of the activity of LDH as a function of the residual moisture content.

The work of Jiang and Nail is described here in some detail because it quantifies the effects of freezing and freeze-drying on proteins systematically without the influence of cryo- and lyoprotectants. Some data, for example, Figure 3.4, may need additional information: Immersion in LN_2 can result in very nonuniform freezing rates in one vial and between different vials; the transfer to −40 °C is equal to a thermal treatment at that temperature for an undefined time span allowing freeze concentration in a nonuniform structure. The differences between columns B and C in Figure 3.4 can be related to spontaneous crystallization in B (as the authors indicate) and/or in freeze concentration in B. Similar questions can be raised with respect to Figure 3.6, where the relative activity at the end of drying is ~47% in part (a) and ~32% in part (b) but ~70% if $T_{sh} = 0$ °C (not shown). The activity depends strongly on RM (Figure 3.7): Are the RMs at the end of drying in Figure 3.6 comparable?

Ru *et al.* [14] described the effect of lyophilization on salt-induced activation of enzymes in organic solvents. Amounts of 50 mg of subtilisin Carlsberg (SC), 50 mg of K_2HPO_4, and 4.9 g of KCl were dissolved in 200 mL of nanopure H_2O, frozen in LN_2 and freeze-dried at a pressure of ~0.25 mbar and $T_{co} = -50$ °C (T_{sh} unknown). Samples were removed at different time intervals for measurement of RM by the Karl Fischer method; average of eight independent measurements were used. Kinetic parameters for transesterification in hexane, for example, as a function of RM show a maximum between 5.5 and 7% RM. The presented function of the drying time may be a function of RM, including the fact that the maxima decreases rapidly (e.g., by 50%) with a decrease in RM of only 1–2%.

As shown in Table 3.4, the selection of the excipient also defines T'_g and the amount of unfreezable water (UFW) in the glass phase.

The data for a mixture of two or more excipients cannot be calculated from the individual data, as shown in Figure 3.8 for a sucrose–citrate solution. This can also be seen in Figure 3.9: The pure solution (without factor VIII) (part (a)) would have

Table 3.4 T'_g and UFW of some excipients.

Excipient	T'_g (°C)	UFW (%)
Sucrose	−32, −33.6[a)]	35.9
Maltose	−30	20
Lactose	−28, −29.7[a)]	40.8
Trehalose	−30	16.7
Fructose	−42	49.0
Glucose	−43	29.1
Glycerol	−65	45.9
Sorbitol	−43	18.7
Dextran	−9	
P beta CD	−8	
Albumin	−10	
PVP	−19,5, −21.1[a)]	
PEG	−13	
Sodium citrate–citric acid	−40	
Na_2PO_4–KH_2PO_4 (1:1)	−80	

a) Data from Ref. [174] of Chapter 1.

to be dried, according to the plot of d(log R)/dt, below −50 °C, while the solution with factor VIII (part (b)) (following the same rule) could be dried at −43 °C (the minimum of the plot d(log R)/dt shifts by almost 10 °C). Figure 3.10 shows three factor VIII solutions with different excipients: Identical resistance data are found at −55, −51, and −35 °C. Allison *et al.* [15] proposed a combination of disaccharides and dextran to gain the advantages of both: The disaccharides preserve the native conformation of a dried protein but may result in a low T_g; high-molecular-weight carbohydrates, for example, dextran, have a high T_g but fail to preserve the native protein conformation. The combination was tested with actin. During storage of actin formulations containing sucrose, trehalose, or dextran

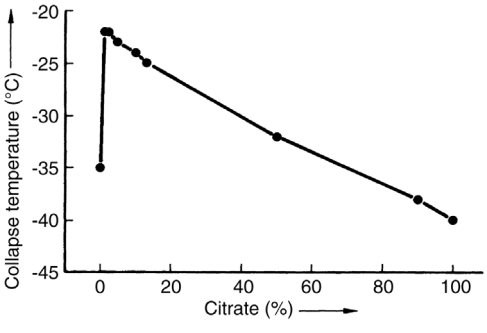

Figure 3.8 Collapse temperature of a sucrose solution as a function of added citrate solution (%). (See also Figure 3 from Ref. [9].)

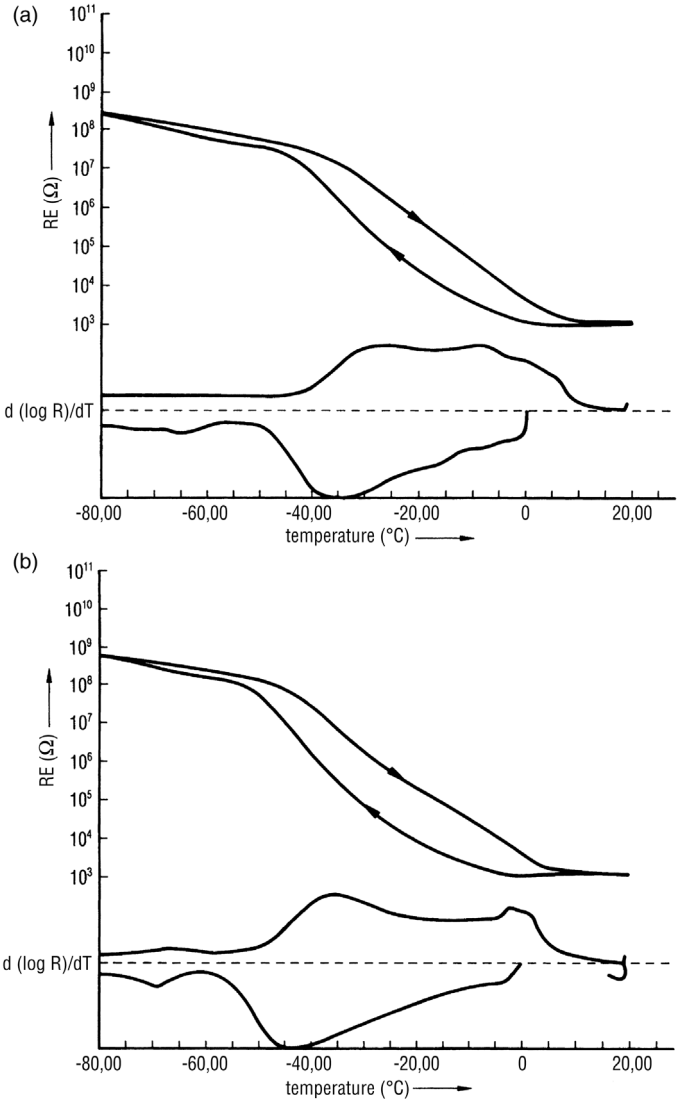

Figure 3.9 Electrical resistance as a function of temperature. (a) Excipient solution. (b) Solution with factor VIII. Cooling rate 15 °C/min. (See also measurements from Ref. [16], not published.)

alone, degradation was noted. The addition of dextran to sucrose or trehalose formulations increased T_g and resulted in improved storage stability. The authors suggested that this strategy of mixing disaccharides with polymeric carbohydrates may optimize protein storage stability.

During secondary drying, a small RM should be reached, since T_g of the dry product increases with decreasing water content. T_g of amorphous, freeze-dried sucrose increases from 16 °C at 8.5% RM to 63 or 64 °C between 1.0 and 0.7% RM. It should be taken into account that RM cannot be taken only at the end of drying,

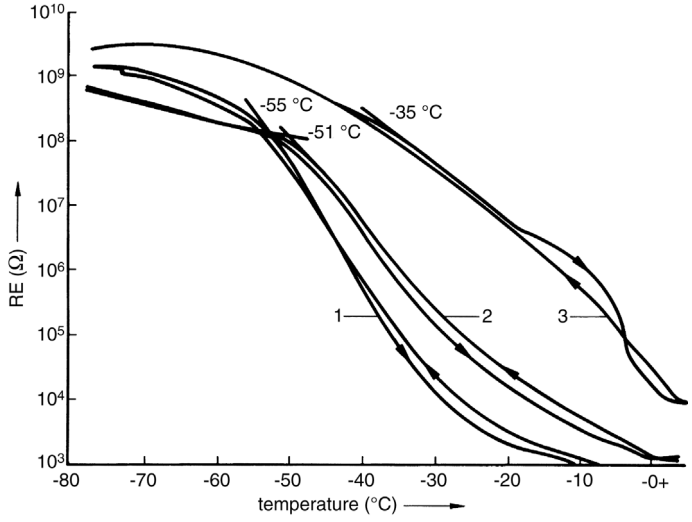

Figure 3.10 Electrical resistance as a function of temperature of three factor VIII solutions with different excipients. (See also Figure 4 from Ref. [16].)

and a possible increase during storage by water desorbed from the stopper must be considered (see Section 1.3.2 and Ref. [17]).

Srabanje also showed that storage below T_g alone is not a sufficient criterion to protect the activity of the protein, since O_2 can have an important influence [18].

The viscosity in the vicinity of T_g follows the Williams–Landel–Ferry equation [19], and also the stability of KS 1/4-DAVBL (deacetylvinblastin hydrazide conjugate), as shown in Figure 3.11.

Jensen [21] and Teeter [22] studied by X-ray diffraction the structure of water molecules in the vicinity of, at the surface of, and inside protein crystals. Jensen used rubredoxin (CEB) crystals to deduce the structure of water from the density distribution of electrons, calculated from diffraction pictures. Jensen found that water molecules that are placed within ~60 nm of the protein surface form a net, which is densest at a distance of a hydrogen bond in the donor or acceptor

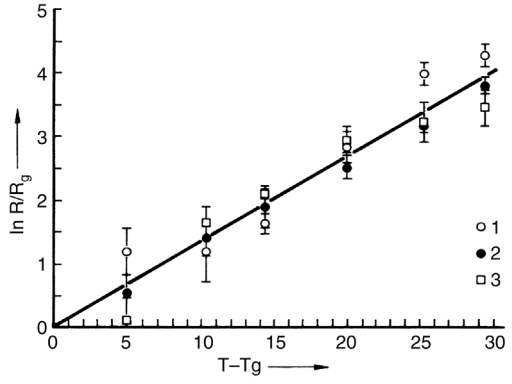

Figure 3.11 Analysis of the degradation of KS1/4 hydrazide conjugate by the Williams–Lande–Ferry glass transition theory. (See also Figure 9 from Ref. [20].) 1, formation of dimers; 2, free vinca generation; 3, decomposition of vinca; R, rate of degradation in %/month at a given temperature and water content; R_g, rate of degradation at T_g. $R_g = 0.10$ (dimer formation), 0.92 (free vinca generation), 3.9 (vinca decomposition).

molecules of a protein. At distances larger than 60 nm, the structure of water becomes increasingly blurred, ending in a structureless phase. Water molecules are also present in the inside of proteins, but are more strongly bound than those on the surface. Teeter [22] used crambin, a hydrophobic protein (MW 4700), to show that at 130 K, two different nets of water exist, one that forms rings of a pentagonal shape and the other in chain-like configurations that are strongly influenced by the surface of the molecule and affect the stability of the molecule. Teeter did not study the water molecules inside a protein.

Hageman *et al.* [23] calculated the absorption isotherms for recombinant bovine somatotropin (rbSt) and found 5–8 g of water in 100 g of protein, which was not only on the surface but also inside the protein molecule. Costantino *et al.* [24] estimated the water monolayer M_0 (g/100 g dry protein) for various pharmaceutical proteins and for their combination with 50 wt% trehalose or mannitol as excipient. They compared three methods of calculating M_0: (i) theoretical (th) from the strongly water binding residues, (ii) from conventional adsorption isotherm measurements (ai), and (iii) from gravimetric sorption analysis (gsa) performed with a microbalance in a humidity-controlled atmosphere. Table 3.5 summarizes the results for three proteins. The methods described can be helpful for evaluating RM data in protein formulations.

Townsend and de Luca studied the influence of lyoprotectants (LP) on ribonuclease (Ri) [25–28] as a model protein. Lyoprotection is defined as stabilization and prevention of degeneration of macromolecules both during freeze-drying and during storage. With phosphate buffer at pH 3–10, Ri in the dry stage loses its activity at 45 °C over time by forming aggregates with covalent bonds. Ficoll 70 is the most effective LP in the pH range 3.0–10.0. All three Ri–LP products were amorphous and not crystalline, although for optimum protection the mass ratio of LP to Ri had to be 6 : 1. The negative influence of phosphate

Table 3.5 Comparison of M_0 for three proteins without and with two excipients, formulated each with 50% w/w of the protein (part of Tables 1 and 2 from Ref. [24]).

Protein	M_0 (th)	M_0 (ai) (g water/100 g dry protein)	M_0 (gsa)
rhIFN-γ	4.5		
+ mannitol		3.1 (3.2)	3.2 (3.3)
+ trehalose		5.0 (6.3)	5.4 (6.3)
rhGH	5.0		
+ mannitol		2.8 (2.7)	2.8 (2.7)
+ trehalose		5.0 (5.8)	4.6 (5.7)
rhDNase	8.0		
+ mannitol		3.4 (3.3)	3.0 (3.3)
+ trehalose		5.1 (6.4)	5.1 (6.4)

The error of (ai) and (gsa) data is given mostly as ±0.2%. The data in parentheses are based on equal contribution from M_0 of the protein and M_0 of the excipient. For mannitol, the value is taken as zero; for trehalose, 6.2 (ai) and 6.0 (gsa).

buffer is attributed to possible heavy metal ions in the buffer. Increasing RM in the dry Ri increases the loss of activity and the aggregation. The same applies with increasing buffer salt concentration, as the amount of air in the closed vials is increased, although Ar or N_2 decreases the denaturation.

Miller *et al.* [29] freeze-dried lactate dehydrogenase (LDH) in the presence of trehalose and trehalose plus sodium tetraborate (TST) to stabilize LDH for storage at high humidity (100%) or warm temperature (45 °C). The freeze-dried LDH with TST had a considerably higher T_g than with trehalose alone and was more stable for several weeks under the conditions given above.

Maa *et al.* [30] used spray drying and spray freeze-drying (see Refs [13,14] in Chapter 5) to produce protein powders for inhalation from deoxyribonuclease (rhDNase) and anti-IgE monoclonal antibody (anti-IgE Mab) with lactose as carrier. Spray freeze-drying produced light and porous protein particles with superior aerosol performance.

Carpenter and Crowe [31] showed by IR spectroscopy that in addition to the H-bonds between protein and carbohydrate, carbohydrate bonds are also necessary to stabilize proteins during drying and reconstitution.

A review by Dong *et al.* [32] provides an overview of how Fourier transform IR spectroscopy can be used to study protein stabilization and to prevent lyophilization-induced protein aggregation. An introduction to the study of protein secondary structures and the processing and interpretation of protein IR spectra is given.

Hora *et al.* [33] described the complexity of protein stabilization with the example of recombinant human interleukin-2 (rhIL-2). Formulations with amino acids and mannitol–sucrose are sensitive to mechanical stress, for example, by pumping. 2-Hydroxypropyl-β-cyclodextrin (HPCD) provides stability, but increases the sensitivity to oxygen. Polysorbate 80 forms a mechanically stable product, but results in oxidation. In both cases contaminants in the HPCD or traces of H_2O_2 in the Polysorbate 80 may have been the starter for the oxidation. Brewster [34] reported that HPCD stabilizes interleukin without forming aggregates and this results in 100% biopotency. Page *et al.* [35] showed that losses in the biological activity of recombinant human interleukin-11 (rhIL-11) at low concentrations may be due to losses by surface adsorption to the glass walls of the container (in addition to other losses). They developed a combination of excipients to stabilize rhIL-11 in glass containers with no loss of potency.

Garzon-Rodriguez *et al.* [36] used sucrose, trehalose, hydroxyethyl-starch (HES), and HES–sugar mixtures to stabilize freeze-dried interleukin-11. Optimum stability was found with HES–sugar formulations. The advantages of the mixture compared with sugar alone were a high T_g, a robust structure, and rapid freeze-drying at increased temperatures.

Prestrelski *et al.* [37] studied the pH conditions and different stabilizers to provide optimum storage stability for IL-2 by Fourier transform IR spectroscopy. Different pH conditions in the absence of excipients change the dry state conformation of IL-2 dramatically. At pH 7, IL-2 unfolds extensively, whereas below pH 5 it remains essentially native. IL-2 at pH 5 is approximately one order of magnitude more stable than at pH 7, taking into account the amount of soluble and insoluble aggregates. A similar pH profile was observed in the presence of

excipients, although excipients change the overall stability profile. Excipients with the capacity to substitute for water during drying preserve the native structure best. Those with a high glass transition temperature provide the highest level of storage stability, but do not prevent unfolding during drying.

Carpenter *et al.* [38] studied the stabilization of proteins by nonionic surfactants. It is known that the critical micelle concentration of the surfactant protects proteins best in aqueous solutions. With certain proteins, for example, human growth hormone, the maximum protection depends upon the surfactant binding stoichiometry. The binding of the surfactant to the protein sterically hinders aggregate formation between protein molecules. During freezing, damage might be caused by the ice–water interface and this could be inhibited by the surfactant.

In contrast to the quoted experiences, Vermuri *et al.* [3] reported for recombinant α-antitrypsin (rAAT) in a phosphate–citrate buffer of pH 7.0 that there was no need for CPAs during freezing, thawing, and freeze-drying. Comparisons of rAAT in lactose, sucrose, and polyvinylpyrrolidone showed generally no significantly better protection. Freezing in LN_2 and an increase in concentration from 10 to 50 mg/mL rAAT did not alter the criteria of stabilization.

Figure 3.12 is a diagram of the freeze-drying of a factor VIII solution (the same solution as used in Figure 3.9).

1) The following facts can be taken from the diagram.
   1.1. The condenser temperature was constant at −52 °C.
   1.2. The temperature at the sublimation front, T_{ice} (Figure 3.13), measured by BTM, was −41 °C after 6 h and −40 °C after 30 h, the controlled operating pressure (p_c) was 0.048 mbar (CA) and 0.078 mbar (TM), respectively, and $T_{sh} = -13$ °C.
   1.3. The product temperature, T_{pr}, measured by two PT 100 s, is an average of −38 °C at the beginning and −31 °C after 30 h.
   1.4. The increase in T_{sh} between 28.5 and 30 h to −4 °C changes T_{ice} in 2 h to −38 °C.
   1.5. After 46 h, pressure rise measurements permitted the raising of T_{sh} to +40 °C, while T_{pr} rose to ∼+20 °C.

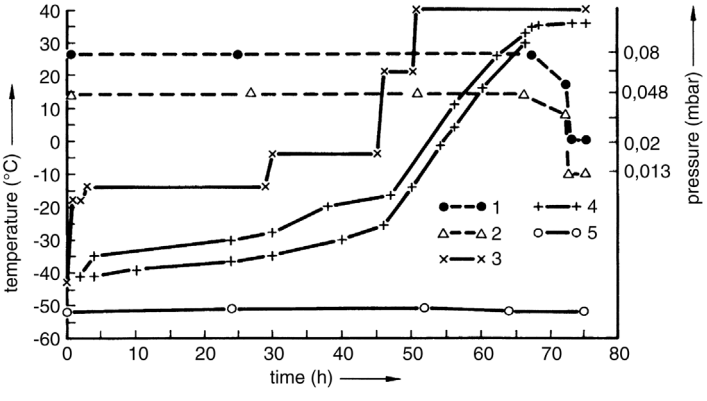

Figure 3.12 Freeze-drying course of factor VIII solution after freezing in LN_2. 1, p_{ch} (TM); 2, p_{ch} (CA); 3, T_{sh}; 4, T_{pr} (two sensors); 5, T_{co}. (See also Figure 7 from Ref. [16].)

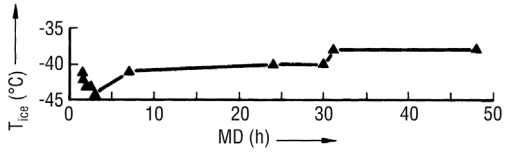

Figure 3.13 Plot of the temperature at the sublimation front (T_{ice}) of the run shown in Figure 3.12. (See also Figure 10b from Ref. [16].)

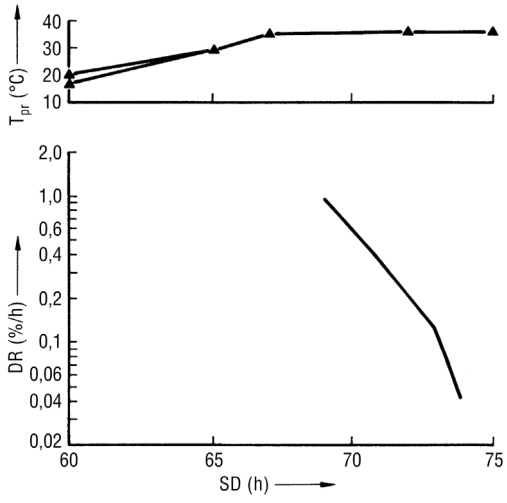

Figure 3.14 Plots of the product temperature and DR values of the run shown in Figure 3.12. (See also Figure 10c from Ref. [16].)

1.6. The pressure rises with increasing T_{sh}, but fall after 52 h and reach 1%/h at 68 h.
1.7. After 66 h, the pressure control could no longer maintain the selected pressure of 0.048 mbar; hence the pressure control is cut off and the pressure drops to 0.012 mbar (CA). The RM measured by the Karl Fischer method was $0.8 \pm 0.06\%$.

2) The following conditions applied to the process.
2.1. Each vial was filled with 30 mL of factor VIII solution, filling height 27 mm.
2.2. The product in the vials was frozen in LN_2 in ~4 min from +22 to −50 °C (~18 °C/min).
2.3. After freezing, the vials rested for 7 h on shelves at −42 °C (Figure 3.15) to simulate the loading of a production plant (growing of crystals in that time).

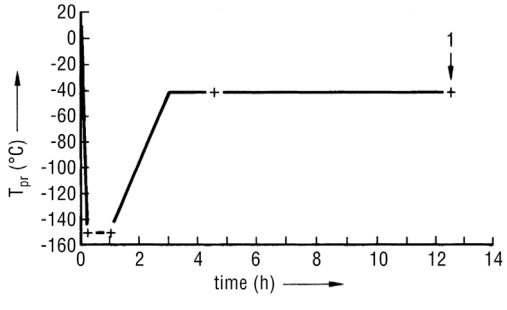

Figure 3.15 Plot of the product temperature during freezing before the course shown in Figure 3.12. 1, start of MD. (See also Figure 10a from Ref. [16].)

2.4. From photographs taken with a cryomicroscope, in which freeze-drying is possible, and from ER measurements (Figure 3.9), the maximum possible T_{ice} was determined as −38 °C and −40 °C is chosen as T_{ice} for the beginning of MD.

3) The following deductions for a shorter drying time can be made from Figures 3.12–3.14 and the RM data.
   3.1. T_{sh} can be raised in one step from −42 to, for example, −6 °C.
   3.2. The pressure difference between the sublimation surface (−40 °C, ∼0.128 mbar) and the chamber pressure (0.048 mbar) is almost a factor of 3, which is unnecessarily large. In choosing a factor of 2 (which is conservative), p_c could be raised to 0.06 mbar, reducing the transported water vapor volume by 25%. Since the heat transfer coefficient in this pressure range depends very little on the pressure, the higher pressure is only advantageous if the vapor transport from the chamber to the condenser is the bottleneck of the process (see Section 1.2.4). At a higher pressure, one could then load more vials in the chamber. In the experiment described, the vapor transport is not the bottleneck; therefore, one cannot expect a reduction in drying time as a result of higher pressure.
   3.3. Based upon the earlier increase in T_{sh} (3.1) and the higher p_c (resulting in a slightly higher T_{ice}), the temperature increase to +20 and +40 °C could be done earlier, probably by a few hours.
   3.4. The temperature in the product rises only slowly, even after the increase in T_{sh}, (in 10 h from −20 to 0 °C and in additional 10 h from 0 to 30 °C). The temperature rise could be accelerated: The shelf temperature is increased, for example, to 50 °C, until the product temperature has reached +25 °C. At that time, T_{sh} is reduced to +40 °C. This temperature increase has taken ∼16 h in the diagram, with a temperature difference $T_{sh} - T_{pr} \approx 30–35$ °C. A greater difference of ∼40–45 °C should again save several hours.
   3.5. The pressure control could be cut off at 66 h instead of 72 h, shortening the drying time by a further 3–6 h.
   3.6. In total, 10–15 h can be saved, resulting in a drying cycle of 64–59 h instead of 72 h, which could mean the completion of a cycle in 3 rather than 4 days. On the other hand, it does not seem likely that one could reduce the drying time under the given conditions (filling height 27 mm and $T_{ice} = -40$ °C) to 40 h or one cycle in 48 h.

This example is only valid with the conditions given. Different types of vials, different filling heights, different excipients with different maximum T_{ice}, and different temperatures during SD will change the data discussed here.

Kreilgaard *et al.* [39] pointed out that an amorphous phase stabilizes recombinant human factor XIII (rFXIII) better than solutes, which crystallize during freeze-drying. However, only amorphous solutes that form hydrogen bonds to the protein and thereby preserve the native structure provide optimum long-term stability. Kreilgaard *et al.* [40] also studied the freeze-drying behavior of recombinant *Humicola lanuginosa* lipase (HLL), a relatively hydrophobic protein. Neither 1 M sucrose, 0.5 M mannitol nor 0.5% w/v dextran altered the secondary

structure of the protein. However, in the presence of 1 M trehalose or 1% w/v Tween 20, the protein formed a white precipitate, an effect not found with more hydrophilic surfaces. The precipitation induced by 1 M trehalose did not alter the secondary structure and dilution with potassium phosphate buffer dissolved the precipitate completely. The precipitate induced by Tween 20 did not dissolve upon dilution with buffer and the native conformation was altered sufficiently to precipitate. Despite this behavior of HLL, the mechanisms accounting for acute and long-term stability are the same as for more hydrophilic surfaces: (i) formation of an amorphous phase containing protein and additive, (ii) additive can form hydrogen bonds and act as a water substitute, and (iii) T_g of amorphous phase above storage temperature.

Ma *et al.* [41] characterized the formulation of tumor necrosis factor (TNF-MAb) for the development of a freeze-drying cycle by DTA, ER, cryomicroscopy, isothermal water adsorption, and RM optimization. The formulation consisted mainly of 20 mg/mL TNF-MAb, 10 mg/mL maltose, and 20 mg/mL glycine. The combination of a stabilizing amorphous sugar (maltose) and a bulking, crystallizing agent (glycine) can be called a ›crystalline matrix.‹ The T'_g of maltose is $\simeq -30\,^{\circ}C$, T'_g of glycine is $\simeq -70\,^{\circ}C$, and $T_{cri,eut} \simeq -22\,^{\circ}C$, which did not crystallize completely during cooling at a rate of 1 °C/min; the crystallization was only finished during warming. The T'_g of the product was $-42\,^{\circ}C$ with the incompletely crystallized glycine. Two thermal treatment cycles were implemented: (i) cooling from 5 to 160 °C, heating to −15 °C, cooling to −165 °C; (ii) heating to 0 °C and cooling again to −160 °C. In the first cycle, the glycine crystallized completely; in the second cycle, the glycine crystals did not melt, acting as a matrix for amorphous maltose–protein product, thereby raising T'_g from −42 to −21 °C. The data were confirmed by cryomicroscopy.

For the secondary drying, the water adsorption isotherm at 22 °C was measured (Figure 3.16) and the stability of the monomers was measured as a function of time at 40 °C with different moisture contents as a parameter (Figure 3.17). From these data, the following production process was recommended: cooling the product slowly (rate <1 °C/min) to −45 °C, slowly warming to −25 °C, and freezing the product back to −45 °C. During the main drying, T_{ice}<−25 °C. Secondary drying terminated when RM was ~0.5%. The authors suggested using the thermal analysis and the strategies used to reduce trial and error experiments in freeze-drying cycle developments for protein pharmaceuticals.

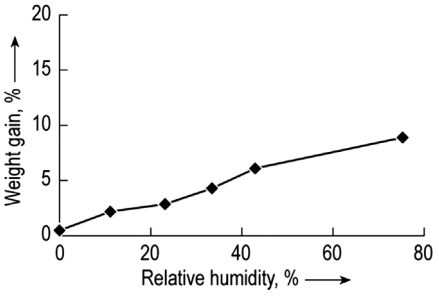

Figure 3.16 TNF-MAb water adsorption isotherm at 22 °C. (From Wang, 2001 [41]. Reproduced with permission of Springer.)

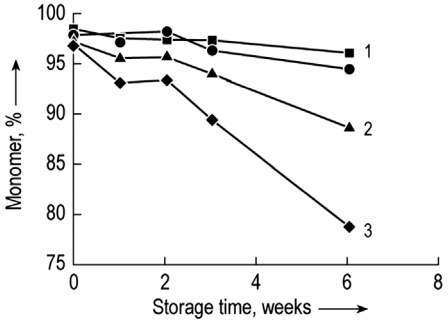

Figure 3.17 Percentage of TNF-MAb monomers for samples stored at 40 °C as a function of storage time. Moisture content 1 2.2; 2 4.7; 3 8.0%. (From Wang, 2001 [41]. Reproduced with permission of Springer.)

3.2 Viruses, Vaccines, Bacteria, and Yeasts

All substances considered in this section can only be dried in the presence of CPAs, if their natural qualities are to be protected. Greiff [42] studied the stability of purified influenza virus of strain PR 8 in physiological saline with calcium lactobionate and human serum albumin (each 1% in the solution). The freezing rate was ~1 °C/min down to −30 °C. During the freeze-drying, the product temperature was raised from −30 to 0 °C in 12–16 h and the product was dried at this temperature. After 24 h, the first 145 vials were removed and additional vials after intervals of 24 h each. The residual moisture content was 3.0, 2.0, 1.5, 1.0, and 0.5%. The stability of the freeze-dried virus (expressed in days during which the titer of the infectivity decreased by a factor of 10) was most unfavorable at 0.4 and 3.2% RM (4 and 7 days, respectively, at +10 °C) and best at 1.7% RM (145 days or more than 1000 days at −10 °C).

Overdrying (0.4% RM) and drying to high RM (3.2%) result in unstable dry products. Overdrying removes bond water, which is essential to keep the protein structure; furthermore, the hydrophilic locations of the protein are exposed to gases, for example, O_2. At too high an RM, free water remains in the dry product and induces reactions that change the protein molecule.

Greiff [43] classified the virus into five categories: (i) nucleic acid-type (either DANN core or RNA core); (ii) sensitivity against lipid solvents; (iii) envelope about the nucleocapsid or not (naked); (iv) pH sensitivity – exposure to pH 3 for 30 min differentiates between those viruses that lose more than a decade in titer and those that lose no titer or less than one decade; (v) heat-sensitive virus cannot be exposed to +50 °C for 30 min.

During the freeze-drying tests, the virus suspensions are either basic salt medium (BSM) or BSM plus calcium lactobionate (CL) plus serum albumin (SN) frozen at −76 °C and dried at either 0 or −40 °C. The activity was evaluated after 30 days storage at −4 or −65 °C. Rehydration was done with distilled water at 0 °C. The results with the freeze-dried viruses indicate the following:

- Al RNA viruses in BSM showed a marked decrease in titer. With the addition of CL and SN, no or only small decreases in titer are found.
- Al DANN virus suspensions in BSM changed only slightly.

- DANN viruses with envelopes, which are solvent sensitive, are less affected by freeze-drying than solvent-resistant, naked DANN viruses.
- pH-sensitive DANN viruses are less affected by freeze-drying than the pH-stable DANN viruses.
- Changes in titer of lyophylized DANN-viruses were independent of temperature sensitivity.

Doner *et al.* [44] studied bovine corona virus (BCV) and respiratory syncytial virus (RSV). Both can be frozen without CPAs at 0.2–0.3 °C/min with no loss of titer. Faster freezing (0.4–30 °C/min) results in an increasing loss of titer of 1–3 decades of infectious units. The freeze-drying experiments were therefore started by freezing at 0.25 °C/min and with the addition of various CPAs. No loss in titer was observed only with 3.6% dextran + 10% sucrose in the suspension for RSV and BCV. RSV could also be dried in 10% sucrose + 1.5% gelatin suspension, without loss of titer. Both viruses belong to the RNA virus group; hence, it should be possible to dry them without loss of titer [43] with CPAs. The results in Ref. [44] show that the conclusions of Greiff cannot be applied to other CPAs without further studies. Bennett *et al.* [45] studied the freeze-drying of varicella zoster viruses (VZV) – a DANN virus with an envelope – that are very labile in cell-free suspensions. Freezing of 0.7 mL in 3 cm^3 vials is performed in LN_2, after which the vials are placed on precooled shelves at −45 °C and the chamber is evacuated to $p_{ch} < 0.07$ mbar for 1 h. The freeze-drying is carried out with three different sets of process data:

	t_{MD} (h)	p_{ch} (mbar)	$T_{sh,MD}$ (°C)	t_{SD} (h)	p_{ch} (mbar)	$T_{sh,SD}$ (°C)	RM (%)
I	3.5	0.31[a)]	−45/+30[b)]	4.5	0.035[c)]	+30	7.1 ± 0.6
II	9	0.091[d)]	−45/+30[b)]	5	0.035[c)]	+30	4.1 ± 1.5
III	40	0.035[c)]	−26[e)]	8	0.035[c)]	+30	0.9 ± 0.4

a) 0.47 mbar TM × 0.65 = 0.31 mbar CA.
b) $T_{sh,MD}$ is raised from −45 to +30 °C during t_{MD}.
c) 0.07 mbar TM × 0.5 = 0.035 mbar CA.
d) 0.14 mbar TM × 0.65 = 0.091 mbar CA.
e) $T_{sh,MD}$ is constant during t_{MD}.

For pressure conversion, see Section 1.2.3. In the above table, CA data are converted from TM data as shown.

Following Eq. (1.14), the t_{MD}, if all data except p_c and T_{sh} are constant, should have a ratio between the three tests as follows:

$$t_{MD\,I} : t_{MD\,II} : t_{MD\,III} = 1/T_{tot\,I}(1/K_{tot\,I}) : 1/T_{tot\,II}(1/K_{tot\,II}) : 1/T_{tot\,III}(1/K_{tot\,III})$$

K_{tot} for II and III are practically independent of the pressure and therefore identical. $K_{tot\ I}$ is approximately twice as large as $K_{tot\ II}$ or $K_{tot\ III}$ as shown in Figure 1.92. With these data, one can conclude that

$$2T_{tot\,I} : T_{tot\,II} : T_{tot\,III} = 1 : 0.388 : 0.088$$

Assuming that at a pressure of 0.3 mbar T_{ice} will be −27.5 °C, one can draw the following picture of the three tests:

	I °C	II °C	III °C
T_{tot} (T_{sh} − T_{ice})	−20	−15.5	−3.5
T_{ice}	−27.5	−23	−29

If the assumed T_{ice} = −27.5 °C is replaced by −22 °C (Table 1.14, column 3), the data are as follows:

	I °C	II °C	III °C
T_{tot} (T_{sh} − T_{ice})	−14.5	−11.2	−2.6
T_{ice}	−22	−18.7	−28.6

The factor 2 as the difference of the two K_{tot} is often confirmed under different conditions.

To complete the picture, the difference in K_{tot} will be assumed as 1.5, resulting in the following data set with T_{ice} = −27.5 °C:

	I °C	II °C	III °C
T_{tot} (T_{sh} − T_{ice})	−20	−11.6	−2.6
T_{ice}	−27.5	−19.1	−28.6

These estimates are simplified. They are made only to show the following:

1) The measured t_{MD} can only be achieved if T_{ice} in test II is 3–8 °C higher than in tests I or III. The short t_{MD} in test I and the long one in test III result from the respective differences between T_{sh} and T_{ice}. The stability and the better yield in test I are not necessarily the result of the residual moisture content, but could also be related to the different T_{ice}. This may also be indicated by a question in Ref. [45]: ›If it is not the water, what else might it be that is leading to higher potency and stability in the short-term drying cycles?‹
2) The unfavorable results in III could also be related to a too small RM.
3) The importance of measuring also T_{ice}.

From the published data, the behavior of the product during desorption cannot be estimated. One could conclude that DR measurements during SD would have given additional information, for example, if test III were to have been terminated after 7% RM had been reached.

Terentier and Kadeter [46] described the freeze-drying of the vaccine *Yersinia pestis* EV 76 in a solution containing 10% sucrose, 1% gelatin, and 0.5% thiourea. The product was frozen on the shelves of a freeze-drying plant at ~8 °C/min to −40 °C. From ER measurements, it was concluded that below −24.4 °C a glass phase started and the eutectic temperature T_e was −17.1 °C. The drying time was determined as 9 h. If T_{sh} was controlled in such a way that T_e was exceeded after 4.5 h, the survival rate fell to ~50%; if T_e was reached after 6 h, the survival rate was ~80%. One can assume that MD should only be terminated after 5 h or more, at which time the temperature could be raised.

Morichi *et al.* [47] showed with 54 different bacteria and bacterial strains that the α-COOH, the α-NH_2, and the guanidino groups played an important role in the protective behavior of arginine. In the opinion of the authors, the common quality of the three groups was their ability to form hydrogen bonds.

Gehrke *et al.* [48] studied the course of freeze-drying on *Escherichia coli* (E) and *Lactobacillus plantarum* (L) with a specially developed plant (Figure 3.18), which permitted the weighing of samples during freeze-drying, the locking of samples from the chamber into an isolator (glove-box), and the measurement of RM in the isolator using the Karl Fischer method. A scheme of the plant is shown, since its design is almost ideal for freeze-drying studies to follow its course quantitatively. For quick freezing of the cultures (1.7–2.2 °C/min), the containers with the samples were placed on precooled shelves at −45 °C. Figure 3.19 shows the process data for drying of E and Figure 3.20 shows the plot of the weight loss of during this test. Figure 3.21 presents the decrease in viable organisms (CFU) per gram of mass during freezing and drying; 10% w/w of skimmed milk and 10% w/w of glycerol were added to the suspensions of cells in all tests. Figure 3.22 shows the drying time for E as a function of T_{sh} and Figure 3.23 shows the sublimation rate in gram of water per unit open surface area of the container as a function of the water content in the product. As shown, the sublimation rate is independent of

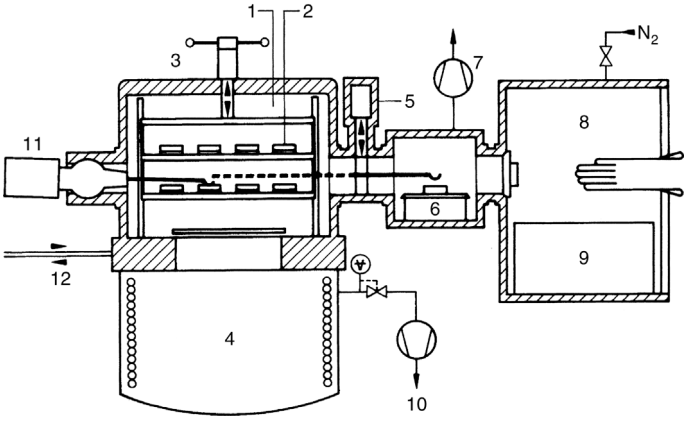

Figure 3.18 Scheme of a laboratory freeze-drying plant. 1, vacuum chamber with tempered shelves; 2, container with probe; 3, lift for shelves; 4, condenser; 5, lockgate; 6, balance in the lock; 7, vacuum pump for the lock; 8, glove-box; 9, Karl Fischer measuring system; 10, pressure-controlled vacuum pump; 11, manipulator; 12, tempered medium. (From Gehrke, 1990 [48]. Reproduced with permission of John Wiley & Sons.)

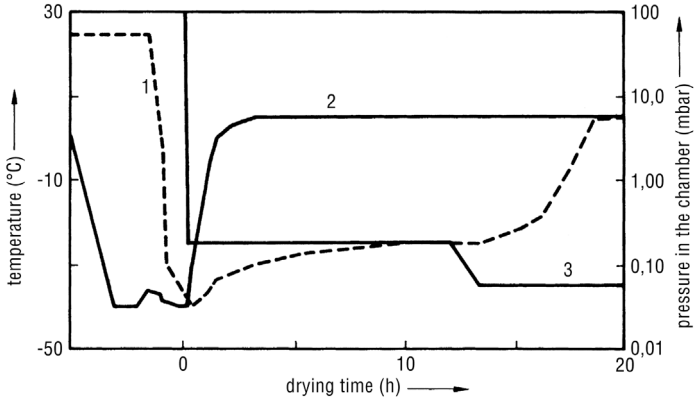

Figure 3.19 Freeze-drying run with *Escherichia coli* (E), $d = 20$ mm. 1, T_{pr}; 2, T_{sh}; 3, p_{ch}. (From Gehrke, 1990 [48]. Reproduced with permission of John Wiley & Sons.)

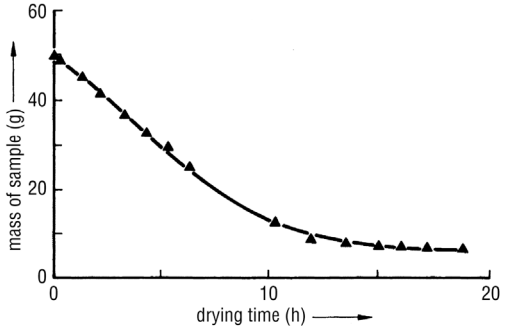

Figure 3.20 Mass of sample as a function of time for E at $p_{ch} =$ 0.18 mbar, $d = 20$ mm. (From Gehrke, 1990 [48]. Reproduced with permission of John Wiley & Sons.)

the layer thickness of the product. This is not possible during MD as shown by Eq. (1.12). The drying time is dependent on *d*. The influence of the operating pressure on the drying time is shown as ~25% shorter at 0.18 mbar than at 0.05 mbar.

Israeli *et al.* [49] found that trehalose is a very good stabilizer for E, even if the freeze-dried suspension of E was stored at 21 °C and 60% relative humidity, and/or was exposed to visible light. In 3 h, the survival rate decreased without trehalose to 0.01% under the influence of light and air; with trehalose, 35% survived. The

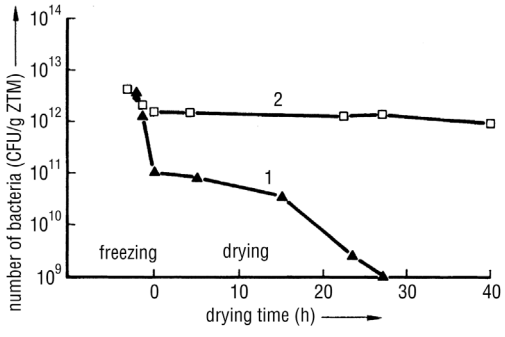

Figure 3.21 Number of bacteria as a function of the drying time for (1) E and (2) L. CFU, measure of number of viable bacteria; ZTM, solids of cells. (From Gehrke, 1990 [48]. Reproduced with permission of John Wiley & Sons.)

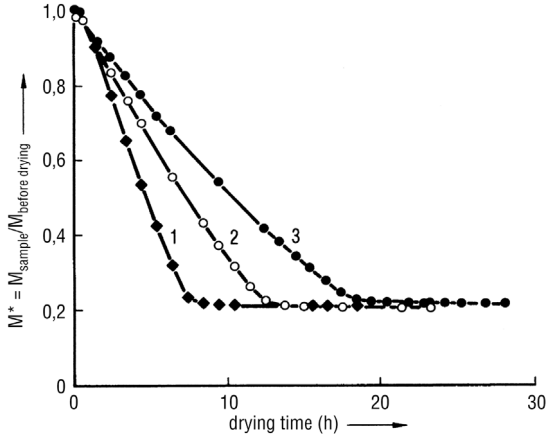

Figure 3.22 Influence of the shelf temperature T_{sh} on the drying time for E. T_{sh} = (1) +13; (2) −5; (3) −13 °C. (From Gehrke, 1990 [48]. Reproduced with permission of John Wiley & Sons.)

optimum trehalose concentration was found to be 100 mM. This corresponded to the number of trehalose molecules necessary to replace the water molecules in the outer membrane of the phospholipid molecules.

To increase the activity and capability of reproduction of *Saccharomyces cerevisiae* (SC), Kabatov *et al.* [50] proposed the addition of 10% skimmed milk, which had been saturated with Ar or N_2. Freezing down to −25 °C was done under pressure and continued down to −55 °C. The freeze-dried suspension did not change its quality during storage at +4 °C.

Pitombo *et al.* [51] found that 0.010 M succinate buffer at pH 4.6 was the best stabilizer for SC. The influence of three different freezing rates (0.5, 1.5, and 5 °C/min)

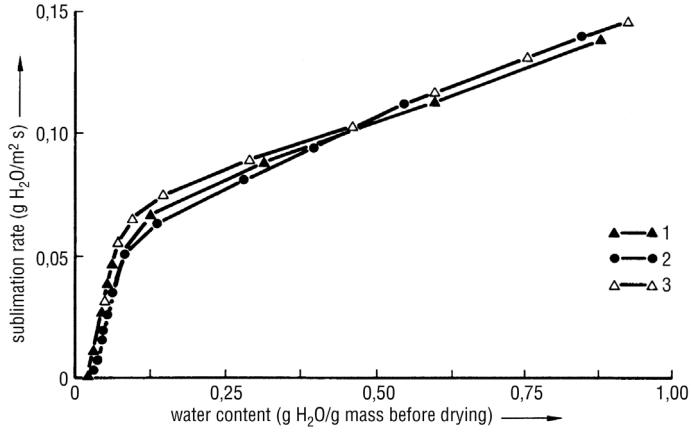

Figure 3.23 Sublimation rate as function of the water content for different product layers: (1), 10; (2), 15; (3) 20 mm. (From Gehrke, 1990 [48]. Reproduced with permission of John Wiley & Sons.) (*Note:* As shown in Eq. (1.12), the drying time is not independent of the product thickness.)

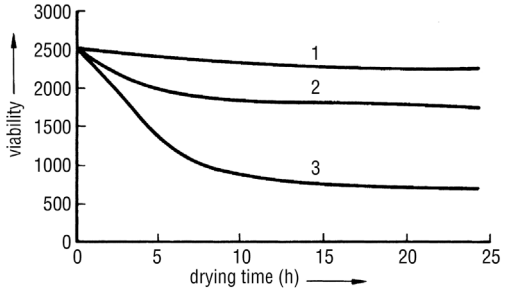

Figure 3.24 Viability of *S. cerevisiae* as a function of drying time, frozen at three different freezing rates: (1) 5; (2) 1.5; (3) 0.5 °C/min. (From Pitombo, 1994 [51]. Reproduced with permission of Elsevier.)

on the capability of reproduction is shown in Figure 3.24. During 235 days of storage at +25 °C, no measurable decrease in invertase activity was observed, if the RM was below 4%. With an RM of ~14%, the invertase activity decreased in 20 days to half and was immeasurable after 57 days, since an insoluble cluster had been formed. A 4% RM correspond at +25 °C to a monomolecular layer of water.

Lodato *et al.* [52] studied the thermal stability of SC (CBS 1171) after freeze-drying and heat treatment (100 min at 70 °C) in 40% w/v solutions of trehalose, maltose, and polyvinylpyrrolidone (PVP) of average mass 10 and 40 kDa and maltodextrin of 3.6 and 1.8 kDa. Samples of 1 mL were frozen at −30 °C and freeze-dried for 24 h at a condenser temperature of −40 °C and a pressure of <0.13 mbar. (*Note:* These data are difficult to understand, as ice at −4 °C has $p_s = 0.128$ mbar, which would leave no pressure difference between the chamber and condenser.) Different RM were obtained by placing the dried samples in the water vapor of saturated salt solutions at 26 °C for 15 days. The freezing rate ensured suitable viability of cells. Without a protecting agent, the viability dropped from 10^9 colony-forming units (CFU)/mL to 8.7×10^3 CFU/mL. Figure 3.25 shows the effect of additives on the survival of SC CBS 1171 after freeze-drying. Figure 3.26 presents the effect of additives of SC CBS 1171 of rehumidified samples after heating at 70 °C for 100 min as a function of moisture content (mc) in % of dry basis (db) and in Figure 3.27 the effect of 100% trehalose (T) (1); maltrodoxin (MD), and their mixtures: (2) MD 1.8 kDa, (2a) 100% MD, (2b) 50% T and 50% MD, (2c) 67% T and 33% MD; (3) MD 3.6 kDa, (3a) 100% MD, (3b) 50% T and 50% MD, (3c) 67% T and 33% MD, on the survival is given after exposure to 33% relative humidity for 15 days at 26 °C and heating at 70 °C for 100 min. The authors conclude that the critical extracellular factors that influence the survival of freeze-dried CS cells subjected to heat treatment are the presence of disaccharides during freeze-drying, their concentration, and the moisture content. The physical state of the extracellular matrices and mobility effects might play only a secondary role in the loss of viability.

Rakotozafy *et al.* [53] compared a drying process at ›surrounding temperature,‹ called ›dehydration by successive pressure drops‹ (DDS) with freeze-drying of commercial compressed SC, baker's yeast, with 165–187% d.b., and a viability of 3.8×10^9 CFU/g d.b. A 10 g amount of product was crumbled in a plastic pot for DDS or in a Petri dish for freeze-drying. The freeze-drying was carried out in a plant with a 400 cm^2 shelf area. The freezing rate was 1 °C/min to −40 °C, and during freeze-drying T_{sh} was 25 °C and T_{co} −55 °C at a chamber pressure of

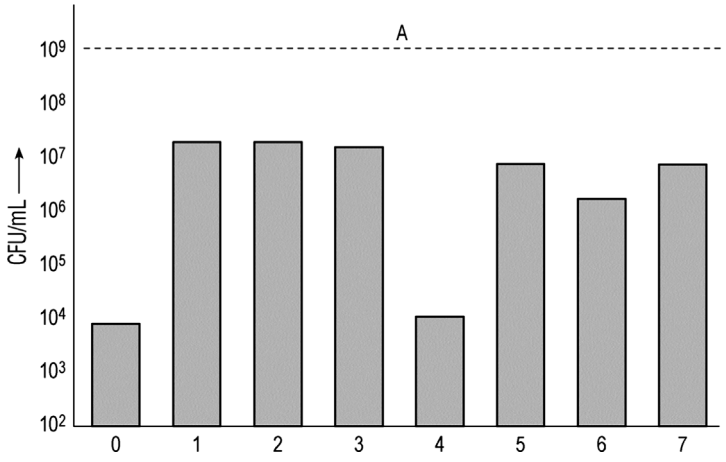

Figure 3.25 Effect of additives on survival of *S. cerevisae* CBS 1171 (SC 1171) after freeze-drying. CFU, colony-forming units; A, CFU/mL before freeze-drying; O, yeast suspension without additives; 1, maltose; 2, trehalose; 3, maltodextrin (MD), average molar mass (am) 1.8 kDa; 4, MD, am 3.6 kDa; 5, PVP, am 10 kDa; 6, PVP, am 40 kDa; 7, 50% MD, 3.6 kDa and 50% trehalose. All solutions with 40% w/v additives. (From Lodato, 1999 [52]. Reproduced with permission of Springer.)

0.3 mbar. The RM at the end of drying was measured with an infrared balance as 4% after 12 h. The same RM with DDS was reached in 4–8 h. The survival rates with DDS were between 31 and 87%, and with freeze-drying 5%. The problems with drying methods using no vacuum or reduced pressures, as here, ~100 mbar, are discussed in Section 1.2.6. With respect to the freeze-drying process used for comparison, a few comments should be made: the initial product contains ~170 g of water on 100 g of solids (or ~37% solids and 63% water) as compared with the usual pharmaceutical products that start with 900 g of water on 100 g of solids. No information was given on the freezing behavior of this form of SC, which is comparable in solid content to concentrated coffee extract. It is well known that products with a high solid content freeze totally differently and may have a higher content of UFW than those with 5–10% solids (see, for example, Figure 1.83 for

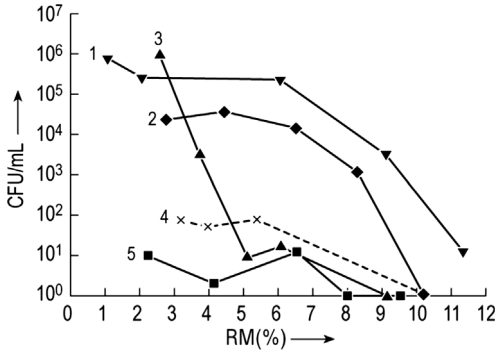

Figure 3.26 Effect as in Figure 3.25 on rehumidified samples heated at 70 °C for 100 min as a function of RM (% of solids). 1, trehalose; 2, maltose; 3, MD, am 1.8 kDa; 4, control; 5, MD, am 3.6 kDa. (From Lodato, 1999 [52]. Reproduced with permission of Springer.)

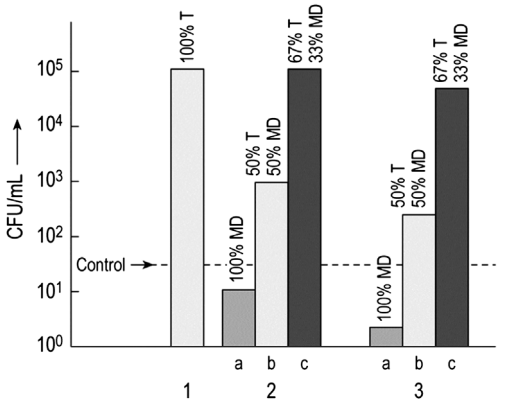

Figure 3.27 Effect of trehalose, MD, and their mixtures as in Figure 3.25 after freeze-drying, exposure at 33% relative humidity during 15 days at 26 °C and heating at 70 °C for 100 min. 1, 100% trehalose; 2, MD 1.8 kDa; 2a, 100% MD; 2b, 50% trehalose and 50% MD; 2c, 67% trehalose and 33% MD; 3, MD 3.6 kDa; 3a, 100% MD; 3b, 50% trehalose, 50% MD; 3c, 67% trehalose and 33% MD. (From Lodato, 1999 [52]. Reproduced with permission of Springer.)

miso sauce and Figure 4.7 for coffee extract). From the data for the freeze-drying step, one can expect T_{ice} is about −25 °C (Figures 2.115 and 2.116). A 10 g amount of product is distributed in a Petri dish, resulting in a layer of a maximum of (used for the following calculation) 2 mm, resulting in a main drying time (Eq. (1.12)) of ∼0.9 h; adding 2 h for secondary drying to 4% RM, the total drying time should not exceed 3 h. The 12 h given in the paper can have two reasons: The product was incompletely frozen and the concentrated ›rubber‹ dried very slowly or the heat transfer from the shelf to the product was very small. The calculation is based on 60 kJ/m^2 h °C (which is low for the pressure of 0.3 mbar). Most likely it is a combination of both factors.

Rindler *et al.* [54] reported an attempt to freeze-dry red blood cells at ultralow temperatures. The cryoprotective solution contained 20% w/w specially purified hydroxyethyl starch (HSE), 5% w/w D-maltose, and 60 mmol/L NaCl in distilled water. Packed red cells and solution were mixed to yield a 10% hematocrit, frozen at a rate of ∼100 °C/min with a sample thickness $d = 1.5$ mm and broken into pieces thereafter. For drying, the product was filled into precooled aluminum tubes, which were placed in an aluminum holder to guarantee optimum heat transfer to the cooled shelf. Between the aluminum tubes and the shelf, a maximum temperature difference of 2 °C was measured. Seven groups of experiments were carried out at T_{sh} between −5 and −65 °C, always at a pressure of 0.02 mbar (*Note:* p_s of ice at −65 °C is $\sim 5 \times 10^{-3}$ mbar, and the mentioned drying pressure and T_{sh} do not appear to correspond). After drying, the samples had been dissolved in an isotonic phosphate-bufferd saline solution (pH 7.2, 37 °C), the rate of extracellular to total hemoglobin concentration, equivalent to the hemolysis, was determined. The difference between the observed hemolysis and 100% is called saline stability, shown in Figure 3.28 as a function of shelf temperature. Table 3.6 summarizes the data and the results of the experiments with the following explanations:

- shelf temperatures (T_{sh});
- measured sublimation temperatures (T_{MD}); the sample height is given as 1.5 mm (for drying) and 2.4 mm (for temperature measurements), the sample

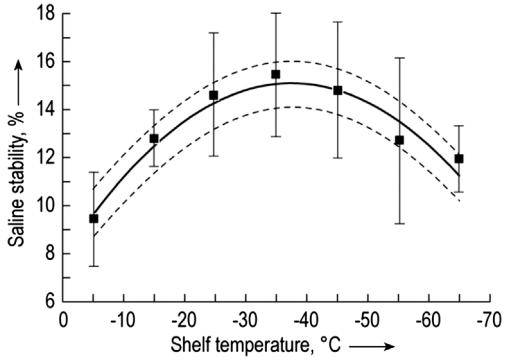

Figure 3.28 Saline stability as a function of shelf temperature. (From Rindler, 1999 [54]. Reproduced with permission of Elsevier.)

shape as broken pieces (for drying) and cylindrical (for temperature measurements);

- measured time of sublimation ($t_{MD,m}$), taken as the time at which the sample temperature (between +12 and +2 °C for $T_{sh} = -5$ and −65 °C, respectively) becomes constant;
- calculated time of sublimation ($t_{MD,c}$), calculated with some assumptions about the amount of radiation energy transferred to the sample;
- calculated temperature during desorption drying (T_{SD}), assuming that the radiation during sublimation and desorption drying follows the same characteristic constants;
- estimated total drying time (t_{tot}), taken as the time at which the relative mass reduction reaches values between 75.3 and 74.6 (±0.2).

This work is quoted as an attempt (i) to freeze-dry red blood cells with measured saline stability and (ii) to use very low temperatures in freeze-drying. The authors offer several critical remarks as to why the stability curve in

Table 3.6 Shelf temperatures (T_{sh}), measured sublimation temperatures (T_{MD}), measured time of sublimation ($t_{MD,m}$), calculated time of sublimation ($t_{MD,c}$), calculated temperature during desorption drying (T_{SD}), and estimated total drying time (t_{tot}) (Tables 1 and 2 from Ref. [54]).

T_{sh} (°C)	T_{MD} (°C)	$t_{MD,m}$ (h)	$t_{MD,c}$ (h)	T_{SD} (°C)	t_{tot} (h)
−5	−33	4.5	4.2	+4	24[a)]
−15	−33	6.0	5.4	−2.5	24[a)]
−25	−33	7.2	6.9	−8.7	24
−35	−35	8.7	–	−14.5	48
−45	−37	10.3	10.5	−20.1	72
−55	−40	13.0	12.7	−25.3	96
−65	−45	14.0	–	−30.1	144

a) Time may be too long (e.g., nighttime).

Figure 3.28 could have its specific shape. Here we may add a note from the freeze-drying process point of view. The calculated T_{DS} and the methods to determine T_{tot} would require a desorption down to 5.2% RM at temperatures as low as −30.1 °C. The authors agree that the relative mass reduction is not accurate enough to determine RM to the necessary degree. The decrease in stability might well be related to incomplete desorption drying at an unknown T_{sd}, unknown because the transfer of radiation conditions from sublimation drying to desorption drying is difficult to prove: The surface area and its optical behavior can be very different. This kind of low-temperature freeze-drying could be done under more controlled conditions in a plant as shown in Figures 2.66–2.68: The product on the shelf ›sees‹ only the shelf temperature, radiation from the walls is eliminated by temperature-controlled shields, the sublimation temperature at the ice front (T_{ice}) is measured by BTM and can be adjusted by a controlled pressure, T_{sh} can be adjusted between −75 and 60 °C, the condenser temperature permits drying at T_{ice} −60 °C, and sublimation and desorption rates and the RM data are permanently measured and calculated. The disadvantage of the plant is the minimum amount of solids needed per run, ∼20 g; 5 g may be possible depending on the required accuracy. The advantages are that no temperature sensors in the product are needed and the process data can be transferred to a larger plant.

A completely different approach to freeze-drying red blood cells (RBCs) and platelets was presented by Bakaltcheva and Reid [55]. RBCs and platelets are pretreated with adonitol, a polyol with similarities to glycerol. The cells were kept for 12 h at 4 °C in a loading solution containing 1800 mM adonitol. The RBCs were frozen and freeze-dried in a solution of 250 mM adonitol, 12 mM dibasic sodium phosphate, 2.9 mM monobasic sodium phosphate, and 20% w/w albumin, either frozen on the precooled shelf at −30 °C at 2.5–5 °C/min or in LN_2 at 70 °C/min. Both frozen products were lyophilized during MD for 30 h at −30 °C and during SD at 15 °C. The LN_2 frozen product was also transferred to the shelf of a freeze-dryer, kept there for 48 h at a drying temperature of −30 °C, and then thawed for 10 min in a water bath at 37 °C. After rapid freezing, the RBC survival was 80% after shelf freezing 15%. After freeze-drying, the survival rate of both freezing methods were equally poor. The survival rate of the LN_2-frozen RBCs during the 48 h of storage at −30 °C is shown in Figure 3.29. The authors conclude that (1) a freezing rate of 2.5–5 °C/min is too slow for RBCs; for optimum survival a rate of ∼100 °C/min is necessary; (2) the damage to the LN_2-frozen RBCs is predominantly a result of the ›warming‹ from −196 to −30 °C on the shelf (Figure 3.29). This hypothesis was

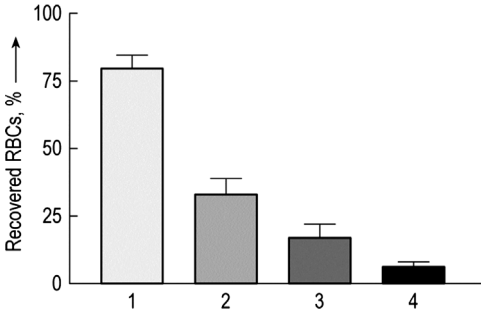

Figure 3.29 Effect of storage time (at −30 °C) on the recovered RBCs (mean values of five measurements ± SEM). (See also Figure 2 from Ref. [55].) 1, RBCs frozen in LN_2; 2, RBCs as in (1) stored at −30 °C for 24 h; 3, RBCs as in (1) stored at −30 °C for 32 h; 4, RBCs as in (1) stored at −30 °C for 48 h.

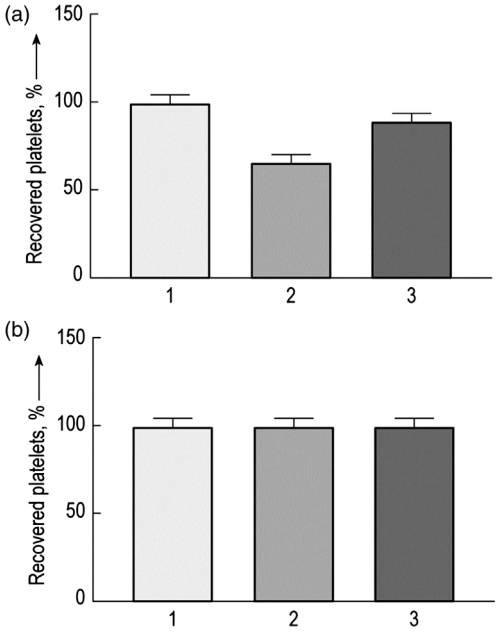

Figure 3.30 Platelets untreated or pretreated with adonitol and frozen at an optimum cooling rate. (See also Figure 3 from Ref. [55].) (a) Frozen to −80 °C and freeze-dried at −30 °C, with a warming step from −80 to −30 °C: 1, platelets control; 2, platelets freeze-dried; 3, as (2) but adonitol treated. (b) Frozen to −30 °C and freeze-dried at −30 °C: (1)–(3) as in part (a).

tested with platelets pretreated or not pretreated with adonitol frozen to −80 °C (Figure 3.30a) with warming to −30 °C and frozen to −30 °C (Figure 3.30b) with no warming before freeze-drying. The recovery of the untreated and the pretreated platelets frozen to −30 °C was 100%. It was subsequently reported that the freeze-drying of pretreated RBCs was successful after freezing at a rate of 100 °C/min to −30 °C and drying at −30 °C at a pressure of 0.4 mbar with no ›warming‹ in between (I. Bakaltcheva, personal communication).

3.3 Antibiotics, Cytostatics, Ibuprofen

The freeze-drying of antibiotics and blood serum largely represented the beginning of industrial lyophilization. Neumann [56] wrote in 1952, ›The (freeze-drying) temperature for the older, not well purified penicillin preparations had to be kept surprisingly low . . . it could not exceed −25 or −40 °C‹ and later, ›Today penicillin is manufactured as crystals without the need for freeze-drying.‹

Other antibiotics still require freeze-drying, for example, Na-cephalotin (Na-CET). Takeda (Ref. [32] of Chapter 1) showed that thermal treatment of Na-CET was not sufficient to produce a pure crystalline product, as the amorphous fraction discolors during storage and must be avoided. Takeda described the production of pure crystalline Na-CET by adding microcrystals of Na-CET to a saturated solution of Na-CET. If this mixture was frozen and freeze-dried, then no amorphous or quasi-crystalline forms were found. Koyama *et al.* [57] reported that after thermal treatment for 24 h, some parts remained incompletely

crystallized. After adding 5% w/w isopropyl alcohol, a thermal treatment of 1 h was sufficient. Furthermore, the product could be dried at a higher pressure. Thus, the drying time could be reduced and 100% of the product could be used.

Ikeda [58] presented a two-stage freezing process for an antibiotic (panipenem), which reacts with another component of the drug (betamipron) and has therefore to be separated until its use. The first substance is filled into vials and frozen. The precooled second substance is then filled into cooled vials and frozen. By this process, the amount of undesirable reaction product could be limited to 0.5% during a 6 months of storage at 40 °C. If the two products were frozen simultaneously, the amount of reaction product was 1.2%.

Jonkman-de Vries *et al.* [59] described the development of a stable parenteral dosage form of the cytotoxic drug E 09. E 09 dissolves poorly in water and its solution is unstable. With the addition of 200 mg of lactose per vial containing 8 mg of E 09, an optimum formulation was developed with respect to solubility, dosage of E 09, and length of the freeze-drying cycle. DSC studies were used to select the most effective parameters. The freeze-dried product remains stable for 1 year when stored at 4 °C in a dark environment.

Kagkadis *et al.* [60] developed an injectable form of ibuprofen [(±)-2-(*p*-isobutylphenyl)propionic acid], which is very slightly soluble in water and has a poor wettability. 2-Hydroxypropyl-β-cyclodextrin (β-HPCD) is used to form a better soluble complex with ibuprofen. This solution has been successfully freeze-dried. The freezing and freeze-drying process were kept uniform in all experiments, although the freezing and freeze-drying cycle itself cannot be discussed from the data presented as an optimum, as the product data as a function of concentration and freezing rate were not given.

3.4 Liposomes and Nanoparticles

Liposome is derived from the two Greek words, "Lipos" meaning fat, and "Soma" meaning body. Liposomes can have a variety of shapes, such as universal-lamellar or multilamellar sizes. The name refers to its structural components – phospholipids – and not to its size. In contrast, the term nanosome refers to the size. A liposome is a vesicle of the same material as a cell membrane.

Liposomes can be used as carriers of active pharmaceutical ingredients (API) to the source of disease in the human organism.

Phospholipids are capable of forming vesicles under certain conditions of excess water and this can be described schematically (Figure 3.31). Liposomes can have a variety of structures (Figure 3.32), as described, for example, by Talsma (Ref. [65] of Chapter 1).

Liposomes can, generally, only be frozen without damage if the suspension is frozen in a glass phase of water. This requires the addition of CPAs, for example, mannitol, dextran, or trehalose and quick freezing (e.g., 10 °C/min by LN_2) [61, p. 363].

Talsma (Ref. [65] of Chapter 1) showed with phospholipon 100 H, a hydrated phosphatidylcholine of soya beans (Nattermann, Cologne), and dicetyl phosphate (DCP) (molar ratio 10 : 1) from which bilayer liposomes have been produced, the

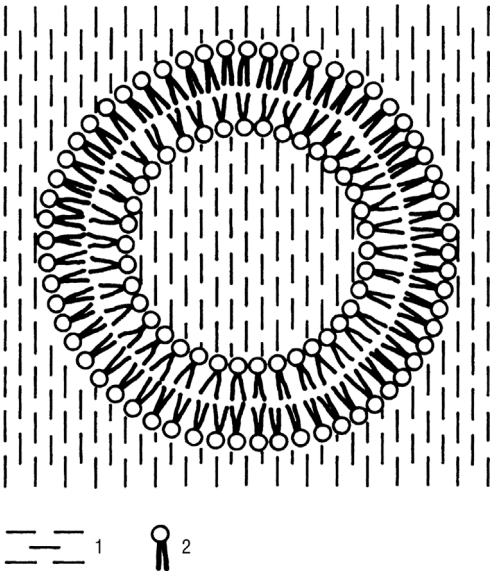

Figure 3.31 Schematic construction of small unilamellar vesicles, 25–100 nm. 1, water; 2, phospholipid. (See also Figure 1 from Ref. [62].)

influence of one CPA (I), of several CPAs (II), of the vesicle size (III), and the cooling rate (IV). In all of the following tests Tris buffer of pH 7.4 was used.

I) In this example, mannitol was applied as CPA. The size of the vesicles was 0.27–0.32 µm and the vesicle concentration was 0.4 per μm^3. The energy flows during cooling (10 °C/min) and rewarming (10 °C/min) were measured by DSC. Figure 3.33a–d shows that peak 2 does not exist if the mannitol is within the liposomes (pure Tris buffer and pure liposome suspension also do not show this peak). *Note:* During the quick freezing of mannitol solutions, not all water crystallizes but forms an amorphous glass phase. During rewarming, the viscosity and specific heat change. This happens, for example, in Figure 3.33b at -33.6 ± 0.6 °C and changes at -22.6 ± 0.3 °C into an exothermic process. At this temperature, the ice is so much softened that water can crystallize and water clusters can now migrate. Only in ~1% mannitol solution can water solidify amorphously under the conditions of the experiment.

In the following table, the temperatures during freezing at which the homogeneous crystallization of ice starts are listed. This is shown by the temperature of pure ice (−41.9 °C): start of homogeneous ice crystallization

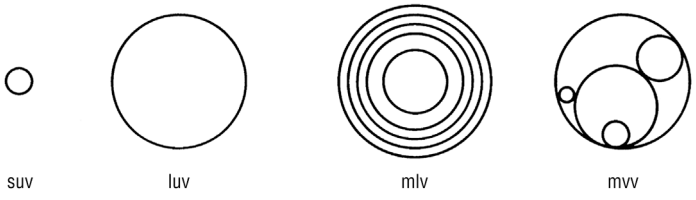

Figure 3.32 Morphology of different liposome structures. Suv, small unilamellar vesicles; luv, large unilamellar vesicles; mLv, multilamellar vesicles; mvv, multivesicular vesicles. (From Talsma, 1991 (Ref. [65] of Chapter 1). Reproduced with permission of Springer.)

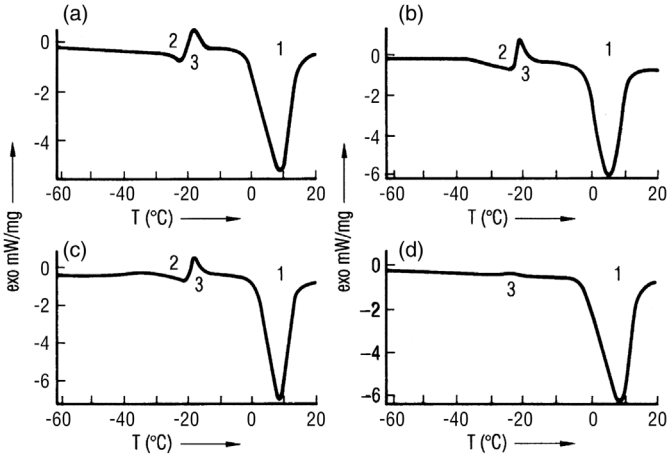

Figure 3.33 Heat flow as a function of time during rewarming of the samples measured by DSC. (a) 11% mannitol in 10 mM Tris buffer, pH 7.4. (b) 35 µmol lipid/mL, 11.2% mannitol in 10 mM Tris buffer, pH 7.4, inside the vesicles as well as in the surrounding medium, particle size 0.32 µm. (c) 33 mmol lipid/mL, 11.2% mannitol in 10 mM Tris buffer, pH 7.4 in the surrounding medium and 10 mM Tris buffer pH 7.4 inside the vesicles, particle size 0.27 µm. (d) 35 µmol lipid/mL, 11.2% mannitol in 10 mM Tris buffer, pH 7.4, inside the vesicles surrounding medium, 10 mM Tris buffer, pH 7.4, particle size 0.32 µm. (From Talsma, 1991 (Ref. [65] of Chapter 1). Reproduced with permission of Springer.)

in different CPAs (lipoid as in Figure 3.33) at a concentration of 30–50 µmol/mL, lipoid size 0.3 µm; 10 mM Tris buffer, pH 7.4; CPA and Tris buffer within or outside the liposomes (Ref. [34] of Chapter 1, p. 68):

CPA (%)	T_{start}	T_c
None	−41.9	
Mannitol 11.2	−44.8	−33.6
Glycerol–mannitol 10/10	−48.7	

T_{start} = extrapolated temperature of start of crystallization, T_c = collapse temperature.

The temperature of the homogeneous crystallization can be changed by changing the CPAs or their mixture.

II) Talsma shows that peak 2 changes only from −39.8 to −40.4 °C (liposomes, liposome concentration, buffer, and cooling rate as in (I), but no mannitol) if the liposome size is decreased from 0.87 to 0.14 µm. With small liposomes, the start of the homogeneous crystallization is delayed. This can also be deduced from the weakly performed crystallization (Figure 3.33d, peak 3), if mannitol is only within the liposome.

III) If the liposomes (as in (I), mannitol within and outside) are cooled at 5 °C/min instead of 10 °C/min, peak 2 starts at ~10 °C higher temperatures and shows a saddle-like form.

Under the conditions described, quick freezing is desirable to produce a maximum of amorphous ice, which can be proven by a crystallization at peak 3. Until now, the freezing criteria have been judged by the changes that they produce during cooling/rewarming. However, the most important goal in the studies of liposomes is to find ways in which water-soluble substances can be encapsulated in liposomes in such a way that they do not leak from the liposomes during transportation and storage and are released in a controlled manner during application.

To test and measure the retention rate of liposomes, carboxyfluorescein (CF) can be used. Ausborn and Nuhn [62] studied different lipid vesicles, for example, egg lecithin (EPC), hydrated egg lecithin (HEPC), cholesterol (CHOL), and mixtures thereof. For centrifuged EPC and for centrifuged HEPC liposomes, a retention rate of 67.5 and 75%, respectively, were found in 0.4 mol/L saccharose with 0.15 mol/L phosphate buffer. Furthermore, the results with different mixtures were reported: HEPC–CHOL with 1 mol/L sucrose has a retention rate of almost 100%, whereas HEPC–liposomes in a 0.4 mol/L saccharose solution reach ~85%. Talsma (Ref. [65] of Chapter 1) established some quantitative connections between retention rates and particle size and storage temperatures. The retention rate of PL 100 H–DCP (10 : 1) (30 µmol/mL) increased from 51 to 98% if the liposome size decreased from 0.2 to 0.12 µm (liposomes in 10% w/w saccharose with 10 mM Tris buffer). The retention rate of the same liposome suspension also depends on the liposome size and the storage temperature after freezing in an acetone–dry ice mixture (Ref. [34] of Chapter 1, p. 92):

Liposome size (µm)	Retention rate for CF (%) after 65 h storage at − 25 °C	in LN_2
0.20	22	47
0.18	41	84
0.12	55	97

To freeze-dry liposomes requires stabilization not only during freezing but also during drying and storage of the dry product. Talsma (Ref. [65] of Chapter 1, p. 106) showed that the retention rate of small liposomes (0.13 µm) was 24.1% and greater than that of large liposomes (0.28 µm), which had only a 7.4% retention rate.

Crowe and Crowe [63] proved that it is sufficient for certain liposomes, for example, egg phosphatidylcholine (DPPC), to be vitrified by trehalose or dextran during freezing and freeze-drying. In trehalose, the retention rate was almost 100% and in dextran more than 80%. This did not apply to egg PC-liposomes: Dextran as CPA alone led to an almost total loss of the CF indicator, but addition of dextran to a trehalose solution (Figure 3.34) also reduced the retention rate of CF substantially, for example, from 90% in a pure trehalose to ~45% if trehalose and dextran were present in equal amounts in the solution. Since the T'_g of dextran is ≃10 °C and that of trehalose is −30 to −32 °C, dextran should form a glass phase at much higher temperatures than trehalose. Therefore, the stabilization of egg PC with trehalose cannot be related to the vitrification. Crowe

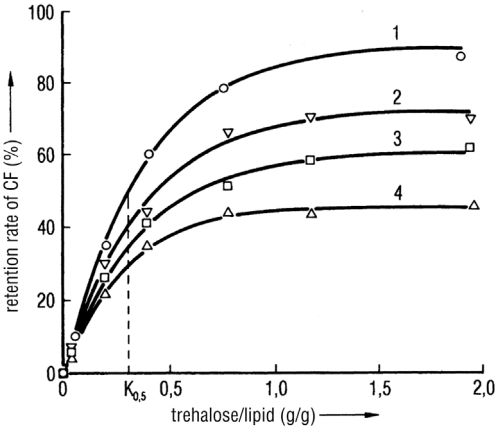

Figure 3.34 Retention of CF as function of the trehalose/lipid concentration with various dextran additions: (1) 0; (2) 0.08; (3) 1.2; (4) 2.0 g dextran/g lipid. (From Crowe, 1994 [61]. Reproduced with permission of Elsevier.)

showed with IR spectroscopy that egg PC freeze-dried with 2 g of trehalose/g lipid had spectrographic characteristics almost identical with those of the hydrous lipid: Trehalose molecules replaced the water molecules and hydrogen bonds were formed between the lipid and trehalose molecules. Thus, the stability of the lipids was preserved even if the water was removed. Crowe and Crowe compared this process with the survival of plants at low temperatures by producing trehalose.

Hauser and Strauss [64] assumed the hydrogen bond between sucrose and phospholipid to be the cause of the integrity of the unilamellar vesicles and showed that enclosed ions cannot migrate to the surroundings.

Ausborn *et al.* [65] confirmed by IR spectroscopy the strong hydrogen bonds between sucrose and SPS monoester (sucrose–palmitate/stearate) with the phosphate head groups, which supports the replacement theory of water molecules.

Suzuki *et al.* [66] concluded from their measurements that glucose and maltose completely prevent the aggregation or fusion of liposomes during freeze-drying, but other maltodextrin support the aggregation owing to their weak hydrophobic behavior.

Jizomoto and Hirano [67] tried to increase the amount of drug inclusions in liposomes by inserting Ca^{2+} ions in dipalmitoylphosphatidylcholine (DPPC) liposomes. The included volume (mL) per gram of liposomes is called V_{cap} and this can be increased as a function of the Ca^{2+} concentration up to 10 times the minimum V_{cap}. The increase in V_{cap} is attributed to the electrostatic repulsion between the Ca^{2+} ions, which reduces the number of lamellae and increases the diameter of the liposomes to a certain extent, but increases V_{cap} substantially. A calculated simulation of this thesis is in reasonable agreement with the measurements.

The inclusion of drugs in liposomes is discussed in four examples:

Gu and Gao [68] reported that freeze-dried cyclophosphamide in liposomes (CPL) reconstitutes well and has a larger antitumor activity and lower toxicity than CPL in aqueous solution.

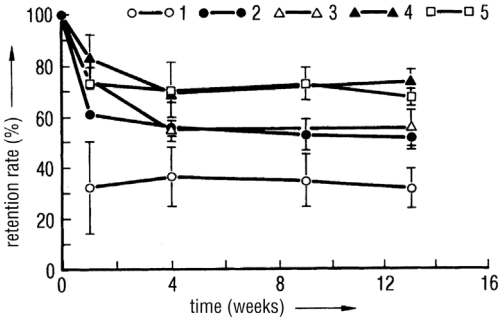

Figure 3.35 Retention rate of liposome-encapsulated hemoglobin as a function of the time elapsed after the reconstitution of the freeze-dried LEH, with different trehalose concentrations as CPA: (1) 0; (2) 10; (3) 50; (4) 150; (5) 300 mM trehalose. (From Rudolph, 1990 [69]. Reproduced with permission of Elsevier.)

Rudolf and Cliff [69] described the inclusion of hemoglobin in liposomes (LEH) to produce a stable blood substitute. The liposomes were formed from a solution of soya bean–phosphatidylcholine (soy PC), cholesterol, dimyristoylphosphatidyl-DL-glycerol (DMPG), and α-tocopherol with a ratio of 10 : 9 : 0.9 : 0.1. The product was dried and rehydrated in a solution of 30 mM trehalose with phosphate buffer, pH 7.4. The evolved multilamellar vesicles were transformed into large unilamellar vesicles (LUV), frozen in LN_2, and freeze-dried. The LEH had an average diameter of 0.4 μm. The retention rate of hemoglobin in freeze-dried LEH is shown in Figure 3.35: After freeze-drying in 150 mM trehalose solution, ~87% of the hemoglobin remained within the liposomes after storage for 13 weeks. In the dry product, stored under vacuum, the level of methemoglobin rose to ~15% after 4 weeks and remained constant at that level up to 12 weeks. That corresponds approximately to the data achieved with liquid LEH stored at +4 °C. The authors expect to develop a storable blood substitute with liposomes.

Foradada and Estelrich [70] studied the encapsulation of thioguanine (TG) in three types of liposomes, produced by extrusion, ethanol injection, and dehydration–rehydration vesicles. The entrapment was examined at three different concentrations (1, 0.1 and 0.01 mM) and three different pH values (4.7, 7.4, and 9.2). The dehydration–rehydration vesicles were found to be the optimum approach to encapsulate TG, independent of the pH value. At pH 4.7, 12 mmol/mol of lipid were entrapped, whereas with the other methods a maximum of 3 mmol/mol of lipid was achieved. The authors related this behavior to the formation of hydrogen bridges between the TG and the liposomes.

Kim and Jeong [71] developed freeze-dried liposomes containing recombinant hepatitis B surface antigen (HbsAg) to enhance the immunogenicity of HbsAg and to produce a stable product during storage. Dehydration–rehydration vesicles with HbsAg were filtered through a 400 nm polycarbonate filter and freeze-dried in a 4 g trehalose/g lipid solution. After 1 year of storage at 4 °C, the vesicles showed a similar size distribution as before freeze-drying and ~70% immunogenicity of HbsAg. Dried liposomes with HbsAg included showed an earlier sero conversion and a higher titer than free HbsAg or a mixture of aluminum phosphate and HbsAg.

van Winden and Crommelin [72] summarized the freeze-drying of liposomes as follows:

The requirements of a liposome drug formulation are

- chemically stable;
- drug remains encapsulated in the liposomes;
- liposome size unchanged during storage.

The freeze-drying of such a formulation is done for two main reasons: (i) The hydrolysis of the phospholipids without most of the water is substantially delayed or avoided. (ii) Other degradation processes are delayed, as the mobility of the molecules is much smaller in the solid state than in the liquid phase. However, damage occurs during the freezing and the freeze-drying process itself. To avoid such damage, in most cases lyoprotectants must be used, although it might be possible to avoid them if certain interactions between the drug and the vesicle can be identified.

The lyoprotectant, for example, disaccharides, forms an amorphous matrix between the liposomes and thus prevents aggregation and fusion during freeze-drying. If the protected liposomes are loaded with drugs that interact with the vesicles, neither separation between drug and liposome nor damage to the liposomes is expected. However, if the drug is water soluble, leakage may even occur at a high ratio of sugar to liposomes (2 g sugar/g liposomes). The retention of the water-soluble carboxyfluorescein (CF) after freeze-drying and reconstitution depends on the lipid composition, vesicle size, and freezing rate.

These influences are described under I–IV at the beginning of this section. The authors concluded from comparisons with freezing and thawing experiments that the leakage may occur during rehydration of the liposomes and not during the freezing process. From FTIR analysis of the freeze-dried cakes, it is further concluded that the influence of size and lipid composition cannot be explained by different levels of bonds between the lyoprotectant and the bilayer component of the liposomes. The CF retention by liposomes based on saturated phospholipid DPPC increases from 42% when slowly frozen (0.5 °C/min) to 80% when frozen in LN_2. DPPC liposomes with cholesterol increase the retention rate from 75 to 90% under the same conditions. On the other hand, no effect of freezing rate was found with liposomes based on unsaturated phospholipid egg phosphatidylcholine (EPC). From these and other experiments, the authors concluded that during freezing the leakage of liposomes may not be induced, but conditions are created that can induce damage during rehydration. Despite the presence of lyoprotectants, ›repacking‹ of the bilayers can occur during and after rehydration.

Studies with the freeze-dried DPPC liposomes in trehalose solution showed that T_g of the amorphous sugar is not the critical temperature during storage, but the bilayer transition temperature T_m for the liposomes determines the short-term stability of the formulation. With trehalose as lyoprotectant and a low residual water content, T_m proved to be 10–30 °C below the onset of T_g; 30 min of heating above T_m but well below T_g decreased the retention of CF after rehydration. T_m after the heating was reduced from 40–80 °C to below 25 °C.

The exact mechanism of leaking induced by heating the dry product above T_m is unclear, but the authors excluded a bilayer phase transition during rehydration or a fusion between the liposomes as a cause of the leakage.

Freeze-dried liposomes loaded with doxorubicin (DXR) have been stored for 6 months at temperatures between −20 and +50 °C. Up to 30 °C, no sign of

degradation was found, but at 40–50 °C, well below the T_g of the dried cake, the total DXR content and the retention of the drug after dehydration decreased, whereas the size of the liposomes increased to a certain extent. The stability with RM below 1% was better than with RM 2.5–3.5%. Lactose, trehalose, and maltose have similar lyoprotectant properties, whereas liposomes with sucrose showed an increase in size.

In summary [72], with an optimized formulation and freeze-drying protocol, liposomes loaded with water-soluble CF or DXR can be freeze-dried with 90% retention upon rehydration. The cake is stable for at least 6 months at temperatures up to 30 °C.

Auvillain *et al.* [73] studied the possibilities of drying nanospheres and nanocapsules without changing their diameter. In addition to a suitable CPA, two conditions during freezing and freeze-drying were decisive: the freezing rate and the melting temperature of the encapsulated oil. The CPA was a 30% trehalose solution (10% was not sufficient). Rapid freezing in an alcohol bath (~4 °C/min) or in LN_2 (~100 °C/min) was necessary to protect the capsule diameter. The included oils did not affect the diameter during freezing and freeze-drying as long as the solidification temperature of the included oil was lower than the essential freezing temperature of the suspension. Oil having a solidification temperature of +4 °C was less suited than one with a temperature of −25 °C, moreover, and a solidification temperature of −65 °C was generally best, as it increased the diameters only marginally or not at all. The authors presumed that the nanocapsules withstood the freezing and drying more easily if the surrounding of the capsules solidified while the oil in the capsule remained soft.

For nanospheres, slow freezing was specified by the authors, although in the opinion of the present author there was a misleading definition of slow freezing. To freeze the nanospheres quickly, the containers with the suspension were placed directly on precooled shelves at −40 °C, producing a ›small number of large crystals.‹ During the ›slow‹ freezing, a natural isolating layer (ice) is built up between the shelves and the containers. This may have led to substantial subcooling followed by an abrupt crystallization, which produced a large number of small crystals. However, such a process should not be denoted ›slow.‹ The freezing may be very fast after a deep subcooling. If this course of events is accepted, the results for nanospheres were comparable to those for nanocapsules. For both nanoparticles, it seems important to produce small crystals quickly. This is possible by freezing in LN_2 and in an alcohol bath with solid CO_2, but subcooling and abrupt freezing can lead to a similar result.

Nemati *et al.* [74] described the freeze-drying of nanoparticles produced from monomeric isohexyl cyanoacrylate (IHCA) in which doxorubicin was encapsulated. The suspension contained: 1% dextran, 70.5% glucose, 10 mg of doxorubicin chlorate, and 50 mg of lactose and the pH was adjusted to 2.3. The product (1.3 mL/vial) was frozen on shelves at −50 °C for 3 h and thermally treated for 24 h at −35 °C. After freeze-drying, the vials with the product were placed for 48 h in a dryer containing P_2O_5. Only after this additional drying did the nanoparticles with doxorubicin have the same diameter after rehydration (351 ± 52 nm) as before freeze-drying (334 ± 55 nm). The present author notes that this second drying

could also be done in the freeze-drying plant, if the condenser temperature is low enough.

Fouarge and Dewulf [75] reported on the freeze-drying of poly(isohexyl cyanocrylate) nanoparticles, which were loaded with dehydroemetine (DHE). The load of absorbed DHE was uniform and reproducible. The stability remained good during 24 months and the acute toxicity of DHE was reduced by combination with nanoparticles, as was the radical concentration.

Fattale *et al.* [76] compared negatively charged liposomes with nanoparticles from poly(isohexyl cyanoacrylate), both of which were loaded with ampicillin. Both carriers were of approximately the same size, 200 nm, but the nanoparticles could be loaded with ~20 times more ampicillin. After freeze-drying and storage at −4 °C, no ampicillin leaked from the nanoparticles, whereas it migrated quickly from the liposomes.

Zimmermann *et al.* [77] developed a freeze-drying process for solid lipid nanoparticles (SLN) loaded with the poorly water-soluble drug RMEZ98 (Novartis). The SLN dispersion contained 2.5% lipids with 99% of all particles smaller than 500 nm. From eight different carbohydrates and two polymers, trehalose and fructose were selected as the most effective CPA. The dried product with fructose had collapsed by visual inspection, but it showed the best results after reconstitution (no comment was made about storage stability). The developed freeze-drying process consisted of the following steps: dilution of the SLN dispersion with trehalose or fructose; cooling in a freezer to −70 °C; thermal treatment at −22 °C for 2 h; cooling to −40 °C for 2 h; MD at 1 mbar with $T_{sh} = -30$ °C for 7 h, −10 °C for 2 h, and 20 °C for 12 h; and SD at 0.001 mbar with $T_{sh} = 30$ °C for 3 h. Some 99% of all particles were smaller than 300 nm before and after freeze-drying and reconstitution for both CPAs. The authors intend to optimize the process further for industrial purposes. The present author notes that since no cake thickness was given, the time schedule cannot be discussed; at a pressure of 1 mbar, one would expect T_{ice} on the order of −20 °C and $T_{sh} = -30$ °C would not be meaningful; it is suggested that a lower pressure and higher temperature during MD, for example, 0.3 mbar and $T_{sh} = 5$ °C, could result in a T_{ice} of, for example, −25 °C and $T_{tot} = 30$ °C (see Figure 2.116). The collapse of fructose under the same process conditions as trehalose is understandable: T'_g of fructose is −42 °C and that of trehalose −30 °C (Table 3.4).

3.5 Antibody

In the human immune system, monoclonal antibodies play an important role in cancer diagnostic and therapy control. Antibodies are protein molecules; they play a role in the immune defense. Another term is immunoglobulin. Today antibodies are indispensable in the treatment of cancer. More than 150 drugs have been approved by the FDA and are free for sale.

Antibody drug conjugates (ADCs), also called immune-conjugates (organic compound), are becoming an increasingly important class of therapeutics. The key feature of the new generation of ADCs is the effective combination of the phototoxicity of natural and synthetic highly potent antineoplastic agents (Gail Phillips, Genentech and Fabric Branle, Hoffmann-La Roche).

Roland Kontermann (University of Stuttgart) reported antibody-conjugates nanoparticles for targeted drug delivery; encapsulation of drugs into liposomal carriers extends plasma half-life and protects the drug from degradation and undesired side effects.

Freeze-drying of antibody drugs needs a very precise process control and monitoring. The freezing process is of particular importance.

Draber *et al.* [78] reported in a research study about "stability of monoclonal IgM antibodies freeze-dried in the presence of trehalose." They describe the use of disaccharide trehalose for the stabilization of monoclonal antibodies during freeze-drying and prolonged storage at elevated temperatures. Application of trehalose for freeze-drying of labile monoclonal IgM antibodies permits convenient long-term storage of large quantities of antibodies and facilitates their transport at ambient temperature. Pikal *et al.* [79] also published stability studies and mechanism of protein stabilization by sugar during freeze-drying and storage. The purpose of this study is to investigate the mechanism of protein stabilization by sugar in the solid state. It explores whether the stabilization is controlled by "glass dynamics" or by structure preservation through "specific interaction" between sugars and protein. For this, IgG1 antibody and recombinant human albumin (rHSA) were formulated with sorbitol, trehalose, and sucrose.

Freeze-drying is the method of choice for the stabilization of labile materials. Although many of the biotechnology products are freeze-dried to achieve adequate shelf-life, proteins may be unstable during the freeze-drying process and/or during storage. In-process degradation is normally minimized by rapid freezing and drying below the relevant glass transition temperature to the optimum residual moisture, usually less than 1%.

Before starting a freeze-drying process, it is imperative to measure freezing behavior and collapse temperature (T_c), T_c, and T'_g were measured by modulated DSC (Sections 1.1.5.3 and 1.1.5.4). In Ref. [80], the process parameter were as follows: freezing below −40 °C (shelf temperature −45 °C), shelf-temperature during primary drying −30 °C, and a chamber pressure of 60 mTorr (0.085 mbar). The product ranged from −39 °C initially to −35 °C at the end of primary drying, as measured with thermocouples in the sorbitol formulation. Primary drying was conducted below T'_g for all the formulations, except for the sorbitol formulation, which finished primary drying at 1 °C above T'_g. Secondary drying was carried out for 4 h at 40 °C.

The water content (residual moisture) for each formulation was determined to be less than 1% using Karl Fischer colorimetric titration. The conclusion is that the presence of sugar in the formulation can improve protein stability and preserve the native structure of protein.

3.6 Transplants, Collagen

The freezing and conservation of viable cells or organs are not discussed here, but only the freezing and freeze-drying of transplants, in which preservation of the structure and its chemical composition is the goal.

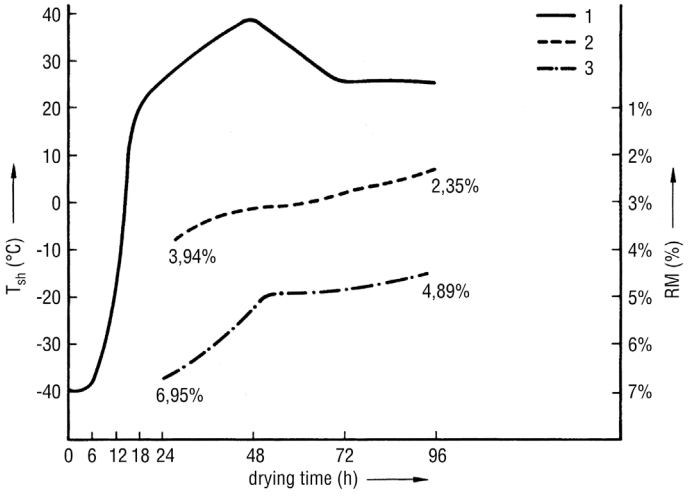

Figure 3.36 Shelf temperature (T_{sh}) as a function of drying time during the freeze-drying of bone corticalis and spongiosa and the related residual moisture content (RM): 1, T_{sh}; 2, RM in spongiosa; 3, RM in bone corticalis. (See also Figure 14 from Ref. [81].)

Hyatt [81] showed a typical temperature and residual moisture course during the freeze-drying of spongiosa and bone corticalis (Figure 3.36). The long drying times are due to three reasons:

- The heat transfer from the shelves to the sublimation front is much smaller compared with the transfer to vials with frozen liquids, as the material has an irregular form and the heat must be transferred through the already dried material (see Section 1.2.1).
- Furthermore, the transplants are often packed in aluminum boxes, which are sealed with sterile filters permeable to water vapor. Even if the box can be designed with a negligible resistance to water vapor flow, the heat transfer is substantially reduced.
- In addition, the transplants may have a larger layer thickness to be dried than in other freeze-drying processes. It is recommended in one charge to freeze-dry transplants of similar layer thickness (the size can vary).

Bassett [82] specified that the transplants be cooled quickly to −78 °C or lower. The transplants should be stored at this temperature for a maximum of 1 year before freeze-drying. The drying process should be terminated only after 1–3% RM is reached. Krietsch *et al.* [83] list 15 different freeze-dried preserves, which had been produced over a period of 10 years, in which bone chips are the largest group with 34%, followed by spongiosa with 22%, dura with 19%, and sinew with 11%.

Marx *et al.* [84] described the application of transplants in the jaw area. All transplants were frozen at −70 to −80 °C or in LN_2 and freeze-dried at a pressure of 0.01 mbar for 21 days to RM <5%.

Merika [85] emphasized from his 17 years of experience with the quality control of freeze-dried transplants the importance of sterility and residual

moisture control as the decisive characteristics. Furthermore, the leak tightness of the storage containers was constantly controlled. Merika did not measure the product temperature during drying, but controlled the process by measuring the water vapor pressure and the temperatures of the shelves and the condenser. The residual moisture content after 2 years of storage must be <5%. All products were sterilized by gamma radiation.

Malinin *et al.* [86] discussed the measurement of RM in freeze-dried bones and compared three methods: gravimetry, Karl Fischer titration, and NMR spectroscopy. The three methods are discussed in Section 1.3.1. All transplants in this comparison were frozen in LN_2 and remained at this temperature for several weeks. The temperature of the condenser during freeze-drying was −60 to −70 °C. The shelves were kept at −30 to −35 °C for the first 3 days. During the last days of the drying, the shelf temperature was raised to +25 or to +35 °C. The chamber pressure (p_{ch}) was 0.1 mbar. During the initial phase of the process, the amount of water vapor transported to the condenser was so large that the ice surface on the condenser was 20 °C warmer than the refrigerant. After 3 days, cooling of the shelves was terminated and the transplant temperature rose to −15 °C. The RM of the dried product was measured at 50 °C over P_2O_5 or in an oven with circulating air at 50 °C or in the same oven at 90 °C over silica gel. Identical measurements were made with fresh bones. For NMR measurements, a known amount of D_2O was added to the bone in a glass container. After equilibrium between D_2O and H_2O had been reached, a known amount of the product was removed from the solution and studied in a Perkin-Elmer NMR spectrometer. In Figure 3.37, the water contents of fresh and freeze-dried bones are listed as measured by NMR and the gravimetric methods at 90 °C. The data show that only a certain amount of the total water can be removed at 90 °C, while another portion is so strongly bound that it cannot be removed by heating. The data also show that the sum of the water measurable by gravimetry and by NMR agrees with the total amount of water.

The merit of Malinin *et al.*'s work is the comparative study of the water content of bones by reproducible methods. The measurement of water vapor pressure during drying cannot be used directly to determine the RM, as Malinin *et al.* correctly state. Measurement of the desorption rates (DR) provides a means to follow quantitatively the course of desorption drying. The method is described in Section 1.2.2, but cannot be applied in an installation as used by Malinin *et al.* because the condenser cannot be separated from the chamber by a valve.

By using the data given in the paper by Malinin *et al.*, it is possible to estimate the freeze-drying process of bone transplants as follows. In the first 3 days, T_{sh} was −30 to −35 °C and T_{co} between −60 and −75 °C. In the early stages of the process, so much water was transported to the condenser that a thick ice layer condensed on the surface, producing a surface temperature of −50 °C. This amount of water cannot sublime from the bones. At T_{sh} −35 °C and T_{pr} −35 °C, only such ice as was condensed during the loading on the cold shelves and transport boxes was sublimed. This was also confirmed by the temperature rise in the bones from −70 to −65 °C by 5–10 °C after commencing evacuation and a further increase in bone temperature to −35 °C. If the water were to sublime in large amounts from the bones, their temperature should be lowered by the energy of sublimation. The

Type of bone	1 Total water by NMR (%)	2 Water removed at 90 °C (%)	3 Water content by NMR after 2 (%)	4 Sum of water 2 + 3 (%)
Fresh, ground corticalis (tibia)	17.34	12.56	4.43	16.99
Fresh, ground corticalis (femur)	20.5	14.62	5.28	19.90
Freeze-dried, ground corticalis	7.55	5.73	4.20	9.93

Figure 3.37 Water content of fresh and freeze-dried bone corticalis: 1, water content measured by NMR; 2, water removed in an oven at 90 °C over P_2O_5; 3, water content measured by NMR after the drying according to (2) has been completed; 4, sum calculated from (2) and (3). (Part of Table 16-3 from Ref. [86].)

temperature increase showed that the water did not come from the bones. This ice load of the condenser and the time taken may be avoided. The transportation boxes should be isolated during transport as much as is practicable and the door of the installation opened for only a short time. During this short period, a small stream of dry (dew point −40 °C) and sterile air should flow through the chamber, producing a small positive pressure (a few millimeter water column). If the condenser can be separated from the chamber by a valve, as assumed in the further discussion, no water vapor could condense on the condenser during the loading of the chamber. After 3 days, cooling of the shelves was terminated and the temperature of the bones rose to −15 °C. The operating pressure in the plant was always 0.1 mbar or less. The first 3 days can be saved, since at T_{pr} −35 °C, p_s is ~0.2 mbar. The amount of water sublimed during these 3 days was small compared with the amount sublimed thereafter at T_{pr} −15 °C, since $p_s \approx$ 1.5 mbar. From the third day on, seven times more water per unit time can be sublimed than in the previous days. Therefore, it is recommended to increase T_{sh} from the beginning to −15 °C. The ice temperature at the sublimation front, T_{ice}, established under these conditions can be measured by BTM, as shown in Section 1.2.1.

The easiest way to control T_{ice} is via the operating pressure. T_{ice} depends on only two processes:

- heat transfer from the shelves to the sublimation front;
- mass transfer from the sublimation front to the condenser.

Heat transfer from the shelves to the sublimation front depends on the pressure and the distance between shelf and product (Figure 1.58). Mass transfer (g/s) increases with pressure, but also depends on the flow resistance of the already dry product and of the packing of the bones. If the maximum tolerable T_{ice} is defined, the drying time depends only on the two processes mentioned above. It cannot be shortened under a given geometric situation and the chosen T_{ice}. This method of T_{ice} control does not require thermocouples and does not contaminate the product.

Selection of the maximum tolerable T_{ice} cannot be done by the methods described in Section 1.1.5 as no uniform mass exists. Willemer [87] concluded

from measurements of homogenized tissue that the maximum T_{ice} is −25 °C, whereas Malinin *et al.* [86] suggested −15 °C after 3 days. The present author notes that −15 °C may not represent T_{ice}, but the surface temperature of a bone.

During MD, T_{ice} can be closely controlled and the change from MD to SD documented and, if required, automatically executed. During SD, the pressure control can be switched off, the pressure will drop, and the progress of SD can be followed by DR measurements. DRs give the amount of water desorbed/h in % of solids. By integration over time, it can be decided when, for example, 5% desorbable water is reached and which result can be expected in a further 48 h of drying.

Figures 3.38 and 3.39[1] present the data for the freeze-drying of 622 g of bone corticalis from swine, which were cut into pieces of 6 × 11 cm and 2 cm thickness or 2.5 × 4.5 cm and 3 cm thickness. The pieces were placed in aluminum trays. Three thermocouples were fixed into holes bored in the bones. Cooling from +20 to −45 °C took ~2.5 h. After the evacuation, T_{sh} was raised to +22 °C and the operating pressure controlled at 1.2 mbar TM, corresponding to 0.8 mbar CA. After 2 h, an equilibrium was reached between shelf temperature, product temperature, surface temperature, and T_{ice} at ≃35 °C. This remained for slightly less than 5 h between −32 and −35 °C, while the temperatures on the bones increased to −5 °C. After 19 h, the controlled operating pressure could no longer be kept constant and DR measurements showed, after 21 h at a constant T_{pr} of

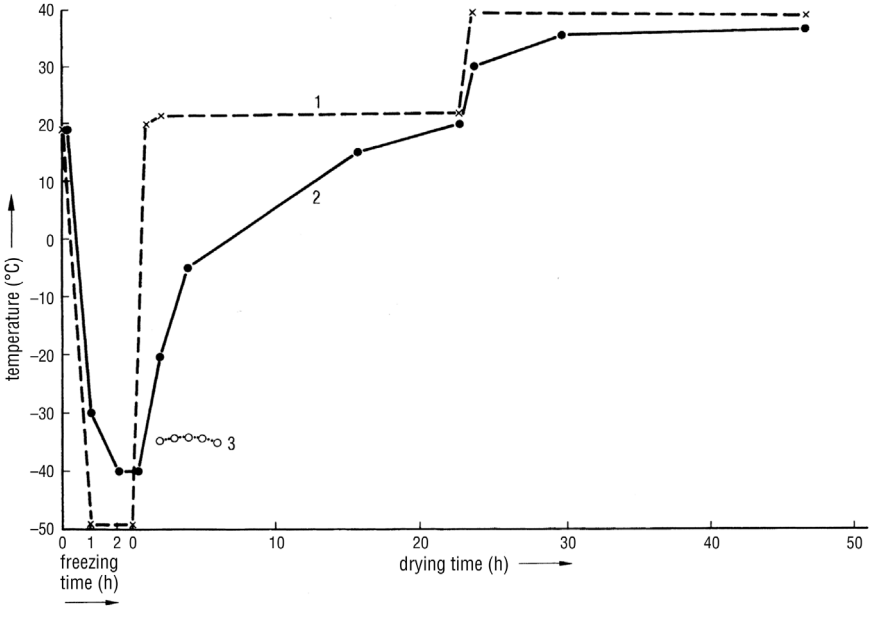

Figure 3.38 Course of the freeze-drying of 622 g of corticalis of pork: 1, temperature of the shelves; 2, average temperature of the bones (three sensors); 3, temperature of the sublimation front (T_{ice}), measured by BTM. (Measurements by Steris GmbH, Hürth, Germany.)

1 Measurements by Steris GmbH, Hürth, Germany.

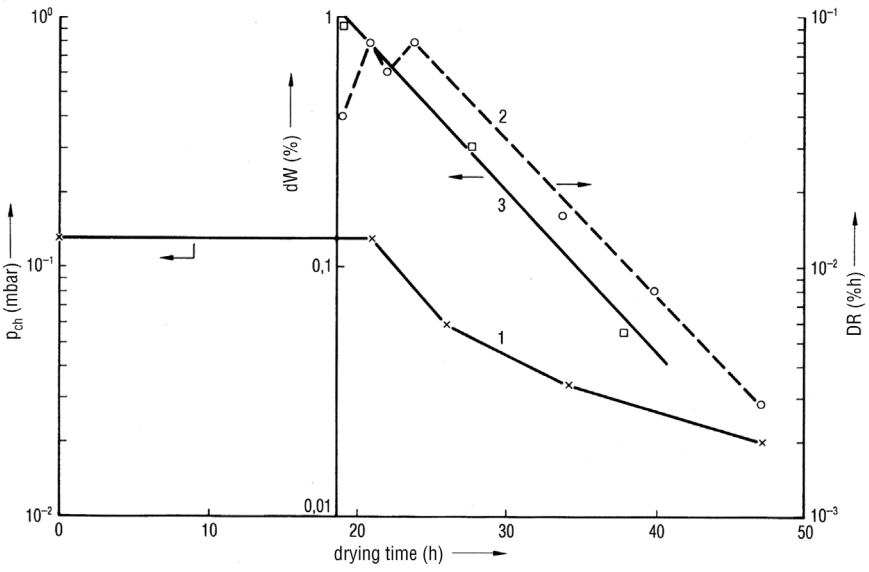

Figure 3.39 Plots of pressure, DR and dW during the drying shown in Figure 3.38. 1, Chamber pressure p_{ch}, left ordinate; 2, desorption rate, DR = water desorbed in % of solids/h, right ordinate; 3, desorbable water, dW = water in % of solids (residual moisture at the given T_{pr}). (DR and dW calculated from pressure rise measurements by Steris GmbH, Hürth, Germany.)

~+20 °C, a falling tendency. The increase in T_{sh} to +40 °C can be seen in the DR data (Figure 3.39). From the DR data, it is possible to estimate the amount of desorbable water (dW) after 19 h (in % solids), as shown by the straight line in Figure 3.39. At 19 h, dW was ~0.9%, at 28 h ~0.24% and at 38 h ~0.05%. Any further drying would not reduce the dW data measurably. The dW data, in this example at 37 °C, provided the information on the time at which the drying could be terminated. At a different temperature, for example, +90 °C, a different equilibrium will be aimed for. DW data and the RM measured by Malinin *et al.* at +90 °C in a vacuum oven and by NMR spectroscopy [86] are different numerical quantities, but can be combined:

Residual moisture content in % of solids:

1.	dW at +37 °C	0.06
2.	Removable water at 90 °C in a vacuum oven over silica gel	4.60
3.	Water content by NMR after operation 2 is concluded	2.49
	Total water content after freeze-drying	7.15

At the end of the freeze-drying process shown in Figure 3.38, four pieces of bone were weighed and had lost 24.5, 24.2, 20.9, and 26.5% (average 24.4%) of their original weight. Drying was then continued for additional 40 h, at which time the average weight loss was 24.6%. The desorbable water dW could not be reduced any further after 46 h of the first drying.

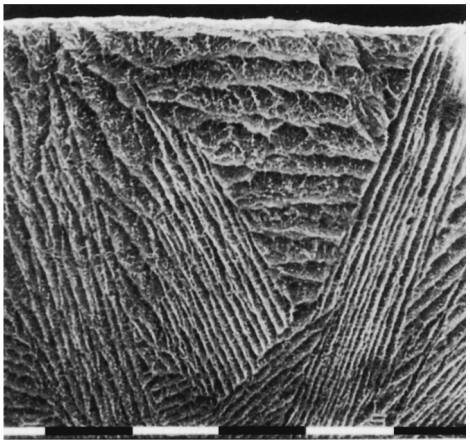

Figure 3.40 Porous structure of collagen sponge produced by freezing in a cryogenic bath at −25 °C and subsequently freeze-dried (scanning electron microscope, white bar = 1 mm). (Schoof, H., Apel, J., Heschel, I., and Rau, G. Influence of the freezing process on the porous structure of freeze-dried collagen sponges. Unpublished results, Helmholtz-Institute, Aachen.)

Schoof *et al.* (Schoof, H., Apel, J., Heschel, I., and Rau, G. Influence of the freezing process on the porous structure of freeze-dried collagen sponges. Unpublished results, Helmholtz-Institute, Aachen) described the development of a collagen product with homogeneous pores whose sizes can be determined by the freezing conditions. The authors quoted several publications in which the homogeneous pore size distribution was shown as essential to optimize the population of the implanted collagen by living cells. The desirable sizes varied between 20 and 125 µm. The collagen suspension, supplied by Dr Otto Suwelack Nachf. GmbH & Co., Billerbeck, Germany, contained 1.8% collagen, water, and HCl at pH 3.2. Furthermore, 3.8% acetic acid was added (pH 2.5). The samples were frozen by the Power-Down process, in which a temperature gradient is applied between the two ends of the sample. Subsequently, the end temperatures are lowered with a constant cooling rate while the temperature gradient is kept constant. In comparison, the same collagen suspension containing 3.8% acetic acid was conventionally frozen in a cold bath at −25 °C. The frozen samples were freeze-dried. Figure 3.40 shows the structure of freeze-dried collagen sponges that were conventionally frozen and freeze-dried. In Figure 3.41, the collagen was frozen by the Power-Down method and freeze-dried; Figure 3.42 shows a part of

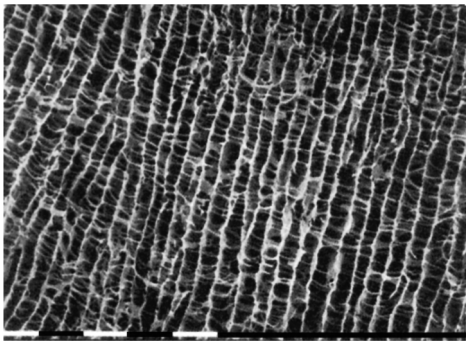

Figure 3.41 Porous structure of collagen sponge produced by directional solidification according to the Power-Down method and subsequently freeze-dried (scanning electron microscope, white bar = 1 mm). (Schoof, H., Apel, J., Heschel, I., and Rau, G. Influence of the freezing process on the porous structure of freeze-dried collagen sponges. Unpublished results, Helmholtz-Institute, Aachen.)

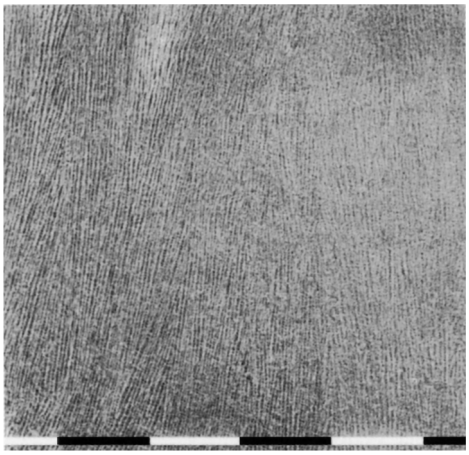

Figure 3.42 Magnification of the defined and homogeneous porous structure of a collagen sponge produced by directional solidification according to the Power-Down method and subsequent freeze-drying (scanning electron microscope, white bar = 0.1 mm). (Schoof, H., Apel, J., Heschel, I., and Rau, G. Influence of the freezing process on the porous structure of freeze-dried collagen sponges. Unpublished results, Helmholtz-Institute, Aachen.)

Figure 3.41 enlarged ~10 times. The pore size can be influenced by the acetic acid content: From 3.8 to 1.5% w/w the size was reduced from ~40 to 20 µm; the temperature gradient was 50 K/cm in this experiment.

3.7 Freeze-Drying Subject Terms – Overview and Summary

Freeze-drying or lyophilization is a dehydration process in which a solution or suspension is frozen and is subsequently dried. The goal is to withdraw the water from the product (water is the reactant partner) and thus chemical reactions (hydrolysis, rearrangements, oxidations, and especially proteins and peptides and ß-elimination) to avoid or reduce them (see Sections 1.1.6 and 3.1).

Solvent: In 95% of all formulations, water is the solvent. Another known solvent is *tert*-butanol (*t*-BA), used in combination with water.

Crystal structure: amorphous and crystalline. Crystalline systems show sharp peaks, their position and the intensity of the crystal compound are a characteristic. Amorphous systems show no sharp peaks in the diffractogram, only "amorphous hills." The freezing behavior of an aqueous amorphous solution has been described in the literature as follows: After supercooling of the solution and subsequent nucleation, the temperature of the solution increases up to equilibrium freezing point. As a general rule, it can be seen that a first fast freezing in a range of <15 °C/min results in fully amorphous structure. Afterward an annealing step can be used for recrystallization of the product. Slow freezing of a product facilitates the formation of a crystalline structure. In connection with annealing, a homogeneous ice structure is reached (see Section 2.1.6)

Crystalline structure former: The freezing of complex solutions and suspensions is often difficult and needs structure formers (Section 1.1.5) trehalose, mannitol, lactose, dextran, and saccharose.

Cryoprotection agents (CPA): Labile products like proteins, peptides, and viruses need CPAs for stabilization (Section 1.1.2).

Excipients: These are added to an active component to overcome the instability issues. Excipients can be categorized in bulking agents, stabilizers, buffers, surfactants, and miscellaneous, depending on their role in the formulations (Sections 1.1.3 and 3.1).

Bulking agents: These should provide cake stability and an attractive appearance. Mannitol and glycine belong to this class, but they tend to readily crystallize. However, it is essential to ensure complete crystallization of these agents during the freezing step and avoid stability problems of the final product.

Stabilizer: Protection against denaturation (Table 1.12).

Unfreezable water (UFW): UFW is water that cannot freeze, even at ultradeep temperatures (Tables 1.2 and 1.3). Almost each product contains a certain amount of UFW. In most cases, this amount does not interfere. The amount is too small to affect the freezing or drying process.

Eutectic point/temperature: The eutectic point/temperature denotes the point where all liquid components of a solution are converted into the solid aggregate state. It is known that some components cannot be frozen → UFW.

Glass transition: It is always a temperature range and not a single temperature value.

Ice structure: Crystalline, amorphous, and semihexagonal.

Annealing – simplified definition: Annealing refers to the temporary residence of the product at a temperature below the freezing point, but above the glass transition. The purpose of annealing is to assist the crystallization process of API or excipients such as mannitol or glycine (Section 1.1.5.4). *Typical annealing step:* Complete freezing of the product, perhaps in two to three steps (equilibrium phase), increasing the shelf temperature to a minimum 10–20 °C above T_c and keep or hold this temperature for a couple of hours. After the hold time has elapsed, the shelf temperature is lowered to the final shelf temperature. The lyophilization process can start.

Thermal treatment: See **Annealing**.

Residual moisture (RM): The residual moisture content in a lyophilized product is an important quality characteristic. Not only the quality but also the stability and the shelf life are determined by the residual moisture content. The "gold standard" with regard to residual moisture content in a freeze-dried cake is less than 1%. However, some proteins are more stable with higher residual moisture content. Residual moisture content can be determined by Karl Fischer titration or if that is not possible, thermal analysis, like DSC or TGA (Section 1.1.5.4), which can overcome the limitations of KF. The ice structure – amorphous or crystalline – may influence the residual moisture content.

Buffer: Mannitol, trehalose, sucrose, and dextrose. See also **Excipients**.

Water cluster: In water that is very well cleared of all foreign particles, the clusters begin to crystallize in subcooled water at −39 °C; this is known as homogeneous nucleation.

Differential Scanning Calorimetry (DSC) (Section 1.1.5.4)**:** With DSC, melting, crystallization, glass transitions (T'_g; T_g), heat capacity of a substance (C_p), aging of a material, purity, protein denaturation, and others can be measured.

References

1 Schiffter, H. (2008) Proteine und Peptide, die Arzneimittel der Zukunft. Freeze-Drying Seminar, University Erlangen-Nuernberg, Germany.
2 Jiang, S. and Nail, S.L. (1998) Effect of process conditions on recovery of protein activity after freezing and freeze-drying. *Eur. J. Pharm. Biopharm.*, **45**, 249–257.
3 Vermuri, S., Yu, C., and Roosdorp, N. (1994) Effect of cryoprotectants on freezing, lyophilization and storage of lyophilized recombinant alpha-antitrypsin formulations. *PDA J. Pharm. Sci. Technol.*, **48**, 241–246.
4 Carpenter, J.F., Crowe, J.H., and Arakawa, T. (1992) Comparison of solute-induced protein stabilization in aqueous solution and in the frozen and dried states, in *Developments in Biological Standardization*, vol. 74 (eds J.C. May and F. Brown), Karger, Basel, pp. 225–239.
5 Craig, D.Q.M., Royall, P.G., Kett, V.L., and Hopton, M.L. (1999) The relevance of the amorphous state to pharmaceutical dosage forms: glassy drugs and freeze-dried systems. *Int. J. Pharm.*, **179**, 179–207.
6 Hatley, R.H.M. and Blair, J.A. (1999) Stabilization and delivery of labile materials by amorphous carbohydrates and their derivatives. *J. Mol. Catal. B*, **7**, 11–19.
7 Remmele, R.L., Stushnoff, C., and Carpenter, J.F. (1994) Real-time spectroscopy analysis of lysozyme during lyophilization: structure–hydration behavior and influence of sucrose. *Formulation and Delivery of Proteins and Peptides*, ACS Symposium Series, vol. 567, pp. 170–192.
8 Franks, F., Hatley, R.H.M., and Mathias, S.F. (1991) T_g values for glass forming anhydrous carbohydrates. *Pharm. Technol. Int.*, **3**, 24–34.
9 Skrabanja, A.T.P., de Meere, A.L.J., de Ruiter Rien, A., and van der Oetelaar, P.J.M. (1994) Lyophilization of biotechnology products. *PDA J. Pharm. Sci. Technol.*, **48**, 311–317.
10 Pikal, M.J. (1990) Freeze-drying of proteins, part II, formulation selection. *Bio-Pharm.*, **3**, 26–30.
11 Izutsu, K., Yoshioka, S., and Takeda, K. (1991) The effect of additives on the stability of freeze-dried ›beta-galactosidase‹ stored at elevated temperature. *Int. J. Pharm.*, **71**, 137–146.
12 De Luca, P.P. (1992) Development of lyophilization formulations. International Colloquium on Ind.-Pharm. Lyophilization, Gent.
13 Jiang, S. and Nail, S.L. (1998) Effect of process conditions on recovery of protein activity after freezing and freeze-drying. *Eur. J. Pharm. Biopharm.*, **45**, 249–257.
14 Ru, M.T., Dordick, J.S., Reimer, J.A., and Clark, D.S. (1999) Optimizing the salt-induced activation of enzymes in organic solvents: effects of lyophilization time and water content. *Biotechnol. Bioeng.*, **63**, 233–241.
15 Allison, S.D., Manning, M.C., Randolph, T.W., Middleton, K., Davis, A., and Carpenter, J.F. (2000) Optimization of storage stability of lyophilized actin using combinations of disaccharides and dextran. *J. Pharm. Sci.*, **89**, 199–214.
16 Willemer, H. (1996) Freeze-drying process data determination for human blood derivatives with factor VIII as example. PDA Fourth International Congress, Vienna, pp. 142–151.

17 Pikal, M.J. and Shah, S. (1992) Moisture transfer from stopper to product and resulting stability applications, in *Developments in Biological Standardization*, vol. 74 (eds J.C. May and F. Brown), Karger, Basel, pp. 165–179.
18 Pikal, M.J., Dellermann, K., and Roy, M.L. (1992) Formulation and stability of freeze-dried proteins: effects of moisture and oxygen on the freeze-dried formulation of human growth hormones, in *Developments in Biological Standardization*, vol. 74 (eds J.C. May and F. Brown), Karger, Basel, pp. 21–38.
19 Williams, M.L., Landel, R.F., and Ferry, J.D. (1955) The temperature dependence of relaxation mechanisms in amorphous polymers and other glass forming liquids. *J. Am. Chem. Soc.*, **77**, 3701–3707.
20 Roy, M.L., Pikal, M.J., Rickard, R.C., and Maloney, A.M. (1992) The effects of formulation and moisture on the stability of freeze-dried monoclonal antibody–vinca conjugate: a test of the WLF glass transition theory, in *Developments in Biological Standardization*, vol. 74 (eds J.C. May and F. Brown), Karger, Basel, pp. 323–340.
21 Jensen, L.H. (1992) The structure of water in protein crystals, in *Developments in Biological Standardization*, vol. 74 (eds J.C. May and F. Brown), Karger, Basel, pp. 53–61.
22 Teeter, M.M. (1992) Order and disorder in water structure of crystalline proteins, in *Developments in Biological Standardization*, vol. 74 (eds J.C. May and F. Brown), Karger, Basel, pp. 63–72.
23 Hageman, M.J., Possert, P., and Bauer, J.M. (1992) Prediction and characterization of the water sorption isotherm for bovine somatropin recombinant. *J. Agric. Food Chem.*, **40**, 342–347.
24 Costantino, H.R., Curley, J.G., and Hsu, C.C. (1997) Determining the water sorption monolayer of lyophilized pharmaceutical proteins. *J. Pharm. Sci.*, **86**, 1390–1393.
25 Townsend, M.W. and de Luca, P.P. (1988) Use of lyoprotectants in the freeze-drying of a model protein, ribonuclease A. *J. Parenteral Sci. Technol.*, **42**, 190–196.
26 Townsend, M.W., Byron, P.R., and de Luca, P.P. (1990) The effects of formulation additives on the degradation of freeze-drying ribonuclease A. *Pharm. Res.*, **7**, 1086–1091.
27 Townsend, M.W. and de Luca, P.P. (1990) Stability of ribonuclease A in a solution and the freeze-dried state. *J. Pharm. Sci.*, **79**, 1083–1086.
28 de Luca, P.P. and Townsend, M.W. (1989) Stability of ribonuclease-A in solution and the freeze-dried state. *Congr. Int. Technol. Pharm. 5th*, **1**, 457–465.
29 Miller, D.P., Anderson, R.E., and De Pablo, J.J. (1998) Stabilization of lactate dehydrogenase following freeze–thawing and vacuum-drying in the presence of trehalose and borate. *Pharm. Res.*, **15**, 1215–1221.
30 Maa, Y.-F., Nguyen, P.-A., Sweeney, T., Shire, S.J., and Hsu, C.C. (1999) Protein inhalation powders: spray drying vs spray freeze-drying. *Pharm. Res.*, **16**, 249–254.
31 Carpenter, J.F. and Crowe, J.H. (1989) An infrared spectroscopy study of the interactions of carbohydrates with dried proteins. *Biochemistry*, **28**, 3916–3927.

32 Dong, A., Prestrelski, S.J., Allison, S.D., and Carpenter, J.F. (1995) Infrared spectroscopy studies of lyophilization- and temperature-induced protein aggregation. *J. Pharm. Sci.*, **84**, 415–424.

33 Hora, M.S., Rana, R.K., Wilcox, C.L., Katre, N.V., Hirtser, P., Wolfe, S.V., and Thomson, J.W. (1992) Development of lyophilized formulation of interleukin-2 (rhIL-2), in *Developments in Biological Standardization*, vol. 74 (eds J.C. May and F. Brown), Karger, Basel, pp. 295–306.

34 Brewster, M.E. (1991) Use of 2-hydroxypropyl-beta-cyclodextrin (HPCD) as a solubilizing and stabilizing excipient for protein drugs. *Pharm. Res.*, **8**, 792–795.

35 Page, C., Dawson, P., Woollacott, D., Thorpe, R., and Mire-Sluis, A. (2000) Development of a lyophilization formulation that preserves the biological activity of the platelet-inducing cytokine interleukin-11 at low concentrations. *J. Pharm. Pharmacol.*, **52**, 19–26.

36 Garzon-Rodriguez, W., Chongpraset, S., Koval, R., Krishnan, S., Randolph, T.W., Warne, N., and Carpenter, J.F. (2001) Use of polymer/sugar mixtures to optimize storage stability of freeze-dried recombinant human interleukin-11. Abstr. Pap. Am. Chem. Soc. 221st, BIOT-014.

37 Prestrelski, S.J., Pikal, K., and Arakawa, T. (1995) Optimization of lyophilization conditions for recombinant interleukin-2 by dried state conformational analysis using Fourier-transform infrared spectroscopy. *Pharm. Res.*, **12**, 1250–1259.

38 Carpenter, J.F., Kreilgaard, L., Jones, L.S., Webb, S., and Randolph, T.W. (1998) Mechanisms of protein stabilization by non-ionic surfactants. Freeze-Drying of Pharmaceuticals and Biologicals, National Science Foundation, Industry/University Cooperative Research Center for Pharmaceutical Processing, CPPR, Brownsville, VT.

39 Kreilgaard, L., Frokjaer, S., Flink, J.M., Randolph, T.W., and Carpenter, J.F. (1998) Effects of additives on the stability of recombinant human factor XIII during freeze-drying and storage in the dried solid. *Arch. Biochem. Biophys.*, **360**, 121–134.

40 Kreilgaard, L., Frokjaer, S., Flink, J.M., Randolph, T.W., and Carpenter, J.F. (1999) Effects of additives on the stability of *Humicola lanuginosa* lipase during freeze-drying and storage in the dried solid. *J. Pharm. Sci.*, **88**, 281–290.

41 Ma, X., Wang, D.Q., Bouffard, R., and MacKenzie, A. (2001) Characterization of murine monoclonal antibody to tumor necrosis factor (TNF-MAb) for freeze-drying cycle development. *Pharm. Res.*, **18**, 196–202.

42 Greiff, D. (1971) Important variables in the long term stability of viruses dried by sublimation of ice *in vacuo*. XIIIth International Congress of Refrigeration, International Institute of Refrigeration (IIR), Washington, DC, pp. 657–667.

43 Greiff, D. (1982) The cryobiology of viruses classified according to their chemical, physical and structural characteristics. International Institute of Refrigeration (IIR) (Comm. C 1), pp. 8–11.

44 Doner, T., Dundrarova, D., Teparicharova, I., Orozeva, M., Bustandzieva, R., and Mitor, B. (1989) Choice of cryoprotective media and freeze-drying parameters of bovine corona-virus and respiratory syncytial virus. IVth International School Cryobiology and Freeze-Drying, Sofia, pp. 31–32.

45 Bennett, P.S., Maigetter, R.Z., Olson, M.G., Provost, P.J., Scattergood, E.M., and Schofield, T.L. (1992) The effects on freeze-drying of the potency and stability of

live varicella virus vaccine, in *Developments in Biological Standardization*, vol. 74 (eds J.C. May and F. Brown), Karger, Basel, pp. 215–221.
46 Terentier, A.N. and Kadeter, V.V. (1989) Freeze-drying of the vaccine strain *Yersinia pestis* EV 76. IVth International School Cryobiology and Freeze-Drying, Sofia, pp. 29–30.
47 Morichi, T., Irie, R., Yano, N., and Kembo, H. (1965) Protective effect of organic and related compounds on bacterial cells during freeze-drying. *Agric. Biol. Chem.*, **29**, 61–65.
48 Gehrke, H.-H., Krützfeld, R., and Deckwer, W.D. (1990) Gefriertrocknen von Mikro-organismen. I. Experimentelle Methoden und typische Ergebnisse. *Chem. Ing. Tech.* doi: 10.1002/cite.330620229.
49 Israeli, E., Shaffer, B.T., and Lighthart, B. (1993) Protection of freeze-dried *Escherichia coli* by trehalose upon exposure to environmental conditions. *Cryobiology*, **30**, 510–523.
50 Kabatov, A.I., Nikonov, B.A., Sventitskii, E.N., and Afanasi, E.S. (1991) Working out the means of recreating the biological activity of *Saccharomyces cerevisiae* yeast at sublimation drying. *Biotekhnologiya*, **1**, 45–46.
51 Pitombo, R.N.M., Spring, C., Passos, R.F., Tonato, M., and Vitalo, M. (1994) Effect of moisture content on the interface activity of freeze-dried *S. cerevisiae*. *Cryobiology*, **31**, 383–392.
52 Lodato, P., Segovia de Huergo, M., and Buera, M.P. (1999) Viability and thermal stability of a strain of *Saccharomyces cerevisiae* freeze-dried in different sugar and polymer matrices. *Appl. Microbiol. Biotechnol.*, **52**, 215–220.
53 Rakotozafy, H., Louka, N., Therisod, H., and Allaf, K. (2000) Drying of baker's yeast by a new method: dehydration by successive pressure drops (DDS). Effect on cell survival and enzymatic activities. *Drying Technol.*, **18**, 2253–2271.
54 Rindler, S., Luneberger, P., Schwindke, I., and Rau, G. (1999) Freze-drying of red blood cells at ultra-low temperatures. *Cryobiology*, **38**, 2–15.
55 Bakaltcheva, I. and Reid, T. (2002) Lyophilization of blood cells. International Conference on Lyophilization–Freeze-Drying, Amsterdam, October 2002, International Society of Lyophilization–Freeze-Drying, Bala Cynwyd, PA.
56 Neumann, K.H. (1952) *Grundriss der Gefriertrocknung, 2. Auflage*, Musterschmidt Wissenschaftlicher Verlag, Göttingen, pp. 102–103.
57 Koyama, Y., De Angelis, R.J., and De Luca, P.P. (1988) Effect of solvent addition and thermal treatment on freeze-drying of cefazolin. *PDA J. Parenteral Sci. Technol.*, **42**, 47–52.
58 Ikeda, M. (1994) Development of a multilayer lyophilization technique for parenteral dosage forms. PDA Asian Symposium, Tokyo, pp. 261–266.
59 Jonkman-de Vries, J.D., Talsma, H., Henrar, R.E.C., Kettenes-van den Bosch, J.J., Bult, A., and Beijnen, J.H. (1994) Pharmaceutical development of a parenteral lyophilized formulation of the novel indoloquinone antitumor agent E 09. *Cancer Chemother. Pharmacol.*, **34**, 416–422.
60 Kagkadis, K.A., Rekkas, D.M., Dallas, P.P., and Choulis, N.H. (1996) A freeze-dried injectable form of ibuprofen: development and optimization using respond surface methodology. *PDA J. Pharm. Sci. Technol.*, **50**, 317–323.
61 Crowe, J.H., Leslie, S.B., and Crowe, L.M. (1994) Is vitrification sufficient to preserve liposomes during freeze-drying? *Cryobiology*, **31**, 355–366.

62 Ausborn, M. and Nuhn, P. (1991) Möglichkeiten und Probleme der Stabilisierung von Liposomen durch Frier- und Lyophilisationsverfahren. 2. Mitteilung:Einfluss von Saccharose und Saccharose-Fettsäureestern auf das Verhalten von Lecithin-Cholosterol-Liposomen. Pharm. Ztg. Wiss., No. 1–4/136. Jahrgang, Govi–Verlag, Eschborn, pp. 17–24.

63 Crowe, L.M. and Crowe, J.H. (1992) Stabilization of dry liposomes by carbohydrates, in *Developments in Biological Standardization*, vol. 74 (eds J.C. May and F. Brown), Karger, Basel, pp. 285–294.

64 Hauser, H. and Strauss, G. (1988) Stabilization of small unilamellar phospholipid vesicles by sucrose during freezing and dehydration. *Adv. Exp. Med. Biol.*, **238**, 71–80.

65 Ausborn, M., Schreier, H., Brezesinnski, G., Fabian, H., Meyer, H.W., and Nuhn, P. (1994) The protective effect of free and membrane-bound cryoprotectants during freezing and freeze-drying of liposomes. *J. Controlled Release*, **30**, 105–116.

66 Suzuki, T., Komtatse, H., and Miyajima, K. (1996) Effects of glucose and its oligomers on the stability of freeze-dried liposomes. *Biochim. Biophys. Acta*, **1278**, 176–182.

67 Jizomoto, H. and Hirano, K. (1989) Encapsulating of drugs by lyophilized empty dipalmitoylcholine (DPPC) liposomes: effects of calcium ion. *Chem. Pharm. Bull.*, **37**, 3066–3069.

68 Gu, X.Q. and Gao, X.Y. (1989) A novel procedure for preparing liposome entrapment of cyclophosphamine (CPL) in its reconstituted form, the properties and antitumor activities of the reconstituted CPL. Congr. Int. Technol. Pharm. 5th, vol. 3, pp. 60–65.

69 Rudolph, A.S. and Cliff, R.O. (1990) Dry storage of liposome-encapsulated hemoglobin: a blood substitution. *Cryobiology*, **27**, 585–590.

70 Foradada, M. and Estelrich, J. (1995) Encapsulation of thioguanine in liposomes. *Int. J. Pharm.*, **124**, 261–269.

71 Kim, Ch.K. and Jeong, E.J. (1995) Development of dried liposomes as effective immuno-adjuvants for hepatitis B surface antigen. *Int. J. Pharm.*, **115**, 193–199.

72 van Winden, E.C.A. and Crommelin, D.J.A. (1998) Freeze-drying of liposomes. International Conference on Freeze Drying, National Science Foundation, Industry/University Cooperative Research Center for Pharmaceutical Processing, CPPR, Brownsville, VT.

73 Auvillain, M., Caré, G., Fessi, H., and Devissaguet, J.P. (1989) Lyophilisation de vecteurs colloidaux submicromiques. *S.T.P. Pharma*, **5**, 738–747.

74 Nemati, F., Cave, G.N., and Couvreur, P. (1992) Lyophilization of substances with low water permeability by a modification of crystallized structures during freezing. Assoc. Pharm. Galenique Ind., Chatenay Malabry, vol. 3, pp. 487–493.

75 Fouarge, M. and Dewulf, D. (1989) Development of dehydroematine (DHE) nanoparticles for the treatment of visceral leishmaniasis. *J. Microencapsulation*, **6**, 29–34.

76 Fattale, E., Rojas, J., Roblot-Treupal, L., Andremont, A., and Couveur, P. (1991) Ampicillin-loaded liposomes and nanoparticles: comparison of drug loading, drug release and *in vitro* antimicrobial activity. *J. Microcapsulation*, **8**, 29–36.

77 Zimmermann, E., Müller, R.H., and Mader, K. (2000) Influence of different parameters on reconstitution of lyophilized SLN. *Int. J. Pharm.*, **196**, 211–213.
78 Draber, P., Draberova, E., and Novakova, M. (1995) Stability of monoclonal IgM antibodies freeze-dried in the presence of trehalose. *J. Immunol. Methods*, **181** (1), 12.
79 Pikal, M.J., Rigsbee, D., and Roy, M.L. (2005) The stability of freeze-dried biosynthetic human growth hormone (hGH) I. The effect of formulation on storage stability. *Pharm. Res.*, **14**, 1379–1387.
80 Pikal;, M.J., Chang, L., Shepherd, D., Sun, J., Quellette, D., Grant, K.L., and Tang, C. (2005) Mechanism of protein stabilization by sugar during freeze-drying and storage: native structure preservation, specific interaction, and/or immobilization in a glassy matrix. *J. Pharm. Sci.*, **94** (7), 1427–1444.
81 Hyatt, G.W. (1960) Procédés employés pour obtenir des tissus humain à usage chirurgical et, en particulier, méthode de conversion par lyophilisation, in *Traité de Lyophilisation* (eds L. Rey *et al.*), Hermann, Paris, pp. 279–301.
82 Bassett, C.A.L. (1964) A survey of the current status of tissue procurement, processing and use, in *Aspects Theoriques et Industriels de la Lyophilisation*, Hermann, Paris, pp. 332–339.
83 Krietsch, P., Hackensellner, H.A., and Näther, J. (1965) 10 jährige Erfahrung bei der Herstellung und Anwendung von Gewebekonserven in der DDR. 6. Gefriertrocknungstagung Leybold-Hochvakuum-Anlagen, Köln.
84 Marx, R.E., Kline, S.N., Johnson, R.P., Malinin, T.I., Matthews, J.G., II, and Gambil, V. (1981) The use of freeze-dried allogeneic bone in oral and maxillofacial surgery. *J. Oral Surg.*, **39**, 264–274.
85 Merika, P. (1983) Quality control of freeze-dried tissue grafts. International Institute of Refrigeration (IIR) (Comm. C1), Paris, pp. 102–105.
86 Malinin, T.I., Wu, N.M., and Flores, A. (1983) Freeze-drying of bone for allotransplantation, in *Osteochondral Allografts* (eds G.E. Friedlaender, H.J. Mankin, and K.W. Sell), Little, Brown & Co., Boston, pp. 183–192.
87 Willemer, H. (1991) Data to be considered for freeze dryers to be used in freeze-drying of transplants (especially bones). 1st European Congress of Tissue Banking and Clinical Application, Berlin, October 1991.

4

Metal Oxides, Ceramic Powders

Dogan and Hausner [1] presented a survey of the applications of freeze-drying in ceramic powder processing; three main objectives have been pursued:

- Freezing and freeze-drying of metal salt solutions, to obtain a homogeneous mixture of different components.
- Freezing and freeze-drying of precipitates to minimize agglomeration during drying.
- Injection molding of powder-liquid mixtures at temperatures below the freezing point of the liquid and freeze-drying of the frozen parts.

The metal solutions are sprayed into cold liquids for rapid freezing, after which the droplets are freeze-dried and decomposed to metal oxides. Owing to the homogeneous distribution of the components, the reactions in the solid state occur at lower temperatures compared with conventionally produced powders.

The drying of the precipitates conventionally leads to hard agglomerates, which densify still more during the calcination to oxides. In the freeze-dried precipitates, only soft agglomerates are formed with fine pores, as shown in Figure 4.1. During sintering of this product, a high relative density can be achieved at substantially lower temperatures (300–400 °C), as shown in Figure 4.2.

Conventionally, a large amount of organic binders must be used for the injection molding of ceramic parts. By injecting a mixture of water and organic solvents with the ceramic powder into the cold mold, small amounts of organic binders are necessary, allowing high heating rates during firing.

Yavuz *et al.* [2] compared the production of Bi–Pb–Sr–Ca–Cu–O powder precursors by freeze-drying, spray-drying, and thermal decomposition. The most reactive precursor was obtained by freeze-drying. The freeze-dried powder was sintered for 60 h at 850 °C, resulting in 91% single-phase Bi-2223, the thermal decomposition product yield was 77% after sintering for 83 h at 850 °C, and by spray drying the maximum amount of Bi-2223 phase was 55% after sintering for 150 h at 850 °C. Tachiwaki *et al.* [3] described the supercritical fluid drying of Y–Ba–Cu oxides from an aqueous alcohol suspension using CO_2. The 2-propanol suspension of the oxides could not be freeze-dried since the freezing point of 2-propanol is −88.5 °C. The supercritical fluid drying is described, but the resulting cation ratio in the dried powder was Y:Ba:Cu = 1 : 6.9 : 3.8 instead of the expected 1 : 2 : 3 and the diameters of the dried powders were larger than expected. The

Freeze-Drying, Third Edition. Peter Haseley and Georg-Wilhelm Oetjen.

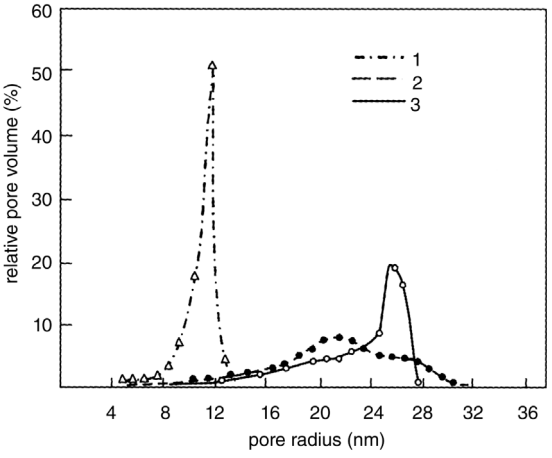

Figure 4.1 Pore-size distribution of MgO compacts. 1: freeze-dried after precipitation and washing; 2: chamber drying at 120 °C after precipitation and washing; 3: commercially available product. (Figure 1 from Ref. [1]. Reprinted with permission of the American Ceramic Society, Westerville, OH. Copyright 1988, American Ceramic Society. All rights reserved.)

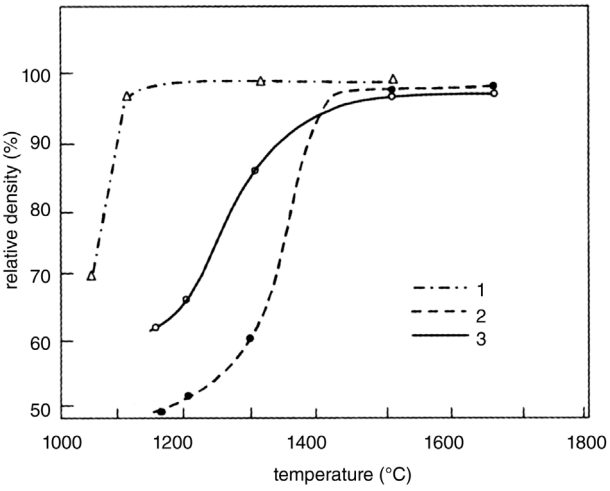

Figure 4.2 Relative density of sintered MgO compact. 1, 2, 3 as in Figure 4.1. (See also Figure 2 from Ref. [4].)

authors expect to develop process conditions that will produce the expected ratio of 1 : 2 : 3.

Itatani *et al.* [5] described a process called ›ultrasonic spray freeze-drying (USFD)‹ with two injection nozzles (Figure 4.3). The two components Ca $(CH_3COO)_2$–(hydrolyzed)$PO(OCH_3)$ (CaPO) and $ZrOCl_2$–YCl_3 (ZrY) were introduced by a flow of He in the two ultrasonic systems (4 in Figure 4.3), which formed droplets. They were simultaneously frozen on a liquid nitrogen-cooled bottle (5 in Figure 4.3). After freezing, parts 1–4 were removed and the chamber

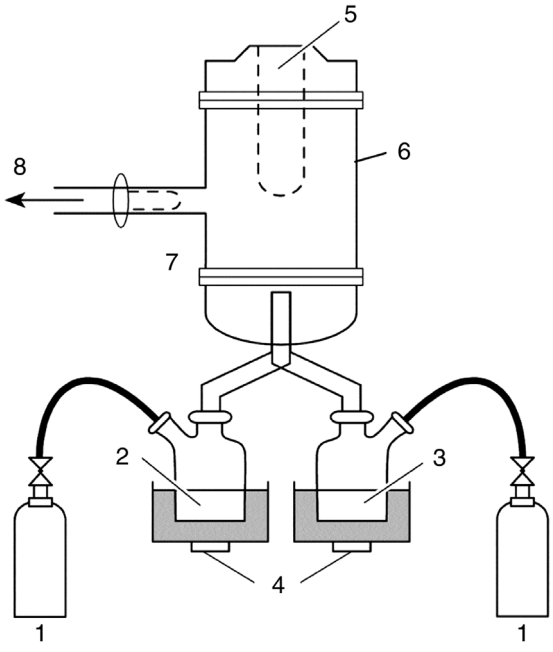

Figure 4.3 Schematic diagram of the ultrasonic spraying freeze-drying apparatus. 1: bottle for He carrier gas; 2: $Ca(CH_3COO)_2$–(hydrolyzed)$PO(OCH_3)$ system; 3: $ZrOCl_2$–YCl_3 system; 4: droplets formed by ultrasonic vibrators; 5: simultaneous freezing of droplets from 1 and 2 on the liquid nitrogen-cooled bottle; 6: chamber (i.d. 95 mm, height 300 mm); 7: filter, to avoid evacuation of frozen material; 8: pumping system, oil diffusion, and rotary pump. (From Itatani, 2000 [5]. Reproduced with permission of Elsevier.)

was closed with a cover and evacuated by a rotary and oil diffusion pump. After the initial 3 h, the liquid nitrogen was replaced by dry ice for 15 h. During the last 72 h, no cooling was used. Thereafter, the product was heated for 24 h at 150 °C. A 0.35 g amount of the product was pressed into cylinders of 10 mm diameter and 4 mm thickness and sintered (a) at 1150 °C pressureless for 5 h and (b) at 1100 °C at a pressure of 300 bar for 1 h. At −100 °C, $p_{s,ice} \approx 1.4 \times 10^{-5}$ mbar and at −80 °C, $p_{s,ice} \approx 5 \times 10^{-4}$ mbar. A diffusion pump connected to this size of chamber can have a pumping capacity of ∼100 L/s or at a pressure of 5×10^{-4} mbar and ∼0.15 g/h, in 15 h ∼2.3 g. If the total amount of product is ∼3 g, the freeze-drying process is feasible. The hot-pressed compacts had a relative density of ∼95%; the grains with sizes below 0.5 μm were dispersed on boundaries of grains with sizes 1–2 μm.

Yokota *et al.* [6] described the spray freeze-drying of a magnesium sulfate solution with 3.5 mol% aluminum added. The solution was sprayed through a nozzle with nitrogen gas into a fluid *n*-hexane solution at −60 °C flowing over the walls of a column. The frozen particles had an average diameter of 42 μm. The pores inside the dried grains had a diameter in the micron range. It was shown that the addition of aluminum produced small amounts of $MgAl_2O_4$ at the grain boundary of the MgO. The porosity was 87–90% and the surface area was >20 m^2/g after exposure to 1300 °C for 20 h.

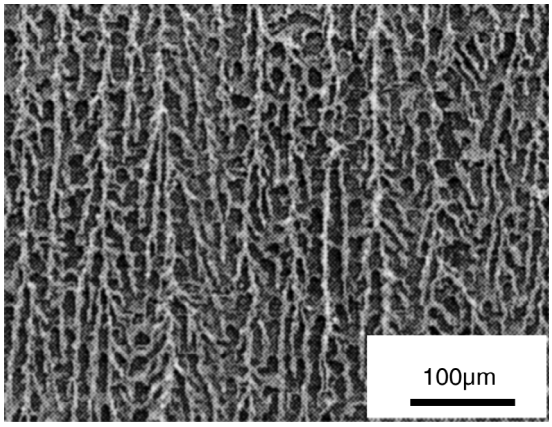

Figure 4.4 Microstructures of porous ceramic from a 28 vol% slurry concentration, cross section parallel to the macroscopic ice growth direction. (From Fukasawa, 2001 [7]. Reproduced with permission of John Wiley & Sons.)

Another method of performing a controlled freezing process was studied by Fukasawa *et al.* [7]. With alumina powder, a dispersant and water slurries with concentrations between 28.0 and 45.0% were prepared and filled into a container. The bottom of the container was made from metal with a high thermal conductivity and the walls from fluororesin. Just the metal bottom was placed in ethanol, its temperature being controlled at −20, −50, and −80 °C. Thus, the ice was stimulated to grow macroscopically from the bottom to the top. Figure 4.4 shows the microstructure parallel to the ice growth direction of the 28 vol.% sample sintered at 1500 °C and Figure 4.5 shows the same product sintered at 1400 °C, frozen at (a) −20 and (b) −80 °C in the ethanol bath. The porosity in both products was 61.6%. One-directional freezing permits one to produce porous ceramics with macroscopically aligned open pores exceeding 10 μm in size, containing pores of ~0.1 μm in their internal walls.

Reetz and Haase [8] used different freezing rates to freeze ZrO_2 and found that slow freezing of this product resulted in better technological qualities, for example, free-flow and sinter ability, than quick freezing. On the other hand, complex Zn solutions can only be frozen quickly to arrive at a product homogeneous in chemical structure and grain size distribution.

Nagai and Nishino [9] froze solutions of K_2CO_3, Na_2CO_3, $MgSO_4$, and $Al_2(SO_4)_3{\cdot}18\ H_2O$ by spraying them into LN_2 and freeze-dried the frozen droplets at 0.13 mbar and 100 °C for 2–3 days. The dry product consisted of hollow and porous balls with a diameter of 150–200 μm and had to be milled for 16 h in a ball mill to make it workable. The calcined product had a spherical (0.1 μm diameter) or plate-like form of 0.2–2 μm.

Torikai *et al.* [10] sprayed aqueous solutions of Mn^{2+}, Co^{2+}, and Ni^{2+} sulfate into LN_2 and produced uniform, spherical particles, which were freeze-dried in a bottle at −80 °C. This was connected to two cold traps (LN_2), a diffusion pump and a backing pump. Freeze-drying of ~10 g took 2–3 days. The dry product in the form of $Mn_3CO_2Ni(SO_4)_6{\cdot}15–16H_2O$ could be transformed into a fine spinel powder at 900–1000 °C in 1 h.

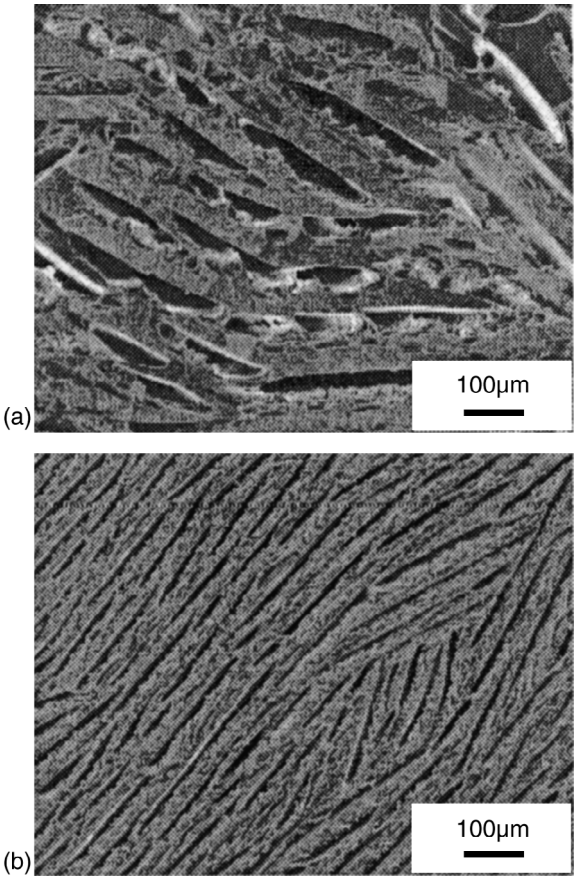

Figure 4.5 Microstructures of the samples from a 28 vol% slurry concentration, sintered at 1400 °C, (a) frozen at −20 °C, and (b) frozen at −80 °C. Both materials had the same porosity of 61.6%. (From Fukasawa, 2001 [7]. Reproduced with permission of John Wiley & Sons.)

Nikolic *et al.* [11] synthesized ZnO and $Bi_{1.8}Pb_{0.2}Sr_2Ca_2Cu_3O_x$ (Bi) powders by spraying the respective solutions in LN_2. The mean droplet sizes were 70 and 61 μm, respectively. The shelf temperature in the freeze-dryer was between −30 and −20 °C and the pressure was 0.13–0.2 mbar. The ZnO powders were heat treated for 2 h at 275 °C in air. The Bi precursor was placed in a furnace preheated to 200 °C and decomposed at temperatures up to or at 840 °C. The ZnO powder obtained was highly reactive and the sintering occurred at 275 °C followed by hard agglomerate formation. The aggregate dimensions were 15–20 μm and the average ZnO crystallite size was 25.9 nm. The Bi powders contained 2212 and 2223 phases. The BET surface area was 2.5 m^2/g and the mean crystallite size 231 nm.

Milne and Mostaghaci [12] compared the consequences of different drying methods on the density, the sinter rate, and microstructures of sublimed TiO_2 suspensions. Evaporation of water in a micro-oven and by radiation heating led to strongly bound agglomerates, whereas freeze-drying resulted in weakly bound

secondary clusters. In 2 h of sintering, the freeze-dried powder reached 98% of the theoretical density, whereas differently dried powders needed twice as much time and had a less fine microstructure.

Kimura *et al.* [13] and Ito *et al.* [14] produced superconducting $YBa_2Cu_3O_{7-\delta}$ and $YBa_2Cu_3O_{7-x}$ ceramic plates, respectively, from freeze-dried carbonate and nitrate solutions, respectively, of ytterbium, barium, and copper. After calcination and sintering, small plates of approximate size $2 \times 5 \times 20\,\mu m$ with high packing density were formed without pressing [13], having a superconductivity equal to that of monocrystalline $YBa_2Cu_3O_{7-x}$ [14].

Lacour *et al.* [15] produced the starting material for YBaCuO from freeze-dried acetate solutions. The strong dependence of the electrical qualities on the salt concentrations was considered surprising (note: the salt concentration strongly influences the structure of any freezing product).

Kimura *et al.* [16] produced spherical $YBa_2Cu_3O_{7-\delta}$ material with a diameter between 20 and 30 μm from freeze-dried nitrate solutions and its thermal decomposition.

Kondou *et al.* [4] compared the production of $Pb(Zr_xTi_{1-x})O_2$ (PZT) by solid-state reaction between TiO_2, ZrO_2, and PbO and the freeze-drying of the nitrate salt solution. The solid-state reaction requires 1100 °C, but the transformation of the freeze-dried nitrates only 580 °C. Furthermore, the freeze-dried product could be sintered better and showed at the Curie temperature a twofold larger dielectric constant than the PZT produced by solid-state reaction.

Sofie and Dogan [17] injection molded parts from lead lanthanum zirconium titanate (PLZT) slurries in *tert*-butanol (TBA), (melting point 25 °C, vapor pressure at 25 °C 55 mbar) as solvent. Compared with an aqueous slurry, the authors suggested the following advantages of TBA: the expansion of water during freezing makes it difficult to obtain high green densities and causes separation of solids and solvent (note: due to slow freezing). The crystalline structure of frozen TBA fades at high solid loading during sintering, resulting in a highly dense microstructure.

To summarize: the freezing method, freezing rate, and thermal treatment (annealing) determine the structure of the dry powder; it cannot be modified during main and secondary drying. Micro- or visual collapses during drying can change or destroy the structure. The methods described in Section 1.1.5 should be used to analyze the results of the freezing procedure and to determine the critical temperatures during drying.

References

1 Dogan, F. and Hausner, H. (1988) The role of freeze-drying in ceramic powder processing. *Ceram. Trans.*, **1** (*Ceram. Powder Sci.*, Part A), 127–134.

2 Yavuz, M., Maeda, H., Vance, L., Liu, H.K., and Dou, S.X. (1998) Powder production methods of Bi–Pb–Sr–Ca–Cu–O superconductors. *Supercond. Sci. Technol.*, **11**, 1166–1172.

3 Tachiwaki, T., Takase, Y., Sugimoto, J., Oda, M., and Kawanaka, S. (1998) An experimental study of supercritical fluid drying of Y–Ba–Cu oxides powder from

aqueous alcohol suspension using carbon dioxide. *Part. Sci. Technol.*, **16**, 109–124.

4 Kondou, S., Kakojawo, K., and Sasaki, Y. (1990) Synthesis of $Pb(Zr_xTi_{1-x})O_3$ by freeze drying method. *Nippon Kagaku Kaishi*, **7**, 753–758.

5 Itatani, K., Akiyama, K., Aizawa, M., Scott Howell, F., and Okada, I. (2000) Sinterability of apatite–zirconia composite powder prepared by ultrasonic spray freeze-drying technique. *J. Soc. Inorg. Mater. Jpn.*, **286**, 194–202.

6 Yokota, T., Takahata, Y., Katsuyama, T., and Matsuda, Y. (2001) A new technique for preparing ceramics for catalyst support exhibiting high porosity and high heat resistance. *Catal. Today*, **69** (1–4), 11–15.

7 Fukasawa, T., Ando, M., and Ohji, T. (2001). Fabrication of porous ceramics with complex pore structure by freeze drying process. *Ceram. Trans.*, **112** (Innovative Processing/Synthesis: Ceramics, Glasses and Composites IV), 217–226.

8 Reetz, T. and Haase, I. (1988) The influence of freezing process on the properties of freeze-dried powders, in Proceedings of the International Conference on Ceramic Powder Process. Sci., (eds H. Hausner, G.L. Messing, and S. Hirano), pp. 641–648.

9 Nagai, M. and Nishino, T. (1985) II Alumina ceramics fabricated by the spray-froze/freeze-drying method. International Institute of Refrigeration (IIR) (Comm. C1), Tokyo, pp. 186–190.

10 Torikai, N., Mejuro, T., Nakayama, H., Yokogama, Y., Sasamoto, T., and Abe, Y. (1985) Preparation of fine particles of spinel-type Mn–Co–Ni oxides by freeze-drying. International Institute of Refrigeration (IIR) (Comm. C1), Tokyo, pp. 177–183.

11 Nikolic, N., Mancic, L., Marinkovic, Z., Milosevic, O., and Ristic, M. (2001) Preparation of fine oxide ceramic powders by freeze drying. *Ann. Chim. (Paris)*, **26**, 35–41.

12 Milne, S.J. and Mostaghaci, H. (1990) The influence of different drying conditions on powder properties and processing characteristics. *Mater. Sci. Eng. A*, **130**, 263–271.

13 Kimura, Y., Ito, T., Yoshikawa, H., Tachiwaki, T., and Hiraki, A. (1990) Growth and characterization of homogeneous yttrium–barium–copper oxide ($YBa_2Cu_3O_{7-x}$) powders prepared by freeze-drying method. *Jpn. J. Appl. Phys., Part 2*, **29**, L1409–L1411.

14 Ito, T., Kimura, Y., and Hiraki, A. (1991) High-quality yttrium barium copper oxide ($YBa_2Cu_3O_{7-x}$) ceramics prepared from freeze-dried nitrates. *Jpn. J. Appl. Phys., Part 2*, **30**, L1253–L1255.

15 Lacour, C., Laher-Lacour, F., Dubon, A., Lagues, M., and Mocaer, P. (1990) Freeze-drying preparation of yttrium barium copper oxide: correlations between electrical and microstructural properties. *Physica C*, **167**, 287–290.

16 Kimura, Y., Ito, T., Yoshikawa, H., and Hiraki, A. (1991) Superconducting yttrium barium, copper oxide ($YBa_2Cu_3O_{7-x}$) particles prepared from freeze-dried nitrates. *Jpn. J. Appl. Phys., Part 2*, **30**, L798–L801.

17 Sofie, S. and Dogan, F. (2000) Ceramic shape forming by freeze-drying of aqueous and non-aqueous slurries. *Ceram. Trans.*, **108** (Innovative Processing/Synthesis of Ceramics, Glasses and Composites III), 235–243.

5

Trouble Shooting

In Section 2.2.11, possible failures during the freeze-drying process are classified in four categories and the preventions and necessary actions briefly discussed. In this chapter, some unexpected or undesirable events are studied, which, by experience, may happen. The problems listed here are selected from the course of the freeze-drying process. A breakdown of single components, for example, pumps, compressors, or valves, is not included. The list is incomplete, but an attempt has been made to mention some of the more frequent events. The problems with leaks and their hunting are discussed in Sections 2.2.9 and 2.2.11.

5.1 Prolonged Evacuation Time

The evacuation of the plant takes longer than calculated from the volume and the pumping capacity, in spite of regular leak checks. The event is most likely related to the formation of ice, which is condensed during loading on the precooled shelves. The extent of this depends on the shelf temperature during loading and the moisture content of the gas in the chamber. One of the possible courses of actions could be as follows: Check the condenser temperature in relation to the pressure reached. If the condenser temperature is, for example, −42 °C, $p_s \approx 0.1$ mbar, but the lowest pressure reached in the chamber is only ~0.5 mbar, then the condenser capacity is not the bottleneck, but the slow sublimation of some ice. Raising T_{sh} from, for example, −40 °C could be started very slowly in such a way that the pressure in the chamber does not exceed p_s of the maximum tolerable T_{ice}, for example, −22 °C ($p_s \approx 0.85$ mbar). This may take one or more hours, depending on the heat transfer to the undesired ice. When all excess ice has been removed, the pressure will drop quickly to the value close to p_s of the ice on the condenser and the normal cycle can be started. If, in another example, the condenser temperature is the limiting factor, then the condenser is at capacity limit and one has to delay the heating until the condenser temperature falls. All this can be avoided if the door of the chamber is only partially opened during loading (Section 2.4) and a low pressure of dry gas is kept in the chamber.

Freeze-Drying, Third Edition. Peter Haseley and Georg-Wilhelm Oetjen.

5.2 Sublimation Front Temperature Too High

After evacuation and at the start of heating, the trend of T_{ice} approaches too close to the maximum tolerable T_{ice}. A reduction in the operation control pressure (p_c) will immediately stop this trend (Figure 2.121) (if the desired T_{ice} is not reached, p_c could be raised). The slope of the function $T_{ice} = f(p_c)$ can become unfavorably steep. In this case, the shelf temperature should also be lowered or raised, but the effect of this change will take time before an equilibrium state is reached again (e.g., 0.5–1 h), depending on the heat transfer conditions and the heat capacity of the shelves and the heat transfer medium.

5.3 Sublimation Front Temperature Irregular

T_{ice} data fluctuate and the standard deviation of the measurements becomes larger than ~0.3–0.5 °C. The monitored p_c, T_{sh}, and T_{co} are stable, but the pressure rise measurements change and vary as shown in Figure 2.23. Most likely, the valve between the chamber and the condenser does not close reproducibly. If the drive of the valve has been checked externally as far as possible, the run cannot be finalized automatically and manual operation should be used, if the time course of the program has been already established.

5.4 Slow Pressure Increase in the Chamber during Main Drying

In spite of a constant or decreasing condenser temperature, the pressure in the chamber rises after main drying has started correctly. This may be due to the development of a leak, although this is unlikely in a plant leak-tested before the run, and a newly developed leak may alter the pressure slightly. In addition, a leak that worsens constantly during the run is possible, although unlikely. Among other reasons, rising pressure may occur due to a constant increase in the pressure of permanent gases. This will increasingly hinder transport of water vapor and reduce the condensing effectiveness of the condenser (Figure 2.19). The increase may occur because of two reasons: After the start of main drying, air dissolved or included in the frozen ice is freed as the ice is sublimed. The amount of included gas can vary by a factor of almost 100, depending on the material used and its fabrication history (see Section 1.2.1). If the capacity of the vacuum pump is smaller than the amount of freed gas at the desired pressure, the condenser is increasingly filled by permanent gases. The other possibility is a misplaced suction pipe of the vacuum pump at the condenser. The common permanent gases have a higher density than water vapor. If the vacuum connection is not in the lowest area of the condenser, the gas will slowly fill the condenser chamber from the bottom up to the suction level of the pump, thus reducing the condenser efficiency to a greater or lesser extent. The suction pipe should be connected as shown in Figure 2.20.

5.5 Stoppers ›Pop Out‹ or Slide into the Vials

The ›pop out‹ of stoppers occurs mostly during evacuation. If the product is not completely frozen and contains highly concentrated, but not solidified, inclusions, their water content may evaporate explosively when the vacuum is applied. This abrupt evaporation will also blow some product particles to the walls of the vial, as can be seen in the vials after drying.

Stoppers may also slide into the vials and cause their virtual closure. This can happen during freezing of the product, especially if the shelf temperatures are very low. The dimensions of the stoppers need to be tested not only for the pressure to close them after drying, but also for shrinking at low temperatures.

5.6 Traces of Highly Volatile Solvents (Acetone, Ethanol)

The presence of such traces always requires some special steps, depending on the amount of the volatile component. If the traces cannot be removed before freezing and drying, they can (i) influence the structure during freezing, (ii) disturb the condensation of ice, and (iii) contaminate the oil in the vacuum pump. As shown in Figure 5.1, the vapor pressures of ethanol and acetone

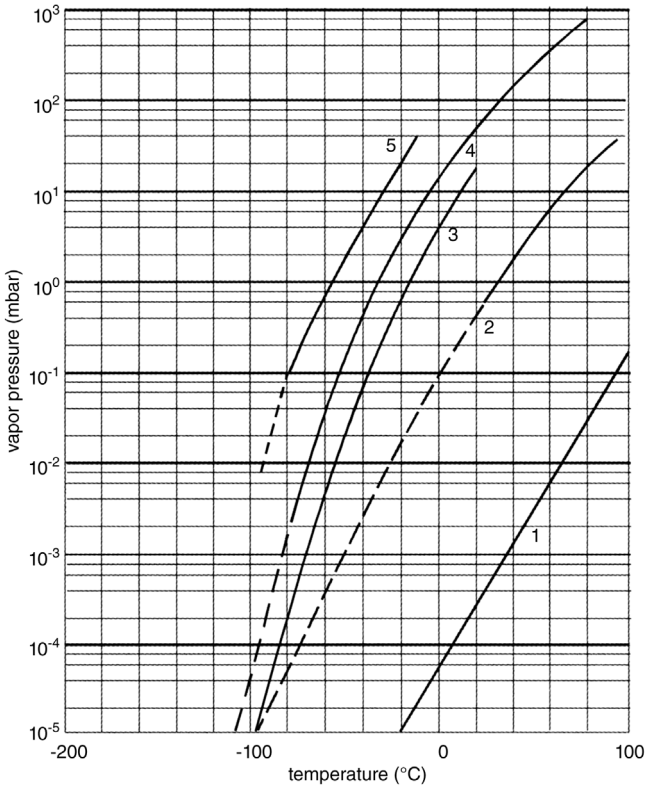

Figure 5.1 Vapor pressures of solvents as a function of temperature. 1: glycerin; 2: dimethyl sulfoxide ($C_3H_8O_3$); 3: water; 4: ethanol; 5: acetone.

at −70 °C are approximately 2×10^{-2} and 3×10^{-1} mbar, respectively (ice 3×10^{-3} mbar). Ethanol melts at −114 °C and acetone at −95.5 °C. If the amounts are small, a very quick freezing might help to distribute the solvents very uniformly in the ice. If the amounts are large enough, they will form a veil on the condenser surface, disturbing the efficiency of the condenser, drip as a liquid from the condenser surface and evaporate from the warmer condenser wall. Furthermore, gauges with hot wires (thermal conductivity gauges) should not be used and finally the oil of the vacuum pumps must be recycled and cleaned or it will be contaminated by the solvents and the pumps will no longer discharge the solvent vapors. These problems may be reduced by placing an LN_2-cooled trap between the condenser and vacuum pump set. Of course, some ice will also condense in the trap, but this amount will be small, as the water vapor pressure of ice in the condenser is very low compared with the vapor pressure of the solvent at the condenser temperature. However, this trap solves the problems in the condenser, mentioned before, only if it is designed also for this task. A substantial effort is justified to remove such solvents before freezing starts.

5.7 Different Structures of the Dried Product in the Center and Border of a Shelf

The outer vials are influenced (if the shelf temperature is uniform) by a different temperature of the walls and the door of the chamber. If the chamber walls and the door are not kept at shelf temperature, the outer vials must be shielded or they may be too warm during freezing (e.g., freezing differently) or too cold during secondary drying (see Figures 1.102–1.105) and this may lead to a different residual moisture content from that in inner vials.

6

Regulatory Issues

Qualification and Validation of Processes and Installations

In the Validation Documentation Inspection Guide, US Department of Health and Human Services, Food and Drug Administration, 1993, the process validation is defined as follows:

- Establishing documented evidence, which provides a high degree of assurance that a specific process will consistently produce a product meeting its predetermined specifications and quality attributes.

The Guide to Inspections of Lyophilization of Parenterals, published by the US Food and Drug Administration, July 1993, contains among others chapters entitled ›Lyophilization Cycle and Controls‹, ›Cycle Validation‹ and ›Lyophilizer Sterilization/Design‹.

In the European Union, the Directive 91/356 EEC provides the principles and guidelines of Good Manufacturing Practice (GMP). In a series of Annexes, supplementary guidelines are covered in Ref. [15] of Chapter 2.

The following are a few of the most important European and US guidelines [1]:

- GAMP = Good Automation Manufacturing Practice [2].
- EC-GMP Guidelines and Annex 15-PIC/S PI 006-1 and FDA Regulations (PIC/S = Pharmaceutical Inspection Convention) [3].
- User Requirements DIN 69905 [1].
- ISPE Commissioning and Qualification [4].
- The Parenteral Society Specification and Validation of Freeze_Dryers No. 9.
- GXP = Good Practices for Computerized Systems in Regulated GXP Environments [1].
- FDA: 21 CFR Part 211, §211.68 (a, b); 21 CFR Part 11, ›Electronic Signature, Electronic Records‹ [5].
- ISO: 100 11 Guidelines for Auditing Quality Systems [1].

Over the years and various experiences, the FDA and the European Union changed their somewhat rigid rules adapted to economic considerations.

Freeze-Drying, Third Edition. Peter Haseley and Georg-Wilhelm Oetjen.

Users – pharmaceutical manufactures – should take advantage of the benefits they achieve by applying QbD (Quality by Design)[1] and PAT (Section 6.1).

FDA announces first step in reducing regulatory burdens for manufactures using practical analytical technologies (PAT) – the elimination of a requirement for three validation batches to demonstrate process validation. ". . . it may not be necessary for a company to manufacture multiple conformance batches prior to initial distribution (if advanced pharmaceutical science and engineering principles and manufacturing control technologies are used)."

Powell-Evans [6] provided a range of advice on how to ›streamline validation‹, which he calls ›one of the most time-consuming and costly exercises faced by pharmaceutical manufacturers‹.

In the following text, an attempt is made to give an example of the types of documentation that must be prepared within the validation master plan (VMP) for the design qualification (DQ), the installation qualification (IQ), and the operational qualification (OQ). Performance qualification (PQ) should follow the successful completion of installation qualification and operational qualification.

Annex 15 PIC/S corresponds in form and regulation depth to the EC Guidelines. As a rule, the EC-GMP Guidelines indicate what must be done, but not how it should be done. The demands shown in Annex 15 with respect to qualification and validation are sufficient to attain the goals of such regulations with present state-of-the-art technology without limiting the manufacturer in his possibilities.

At the beginning of any qualification and validation, a validation master plan must be worked out. The FDA defines ›validation plan‹ as a ›validation protocol‹ (guideline of principles of general process validation) [7].

The validation plan should contain the following (see Figures 6.1 and 6.2):

1) Qualification and validation principles [12]
2) Planning for validation
3) Documentation
4) Qualification
5) Process validation
6) Cleaning validation [8]
7) Sterilization validation [8]
8) Change control
9) Revalidation
10) Risk analysis
11) Worst-case scenario

1) Qualification and validation principles

   This describes the principles of qualification and validation that are applicable to the manufacturer of medical products. It is a GMP requirement that manufacturers identify the validation work needed to prove control of the critical aspects of their particular operations. Significant changes for the facility, the equipment, and the processes that may affect the quality of the product should be validated. A risk assessment approach should be used to determine the scope and extent of validation.

1 PDA/FDA Joint Regulatory Conference, 9/24/2007.

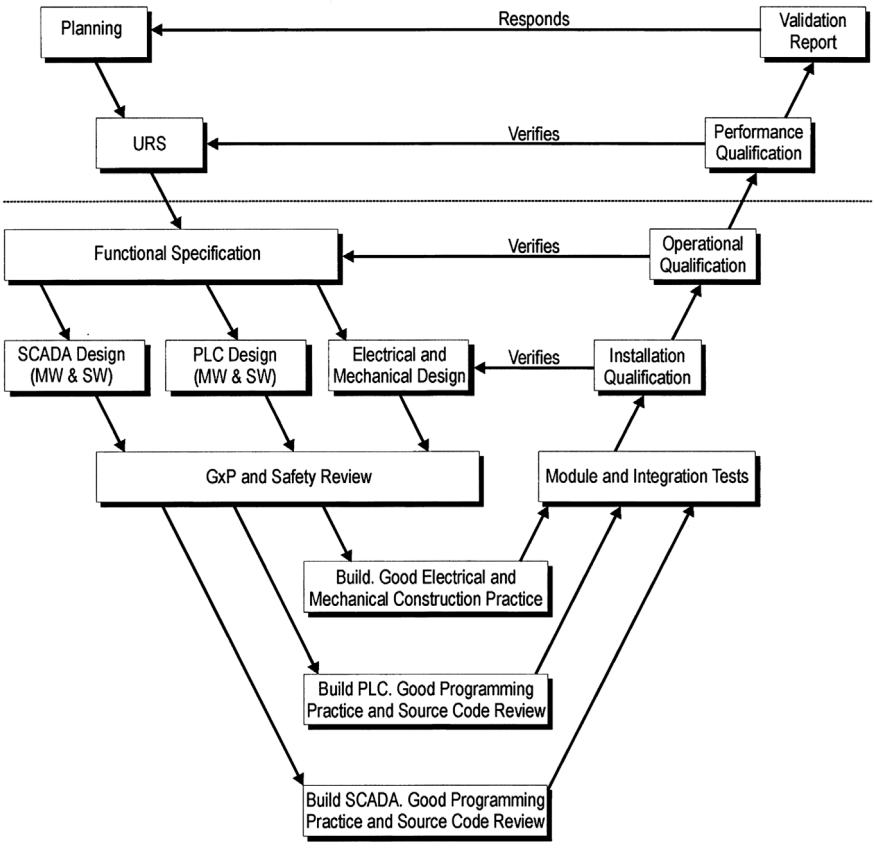

Figure 6.1 Validation concept following GAMP V-diagram.

2) Planning for validation

   All validation activities should be planned. The key elements of a validation program should be clearly defined and documented in a validation master plan. The VMP should be a summary document that is brief, concise, and clear. The plan should contain at least the following: validation policy, organizational structure of validation activities, summary of facility systems, equipment and processes to be validated, documentation format, planning and scheduling, change control, and reference to existing documents.

3) Documentation

   A written protocol should be established that specifies how qualification and documentation will be conducted. The protocol should be reviewed and approved. The protocol should specify critical steps and acceptance criteria.

   A report that cross-references the qualification and/or validation protocol should be prepared, summarizing the results obtained, commenting on any deviation observed, and drawing the necessary conclusions, including recommended changes necessary to correct deficiencies. Any changes in the plan as defined in the protocol should be documented with the appropriate justification.

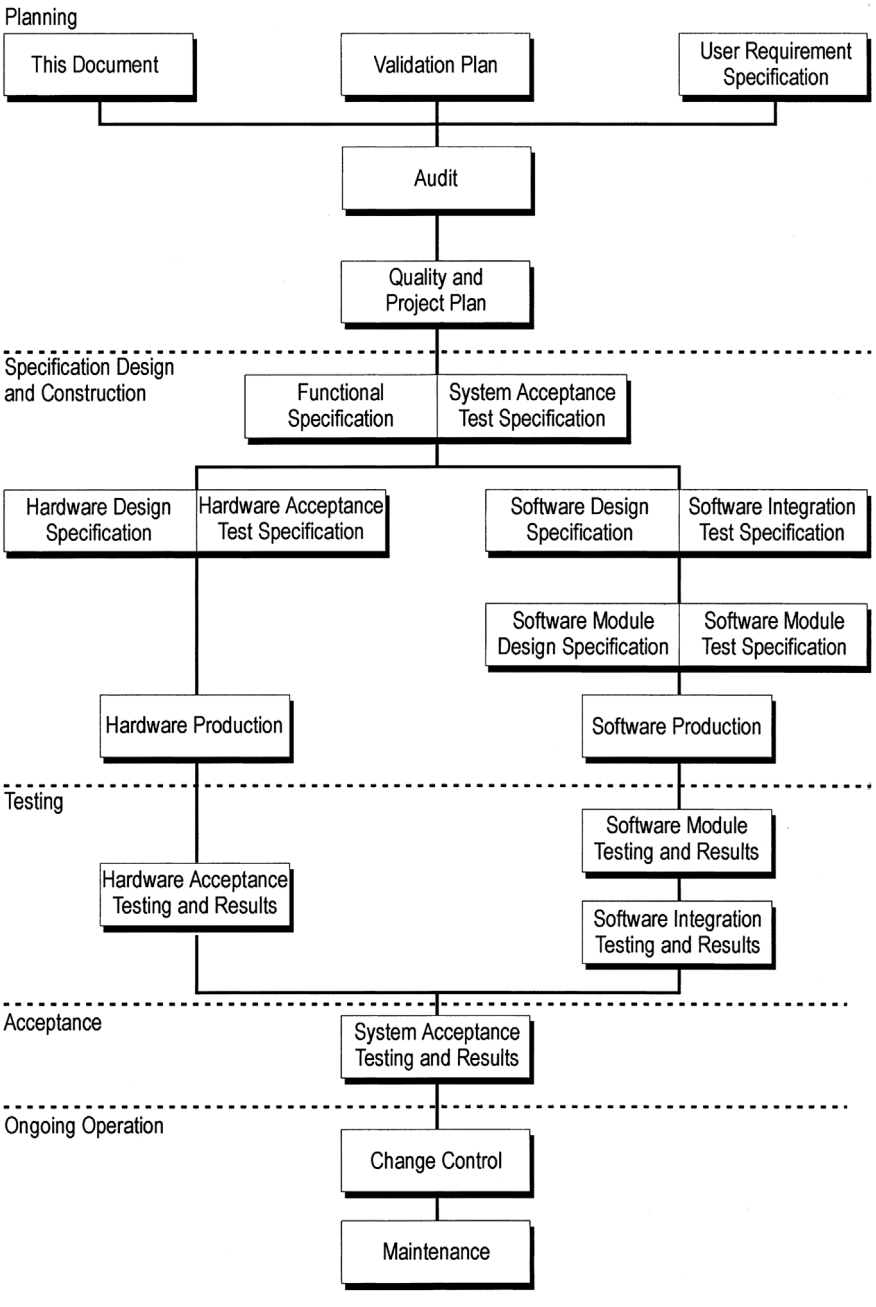

Figure 6.2 Qualification model following GAMP guidelines.

After completion of a satisfactory qualification, a formal release for the next step in qualification and validation should be made as a written authorization.

4) Qualification

4a Design qualification

The first element of a validation system or equipment should be design qualification. The compliance of the design with GMP should be demonstrated and documented.

4b Installation qualification

IQ should be performed on new or modified systems and equipment. IQ should include, but not be limited to, the following:

- Installation of the equipment, piping, services, and instrumentation checked to current engineering drawing and specifications.
- Collection and collation of supplier operating and working instructions and maintenance requirements.
- Calibration requirements.
- Verification of materials of construction.

4c Operational qualification

OQ should follow installation qualification. OQ should include, but not be limited to, the following:

- Tests that have been developed from knowledge of processes, systems, and equipment.
- Tests to include a condition or a set of conditions and encompassing upper and lower operation limits, sometimes referred to as ›worst-case‹ conditions.

The completion of a successful OQ should allow finalization of calibration, operating, cleaning and sterilization procedures, operator training, and preventative maintenance requirements. It should permit a formal ›release‹ of the systems and equipment.

4d Performance qualification

PQ should follow successful completion of IQ and OQ. PQ should include, but not be limited to, the following:

- Tests using production materials, qualified substitutes, or simulated products that have been developed from knowledge of the process and the systems or equipment.
- Test to include a condition or set of conditions and encompassing upper and lower operating limits.
- Although PQ is described as a separate activity, it may also in some cases be appropriate to perform it in conjunction with OQ.

5) Process validation

This is the documented evidence that the process, operating within established parameters, can perform effectively and reproducibly produce a medical product that meets predetermined specifications and quality attributes.

6) Cleaning validation

For cleaning validation, the cleaning process must be defined and the parameters described in writing. The limits and test procedures must be described. The process is then run and the records cross-checked against

the parameters. The results are then evaluated. This process is repeated three times to prove the reproducibility of the process.

7) Sterilization validation

For sterilization validation, the sterilization process must be defined and the parameters described in writing. The limits and test procedures must be described. The process is then run and the records cross-checked against the parameters. The results are then evaluated. This process is repeated three times to prove the reproducibility of the process.

8) Change control

Written procedures should be in place to describe the actions to be taken if a change is proposed to a starting material, product component, process equipment, process environment, method of production or testing, or any other change that may affect product quality or reproducibility of the process.

9) Revalidation

This is a repeat of the process validation to provide an assurance that changes in the process/equipment introduced in accordance with change control procedures do not adversely affect process characteristics and product quality.

10) Risk analysis

This is a method to access and characterize the critical parameters in the functionality of an equipment or process.

In-process controls are as follows:

- Recording of actual and target values of temperature and pressure
- Shelf temperature
- Condenser temperature
- Chamber pressure (vacuum)
- Chamber pressure (overpressure SIP)
- Pressure rise measurement (PRM) to determine the transition point from PD (primary drying) to SD (secondary drying). PRM is controlled automatically.
- The data records of process parameters require calibrated measuring systems and sensors.

Risk analysis	Reason	Precautions
Leak at the door	Door seal defective or incorrect seating	Visual inspection before every door closing. Seal change at regular intervals
Set point chamber vacuum is not reached	Defective vacuum sensor	Is reported as an alarm
	Residual water/condensate in the condenser	Extend automatic drain time in this process step
	Leakage in the system	Start leak test
Choice of wrong recipe/program from the archives	Inattention/distraction/ not authorized	Set access permission and recipe management new and protect it by password. Perform repetitive training courses
Technical failure due to failure of a resource	Power failure	Ensure emergency power supply
	Cooling water shortage	Switching over to emergency supply
	Compressed air for valves has failed	Switching over to emergency supply

11) Worst-case scenario

This is a condition or set of conditions encompassing maximum and minimum processing limits and circumstances within standard operating procedures that pose the greatest chance of a product or process failure when compared to ideal conditions. Such conditions do not necessarily induce product or process failure.

The examples given are restricted to the process and installation engineering aspects and exclude the many other aspects, for example, sterility, biological or chemical requirements, corporate policies, or the production environment.

The information described is organized in seven categories:

6.1 PAT (Practical Analytical Technology)
6.2 Quality of the product to be manufactured
6.3 Description of the process developed for the manufacturing of the product
6.4 Description of the production installations and their handling
6.5 Equipment performance tests
6.6 Qualification of the installations to document the ability of the equipment to operate the process described in Section 6.3
6.7 Documentation of the quality of the manufactured product and its comparison with Section 6.2

6.1 PAT (Practical Analytical Technology)

US FDA: PAT are tools and systems that utilize real-time measurements or rapid measurements during processing of evolving quality and performance attributes of in-process materials to provide information to ensure optimal processing to produce final product that consistently conforms to established quality and performance standards.

FDA-PAT initiative:

- 2002 Guideline: Pharmaceutical cGMs for the twenty-first century – a risk-based approach.
- 2004 Guidance for industry: PAT – a framework for innovative pharmaceutical development, manufacturing, and quality assurance. Increased focus on "quality by design."
- 2008 Compliance Policy Guide – Process Validation Requirements for Drug Products and Active Pharmaceutical Ingredients Subject to Pre-Market Approval.

PAT is a tool to scale up a freeze-drying process and help to reduce costs and manufacturing times. The freeze-drying process is known as a time-consuming process and therefore expensive. In order to lower costs during manufacturing, the effective cycle time must be reduced.

PAT as well as "quality by design" [14] are important elements to ensure economics of scale, reduce time to market, and facilitate cost-intensive trials on production size lyophilizers. Applying PAT in the laboratory can provide valuable

information about product and process behavior and help identify the critical process parameters during cycle development and optimization.

The pharmaceutical industry and the FDA have come to realize that testing quality in the final product is inhibiting the rate of introducing important new drugs. With this PAT tool, the FDA is encouraging the pharmaceutical industry to produce drugs more effectively and with higher quality.

The objective is to produce a freeze-dried cake with the desired characteristics: moisture content, stability, and reconstitution. This often requires a number of test trials, each one requiring the necessary facilities, time, personnel, and media (power, WFI, etc.). Critical process parameters must be specified and controlled within predefined limits. These parameters (specificators) must be set by performing experiments in the laboratory and using PAT tools that are capable of describing all of the important process parameters with acceptable accuracy. PAT can be seen as a toolbox that includes the use of "smart sensors" (see Tempris, Section 1.2.3.1) that may enhance process monitoring. Other tools are BTM (barometric temperature measurement → Oetjen; Figure 1.119) and (PRM) pressure rise measurement and TLC (thermodynamic lyophilization control → Section 2.6.2.2)

Scale-up processes often require two stages: first, scale-up is done in a laboratory lyophilizer, here the focus is more on process understanding, and in a second step pilot production and from pilot production to full commercial volumes. The pilot production is required to produce sufficient product under relevant GMP conditions for clinical validation [10]. A rule of thumb for size categorization is as follows:

- Laboratory lyophilizer (shelf area<0.25 m^2)
- Pilot lyophilizer (shelf area from 1 to 5 m^2)
- Production lyophilizer (shelf area from 5 to 50 m^2)

The choice of process depends on the requirements of each application and, therefore, a flexible approach is required to ensure the best security of outcome.

The definition of a scale-up process can be described as follows: The outcome from the pilot stage process must be recreated in the production lyophilizer.

First stage – laboratory lyophilizer: Basic understanding that freeze-drying must be considered as a "multiprocess" taking place in each vial (container) in a variation range. Freezing phase is mostly driven by statistic nucleation effects (crystallization). Amorphous structure needs to be considered. Ice temperature during sublimation depends on shelf temperature, chamber pressure, and equipment design. Desorption depends on product properties and previous accomplished cycle.

Principles for primary drying:

Procedure	Principle	Result
BTM (product parameter)	Indirect calculation of T_{ice} by pressure rise analysis	Direct control of temperature at the sublimation front
Gas flow (process parameter)	Indirect calculation of sublimation rate by detecting vapor velocity	Determination of end point of sublimation phase
Gas moisture (process parameter)	Direct measurement of partial vapor concentration	Determination of end point of sublimation phase

Principles for secondary drying:

Parameter	Direct control	Device
Residual moisture (product parameter)	Process progress	NIR – probe (near-infrared spectroscopy)
Desorption rate (process parameter)	Process progress	BTM (TLC), gas flow, gas moisture

Parameters of process: Ice temperature at sublimation front is the only direct product parameter, enabling full process control and full product protection – "true PAT." Measurement of gas velocity or gas moisture in the chamber determines the end points.

Second stage – pilot lyophilizer: There are several other influencing factors that have enormous impact on the process: The formulation, finding excipients (Section 1.1.5) with sufficient interaction between buffers, bulking agents, preservatives, monotonicity agents, stabilizers, solubilizing agents, and antioxidants, is the most difficult step in recipe creation and lyophilization. The intention is to avoid changing the formulation during scale-up as much as possible, but this is very difficult to achieve.

The chamber vacuum profile during PD (primary drying) and SD (secondary drying) influences the sublimation and desorption process. Other influences factors are as follows: the vapor pressure difference between the product ice front and chamber, the vapor pressure at the condenser surface, and the method used for vacuum control (the instrumentation is important in achieving comparable conditions for vacuum regulation). The shelf temperature, heat fluid in the shelves, and the condenser cooling have huge impact on the process performance. Other factors are heat input and vapor transport out of the product; pore diameter, the contact conditions from vials (containers) to the shelves; radiation and heat convection of surrounding areas; temperature gradient from product to the ice condenser and the temperature difference within and between the shelves. Only one, or a combination of those influencing parameters, can lead to differences in the speed of freezing, final drying, and product outcome.

The overall goal of a freeze-drying cycle optimization is to keep the product temperature (T_{ice}) close to the critical temperature during primary drying to cut cycle time. The critical temperature is known to be the collapse temperature (T_c) [11].

Technical design parameters and dimensions are the other influencing factors: mainly the pathways for a free water vapor flow (for sublimation performance, see Section 2.2.4, Figure 2.18 → Vakutec) inside the system. This includes the position of the condenser, the design of the evaporator, the condensing surface, the size and interdistance of the shelves, and the areas around the shelf package.

The ratio of heat transfer flow media to the amount of product has an influence on the dry product. The amount of required thermal energy depends on the shelf area and the amount of product to be brought to the required temperature (heating and cooling). Fine-tuning of the parameters pressure and temperature ramping is essential, to avoid overshoots and control accuracy of set values.

The instrumentation used for process control, such as product temperature probes (PT 100 or thermoelements) have limitations (Oetjen, Figure 1.117) in Ref. [58] of Chapter 1. A better solution are wireless temperature sensors (see Tempris, Section 1.2.3.1). The type of vacuum control, whether capacitance or Pirani, has a huge influence as well. Another major influence does the vacuum regulation in the chamber, by mass flow controllers (calibrated leak) compared with the option of opening and closing the vacuum valve between condenser and vacuum pump set.

Conclusion: The product temperature at the sublimation interface is perhaps the most critical process parameter during freeze-drying, followed by the product resistance. Therefore, a PAT technology used during cycle development or optimization should be capable of a measurement of these two important parameters. Manufacturers of lyophilizers invest a lot of time and money in the design and control of their equipment to streamline the process of scale-up from the laboratory, through the pilot phase, and on the production equipment. Pharmaceutical companies would do well to leverage that experience, involving their supplier partners at the earliest stage of new product development, to minimize development time [13].

6.2 Quality of the Product

The qualities of the product and their tolerances must be deduced from the protocols of the development. The methods to measure the qualities must be described as documented in the development protocols. The directives (a) to (t) are not detailed here. They must be written in accordance with company policies and the Quality Systems Manual for each individual production. The tolerances are given in braces, for example, {±1 °C}.

6.2.1 The product to be frozen can be stored and handled at maximum XX °C {±YY °C} for a period of maximum XX hours {±YY hours}. If the temperature limits and/or time limits are exceeded, directive (a) must be applied.

6.2.2 The product subcools by 4–8 °C, if cooled at a cooling rate of 1 °C/min {±0.2 °C/min}. *Warning:* If subcooling does not occur, the frozen product may have an undesirable structure, for example, highly concentrated, highly viscous inclusions, which might dry slowly and will raise T_{ice}. If the subcooling cannot be confirmed by measuring T_{pr} during freezing (e.g., due to automatic loading), the method given in directive (b) is to be applied. If a subcooling between 4 and 8 °C cannot be proven, directive (c) is to be applied.

6.2.3 After cooling the product to minimum −40 °C {+0 °C, −5 °C}, the product has a uniform, fine structure. This product could be well but slowly dried. To induce some growing of the ice crystals, the product must be kept for XX min {−0 min, +YY min} at a temperature of, for example, −30 °C {−3 °C, +0 °C}. With this tempered structure, t_{md} = XX hours {±0.5 h}. If t_{md} is shorter than or exceeds this time, directive (d) is to be applied.

6.2.4 The collapse temperature of the product frozen, treated as described in Section 6.2.1.3, T_{ice} = −28.0 °C {±1.5 °C}.

6.2.5 The product temperature during secondary drying must reach $T_{pr,sd}$ +35 °C {+0 °C, −4 °C}. If $T_{pr,sd}$ is not measured directly, directive (e) must be applied.

6.2.6 At the end of secondary drying, dW of the product must be 0.6% {±0.3%} at +35 °C. If 0.6% is not achieved, directive (f) must be followed. The residual moisture content (RM) of the product in the closed vials measured by the methods given in directive (g) must be 1% {standard deviation of all vials measured 0.4 °C or smaller}.

6.3 Description of the Process Developed for Manufacturing of the Product

The process has been developed in a pilot plant with the following specification: volume of the drying chamber *V*, shelf area *A*, shelf temperature controlled between −50 °C and +70 °C, maximum cooling rate of the empty shelves down to −40 °C is 2.5 °C/min, heating rate from 0 to +40 °C is 3 °C/min, temperature variation on each shelf <±1 °C, roughness of the shelf surface in Ra-Standard 1.5 (1.0–1.5 µm), condenser T_{end} −65 °C, surface of the condenser coils XX m^2, vapor flow density ($s^{\#}$) from the chamber to the condenser at XX $p_{ch,H2O}$ = XX (g/s cm^2), and at XX $p_{ch,H2O}/10$ = XX/30 (g/s cm^2) (*Note*: if the pressure decreases by a factor of 10, the vapor flow density decreases more, for example, by a factor of 30; see Figure 1.142), and two stage vacuum pump set, with gas ballast at XX p_{ch} S = XX (m^3/h). All vacuum gages measure the changes of a capacitance, type CA, T_{ice} by automatic BTM, DR by automatic pressure rise measurement, dW calculated by computer from DR data, automatic operation pressure control operates from 0.02 to 0.5 mbar, leak rate of chamber, and condenser <XX (mbar L/s).

Filling of vials: Vials of type (B) of the manufacturer (C) have been selected as documented in file (D) and used exclusively during the process development. The required subcooling and the cooling rate are only ensured if the filling height in the vials B is XX mm {−0%, +2%}. The time for filling and loading of XX vials in the pilot plant has been XX hours {±10%}. For each development run, XX number of vials have been used, filling 50% of the available shelf area.

The chosen T_{ice} has been reached in the pilot plant at p_c mbar {±5%} and at T_{sh} = −10 °C. *Note*: In a freeze-drying plant with different dimensions and different number of vials, p_c will be slightly different to achieve the desired T_{ice}. Therefore, p_c must be modified accordingly. In the pilot plant, a change of p_c to 1.1p_c {±5%} increases T_{ice} by 0.5 °C. In the pilot plant, p_c has been controlled by closing the valve between the condenser and the vacuum pump set.

After XX h of main drying, T_{ice} decreases in two measurements in succession by more than 2 °C from the maximum of all average T_{ice} calculated (called max. $T_{ice,ave}$) and the controlled operation pressure p_c can no longer be kept constant. The control of the operation pressure is terminated automatically. The chamber pressure decreases during several minutes to less than $p_c/8$. At that time, T_{sh} is automatically increased to +33 °C {±1 °C} and the DR–dW measurement switches on. After XX hours, DR shows a value of 0.05%/h and dW was calculated as 0.8%. Since the preset dW must be smaller than 0.8% but larger than 0.6%, the

secondary drying has been continued until dW = 0.71 has been reached. At that time, the plant has been vented with gas G [specification in directive (h)] to atmospheric pressure and the vials have been closed. The data for three repeated runs are documented in file (E) and the data for p_{ch}, p_{co}, T_{ice}, T_{pr}, T_{sh}, DR and dW as a function of drying time shown as graphs.

In three additional test runs (each repeated three times), the following has been demonstrated:

1) p_c has been increased until T_{ice} reached −28 °C {standard deviation 0.34 °C}. This happens if p_c is increased by a factor of 1.25 (e.g., from 0.10 to 0.125 mbar). This higher T_{ice} decreases t_{md}, but cannot be accepted since $T_{ice} = -28\,°C \pm 1.5\,°C$. For safety reasons, $p_c + 0.5\%$ must remain the maximum tolerance (in this example).
2) The main drying has been terminated when T_{ice} had decreased for the first time from max. $T_{ice,ave}$ by 1.5 °C followed by a secondary drying as described. The desired dW was not reached measurably early than by the change of 2 °C in two successive measurements. The decision remains to change after two successive measurements showing T_{ice} reduced by 2 °C.
3) T_{sh} has been increased to +40 °C, but only until T_{pr} reached +25 °C, at which time T_{sh} was reduced to +30 °C. By this step the total drying time was reduced by 15%. The visual inspection of the dried product from XX vials (cut open) did not show signs of collapsed occlusions. The solubility of the product in XX tested vials satisfied the directive (i).

Based on the product quality (Section 6.2) and the process development above, the following process has been adopted:

1) The filling height in the vials type B must be XX mm {−0%, +2%}.
2) The filling and transfer times of the vials as carried out in the development are well below the specification in Section 5.1 and the temperature during this time did not exceed the specified maximum as proved in file (E).
3) The subcooling in the documented runs was between 4 and 6 °C (average 5.3 °C). If the subcooling of 4–8 °C is not achieved, directive (c) must be followed. If the subcooling cannot be measured during production, directive (b) must be applied.
4) The cooling rate down to below −40 °C must be between 0.8 and 1.2 °C/min. If it is outside this range, directive (c) must be followed.
5) After T_{pr} is below −40 °C, it has to be increased to −30 °C {+0 °C, −3 °C} for XX min {−0 min, +YY min}.
6) The controlled operation pressure during the main drying is p_c mbar {−0%, +10%}, $T_{sh} = -10$ °C. With these data, T_{ice} has been −29.5 °C {standard deviation 0.38 °C) in the pilot plant. The production department must check the function $T_{ice} = f(p_c)$ for the production plant and modify p_c if necessary to achieve $T_{ice} = -29.5$ °C {standard deviation <0.4 °C}.
7) The main drying time has to be t_{md} = XX hours {±0.5 h}. If t_{md} is shorter or longer, directive (d) has to be applied.
8) The main drying is to be terminated automatically if the measured T_{ice} becomes (by two successive measurements) 2 °C smaller than max. $T_{ice,ave}$.

At that time, the automatic pressure control is terminated and T_{sh} raised to +35 °C {+0 °C, −1 °C}. After the pressure control has been terminated, the pressure must drop to $p_c/8$ within 10 min. If the pressure remains higher or it takes a longer time to reach this level, directive (j) must be followed.

9) During the secondary drying, $T_{pr,sd}$ must reach +33 °C {+2 °C, −3 °C}.
10) If $T_{pr,sc}$ is not measured directly, directive (e) has to be applied.
11) The end of SD is reached when dW is 0.6% {±0.3%). If the dW is not reached in XX hours {±0.5 h), the drying can be prolonged by YY h. If dW is not reached at that time, directive (f) should be followed.
12) After the drying is terminated, the valve between chamber and condenser is closed and the chamber vented with gas (G), specification in directive (k) to atmospheric pressure. Thereafter, the vials are closed with the stoppers, which have been treated as specified in (l).
13) The residual moisture content of the product in the vials is checked as specified in directive (m). The product in all vials measured has to have an RM 1% {standard deviation <0.4 °C}. If this is not the case, directive (n) should be followed.
14) If, during stoppering, one or more vials break, directive (o) must be applied.
15) The visual inspection of XX vials cut open does not show any sign of skin on the cake surface and of collapsed inclusion near the bottom of the vial. The solubility test, described in directive (p), will be satisfactory for the dried product in all vials tested.

6.4 Description of Production Installations and Their Handling

6.4.1 The following documents supplied by the manufacturer can be used as part of this qualification: description and instruction manual, installation drawings and instructions, test and takeover certificates, and software documentation. It is recommended to list and specify all necessary documents and their format in the purchase order, as this reduces time and effort for both the buyer and the seller.

The installations have been taken over from the seller at (date and time). Before the takeover, the seller has successfully corrected complaints listed in Appendix 1 of the takeover protocol. The freezing and freeze-drying plant is registered as GF 50/95/1 and the loading and unloading system as GF 50/95/2.

6.4.2 The electrical power of both plants (XX kW) is supplied by the main power supply of building (F). An emergency diesel power supply of YY kW is installed, which switches on 1 min after a power break (if YY is not equal to XX, the sequence of components to be connected to the emergency set is listed in directive (q), deposited at the control center).

The control and calculating systems of both plants are connected by shielded cables to an independent power supply system, called computer power, that excludes influences of power variation or breakdown.

6.4.3 The cooling water (maximum XX m^3/h, maximum temperature +32 °C) is taken from the central supply system, which is protected against power

failure and has an ample reservoir. No compressed air is used by GF50/95/1. All drives are electric or hydraulic.

6.4.4 The training of the personnel on installations GF 50/95/1 and 2 is organized as laid down in directive (r).

6.4.5 The calibration of all instruments of the installations is carried out by the calibration service of the quality department, following the rules of that service. The computer programs used in the two installations are permanently tested by a program tested and accepted by the quality department. Errors or deviations are recorded and must be evaluated by the quality department as given in directive (s).

6.4.6 Changes in the program must be carried out as described in directive (t). If one or more of the following data are not supplied by the manufacturer, it is recommended to measure and to include them in the qualification document of the plants:

- The calculated evacuation time for the chamber and the condenser volume by the described pump set, for example, XX min down to 1 mbar, YY min down to 0.1 mbar, and ZZ min down to 0.03 mbar.
- The leak rate of chamber and condenser measured as proposed in Section 2.2.6.
- The flow of water vapor between chamber and condenser at least at two different pressures, as proposed in Section 1.2.4, for example, $p_{ch,H2O} = 0.5$ and 0.05 mbar.
- The temperature differences between the product of 10 different vials filled with specified product and the specified filling height, for example, five of these vials placed in the center and five at the border of the shelf. It is recommended to measure these differences during freezing and secondary drying with and without the shielding described in Section 1.2.1 (see Figure 1.103). The temperatures during freezing and secondary drying should be as specified in the process qualification. The results will give information on whether the applied shielding method is satisfactory for the process or requires improvements.

6.5 Equipment Performance Tests

6.5.1 The leak test described in directive (u) has been carried out twice in a row and on a third occasion 24 h later. The leak rates 2.0×10^{-3}, 2.3×10^{-3}, and 2.5×10^{-3} mbar L/s are below the requirements in directive (u). At the same time, the evacuation time has been measured. The averages of the three measurements have been 1.1 *a* min (±0.2 min) to 1 mbar, 1.3 *b* min (±0.2 min) to 0.1 mbar, and 2.2 *c* min (±0.4 min) to 0.03 mbar (*a*, *b*, and *c* are the calculated evacuation times). The results are acceptable (the degassing of the walls starts below 1 mbar). The final pressure after XX h of pumping has been between 0.015 and 0.025 mbar, which is below the manufacturer's specification.

6.5.2 The roughness of the shelves and the maximum pressure at the stoppering device have been documented in the takeover protocol. The maximum

cooling rate of the empty shelves has been 2.2 °C/min from 0 to −40 °C. The maximum heating rate from 0 to +40 °C is 2.5 °C/min. Both data meet the specification. The temperature differences on all shelves are smaller than ±1 °C in the temperature range between −40 and +40 °C, which corresponds to the specification.

6.5.3 The water vapor flow has been measured at two different pressures by using the instructions given in 6.4.6. In the calculated data, the time for evacuation is not taken into account; therefore, the data may have an error of ±10%. The vapor flow has been at a pressure $p_{ch} = 0.9S_m^{\#}$ (g/h) and at $0.1p_{ch} = 0.8S_m^{\#}$ (g/h), where $S_m^{\#}$ is the maximum possible flow at the tested pressure for a ratio $l/d = 2.5$ given in Figure 1.142 (the data given in the figure have to be multiplied by the free surface area of the connection between the chamber and condenser). The factors 0.9 and 0.8 show that the accuracy of such a test cannot be only a few percent, but the fact that both values are clearly below 1.0 indicates that the ratio l/d is larger than 2.5. In summary, the vapor flow performance of the plant can be accepted.

At the end of both tests, the condenser surface has been covered by an ice layer of ∼1.5 cm (by calculation). The visual inspection confirmed this as far as possible. Before both tests and after the second test, the condenser temperature has been T_{co} with changes smaller than ±1.5 °C. The defrosting time for the condenser by steam has been ∼XX min. The condenser performance is within the specifications.

6.5.4 The warning of undesirable trends during the process has been tested by providing undesirable trend data manually for the following trend measurements:

- cooling speed during freezing;
- T_{ice} at constant p_c;
- T_{ice} changes of more than 0.6 °C between two measurements after 2 h of MD until 8 h of MD (*Note*: in the first 2 h, the thermodynamic equilibrium is not reached and after 8 h MD comes to the end at which T_{ice} decreases anyway);
- the pressure decreases after SD has started does not reach $0.15p_c$ in 10 min.

In all cases, the trend warning has been activated, indicating the maximum tolerance of the trend.

6.5.5 The alarm system has been tested by applying by hand data outside the preset tolerances for the following process data:

- T_{pr} at the end of freezing;
- t_3 during which T_{pr} must be reached;
- T_{ice};
- $T_{sh,md}$;
- p_c;
- T_{co};
- t_{md};
- $T_{sh,sd}$;
- $p_{ch,sd}$;
- t_{sd}.

All alarm signals showed the correct identification and the acoustic alarm warned about the event.

All tests within the activities of Section 6.5 are recorded and documented in file (F).

A similar test protocol for the loading and unloading installation GT50/95/2 must be established. However, no example can be given, since this kind of equipment can be based on very different design layouts.

Media Fill Test (MFT)

Such a test is performed to check whether an aseptic freeze-drying process can be carried out.

Requirement: The lyophilizer preferably should have its own MFT program. If not, a manually freeze-drying program must be developed. The lyophilizer equipment is prepared for the MFT, which means it is cleaned (CIP) and sterilized (SIP). The same applies for the product trays. The clean room or isolator – class A – is qualified and in operation.

Generally, the MFT runs like a lyophilization process; there are usually parameters used. It is optional to use sterile air or nitrogen gas (N_2) to vent the chamber at the end of MFT.

All pressure/vacuum set points are multiplied by the factor 1.000.

Example: 0.25 mbar × 1.000 = 250 mbar [9]
0.01 mbar × 1.000 = 10 mbar [9]

At these values, there is danger that too much water is evaporated. Therefore, a pressure set point between 900 and 800 mbar should be used and controlled for the MFT. A fixed rule for the selected pressure does not exist; most of the range between 900 and 10 mbar applies.

Purpose of the MFT is to prove that in the process path → filling the product trays → loading the trays into the lyophilizer → freeze-drying → unloading the lyophilizer, no contamination occurs.

Proposal for a MFT program:

- loading the lyophilizer with 5–8 trays, each one filled with 0.5 to 1.0 L;
- of product (for example, bouillon);
- trays are placed on different shelves and different positions;
- shelf temperature during loading 10 °C;
- cooling (freezing process) at 10 °C;
- start PD (primary drying):
  - chamber pressure 900 mbar;
  - shelf temperature 10 °C;
  - time 22 h;
- pressure rise measurement (PRM) at end of PD:
  - time 2 s (no max. set value);
  - number of PRM: 1;
- start SD (secondary drying):
  - chamber pressure 900 mbar;
  - time 1:5 h;

- process end: venting with sterile air or N_2;
- examine product on contamination.

6.6 Quality of Installation to Document the Ability of Equipment to Operate Processes (Described in Section 6.3)

In the following table, the important process steps (Proc. No.), the process description (Process quantity (measure)), the related target data (Target data), and their tolerances (tolerances) are listed and compared with average data measured in three runs (Ave. act. data) and the minimum and maximum data measured in the three runs (min./max.). The last two data have to be taken from the protocols and listed. In the last column, the identification numbers of the runs in which the two extreme data are measured are listed (Ident. No.). Data for the last two columns are not given, with the exception of Proc. No. 1.1 as an example. The table is a proposal of how the comparison could be made. The list may not be complete in all possible cases and is concentrated on the time, pressure, and temperature data. Other methods may be preferred to make the ability of the equipment transparent.

Proc. No.	Process quantity (measure)	Target data (tolerances)	Ave. act. data (min./max.)	Ident. No.
1.1	Time between product being finished and start of freezing (h)	t (+10%)	$0.93t$ ($0.85t$/$1.01t$)	001/003
1.2	Temperature during 1.1 (°C)	T (±3 °C)		
1.3	Filling height in vials (mm)	XX (0%, +2%)		
2.1	Leak rate of chamber and condenser (mbar L/s)	<XX (+0)		
2.2	Subcooling (°C)	4–8 (±0)		
2.3	Cooling rate down to −40 °C (°C/min)	0.8–1.2 (±0)		
2.4	Resting time at −30 °C (min)	XX (−0, +YY min)		
2.5	Temperature during 2.4 (°C)	30 (−3, +0 °C)		
3.1	Condenser temperature during MD	≤45 °C (+0)		
3.2	Time of evacuation to p_c (min)	XX (+30%)		
3.3	Controlled pressure during MD (mbar)	p_c (−0, +10%)		
3.4	T_{sh} after 3.2 completed (°C)	−10 (±1.5 °C)		
3.5	T_{ice} 1 h after 3.2 (°C)	−30 °C (+0, −1 °C)		
3.6	Standard deviation of 3.5	<0.4 °C		
3.7	Duration of MD from 3.2 to 4.1	t_{md} (±0.5 h)		
4.1	Change from MD to SD	T_{ice} = max. $T_{ice,ave}$ −2 °C		

(*continued*)

(*Continued*)

Proc. No.	Process quantity (measure)	Target data (tolerances)	Ave. act. data (min./max.)	Ident. No.
4.2	p_{ch} 10 min after 4.1 (mbar)	$p_c/8$ ($<p_c/7$)		
4.3	T_{St} during SD (°C)	+35 (+0, −1 °C)		
4.4	T_{pr} during SD to reach	33 (−3, +2 °C)		
4.5	T_{co} during SD	≤55 (+0)		
4.6	DR after 1.5 h of SD (%/h)	3 (1–5%/h)		
4.7	dW at the end of MD (%)	0.6 (±0.3%)		
4.8	Time of SD (h)	t_{sd} (±0.5 h)		
5.1	Time of venting with gas (G) (min)	XXX (−0, +20%)		

Such a (or a similar) comparison not only proves that the process in the installations can be completed reproducibly within the given tolerances, but also that the information may be helpful:

- To assess the target data and their tolerances. If the average data of all three runs are approximately in the middle of the tolerances, the target data and their tolerances are an optimum.
- To assess the reproducibility of the total process. If the maximum and minimum actual data relate mostly to the same run, reproducibility is just within the tolerances. If one run is not referred to at all, this run would be the best and one can try to find the reasons why this has happened.
- To select such process numbers whose average actual data are very close to the target data and study, whether the tolerances can be reduced or enlarged if the maximum and minimum data are close to the tolerances in all three runs.
- To calculate the standard deviations of the average actual data and use these in future runs as a trend warning when the standard deviation with new data added changes measurably.

6.7 Documentation of the Quality of the Products Manufactured (in Comparison with Section 6.2)

The product development department and/or quality assurance department prove and document that the products manufactured in the runs described above have the specified quality.

References

1 GMP-/FDA-gerechte Validierung (2002) Qualifizierung von Anlagen und Validierung von Prozessen und Systemen, Pharma-Technologie Journal, Editio Cantor Verlag, Concept Heidelberg, Heidelberg, Germany.

2 GAMP (2017) Information: http://www.ispe.org/gampinfo/htm.
3 PIC/S Validation Guide (2011) Validation of aseptic processes. Available at http://www.picscheme.org/pubs/htm.
4 ISPE (2001) Baseline Pharmaceutical Engineering Guides, Vol. 5, Commissioning and Qualification Guide.
5 GMP-Gesetze der USA (2002) 21 CFR 210/211 cGMP for Finished Pharmaceuticals, 21 CFR 11 Electronic Records, Electronic Signature. Maas & Peither GMP-Verlag, Schopfheim.
6 Powell-Evans, K. (1998) Streamlining validation. *Pharm. Technol. Eur.*, **10** (12), 48–52.
7 FDA (1987) FDA Guideline on General Principles of Process Validation.
8 FDA (1983) FDA Guide to Inspections of Validation of Cleaning Processes.
9 FDA (2006) FDA/ORA Compliance Policy Guide. Sub chapter 490.100. Process Validation Requirements for Drug Products and Active Pharmaceutical Ingredients Subject to Pre-Market Approval (CPG 7132c.08).
10 Gieseler, H. (2007) PAT for freeze-drying cycle optimization in the laboratory. Department of Pharmaceutics, University of Erlangen-Nuernberg; *European Pharmaceutical Review*, Issue 1.
11 Hussain, A.S. (2001) Emerging science issues in pharmaceutical manufacturing: practical analytical technologies. FDA Science Board Meeting, Nov. 2001.
12 Guttzeit, M. (2011) Team Leader, Validation, GEA Lyophil GmbH, Huerth/Germany.
13 Fricke, G., Boeckem, M., and Steiner, M. (2007) PDA Global PAT Conference, Bethesda, Maryland USA, May 2007.
14 Winkle, H. (2007) Implementing quality by design. PDA/FDA Joint Regulatory Conference, 9/24/2007.

Appendix: Abbreviations, Symbols, and Unit of Measure

Symbol	Meaning	Unit of measure
Å	Ångström unit	0.1 nm
ANSI	American National Standardization Institute	
ASME	American Society of Mechanical Engineers (American authority for pressure code regulations)	
AV	average value	
α	heat transfer coefficient	kJ/(°C m^2 h), J/(°C cm^2 s)
a_w	water activity	p/p_s
BTM	barometric temperature measurement	
b/μ	permeability of water vapor through the dried product	kg/(h m mbar)
CA	capacitive vacuum gauge	
cGMP	current Good Manufacturing Practice	
CIP	Clean-in-Place	
CPA	cryoprotective agent	
c_f	specific heat of solids	kJ/(kg °C)
c_g	concentration of solids at T_g	% (w/w)
$c_{g'}$	concentration of solids at $T_{g'}$	% (w/w), g/g
c_{ice}	specific heat of ice	kJ/(kg °C)
c_p	specific heat of gas (constant pressure)	kJ/kg °C)
c_w	specific heat of water	kJ/(kg °C)
d.b.	dry basis	
DE	demineralized water	
DR	desorption rate, desorbed water in % of solids per hour	%/h
DSC	differential scanning calorimetry	
DTA	differential thermal analysis	

(*continued*)

Freeze-Drying, Third Edition. Peter Haseley and Georg-Wilhelm Oetjen.

(*Continued*)

Symbol	Meaning	Unit of measure
d	thickness of layer, diameter	cm, m
dp	pressure rise	mbar
dt	time of dp	s, h
dT	temperature difference	°C
dW	desorbable water in % of solids	%
E	enthalpy	kJ/kg
ER	electrical resistance	Ω
ESM	electron scanning microscopy	
ε	radiant efficiency, radiance of the emitter/radiance of a black body	
F	area	m^2, cm^2
FDA	US Food and Drug Administration	
F_{sh}	shelf area in a drying chamber	m^2, cm^2
H_2O_2	hydrogen peroxide	
Hz	frequency	Hz
h	hour(s)	h
GAMP	Good Automation Manufacturing Practice	
Ic	ice, cubic	
Ih	ice, hexagonal	
ISPE	International Society for Pharmaceutical Engineering	
J_{nmr}	coupling constant, measure of the splitting of lines in NMR measurements	
J^*	nucleation rate	nuclei/(volume time)
K	thermodynamic temperature	K
K_{su}	heat transfer coefficient from the heating medium to the freezing zone	kJ/(m^2 h °C)
K_{tot}	heat transfer coefficient from the heating medium to the sublimation front s	kJ/(m^2 h °C)
LN_2	liquid nitrogen	
L	liter	liter
LR	leak rate of a plant	mbar L/s
LR_{max}	maximum tolerable leak rate of a plant	mbar L/s
LS	sublimation energy of water	kJ/kg
LSKM	Limited Spearman Karber Method	
LW	evaporation energy of water	kJ/kg
l	length	m, cm, µm, nm
Λ	wave length of light	nm

(*Continued*)

Symbol	Meaning	Unit of measure
λ	thermal conductivity	kJ/(m h °C)
λ_g	thermal conductivity of frozen product	kJ/(cm s °C)
λ_{tr}	thermal conductivity of dried product	kJ/(cm s °C)
M	molar mass	g/mol, L/mol
MD	main drying, sublimation drying	
m	mass	kg
mM	quantity of particles	
m_{H_2O}	mass of water, sublimate during MD	kg
m_{ice}	mass of water frozen to ice	kg
m_{solid}	mass of solids	kg
Δm	part of frozen water	kg/kg
min	minute(s)	min
n	Amount of substance	mol
NA	Avogadro constant	
NIR	near infrared spectroscopy	
NMR	nuclear magnetic resonance	
NODT	nucleation on demand technology	
OPC	operation pressure control	
OQ	operational qualification	
p	pressure	bar, mbar
p_c	controlled operation pressure during MD	mbar
p_{ch}	pressure in the drying chamber	mbar
p_{co}	pressure in the condenser	mbar
p_{end}	end pressure	mbar
$p_{H_2O,ch}$	partial water vapor pressure in the chamber	mbar
p_{ice}	p_s of ice	mbar
p_{md}	pressure during MD	mbar
p_{pg}	pressure of permanent gases	mbar
p_s	saturation vapor pressure	mbar
p_t	total pressure	mbar
Δp	$p_s - p_{H_2O,ch}$	mbar
PAT	practical analytical technology	
PLC	programmable logic controller	
PP	pilot plant	
P1	production plant (smaller plant)	
P2	production plant (bigger plant)	

(*continued*)

(*Continued*)

Symbol	Meaning	Unit of measure
PRM	pressure rise measurement	
PT 100	temperature resistance sensor	
PQ	performance qualification	
Q	quantity of heat	J, kJ, W s
Q_e	melting energy of ice	kJ/kg
Q_{tot}	total quantity of heat	kJ
q	density of heat flow	W/m^2
qL	leak rate	mbar L/s
qpv	suction capacity	mbar L/s
Ra	surface roughness	µm
Re	Reynolds number	
RF	Karl Fischer titration	
RM	residual moisture content	% (water in % solids)
RMIR	residual moisture measurement by NIR	
RTD	resistance temperature gauge	
r	radius	m, cm
ρ_g	mass density of a frozen product	kg/m^3, g/cm^3
S	suction speed of the plant vacuum system	m^3/h, L/s
S_{LS}	suction speed after the trottle L	m^3/h, L/s
S^*	spin	
S^{**}	magnetic field strength	G
$S^\#$	gas or vapor stream	g/h, g/s
SA	standard deviation	
SD	secondary drying	
SEM	scanning electron microscope	
SIP	sterilization-in-place	
S_W	surface of the chamber walls; door; shelves; condenser walls; evaporator	m^2
s	second(s)	s
$s^\#$	gas or vapor stream density	$g/(cm^2\ s)$
σ	unit conductance	$kJ/m^2\ h\ K^{-4}$
T	temperature	°C
T_o	freezing temperature of water	°C
T_1	temperature of water at process start	°C
T_{am}	"antemelting" temperature	°C
T_c	collapse temperature	°C
T_{co}	condenser temperature	°C

(*Continued*)

Symbol	Meaning	Unit of measure
T_d	devitrification temperature	°C
T_e	eutectic temperature	°C
T_{end}	final/end temperature of the condenser	°C
T_g	glass transition temperature	°C
$T_{g'}$	glass transition temperature if all freezable water is crystallized	°C
T_{tot}	time-weighted average of temperature difference ($T_{sh} - T_{ice}$) during MD	°C
T_h	crystallization temperature of hexagonal ice	°C
T_{hc}	temperature of homogeneous crystallization	°C
T_{ice}	temperature of ice at the sublimation front	°C
$T_{ice/n}$	sum of all n T_{ice} measurements divided by n	°C
T_{im}	"incipient melting" temperature	°C
T_k	crystallization temperature of hexagonal ice	°C
T_m	melting temperature	°C
$T_{m'}$	temperature of bilayer transition	°C
T_{md}	temperature during MD	°C
T_{me}	temperature of the heating and cooling medium	°C
T_{pr}	product temperature	°C
$T_{pr,SD}$	product temperature during secondary drying	°C
T_r	recrystallization temperature	°C
T_{sc}	temperature to which a product subcools	°C
T_{sh}	shelf temperature	°C
$T_{sh,\ SD}$	shelf temperature during secondary drying	°C
T_{str}	temperature of a radiant surface	°C
T_{tb}	tray bottom temperature	°C
TG	thermogravimetric method	
Th	thermocouple	
TM	heat conductivity vacuum gauge	
TUEV	Technischer Überwachungsverein (German authority for pressure code regulations)	
t	time (space of -)	h, min, s
t-BA	*Tert-butanol*	
t_e	freezing time	h, min
t_{md}	main drying time	h
t_{sd}	secondary drying time	h
t_{SGR}	spin–lattice relaxation	s

(*continued*)

(*Continued*)

Symbol	Meaning	Unit of measure
t_{SR}	spin–spin relaxation	s
t_{to}	total drying time	h
UFW	"unfreezable water"	% (of total water)
VMP	Validation Master Plan	
VPM	vapor pressure moisture technology	
V	volume	m^3, L, cm^3
V_{ch}	volume of a drying chamber	m^3, L
ν	speed	m/s
ν_c	growing speed of nuclei	cm/s
ν_f	cooling rate	°C/s
ν_k	Speed of crystallization	m/s
ν_T	Speed of temperature changes	m/s per °C
ν_t	Speed per time unit	m/s
x_f	part of solids	kg/kg, %
x_w	part of water above 0 °C	kg/kg
$x_{w'}$	part of ice	kg/kg
ζ_w	part of water in the dry product	kg/kg
ξ_w	part of water	kg/kg
WFI	Water for Injection	

Explanation Power-Down Process:

Collagen in form of a plate with a thickness from about 5 to 40 mm is placed between two shelves (Sandwich principle) that can be cooled and heated. One of these plates (shelves) is movable. The plates (shelves) are moved together and the cooling process starts. The heat transfer (freezing) starts from both sides – Power-Down method.

Index

Freeze-Drying, Third Edition. Peter Haseley and Georg-Wilhelm Oetjen.

d

g

h

WILEY END USER LICENSE AGREEMENT

Go to www.wiley.com/go/eula to access Wiley's ebook EULA.